AN INVESTIGATION OF SPLAYING
IN REDRAWING

by

JOHN ARTHUR WALTERS, B.Sc.

Submitted in fulfilment of the requirements for the degree of Doctor of Philosophy.

The University of Aston in Birmingham

June, 1971.

Thesis
621.77
WAL

-8DEC71 145471

SUMMARY

Experimental and theoretical studies were made of splaying behaviour in the direct redrawing process. Cup diameter/thickness ratio governs whether redrawing is conducted with or without a hold-down punch to prevent wrinkling during deformation. Both situations, (termed constrained redrawing and unconstrained redrawing respectively), were investigated from a splaying aspect.

Splaying was related to that deformation in the cup which precedes die contact during steady-state redrawing conditions, and was associated with a reduction in redraw load. The phenomenon was explained by the principle of minimum energy of deformation.

In unconstrained redrawing splaying increased as cup diameter/thickness ratio diminished, whereas in the constrained situation severity of bending around the hold-down punch profile radius was the predominant parameter, diameter/thickness ratio having only a weak influence. For constrained redrawing die geometry did not directly influence the potential for splaying but dies of small angle prematurely terminated the splaying phase. For unconstrained redrawing die geometry both influenced splaying potential and restricted maximum splaying. Dies of large angle will therefor generally promote greatest splaying.

Experimental results implied that splaying decreases as the rate of work-hardening increases. Greatest splaying was 4 - 4.5% and occurred in constrained redrawing with the combination of a small hold-down punch profile radius, large die angle and work-hardened cups.

Theory correctly predicted all experimental trends. Two expressions for maximum splaying are proposed, one providing an over-estimate and the other an under-estimate. Experimental results were spread between the limits of these expressions.

The use of a guide to prevent splaying did not produce a reduction in redraw load. There was evidence to suggest that the contrary was true.

Results of research should be equally applicable to the reverse redrawing process.

AN INVESTIGATION OF SPLAYING IN REDRAWING.

Contents.

Contents (continued.)

Contents (continued.)

Contents (continued.)

Contents of appendices.

NOMENCLATURE IN THESIS

Symbols of geometry

t_o, r_o - Wall thickness and radius of blank before cupping or wall thickness and mean radius of entering cup in redrawing.

t, r - Wall thickness and mean radius of an element at any stage during cupping or redrawing.

t_e, r_e - Final wall thickness and mean radius of cup after cupping or redrawing.

R - Current radius of bending or unbending.

R_n - Current radius of neutral surface in bending or unbending when this is not coincident with R.

R_o - Mean radius of bending of cup wall at die entry during steady-state redrawing for either constrained or unconstrained conditions.

R_c - Mean radius of bending of cup wall around hold-down punch in constrained redrawing.

R_f - Mean free radius of bending of cup wall at die entry in unconstrained redrawing.

R_d - Mean radius of bending of cup wall over die profile radius in cupping or redrawing.

R_p - Mean radius of bending of cup base around draw punch nose.

θ - Angle between planes of reference in bending or drawing along a circular path.

ϕ - Angle between planes of reference around cup circumference.

λ	-	Shift of neutral surface from central surface when bending or unbending under tension.
y	-	Radial distance of any element from the neutral surface of bending or unbending.
y_b	-	Radial distance of elastic/plastic interface from the neutral surface in bending or unbending.
α	-	Die and hold-down punch semi-angle in redrawing.
γ	-	Draw ratio in cupping or redrawing $= \frac{r_o}{r_e}$
l_o	-	Initial length of cup wall involved in splaying.
l	-	Current length of cup wall involved in splaying.

Symbols of stress and strain

σ	-	Normal stress.
ε	-	Normal plastic strain.
e	-	Normal elastic strain.
$\sigma_1, \sigma_2, \sigma_3$	-	Cup wall stresses in the radial, through-thickness and circumferential directions respectively.
$\varepsilon_1, \varepsilon_2, \varepsilon_3$	-	Cup wall plastic strains in the radial, through-thickness and circumferential directions respectively.
Y	-	Uniaxial yield stress.
$\bar{\sigma}$	-	Equivalent stress.
$\bar{\varepsilon}$	-	Equivalent plastic strain.
σ'	-	Deviatoric stress.
σ_m	-	Hydrostatic stress.
τ	-	Shear stress.
S	-	Radial splay in an element.
ΔS	-	Fractional circumferential strain induced in an element by splaying.

Symbols of forces and moments

P	-	Punch load in cupping or redrawing.
H	-	Hold-down force in cupping or redrawing.
M	-	Bending moment.

Symbols of energy

w_s, w_b, w_r	-	Specific plastic work components associated with splaying.
W_s, W_b, W_r	-	Bulk plastic work components associated with splaying.

Symbols of constants

a	-	Gradient of equivalent stress-strain curve.
m	-	Constant for adjusting Tresca's yield criterion.
μ	-	Coefficient of friction.
E	-	Modulus of elasticity.
ν	-	Poisson's ratio.

I. INTRODUCTION.

The term 'splaying' is used to describe a redundant deformation occurrent in the redrawing process. For certain materials at high plastic-strain levels splaying may be a source of product failure and rejection. Although reported observations of splaying have usually been made when redrawing by the direct method, the phenomenon is apparently not confined to this arrangement, and may also be troublesome in reverse redrawing. It is probable that the basic causes of splaying are common to both types of redrawing, and therefore a study of either one type should provide information generally relevant to the other. Since direct redrawing is used at Tube Investments Limited, this method was selected for the research reported in this thesis.

FIG. 1. illustrates a typical direct redraw arrangement where the entering cup of radius r_o is reduced to radius r_e by a punch drawing the cup through a die. Direct redraws may broadly be classified into two groups, namely constrained and unconstrained (or free). In the first category, comprising thin-walled cups, a hold-down punch is used to apply a compressive force to the plastically deforming cup flange and thus suppress a tendency for the flange to wrinkle. In the second category, comprising relatively thick-walled cups, the flange-wrinkling tendency is absent and a hold-down punch becomes unnecessary. Splaying has been observed in both categories, inferring that the underlying mechanism is fundamental to the redraw process rather than a particular tooling configuration.

Whilst the entering portion of the partially redrawn cup is long, it is sufficiently rigid to resist any flexural tendencies arising from plastic deformation prior to contact with the die mouth. As the redraw proceeds however and the length of entering cup becomes progressively shorter, a stage is reached where this shortened length is incapable of supplying the constraint necessary to maintain the previous

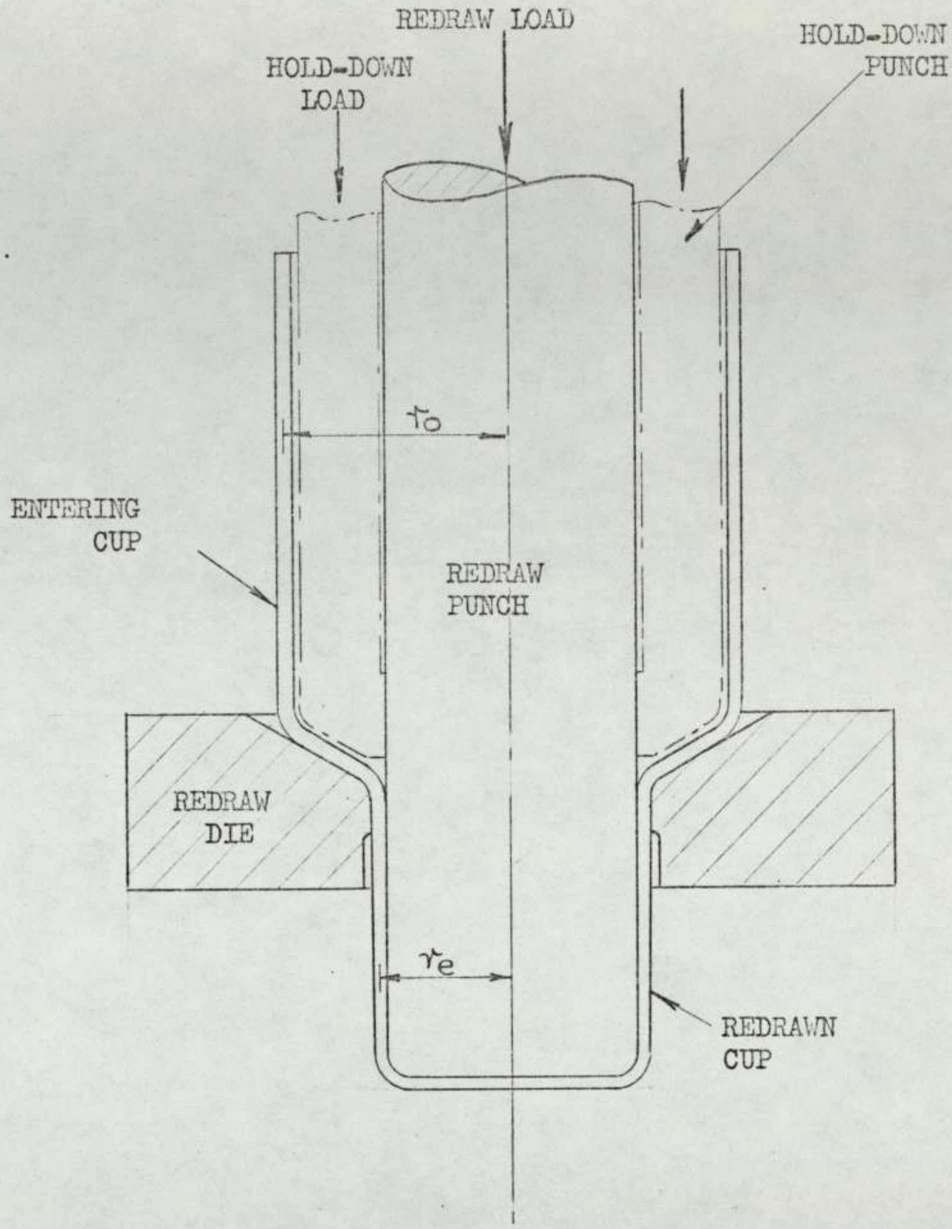

FIG. 1 A TYPICAL DIRECT REDRAWING OPERATION.

equilibrium. The entering cup wall then proceeds to deform radially outwards to produce the effect known as splaying illustrated in FIG. 2. High tensile circumferential stresses developed in the region of the cup rim may promote longitudinal splitting.

A deep-drawing process is currently under development at Tube Investments Limited, whereby a flat circular blank is sequentially drawn through a number of diameter reducing stations, without interstage annealing, to produce an elongated cup. The overall plastic strain suffered by the blank is much more severe than that encountered in conventional deep-drawing operations, and consequently in the latter stages of the process, most of the commonly deep-drawn materials possess little residual ductility. In 1967 a research and development programme was initiated with stainless-steel to determine maximum draw ratios per stage in a four-draw schedule. Early in the programme it was found that although cups were processed without failure in the tools, a high proportion of the finished cups were unacceptable due to longitudinal splits extending into the cup body from the rim. Observations made on the forming process revealed that splaying occurred in every redraw, and that fractures in the cup rim usually occurred in the third and final draw stages as a consequence of splaying.

A literature survey revealed that during studies of the deep-drawing process Swift[1] and others observed splaying in direct redrawing and concluded its effect was to increase punch load, causing cup failure as a result of excessive drawing stress. By modifying the redraw tooling arrangement to provide a guiding section at die entry, Swift prevented splaying, and eliminated the increased redraw load corresponding to splaying.

After Swift's example the conventional redraw dies in use for the stainless-steel programme were replaced by guided redraw dies, of a type such that the guiding section was an integral part of the die proper. Further drawing experiments gave a high failure rate in the

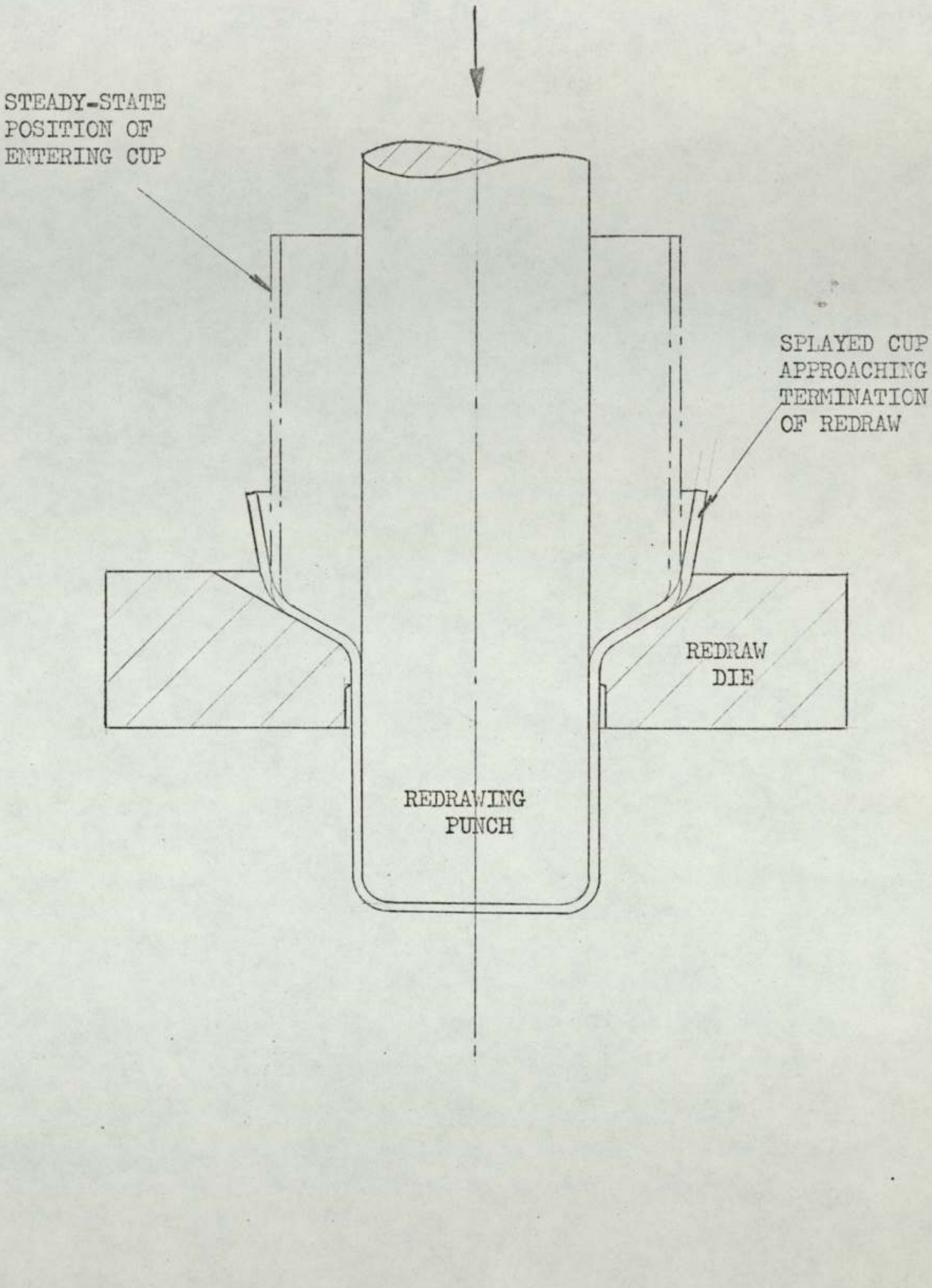

FIG. 2 SPLAYING OF A CUP IN REDRAWING

tools, failures being of the burst-bottom type characteristic of excessive drawing stress. Load measurements subsequently taken confirmed that redraw loads with guided dies exceeded those with conventional, unguided dies. At that juncture the stainless-steel series of experiments were discontinued leaving the apparent anomaly with Swift's results unresolved.

To provide further information on the effects of guiding in redrawing, an experimental study was carried out at Tube Investments Research Laboratories in 1968. In these tests aluminium-alloy cups were redrawn with a tooling geometry widely different from that used in the stainless-steel programme. However it was again concluded that guided redraws required higher drawing loads than their unguided counterparts.

A further, more comprehensive search of deep-drawing literature provided little additional information, and indicated that although splaying was recognised as a troublesome feature of redrawing, the mechanics of the phenomenon were not fully understood. In January 1969, a programme of research was initiated with the broad objective of increasing knowledge of splaying in redrawing. This thesis is a record of that work.

The thesis is compiled in accordance with chronological sequence of activity. Thus the bulk of theoretical work on splaying was undertaken after the first and second experimental programmes were completed, when evidence was available on which to base key assumptions made in developing theories. The third, final, experimental programme was designed to test theories under conditions resembling those in deep drawing at Tube Investments.

2. SURVEY OF DEEP DRAWING LITERATURE.

2.1. INTRODUCTION.

The survey comprises a variety of papers embracing various aspects of deep drawing science with which the writer became acquainted during the course of research, and drew upon, either directly or indirectly, in formulating investigational programmes and developing theoretical analyses.

Only the last of eight sections presented is concerned with papers on splaying, and is largely of a descriptive nature reflecting the general lack of knowledge on the subject.

The first two sections are devoted to cupping and redrawing theory and experiment, in which the works of Chung and Swift form major contributions. Flange wrinkling is the subject matter of the third section. The remaining sections briefly discuss anisotropy, residual stresses, friction, lubrication and speed effects, and simulative tests in the context of their significance to deep drawing.

2.2. CUPPING EXPERIMENT AND THEORY

(a) Introductory comments.

Cupping is the oldest and most widely used deep drawing operation, and is characterised by the radial drawing of a flat blank to form a cup-like component with closed bottom and open top. Usually, but not always, products of the process are cylindrical, being formed from a circular blank. When fully exploited the process provides a cup whose depth is equal to or slightly less than its diameter. If no deliberate attempt is made to control wall thickness, the latter varies from closed to open end, being approximately equal to blank thickness near the closed end and of greater thickness near the open end.

Cupping is a complex metal forming operation, not lending itself readily to theoretical analysis. The forming load is developed as a result of deformation at the die, whilst under unfavourable conditions failure of the cup usually occurs adjacent to the punch nose radius. The situation is further complicated by the process being of a non-steady state nature. Mechanics of deformation at the die are now well understood, but no comprehensive theory exists for accurately predicting deformation at the punch nose.

Crane (1938)[2], Jevons (1940)[3], and Sachs (1951)[4] have published extensive works on cupping. The largest contribution to an understanding of the process however, resulted from work conducted at Sheffield university under the guidance of Swift during the period 1940 - 1950. This culminated in a two-part paper by Chung and Swift[5] in 1951. The first part of the paper described an experimental investigation into various process parameters. Strain development in the punch nose vicinity was closely observed. The second part of the paper comprised a theoretical study of stresses and strains developed in a cup radially drawn from a circular blank. Their approach, now regarded as classical, has been followed in numerous subsequent theoretical treatments of deep drawing operations.

Although the theory of Chung and Swift gives excellent correlation with experimental evidence it is intractable and unsuitable for rapid calculations. It was thus an attractive proposition to simplify the theory and so obtain more rapid, though less accurate means of computation. A good example of this is the analysis of Barlow[6], who provided an approximate method of estimating maximum draw ratios in cupping.

The practical aspects of Swifts work on cupping were covered by Willis[7], whilst Alexander[8] has written a comprehensive review on the theories of Chung and Swift.

The remainder of this section is devoted to discussing in more detail the works of Chung and Swift, and Barlow.

(b) Experimental work of Chung and Swift.

The investigation was conducted on a 50 Tonf. mechanical press producing cups 4 inches diameter from blanks ranging from 0.025 to 0.060 inches thick. The press cycling speed was 8.2 strokes/minute, and graphite-tallow lubricant was used throughout. Most cups were produced in low carbon steel, but for comparison additional cups in aluminium, brass and copper were made.

Aspects of the process investigated were:

(i) Method of blank holding.

(ii) Drawing ratio.

(iii) Die profile radius.

(iv) Punch profile radius.

(v) Punch-die radial clearance.

(vi) Cup material.

(vii) Blank thickness.

(i) Method of blank holding.

Two methods were investigated, constant pressure and constant clearance. In the former, force on the blank-holder was maintained constant throughout any cupping operation but could be adjusted to suit cupping conditions as required. In the latter, the blank-holder was clamped to the die, giving a fixed clearance between the two members.

A series of tests were conducted to determine the effect of varying hold-down pressure on the process. It was found that provided the holding force was above a lower limit (giving wrinkle-free drawing), increasing that force had little effect on either draw load or the condition of drawn cups. The view was held that the increased frictional drawing-load component caused by the higher holding force was offset because the deforming cup flange was thinner and therefore offered less resistance to deformation.

In a further series of tests the merits of each type of blank-holding were compared. It was found that the constant pressure method gave slightly lower drawing loads that that of constant clearance.

(ii) Drawing ratio.

Steel blanks of various diameters were cupped using a constant punch/die diameter. Results indicated that for a given tooling arrangement draw load increased linearly with blank diameter, and that maximum draw load occurred later in the draw-cycle as the blank diameter increased. FIG. 3. shows a typical family of punch load/ travel curves.

Examination of drawn cups revealed the presence of two necks in the vicinity of the bottom-wall junction radius. The upper, smaller neck occurred where the radius merged with the cup wall and is shown as 'A' in FIG. 4. The lower, larger neck located around the radius, was the fracture site when drawing under unfavourable conditions.

(iii) Die profile radius.

The die profile radius was found to exert a significant influence on both punch load/travel characteristics and maximum achievable draw ratio. When the die radius/blank thickness ratio was below 10 a decrease in radius caused an increase in punch load, and wall thinning at the critical lower neck. Little was achieved by increasing the die radius/blank thickness ratio above 10. An upper limit on the ratio was set by a tendency for the cup to wrinkle around the die profile. FIG. 5. shows the relationship between die profile radius and maximum drawable blank diameter.

(iv) Punch profile radius.

In this series of tests the effect of punch profile radius on punch load/travel characteristics and wall thinning were observed. Punch profile radius was varied over the range 1/8 - 2 inches, the latter corresponding to a hemispherical profile.

With small draw ratios it was found that punch load decreased as punch radius increased, but with larger draw ratios the effect was absent, maximum punch load being independent of punch radius. For all

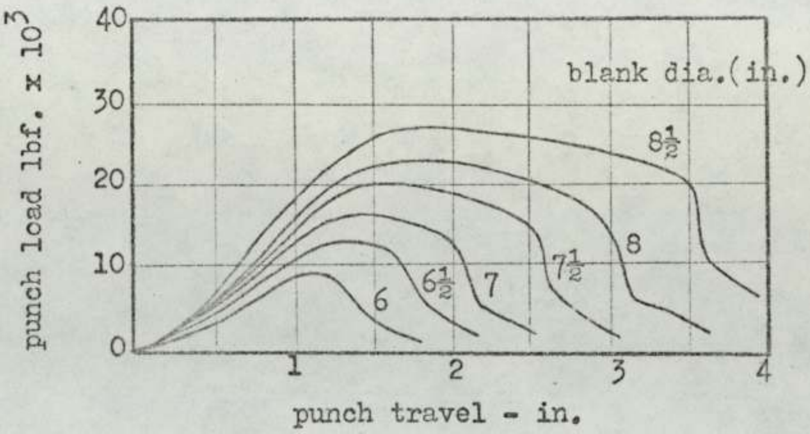

FIG. 3 EFFECT OF BLANK DIAMETER ON PUNCH LOAD-TRAVEL

punch profile radius 1 in.

die profile radius $\frac{3}{8}$ in.

positive pressure holder.

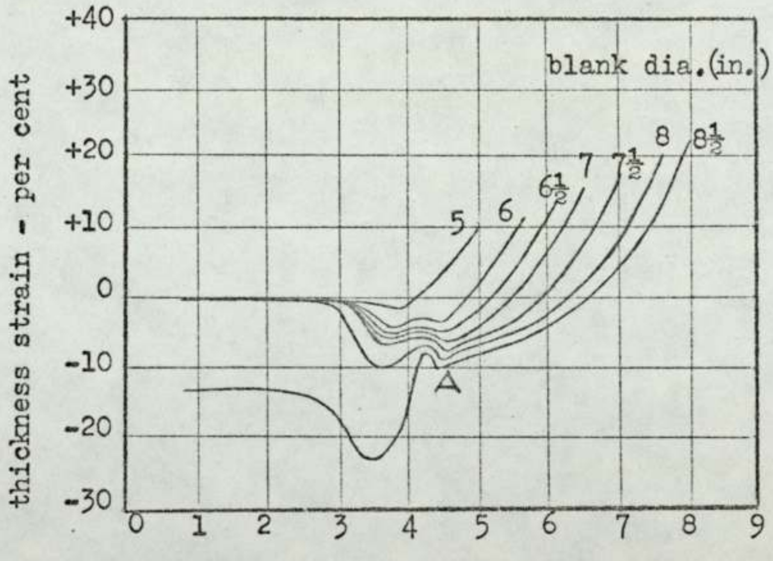

FIG. 4 EFFECT OF BLANK DIAMETER ON THICKNESS STRAIN

punch profile radius $\frac{1}{4}$ in.

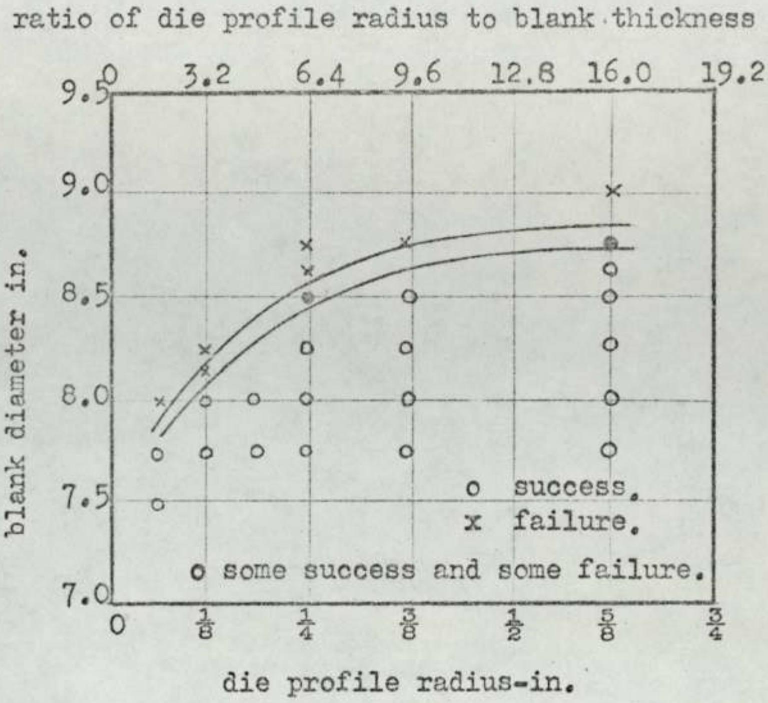

FIG. 5 EFFECT OF DIE PROFILE ON DRAWING CAPACITY

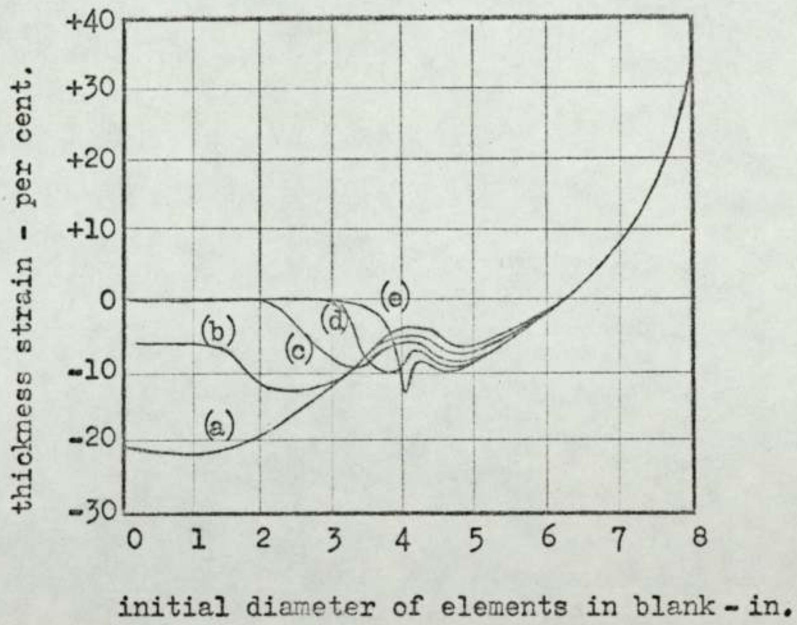

FIG. 6 EFFECT OF PUNCH PROFILE ON THICKNESS STRAINS

a punch profile radius 2 in.

b punch profile radius 1 in.

c punch profile radius ½ in.

d punch profile radius ¼ in.

e punch profile radius ⅛ in.

tests the effect of increasing punch radius was to retard the point of maximum punch load within the draw cycle. The observed retarding effect was attributed to the greater distance travelled by a large-radiused punch whilst initially embedding in the blank. With small draw radius this process continued up to the maximum load point and was responsible for the lower loads recorded. As the draw ratio increased the embedding process was complete with all punch radii investigated before that point in the draw cycle corresponding to maximum punch load. Then all maximum punch loads were comparable.

FIG. 6. illustrates the manner in which punch nose profile was found to influence local thinning in the cup bottom. A small punch radius produced upper and lower necks in the vicinity of the cup radius, the lower neck being most severe. Little thinning occurred over the flat cup base. The effect of a large punch radius was to produce greater general thinning over the base of the cup.

The necking patterns of FIG. 6. were explained in terms of loading conditions at the commencement of cupping when the blank became progressively deformed to the die and punch radii contours. During this period bending at die and punch occurred under tension imposed by the large, as yet undeformed outer blank area, and resulted in thinning at the two regions. On further punch advance the locally thinned metal previously at the die radius became the upper neck observed in the final cup. The form of the lower neck was dependent upon the magnitude of the punch radius. If the latter were small, acute local necking resulted from severe bending under tension. Conversely a large punch radius produced little bending strain but a more general base thinning as the material was stretch-formed under bi-axial tension.

A number of cups were drawn in soft and half-hard aluminium. It was found that a hemispherical punch profile gave the highest draw ratio with the soft material, whereas the smallest punch radius available (1/8 inch) gave best results with the half-hard stock. Cups in the half-hard material were compared with steel cups drawn on the same tooling and found to exhibit similar necking patterns. However steel had previously been shown to draw best on a hemispherical punch. This anomalous behaviour of aluminium could not at the time be explained by Chung and Swift, however subsequent work by Loxley and Freeman indicated that frictional condition over the punch nose was a critical factor.

The uncertainty of friction at the punch nose has prevented accurate theoretical prediction of maximum draw ratios in cupping. Unless frictional conditions are known precisely it is not possible to establish either the site or stress situation of the fracture zone.

(v) <u>Radial clearance between punch and die.</u>

Tests indicated that a 10% clearance caused ironing at the cup rim but no excessive increase in punch load, whereas cups drawn with 70% clearance exhibited bell-mouths. It was concluded that generally 30% clearance provided satisfactory results.

(vi) <u>Cup material.</u>

Tests were conducted on low carbon steel, aluminium (soft and half-hard), copper (half-hard) and 70/30 brass (half-hard). It was found that for a given tooling arrangement the maximum punch load point within the draw cycle was strongly influenced by the work-hardening properties of the materials tested. For a low work-hardening material (half-hard aluminium), the peak load occurred early, whereas a high work-hardening material (70/30 brass) gave a peak punch load when the draw cycle was well advanced.

An examination of the drawn cups revealed that low work-hardening materials exhibited marked upper necks, less severe lower necks and little general base thinning. The converse was true for high work-hardening materials.

(vii) <u>Thickness of blanks.</u>

Steel blanks 0.025, 0.039 and 0.060 inch thick were cupped on tooling with a die radius/blank thickness ratio of 6.5, and a radial die-punch clearance of 30%. It was found that for a given blank diameter punch load was linearly related to blank thickness.

(c) Theoretical treatment by Chung and Swift.[5]

The theory establishes radial drawing stress and principal strains in the cup wall at any stage during the cupping operation. Account was taken of all process parameters influencing this stress including blank-holder friction, plane radial drawing in the flange, plastic bending and unbending at entry to and exit from the die profile radius, and radial drawing in the presence of friction around the die radius. Effects of anisotropy were ignored.

No attempt to analyse stresses and strains in the punch-nose vicinity were made, although these will be strongly influenced by radial drawing stress in the cup wall. The theory provides information on the type and magnitude of strains imposed during cupping and enables press loads and power requirements to be calculated.

(i) Distribution of stress and strain.

The deformation zone was considered to comprise a number of distinct stages. It was assumed that at any instant in the draw cycle the radial stress in the cup wall was the summation of radial stress increments generated at each of the stages. This concept is best described with reference to FIG. 7.

Deformation in the plane flange is such that during drawing the outer rim thickens to a greater extent than elements at a smaller radius. It is therefore assumed that the total blank-holder force always operates at this point, causing resistance to radial drawing and imposing a radial stress σ_{1A} . Radial drawing occurs between points A and B generating a radial stress $\sigma_1'{}_B$ at B. Plane radial drawing ends at B where the flange is assumed to instantaneously bend to the die radius, receiving an abrupt radial stress increment b_1 so that the

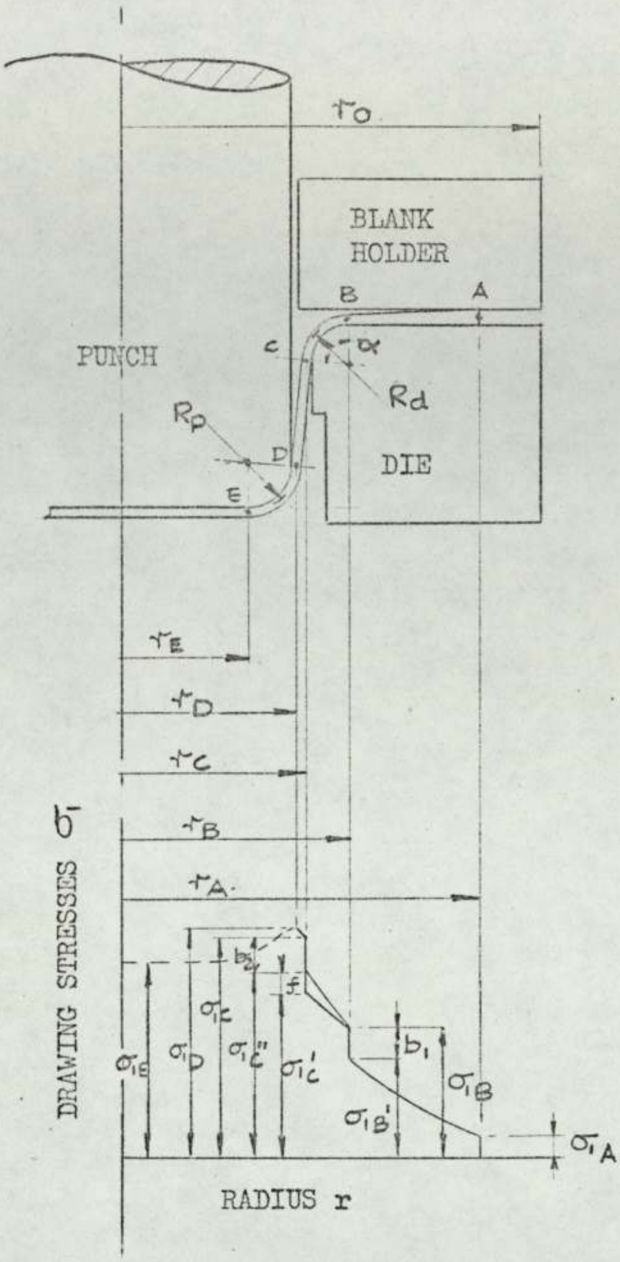

FIG. 7 INSTANTANEOUS DRAWING STRESS DISTRIBUTION IN CUPPING

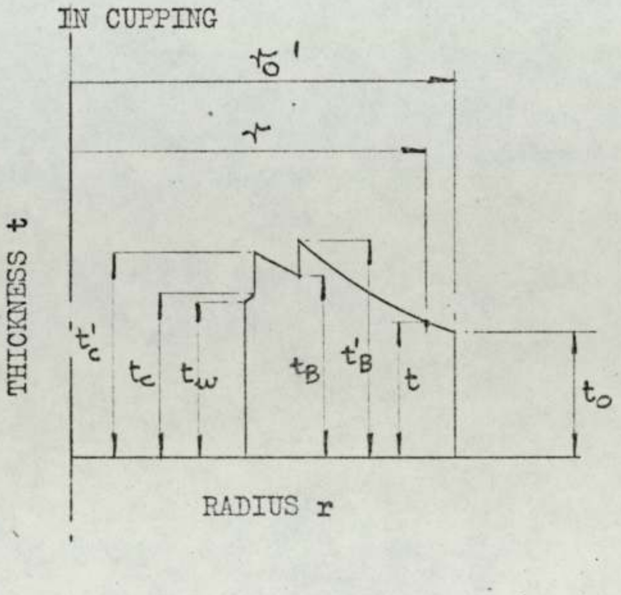

FIG. 8 THICKNESS HISTORY OF AN ELEMENT

radial stress after bending at B is σ_{1B} . Further radial drawing occurs around the die radius profile B - C in the presence of flange-die interface friction. Radial drawing alone produces a radial stress increment $\sigma_{1C}' - \sigma_{1B}$, whilst friction is responsible for an additional increment f . The total increment over the die radius is thus $\sigma_{1C}' - \sigma_{1B} + f$ and the radial stress immediately before unbending at C is σ_{1C}'' . Unbending of the flange into the cup wall at C provides a radial stress increment b_2 which increases the total radial stress at C to σ_{1C} . If the radial stress at C is sufficiently large yielding may occur in the cup wall, causing thinning, work-hardening, and a further slight increase in radial stress to σ_{1D} at D. Stress distribution in the cup bottom is unknown and represented by a dotted line in FIG. 7.

FIG. 8. depicts the thickness strain development of a particular element, originally at radius r_o' in the blank, during passage through the deformation zone. (The thickness strain induced in any element varies widely with its position in the undeformed blank.) Radial drawing operations tend to produce thickening whilst bending and unbending operations are accompanied by an abrupt thinning.

(ii) Plane radial drawing.

Four basic plasticity concepts were employed to provide solutions of stresses and strains across the deforming flange. These included:

1. A study of the force equilibrium of a general element.
2. A criterion of yielding.
3. Plastic stress - strain laws.
4. Compatibility of strains and displacements.

Additionally the concepts of equivalent stress and strain were used to study deformation in an idealised work-hardening material.

The equilibrium equation for an element was written,

$$\frac{d}{dr}(t.\sigma_1) + \frac{t}{r}(\sigma_1 - \sigma_3) - 2\mu\sigma_2 = 0 \quad \text{———} \quad 2.1$$

To solve this equation the stress σ_2 was considered negligable compared with σ_1, σ_3 reducing the problem to one of plane stress. Also, on the basis of experimental evidence, thickness variation across the flange was ignored for the purpose of stress computation. Circumferential stress σ_3 was eliminated from equation 2.1 by use of a yield criterion,

$$\sigma_1 - \sigma_3 = m\bar{\sigma} \quad \text{———} \quad 2.2.$$

Equation 2.2. is a modification of Tresca's yield criterion, the constant m being selected to provide closer agreement with Von Mises criterion. (The latter although giving better agreement with experiment for most materials, is difficult to manipulate mathematically.)

Combining equations 2.1, 2.2 and integrating gives, for a none work-hardening material $\bar{\sigma} = Y$,

$$\sigma_{1(r)} = \sigma_{1A} + mY \ln \frac{r_A}{r} \quad \text{———} \quad 2.3$$

where σ_{1A} is the induced radial stress at the rim due to blank-holder force H. σ_{1A} may be written,

$$\sigma_{1A} = \frac{\mu H}{\pi r_A . t_A} \quad \text{———} \quad 2.4$$

To proceed further with the analysis Levy-Mises stress-strain relationships and the condition of volume constancy were introduced. These provided a differential equation relating flange thickening and circumferential strain,

$$\frac{dt}{t} = -\left[2 + \frac{3}{\frac{\sigma_1}{m\bar{\sigma}} - 2}\right] \frac{dr}{r} \quad \text{———} \quad 2.5$$

In particular at the flange rim equation 2.5 becomes,

$$\frac{d(t_A)}{t_A} = -\left[2 + \frac{3}{\frac{\mu H}{\pi r_A . t_A . mY} - 2}\right] \frac{d(r_A)}{r_A} \quad \text{———} \quad 2.6$$

for a none work-hardening material.

Equation 2.6 was numerically integrated to determine the variation in rim thickness t_A as the flange was drawn in.

In combination with equations 2.3 and 2.4 equation 2.5 may be re-written,

$$\frac{dt}{t} = -\left[2 + \frac{3}{\frac{\mu H}{\pi . r_A . t_A . mY} + \ln \frac{r_A}{r} - 2} \right] \frac{dr}{r} \qquad 2.7$$

to give the thickness change in any flange element at current radius r. The circumferential strain $\int \frac{dr}{r}$ of an element is not immediately known, since on commencing to draw the flange thickness changes. A relationship between r the current radius of an element, and r' its original position in the undeformed blank, was obtained by equating volumes of flange originally between r_0 and r', and currently between r_A and r. This gave an expression,

$$r = \sqrt{r_A^2 - (r_0^2 - r'^2)\frac{t_0}{t_m}} \qquad 2.8$$

where tm is the mean current flange thickness between r_A and r (i.e. $t_m = \frac{t_A + t}{2}$)

Equations 2.7 and 2.8 may be solved alternately by successive approximation to give the thickness history of elements at various positions within the original flange, and the current thickness distribution across the flange. The computation is exhaustive.

Plane radial drawing of a work hardening material was now considered. In establishing the radial stress σ_1 account was taken of the equivalent strain in elements within the deforming flange. Although this quantity is a function of the three principal strains $\varepsilon_1, \varepsilon_2, \varepsilon_3$, Hill showed that for draw ratios less than two, equivalent strain differed from circumferential strain $\varepsilon_3 = \ln \frac{r'}{r}$ by not more than 3%. Chung and Swift utilised this simplification and assumed an idealised equivalent stress-strain relationship

$$\bar{\sigma} = \bar{\sigma}_0 + A\bar{\varepsilon}^n$$

where $\bar{\sigma}_0$, A and n were constants. Radial stress was then written,

$$\sigma_1 = \sigma_{1A} + m\int_r^{r_A}\left[\bar{\sigma}_0 + A\left(\ln \frac{r'}{r}\right)^n\right]\frac{dr}{r} \qquad 2.9$$

Equation 2.9 could not be solved directly since the ratio demanded knowledge of the thickness history of an element. A procedure similar to that for the non work-hardening material was followed to determine thickness changes. First, thickness strains at the rim were computed using equation 2.6 with $\bar{\sigma}_0 + A\left(\ln \frac{r_0}{r_A}\right)^n$ substituted for Y. Radial stress and thickness distribution were then found by alternate numerical integration of equations 2.5 and 2.9. The computation involved was formidable, and Chung and Swift found that only a small error resulted in strain calculations if the constant A in equation 2.9 was taken as zero - inferring that work-hardening had little effect on strain distribution. For purposes of radial stress calculation the work-hardening term must be included.

Stress and strain distributions in the flange during drawing are shown in FIGS. 9. and 10.

(iii) Plastic bending and unbending at the die radius.

The mechanics of bending at the die radius were studied by Swift using a simulative test, in which metal strip was bent under tension around a series of rollers. The work is described by Willis.

On reaching the die radius the cup wall is assumed to bend instantaneously. No circumferential straining accompanies bending which must therefore be a plane strain process. The stress normal to the die was assumed negligible. Bending occurs under back-tension exerted by the plane radial drawing zone and therefore a net radial force equal to this tension must exist across the bent section. In consequence the neutral plane of bending shifts a distance λ from the mid-wall plane in a direction towards the inside of the bend. Since the neutral is not coincidental with the mid-wall plane a tensile

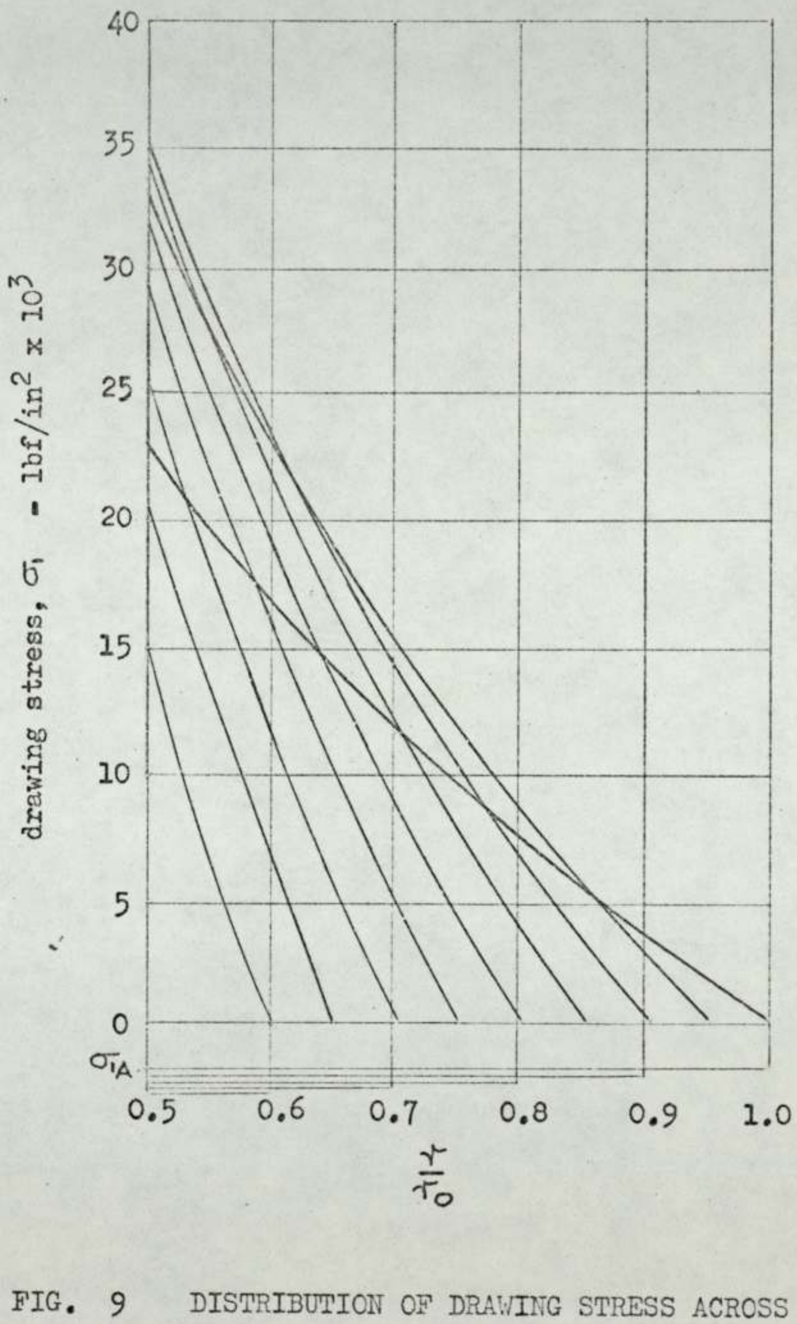

FIG. 9 DISTRIBUTION OF DRAWING STRESS ACROSS FLANGE

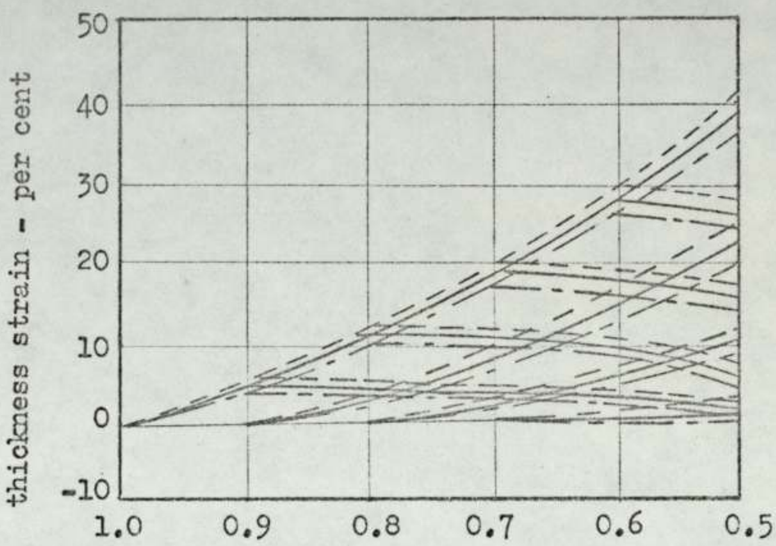

current position of element, $\frac{r}{r_0}$

FIG. 10 DEVELOPMENT OF THICKNESS STRAINS IN PLANE RADIAL DRAWING

upward curves represent a particular element; horizontal curves represent contour at a given stage.

- - - no strain hardening and no hold down pressure

—— typical mild steel with 15,500 lbf hold down and μ = 0.06

— - — - — as above but μ = .13

strain occurs on the latter, and as the bending is plane strain an equal amount of wall thinning occurs simultaneously. FIG. 11. shows conditions during bending under tension.

Unbending at exit from the die radius was treated by Chung and Swift in a similar manner to bending and is therefore not discussed separately at this juncture.

Strains imposed by bending are small and flange material has incurred previous strain on reaching the die. Use of a linear equivalent stress-strain relationship of the type,

$$\bar{\sigma} = \bar{\sigma}_1 + a\bar{\varepsilon}$$

was therefore considered justified by Chung and Swift. For the assumed plane strain conditions Von Mises yield criterion gives,

$$\sigma_1 = \frac{2}{\sqrt{3}} \cdot \bar{\sigma}$$

Shift in the neutral axis λ was found by equating the net bending force to the back-tension and provided the expression,

$$\lambda = \frac{\sigma'_{1B} . t_B}{\frac{4}{\sqrt{3}}\bar{\sigma} + \frac{4}{3}\frac{a t_B}{R_n}} \qquad \text{—————} \qquad 2.10$$

t_B and R_n are not immediately known and equation 2.10 must be solved by successive approximation .

Radial tensile strain on the mid-wall plane is given approximately by,

$$\varepsilon_1 = \frac{\lambda}{R_n} \qquad \text{—————} \qquad 2.11$$

and this is numerically equal to the thinning strain which accompanies bending.

The increment of radial stress b required to produce bending was found by equating plastic work of bending an elemental length of cup wall $R_d . \delta\theta$ to the work done by the radial force in moving through the same distance. If W_b is the work of plastic bending the elemental length, then,

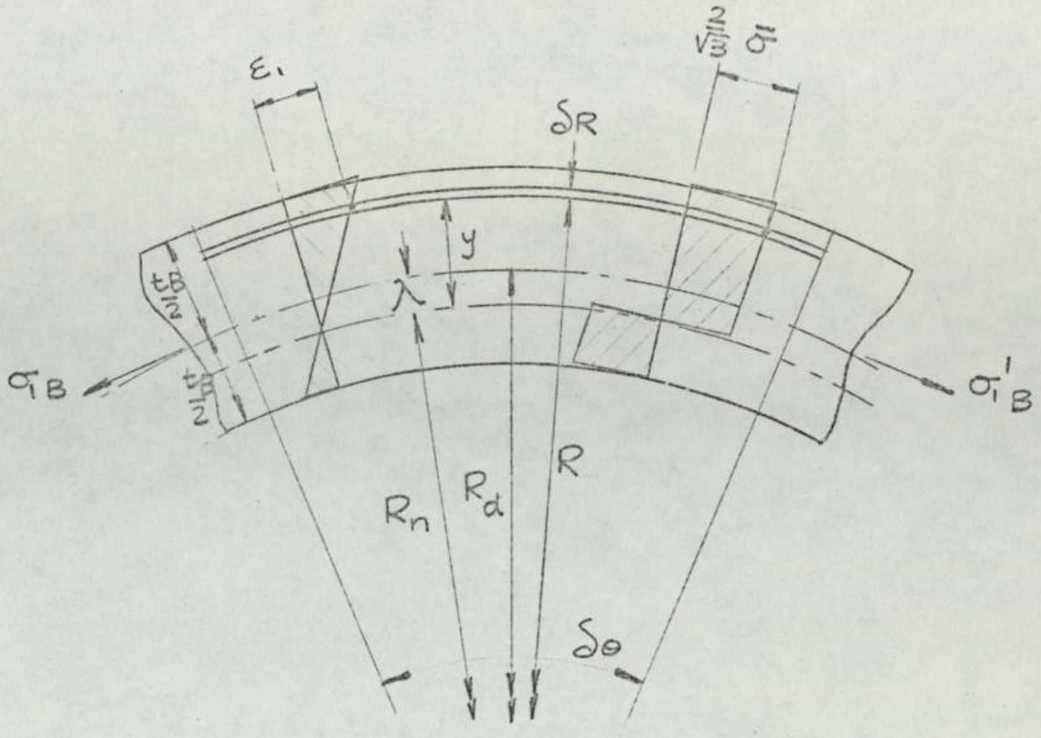

FIG. 11 CONDITIONS DURING BENDING UNDER TENSION

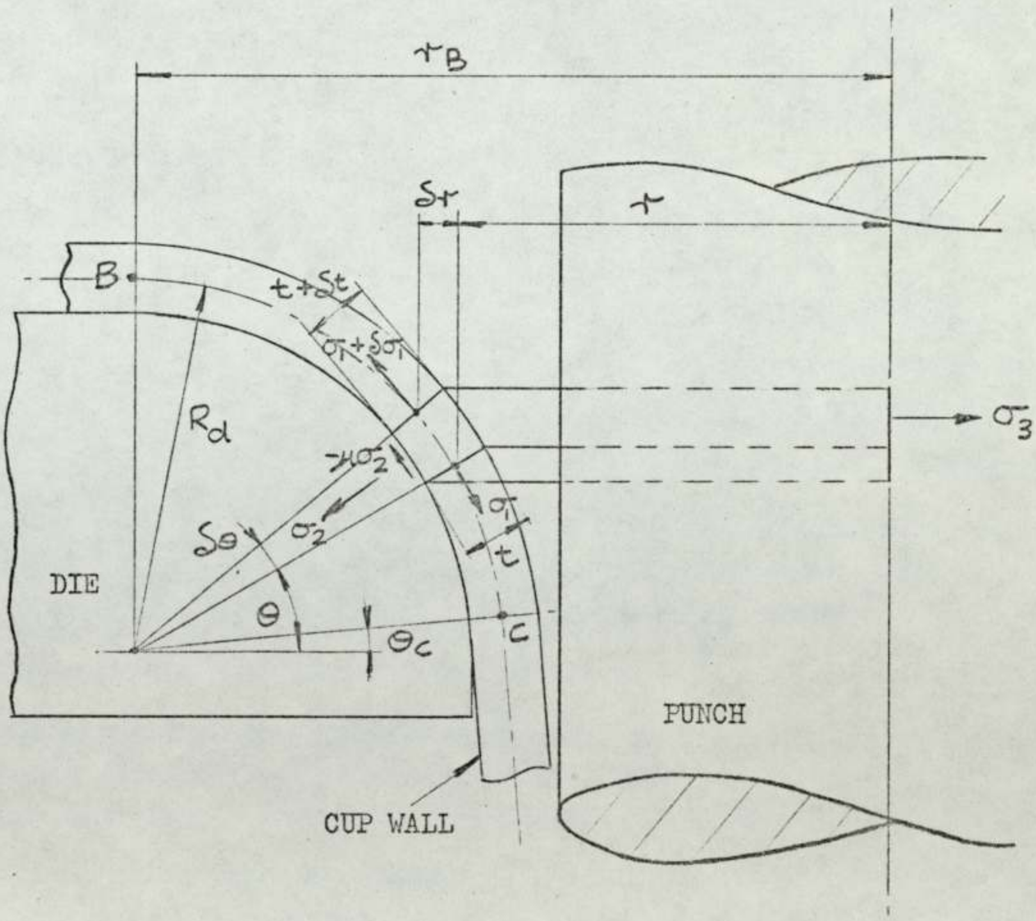

FIG. 12 RADIAL DRAWING AROUND DIE PROFILE

$$W_b = b.R_d.\delta\theta.t_B \qquad \text{———} \qquad 2.12$$

Referring to FIG. 11. the work of bending an elemental wall layer thickness δR, volume δv, is

$$\delta W_b = \bar{\sigma}.\ \delta\bar{\varepsilon}.\delta v.$$

For the assumed plane strain conditions,

$$\delta\bar{\varepsilon} = \frac{2}{\sqrt{3}}.\delta\varepsilon_1 \quad \text{where} \quad \delta\varepsilon_1 = ln\frac{R}{R_n} \simeq \frac{y}{R_n}$$

Thus,

$$\delta W_b = \frac{2}{\sqrt{3}}\left(\bar{\sigma}_1 + \frac{2}{\sqrt{3}}a.\frac{y}{R_n}\right)\frac{y}{R_n}\left(R_n \pm y\right)\delta\theta.\delta y$$

Where the $\pm$ sign notes elements above and below the neutral axis respectively. W_b is then given by,

$$\frac{W_b}{\delta\theta} = \int_0^{\frac{t_B}{2}+\lambda} \frac{2}{\sqrt{3}}.\left(\bar{\sigma}_1 + \frac{2}{\sqrt{3}}\frac{ay}{R_n}\right)\left(R_n+y\right)\frac{y}{R_n}.dy$$

$$+ \int_0^{\frac{t_B}{2}-\lambda} \frac{2}{\sqrt{3}}.\left(\sigma_1 + \frac{2}{\sqrt{3}}\frac{ay}{R_n}\right)\left(R_n-y\right)\frac{y}{R_n}.dy \qquad \text{———} \qquad 2.13$$

Equations 2.12 and 2.13 when combined give the increment of radial stress b to cause bending.

(iv) <u>Radial drawing over the die profile radius.</u>

After bending at B (FIG 12.) the cup flange is radially drawn around the die radius profile in the presence of friction at the die-flange interface. In earlier work Swift had compared frictional conditions in the zone to those existing in a belt transmitting power to a pulley. The stress at B then becomes analogous to the back-tension in a belt, whilst the stress at C to overcome <u>friction alone</u> is given by an equation of the type,

$$\frac{\sigma_{1C}}{\sigma_{1B}} = e^{\mu\theta}$$

The general approach to stress and strain determination was similar to that for the plane radial drawing zone, but was complicated by the zone's curved nature. Equilibrium of an elemental ring of the deforming flange in the direction of the punch axis was considered, to provide an equation relating σ_1 and σ_2. A further equation relating σ_1, σ_2 and σ_3 was obtained by considering the equilibrium of a half-ring in the direction normal to the punch axis. These two equations were then combined to eliminate σ_2, and assuming, (as for the plane flange), that at any instant the thickness variation over the zone was negligible, a single equilibrium equation was written,

$$\sigma_3\left(1+\mu\cot\theta\right)-\frac{d}{dr}(\sigma_1 . r)-\mu\sigma_1 . r . \frac{d\theta}{dr}=0 \qquad 2.14$$

The modified Tresca yield criterion $\sigma_1 - \sigma_3 = m\bar{\sigma}$ was introduced to eliminate σ_3, and by putting $dr = R_d \sin\theta . d\theta$ equation 2.14 became,

$$d\sigma_1 = -m\bar{\sigma}\frac{dr}{r} - \frac{\mu R_d \cos\theta}{r}\left[m\bar{\sigma}\cos\theta - \sigma_1\left(\cos\theta - \frac{r}{R_d}\right)\right] \qquad 2.15$$

The first and second terms on the right-hand side of equation 2.15 represent radial stress components to promote pure radial drawing and overcome friction respectively. The equation was solved by successive approximation using numerical integration for the friction term.

Chung and Swift suggested that a simpler though less accurate method of radial stress calculation for the zone was to directly add pure radial drawing components to frictional components given by the 'belt transmission' formula.

Having deduced stress distribution over the zone, corresponding strains were found by a procedure similar to that for the plane flange.

(v) Post die-contact deformation.

The preceding analysis enabled Chung and Swift to calculate radial drawing stress and wall thickness at the die exit (point C FIG. 7.) for any stage of the cupping process. It was pointed out however that during that part of the operation when the drawing stress at C, σ_{1_C} is increasing, a possibility of further thinning in the cup wall currently below C exists, even though the draw ratio is less than maximum.

Suppose that at a particular stage in the cycle radial stress at C is σ_{1_C}. Punch constraint imposes plane strain conditions in the cup wall, therefore,

$$\sigma_{1_w} = \sigma_{1_c} \cdot \frac{t_c}{t_w},$$

Wall thinning occurs if $\frac{\sqrt{3}}{2}\,\sigma_{1_w} > \bar{\sigma}_w$,
until work hardening gives $\bar{\sigma}_w = \frac{\sqrt{3}}{2} \cdot \sigma_{1_w}$.
The equivalent strain increment of thinning is given by,

$$\delta\bar{\varepsilon} = \frac{2}{\sqrt{3}} \ln \frac{t_c}{t_w}$$

over the small strain range involved it was assumed

$$\delta\bar{\sigma} = a\,\delta\bar{\varepsilon}, \quad \text{hence,} \quad \frac{\sqrt{3}}{2}\,\sigma_{1_w} - \bar{\sigma}_w = \frac{2}{\sqrt{3}} a \ln \frac{t_c}{t_w}$$

$$\text{or} \quad \frac{\sqrt{3}}{2} \cdot \sigma_{1_c} \cdot \frac{t_c}{t_w} - \bar{\sigma}_w = \frac{2}{\sqrt{3}} a \ln \frac{t_c}{t_w} \qquad 2.16$$

Equation 2.16 may be used to determine post die- contact thinning.

(vi) Punch load-travel.

Punch load was calculated from,

$$P = 2\pi r_c \cdot t_c \cdot \sigma_{1_c} \cdot \sin\theta .$$

Punch travel was deduced from a knowledge of the current flange dimensions and volume constancy.

(vii) Correlation of theoretical-experimental results.

Comparisons were made on the basis of punch and die profile radii, blank diameter, blank material and lubricant. Graphs of experimental-theoretical correlation were presented for draw loads and strains. Generally the correlation was good, being within about 8% for punch loads. FIG. 13. shows the correlation for punch load-travel with various blank diameters. Strain correlations were within about 15%, and in general were not as close as for punch loads. This was attributed, at least in part, to anisotropy, since for steel, which exhibited marked earing characteristics, strain correlation deteriorated in the upper regions of the cup.

The theoretical treatment of the cupping process by Chung and Swift was necessarily complicated owing to the intractable nature of the problem. Because of this, the treatment was not recommended for general use. It was suggested however that tables could be compiled for use by press and press-tool engineers. Modern computation facilities provide access to theoretical results.

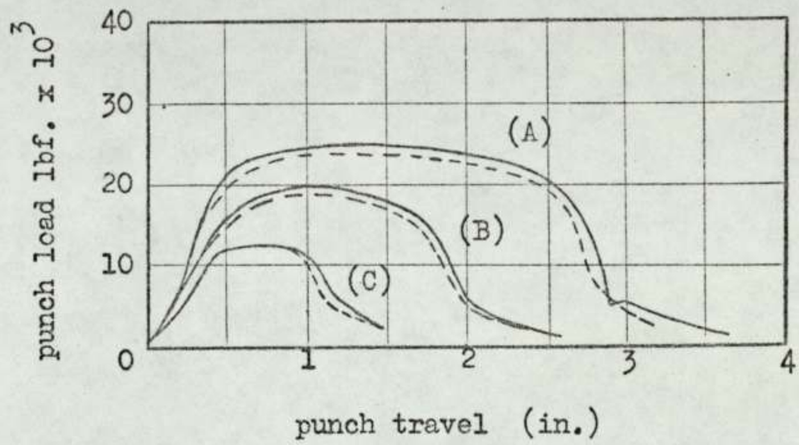

FIG. 13 EFFECT OF BLANK DIAMETER ON PUNCH LOAD

(A) 8 in. diameter blank

(B) 7 in. diameter blank

(C) 6 in. diameter blank

—— experimental curves ---- theoretical curves

Draw data:

material mild steel 0.039 in. thick

punch diameter 4 in., profile radius $\frac{1}{4}$in.

die diameter 4.101 in., profile radius $\frac{1}{4}$in.

(d) Theoretical treatment by Barlow.[6]

The general approach of Chung and Swift was used in estimating the maximum draw ratio in cupping. It was proposed that the latter occurs when maximum drawing stress in the cup at die exit attains a value equal to the ultimate tensile stress of the un-worked lower cup wall. Simplifications involving major assumptions were made both in drawing stress determination and mode of fracture in lower cup wall. The validity of a number of assumptions is arguable but results showed an experimental-theoretical correlation for draw ratio within 8% , theory generally giving an underestimate.

Derivation of drawing stress.

With a work-hardening material the point in a draw cycle at which maximum drawing stress (and draw load) occurs is not immediately known, and therefore the deforming flange geometry at the point is also unknown. Without knowledge of the latter maximum drawing stress cannot be calculated directly. For a particular draw ratio (near to the maximum) Barlow calculated drawing stress at various points within the cycle and hence determined its maximum value by interpolation. Drawing stress at die exit was considered to comprise components due to,

(i) radial drawing.

(ii) bending and unbending at the die radius.

(iii) friction at the blank-holder.

(iv) friction at the die radius.

(i) Radial drawing.

A plane stress situation with $\sigma_2 = 0$ was assumed, and thickness variation over the deforming flange at any instant ignored in deriving an expression for the 'pure' radial drawing stress component,

$$_{r}\sigma_{1} = -m\int_{r_A}^{r_e} \bar{\sigma}\,\frac{dr}{r} \qquad 2.17$$

Where r_A is the current rim radius. The constant m was taken as 1.1.

Both of the above assumptions were shown by Chung and Swift to be reasonable.

The value of $\bar{\sigma}$ in equation 2.17 varies over the flange width for a work hardening material. Barlow obtained values of equivalent stress at inner and outer current flange extremities from a knowledge of equivalent strains at these points, and hence deduced a mean value of $\bar{\sigma}$ across the flange at any instant. In finding equivalent strain at the inner flange edge the procedure of Chung and Swift was used, allowance being made for flange thickening.

(ii) <u>Bending and unbending at the die radius.</u>

A much simplified version of Chung and Swift's treatment was used, no account being taken of back tension and hence thinning. It was then possible to write the increment of radial stress for the two processes solely in terms of current equivalent stress and bending geometry, ie.,

$$_b\sigma_1 = \frac{\frac{2}{\sqrt{3}}\,\bar{\sigma}.t}{4\,R_d} \qquad \text{———————} \qquad 2.18$$

In equation 2.18 t was taken as the original blank thickness and $\bar{\sigma}$ as for equation 2.17. By stipulating a bending geometry $\frac{R_d}{t}$ of 10 equation 2.18 was re-written.

$$_b\sigma_1 = 0.029\,\bar{\sigma}.$$

The consequences of ignoring back-tension and thickening in this analysis would be an underestimation of the radial stress component.

(iii) <u>Friction at the blank-holder.</u>

The blank-holder was assumed to act only on the outer flange rim where a radial stress,

$$\sigma_1 = \frac{\mu H}{\pi r_A . t_A} \qquad \text{is induced.}$$

Barlow referred this stress directly to the inner flange rim, and by putting the thickness there equal to the blank thickness t_o,

$$_h\sigma_1 = \frac{\mu H}{\pi r_e \cdot t_o}$$

(iv) Friction at the die radius.

The 'belt-transmission' analogy drawn by Swift was utilised, back-tension at zone entry comprising that due to radial drawing, blank-holder friction, and bending. For 90 degree contact over the radius, radial stress at zone exit was written,

$$\sigma_1 = e^{\frac{\mu\pi}{2}}\left({}_r\sigma_1 + {}_h\sigma_1 + {}_b\sigma_1\right)$$

Total drawing stress.

The radial stress increment for pure radial drawing ${}_r\sigma_1$ as given by equation 2.17 was for an instantaneously uniform flange thickness $t_m > t_o$. Although no account was taken of thinning during bending/unbending Barlow acknowledged that thinning occurred in these operations, and assumed that on leaving the die radius cup wall thickness was approximately t_o. The radial stress increment for pure drawing thus increased to,

$$_r\sigma_1 = 1.1\,\bar{\sigma}\,\frac{t_m}{t_o}\ln\frac{r_A}{r_e}$$

Unbending into the cup wall was assumed to give an increase in radial drawing stress,

$$_u\sigma_1 = 0.029\,\bar{\sigma}$$

giving a final nominal cup wall drawing stress of,

$$\sigma_w = e^{\frac{\mu\pi}{2}}\left(1.1\,\frac{t_m}{t_o}\,\bar{\sigma}\ln\frac{r_A}{r_e} + \frac{\mu H}{\pi r_e . t_o}\right) + \left(e^{\frac{\mu\pi}{2}}+1\right)0.029\,\bar{\sigma}$$

Forming limits.

Barlow assumed that failure occurred in the cup where the base radius merged with the wall, and that ultimate tensile strength in this region was the failure criterion. The validity of this assumption has been shown doubtful by a number of investigators, who found that punch nose profile and lubrication condition exerted an influence on maximum draw ratio. No weight was given to either of these factors by Barlow. Fracture at the assumed site infers a flat bottomed punch with small corner radius, but such a punch would induce acute bending strains causing local necking and failure.

Table 1 gives experimental-theoretical correlation of maximum diameter reduction (an expression of draw ratio) for a number of aluminium alloys.

TABLE 1 CALCULATED AND EXPERIMENTAL VALUES FOR MAXIMUM REDUCTION IN CUPPING (BARLOW)

Aluminium Alloy	Maximum reduction in cupping %	
	Calculated	Experimental
1C - O	49.8	50
N3 - O	48.6	46.7
N3 - $\frac{3}{4}$H	51.9	48.7
N5 - O	53.2	54.3
H20 - O	48.3	51.5
H20 - FW (Freshly quenched)	48.1	51.5
H20 - W	47.5	51.5
H20 - WP	47.6	51.5
H15 - W	47.3	48.7
H15 - WP	47.0	48.7

2. 3. REDRAWING EXPERIMENT AND THEORY

(a) Introductory comments.

The maximum length/diameter ratio of a cup drawn directly from a blank is, for most common engineering materials, slightly less than unity. When higher ratios are required additional forming operations become necessary. The redraw process falls into this category.

Redrawing is similar in many respects to cupping. A punch forces an existing cup through a die to cause a reduction in diameter and consequent elongation. The wall thickness of the cup may or may not be deliberately controlled. Depending upon cup geometry, die geometry and redraw ratio, hold-down pressure may be necessary to prevent flange-wrinkling. The main difference between cupping and redrawing is that in the latter a steady state draw ratio is achieved. Therefore provided the entering cup is of uniform properties throughout its length redraw load remains substantially constant. This situation arises when redrawing an annealed cup. Conversely if a work-hardening as-drawn cup is redrawn maximum redraw load occurs late in the cycle, since material in the upper cup walls has received greater prior strain and hence offers correspondingly higher resistance to further deformation.

Redrawing gives more scope for tooling variations than cupping, but falls broadly into two classes;

(a) direct redrawing.

(b) reverse redrawing.

These are illustrated in FIG. 14. The direct method of redrawing would appear to be the most widely used, but the reverse method offers the possibility of both cupping and redrawing in one stroke of a double-action mechanical press. Direct redraws are characterised by four bending operations, bending and unbending occurring at both the hold-down punch and die profile radii, whereas reverse-redraw tooling may be designed to eliminate one of the bending/unbending operations which

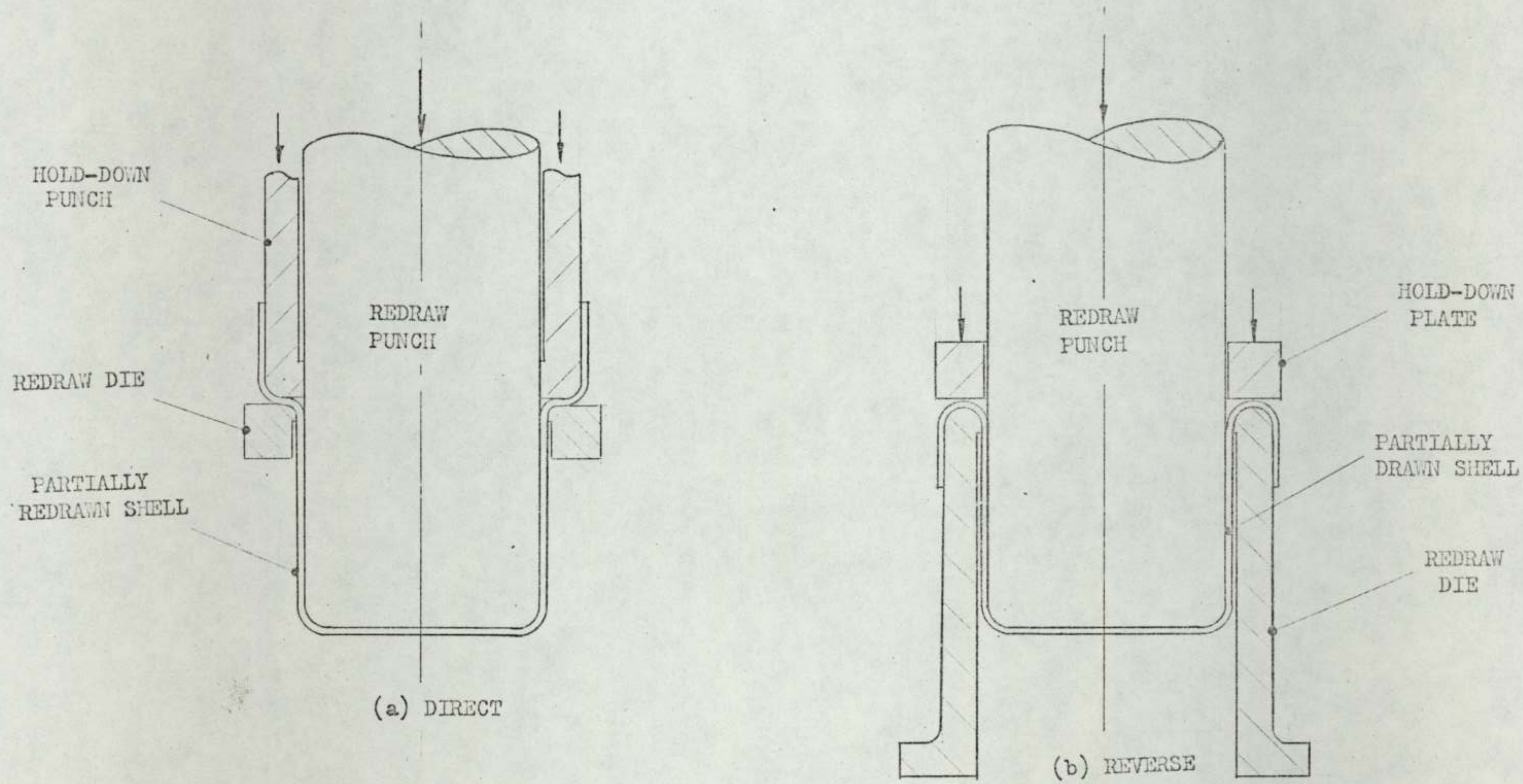

FIG. 14 DIRECT AND REVERSE REDRAW METHODS.

inevitably occurs in direct-redrawing. FIG. 14. shows such an arrangement.

The remainder of this section is devoted to discussing three papers on redrawing.

(i) The experimental work of Chung and Swift.[9] (1958)

(ii) A theoretical treatment of reverse redrawing by Chung.[10] (1951)

(iii) A theoretical treatment of direct redrawing in the absence of hold-down by Fogg.[11] (1968)

(b) The experimental work of Chung and Swift.

Three redraw arrangements were investigated comprising direct and reverse methods. Where employed, hold-down was of the 'constant pressure' type. Materials investigated included 0.08% carbon steel and 70/30 brass, both in annealed (blank) condition, and 99% pure aluminium in soft and half-hard tempers. Tests conducted on these materials revealed no significant directional properties. (Tensile tests were carried out at 0, 45, and 90 degrees to the rolling direction, different strain levels being generated in the strip material by cold-rolling. It is unlikely that such tests would give an indication of normal plastic anisotropy.) Details of first-stage cup manufacture are given in table 2. Similar press speeds and lubricants were used for redrawing.

Variation in overall draw ratio with cupping draw ratio.

Brass and steel blanks of various diameters were cupped and then redrawn without interstage annealing. The upper limit of cupping draw ratio was taken as that at which failures occurred. Cups were redrawn with tooling configurations as shown in FIG. 14. For both materials and both redraw types maximum overall draw ratio occurred with a maximum cupping draw ratio, although a higher redraw ratio was possible with lower cupping draw ratios. Of the two types of redrawing the reverse method gave highest overall draw ratio (2.9) which occurred with steel. Maximum cupping draw ratios for brass and steel were

TABLE 2 DATA FOR FIRST-STAGE DRAWING (CHUNG AND SWIFT)

Press	Stroke 10 in., 8.2 strokes per minute.
Lubricant	Graphite in tallow ($\frac{1}{3}$ by weight).
Blank-holder	Positive pressure type.
Blank thickness	.039 in.
Punch diameter	4 in.
Punch profile radius	3/16, 7/32, 1/4, 9/32, or 5/16 in. according to redrawing punch diameters.
Radial clearance	30 % of blank thickness
Die profile radius	$\frac{1}{4}$ in.

similar (2.1) .

Chung and Swift concluded that cupping performance could not be taken as a guide to redrawing performance and that materials which work-harden rapidly were less suitable for redrawing. The superiority of reverse redrawing was attributed to lower bending work with this arrangement.

In a further series of tests direct redrawing was conducted with a 15 degree semi-angle die, and hold-down punch raised clear of the die to act only as a guide for the entering cup. This arrangement gave higher draw ratios than either the previous direct or reverse methods.

Effect of interstage annealing.

Brass and steel cups were drawn and annealed before redrawing by the direct and reverse methods shown in FIG. 14. Results were compared with those obtained when redrawing as-drawn cups. For both annealed materials the reverse redraw ratio was limited to 1.5 only by available tooling, whereas with as-drawn cups maximum redraw ratios for brass and steel were 1.32 and 1.37 respectively.

Effect of punch profile radius.

The punch profile was varied from flat-bottomed with small corner radius to hemispherical. Results were similar to those obtained in cupping regarding punch load build-up and thickness strains over the punch nose. (The reader is referred to page 9 of the thesis.) Punch profile was found to exert no influence on maximum redraw load.

Effect of first-draw radial clearance.

In previous work Chung and Swift had found that deliberate ironing of the thickened upper cup walls in cupping gave no increase in punch load (since maximum punch load occurred earlier in the cycle.) This practice was found to be of direct benefit when redrawing since with unironed cups the thickened upper walls combined with the high prior strain levels in this region to give excessive punch load near the termination of the redraw cycle.

Effect of blank material and prior cold work.

Materials investigated were soft brass, steel and aluminium, and half-hard aluminium. Maximum cupping draw ratios for these materials were 2.13, 2.13, 2.0 and 2.06 respectively. In redrawing however, a draw ratio of 1.37 was unsuccessful with brass and soft aluminium but successful with steel and half-hard aluminium. Further work showed that a redraw ratio of 1.44 was possible with half-hard aluminium, but not with steel. The general conclusion was formed that materials which work harden rapidly give best results in cupping, whereas the converse is true for redrawing.

(c) Chung's theoretical treatment of reverse redrawing.[10]

The redraw arrangement considered is shown in FIG. 15.a., the die profile being of hemispherical form. The hold-down force was assumed to act at a circle described by point B. Deformation was taken to be fully plastic and characterised by;

(i) bending at A.

(ii) radial drawing between A and C with friction at the cup flange/die interface.

(iii) unbending into the final cup wall at C under back tension.

The analysis was simplified by a number of assumptions. Thickness changes were ignored for the purpose of radial stress derivation, and an approximate allowance made for friction over the die profile by utilising the 'belt-transmission' formula. Work hardening was taken into account by determining a mean yield stress for the deforming flange. Comparison between theoretical and experimental punch loads indicated a correlation to within about 10 - 15%, the theory giving an underestimate.

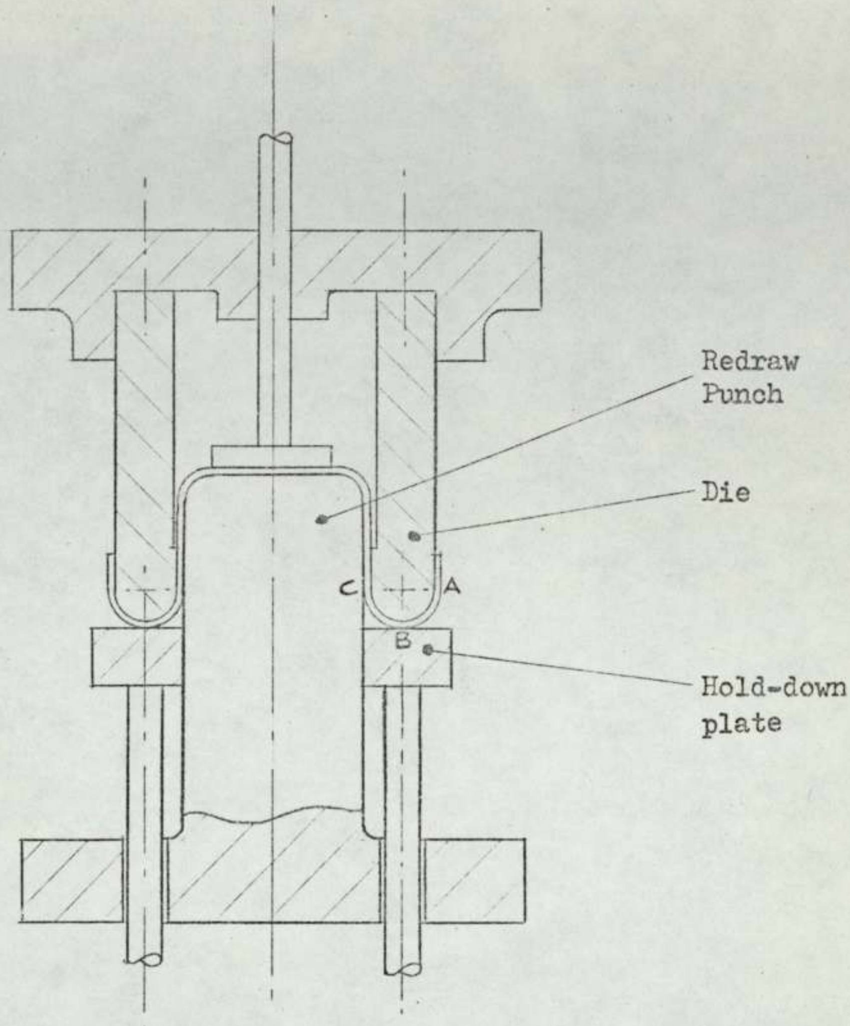

FIG. 15a ARRANGEMENT FOR REVERSE REDRAWING

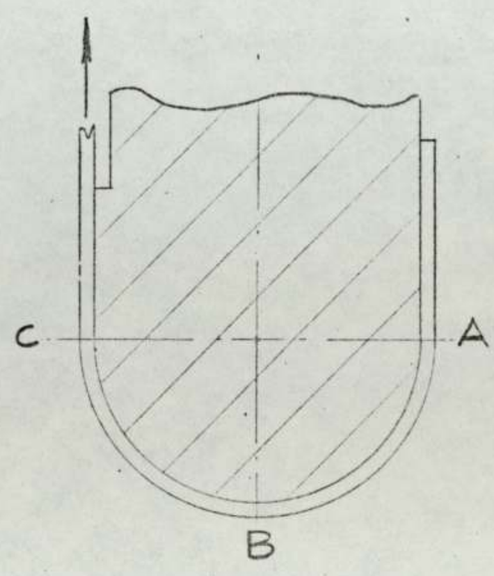

FIG. 15b DETAIL OF DEFORMATION ZONE

Bending and unbending components of radial stress.

The general approach developed by Chung and Swift for cupping was followed. Bending at A (FIG. 15.b.) occurs without back tension and gives rise to a radial stress component,

$$_b\sigma_A = \frac{Yt}{4R_d} \qquad (2.19)$$

In deriving this expression Chung adopted Tresca's yield criterion which gives no weight to the assumed plane strain conditions.

It was assumed that unbending at C also produced a radial stress component as equation 2.19. By adopting this procedure Chung ignored the effect of back-tension at C on increasing the unbending stress component.

Radial stress component for pure radial drawing.

The radial stress component to give frictionless radial drawing between points A and B (FIG. 15.) for a none work hardening material was computed to;

$$_r\sigma_C = Y \ln \frac{r_o}{r_e} \qquad (2.20)$$

and found to be independent of the strain path.

Friction due to hold-down force.

The hold-down force H acting on point B induces a frictional drag $2\mu H$ on the cup flange, since both inside and outside surfaces are affected. Therefore, the component of radial stress at B required to overcome this drag was found to be,

$$_h\sigma_B = \frac{\mu H}{\pi r_B t} \qquad (2.21)$$

Friction at the die profile.

Each of the radial stress components given as equations (2.19), (2.20), (2.21) has an associated frictional component due to the curvature of the die profile. Chung referred each component to the die exit at point C (FIG. 15.) making allowance for die profile friction.

When referred to C equation 2.19 becomes,

$$_b\sigma_{1C} = \frac{Yt}{4R_d} e^{\mu\pi},$$

and the total stress component for bending and unbending when referred to C is thus,

$$_{b,u}\sigma_{1C} = \frac{Yt}{4R_d}\left(1 + e^{\mu\pi}\right) \qquad (2.22)$$

Hold-down contribution to radial stress at C becomes.

$$_h\sigma_{1C} = \frac{\mu H}{\pi r_B t} e^{\frac{\mu\pi}{2}} \qquad (2.23)$$

The frictional component arising from pure radial drawing could not readily be taken into account, since radial drawing stress $_r\sigma_1$ increases from zero to $_r\sigma_{1C}$ around the die profile. Chung assumed that the mean radial drawing stress $_r\frac{\sigma_{1C}}{2}$ acted at point A when finding the associated friction component, and gave rise to a stress component at C,

$$_f\sigma_{1C} = {}_r\frac{\sigma_{1C}}{2}\left(e^{\mu\pi} - 1\right)$$

Hence the total contribution of radial drawing to the radial stress at C was,

$$_f\sigma_{1C} + {}_r\sigma_{1C} = \frac{1}{2} Y \ln\frac{r_0}{\bar{r}_e}\left(e^{\mu\pi} + 1\right) \qquad (2.24)$$

Summation of the equations (2.22), (2.23), (2.24) provides the drawing stress in the cup wall at C, σ_{1C}.

Survey note.

When referring radial stress terms to the die exit, Chung ignores the 'area' effect involved and its influence on increasing the radial stress.

Characteristics of the reverse redrawing arrangement.

With the arrangement shown in FIG. 15a, the die profile radius directly effects both bending/unbending severity and draw ratio, and so also exerts a marked influence on draw load characteristics. FIG. 16 shows the drawing stress ratio $\frac{\sigma_{1c}}{Y}$ as a function of $\frac{r_e}{r_o}$, with $\frac{r_o}{t_o}$ as a parameter. In obtaining this relationship hold-down (as given by equation 2.23) was ignored. The curves of FIG. 16 are explained as follows; for very small draw ratios bending is severe, and hence an increase in draw ratio causes a fall in bending work greater than the increase in radial drawing work. For higher draw ratios however, increases in draw ratio produce only small decreases in bending work and hence the radial drawing work term predominates.

Punch load calculations.

Punch load P was calculated from,

$$P = 2\pi r_e . t_o . \sigma_{1c}$$

FIG. 17 shows typical punch load-travel diagrams. With annealed cups steady-state conditions are attained whilst the deforming flange width remains constant. As-drawn cups exhibit a rising redraw characteristic due to the increase in yield stress up the cup wall.

Correlation of theory and experiment.

Experimental redraws were conducted in steel and aluminium at a logarithmic strain-rate of about 1 unit/second, and with hold-down force constant at 2300 lbf. Table 3 gives principal test data. In tests 1, 2, 3, 4 theory underestimated redraw load by 9, 8, 4 and 17% respectively. (If the 'area' effect mentioned previously had been taken into account theoretical load would have been greater.)

Approximate allowance was made for work hardening by using a mean value of yield stress for the deforming flange. For as-drawn cups it was necessary to determine prior strain in the upper cup walls.

(d) Fogg's theoretical treatment of direct redrawing.[11]

A theory was proposed for direct redrawing through conical dies

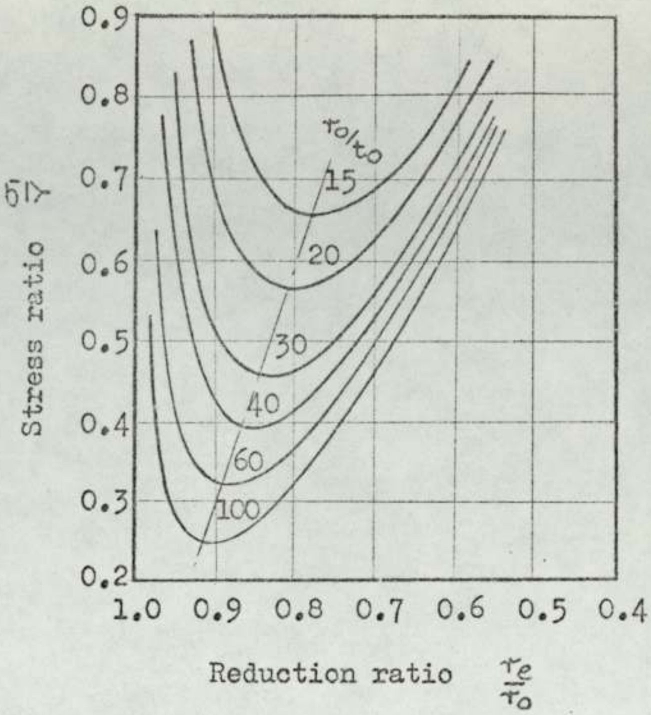

FIG. 16 CHARACTERISTIC CURVES OF REVERSE REDRAWING (CHUNG)

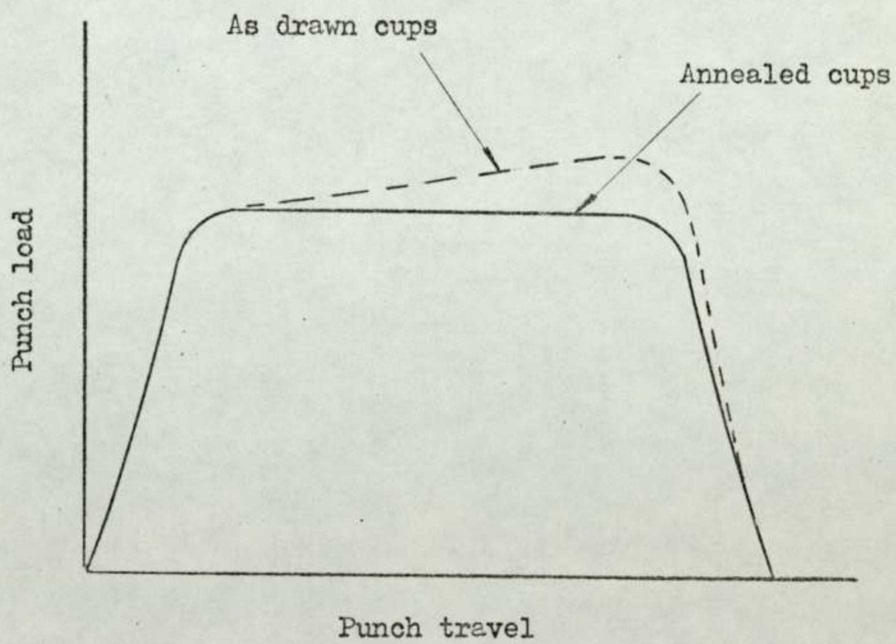

FIG. 17 PUNCH LOAD CHARACTERISTICS FOR REVERSE REDRAWING WITH ANNEALED AND AS-DRAWN FIRST STAGE CUPS.

TABLE 3 REVERSE REDRAWING DATA (CHUNG)

Test No.	1	2	3	4
Punch diameter, (in.)	2.916	2.916	2.916	2.666
Die throat diameter, (in.)	3.033	3.033	3.033	2.785
Draw die radius, (in.)	0.242	0.242	0.242	0.304
Entering cup diameter, (in.)	4.047	4.047	4.049	4.037
Cup wall thickness, (in.)	0.047	0.047	0.049	0.037
Inter-stage annealing	YES	NO	NO	YES
Material	STEEL	STEEL	ALUMINIUM	STEEL
Coefficient of friction	0.10	0.10	0.05	0.10
Experimental maximum punch load, (lbf)	14,500	20,500	5,100	13,000
Theoretical maximum punch load, (lbf)	13,200	18,900	4,900	10,800

in the absence of a hold-down punch. For the purpose of analysis the deformation zone, considered fully plastic, was divided into stages comprising four bending operations and three regions of radial drawing. Referring to FIG. 18A the deformation stages are, in sequence:

(i) Bending at A.

(ii) Frictionless radial drawing between A and B.

(iii) Unbending at B with back tension.

(iv) Radial drawing between B and C with friction at the cup/die interface.

(v) Bending at C with back tension.

(vi) Radial drawing between C and D with friction at the cup/die profile radius interface.

(vii) Unbending into the cup wall at D with back tension.

The general approach to the problem was that developed by Chung and Swift for cupping. Starting at point A, radial stress and thickness strain of an element were traced through the deformation zone. The paper amply illustrates the mathematical complexity involved in a rigorous analysis of direct redrawing. Four aspects of Fogg's work are considered particularly noteworthy and it is with these that the current survey is largely concerned. Firstly, a linearised adjustable yield criterion was employed throughout the analysis to provide closer agreement with Von Mises criterion than does the modified Tresca criterion used by previous investigators. Secondly, the linearised yield criterion was treated as a plastic potential for deducing plastic strain ratios, and hence for tracing thickness strain development. Thirdly, work hardening was taken into account by linearising the equivalent stress-strain curve over each of the various deformations describing the process. Fourthly, geometry of the unconstrained zone A B in FIG. 18A was deduced by utilising the principal of minimum energy of plastic deformation. This latter feature of Foggs work is of special interest

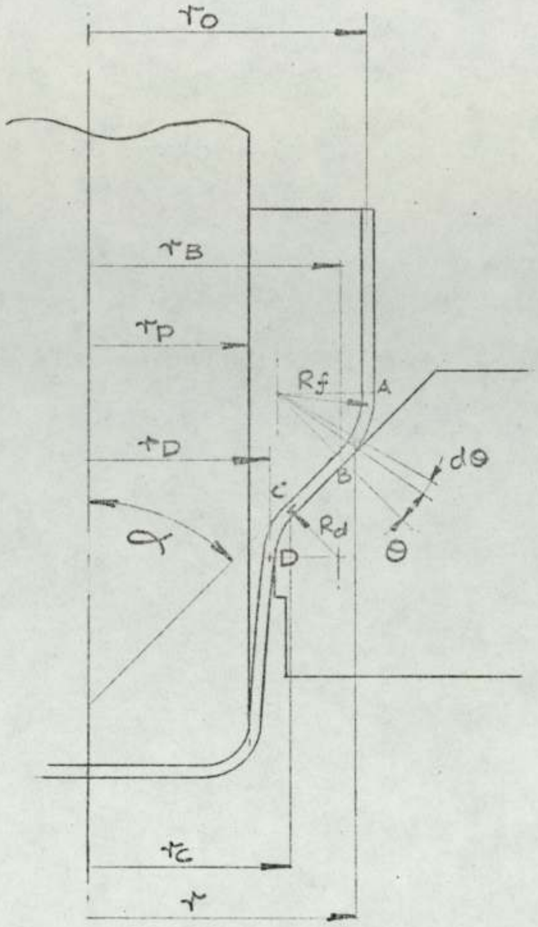

(A) REDRAWING GEOMETRY

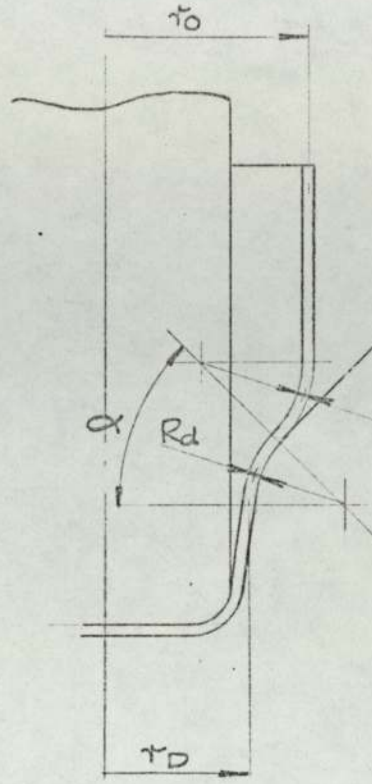

(B) MINIMUM CONDITION FOR THEORY

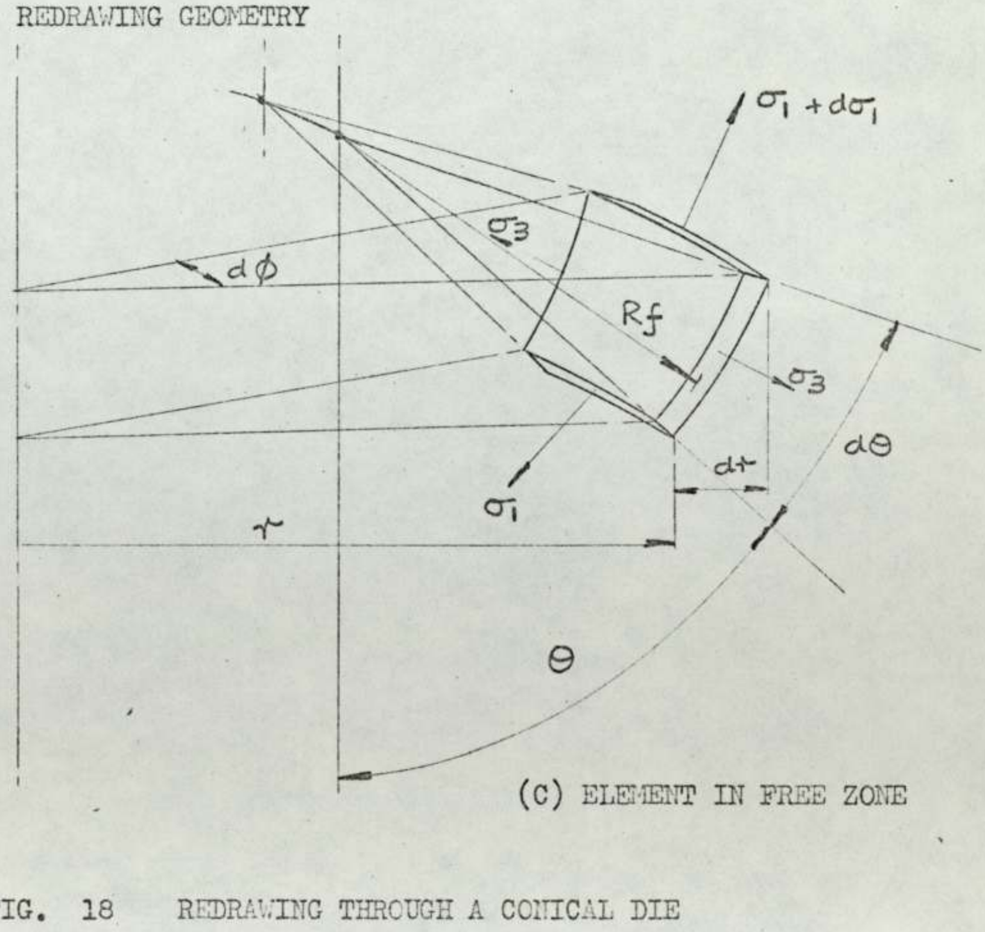

(C) ELEMENT IN FREE ZONE

FIG. 18 REDRAWING THROUGH A CONICAL DIE

to the writer, since splaying in unconstrained redrawing was found to be strongly influenced by the bending severity in this zone.

In developing the theory it was assumed that,

(1) The entering cup wall was of uniform thickness and yield strength, so that steady-state redrawing conditions were attained.

(2) The analysis was limited to a pre-drawn cup diameter/thickness range of 40-100. Within this range it was assumed that plane-stress drawing conditions were attained and that no flange wrinkling would occur.

(3) Anisotropy and the Bauschinger effect were ignored.

Linearised yield criterion.

It was argued that the use of Tresca's yield criterion in conjunction with Levy-Mises stress-strain equations did not conform to the principle of maximum plastic work, and a closer approximation to the ideal but intractable Von Mises/Levy-Mises combination could be obtained for plane stress problems by linearising Von Mises criterion with a method suggested by Prager.[12]

Von Mises yield criterion for plane stress is given by,

$$\sigma_1^2 - \sigma_1 . \sigma_3 + \sigma_3^2 = Y^2 \left(= \bar{\sigma}^2\right) \qquad (2.26)$$

In radial drawing the principal stresses σ_1, σ_3 are always positive and negative respectively, and Von Mises criterion of yielding is represented by a curved line shown in FIG 19. Over a small stress ratio range Prager's linearisation gives a closer fit than either of the Tresca lines, and may be expressed,

$$c_1 \sigma_1 - \sigma_3 = c_2 \bar{\sigma} \qquad (2.27)$$

where C_1, C_2 are treated as constants over the stress range of interest. (In his paper Fogg wrongly shows C_1 as the complementary slope to that in Fig. 19. This error, unless corrected, may have resulted in incorrect values for plastic strains.)

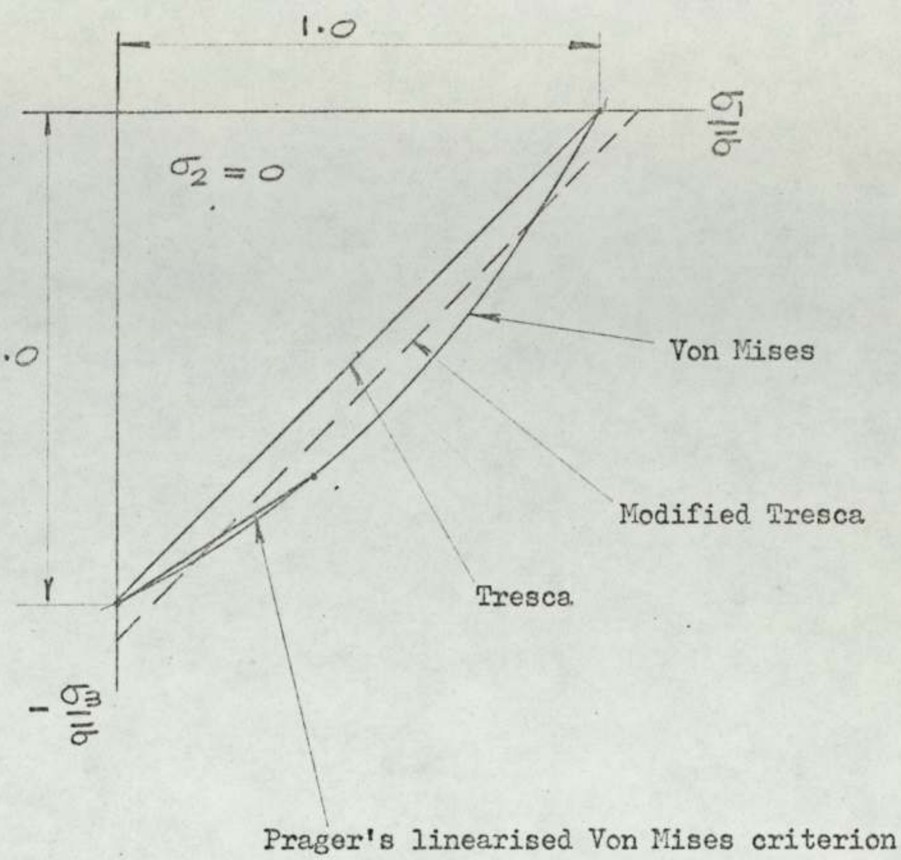

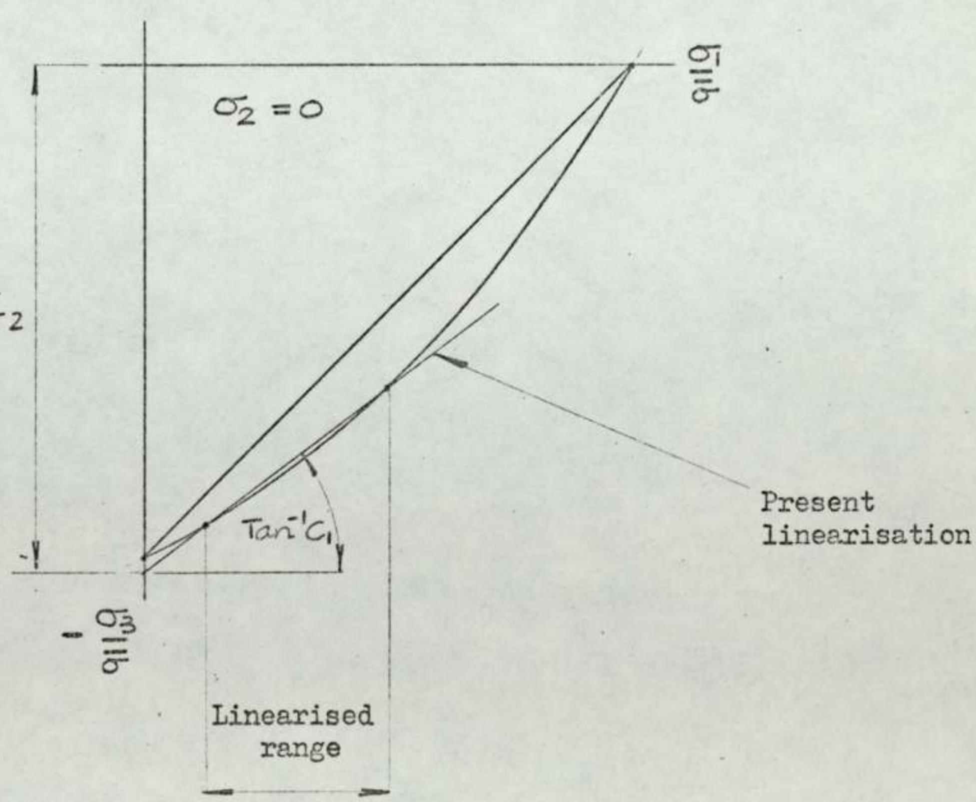

FIG. 19 PRAGER'S METHOD OF LINEARISING THE VON MISES ELLIPSE

Plastic strain ratios.

Equation (2.27) was treated as a plastic potential for deriving plastic strains.

If $f(\sigma ij) = c_1\sigma_1 - \sigma_3 - c_2\bar{\sigma} = 0$, then

$$d\varepsilon ij = \frac{\partial}{\partial \sigma ij} f(\sigma ij)\, d\lambda' \qquad \text{———————— (2.28)}$$

where $d\lambda'$ is an instantaneous non-negative constant.

Equation 2.28 was used to obtain $d\varepsilon_1$, $d\varepsilon_3$, and $d\varepsilon_2$ was given by the plastic incompressibility condition,

$$d\varepsilon_1 + d\varepsilon_2 + d\varepsilon_3 = 0$$

Linearised equivalent stress-strain curve.

Over each deformation stage work hardening was taken into account by fitting a straight line to the equivalent stress-strain curve. An equivalent stress-strain relationship of the type,

$$\bar{\sigma} = Y_i + a_i\,\bar{\varepsilon}$$

was used where Y_i and a_i were adjustable constants.

Geometry of the unconstrained (free) zone at die entry.

The zone is identified as arc A B in FIG. 18A, and defines deformation in the entering cup before contact with the die mouth. In finding the geometry of this zone Fogg considered that deforming metal would follow a path requiring minimum energy of deformation. It was assumed that;

(1) The material was non work-hardening.

(2) Deformation conformed to a circular arc.

(3) Bending at A and unbending at B occurred instantaneously, and thus under plane strain conditions.

For a given die angle the energy expended in the free zone is a function of bending radius R_f. If the latter was small, bending work would be high whilst radial drawing work would be low. The converse would be true if R_f was large. Fogg's analysis provides a value of R_f between these two extremes, such that combined bending and radial drawing work is a minimum.

FIG. 18C shows an element in the free zone. The specific plastic work for radial drawing is given by,

$$d\omega_r = \sigma_1 . d\varepsilon_1 + \sigma_2 . d\varepsilon_2 + \sigma_3 . d\varepsilon_3 \quad \text{———} \quad (2.29)$$

where the plane stress condition makes $\sigma_2 = 0$. Putting $\bar{\sigma} = Y$ in equations 2.27, 2.28, and substituting for $\frac{d\varepsilon_1}{d\varepsilon_3}, \sigma_3$ in equation 2.29 gives,

$$d\omega_r = - C_2 . Y \frac{dr}{r}$$

Integrating between A and B provides the specific zone work of radial drawing,

$$\omega_r = C_2 Y \ln \frac{r_o}{r_B} \quad \text{———} \quad (2.30)$$

Bending/unbending in the zone was analysed by the procedure of Chung and Swift. The specific work of bending at A which occurs in the absence of back tension is given by,

$$\omega_b = \frac{2}{\sqrt{3}} \frac{Y\, t_o}{4\, R_f} \quad \text{———} \quad (2.31)$$

Although unbending at B occurs under back tension Fogg assumed that this would be small and ignored its effect on increasing unbending work and thinning of the cup wall. With these assumptions unbending work ω_u becomes equal to bending work as provided by equation 2.31.

The free radius R_f was found from the condition,

$$\frac{\partial}{\partial R_f}\left(\omega_r + \omega_b + \omega_u \right) = 0 \quad \text{———} \quad (2.32)$$

For the purpose of differentiation equation 2.30 was written in terms of R_f and α,

$$\omega_r = C_2 Y \ln \frac{r_o}{r_o - R_f(1-\cos\alpha)}$$

which, since the zone draw-ratio is small, was written,

$$\omega_t = \frac{C_2 Y R_f (1-\cos\alpha)}{t_o} \text{ ——————————— } (2.33)$$

Total zone work is given by equations 2.31, 2.33,

$$\omega = Y\left[C_2 \cdot \frac{R_f}{t_o}(1-\cos\alpha) + \frac{t_o}{\sqrt{3}\,R_f}\right]$$

and the condition $\frac{\partial(\omega)}{\partial R_f} = 0$ provided

$$\frac{R_f}{t_o} = \sqrt{\frac{t_o/t_o}{\sqrt{3}\,C_2(1-\cos\alpha)}} \text{ ——————————— } (2.34)$$

C_2 may be ommitted from equation 2.34 since over the stress range involved its value is unity.

Fogg claimed that equation 2.34 gave reasonable agreement with experimentally measured profiles, and pointed out that according to theory R_f was independent of overall redraw ratio, but as the redraw ratio decreases the conical drawing zone B C (FIG. 18A) ultimately reduces to zero. For this special case, shown in FIG. 18B, the redraw ratio may be written,

$$\gamma = \frac{1}{1-\frac{(R_f+R_d)(1-\cos\alpha)}{t_o}} \text{ ——————————— } (2.35)$$

Having deduced free zone geometry for a non work-hardening material Fogg analysed stresses and strains in the complete redraw for a work-hardening material.

Correlation of theory and experiment.

To test the validity of the proposed theory 2 in. diameter, 0.040 in. thick cups in 70/30 brass were redrawn. Equivalent stress-strain diagrams were constructed from plane strain compression tests conducted on specimens cut from the cup walls. Test results were used to determine the linearisation constants C_1, C_2, Y_i and a_i .

Experimental redraw tests were limited to a single variable - the redrawing ratio γ . A die of semi-angle 30 degrees and throat radius 5/16 in. was used throughout.

FIG. 20A shows experimental/theoretical punch load variation with redraw ratio. For both annealed and as-drawn cups theory over-estimated punch loads at low redraw ratios by 16 - 18%. At higher redraw ratios correlation improved. Fogg suggested that the discrepancy was consistent with an overestimation of bending/unbending radial stress components which increase only slightly with redraw ratio and therefore exert a diminished overall influence at higher redraw ratios. In explanation of the effect it was suggested that the plane-strain stress condition assumed in bending may be inaccurate for small redraw ratios where considerable compressive circumferencial stresses exist due to radial drawing. FIG.20B shows experimental/theoretical thickness changes.

Theoretical drawing stress relationships.

The theoretical effect of redraw parameters on drawing stress are shown in FIG. 21 for the particular experimental cup geometry. FIG. 21A indicates that die-angle exerts only a slight influence on drawing stress over the range 15 - 60 degrees, lower die angles generally giving lowest drawing stress. Fogg stated that an optimum die angle of 22½ degrees was found for a redraw ratio of 1.5. The dotted line in FIG. 21A represents the situation where the conical drawing zone degenerates to a single point. Drawing then only occurs over the die radius, and with this particular geometry the free radius R_f may be expressed in terms of die radius R_d and redraw ratio γ by combining equations 2.34, 2.35 to eliminate α . FIG. 21B shows drawing stress variation with die radius for this condition. FIG. 21C shows drawing stress variation with die radius for the optimum 22½ degrees die semi-angle.

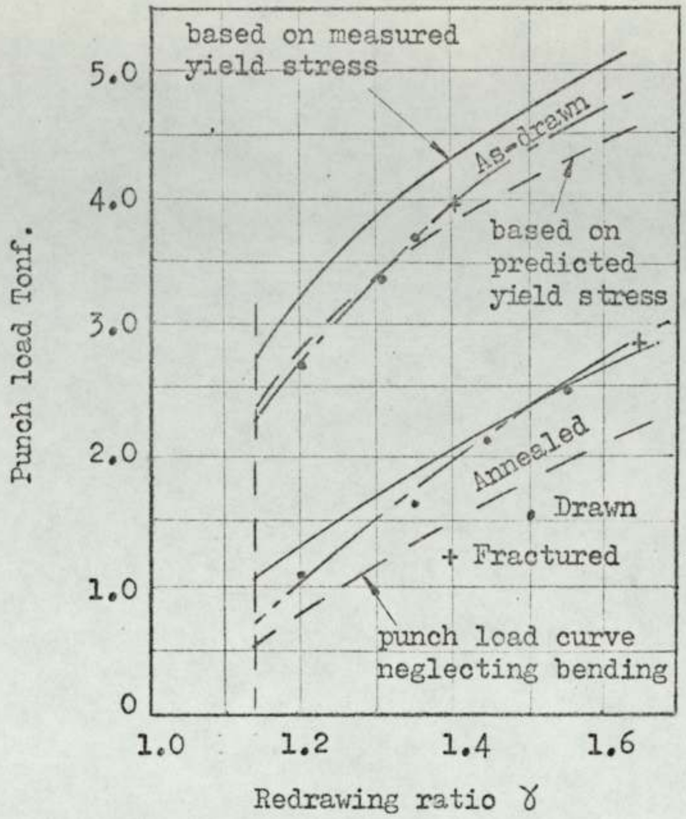

FIG. 20A COMPARISON OF THEORETICAL AND EXPERIMENTAL PUNCH LOADS FOR 70/30 BRASS CUPS (FOGG)

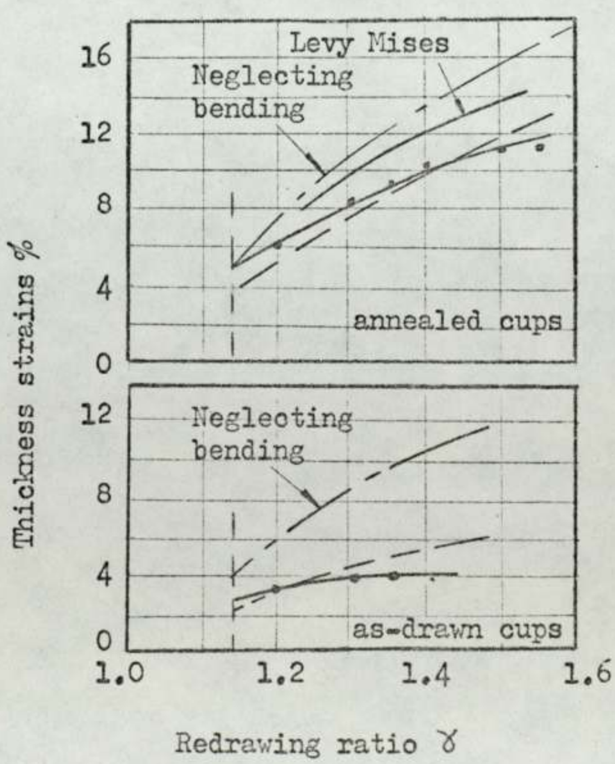

FIG. 20B CHANGE IN WALL THICKNESS WITH REDRAWING RATIO FOR AS-DRAWN AND ANNEALED CUPS (FOGG)

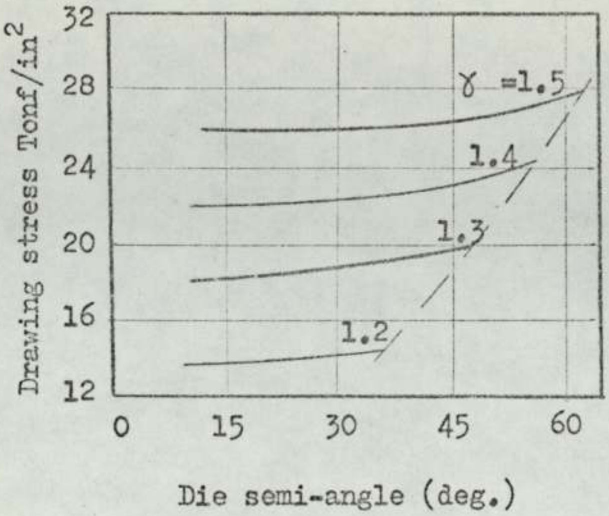

(A) Variation in drawing stress with die semi-angle for different redrawing ratios (Rd = 5/16 in.)

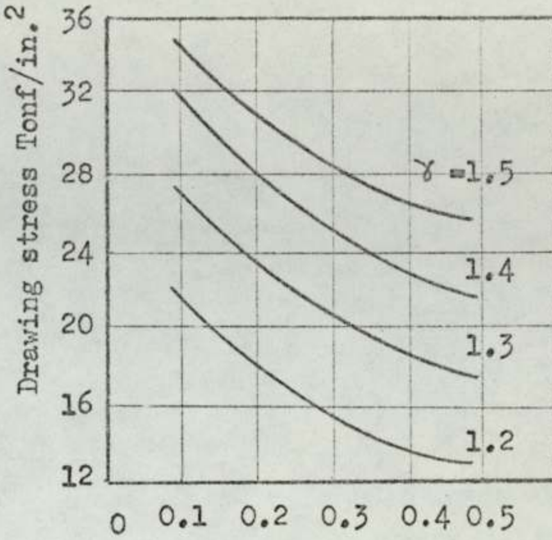

(B) Variation of drawing stress with die radius for single curvature dies

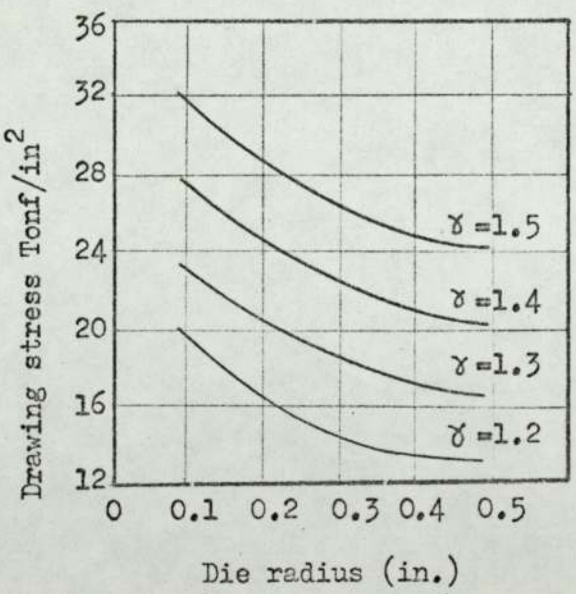

(C) Influence of die radius on drawing stress for different redrawing ratios ($\alpha = 22.5^\circ$)

FIG. 21 THEORETICAL REDRAWING STRESS CHARACTERISTICS WITH CONICAL DIES (FOGG)

2.4. FLANGE WRINKLING IN DEEP DRAWING.

(a) Introductory comments.

Deep-drawing operations are characterised by a plane stress system in the plastically deforming flange, where the radial stress is tensile and the circumferential stress compressive. Under the action of the circumferential stress the flange may become unstable and buckle into a number of wrinkles or waves as shown in FIG.22. When this possibility arises it is common to suppress wrinkling by means of a hold-down agent which, in cupping, is termed a blank-holder, and takes the form of a ring whose annular dimensions correspond to those of the drawing die. The blank-holder may be held in position by either a hydraulic/pneumatic force, in which case the latter is constant, or by springs which exert a force proportional to the wrinkle wave height. In 'constant clearance' blank-holding the tools and supporting press structure act as a very stiff spring and this method therefore falls into the second category above.

Flange wrinkling can become a severe problem in deep drawing. It may promote drawing failure, and at best detracts from the quality of the finished product. The first attempt to theoretically analyse the problem was made by Geckeler (1928), who described the critical buckling compressive flange stress in terms of flange geometry. Baldwin and Howald[13] (1946) converted Geckeler's theory into a more usable form and compared theory with experimental evidence. Baldwin and Howald were concerned with evaluating critical buckling conditions for cupping without a blank-holder. The applicability of their work is limited, since the large draw ratios (2/1) achieved in cupping usually require blank-holding.

Senior[14] (1956) derived expressions for critical wrinkling conditions and number of waves formed when cupping without a blank-holder. An energy approach was adopted to obtain a stability equation. By modifying this equation wrinkling behaviour with a spring-type blank-holder was studied, but a similar approach did not provide directly

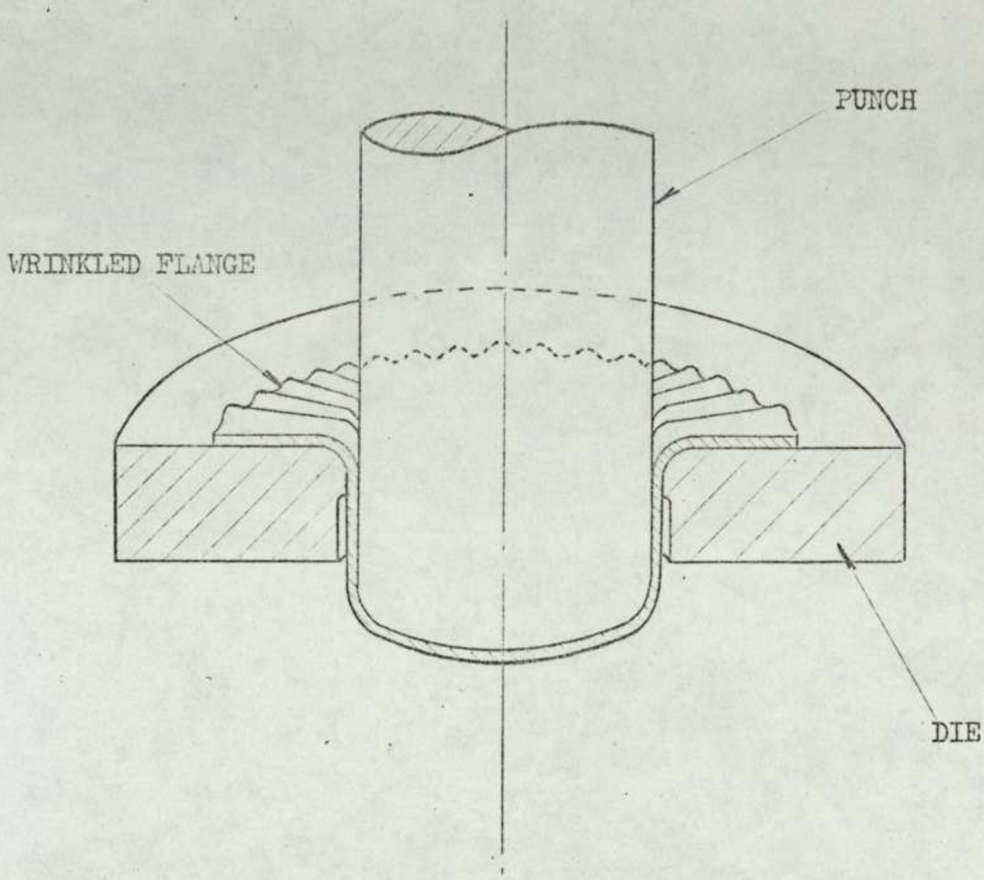

FIG. 22 FLANGE WRINKLING IN CUPPING WITHOUT A BLANK-HOLDER.

useful information on wrinkling with constant pressure blank-holding. Senior's work embraced that of Geckeler and Baldwin and Howald, and was discussed by Alexander.[8]

Siebel[15] (1954) derived an expression for minimum blank-holder pressure for a 'constant-pressure' system of blank-holding. There is a lack of available experimental evidence to verify this theory, and in view of certain assumptions made there must remain reservations about its validity.

The remainder of this part of the survey is given to discussing salient features of Senior and Siebel's work.

(b) Senior's theories of wrinkling.

The conditions causing flange-wrinkling in the absence of blank-holding were first analysed. It was postulated that instability would occur when the energy due to compressive flange stresses reached a level sufficient to form waves, taking account of resistance to wave formation imposed on the inner flange where the cup is constrained between punch and die. The method used to allow for this constraint was fundamental to Senior's approach and so requires special mention; if a radial section is cut through a wrinkle, any point on the section is displaced above the die by an amount proportional to distance from the die throat. The analogy was therefore made to a problem investigated by Morley who deduced elastic deflection in an annular disc clamped at its inner edge and subjected to lateral pressure. Since pressure required to deform the disc resulted from the inner constraint, Senior postulated that the effect of the latter in cupping could be simulated by an equivalent pressure, proportional to mean wave height, acting over the flange area. That is,

$$\frac{q}{\gamma} = 7.47\,\frac{E_o . I}{b^5} = K \qquad (2.36)$$

Where q = normal pressure.

z = wave deflection at any point in the wave around the mean flange circumference.

E_o = plastic buckling modulus.

I = second moment of area of the flange section through its central plane.

b = flange width.

K = a constant.

The plastic buckling modulus E_o takes account of the elastic-plastic nature of the problem, and is a function of elastic and tangent modulii (Johnson and Mellor).[16]

The basic equation for instability was written,

$$U_1 = U_2 + U_3 \qquad (2.37)$$

where U_1 was the energy of flange compression, U_2 the energy to form a wave by bending, and U_3 the energy required to overcome the simulated pressure constraint. In deriving expressions for these terms a half-wave flange segment was considered. It was assumed that;

(1) The wave form was sinusoidal.

(2) The number of generated waves would be large, so that a half-segment could be considered straight.

(3) Deformation was pure bending with no twisting of the section.

(4) The flange thickness t was equal to the blank thickness t_o.

Energy of bending.

For a wave form,

$$z = Z \sin \frac{\pi x}{L} \qquad (2.38)$$

bending work is,

$$U_2 = \frac{1}{2}\int_0^L E_o I \left(\frac{d^2 z}{dx^2}\right)^2 dx \qquad \text{------------} \qquad (2.39)$$

where Z and L are wave amplitude and half-length respectively, and x the co-ordinate along the mean-flange circumference. The half-wave L was written in terms of the mean flange radius a and number of full waves n, $L = \frac{\pi a}{n}$.

Solution of equation 2.39 then gave,

$$U_2 = \frac{\pi E_o I Z^2 n^3}{4a^3} \qquad \text{------------} \qquad (2.40)$$

(The power of n was wrongly given as 2 in Senior's paper.)

Energy of flange compression.

With a mean compressive flange stress σ, force on a section is $\sigma.b.t$. The distance moved by this force in forming a half-wave is approximately,

$$L_o - L = \frac{1}{2}\int_0^L \left(\frac{dz}{dx}\right)^2 dx \qquad \text{------------} \qquad (2.41)$$

Integrating equation 2.41, putting $L = \frac{\pi a}{n}$, and multiplying by the force $\sigma.b.t$ gives,

$$U_1 = \frac{\pi \sigma.b.t.Z^2 n}{4a} \qquad \text{------------} \qquad (2.42)$$

Work done against simulated constraint.

The force acting on a flange element of circumference dx is $q.b.dx$. In generating an increment of wave height dz at x the elemental work is $q.b.dx.dz$, and thus for a half-wave the work is given by,

$$U_3 = \int_0^L \int_0^z b\,q\,dx\,dz \qquad \text{------------} \qquad (2.43)$$

Senior considered q (equation 2.36) could take values between Kz and KZ. Equation 2.43 was integrated for both these conditions to provide upper and lower boundaries for the transition to wrinkling,

$$\check{U}_3 = \frac{\pi . b . K . Z^2 a}{4n} \quad \text{———} \quad (2.44a)$$

$$\hat{U}_3 = \frac{2b . K Z^2 a}{n} \quad \text{———} \quad (2.44b)$$

Critical conditions for wrinkling.

Substituting for U_1, U_2, U_3 in equation 2.37 gave the lower wrinkling threshold,

$$\sigma . b . t . = E_o . I . \frac{n^2}{a^2} + b . K \frac{a^2}{n^2} \quad \text{———} \quad (2.45a)$$

and the upper wrinkling threshold,

$$\sigma . b . t . = E_o . I . \frac{n^2}{a^2} + \frac{8}{\pi} b K \frac{a^2}{n^2} \quad \text{———} \quad (2.45b)$$

Equations 2.45a, b were differentiated with respect to n to determine the number of waves at instability, and hence the circumferential stress σ at this condition. There is some disagreement in the resulting expressions for n and $\frac{\sigma}{E_o}$. In his paper Senior gave;

$$1{\cdot}65 \frac{a}{b} \leq n \leq 2{\cdot}33 \frac{a}{b}$$

$$0{\cdot}46 \left(\frac{t}{b}\right)^2 \leq \frac{\sigma}{E_o} \leq 0{\cdot}64 \left(\frac{t}{b}\right)^2$$

However Alexander stated the expressions should read;

$$1{\cdot}65 \frac{a}{b} \leq n \leq 2{\cdot}08 \frac{a}{b}$$

$$0{\cdot}46 \left(\frac{t}{b}\right)^2 \leq \frac{\sigma}{E_o} \leq 0{\cdot}58 \left(\frac{t}{b}\right)^2$$

According to the writer these expressions should be;

$$1{\cdot}65 \frac{a}{b} \leq n \leq 2{\cdot}08 \frac{a}{b} \quad \text{———} \quad (2.46)$$

$$0.46\left(\frac{t}{b}\right)^2 \leq \frac{\sigma}{E_o} \leq 0.73\left(\frac{t}{b}\right)^2 \qquad (2.47)$$

Equation 2.47 was used to determine critical flange geometry after a method evolved by Baldwin and Howald.[13] The final result is that for a given overall cupping reduction the minimum blank thickness/diameter ratio for wrinkle-free drawing may be computed. The method is identical for both limits of equation 2.47 and is briefly described with the aid of FIG. 23 for the lower limit: For a given overall cupping reduction, the term $0.46\left(\frac{t}{b}\right)^2$ when plotted against current flange rim reduction on a log-log scale, gives a family of curves for various values of $\frac{t_o}{b_o}$. All curves are of identical contour and may be represented by a single curve adjustable along the vertical ordinate. The term $\frac{\sigma}{E_o}$ depends upon mean strain in the cup flange and may also be plotted as a function of current rim reduction to the same log-log scale. To find the instability value of $\frac{t_o}{b_o}$ the representative $\left(\frac{t}{b}\right)^2$ curve is adjusted downwards until tangency occurs with the $\frac{\sigma}{E_o}$ curve. This gives the critical value of $0.46\left(\frac{t}{b}\right)^2$, and the corresponding intercept with the vertical ordinate (ie. zero reduction) provides the critical $0.46\left(\frac{t_o}{b_o}\right)^2$ value, from which the blank thickness/diameter ratio may be readily calculated.

In practice blank geometry is such that maximum cupping reductions are rarely achieved without positive blank-holding. Senior next investigated this situation.

Cupping with a spring-loaded blank-holder.

The constraint offered by this type of blank-holder was similar to that postulated for inner rim clamping, and the two terms were therefore added after converting blank-holder load to an equivalent flange pressure q_1. The energy term U_3 was then written,

$$U_3 = \int_0^L \int_0^\delta b(q + q_1)\, dz . dx$$

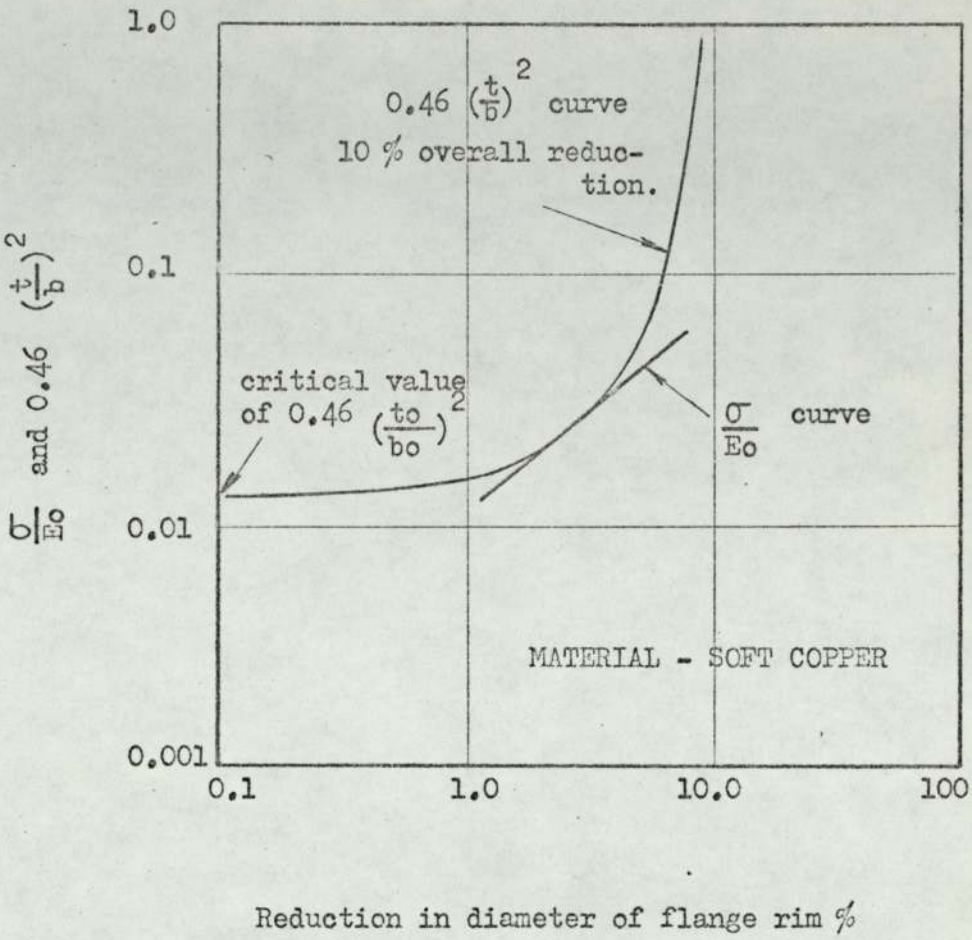

FIG. 23 ILLUSTRATING METHOD OF DEDUCING MINIMUM $(\frac{t_o}{b_o})$ AT A 10 % OVERALL REDUCTION FOR WRINKLE-FREE DRAWING (BALDWIN AND HOWALD)

As for q, q_1 could lie between two limits given by

$$\check{q}_1 = \frac{T_z}{\pi a b} \quad , \quad \hat{q}_1 = \frac{T.Z}{\pi a b}$$

where T is the spring stiffness.

The other terms of the equilibrium equation U_1, U_2 were as equations 2.40 and 2.42, and differentiation with respect to n provided expressions for the number of plastic waves formed.

For the lower limit of constraint,

$$n = a\left[\frac{7.47}{b^4} + \frac{3.82\,T}{E_o.a.b.t^3}\right]^{\frac{1}{4}} \qquad (2.48)$$

and for the upper limit,

$$n = a\left[\frac{19}{b^4} + \frac{9.72\,T}{E_o.a.b.t^3}\right]^{\frac{1}{4}} \qquad (2.49)$$

Equation 2.48 corresponds to Senior's equation 23 which according to Alexander (and the writer) is wrongly written. Senior found that except for low values of T the first terms of equations 2.48, 2.49 could be reasonably ommitted. Equation 2.48 then becomes,

$$n = 1.4a\left[\frac{T}{E_o.b.a.t^3}\right]^{\frac{1}{4}} \qquad (2.50)$$

<u>Experimental-theoretical correlation (spring blank-holder.)</u>

Equation 2.50 was used for comparison with experimental observations. It was found that in the absence of blank-holding the final number of plastic waves equalled the number of initially formed elastic waves, the wave-forming criterion being independent of buckling modulii. With blank-holding however, the number of final plastic waves was sensitive to the plastic buckling modulus. Senior observed that with spring blank-holding a low number of elastic waves formed initially and multiplied on pressing against the blank-holder, so that each initial wave became two or three final waves. For a given reduction equation

2.50 reasonably predicted the effects of blank-holder stiffness, material properties and thickness. Brass cups were drawn with reductions ranging from 20 - 55%. For high reductions the number of waves was insensitive to variations in reduction, but at lower reductions the number of waves increased rapidly as the wrinkle-free condition was approached. It was concluded that the latter condition could be considered as an infinite number of infinitesimally small waves.

Cupping with a constant-load blank-holder.

The energy approach followed in previous work failed to supply useful information on wrinkling characteristics. This resulted from the wave amplitude term Z being inseparable from the number of waves n in the equilibrium equation.

For a blank-holder load Q the load carried by each wave is $\frac{Q}{n}$, and for a wave amplitude Z the total work done against the blank-holder in forming a single wave is,

$$U_4 = 2Z\frac{Q}{n}$$

The terms U_1, U_2, U_3 are as previously found for drawing without blank-holding, and thus the equilibrium equation for the lower instability limit is,

$$\sigma . b . t . = E_o . I . \frac{n^2}{a^2} + bK\frac{a^2}{n^2} + \frac{8Qa}{\pi Z n^2} \qquad (2.51)$$

Senior differentiated equation 2.51 with respect to n to find the number of waves formed. For this operation Z was treated as constant, although as Alexander pointed out Z and n are probably related. The number of waves is then given by,

$$n = \frac{7.47\, E_o . t^3 . a^4 + 30.6\, Q . a^3 . b^3 / Z}{E_o . b^4 . t^3} \qquad (2.52)$$

The constants 7.47, 30.6 were wrongly given in Senior's paper as 1.34 and 2.54.

n could not be found from equation 2.52 since Z was unknown.

Summary of Senior's results.

For cupping without a blank-holder theory and experiment agreed closely. The number of wrinkles formed was found to vary inversely with overall reduction, and the wrinkle free condition corresponded to that for an infinite number of minute wrinkles. Although critical reduction was a function of material properties, the dependence was weak, and it was considered adequate to use a single reduction-blank thickness/diameter curve for all materials and states of prior strain.

When cupping with a spring-type of blank holder the number of final plastic waves formed depended upon blank-holder stiffness, flange geometry and material properties. For a given material and flange geometry it was possible to pre-determine number of wrinkles in terms of blank-holder stiffness.

The energy approach adopted did not provide directly useful information when cupping with a constant pressure blank-holder, since wave amplitude could not be expressed in terms of wave number.

Survey note.

Senior's treatment is for cupping from a flat blank. It would seem that a similar approach may supply information on wrinkling in redrawing, making due allowance for the additional constraining effect of the entering cup at the outer flange.

(c) Siebel's wrinkling theory.[15]

An expression for blank-holder pressure was derived in terms of overall draw ratio and material properties, using a semi-empirical approach involving numerous assumptions and adjustments.

Wave amplitude.

At any stage in the cupping process there is a thickness various over the deforming flange (Chung and Swift). The blank holder acts only at the outer rim, there being a slight gap elsewhere. Siebel proposed that the flange would wrinkle to fill this gap and so exert a force on the blank-holder. Thickness variations over the flange were studied for a number of draw ratios, with the conclusion that the maximum die/ blank-holder gap could be approximately written,

$$2f = 0.024 t_o (\gamma - 1)^2$$

and the mean wave amplitude across the flange was thus,

$$f_m = 0.006 t_o (\gamma - 1)^2 \qquad (2.53)$$

Blank-holder pressure.

The flange buckling mechanism was considered to be that of a simple strut, no account being taken of the constraint at the inner flange edge (Senior). Equilibrium of a half-wave wrinkle was expressed in terms of;

(1) The compressive circumferential force.

(2) The lateral blank-holder constraint.

(3) The fixing couples at each end of a half-wave.

Force (1) was based upon the material yield-stress Y, although the average circumferential stress must be less than this. To determine couples (3) a sinusoidal wave form of amplitude f_m was assumed. Curvature, and hence strain, at the half-wave ends was found from the general expression $\frac{1}{\rho} = \frac{d^2y}{dx^2}$. Bending stresses were obtained in terms of the plastic tangent modulus $\frac{dY}{d\varepsilon}$. Integration over the flange section then provided the bending couples.

Substitution for items (1), (2), (3) in the basic moment equilibrium equation gave an expression,

$$\frac{p}{Y} = 8\left(\frac{t_o}{L}\right)^2\left(\frac{f_m}{t_o}\right)\left[1 - \frac{\pi^2}{3}\left(\frac{t_o}{L}\right)^2 \frac{dY/d\varepsilon}{Y}\right] \qquad (2.54)$$

where p = blank-holder pressure.

L = wave-length of a wrinkle.

Equation 2.54 was then differentiated with respect to $\left(\frac{t_o}{L}\right)$ to give the maximum value of $\left(\frac{p}{Y}\right)$,

$$\frac{\hat{p}}{Y} = 0.6\left(\frac{f_m}{t_o}\right)\frac{Y}{dY/d\varepsilon} \qquad (2.55)$$

After examining stress-strain curves for steel and copper Siebel concluded that equation 2.55 could be re-written.

$$\frac{\hat{p}}{Y} = 0.3\left(\frac{f_m}{t_o}\right) \text{ to } 0.4\left(\frac{f_m}{t_o}\right)$$

Substitution for f_m from equation 2.53 gave

$$\hat{p} = 0.002(\gamma-1)^2 Y \text{ to } 0.0025\,(\gamma-1)^2 Y \quad \text{———} (2.56)$$

'Adjustments' were then made which appear to be concessions to the inadequacy of the theory. It was recommended that Y in equation 2.56 be replaced by the corresponding ultimate tensile strength, and that an allowance be made for variations in f_m arising from die/blank-holder manufacturing errors. Both adjustments had the effect of increasing blank-holder pressure p. Siebel's final equation read,

$$\frac{p}{U.T.S.} = 0.002/0.0025\left[(\gamma-1)^2 + \frac{1}{200}\frac{d}{t_o}\right] \quad \text{———} (2.57)$$

where d = punch diameter.

Application of the theory.

It was claimed that equation 2.57 was a useful guide to blank holder requirements. No independent experimental data have been found by the writer to either prove or disprove this claim, but in view of the empirical nature of the work, and the assumptions and adjustments made in reaching equation 2.57, it seems unlikely that the theory could be relied upon for accurate predictions.

2.5 ANISOTROPY AND ITS RELEVANCE TO DEEP DRAWING.

(a) Introductory comments.

A body possessing different properties in different directions is said to be anisotropic. Forged, rolled and drawn products usually become anisotropic as a result of the manufacturing process, and are often produced to offer maximum strength in certain directions. Directional properties may be introduced into a material by deliberately restricting slip on crystallographic planes to certain directions. The material is then said to possess a 'texture'. Different atomic lattice structures inherently exhibit different degrees of anisotropy. However, a certain degree of anisotropy may be introduced in all materials during fabrication, and this particularly applies to rolled sheet. Consequently deep drawn products are usually anisotropic.

Two approaches, termed 'macroscopic' and 'microscopic', are used to investigate deformation in anisotropic materials. Hill's plasticity theory[17] forms the basis of the macroscopic approach and was developed by assuming certain general properties for the aggregate. The theory has been used to explain anisotropic behaviour in deep drawing. The microscopic approach is essentially concerned with slip systems on a crystallographic basis and is used to determine fundamental anisotropic characteristics e.g. why certain materials should inherently possess greater anisotropy than others.

The ratio width strain/thickness strain of a strip specimen in uniaxial tension is termed the coefficient of normal anisotropy R . If the material were isotropic this ratio would be unity, according to the laws of plasticity. For the special case where R is constant for all directions in the plane of a sheet, a cup deep-drawn from the sheet would reveal no visible external signs of anisotropy. If R varied in the plane of the sheet, giving planar anisotropy, the deep drawn cup would exhibit rim irregularities known as 'earing', the earing geometry being indicative of both maximum variation in R and its dependence on direction.

Although earing may cause practical problems in deep drawing, a more fundamental effect of anisotropy is its influence on maximum draw ratio. Correlations have been found to exist between the mean coefficient of normal anisotropy $\bar{R}$ and deep drawing performance. The pioneering work in this direction was by Lankford and others about 18 years ago. A correlation between formability and R was detected when pressing motor car bumpers. Whiteley[18] later established a definite correlation between R and maximum draw ratio in cupping. Information on a wide range of R values for various materials has since accumulated and there is now no serious doubt that normal anisotropy strongly influences deep-drawability.

A number of practical difficulties have been encountered in measuring values of R. To overcome these Atkinson and Maclean[19] suggested a testing procedure.

The remainder of this section of the survey is given to discussing various aspects mentioned above in more detail.

(b) Hill's anisotropic yield criterion.[17]

It was proposed that an anisotropic material has three principal axes of anisotropy x, y, z along which it possesses different tensile yield-strengths. Hill's criterion is an extension of Von Mises isotropic criterion which may be written in terms of the three principal stresses, $\sigma_1, \sigma_2, \sigma_3$,

$$(\sigma_1 - \sigma_2)^2 + (\sigma_2 - \sigma_3)^2 + (\sigma_3 - \sigma_1)^2 = \text{constant},$$

or in terms of the three normal and shear stresses

σ_x, σ_y, σ_z, τ_{xy}, τ_{yz}, τ_{zx}, as,

$$(\sigma_x - \sigma_y)^2 + (\sigma_y - \sigma_z)^2 + (\sigma_z - \sigma_x)^2 + 6(\tau_{xy}^2 + \tau_{yz}^2 + \tau_{zx}^2) = \text{constant} \quad \text{——(2.58)}$$

making use of the stress invariants I_1, I_2 .

By analogy with equation 2.58 Hill's criterion was written,

$$2f(\sigma_{ij}) = F(\sigma_y-\sigma_z)^2+G(\sigma_z-\sigma_x)^2+H(\sigma_x-\sigma_y)^2+2L\tau_{yz}^2+2M\tau_{zx}^2+2N\tau_{xy}^2=1 \quad (2.59)$$

where $F, G, H, L, M, N,$ are characteristics of the current state of anisotropy. Hill showed that if X, Y, Z and R, S, T were the yield strengths in tension and shear respectively along the principal axes;

$$\left.\begin{aligned} 2F &= \frac{1}{Y^2}+\frac{1}{Z^2}-\frac{1}{X^2} & \quad 2L &= \frac{1}{R^2} \\ 2G &= \frac{1}{Z^2}+\frac{1}{X^2}-\frac{1}{Y^2} & \quad \text{and} \quad 2M &= \frac{1}{S^2} \\ 2H &= \frac{1}{X^2}+\frac{1}{Y^2}-\frac{1}{Z^2} & \quad 2N &= \frac{1}{T^2} \end{aligned}\right\} \quad (2.60)$$

It was further shown that equation 2.59 reduced to 2.58 when $F = G = H$ and $L = M = N = 3F$

Equation 2.59 was treated as a plastic potential to give plastic strain-increments in terms of stresses.

For the purpose of observing the effects of anisotropy in deep-drawing it is convenient to consider a sheet of zero planar anisotropy so that $X = Y$ and $F = G$. The strain ratios $d\varepsilon_x : d\varepsilon_y : d\varepsilon_z$ obtained along the x axis in a tensile test are then identical to those for a similar test along the y axis and are given by,

$$G+H : -H : -G$$

For the particular case where $\sigma_x, \sigma_y, \sigma_z$ are principal stresses equation 2.59 becomes,

$$(\sigma_y-\sigma_z)^2+(\sigma_z-\sigma_x)^2+\frac{H}{G}(\sigma_x-\sigma_y)^2 = \frac{1}{G} \quad (2.61)$$

Now for a strip specimen tensile tested along the x axis $H:G$ is the width/thickness strain or the normal anisotropy coefficient R. Furthermore from equations 2.60,

$$\frac{1}{G} = 2Z^2 = \left(1 + \frac{H}{G}\right)Y^2 = (1+R)Y^2$$

Equation 2.61 may therefore be re-written,

$$(\sigma_y - \sigma_z)^2 + (\sigma_z - \sigma_x)^2 + R\,(\sigma_x - \sigma_y)^2 = (1+R)Y^2 \qquad (2.62)$$

and is useful for predicting the influence of R in stress systems encountered in deep drawing.

(c) <u>Application of Hill's yield criterion to deep drawing.</u>

Limiting draw ratio conditions occur in cupping when the drawing load due to deformation at the die equals the maximum load bearable in the lower cup wall near the punch nose radius. It is therefore of interest to observe the effects of anisotropy in these two zones.

The largest component of drawing stress arises from radial drawing in the plane flange (Chung and Swift), where the radial stress system is approximately plane and the material strains in all three principal directions

For this situation equation 2.62 becomes,

$$\sigma_x^2 + \sigma_y^2 - \frac{2R}{1+R}\sigma_x.\sigma_y = Y^2, \quad \text{since} \quad \sigma_z = 0$$

σ_x, σ_y are always tensile and compressive respectively. The largest value σ_x may attain occurs when σ_y approaches zero. Therefore σ_x will not exceed Y, and R will not influence maximum drawing load.

The stress-strain conditions attendant at fracture near the punch nose are generally uncertain. Holcomb and Backofen,[20] and Moore and Wallace[21] assumed plane-strain fracture in the lower cup wall when analysing the effects of anisotropy, whilst Chung and Swift[5] found that fracture usually occurred at the lower of two necks situated around the base corner profile. Wilson[22] also subscribed to that view. In the latter case fracture would be in biaxial tension.

For biaxial tension over the punch nose $\sigma_x = \sigma_y$ with $\sigma_z = 0$

Substitution in equation 2.62 gives

$$\frac{\sigma_x}{Y} = \sqrt{\frac{1+R}{2}} \qquad (2.63)$$

Equation 2.63 implies that the load carrying capacity at the assumed fracture site increases with R, and that when R exceeds unity wall strength exceeds that in uniaxial tension.

For plane-strain tension in the lower cup wall $d\varepsilon_y = 0$ and therefore $d\varepsilon_z = -d\varepsilon_x$. Also $\sigma_z = 0$. By substituting these values in the stress-strain increment equations derived from the anisotropic yield criterion it may be shown that,

$$\sigma_y = \frac{R}{R+1} \cdot \sigma_x$$

Substitution for σ_y in equation 2.62 then gives,

$$\frac{\sigma_x}{Y} = \frac{1+R}{\sqrt{1+2R}} \qquad (2.64)$$

Equation 2.64 was derived by Backofen and reduces to Von Mises plane-strain yield stress $\frac{2}{\sqrt{3}}Y$ when R = 1. Thus the load carrying capacity of the cup wall is increased purely by the plane strain condition, and is further enhanced as R increases above unity.

For both cup failure modes examined Hill's criterion predicts an increase in drawability with R value.

(d) Microscopic (or crystallographic) approach to anisotropy.

The approach is more fundamental than Hill's in that deformation on a microscopic scale within single crystals is studied and results applied to explain bulk anisotropic behaviour of an aggregate. The Schmid law,

$$\sigma = \frac{\tau}{\cos\beta . \cos\psi} \qquad (2.65)$$

relates the direct stress σ applied to a crystal to the critical resolved shear stress τ in an active slip system. Equation 2.65

defines a three dimension state. The angle β defines the component of σ, σ' resolved on to the slip plane, and ψ resolves σ' in the slip direction. If τ is the shear stress required to cause plastic flow on the slip plane the magnitude of the applied stress σ depends upon its orientation defined by β, ψ. Generalising, a textured material will appear strong or weak depending upon the direction of the applied stress. The above argument implies that anisotropic behaviour will be strongly influenced by atomic lattice structure and therefore that certain materials exhibit greater anisotropy than others.

Studies of anisotropy in single crystals have been made by Roberts and Vieth and Whiteley. Unfortunately such results are not readily applied to aggregates, where even if orientation is perfect, grain boundary constraint may initiate secondary slip systems. Blade studied the behaviour of several textures in single crystals and so predicted behaviour in an aggregate making allowance for differing texture proportions. Wilson[22] has discussed this approach.

Dillamore pointed out that R values as determined from a uniaxial tensile test merely express a relationship between strains for a particular orientation under a particular stress condition, and that under a different stress system the material may behave in a very different manner.

(e) <u>Experimental correlation between R value and deep drawability.</u>

Whiteley[18] (1959) measured R values for a number of materials. Where a high degree of planar anisotropy was present an average R value ($\bar{R}$) was taken. Each material was then cupped and the limiting draw ratio established. Whiteley concluded that limiting draw ratio increased in direct proportion to $\bar{R}$ for all materials investigated. It is interesting to note that in these tests aluminium killed steel gave higher draw ratios than either brass or stainless steel. Swift had earlier concluded that draw ratio improved with a high work-hardening rate, and on this basis brass and stainless steel should have performed better than steel. Swift did not investigate anisotropic behaviour.

Lilet and Wybo[23] (1964) investigated the effect of R in a number of standard tests comprising cup drawing and stretch forming. A definite correlation between R and draw ratio was found in the cupping tests. The cups, drawn from different steels, showed a wide variation in earing characteristics but this did not affect the correlation provided a mean R value was taken. No correlation was observed for the stretch forming tests, the assessment criterion adopted being strain to fracture. In further tests steel cups with similar earing patterns but different ear heights were drawn. It was found that materials of similar mean R value could possess widely differing degrees of planar anisotropy, and that in this situation materials with the highest minimum R value performed best in drawing.

Atkinson and Maclean[19] (1965) investigated factors affecting the test for R values and attempted to improve correlation between R and limiting draw ratio by controlling frictional conditions in cupping.

In deriving R values thickness strains were found indirectly by measuring elongation and width strains. This method was found to be more accurate than measuring thickness strain directly. R was expressed,

$$R = \ln \frac{w_1}{w_2} \Big/ \ln \frac{w_2}{w_1} \cdot \frac{l_2}{l_1}$$

A large test piece gauge length ($7\frac{1}{2}$ in.) was used to take into account any local inhomogeneity present in the sheet, and was divided into 15 - $\frac{1}{2}$ in. segments. Width and length strains were measured in each segment for extensional strains of 10, 15 and 20 %. A significant variation in results occurred over the gauge-length and increased with strain level. The following procedure was recommended for R value determination;

(1) The gauge length should be large.

(2) Tensile elongation should approach the limit of uniform elongation.

(3) Width and length strains should be measured in preference to thickness strain.

(4) Width measurements should be made at intervals not greater than $\frac{1}{2}$ in. along the gauge length.

(5) Measuring techniques should be precise.

Atkinson and Maclean suggested that experimental scatter in previous experimental investigations of R - drawability correlation resulted from variable frictional conditions. To test this theory steel cups were drawn using polythene sheet and oil as lubricants. An average R value

$$\bar{R} = \frac{R_0 + R_{90} + 2R_{45}}{4}$$

was taken over the sheet. It was found that a strong correlation existed between $\bar{R}$ and maximum draw ratio with polythene irrespective of the blank surface finish, whereas the correlation with oil deteriorated as the blank surface finish was varied. In further tests it was demonstrated that when $\bar{R}$, yield strength, tensile strength and ductility were varied only $\bar{R}$ had a significant effect on draw ratio.

Various investigators have shown graphical correlations between R and drawability. That of Wilson is reproduced as FIG. 24 and also illustrates the lack of sensitivity of draw ratio to tensile elongation properties. Attention is drawn to the spectacular limiting draw ratio possible with titanium by virtue of its high R value.

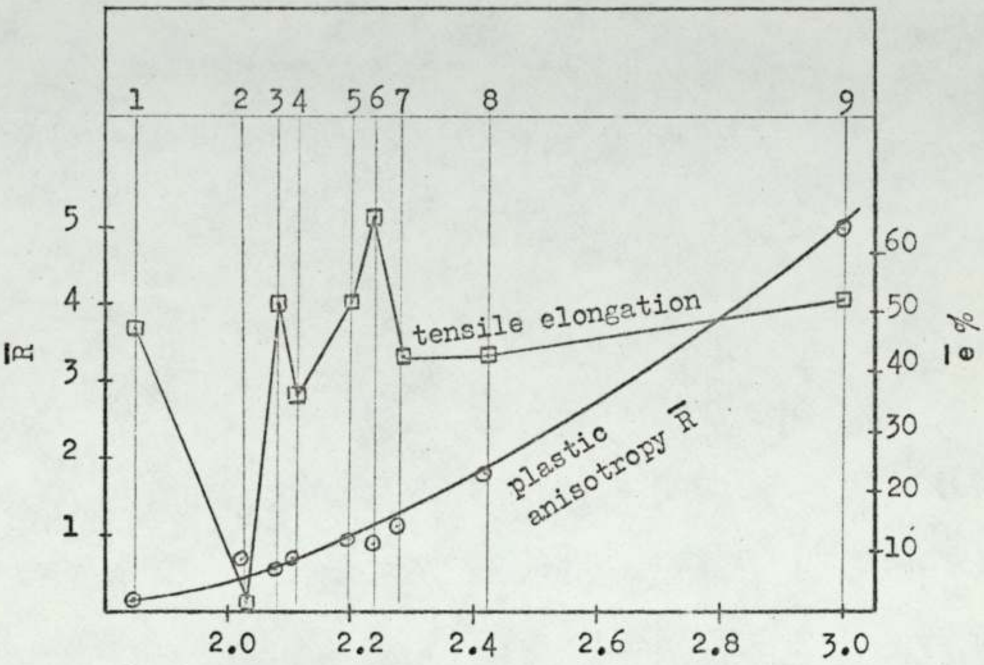

FIG. 24 LIMITING DRAW RATIO AS A FUNCTION OF MEAN COEFFICIENT OF NORMAL ANISOTROPY $\overline{R}$ AND MEAN TENSILE ELONGATION TO FRACURE $\overline{e}$ (WILSON)

1. Commercial zinc, rolled 85 % and annealed at 200°C.
2. Cube-texture tough-pitch copper.
3. Commercial aluminium $\frac{3}{4}$-hard.
4. Commercial aluminium annealed at 300°C.
5. "Balanced-texture" tough-pitch copper.
6. 70/30 Brass annealed at 700°C.
7. Box-annealed open-hearth rimming steel.
8. Box-annealed aluminium-stabilized steel.
9. Annealed titanium grade 115.

2.6 FRICTION, LUBRICATION AND SPEED EFFECTS IN DEEP DRAWING.

(a) Inroductory comments.

The role of a lubricant in metal-forming processes is three-fold, it should reduce forming loads to a minimum, minimise tool wear, and assist in imparting a good surface finish to the product. The relative importance of these three requirements may vary. In all drawing operations improved lubrication provides a decrease in forming load. It does not follow however that potentially higher useful deformation will result. This particularly applies to drawing tubular components with a mandrel or punch where the success of the process often depends upon friction between the workpiece and inner tool; whilst improved lubrication leads to lower forming loads it also reduces friction at this interface.

Frictional effects in deep drawing do not depend solely on the type of lubricant used. Tool and work-piece surface finish can also play a significant role. Failure to recognise this led to difficulties in early attempts to establish correlations between drawability and desirable material properties. The paper by Kemmis well illustrated this point. It seems that frictional effects in deep drawing were not generally appreciated until the late 1940's. Since that time the problem has received considerable attention.

(b) Lubrication mechanisms in metal forming.

Two broad classes of lubrication occur in metal forming and are identified as "full-film" and "boundary" . Full-film lubrication exists when the tool/workpiece interface becomes completely separated by a lubricant layer, whilst boundary conditions occur when metal to metal contact is prevented only by a minutely thin lubricant film whose thickness is less than variations in surface topography of the rubbing surfaces.

Since surfaces do not contact with full-film lubrication little surface modification of the workpiece occurs, coupled with a small amount of tool wear. Full film lubrication only exists when the lubricant film is capable of remaining stable under the applied normal pressure. To achieve this situation the lubricant must have high compressive strength/low shear strength characteristics or alternatively external means are necessary for preventing lubricant expulsion from the tool/workpiece interface. Hydrodynamic lubrication falls into the second category and exists when pressure build-up in the lubricant at die entry becomes equal to the normal pressure between tool and workpiece. Pressure build-up depends upon sliding velocity, geometry of the tool entry zone and viscous properties of the lubricant. Wistreich showed that hydrodynamic conditions occurred in high speed wire drawing whilst Christopherson (and others) achieved similar conditions in tube drawing by contriving a simple means of pressure generation at die entry.

Boundary lubrication conditions are identified by a drastic modification of the workpiece surface in plastic deformation, the final product having a burnished appearance. Mechanisms involved in boundary lubrication are complex since topography of the contacting surfaces assumes importance, and the workpiece surface continuously modifies throughout the deformation zone. This aspect was discussed by Fogg.[24] On a microscopic scale metal surfaces appear as undulations of peaks and valleys, and when two such surfaces are pressed together the real contact area is only a small proportion of that apparent. If the compressive force is sufficiently high local contact points become plastically deformed, so providing a larger load supporting area. Bowden, Leben and Tabor showed that when surfaces were chemically clean, or even poorly lubricated, pressure welding could occur at local points of contact. They concluded that a lubricant film of even molecular proportions was sufficient to prevent welding.

FIG. 25. illustrates the two lubrication classes in metal forming, the tool/workpiece surfaces being drawn to a microscopic scale. FIG. 25(a) shows the workpiece at entry to the deformation

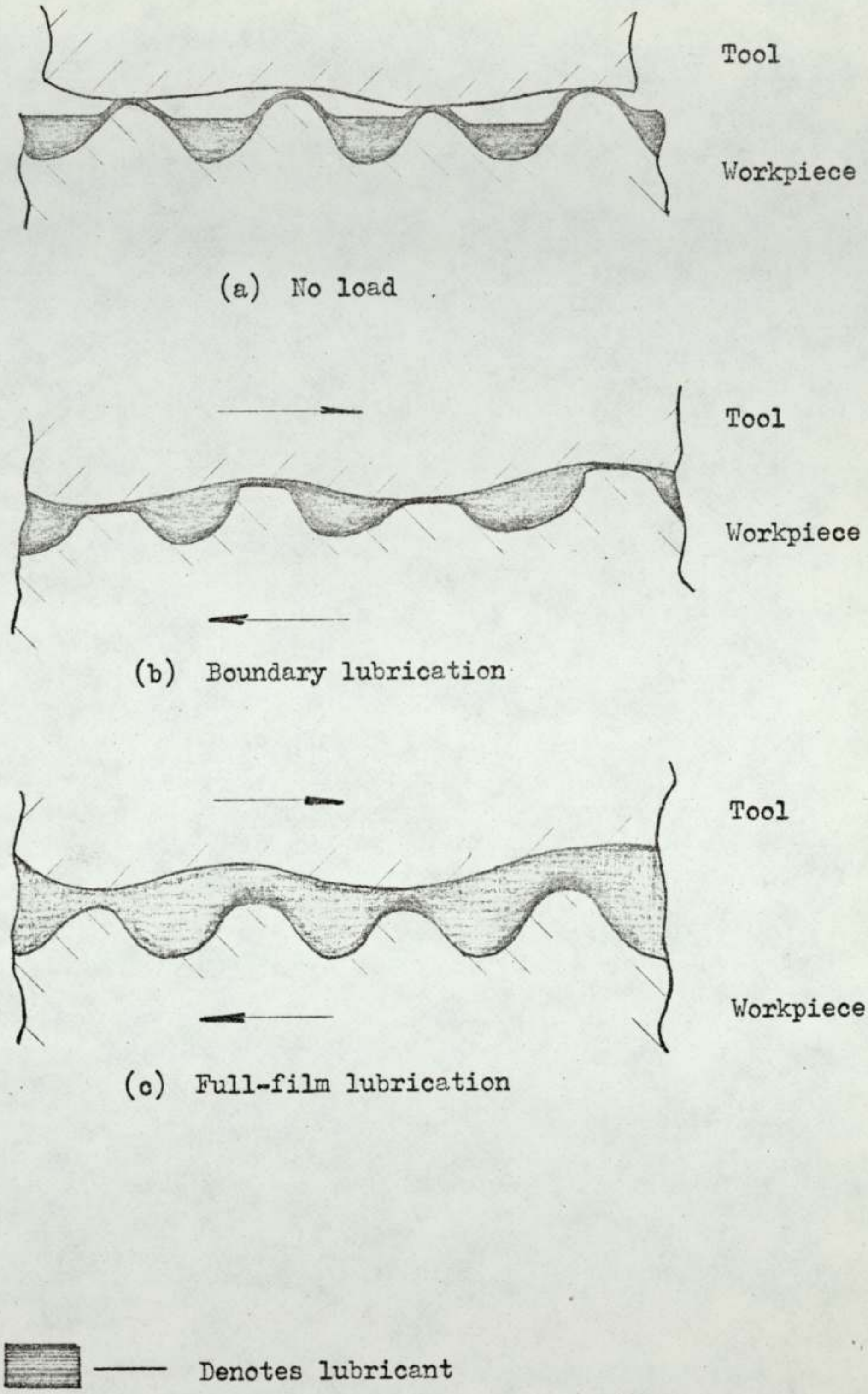

FIG. 25 BOUNDARY AND FULL-FILM LUBRICATION MECHANISMS

zone with zero normal pressure. FIG. 25(b) represents boundary lubrication during plastic deformation. The normal pressure causes modification at the peak tips which become flattened until lubricant pools in asperity valleys are pressurised and hence support load. In addition leakage from the pools supplies lubricant to the areas of surface contact, and if this supply is adequate fusion (or pick-up) at the asperity peaks will not occur. Under boundary lubrication conditions the conventional coefficient of friction defined as shear force/normal force only provides an overall, inadequate, impression. FIG. 25(c) shows full-film lubrication with sliding surfaces completely separated.

(c) Lubrication and tool-workpiece surface finish in deep drawing.

Swift found that when cupping aluminium with a hemispherically nosed punch softer blank tempers gave highest limiting draw ratio (L. D. R.), whereas when using a flat bottomed punch harder tempers performed best. Loxley and Freeman[25] (1954) investigated this behaviour. Cupping tests were conducted on aluminium blanks in a variety of tempers using different lubrication conditions. With a hemispherical punch and good lubrication L. D. R. was highest with low tempers, confirming Swift's findings. When using a flat bottomed punch however the relationship between temper and L. D. R. could be varied by changing lubrication conditions. With no lubricant present L. D. R. increased with temper; with fair lubrication L. D. R. first increased with temper but at higher tempers the trend reversed; with good lubrication L. D. R. decreased as temper increased. It was concluded that the behaviour earlier reported by Swift could be explained in terms of frictional conditions.

In further tests deformation over a hemispherical punch nose was studied by bulging blanks to failure, and observing the effect of lubrication on the fracture site. Even with good lubrication fracture never occurred at the pole (as would be predicted under frictionless conditions) but at a point on the punch profile. As lubrication became poorer the fracture site moved systematically away from the pole demonstrating the effect of friction on the process.

Finally steel cups were drawn with both hemispherical and flat-bottomed punches. Lubrication was applied to the blank either on (a) both sides (b) punch side only, (c) die side only, (d) neither side. The resulting L. D. R. values were, highest to lowest, (c), (a), (d) and (b), for both types of punch nose.

Wallace[26] (1960) investigated the effect of punch surface finish on L. D. R, using a flat nosed punch and graphite-tallow lubricant. Various surface finishes were obtained by shot-blasting. Two qualities of steel were drawn, 'extra-deep drawing' and 'deep drawing'. It was found that L. D. R. increased with punch roughness for both materials, and that the increase in L. D. R. due to roughening was higher than that due to different material qualities. Further investigations showed that with smooth punches L. D. R. was highest when punch-lubrication was ommitted, but with rougher punches the effect was not significant.

Whitton and Mear[27] (1960) investigated the effect of blank and tool surface finish in the Swift cupping test, to check if a test procedure earlier written by Kemmis[28] was sufficiently rigorous in controlling process variables. The maximum range of tool surface finish suggested in the procedure was 0 - 20 micro in. (C. L. A.) . Whitton and Mear used punch/die combinations at the two extremes of the range with a blank-holder finished to 10 micro in. (C. L. A.) . Controls on blank surface finish were not specified by Kemmis but each test material, aluminium, brass and steel, was artificially roughened to simulate commercially produced rough and smooth sheets. It was generally concluded that variations in tool surface finish within the range 0 - 20 micro in. (C. L. A.) could cause variations in L. D. R. - mechanical property correlations.

Fukui[29] and others (1963) investigated the effects of tool surface finish, blank surface finish , oil viscosity and drawing speed on drawability. The interaction of these variables made clear-cut trends difficult to discern. The criterion of drawability was not limiting draw ratio but the amount by which an oversize blank was drawn before failure occurred. (Although this procedure only requires one blank size to cover all tests, it is considered by the writer to be artificial and a poor substitute for a cupping test like Swift's.) Tests indicated that with low viscosity oil drawability improved with tool roughness, but with higher viscosities smooth tools were better. The trend became less marked at higher drawing speeds (40 feet/minute). It was stated that dies roughened radially gave better results than those roughened circumferentially, but this statement did not appear substantiated by Fukui's graphs. Drawability decreased with increasing blank roughness for low viscosity oils, especially at high drawing speeds. With high viscosity oils optimum drawability depended upon both sheet and tool roughness. It was concluded that speed and viscosity had similar effects on friction at the punch nose; at low speed oil was squeezed from the punch nose/blank interface giving desirable friction effects, but at higher speeds this oil became trapped.

(d) Lubricants in deep drawing.

Evans, Silman and Swift[30] (1947) pointed out that metal-working lubricants should possess high film strength to resist expulsion from the tool/workpiece interface under the high pressures and temperatures developed in metal forming. To achieve this requirement most lubricants possess in addition to the basic lubricity;

(a) 'Fillers' to increase viscosity and assist in tool/workpiece separation.

(b) Additives to chemically react with the workpiece surface and form a semi-solid molecular film providing a key for the main lubricating constituent, the film itself possessing lubricating properties.

Lloyd[31] discussed developments in deep drawing lubricants since World War II, the merits of full-film over boundary lubrication, and how practical considerations of application and removal may influence lubricant choice.

Willis[7] 1954 gave a detailed account of Swift's work on lubricant evaluation: cups in steel, brass and aluminium were drawn with a wide range of lubricants comprising most of those in common use during the early 1950's. It was concluded that lubricants containing 'filler' constituents were more effective than lower viscosity liquids. Drawing speeds of 1 inch/minute and 17 feet/minute were used. The higher speed was found to increase punch load by 7 - 10% but no deterioration in drawability was detected.

Mear, Topper and Ford[32] (1963) investigated polymers as lubricants in deep drawing. Cups were produced in the new materials titanium, zirconium, niobium, tantalum and vanadium at a drawing speed of 8.75 feet/minute. The polymer films polythene, polypropylene and P.T.F.E. gave better results than chlorinated mineral oil. However at higher drawing speeds the polymers were no more effective than a low viscosity oil. It was suggested that the desirable low speed effect corresponded to full-film separation but this mechanism broke down due to heat generation at higher speeds.

Coupland and Holyman[33] (1965) compared dry-film lubricants with extreme pressure oils in deep drawing. Draw load was the assessment criterion. The dry-film lubricants comprised polymers, soap and alkali, fatty acids, resins, silicones, molybdenum disulphide and spirit based drawing oils. Cups were drawn in mild steel, tin plate and zinc coated mild-steel. It was concluded that in general dry-film lubricants were superior to conventional drawing oils, and that of all lubricants tested polythene gave lowest forming loads.

(e) <u>Speed effects in deep drawing.</u>

In an investigation at P.E.R.A. (1954) steel cups were drawn with a range of lubricants at a speed between 20 - 60 feet/minute. An increase in speed was found to give a small punch load reduction and an increase in limiting draw ratio. Best results were obtained with viscous oil having sulphurised and chlorinated additives.

Wallace (1955) drew steel cups in the speed range 1 - 30 feet/minute. Flat and hemispherical-bottomed punches were used. With the 'flat' punch limiting draw ratio increased with speed when using mineral oil lubricant, but no improvement occurred when drawing with graphite/tallow or no lubricant. The 'hemispherical' punch gave no speed effect with either lubricant.

Coupland and Wilson[34] (1958) conducted a thorough investigation into the effects of speed in deep drawing. Steel and 70/30 brass cups were drawn at 10, 35 and 90 feet/minute on flat and hemispherical-bottomed punches. Lubricants investigated were;

(a) four mineral oils of differing viscosities.

(b) colloidal graphite.

(c) oil with extreme pressure additives.

Limiting draw ratio (L. D. R.) was the assessment criterion.

Initially steel cups were drawn with lubricants (a) and (c). When using the flat -bottomed punch L. D. R. increased with speed and viscosity. The reverse trend occurred with the hemispherical punch. Draw load decreased with speed especially with the higher viscosity oils. It was concluded that lubrication at the die improved with speed, accounting for the lower loads, but with the hemispherical punch the improvement in punch-nose lubrication was even more marked resulting in a reduction in L. D. R. Conversely the 'flat' punch was relatively insensitive to lubrication condition giving an increase in L. D. R.

Further tests were conducted to isolate lubrication effects from any possible strain-rate effects. Graphite was known to be a lubricant insensitive to speed and was used to study strain-rate effects, whilst 70/30 brass was known to show little strain-rate effect and so was used to study lubricant-speed behaviour. Steel and brass cups were drawn with graphite. L. D. R. trends with steel were similar, though less marked, than those with oil previously found. There was a tendency for draw load to increase with speed. This was attributed to an increase in yield strength with strain-rate. It was suggested that opposite trends found with the two punch-nose types were due to different straining conditions over the nose. Greater thinning occurred with the 'hemispherical' punch at higher speeds whereas straining over the 'flat' punch nose was relatively unaffected by speed. No speed effect with either punch was observed with brass. Tests were then carried out drawing brass with oils (a) and (c). Results were similar to those obtained for steel. By applying oil to the 'die-side' only it was possible to reverse the earlier trend with the hemispherical punch.

Overall conclusions were that for steel, lubrication and strain-rate effects on L. D. R. were complimentary; an increase in speed causing an increase in L. D. R. for a flat-bottomed punch and a decrease in L. D. R. for a hemispherical-bottomed punch. Their effects on draw load were opposite, but on balance the lubrication effect was dominant providing a decrease in load with increased speed. Coupland and Wilson pointed out that the effects of speed on working temperature had not been investigated, and that any work-softening in the deforming flange would be beneficial. Conversely temperature increase may influence lubrication adversely.

2.7. RESIDUAL STRESSES IN DEEP DRAWING.

(a) Introductory comments.

Residual stresses are defined as those stresses retained in a component after fabrication is complete and all external forces and constraints are removed. They are usually regarded as undesirable process features. Residual stresses are frequently found in cold-formed products and those which undergo differential heating or cooling rates in manufacture. The current survey is restricted to discussing cold-formed thin-walled products.

(b) Character of residual stresses.

Residual stresses can only occur after plastic deformation, and then only when strains induced are of a non-uniform nature. Bending, twisting, and cylinders under internal pressure are examples of non-uniform straining processes. Therefore a manufacturing route comprising any of these elements is likely to promote residual stresses. Johnson and Mellor[16] stated that residual stresses in cold-drawn tube did not increase with reduction severity and that there was evidence to suggest the converse was true. Sachs[4] claimed that the level of residual stress could be reduced by stretching the component to about 2% uniform elongation. Failures due to residual stress often occur after the forming operation is complete - Jevons[3] quotes an example where an 18/8 stainless steel cup fractured an half-hour after drawing. Residual stresses possess two properties which are used in their evaluation;

(1) Their integrated or resultant values in any direction is zero. They provide zero net force.

(2) Their integrated or resultant moment about any axis is also zero.

(c) Methods of detecting residual stress.

Three experimental techniques are used to study residual stress distribution and comprise ;

(i) X-ray methods.

(ii) Metal removal methods.

(iii) Selective slitting methods.

In method (i) X-rays are used to supply information on crystal lattice distortion, from a knowledge of which elastic strains and hence stresses are computed. Method (ii) exploits the fact that a residually stressed component distorts when part of the component is removed. It is possible to relate this distortion to the residual stress formerly in the removed material. The method is applied to components with rotational symmetry about an axis i.e. round bars and thick-walled tubes. Sach's and Espey[35] developed a technique whereby circumferential layers were successively removed from a tube bore and corresponding strains measured on the outside surface. Denton[36] discusses more recent developments in the technique. The situation may arise where layer removal causes yielding in the remaining body. The method then becomes invalid.

Residual stress determination by method (iii) is widely used for cold-drawn thin-walled components for which the approximate residual stress distribution may be assumed. This method forms the basis of the following survey.

(d) <u>Determination of residual stress in thin-walled tubular components by slitting.</u>

Cold-drawn tubular components exhibit a residual stress distribution which is approximately linear across the wall section and is tensile on one surface (usually the outer) and compressive on the other. By assuming this distribution the magnitude of residual stresses may be estimated by a method devised by Sachs and Espey.[35] The method cannot be applied indescriminately to all types of residual stress systems.

Sachs and Espey assumed that a longitudinal slit would remove a high proportion of the circumferential residual stress σ_3 , without interfering with any longitudinal stress σ_1 which may be present. The maximum value of σ_3 was then calculated by finding the moment required to re-bend the sprung section elastically to its original dimensions. To determine longitudinal residual stress σ_1 two parallel longitudinal slits were made part way into the tube to separate a tongue from the tube proper. The tongue, being free from circumferential constraint, elastically deflects radially by an amount proportional to the release of the longitudinal residual stress. In finding σ_1, σ_3 the through-thickness stress σ_2 was considered negligible.

The bending moment released by a single longitudinal slit is given by,

$$M = \frac{E.I}{1-\nu^2} \cdot \frac{1}{r_e} \qquad (2.66)$$

where I = second moment of area for circumferential bending.

r_e = equivalent radius of bending from sprung tube radius r_o' to original unslit radius r_o.

$1-\nu^2$ = a term accounting for the constraint on anticlastic bending in the longitudinal direction due to tube geometry.

The equivalent curvature $\frac{1}{r_e}$ may be expressed,

$$\frac{1}{r_e} = \frac{1}{r_o} - \frac{1}{r_o'}$$

Substituting for r_e in equation 2.66 gives,

$$M = \frac{E.I}{1-\nu^2}\left(\frac{r_o' - r_o}{r_o'.r_o}\right) \qquad (2.67)$$

The circumferential residual stress σ_3 at any distance x from the tube outer surface may now be found by substituting M in the general equation of elastic bending.

$$\sigma_{3_x} = \frac{E}{1-\nu^2}\left(\frac{t}{2} - x\right)\left(\frac{r_o' - r_o}{r_o'.r_o}\right) \qquad (2.68)$$

when d = diameter, $r_o' - r_o = \frac{\Delta d}{2}$

and if $\bar{d} = r_o' + r_o$, $r_o'.r_o \simeq \frac{\bar{d}^2}{4}$

Equation 2.68 may therefore be written in terms of maximum residual stress,

$$\sigma_3 = \pm \frac{E}{1-\nu^2} . t . \frac{\Delta d}{\bar{d}^2} \qquad (2.69)$$

σ_3 may be determined by slitting a tube and measuring Δd, $\bar{d}$.

The longitudinal residual stress σ_1 was found by measuring the deflection δ at the free end of a tongue length L which was assumed to bend to radius R .

From Pythagoras,

$$\frac{1}{R} \simeq \frac{2\delta}{L^2}$$

and the equation of bending gives,

$$\sigma_{1_x} = E(t-2x)\frac{\delta}{L^2}$$

which attains a maximum value at the inner and outer surfaces,

$$\sigma_1 = \pm E.t.\frac{\delta}{L^2} \qquad (2.70)$$

The term $1-\nu^2$ is absent from equation 2.70 since there is no anticlastic constraint.

A cold-drawn tube usually springs open rather than closed when slit. According to equations 2.69 and 2.70 both circumferential and longitudinal bending stresses are then tensile at the outer face and compressive at the inner face.

Sachs and Espey suggested a length/diameter testpiece ratio of at least 3, since ratios lower than this gave low amounts of springing. Denton explained the behaviour as interaction between circumferential and longitudinal residual stresses in that with short tubes, longitudinal stress was largely dissipated on slitting, and this caused a relaxation of circumferential stress. The type of slit made was also found to influence springing-specimens cut with a fine jeweller's saw sprang more than those cut with a normal hack-saw. This effect was explained as stress-relief near the cut. Deflection of a longitudinal tongue was strongly influenced by the ratio tongue width/tube diameter which for maximum flexing lay between 0.1 and 0.2. Narrower tongues were stress-relieved by cutting, whilst wider tongues resisted flexing by virtue of their curvature. Denton and Alexander recommended a modified test to circumvent problems of circumferential and longitudinal stress interaction on slitting. The test also obviated cutting a tongue. Their method was to slit long and short tubes and compute circumferential residual stresses $\hat{\sigma}_3$ and $\check{\sigma}_3$, the difference $\hat{\sigma}_3 - \check{\sigma}_3$ being due to interference of longitudinal stress relaxation with the short tube. A longitudinal stress σ_1 would induce a circumferential stress $\nu\sigma_1$, and therefore $(\hat{\sigma}_3 - \check{\sigma}_3) = \nu\sigma_1$, from which σ_1 may be found.

Derivation of residual stress directly from the slitting method requires the assumption that residual stresses are completely released on splitting. This is only approximately true since the slit tube usually springs further if circumferential layers are removed from inner or outer faces. Sachs and Espey[37] described a procedure where, after slitting, layers were successively removed by pickling. Additional residual stresses released were computed from a knowledge of flexing in the specimen. FIG. 26. compares residual stress distribution obtained by slitting only, with that for the slitting plus layer removal method.

(e) <u>Residual stresses in deep drawn cups.</u>

The methods of residual stress determination proposed by Sachs and Espey apply when residual stress distribution is constant with specimen length. Although the method may be suitable for redrawn cups annealed before redrawing, it cannot be immediately applied to drawn cups owing to the different strain histories undergone by each wall element. Sachs and Espey described a drawn cup as "an assembly of a sequence of differently strained thin-walled

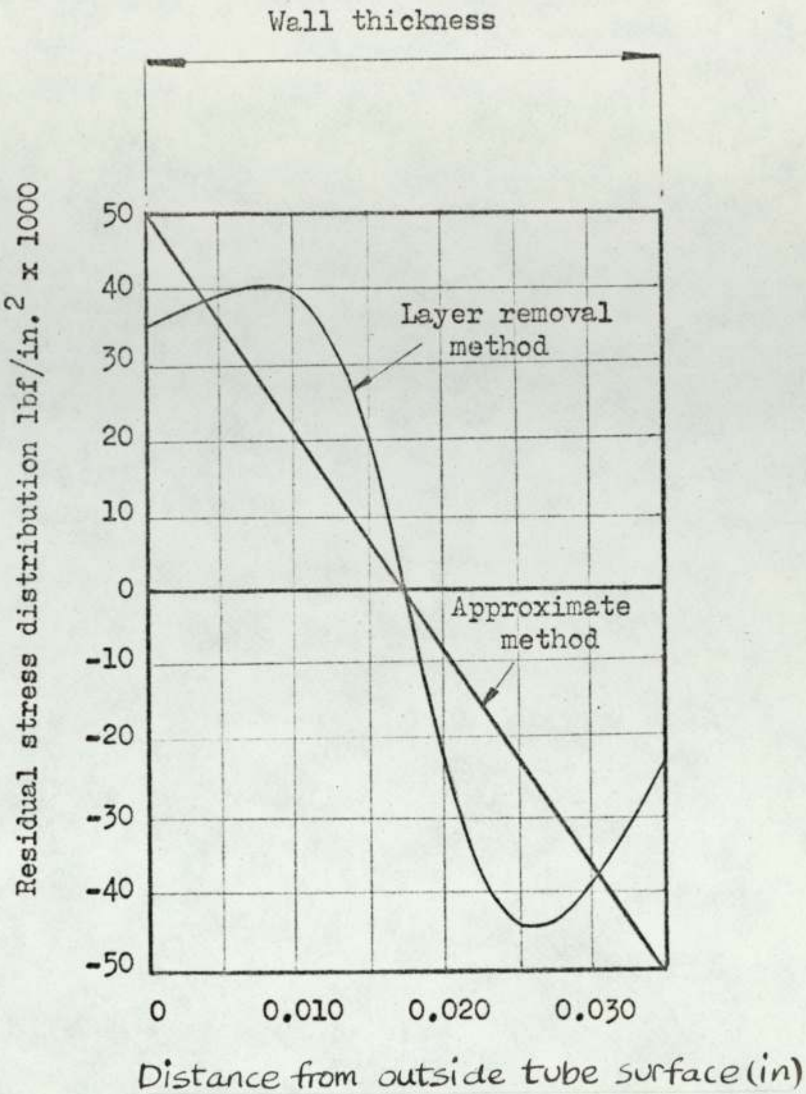

FIG. 26 RESIDUAL CIRCUMFERENTIAL STRESS IN A BRASS TUBE 0.500 in. OUTSIDE DIAMETER, 0.0345 in. WALL THICKNESS, SUNK FROM 0.625 in. OUTSIDE DIAMETER THROUGH A 12.5 deg. SEMI-ANGLE DIE. (SACHS)

tubes" and continued " the residual stresses consist of a portion corresponding to those in uniform tubing and another portion originating from the mutual effect of the various layers."

Swift[38] investigated residual stresses in cups. In view of the heterogeneous strain histories of wall elements a radial shear stress τ was postulated on planes normal to the cup axis, its existence depending upon a circumferential stress σ_3 in the cup wall such that,

$$\frac{d\tau}{dx} = \frac{\sigma_3}{r_0}$$

where x is the distance of an element from the open end. The shear force on an element circumferential length $r_0 \Delta\phi$ is,

$$dF = \sigma_3 . t . \Delta\phi . dx = \sigma_3 . t . \frac{\omega}{r_0} . dx \qquad \text{when} \quad \omega = r_0 \Delta\phi$$

If a longitudinal tongue width ω is cut from the cup wall the bending moment released is given by,

$$M = \int F\, dx = EI \frac{d^2y}{dx^2}$$

$$\text{or} \quad EI \frac{d^4y}{dx^4} = \frac{dF}{dx} \qquad \text{giving} \quad \frac{d^4y}{dx^4} = \frac{12\sigma_3}{E.t^2.r_0} \quad \text{——} (2.71)$$

where y is the tongue deflection at x and $I = \frac{\omega t^3}{12}$

Swift measured tongue deflection and deduced the variation of σ_3 with x by graphical differentiation. The method did not allow an accurate assessment of σ_3 but indicated that its value changed from high tensile near the open end to high compressive $\frac{3}{8}$ in. into the cup. Further down the wall stresses diminished rapidly.

To obtain a more accurate assessment of circumferential stress, σ_3 was assumed constant over a tongue length L.

The shear force was then written,

$$F = \int_0^L \bar{\sigma}_3 . \frac{t . \omega . dx}{r_0} = \frac{\bar{\sigma}_3 t . \omega . L}{r_0}$$

The problem was thus similar to a cantilever with a uniformly distributed load,

$$\frac{F}{L} = \frac{\bar{\sigma}_3 . t . \omega .}{r_0}$$

and deflection at the free end was,

$$\delta = \frac{3 L^4 \bar{\sigma}_3}{E r_0 t^2} \qquad (2.72)$$

L was increased in stages, δ measured, and $\bar{\sigma}_3$ calculated from equation 2.72. Results for a 2 in. diameter steel cup drawn from a 4 in. diameter 0.038 in. thick blank are shown in table 4 . The results imply a reversal in $\bar{\sigma}_3$ between 3/16 and 3/8 in. from the cup rim.

Swift next considered the possibility of a pure bending stress σ_3' existing in the wall as for a plain drawn tube. An equation similar to 2.69 was used to determine σ_3' , the term $1-\nu^2$ being omitted since the cup was too short to exercise anticlastic constraint.

Total circumferential residual stress $\sigma_3 + \sigma_3'$ was found to have a maximum tensile value near the cup rim. Rings cut from cups sprang open on slitting, indicating tensile and compressive stresses at outer and inner surfaces respectively. A study was made of the effects of process parameters on residual stress level in drawn cups. Results are summarised below.

punch profile	-	no influence.
die profile	-	residual stress higher with larger radii.
lubricants	-	residual stress higher with good lubricants.
materials	-	low elastic modulus with high yield stress gave highest residual stress.
reduction	-	little influence.

TABLE 4 AVERAGE RESIDUAL HOOP STRESS VARIATION WITH DEPTH OF TONGUE (SWIFT)

DEPTH OF TONGUE (in.)	AVERAGE CIRCUMFERENTIAL STRESS ($Tonf/in.^2$)
0 - 3/16	28
0 - 3/8	10.5
0 - 9/16	3.5
0 - 3/4	1.4
0 - 15/16	1.0
0 - 1.1/8	0.6

ageing - residual stress increased in cups over a one-month period.

Survey note.

The above results indicate that factors influencing residual stress are not always obvious. Results with die-profile, lubricants and reduction may be tentatively explained by an increase in drawing stress causing greater stretching in the cup wall and so partially relieving residual stress (Sachs). The level of residual stress should be viewed in context with the material's yield or fracture stress.

2.8. SIMULATIVE DEEP DRAWING TESTS.

(a) Introductory comments.

The object of simulative deep drawing tests is to furnish information on the probable behaviour of material in actual production forming operations without involvement in complex and costly tooling. An ideal simulative test would truly represent mechanics of the forming process and indicate variations in material properties which influence formability.

Various tests have been devised for assessing sheet forming properties. These fall into two classes: stretch-forming tests and drawing tests.

Criterion of performance in a stretch-forming test is the maximum biaxial strain undergone by a sheet before fracture. Jevons[3] concluded that results from such tests were not generally applicable to deep drawing, although useful in press work if applied discriminately.

The most common kind of simulative drawing test is that in which a circular cup is drawn from a flat circular blank under closely controlled conditions, materials being assessed on the basis of the deepest drawable cup. Swift's cupping test is typical. Sach's (1930) suggested a wedge drawing test which simulates conditions in the plane flange of a partially drawn cup. Friction makes this test somewhat unreliable.

(b) Stretch-forming tests.

Erichsen test.

The test compares the formability of different materials, or different batches of the same material. A blank, rigidly clamped above a circular die, is bulged to fracture by a descending ball-headed punch. Test criterion is the depth of bulge at fracture. Potential sources of test unreliability are;

(i) Variations in clamping force may allow an element of radial drawing to occur.

(ii) The test end-point is not readily observed.

(iii) Punch profile surface roughness may influence straining.

(iv) Results vary with the type of lubrication.

Olsen and Amsler tests.

These tests are similar to the Erichsen test and suffer from the same sources of error. The only differences are in tool dimensions.

Avery test.

This is a two part test, the first part being similar to Erichsen's. In the second part, die and clamping ring are replaced by similar tools with interlocking annular serrations which prohibit radial drawing. A comparison of bulge-depths in the two tests is supposed to provide useful information on forming properties.

Guillery test.

Punch/die clearances are greater than in the Erichsen test, otherwise tests are similar.

Jovignot test.

Bulging is carried out by oil under pressure, the blank rim being tightly clamped to provide a seal.

Kaiser Wilhelm Institute (K.W.I.) test.

A square sheet test-piece is clamped above a die and bulged by a flat-headed punch, a projection on the punch locating a hole in the blank centre. The K.W.I. value is taken as the increase in hole diameter at a point when radial cracks appear from the hole. It is claimed that the test gives a better guide to directional properties than the Erichsen test.

Survey comment.

Stretch forming tests are primarily concerned with strains to fracture - or ductility. There are other even more important property requirements in deep drawing, for example normal anisotropy (FIG. 24.)

(c) <u>The Swift cupping test.</u>

As a result of research Swift concluded that there was no better test for deep drawability than to conduct the operation itself under controlled experimental conditions. It was proposed therefore that standard diameter cups should be drawn on standard tools, with the test criterion being the largest blank drawable without fracture and the ratio largest blank diameter/punch diameter defining the limiting draw ratio (L. D. R.) Limitations of the test were fully appreciated but it was felt that the test could be a useful guide to the comparative drawability of various materials and tempers.

Although Swift's test is simple in concept its practical application requires careful control over process variables. Failure to appreciate this lead to disappointing results when the test was first introduced to industry. A comprehensive investigation by B.I.S.R.A. during 1950-1954 resulted in a formal Swift cupping test procedure, reported by Kemmis,[28] which stipulated controls on:

Punch and die diameters.

Punch and die radii.

Punch/die clearance.

Tool surface finish.

Blank-holder pressure.

Lubrication.

Drawing speed.

Tool material.

Blank preparation.

It was proposed that near the limiting draw ratio at least five blank at each diameter should be drawn.

Whitton and Mear[27](1960) showed that sheet surface finish could affect L. D. R. and that the tool surface finish range suggested by Kemmis was too wide. Atkinson and Maclean[19] (1965) demonstrated how polythene sheet could make test results less sensitive to blank surface finish. Wallace[39] (1962) was doubtful about the general applicability of Swift test results and argued that factors of scale, tool geometry and friction could not be adequately simulated.

Recently the Swift cupping test procedure recommended by Kemmis has been revised in view of a changed attitude towards the test (Hawtin 1969)[40]. Tolerances on tool dimensions and surface finish have been tightened. It was previously believed that performance in various press-shop operations could be correlated with L. D. R., but this is now regarded as a misconception.

(d) The wedge drawing test.

The essential features of the test are shown in FIG. 27. During cupping the deforming flange may be considered to comprise a number of sectors (FIG 27 a), the flow in each sector being radial. Sachs suggested that deformation within a sector could be simulated by a wedge-shaped die (FIG 27 b), with the deepest wedge drawable without fracture being representative of performance in actual deep drawing operations. In view of general interest shown in the test following its introduction, Loxley and Swift[41] (1944) carried out an experimental investigation.

Tests were conducted with steel and aluminium bronze at a drawing speed of 1.3 inches/minute, using an included wedge angle of 20 degrees. Colloidal graphite and tallow were the drawing lubricants. A linear relationship between draw load and wedge draw ratio was found, but the maximum draw ratio was only about 80% of that in cupping, even though in the latter additional bending/unbending operations occur. Maximum draw ratio was also found to be more sensitive to lubrication conditions than was the maximum ratio in cupping. All specimens drawn

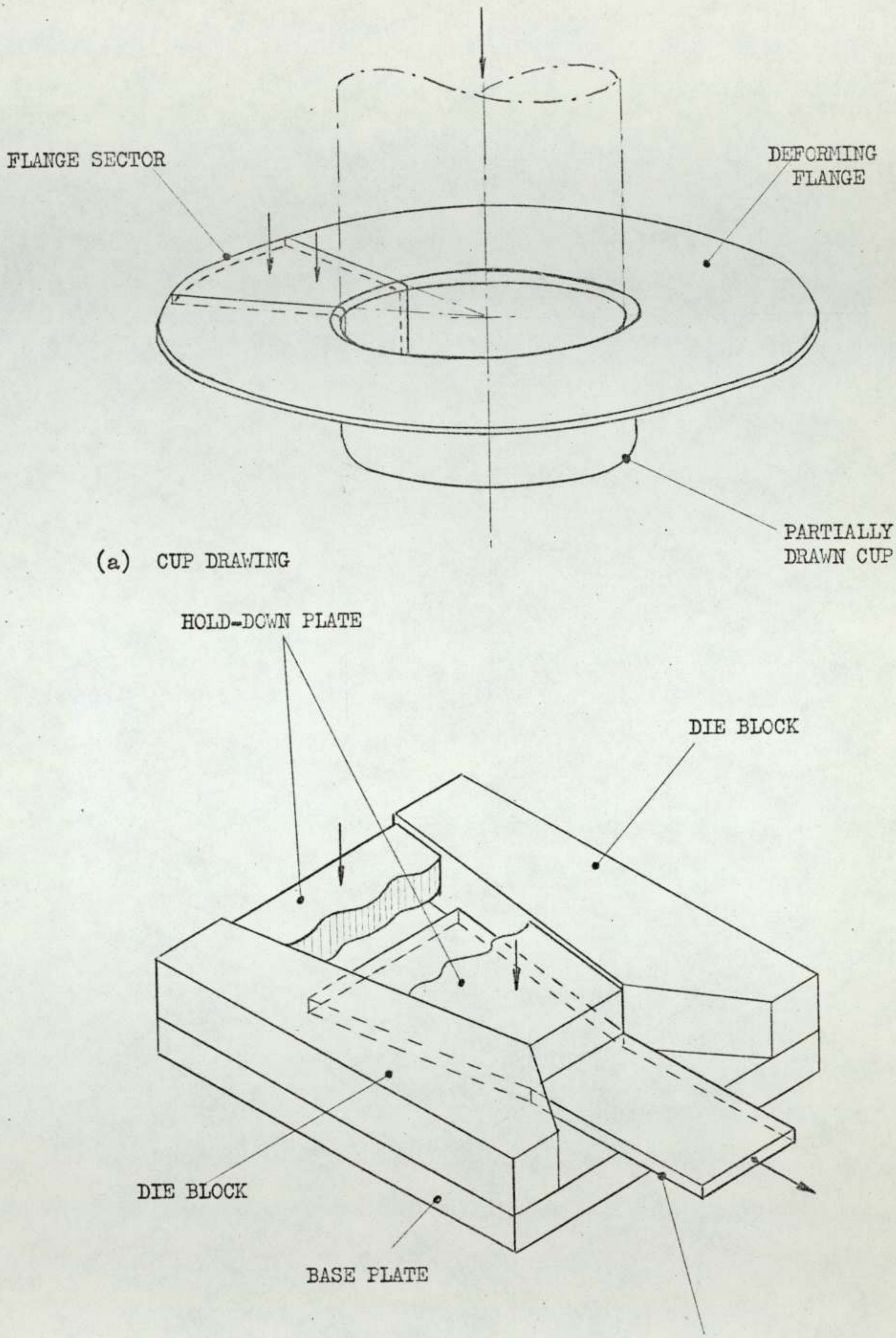

(a) CUP DRAWING

(b) THE WEDGE DRAWING TEST

FIG. 27 SIMULATED PLANE RADIAL DRAWING BY THE WEDGE DRAWING TEST.

on the wedge-test exhibited back-end "fish-tailing" , an indication of high friction at the wedge sides. Hardness readings on drawn samples revealed that the edges were work-hardened more than the centre. It was concluded that friction dominated the test and made it unreliable for predicting deep drawing performance.

The effects of friction on the wedge test were theoretically studied by considering equilibrium under the action of the drawing force, side pressure forces, and side friction forces. It was shown that an increase in the coefficient of friction from 0 to 0.10 increased draw load by 60% whilst an increase from 0 to 0.16 caused an increase of 100%.

Survey note.

With recent improvements in dry-film lubrication the test may now give closer correlation with cupping test results.

2.9. SPLAYING IN REDRAWING.

(a) Introductory comments.

The problems experienced with splaying at Tube Investments Limited, as discussed in Section I of the thesis, have probably been encountered by other concerns active in deep drawing. A thorough search of openly published literature however has provided little detailed information on the problem and references obtained are mainly of a descriptive content. Usually splaying has been observed whilst conducting investigations into some other aspect of redrawing and has therefore received only brief mention. To the writer's knowledge no previous direct study of splaying in redrawing has been made apart from a short exploratory investigation at Tube Investments Research Laboratories in 1968.

(b) Survey of available literature.

Swift[42] carried out a series of deep-drawing trials in 1940 to determine factors influencing the overall draw ratio when cupping was followed by a single redraw operation. Steel blanks 4 in. diameter 0.036 in. thick were cupped on a 2 in. diameter flat-headed punch and then redrawn. Redraw tooling comprised a $1\frac{3}{8}$ in. diameter draw punch, a 90 degree semi-angle die with $\frac{3}{8}$ in. profile radius, and a flat-headed hold-down punch with $\frac{1}{8}$ in. profile radius.

Redraw load-travel diagrams exhibited a peak just before the end of drawing. This peak could not be fully explained in terms of the normally expected sequence of events, but on closely observing the process it was seen to correspond with splaying of the upper cup wall just before the cup rim entered the die. Swift commented "This was no doubt owing to the diminution of its flexural stiffness as its depth reduced." FIG. 28 a shows a typical punch load-travel diagram obtained by Swift, splaying being observed in zone C. (Even under non-splaying conditions maximum load would normally occur in this region with an as-drawn first stage cup.) To observe the effect of hold-down

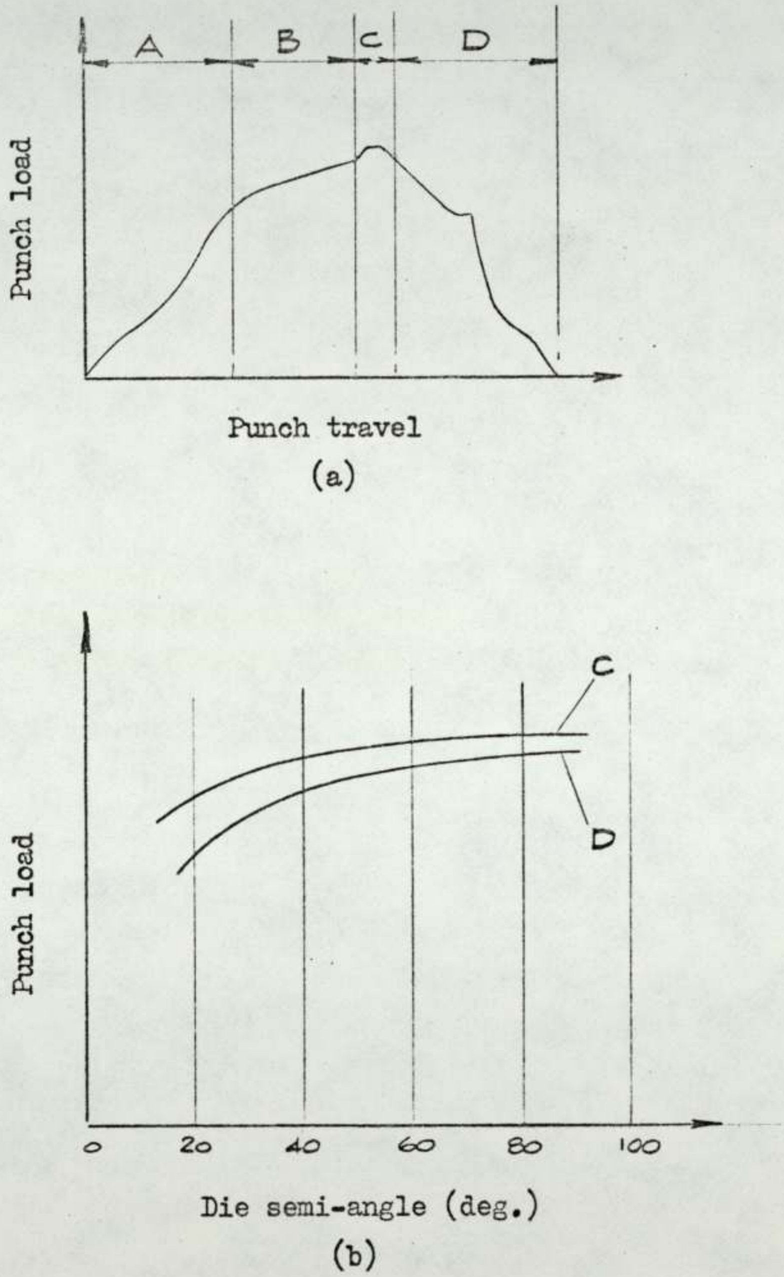

FIG. 28 PUNCH LOAD CHARACTERISTICS IN REDRAWING

(a) RELATION TO PUNCH TRAVEL
(b) RELATION TO DIE ANGLE (SWIFT)

punch profile radius on splaying the latter was increased from $\frac{1}{8}$ to 5/16 in. A slight reduction in peak load was noted. The hold-down punch was then retracted to act merely as a guide, and an even greater reduction in peak load occurred. (It would appear that the redraw exhibited no wrinkling tendencies and therefore a hold-down punch was really superfluous.) The 90 degree die was then replaced by one of 60 degrees semi-angle, other conditions remaining constant. This arrangement provided a higher overall draw ratio than was previously possible, but second stage cups produced from the larger blanks showed signs of longitudinal cracking. (which may have been due to splaying.)

In view of the 60 degree die result the effect of die angle was investigated more thoroughly. 3.9 in. diameter steel and 3.7 in. diameter aluminium blanks were cupped and then redrawn through dies with semi-angles ranging 15 - 90 degrees. Steel showed a definite trend for draw load to diminish as die angle decreased, but the effect with aluminium was not so marked. It was observed that as die angle decreased the <u>difference</u> in load in zones C and D (FIG. 28 a) increased. This result is illustrated in FIG. 28 b . Swift suggested that the peak in zone C was due to splaying, which infers that splaying increases at lower die angles.

In summary the main findings on splaying behaviour were:

(i) Splaying caused a peak in redraw load.

(ii) When using a hold-down punch to influence metal flow into the die the peak redraw load (corresponding to splaying) depended upon the severity of bending around the hold-down punch radius.

(iii) By raising the hold-down punch above the die to act merely as a cup guide the peak redraw load was further reduced.

(iv) By decreasing the redraw die angle maximum punch load was also reduced but apparently splaying increased.

In a further series of tests during 1940 Swift[1] again encountered splaying when redrawing brass and steel cups. Brass was observed to splay more than steel. The effect of using an external guide ring to prevent splaying was studied. (In practice a guide ring may be either a separate component secured to the die or an integral part of the die as shown in FIG. 29. Its function is identical in both cases.) Mild steel blanks 4.15 in. diameter 0.036 in. thick were cupped on a 2. in. diameter flat-headed punch and then redrawn on tooling comprising a 1.7/16 in. diameter punch and 30 degree semi-angle die.

When the hold-down punch was fully inserted fracture occurred in redrawing at a punch load of 10,000 lbf., but with the hold-down punch raised clear of the die redrawing was successfully accomplished with a maximum punch load of 9,080 lbf. On installing the guide ring redraw load reduced to 8,720 lbf.

Tests were repeated with brass blanks 4.10 in. diameter 0.036 in. thick. Results were similar to those with steel.

To summarise;

(i) Brass showed a greater tendency to splay than steel.

(ii) By allowing the cup to enter the die freely redraw load was reduced.

(iii) An external guide ring prevented splaying and also gave a reduction in punch load.

When introducing their paper on redrawing Chung and Swift[9] referred to the use of a specially profiled hold-down plate to prevent splaying in reverse redrawing. FIG. 30 is constructed from their description.

In 1967 an investigation was carried out at Tube Investments to determine deep-drawability of austenitic stainless steel. Splaying was found to be a source of fracture in the upper cup walls and to overcome the problem guided redraw dies of the integral type were used.

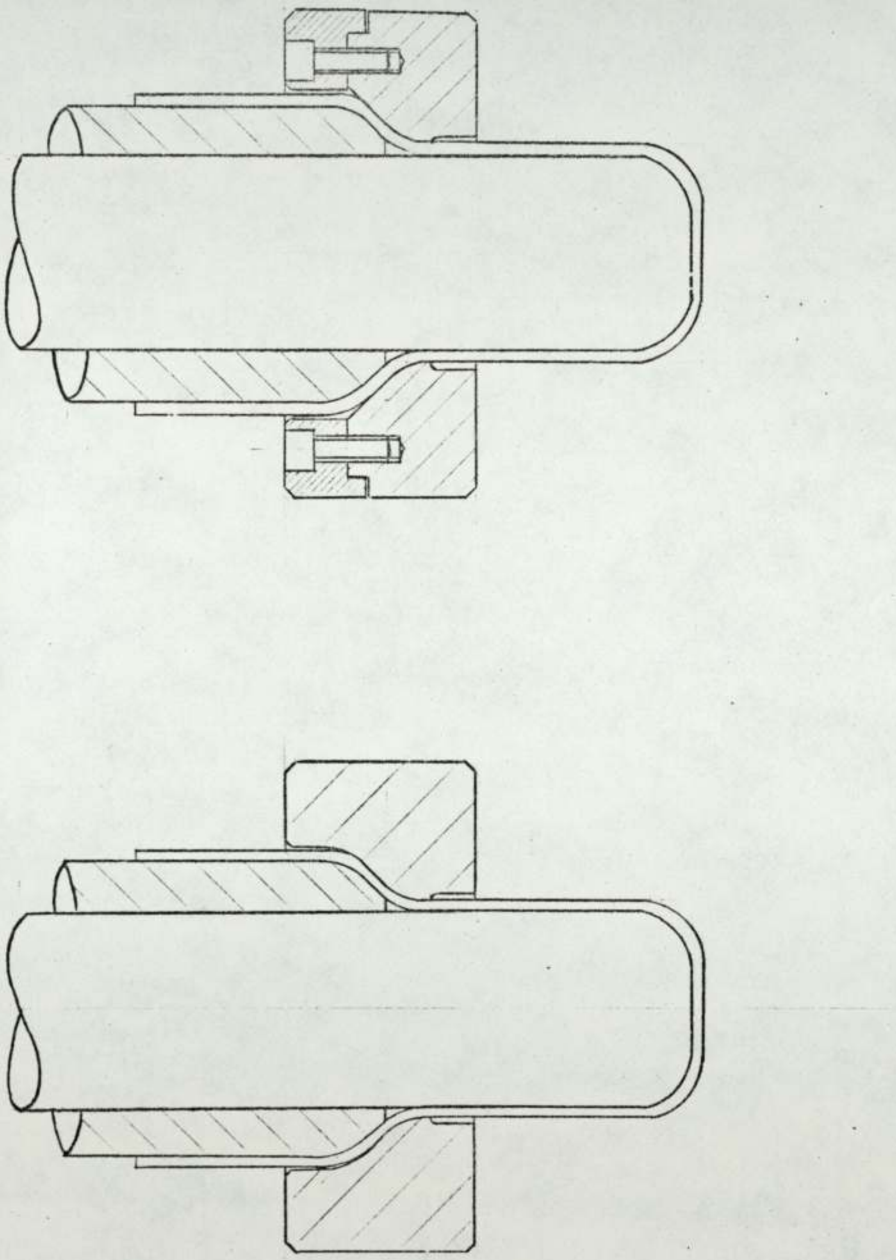

FIG. 29 REDRAWING WITH GUIDED DIES

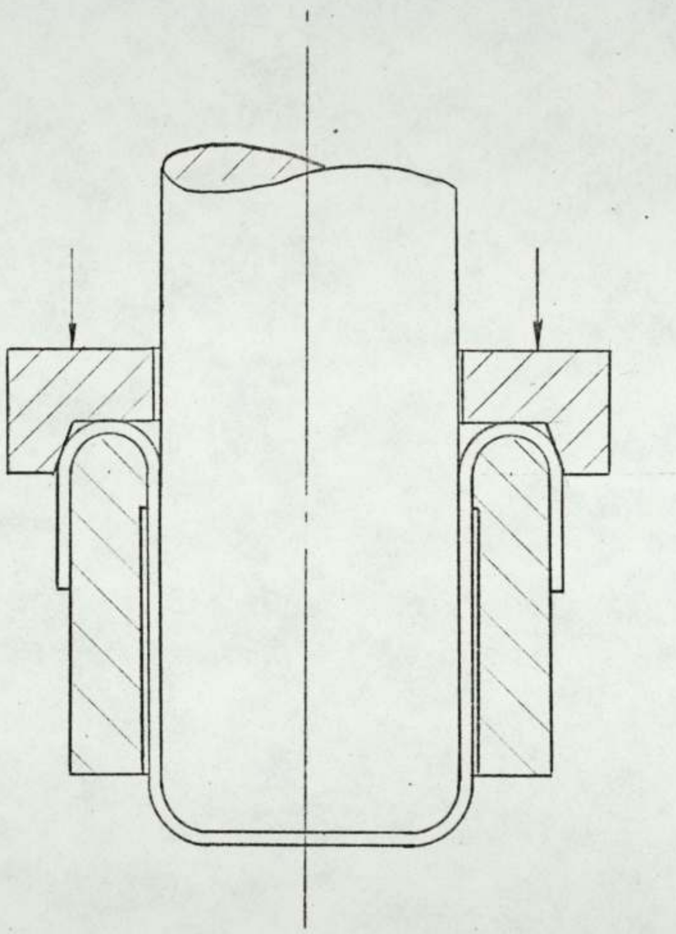

FIG. 30 PREVENTION OF SPLAYING IN REVERSE REDRAWING BY USE OF CONICAL HOLD-DOWN PLATE.

It was then found that punch load became excessive causing the cup bottom to fracture. This result was at variance with the earlier findings of Swift, and to provide additional information a short experimental study of the effects of guiding on punch load was conducted at Tube Investments Research Laboratories by Norman in 1968.[43] N.S.3 aluminium alloy blanks $3\frac{3}{4}$ in. and $3\frac{1}{4}$ in. diameter 0.022 in. thick were cupped with a 1.969 in. diameter punch and subsequently redrawn using a 1.408 in. diameter punch and a 90 degree semi-angle die with $\frac{1}{8}$ in. profile radius. A hold-down punch was used to prevent flange wrinkling. External guiding was by means of a short thick-walled brass tube whose bore was 0.010 in. larger than the first stage cups. When attempting to redraw cups from the larger blank size success without the guide was marginal. With the guide in position failure occurred consistently. The smaller blanks were used to observe the effect of guiding on punch load-travel characteristics, and it was found that guiding not only increased punch load but also caused its peak value to occur earlier in the redraw. These results are expressed graphically in FIG. 31. The increase in load due to guiding was about 8 % using an oil lubricant but this figure was reduced with polythene film lubrication. Changing the lubricant had little effect on the peak load displacement 'X' in FIG. 31.

Norman's results supported those obtained in the stainless-steel trials and indicated that guiding may increase redraw load, contrary to Swift's findings. The anomaly may be partly explicable in terms of the different tooling arrangements in that work at Tube Investments was carried out with an effective hold-down condition whereas Swift used a raised (ineffective) hold-down punch in his tests. Further work was necessary to resolve the situation.

Fogg[11] (1968) studied deformation in the entering cup prior to die contact when redrawing without hold-down. By assuming that deformation would be according to the principle of minimum plastic work an expression was derived for 'free' zone geometry,

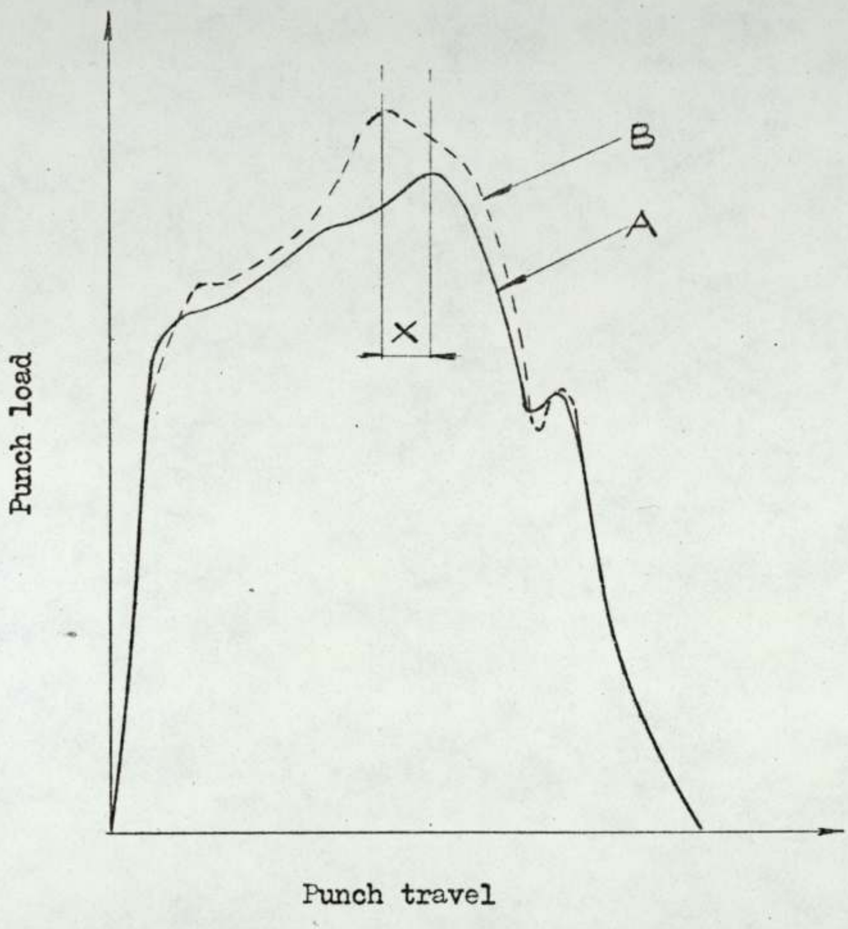

FIG. 31 PUNCH LOAD CHARACTERISTICS IN REDRAWING
CURVE (A) CONVENTIONAL REDRAW DIE
CURVE (B) WITH GUIDE AT DIE ENTRY.

$$\frac{R_f}{t_o} = \sqrt{\frac{{}^{t_o}/_{t_o}}{\sqrt{3}\,(1-\cos\alpha)}}$$

The expression predicts that bending becomes more severe at larger die angles.

Swift found that as hold-down punch radius increased peak redraw load decreased. It was implied that splaying also decreased which suggests a tendency for splaying to increase with bending severity. However when redrawing with the hold-down raised it was found that the 'splay' peak in FIG. 28 a tended to increase as die angle diminished. But according to Fogg bending severity decreases as die angle decreases, which suggests that splaying should also decrease. This apparent anomaly is probably due to Swift not actually measuring splaying but inferring its magnitude from its effect on redraw load.

Busby and Fogg[44] (1969) encountered splaying when investigating the deep-drawability of high-speed and low-tungsten tool steels. Blanks were cupped and redrawn without interstage annealing. Results were not encouraging, a major problem being cracks in the redrawn cup walls. Cupping draw ratios of 1.8, 2.0, and 2.2 were followed by a redraw of either 1.15 or 1.25 through single curvature dies of profile radius/cup wall thickness ratio = 5. Initial trials were conducted on a crank press operating at 20 strokes/minute. After redrawing, cups exhibited a high degree of splitting and fragmentation, especially those in high-speed steel. To study the cause of the failure mode further redraw tests were carried out at slow speed. It was then observed that splitting near the cup rim occurred as a result of splaying, the increase in cup rim diameter being about 2 %. By installing a guide ring better results were obtained, but splitting was not completely eliminated.

3. OBJECTIVES OF RESEARCH.

I. To conduct an experimental and theoretical investigation into the causes of splaying in redrawing, and hence relate splaying to the principal process parameters;

(a) Die profile geometry.

(b) Hold-down punch geometry.

(c) Cup geometry.

(d) Cup material properties.

II. To determine conditions of redrawing which cause greatest and least degrees of splaying.

III. To study the effect of splaying on redraw punch load.

IV. To prevent splaying by using a guide ring, and observe its effect on redraw punch load.

V. As an outcome of the investigation, to suggest optimum redrawing conditions for relief from splaying and any associated problems.

4. EXPLORATORY THEORETICAL INVESTIGATIONS.

4.1. Introductory comments.

Exploratory theoretical studies were undertaken with the broad objective of identifying the splaying problem and deciding which areas required further investigation. In particular it was necessary to determine those elements of the redraw process involved in or affected by splaying, and take into account all process parameters which could influence the phenomenon. With an appreciation of these factors experimental programmes could be designed to supply useful information. It was equally important to explore various theoretical approaches with a view to eliminating those unlikely to provide a basis for further development.

In this section the direct redrawing process is briefly reviewed, and parts of the process involved in splaying identified. Deformations contained in those parts are then analysed in more detail. Finally a theoretical approach suitable for investigating splaying is discussed.

4.2. Brief theoretical review of the direct redraw process.

FIG. 32 illustrates a typical direct redrawing operation. The force P applied to the redraw punch is that necessary to maintain plastic deformation in the zone A - D under the attendant frictional conditions. If a hold-down punch is required its force H is normally just sufficient to prevent wrinkling between A and C.

An element of the cup wall entering the deformation zone at A bends under the action of a moment supplied by tension in the wall below A, and a fixing moment supplied by the rigid undeformed cup wall above A. The radius of bending will either be R_f if the redraw is free or R_c in the event of a hold-down punch being used for which $R_c < R_f$. The increment of radial stress to cause bending at A may be found by a method proposed by Chung and Swift[5] which leads to the equation,

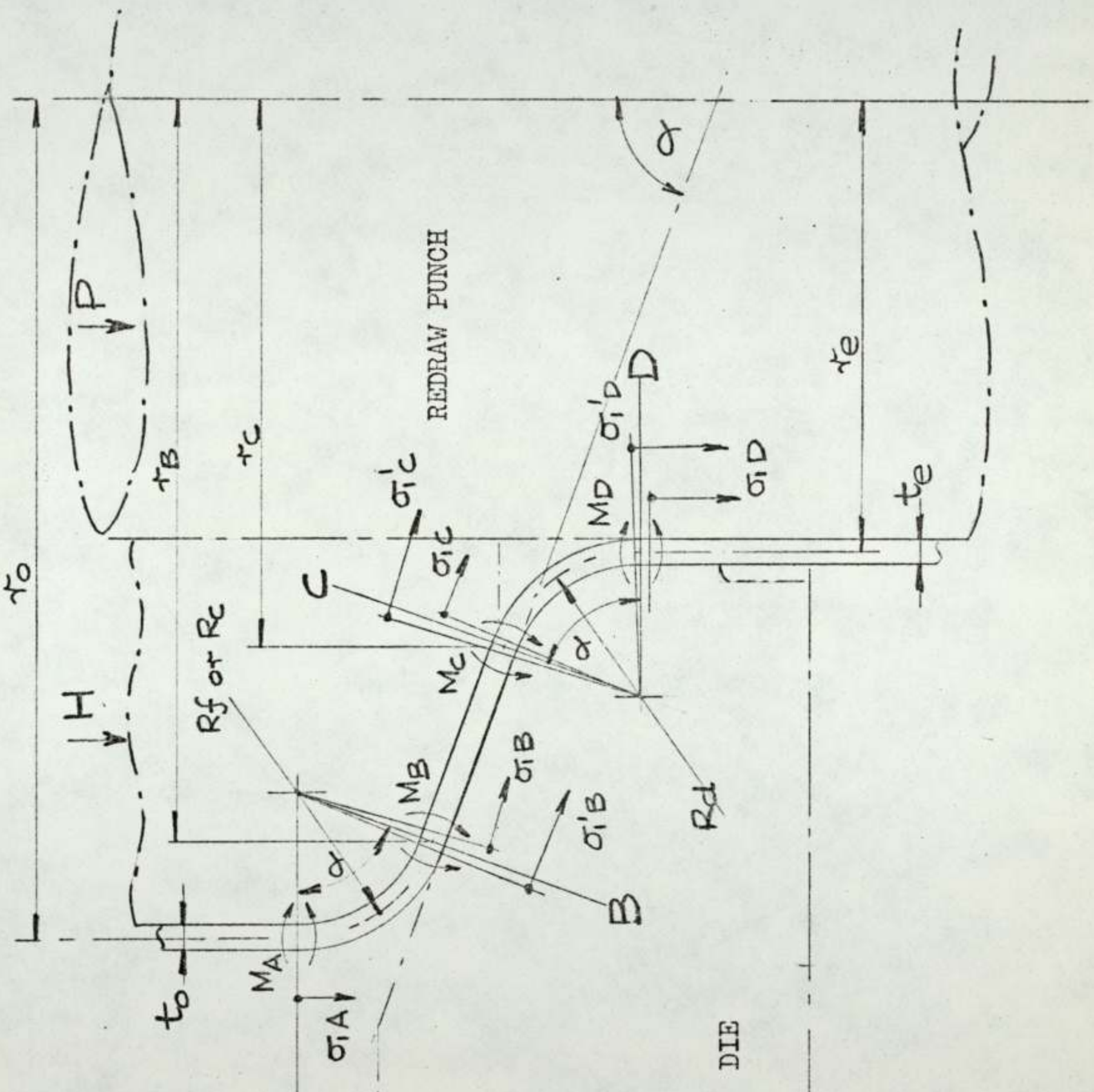

FIG. 32 RADIAL STRESS DESIGNATION DURING REDRAWING

$$\frac{2\Delta\theta}{R}\int_0^{\frac{t_o}{2}} \frac{2\bar{\sigma}}{\sqrt{3}}(R+y)\,y\cdot dy = \sigma_{1A}.t_o.R.\Delta\theta \qquad (4.1)$$

σ_{1A} as given by equation 4.1, increases as R decreases although the bending moment M_A of a rigid/perfectly plastic material is independent of R . The bending process is assumed to be plane-strain with $\varepsilon_3 = 0$, and since there is no overall radial strain, there is no change in wall thickness.

Radial drawing occurs in the zone A - B with the radial stress increasing from σ_{1A} to $\sigma_1{'}_B$ at B in accordance with the differential equation,

$$r\frac{d\sigma_1}{dr} + \sigma_1 - \sigma_3 = 0 \qquad (4.2)$$

Plastic strains may be deduced using Levy/Mises stress-strain increment equations,

$$\frac{d\varepsilon_1 - d\varepsilon_2}{\sigma_1 - \sigma_2} = \frac{d\varepsilon_2 - d\varepsilon_3}{\sigma_2 - \sigma_3} = \frac{d\varepsilon_3 - d\varepsilon_1}{\sigma_3 - \sigma_1}$$

in conjunction with the condition of plastic incompressibility,

$$d\varepsilon_1 + d\varepsilon_2 + d\varepsilon_3 = 0$$

The radial stress in zone A - B is usually small and an element passing through the zone tends to thicken.

Unbending at B requires a moment M_B which is supplied by the radial drawing stress below B, σ_{1B}. The equal and opposite fixing couple is supplied by the cup wall above B in unconstrained redrawing. It is not clear if the hold-down punch contributes to the fixing effect when $R_c < R_f$. Unbending occurs under back tension $\sigma_1{'}_B$, the effect of which is to increase the radial stress increment required for unbending, and cause a general extension of the cup wall. Plane-strain conditions $d\varepsilon_3 = 0$, therefore imply wall thinning. The method of finding radial stress increment for bending/unbending under tension was developed by Chung and Swift[5], and is discussed in section 2.2.C of the thesis. It leads to the expression,

$$(\sigma_B - \sigma_{1B}')\,t.R.\Delta\theta = \frac{2}{\sqrt{3}}\bar{\sigma}\Delta\theta \int_0^{\frac{t}{2}+\lambda} \frac{y}{\bar{R}_n}(R_n + y)\,dy$$

$$- \frac{2}{\sqrt{3}}\bar{\sigma}_o \Delta\theta \int_{-(\frac{t}{2}-\lambda)}^{0} \frac{y}{\bar{R}_n}(R_n - y)\,dy \quad \text{———} (4.3)$$

Between B and C (FIG. 32) radial drawing occurs along the conical die face, and the radial stress increases from σ_{1B} at B to σ_{1C}' just before re-bending at the die throat radius. In constrained redrawing most of the hold-down force is reacted over this zone and increases the frictional component of radial stress. For unconstrained redrawing equilibrium of a zone element occurs when,

$$\frac{d}{dr}(\sigma_1.t.r) - \sigma_3.t\,(1 + \mu \cot\alpha) = 0 \quad \text{———} (4.4)$$

where μ is the coefficient of friction at the cup/die interface. Swift[45] has shown that neglect of the thickness term in equation 4.4 makes little difference in the solution for radial drawing stress. For constrained redrawing a problem arises in designating the point of application of hold-down force, since during radial drawing between B and C the wall thickness tends first to increase and then decrease, depending upon the relative magnitudes of σ_1, σ_3, and hence upon the draw ratio. Hold-down force will be concentrated at the thickest point of the zone and this point is not immediately known. An alternative approach is to assume the hold-down force to be uniformly distributed over the flange area, giving rise to a normal pressure,

$$\sigma_2 = \frac{H \sin\alpha}{\pi(r_B^2 - r_C^2)}$$

Equilibrium of a zone element is then given by,

$$\frac{d}{dr}(\sigma_1.t.r) - \sigma_3.t - \frac{2\mu\sigma_2 r}{\sin\alpha} = 0 \quad \text{———} (4.5)$$

Plastic strains may be found by a procedure similar to that for zone A - B . Swift[45] found that work-hardening and friction made little difference to thickness strains in the analogous process of tube sinking.

The mechanics of re-bending to the die radius at C are similar to those for unbending at B, only the back tension $\sigma_1{'}_C$ is now greater causing more wall thinning. The bending moment M_C is supplied by tension in the wall below C, and the fixing moment by the cup wall above C for unconstrained drawing. In constrained redrawing the hold-punch may contribute toward the fixing moment. Re-bending increases the radial stress at C to σ_{1C} .

Between C and D elements are radially drawn to become part of the final cup wall after unbending at D. The increment of radial stress to provide frictionless drawing may be found from equation 4.2, but zone friction is usually high and its influence on radial stress cannot be ignored. Chung and Swift[5] provided two methods for calculating radial stress increment in this region. In the first method, equilibrium of a curved element was considered to give,

$$d\sigma_1 = -m\bar{\sigma}\frac{dr}{r} - \mu R_d \cdot \frac{\delta\theta}{r}\left[m\bar{\sigma}\cos\theta - \sigma_1\left(\cos\theta - \frac{r}{R_d}\right)\right] \quad \text{—(4.6)}$$

Equation 4.6 may be solved numerically using successive approximation. The second method was less rigorous though easier to apply, components of radial stress increment due to radial drawing and friction being computed separately and added to give the total increment. Radial stress increment due to friction was found from the slow-speed belt transmission formula and gave

$${}_f\delta\sigma_1 = \sigma_{1_C}\left(e^{\mu\theta} - 1\right)$$

${}_f\delta\sigma_1$ was then added to the frictionless drawing component from equation 4.2. to give the total radial stress increment. Having determined stress distribution over the zone, strains may be found as for the previous radial drawing zones A - B and B - C.

Unbending into the cup wall at D under the action of bending moment M_D increases radial drawing stress to σ_{1_D}, and causes further wall thinning.

Punch load is given by,

$$P = 2\pi r_e . t_e . \sigma_{1_D}$$

Radial drawing stress distribution across the complete plastic deformation zone is shown in FIG. 33, whilst thickness strain development of a typical element passing through the zone is shown in FIG. 34.

4.3. Zone of splaying.

Splaying is not a random phenomenon of redrawing. Its causes lie in the physical conditions imposed on the deforming cup during the process, and it is explicable in terms of these conditions. The starting point of any theoretical analysis must be an appreciation of factors controlling deformation during steady-state conditions in that part of the cup ultimately involved in splaying. In all probability these factors are closely associated with the degree of eventual splaying which occurs when constraint supplied by the entering cup is gradually removed.

FIG. 32 illustrates a typical direct redrawing operation. When redrawing is unconstrained Fogg[11] showed that during steady-state conditions die and cup geometry define the radius of curvature of zone A - B. Attention is drawn to the way in which a hold-down punch, introduced to prevent wrinkling in the region B - C, may influence deformation A - B. Two possibilities arise, firstly provided the hold-down punch radius R_c' is greater than the free inner radius R_f', deformation will occur as though no hold-down punch was present. Secondly, if the mean radius of bending around the hold-down punch R_c is less than the free radius R_f, deformation in A - B will be directly affected. In following work the term 'constrained redrawing' will be used when the hold-down punch directly affects the geometry of deformation A - B.

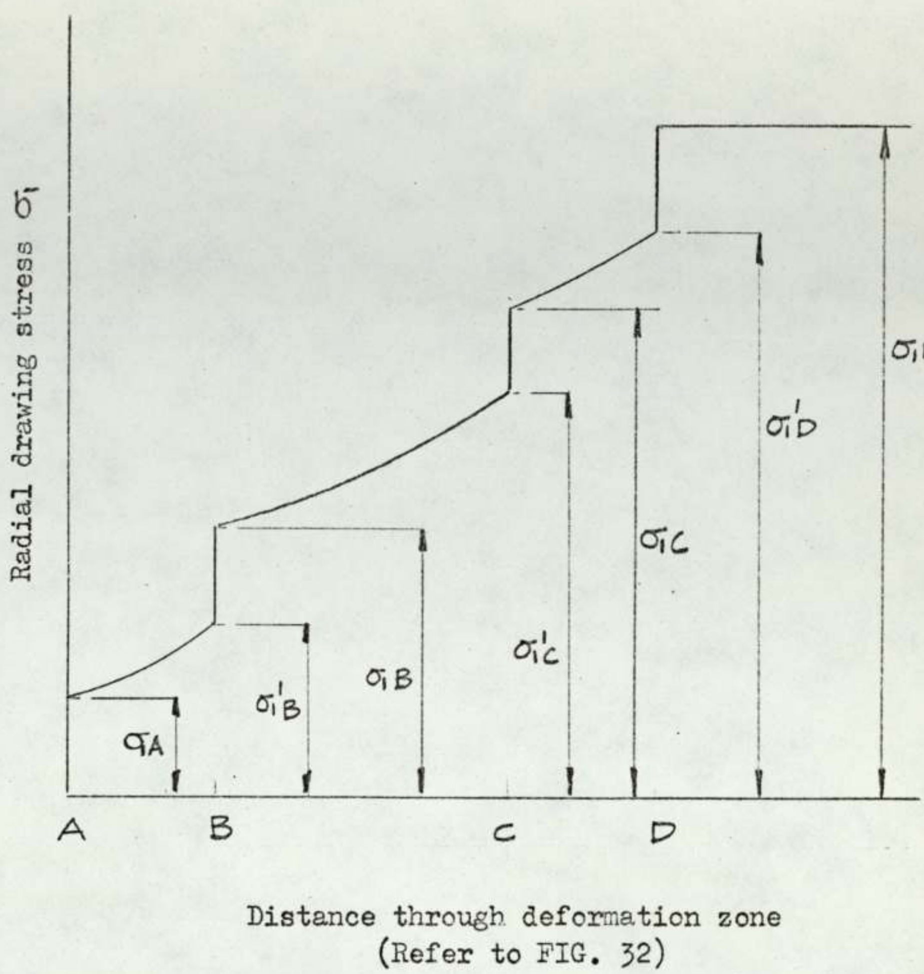

FIG. 33 RADIAL DRAWING STRESS ACROSS DEFORMATION ZONE DURING A TYPICAL REDRAWING OPERATION

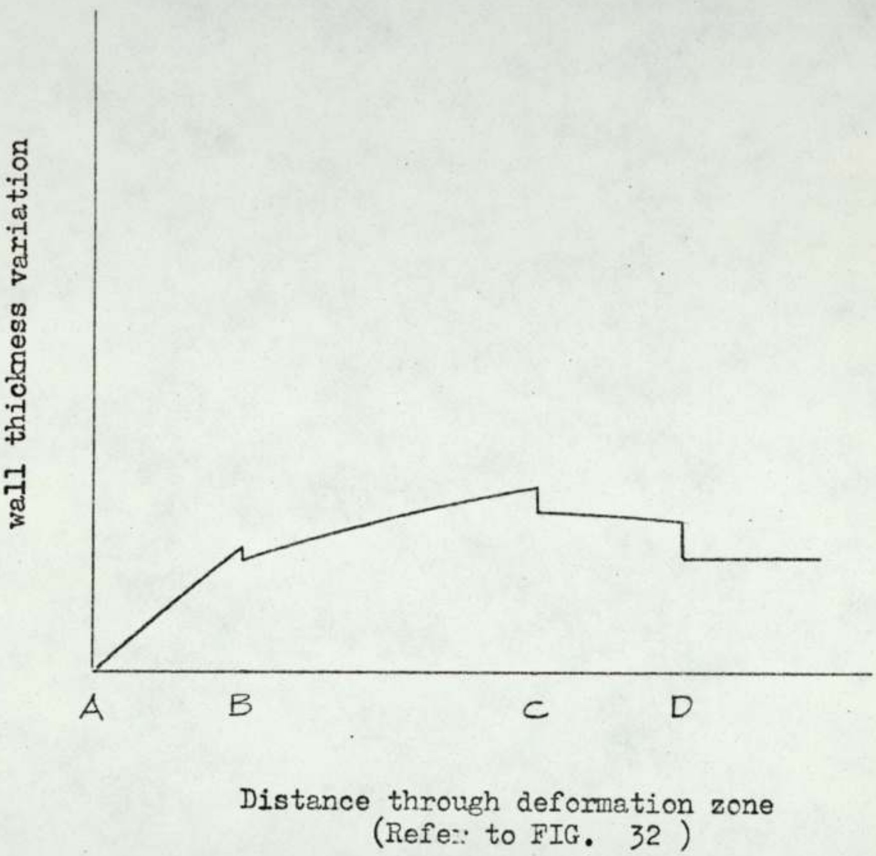

FIG. 34 CUP WALL THICKNESS VARIATION ACROSS DEFORMATION ZONE DURING A TYPICAL REDRAWING OPERATION

When redrawing is constrained only that part of the entering cup above point B is free to splay or be influenced by splaying, since elements below B are compelled to follow the die contour by the hold-down punch. Moreover it is unlikely that B will travel up the die face on splaying since this would tend to increase zone curvature and hence zone work. It therefore seems reasonable to assume that during splaying point B will remain fixed.

When redrawing is unconstrained point B is defined by tool and cup geometry. By a similar argument to that advanced above it is unlikely that point B will move up the die face on splaying. Conversely, appreciable movement down the face would involve an increase in free radial drawing work. For the present therefore, subject to later experimental confirmation, it will be assumed that as for constrained redrawing point B will remain fixed throughout the splaying phase. In other words it is assumed that deformation occurring after point B will not influence splaying, which must therefore be brought about by deformation taking place before B is reached during steady-state conditions. This region of the cup is shown in more detail by FIG. 35.

Deformation in the zone A - B (FIG. 35.) comprises, bending at A to R_f or R_c, radial drawing between A and B, and unbending to the die face at B. The bending moment operating at A demands a fixing moment of equal magnitude to be supplied by the entering cup which as a consequence will tend to flex outwards. Thus bending at zone entry promotes splaying conditions, ignoring for the present the possibility of contributions from radial drawing and unbending at zone exit. Under the action of the bending moment at A a system of tensile circumferential stresses will develop in O A of sufficient intensity to supply a fixing moment. While O A is long, it is unlikely that this system will extend to the cup rim. The alternative hypothesis is that tensile circumferential stresses are generated over a comparatively short distance above A, and that during steady-state redrawing conditions the system is of a constant nature.

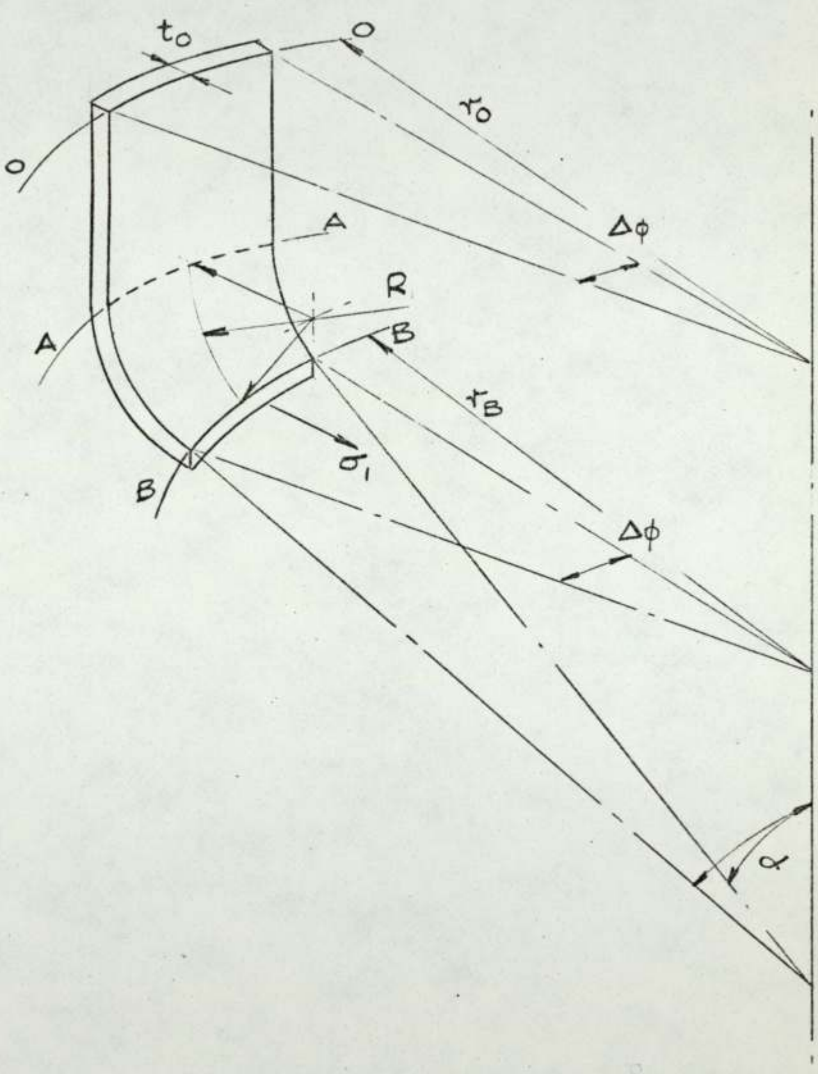

FIG. 35 CIRCUMFERENTIAL ELEMENT OF CUP AT THE BEGINNING OF REDRAWING

Since radial drawing commences near A and involves high circumferential compressive stresses the tensile 'fixing' system must terminate rather abruptly in this region. The upper boundary of the system will probably be less well defined. The envisaged tensile stress system above A must be accompanied by strains. This implies a bulge through which wall elements pass during steady-state conditions, the bulge being of small amplitude and probably of an elastic nature. Elements situated above the bulge will be stress-free and make no contribution to the fixing moment M_A. The situation will persist until the cup rim reaches the bulge. Then elements in the region O A are no longer compelled to follow the previously enforced path into zone A - B, which will itself modify. Splaying will commence and continue as the length O A decreases until finally the cup rim is drawn in.

The precise effect on splaying of unbending at B is less easily appreciated, but the moment causing unbending is of opposite character to that operating at A and must tend to induce circumferential compression above B. However the manner in which this compression is distributed is not readily ascertained. For constrained redrawing the hold-down punch is capable of supplying the fixing moment M_B (FIG. 32.) so long as contact is made with the profile radius, but with unconstrained redrawing the moment must be completely reacted in the radial drawing zone above B during both steady-state and splay phases. The only aspect of unbending at B immediately clear is that it will not contribute towards splaying.

Stress analysis of the radial drawing zone A - B was greatly oversimplified in section 4.2, particularly for the case of unconstrained redrawing where compressive circumferential strains are induced in the complete absence of any normal tool constraint. This contrasts markedly with the popular concept of tube-sinking where the die surface, in exerting normal pressure, provides equilibrium in the direction normal to drawing. The terminal couples M_A, M_B give rise to shear stresses on planes carrying the radial stress σ_1 which cannot therefore be a principal stress. To investigate the possibility of deformation in this zone contributing to splaying it was necessary to conduct separate studies of zone equilibrium for constrained and unconstrained conditions.

4.4. Elastic-plastic bending theory.

In section 4.3 it was found that bending at point A (FIG. 35) during steady-state redrawing could have an important influence on splaying. It was therefore of interest to examine the bending process in detail, taking account of the elastic-plastic nature of the problem rather than assuming fully plastic conditions as is usually done in deep drawing theory.

Under the action of a bending moment there exists within the bent section a neutral surface upon which zero strain occurs, strain in other elements being proportional to their distance from this plane. All engineering metals are to some extent elastic and there is thus always a part of the bent section near the neutral surface which remains elastic regardless of bending severity.

The element of cup wall shown in FIG. 35 may be considered of rectangular cross section. When subjected to an increasing bending moment the section will first plastically yield at its outer extremities, and the elastic/plastic boundaries will converge on the neutral surface. A knowledge of the currently applied bending moment enables the boundary positions and current radius of curvature to be calculated. The following analysis examines the inter-relation of these factors for the plane-strain bending condition usually assumed in deep drawing.

The assumptions made are;

(1) A pure bending moment operates and the neutral plane is the central plane.

(2) Transverse planes remain plane during bending.

(3) The material yield strength is equal in tension and

compression.

(4) There is a linear equivalent stress-strain relationship within the plastic range, $\bar{\sigma} = \bar{\sigma}_o + a\bar{\varepsilon}$

FIG. 36 a shows the elastic/plastic state for a mean radius of bending R . At any distance y from the neutral surface $\varepsilon_1 = \ln(1+\frac{y}{R})$ and $\hat{\varepsilon}_1 = \ln(1+\frac{t}{2R})$. During redrawing operations $\frac{t}{R}$ seldom increases above about $\frac{1}{5}$, and therefore the current analysis is interested in $0 < \frac{t}{R} < \frac{1}{5}$. Within this range $\ln(1+\frac{y}{R})$ is reasonably approximated by $\frac{y}{R}$, making longitudinal strain ε_1 directly proportional to distance from the neutral surface as shown in FIG. 36 b.

For the assumed plane-strain bending condition, $e_3 = \varepsilon_3 = 0$. Also the through-thickness stress σ_2 may be ignored.

From the elastic stress-strain equations $\sigma_3 = \nu\sigma_1$, giving,

$$\sigma_1 = \frac{E.e_1}{1-\nu^2} \qquad (4.7)$$

From Levy-Mises plastic stress-strain increment equations and the condition $d\varepsilon_2 = -d\varepsilon_1$, $\sigma_3 = \frac{1}{2}\sigma_1$. Theory therefore predicts a discontinuity in σ_3 across the elastic/plastic boundary since in general $\nu \neq \frac{1}{2}$. It becomes debatable which value of σ_3 to use in Von Mises yield criterion. (This problem would not arise with Tresca's criterion). Putting $\sigma_3 = \frac{1}{2}\sigma_1$ in Von Mises criterion gives,

$$\sigma_1 = \frac{2}{\sqrt{3}}.\bar{\sigma} \qquad (4.8)$$

For continuity of the stress σ_1 across the elastic/plastic boundary equations 4.7, 4.8 are equal when $y = y_P$ (FIG. 36 b). But $e_1 = \frac{y_P}{R}$, therefore,

$$y_P = \frac{2}{\sqrt{3}}.\bar{\sigma}_o\frac{R}{E}.(1-\nu^2) \qquad (4.9)$$

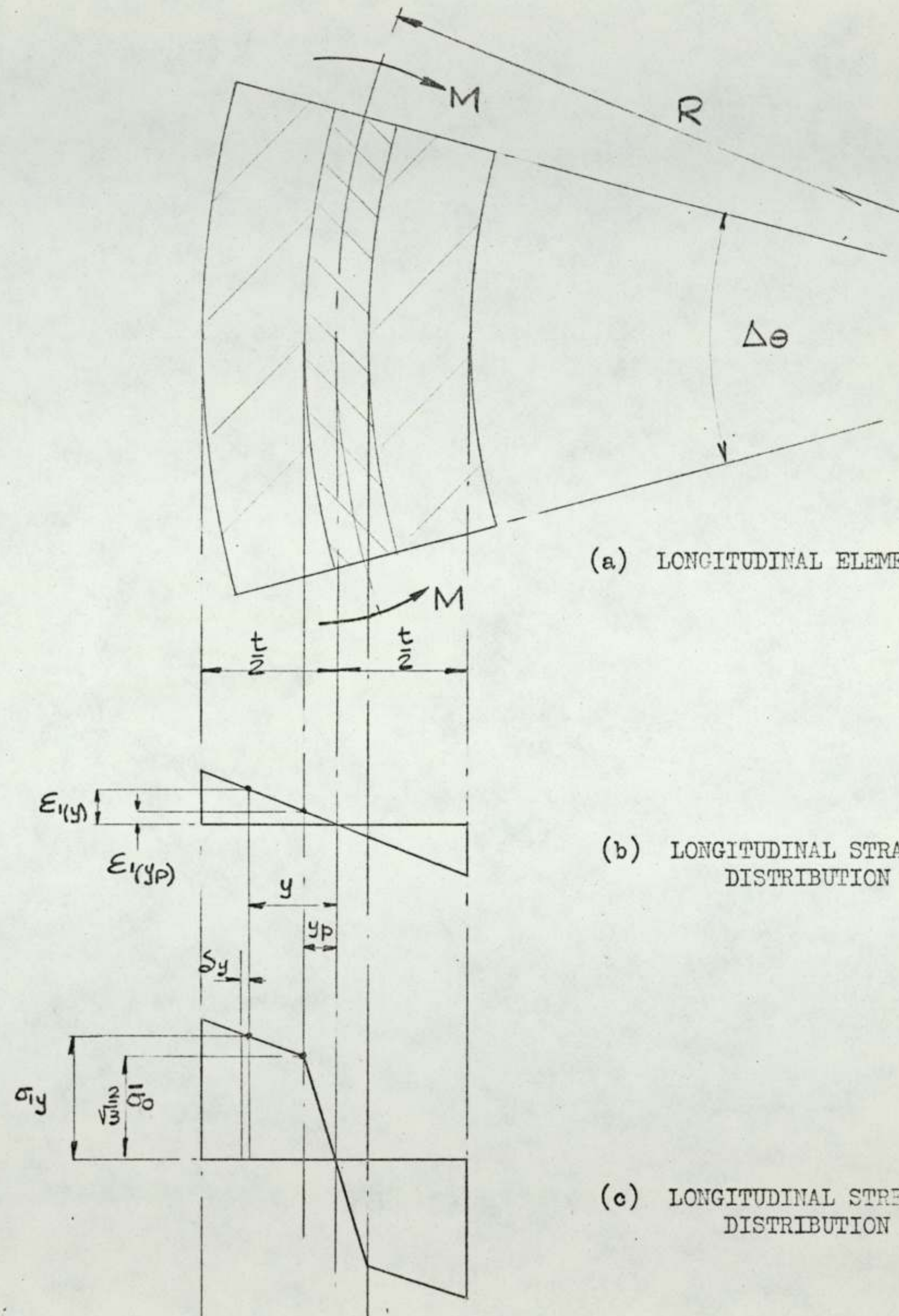

(a) LONGITUDINAL ELEMENT

(b) LONGITUDINAL STRAIN DISTRIBUTION

(c) LONGITUDINAL STRESS DISTRIBUTION

FIG. 36 ELASTIC - PLASTIC BENDING

Equation 4.9 gives the current boundary position when the curvature is $\frac{1}{R}$ For any element within the plastic region $y > y_P$ the total strain $e_1 + \varepsilon_1 = \frac{y}{R}$, and the plastic strain $\varepsilon_1 = \frac{1}{R}(y - y_P)$ Since equivalent strain $\bar{\varepsilon} = \frac{2}{\sqrt{3}} . \varepsilon_1$, the equivalent stress for any element is,

$$\sigma = \bar{\sigma}_0 + \frac{2}{\sqrt{3}} \cdot \frac{a}{R} (y - y_P) \qquad (4.10)$$

Equivalent stress-strain relationships in bending are shown by FIG. 37. From equations 4.8 and 4.10,

$$\sigma_y = \frac{2}{\sqrt{3}} \left[\bar{\sigma}_0 + \frac{2}{\sqrt{3}} \cdot \frac{a}{R} (y - y_P) \right] \qquad (4.11)$$

Stress distribution in elastic and plastic zones is shown in FIG.36 c.

The external bending moment applied to the section M is given by the sum of elastic and plastic moments M_e and M_P respectively.

$$M_e = 2 \int_0^{y_P} \sigma_1 . y . dy \qquad \text{per unit width.}$$

Substituting for σ_1 from equation 4.7, y_P from equation 4.9, and integrating gives,

$$M_e = \frac{16 \bar{\sigma}_0{}^3}{9\sqrt{3}} \left[\frac{R(1 - \nu^2)}{E} \right]^2 \qquad (4.12)$$

$$M_P = 2 \int_{y_P}^{\frac{t}{2}} \sigma_1 . y . dy \qquad \text{per unit width.}$$

Substituting for σ_1 from equation 4.11 and integrating gives,

$$M_P = \frac{4}{\sqrt{3}} \left[\frac{\bar{\sigma}_0}{2} \left(\frac{t^2}{4} - y_P{}^2 \right) + \frac{2a}{3\sqrt{3}R} \left(\frac{t^3}{8} - y_P{}^3 \right) + \frac{a}{\sqrt{3}R} \left(y_P{}^3 - \frac{t^2}{4} . y_P \right) \right] \qquad (4.13)$$

where y_P is provided by equation 4.9 .

It is of interest to examine the dependence of bending moment on current curvature. Analysis is complicated by a being capable of assuming a wide range of values, however splaying is likely to be a problem when the cup is severely work-hardened, and for this

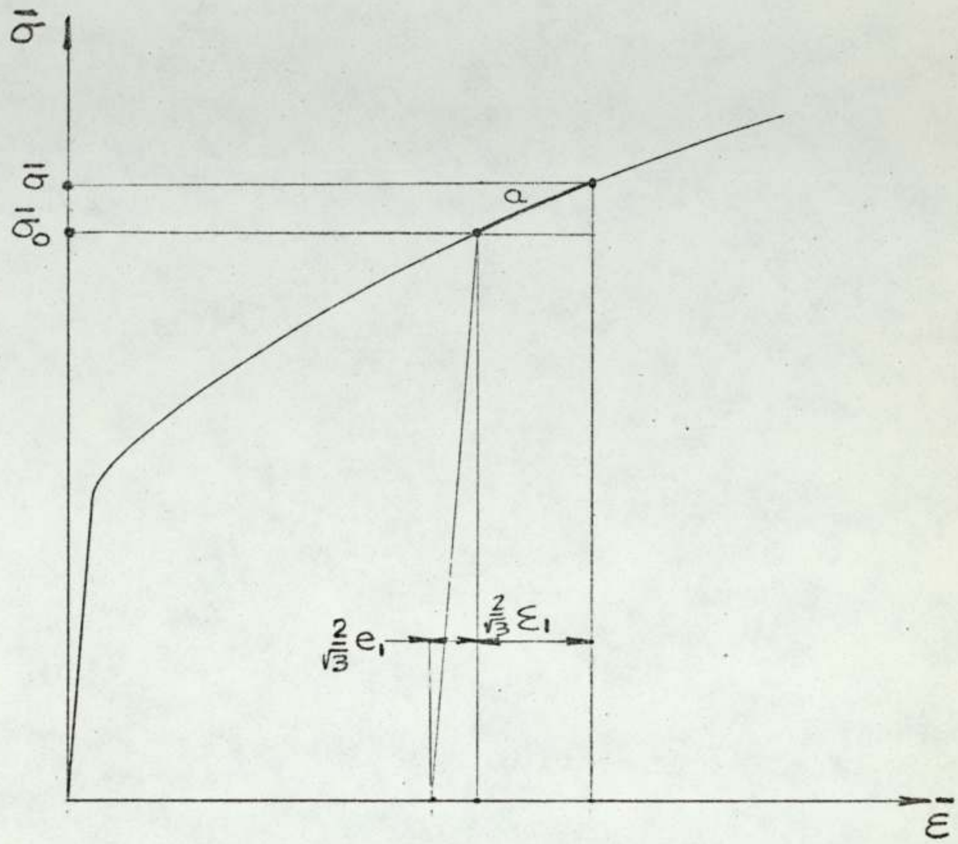

FIG. 37 EQUIVALENT STRESS-STRAIN RELATIONSHIP IN BENDING THEORY

situation a may be taken as zero for a first approximation. The bending moment M then becomes,

$$M = M_e + M_p = \frac{2}{\sqrt{3}}\bar{\sigma}_0\left(\frac{t^2}{4} - y_p^2\right) + \frac{2}{\sqrt{3}}\cdot\frac{8}{9}\,\bar{\sigma}_0^3\left[\frac{R(1-\nu^2)}{E}\right]^2$$

Substituting for y_p from equation 4.9

$$M = \frac{2}{\sqrt{3}}\,\bar{\sigma}_0\frac{t^2}{4}\left[1 - \frac{16R^2}{9t^2}\cdot\bar{\sigma}_0^2\left(\frac{1-\nu^2}{E}\right)^2\right] \qquad (4.14)$$

Now at first yielding $y_p = \frac{t}{2}$ and suppose $R = R_p$

Then from equation 4.9.,

$$\bar{\sigma}_0^2\left(\frac{1-\nu^2}{E}\right)^2 = \left(\frac{\sqrt{3}}{4}\cdot\frac{t}{R_p}\right)^2$$

Equation 4.14 may therefore be re-written,

$$\frac{M}{\hat{M}} = 1 - \frac{1}{3}\left(\frac{R}{R_p}\right)^2 \qquad (4.15)$$

where $\hat{M}$ is the fully plastic bending moment $\frac{2}{\sqrt{3}}\cdot\frac{\bar{\sigma}_0 t^2}{4}$.

The current degree of plasticity in the section $\frac{t/2 - y_p}{t/2}$ may be expressed $1 - \frac{R}{R_p}$.

FIG. 38 shows the ratio $M/\hat{M}$ and degree of plasticity as functions of R/R_p. The magnitude of the bending moment induced at zone entry in redrawing may now be studied. The minimum radius of bending to initiate yielding is given by,

$$R_p = \frac{\sqrt{3}}{2}\cdot\frac{1}{1-\nu^2}\cdot\frac{E}{\bar{\sigma}}\cdot\frac{t}{2} \simeq \frac{E}{\bar{\sigma}}\cdot\frac{t}{2}$$

If the radius of bending at zone entry is written $R = n.t$ then,

$$\frac{R}{R_p} = 2n\frac{\bar{\sigma}}{E},$$

where n will not exceed about 10. This figure together with typical values of $\bar{\sigma}$ and E were used to calculate values of R/R_p for low carbon steel, stainless steel and 70/30 brass. Results are shown in table 5. When viewed in connection with FIG. 38 these figures show that it is justifiable to assume fully plastic conditions

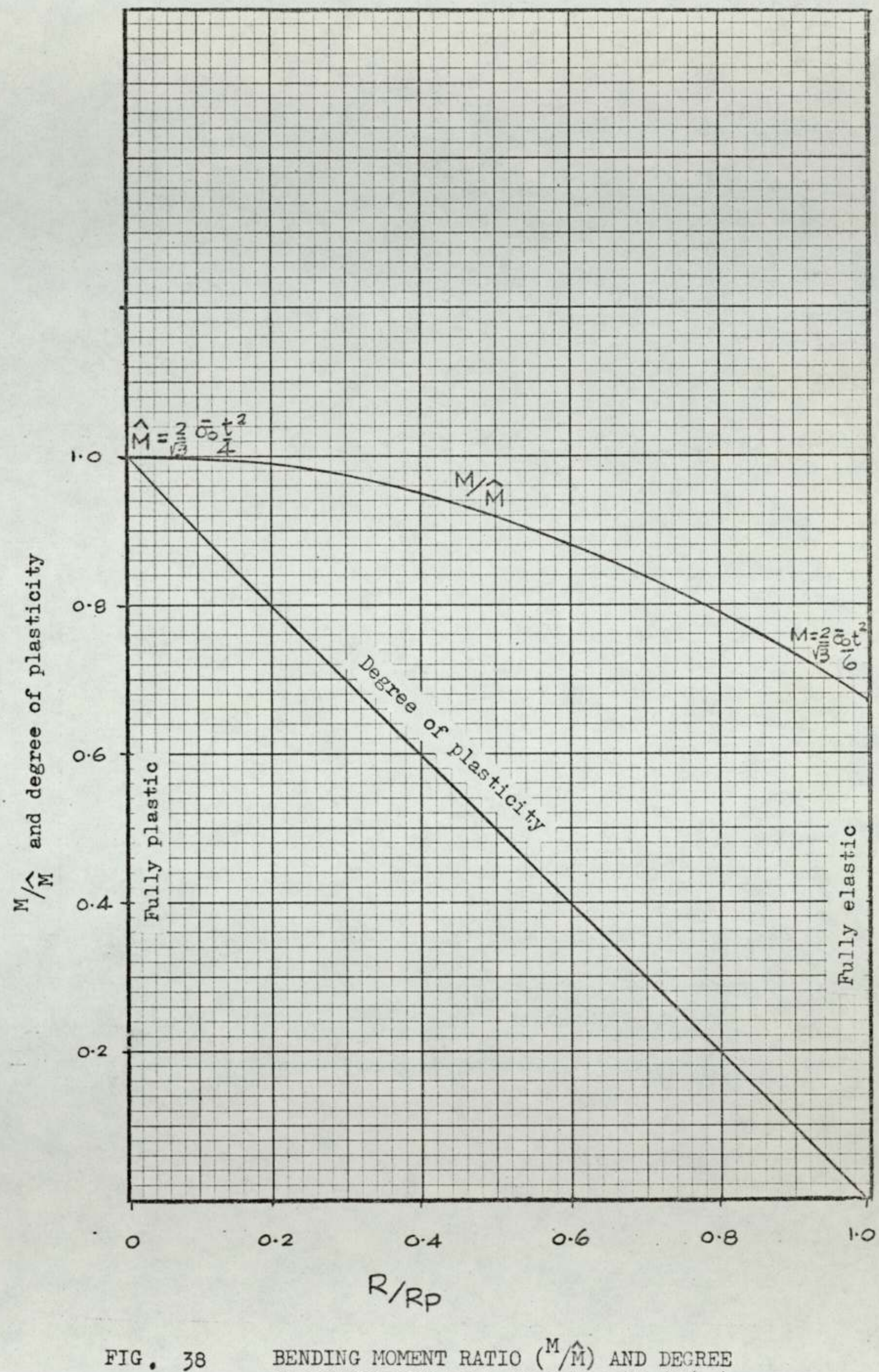

FIG. 38 BENDING MOMENT RATIO ($M/\hat{M}$) AND DEGREE OF PLASTICITY AS A FUNCTION OF (R/R_P), THE RATIO OF CURRENT RADIUS OF BENDING TO RADIUS OF BENDING AT FIRST YIELD.

TABLE 5 VALUES OF R/RP CALCULATED FOR

R = 10 x SECTION THICKNESS

MATERIAL	CONDITION	R/RP
Low carbon steel	Soft Hard	.020 .066
Austenitic stainless steel	Soft Hard	.020 .133
70/30 Brass	Hard	.200

for calculating bending moments. The elastic core, although defining curvature, contributes a negligible amount to the bending moment which is in the present context independent of curvature.

4.5. Onset of splaying.

During steady-state redrawing a system of tensile circumferential stresses exist in the entering cup wall above the point of bending into the deformation zone A - B (FIG. 35). As the cup rim approaches A the system becomes unbalanced, and splaying commences. It has been argued that the bending moment at zone entry will contribute towards the splaying effect, whilst the bending moment at zone exit cannot promote splaying. The effect of radial drawing in the zone on splaying has not yet been established. For the present, only the effect of initial bending is studied.

At splaying onset little modification will have occurred to zone A - B, and the bending moment at A may be considered fully plastic. The cup wall O-A is similar to a cantilever of length ℓ_0, operated upon by a known moment M_A as indicated in FIG. 39 a. A fixing moment supplied by stresses σ_3 in the cup wall is accompanied by a shear force F_A at A (FIG. 39 b). The cup rim is a free surface and carries no stress. The shear force F_A is given by,

$$F_A = \int_0^{l_0} \sigma_3 t_0 \Delta\phi . dx,$$

and the fixing moment M_A by,

$$M_A = \int_0^{l_0} \sigma_3 t_0 \Delta\phi . x . dx.$$

The fully-plastic bending moment at A is given by,

$$M_A = \frac{2}{\sqrt{3}} . \frac{Y t_0^2}{4} . r_0 \Delta\phi.$$

Therefore

$$\frac{2}{\sqrt{3}} . \frac{Y t_0 r_0}{4} = \int_0^{l_0} \sigma_3 . x . dx \qquad (4.16)$$

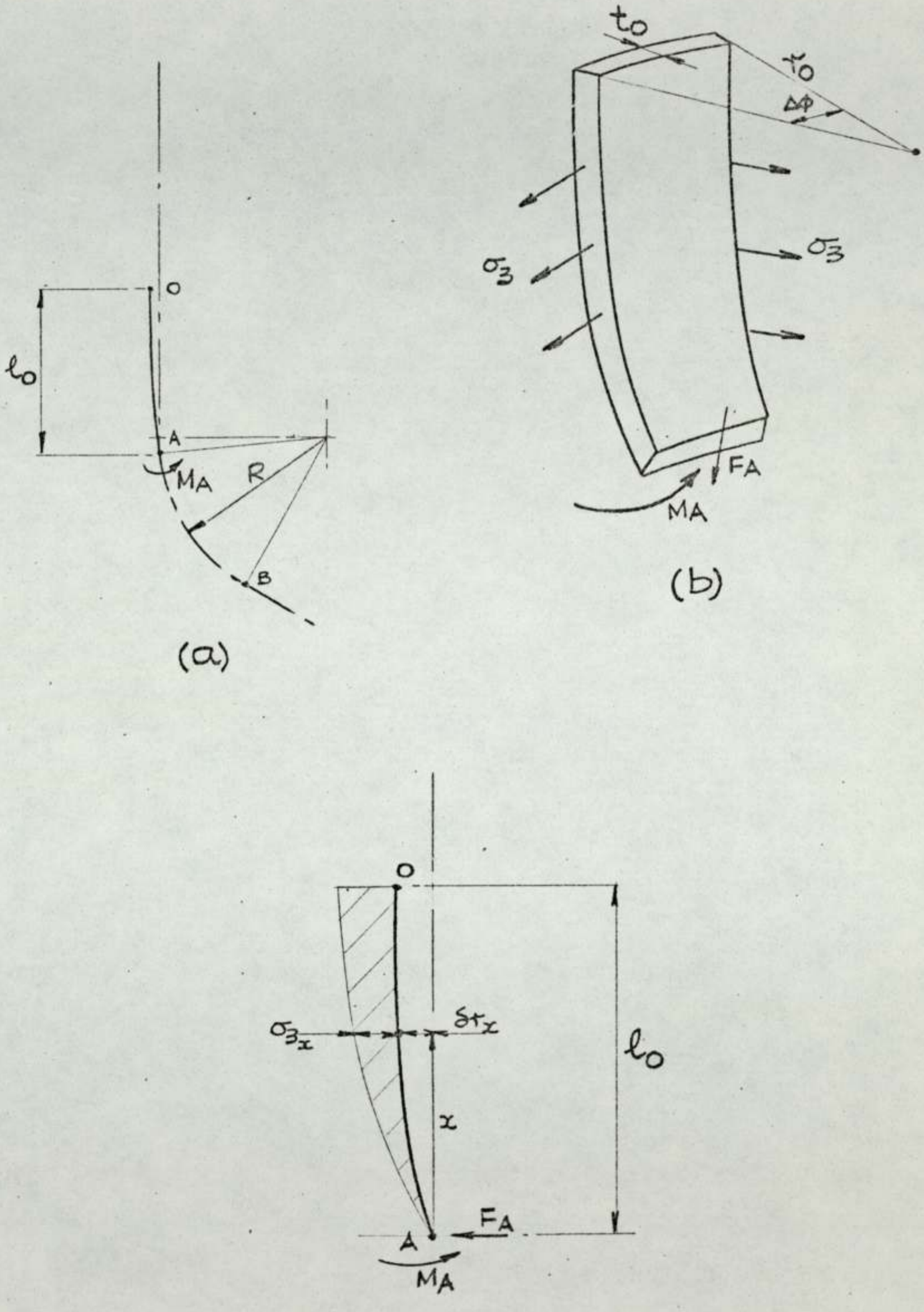

FIG. 39 ENTERING CUP WALL AT ONSET OF SPLAYING

The values of σ_3 in equation 4.16 depend upon the assumed stress-strain relationship. Two approaches are possible.

(i) <u>fully plastic entering cup.</u>

Assuming σ_3 is a principal stress, its value in the splayed cup will be Y for all values of x in FIG. 39 c. Integration of equation 4.16 with $\sigma_3 = Y$ then gives,

$$l_o = \sqrt{\frac{r_o . t_o}{\sqrt{3}}} = 0.76 \sqrt{r_o . t_o} \qquad \text{——— (4.17a)}$$

(ii) <u>fully elastic entering cup.</u>

At the commencement of splaying all circumferential strain in the length l_o may be considered elastic. Then,

$$\sigma_3 = E \cdot \frac{\delta r_x}{r_o}$$

To proceed further a relationship between δr_x and x is required. Since there is no a priori means of achieving this, assumptions regarding the deflected profile are necessary.

Assuming a profile $\delta r_x = \frac{x}{l_o} . \delta r_{l_o}$, σ_3 is given by,

$\sigma_3 = \frac{E}{r_o} \frac{x}{l_o} . \delta r_{l_o}$, and equation 4.16 becomes, after integrating,

$$\frac{2}{\sqrt{3}} . \frac{Y t_o . r_o}{4} = \frac{E . l_o^2 \delta r_{l_o}}{3 r_o}$$

Yielding will occur at the rim when $\delta r_{l_o} / r_o = Y/E$, and therefore the length of cup wall involved in splaying is,

$$l_o = \sqrt{\frac{\sqrt{3}}{2} . r_o . t_o} = 0.93 \sqrt{r_o . t_o} \qquad \text{——— (4.17b)}$$

Assuming a profile $\delta r_x = \delta r_{l_o} . \sin \frac{\pi x}{2 l_o}$ gives,

$$\sigma_3 = \frac{E . \delta r_{l_o}}{r_o} . \sin \frac{\pi x}{2 l_o}$$

Substituting for σ_3 in equation 4.16, integrating, and applying the yield condition gives,

$$l_o = \frac{\pi}{4}\sqrt{r_o . t_o} = 0.84\sqrt{r_o . t_o} \qquad (4.17c)$$

It was of interest to compare predictions of the above theory with experimental evidence available at that time. Although no experimental work had as then been undertaken by the writer, the work of Norman[43] discussed in Section 2.9 appeared to indirectly supply information on the onset of splaying: the work was primarily concerned with observing the effect of guiding on redraw punch load, the guide ring being a loose fit over the entering cup (0.010 in. diametral clearance), and apparently incapable of exerting any influence until splaying caused interference between guide and cup. At this stage the load-travel curves taken with and without guiding diverged, the former becoming greater and reaching a clearly defined maximum after a further small increment of punch travel. The actual point of a divergence was not clear, but from Norman's data it was possible to calculate cup rim height above the die when the 'guided' maximum punch load occurred. This was 0.6 inch. It was presumed splaying had commenced just previous to this stage.

From a knowledge of the cup material properties circumferential strain to cause yielding at the cup rim was found to be 0.002, whilst the splay strain necessary to cause contact with the guide was 0.005.

According to equation 4.17 c for the particular cup dimensions l_o was 0.118 in. This, when added to the hold-down punch radius and wall thickness, gave a cup rim height above die of 0.26 in.

Therefore, a wide discrepancy apparently existed between theory and experiment and seemed to indicate that additional unaccounted-for factors were influencing splaying.

4.6. Equilibrium in the radial drawing zone.

The singular nature of radial drawing in the zone A - B (FIG. 35) was discussed in section 4.3. If the zone is broken down into its component deformations, bending, radial drawing, and unbending, and each analysed independently, stress analysis is relatively simple. This is the usual approach to the problem, and was followed by Fogg[11] in deducing zone geometry for unconstrained redrawing. However the true stress situation is complicated since the three components of deformation are mutually dependent and must therefore inter-react.

It was thought that a knowledge of stress distribution within the zone A - B could lead to a clearer understanding of the reasons for splaying. Analysis of zone equilibrium was therefore undertaken for the situations of constrained and unconstrained redrawing.

(i) Unconstrained redrawing.

FIG. 40 a shows an element in the zone A - B . Fogg found that zone curvature was reasonably constant, and could be represented by a radius R_f . This assumption was made in the following analysis.

FIG. 40 b is a three-dimensional view of the element showing the direction of applied stresses. The circumferential stress σ_3 acts on a compound plane and has components in directions parallel and normal to R_f at θ . The angle subtended parallel to R_f at θ is $\Delta\phi'$, and that normal to R_f at θ , $\Delta\phi''$. If the angle subtended normal to the redrawing axis is $\Delta\phi$ then,

$$\Delta\phi' = \Delta\phi \cos\theta \quad , \quad t' = t/\cos\theta$$

$$\Delta\phi'' = \Delta\phi \sin\theta \quad , \quad t'' = t/\sin\theta$$

FIG. 40 c is a view of the element normal to R_f at θ from which,

$$\sigma_3' = \sigma_3 \cos\frac{\Delta\phi''}{2} \simeq \sigma_3 .$$

FIG. 40 d is a view parallel to R_f at θ from which,

$$\sigma_3'' = \sigma_3 \cos\frac{\Delta\phi'}{2} \simeq \sigma_3$$

In the current analysis thickness variation is ignored.

Resolving forces parallel to R_f at θ ,

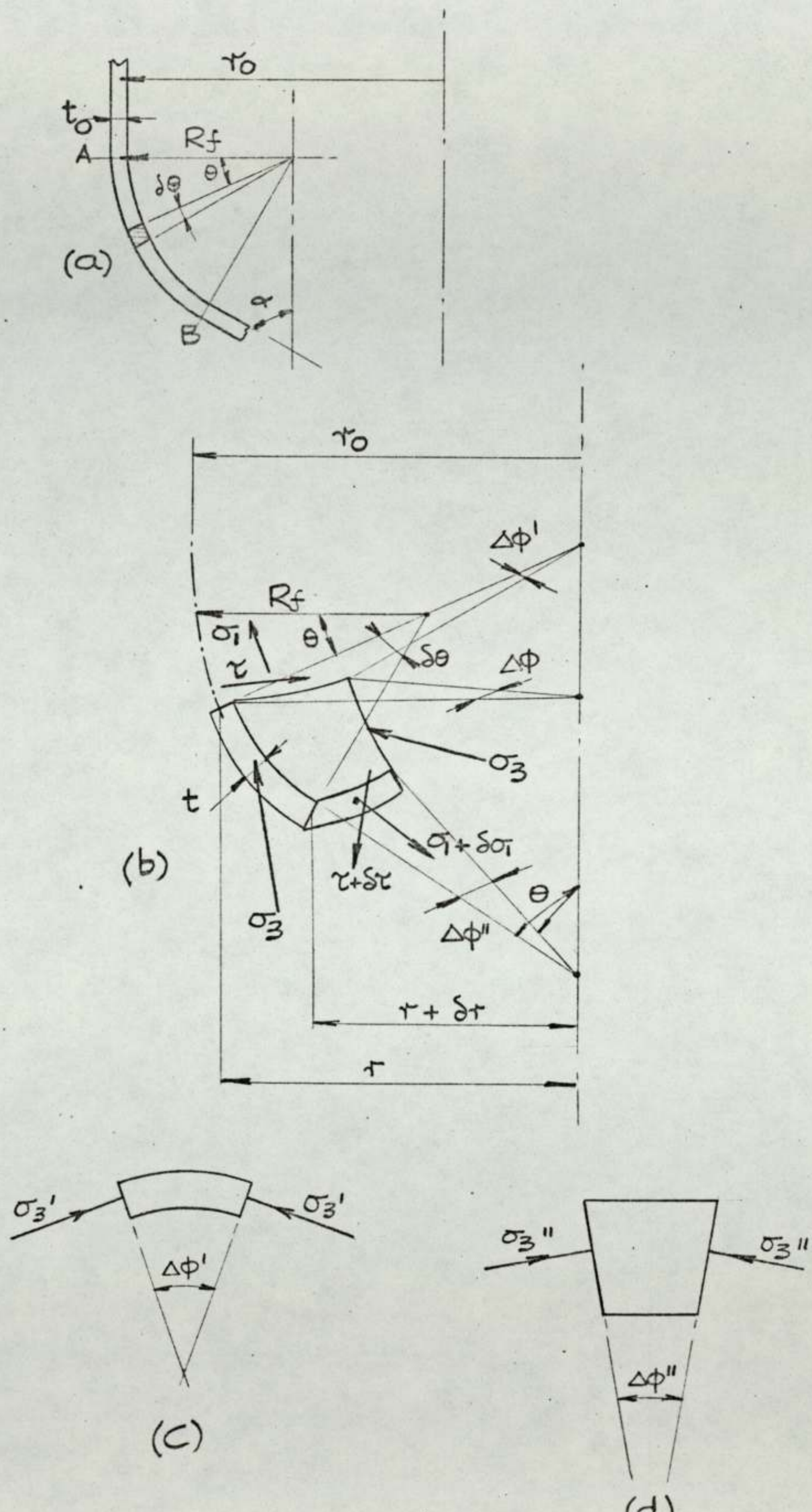

FIG. 40 STRESSES ACTING ON AN ELEMENT IN "ZONE OF SPLAYING" DURING STEADY-STATE REDRAWING WITHOUT A HOLD-DOWN PUNCH.

Force due to $\sigma_3' \left(= \sigma_3\right) = 2\,\sigma_3 . \sin \frac{\Delta\phi'}{2} . R_f . \delta\theta . t .$

$$= \underline{\sigma_3 . R_f . \Delta\phi . t \cos\theta . \delta\theta} - (\mathrm{I})$$

Force due to $\sigma_1 = 2\sigma_1 . \sin\frac{\delta\theta}{2} . \frac{r}{\cos\theta} . \Delta\phi' . t$

$$= \underline{\sigma_1 . \delta\theta . r . t . \Delta\phi} \text{ ——— } (\mathrm{II})$$

The term (I) decreases as θ increases. The term (II) increases with θ providing r is large compared with R_f, since σ_1 must increase with θ. In general therefore $\mathrm{I} \neq \mathrm{II}$, and to maintain equilibrium a shear stress τ exists as indicated in FIG. 40 b. The presence of shear stresses implies that σ_1, σ_2 are not principal stresses, and that a variable bending moment exists throughout the zone.

Force due to τ parallel to R_f at θ is,

$$\left[(\tau + \delta\tau)\cos\frac{\delta\theta}{2}\,(r + \delta r)' - \tau\cos\frac{\delta\theta}{2}\,r'\right]\Delta\phi' . t = \left[r\,\delta\tau - \tau R_f \underline{\sin\theta\,\delta\theta}\right]\underline{\Delta\phi . t} \; (\mathrm{III})$$

since from the zone geometry $r = r_0 - R_f(1 - \cos\theta)$ and

$\delta r = - R_f . \sin\theta . \delta\theta .$

Equilibrium in the direction parallel to R_f at θ is given by the condition $\mathrm{I} - \mathrm{II} + \mathrm{III} = 0$, or,

$$\sigma_3 . R_f . \cos\theta . \delta\theta - r . \sigma_1 . \delta\theta + r\,\delta\tau - \tau . R_f . \sin\theta . \delta\theta = 0 \text{ —— } (4.18)$$

Resolving forces normal to R_f at θ,

Force due to $\sigma_3 = 2\,\sigma_3 . \sin\frac{\Delta\phi''}{2} . R_f . \delta\theta . t$

$$= \underline{\sigma_3 . \Delta\phi \sin\theta . \delta\theta . R_f . t} \text{ —} (\mathrm{IV})$$

Force due to $\sigma_1 = \left[(\sigma_1 + \delta\sigma_1)(r + \delta r)' - \sigma_1 . r'\right]\Delta\phi' . t . \cos\frac{\delta\theta}{2}$

$$= \left[\delta\sigma_1 . r - \sigma_1 R_f \underline{\sin\theta . \delta\theta}\right]\underline{\Delta\phi\, t} \text{ —} (\mathrm{V})$$

Force due to $\tau = \left[(\tau + \delta\tau)(r + \delta r)' - \tau r'\right]\Delta\phi' . t . \sin\frac{\delta\theta}{2}$

$$= \underline{\tau . r . \delta\theta . \Delta\phi . t} \text{ ——— } (\mathrm{VI})$$

Equilibrium in the direction normal to R_f at θ is given by the condition $\mathrm{IV} - \mathrm{V} - \mathrm{VI} = 0$, or,

$$\sigma_3 . \sin\theta . \delta\theta . R_f - \delta\sigma_1 . r + \sigma_1 . R_f . \sin\theta . \delta\theta - \tau . r . \delta\theta = 0 \text{ —— } (4.19)$$

where $r = r_0 - R_f(1 - \cos\theta)$

Equations 4.18, 4.19 together specify equilibrium of an element in terms of the unknown quantities, τ, σ_1, σ_3 and R_f

Von Mises yield criterion may be written,

$$(\sigma_x-\sigma_y)^2+(\sigma_y-\sigma_z)^2+(\sigma_z-\sigma_x)^2+6(\tau^2_{xy}+\tau^2_{yz}+\tau^2_{zx})=2Y^2$$

In the present problem $\sigma_1 \equiv \sigma_x, \sigma_2 \equiv \sigma_y, \sigma_3 \equiv \sigma_z$. Since σ_3 is a principal stress $\tau_{yz} = \tau_{zx} = 0$. Also $\sigma_2 = 0$. The yield criterion may therefore be re-written,

$$\sigma_1^2 + \sigma_3^2 - \sigma_3.\sigma_1 + 3\tau^2 = Y^2 \qquad (4.20)$$

Equation 4.20 is not however easily combined with equations 4.18, 4.19 and even then additional information is required to solve the problem. Shear stress may be expressed in terms of the bending moment derivative $\frac{dM}{d\theta}$ but this does not simplify matters. It was concluded that even for steady-state conditions an equilibrium approach would not provide information on eventual splaying behaviour. On commencement of splaying the non-steady state brings additional complications.

(ii) <u>Constrained redrawing</u>.

The radial drawing zone is as shown in FIG. 40 a but with R_f replaced by R_c . Contact with the hold-down punch profile first occurs at A, and a normal pressure is exerted on the inside of the cup throughout the angle of contact α . The system of circumferential stresses postulated above A cause a shear force at A. This force is assumed to be reacted by the hold-down punch at A. Similarly it is assumed that any shear force due to unbending at B will also be reacted by the punch. On this basis no shear stresses are present on planes carrying the radial stress σ_1 which is therefore a principal stress. σ_2, σ_3 are also considered principal stresses whilst acknowledging that friction is present at the cup-punch interface.

The three dimensional stress distribution is similar to that shown for the element in FIG. 40 b, but with shear stresses absent, a pressure σ_2 on the inner face, and a friction component $\mu\sigma_2$

opposing motion of the element into the zone. Distribution of pressure σ_2 is provided by the following analysis, which ignores thickness changes.

Equilibrium of an element in the direction parallel to R_c at θ is given by,

$$r.\sigma_1.\delta\theta.t - \sigma_3.R_c.\delta\theta.t.\cos\theta - \sigma_2.R_c.\delta\theta.r = 0 \quad \text{——— (4.21)}$$

Equilibrium normal to R_c at θ is given by,

$$(\sigma_3+\sigma_1)\sin\theta.\delta\theta.R_c.t - \delta\sigma_1.r.t + \mu.\sigma_2.R_c.\delta\theta.r = 0 \quad \text{——— (4.22)}$$

Eliminating σ_2 between equations 4.21 and 4.22,

$$(\sigma_3+\sigma_1)\sin\theta.\delta\theta.R_c.t - \delta\sigma_1.r.t + \mu(r.t.\sigma_1\delta\theta - \sigma_3 R_c t\cos\theta\delta\theta) = 0 \quad (4.23)$$

Since σ_3 was assumed compressive Tresca's modified criterion becomes,

$$\sigma_1 + \sigma_3 = mY$$

Substituting for σ_3 in equation 4.23 provides,

$$\delta\sigma_1 = \frac{mY R_c \sin\theta.\delta\theta}{r} + \mu\left[\sigma_1 + \frac{R_c.\cos\theta}{r}(\sigma_1 - mY)\right]\delta\theta \quad \text{——— (4.24)}$$

For the general case $\mu \neq 0$ equation 4.24 requires numerical methods for solution, and is of identical form to an expression derived by Chung and Swift[5] for radial drawing around the die profile in cupping.

For the idealised case where $\mu = 0$ and the material does not work harden, equation 4.24 may be written,

$$\int_{\sigma_{1A}}^{\sigma_1} d\sigma_1 = m.Y.R_c \int_0^{\theta} \frac{\sin\theta}{r_0 - R_c(1-\cos\theta)}.d\theta$$

since $r = r_0 - R_c(1-\cos\theta)$

On integrating,

$$\sigma_1 - \sigma_{1A} = mY \ln\frac{r_0}{r} \quad \text{——— (4.25)}$$

From the yield criterion,

$$\sigma_3 = mY\left(1 - \ln\frac{r_0}{r}\right) - \sigma_{1A}$$

Substitution for σ_1, σ_3 in equation 4.21 gives,

$$\sigma_2 = \frac{t(r + R_c.\cos\theta)}{R_c.r}\left(mY\ln\frac{t_0}{\bar{r}} + \sigma_{1A}\right) - \frac{mY.t.\cos\theta}{r} \qquad (4.26)$$

From Chung and Swift, $\sigma_{1A} = \frac{2}{\sqrt{3}}\frac{Yt}{4R_c}$

Equation 4.26 may be used to study the effect of process parameters R_c/t_0, r_c/t_0 on pressure distribution over the hold-down punch nose. FIG. 41 shows the relationship between σ_2/Y and θ for $r_0/t_0 = 20$, $R_c/t_0 = 4$

Although equation 4.26 could be useful in predicting hold-down force requirements it does not throw any light on the splaying problem. The expression becomes invalid if, on splaying, zone curvature decreases below $1/R_c$. There is no indication when this situation arises.

(iii) Shortcomings of an equilibrium approach to splaying.

The preceding analyses illustrated two important conditions which must be satisfied when applying an 'equilibrium' approach to deformation problems.

(a) The geometry of the zone must be known.

(b) The boundary conditions must be known.

These conditions were reasonably satisfied for constrained redrawing but not for unconstrained redrawing, and in the latter case it was not possible to complete the stress analysis. Once splaying commences neither conditions (a) or (b) are known, and it was therefore concluded that this type of approach to splaying offered little possibility of success.

4.7. Fogg's method of deducing free-zone geometry and its implications to splaying.

As a result of work reported in section 4.6 it was concluded that an 'equilibrium' approach was not applicable to the splaying problem. A different approach was therefore required. Fogg[11] deduced

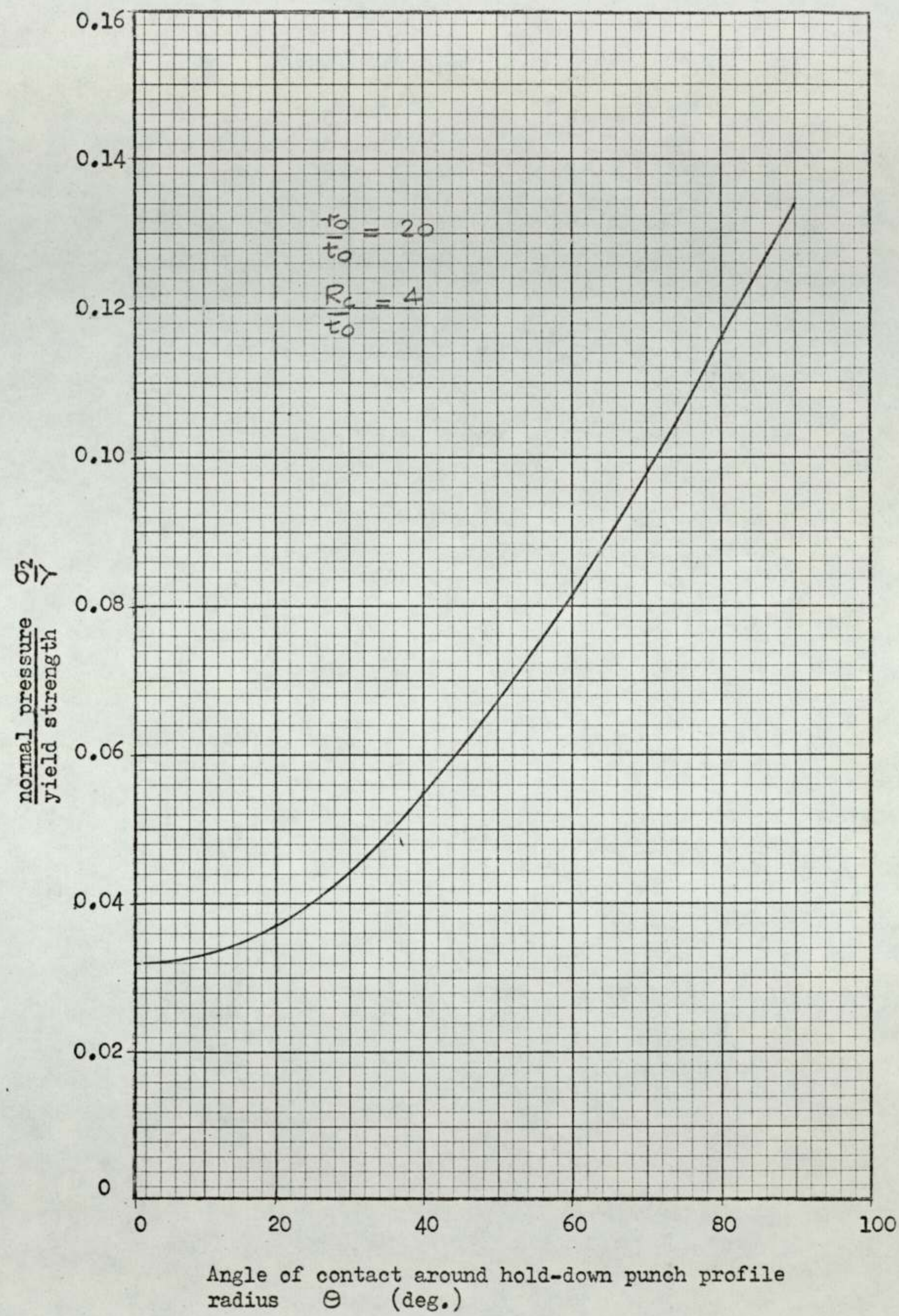

FIG. 41 VARIATION OF NORMAL PRESSURE RATIO WITH ANGLE OF CONTACT ON HOLD-DOWN PUNCH PROFILE RADIUS (θ).

free-zone geometry in unconstrained redrawing by using an 'energy' technique. (The work was discussed in section 2.3 d). The general approach for explaining the zone's existence was considered by the writer to be equally relevant to an explanation of the splaying phenomenon.

The free zone of unconstrained redrawing is shown by arc A - B in FIG. 42. In deducing its geometry Fogg ignored the complexities encountered in section 4.6, and assumed the zone to comprise;

(1) Bending at entry under plane-strain conditions with $\varepsilon_3 = 0$

(2) Radial drawing at constant radius R_f with $\sigma_1, \sigma_2, \sigma_3$ principal stresses.

(3) Unbending at exit under plane-strain conditions with $\varepsilon_3 = 0$

It was postulated that zone geometry would always be such that work of plastic deformation would be a minimum. On the basis of this concept it was shown that,

$$\frac{R_f}{t_o} = \sqrt{\frac{r_o/t_o}{\sqrt{3}\,(1-\cos\alpha)}} \qquad (4.27)$$

The die semi-angle α in equation 4.27 is that at the point of first contact between cup and die. The expression is not limited to dies of conical profile.

Although at present no link has been shown to exist between free-zone geometry and subsequent splaying behaviour it is reasonable to assume that splaying is also explicable by the principle of minimum energy of deformation. Thus it may be argued that during steady-state redrawing (when the entering cup is long) boundary conditions for zone A - B are constant, and for this situation zone geometry as given by equation 4.27 demands least energy. As the entering cup becomes shorter its constraining influence decreases, and splaying takes place in a non-steady state manner such that at any instant the work of deformation is minimal for the imposed constraint.

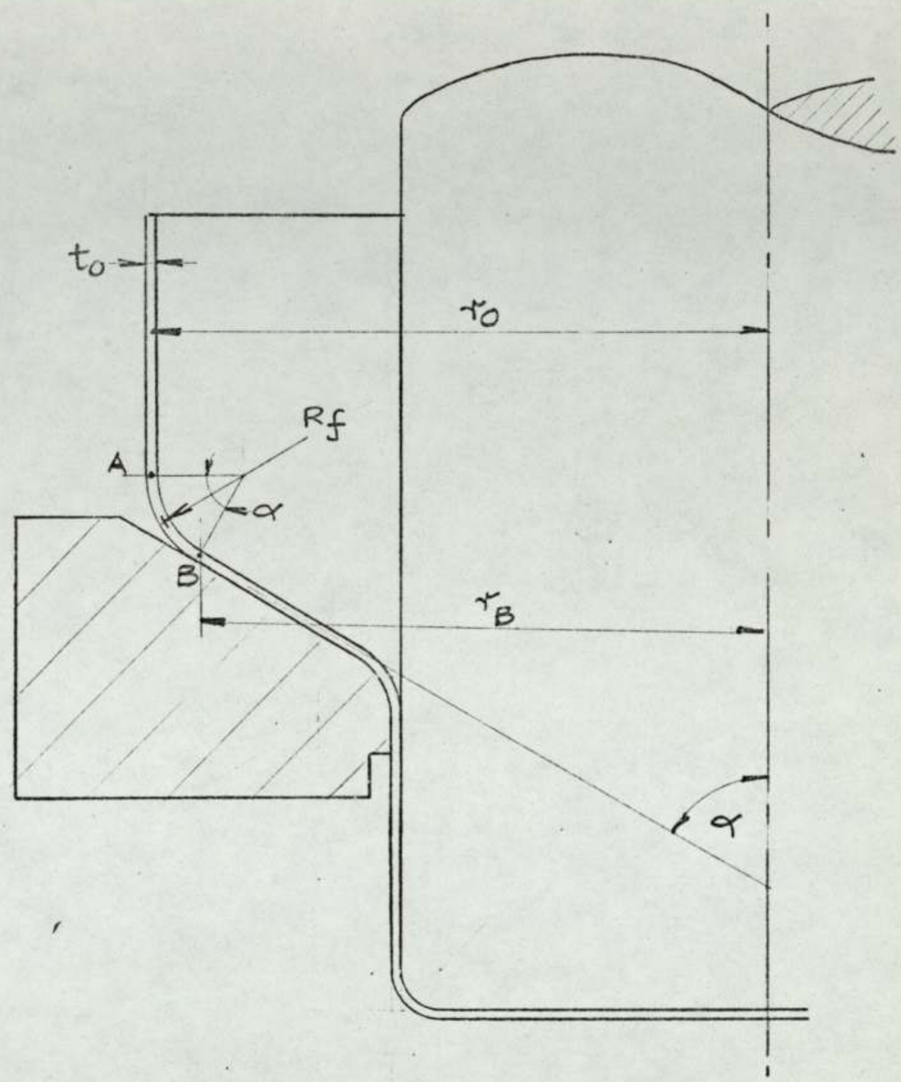

FIG. 42 REDRAWING WITHOUT A HOLD-DOWN PUNCH SHOWING THE FREE ZONE.

Fogg claimed that equation 4.27 gave good agreement with experimental observations but no actual data was provided. In view of the possibility of following a similar energy approach to the splaying problem it was considered important to check the accuracy of equation 4.27 by measuring free-profiles on partially redrawn cups. At that juncture the writer had not carried out any redrawing tests, but a number of samples had been retained from tube sinking trials earlier conducted by Bethel* The trials had been undertaken primarily to determine the effect of die-angle on wall thickness changes, and large die-angles had been used - more characteristic of redrawing than conventional tube sinking. Since tube sinking and redrawing are similar processes it was considered relevant to obtain profiles of the partially sunk tubes and compare free-zone geometry with that predicted by Fogg. Test details and measured profiles are included in appendix A 1 of the thesis. The experimental-theoretical correlation was generally good and gave support to the minimum energy concept adopted by Fogg.

Implications of Fogg's theory.

According to Fogg free-zone geometry depends upon the parameters t_0/t_o and α . FIG. 43 shows this dependence. Although these results are of interest, they do not indicate zone work in relation to t_0/t_o and α , or the relative contributions of bending/unbending work and radial drawing work to total zone work. However this information may be derived;

Specific zone work of bending/unbending is given by,

$$w_b + w_u \simeq 2w_b = 2 \cdot \frac{2}{\sqrt{3}} \cdot \frac{Y t_0}{4 R_f} ,$$

---

* Mr. L. Bethel was formerly at Tube Investments Limited.

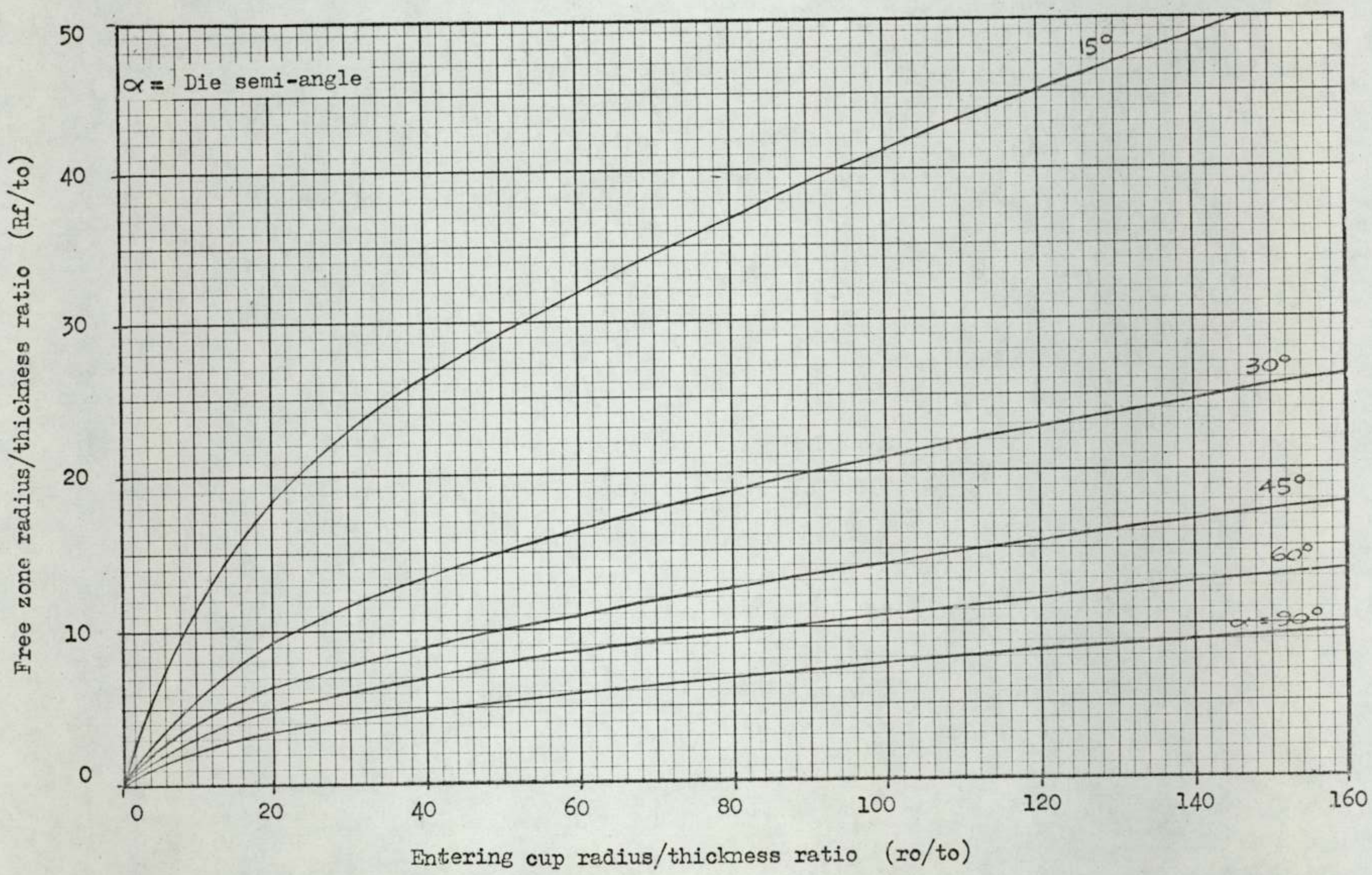

FIG. 43 FREE ZONE RADIUS/THICKNESS RATIO AS A FUNCTION OF CUP RADIUS/THICKNESS RATIO AND DIE ANGLE (AFTER FOGG)

and the specific work of radial drawing by,

$$w_r \simeq \frac{Y R_f}{t_o}\left(1-\cos\alpha\right)$$

Therefore the ratio radial drawing work/bending work is,

$$\frac{w_r}{2w_b} = \frac{\sqrt{3}\ R_f^2(1-\cos\alpha)}{r_o . t_o.}$$

But from equation 4.27. $\quad R_f^2 = \frac{r_o . t_o}{\sqrt{3}\,(1-\cos\alpha)}$

Therefore the free-zone total specific bending work is equal to the specific radial drawing work for all values of r_o/t_o and α . Total specific zone work is given by,

$$w = (w_b + w_u) + w_r = 4w_b = \frac{2}{\sqrt{3}}\cdot\frac{Y\,t_o}{R_f}$$

Substituting for R_f from equation 4.27 provides,

$$\frac{w}{Y} = \frac{2}{(3)^{1/4}}\sqrt{\frac{1-\cos\alpha}{r_o/t_o}} \qquad (4.28)$$

Inspection of equation 4.28 reveals that the work ratio $\frac{w}{Y}$ increases as die angle increases and as cup radius/thickness decreases. Therefore although R_f defines a minimum work condition, the actual magnitude of work varies with r_o/t_o and α . It was considered that this result could have important implications for splaying. FIG. 44 shows a family of curves plotted from equation 4.28. For any particular arrangement $r_o/t_o, \alpha$, zone work would be increased by using a hold-down punch for which $R_c < R_f$.

4.8. <u>General considerations of energy approach to splaying.</u>

During steady-state unconstrained redrawing the free zone remains geometrically unchanged as though defined by a rigid tool arrangement. Elements in the entering cup pass through the zone and receive a constant increment of work. A similar situation exists when redrawing is constrained only then zone work is higher.

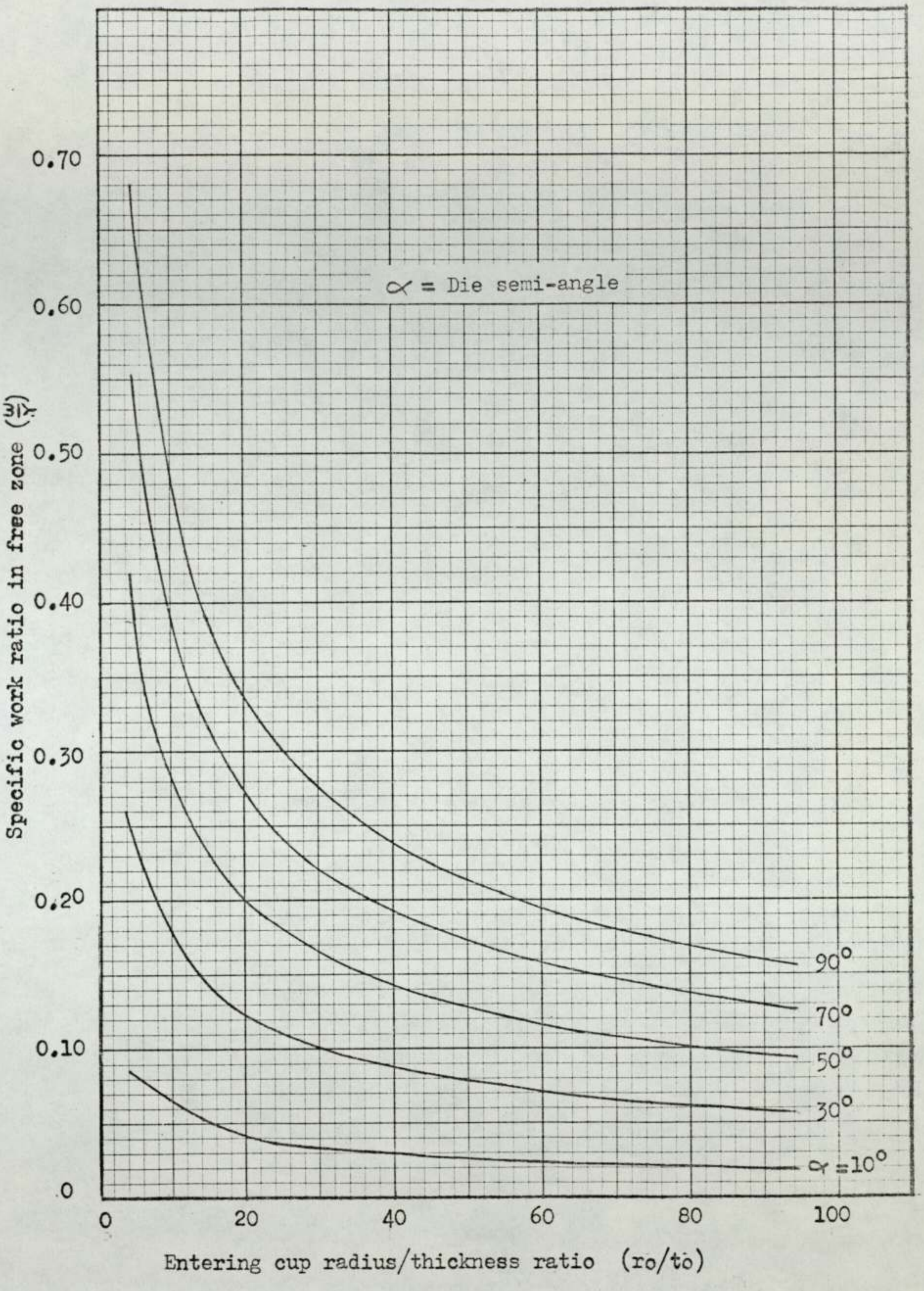

FIG. 44 VARIATION OF SPECIFIC WORK RATIO IN FREE ZONE WITH CUP RADIUS/THICKNESS RATIO AND DIE ANGLE.

Splaying occurs in the absence of any externally applied force. A change in steady- state conditions must represent a change in zone work, otherwise elements would not splay. This change of work to the splayed mode cannot represent an increase in energy, for this would involve additional external work. It may therefore be surmised that elements involved in splaying pass from radius r_0 to r_B (FIG. 40) with less work of deformation than elements during steady-state. This postulate was used as a basis for further theoretical studies.

4.9 Conclusions drawn from exploratory investigations.

(1) Only that part of the cup above the point of first die contact during steady-state redrawing was influenced by or involved in splaying.

(2) During steady-state redrawing a system of tensile circumferential stresses exists in the entering cup wall just above the point where plastic deformation commences. Splaying occurred when this system was disturbed.

(3) The bending moment at entry to the plastic deformation zone contributed towards splaying but there was no contribution from the unbending moment at the point of die contact. The contribution of the radial drawing zone bounded by these two moments was obscure and required further investigation.

(4) For the purpose of calculating bending moments the cup material may be considered fully plastic.

(5) It was possible to predict the length of cup wall involved in splaying in terms of the bending moment at die entry. The theory required verification.

(6) It was not possible to predict splaying behaviour by considering equilibrium of an element in the zone ultimately involved in splaying.

(7) Free-zone geometry deduced by Fogg using a minimum energy concept was in reasonable agreement with experimental evidence.

Fogg's theory implied that specific zone work was a function of entering cup and die geometry.

(8) Specific zone work in the plastic region prior to die contact was influenced by hold-down punch nose geometry.

(9) Splaying was associated with a decrease in process work.

(10) An energy approach was most suitable for a theoretical analysis of the splaying problem.

5. PLAN OF RESEARCH.

5. 1. Introductory comments.

Research programmes were devised to fulfil objectives listed in section 3, the order of investigation being largely dictated by the need to resolve fundamental issues relating to splaying before proceeding with more detailed research into the effects of various process parameters on the phenomenon. In particular it was necessary to determine if splaying was associated with an increase or decrease in process work since a literature survey had revealed differences of opinion on this basic aspect. It was also important to answer early in the research programme certain questions arising from exploratory theoretical considerations discussed in section 4.

Research comprised four programmes the outlines of which are given below in order of execution.

5. 2. Outline of research.

(a) First experimental programme.

Preliminary theoretical studies of splaying indicated that it was deformations occurrent at the beginning of the process which were ultimately responsible for splaying. The effects of bending into the plastic zone were reasonably well understood but the contribution (if any) to splaying from radial drawing prior to die contact remained obscure and required further investigation. It was therefore an attractive proposition to isolate deformations considered responsible for splaying from the redraw as a whole. Some form of simulative test was thus indicated. The first programme comprised experiments designed around this concept.

(b) Second experimental programme.

Experimental programme (a) was intended to give an insight into the basic splaying mechanism. To supply quantitative information actual redraw tests were necessary. A series of tests were therefore devised to indicate at which stage in the redraw process splaying was initiated and thence its precise development in relation to all important redraw variables.

It was realised that studies of splaying in drawn cups would be complicated by non-uniformity near the rim arising from anisotropy, and that due to this the effect of splaying on draw load may be partially masked. To eliminate undesirable features of anisotropy it was planned to redraw specially prepared tubular test-pieces rather than cups prepared from sheet.

(c) Programme of theoretical investigation.

Experimental programmes I and II were designed to contribute information in areas which preliminary investigations had shown to be crucial to an understanding of splaying behaviour. It was planned to use this information as a foundation for comprehensive theoretical studies.

(d) Third experimental programme.

To complete research it was considered important to check the validity of splaying theory under conditions similar to those of actual production. It was therefore planned to redraw cups and test principal theoretical predictions.

5. 3. Testing equipment.

On planning details of research it became clear that simplifications could be achieved by conducting first and second experimental programmes on a common machine using interchangeable test-rigs. Testing procedures demanded that the machine should possess draw speed control, accurate positional control, and static load-holding features. No suitable existing machine was available for the period required by the project and therefore a special-purpose machine was designed and constructed.

An existing hydraulic press was available for the third experimental programme. This was modified to incorporate hold-down facilities and load-measurement instrumentation.

5. 4. Presentation of experimental programme data.

The three experimental programmes, although aimed at a common goal, comprised three distinct investigations. For clarity of presentation each programme is treated as a separate section of the thesis comprising; objects, scope, equipment details, testing procedures and experimental results.

6. TESTING MACHINE FOR FIRST AND SECOND EXPERIMENTAL PROGRAMMES.

6. 1. Design specification.

Machine design was based on the following considerations,

(1) The machine should be a self-contained unit incorporating the precision required for the proposed experimental programmes.

(2) Test rigs mounted on the machine should be easily interchangeable and readily accessible during tests.

(3) The machine should have a maximum draw-load of 2 Tonf. and a working stroke of $4\frac{1}{2}$ in.

(4) The machine should incorporate a strain-gauge load-cell capable of accurately measuring draw-load.

(5) The machine should possess the feature of accurate positional control over the test-piece at any point in the working stroke.

(6) The machine should have infinitely variable speed control in the range 0 - 20 in. / min.

(7) The machine should incorporate the facility of static load-holding.

6.2. General design features.

FIGS. 45, 46 and 47 illustrate design features. Test rigs were mounted on the upper platen, drawing load being transmitted through two vertical columns which also served as guides for a crosshead. A strain-gauge load cell was connected between the crosshead and test-piece gripping dog (FIG. 47), the underside of the crosshead being coupled to the drive mechanism.

Speed control was achieved by means of an electronic speed control unit which is shown on the left-hand-side of the machine in FIG. 45.

Details of the testing machine are given in appendix A_2 .

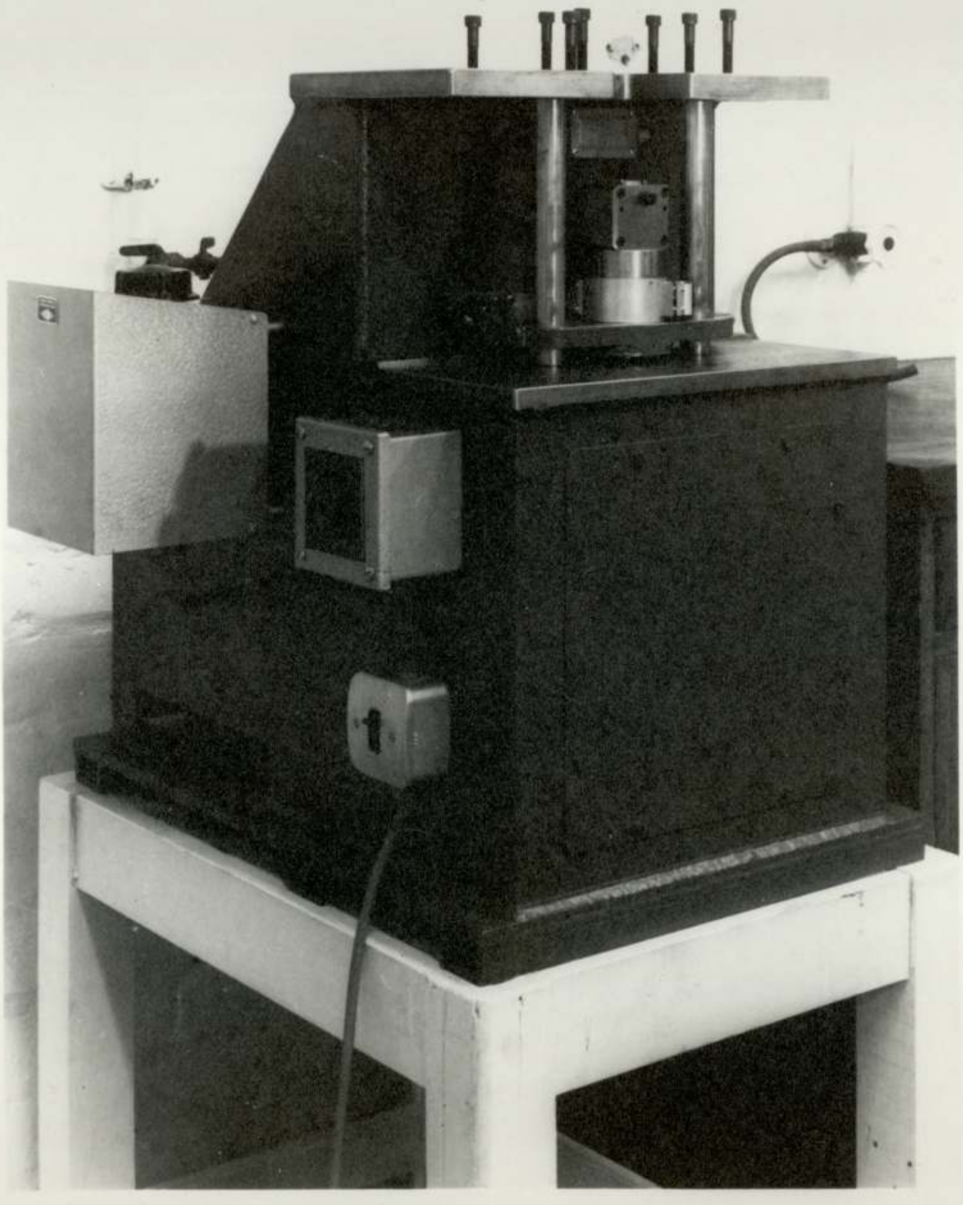

FIG. 45 TESTING MACHINE FOR EXPERIMENTAL PROGRAMMES 1 AND 2.

SIDE -FRONTAL VIEW.

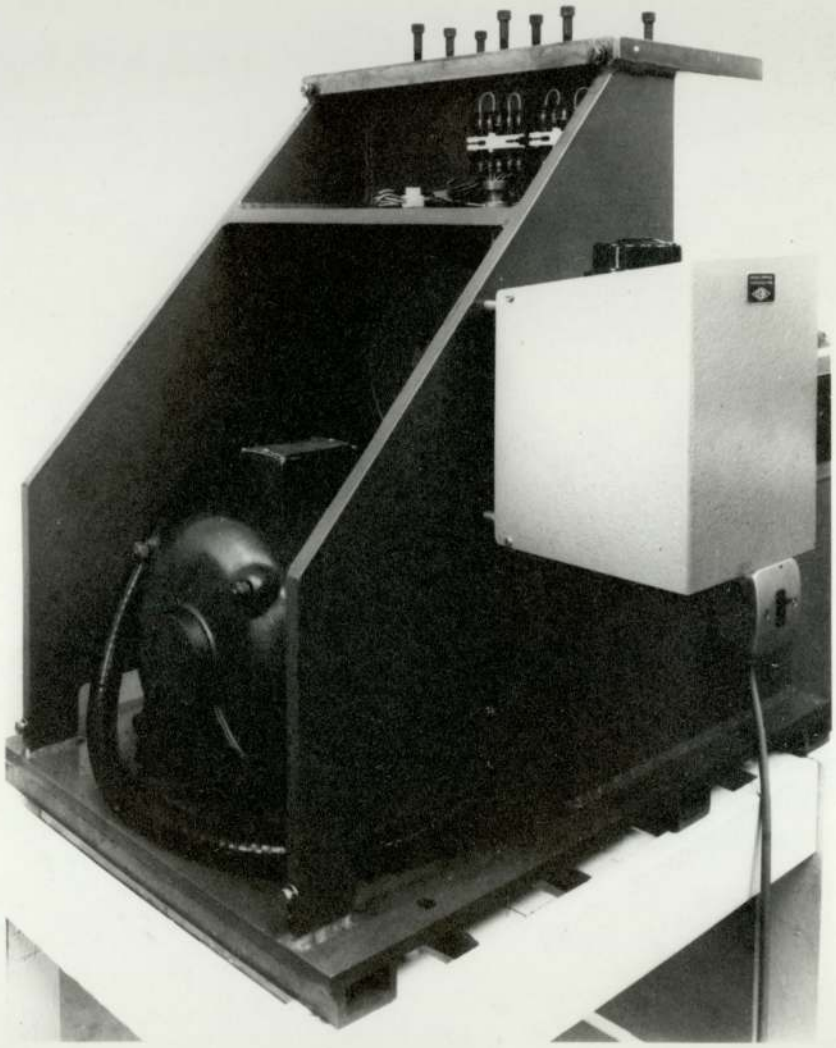

FIG. 46 TESTING MACHINE FOR EXPERIMENTAL PROGRAMMES 1 AND 2.
SIDE-REAR VIEW WITH COVER REMOVED.

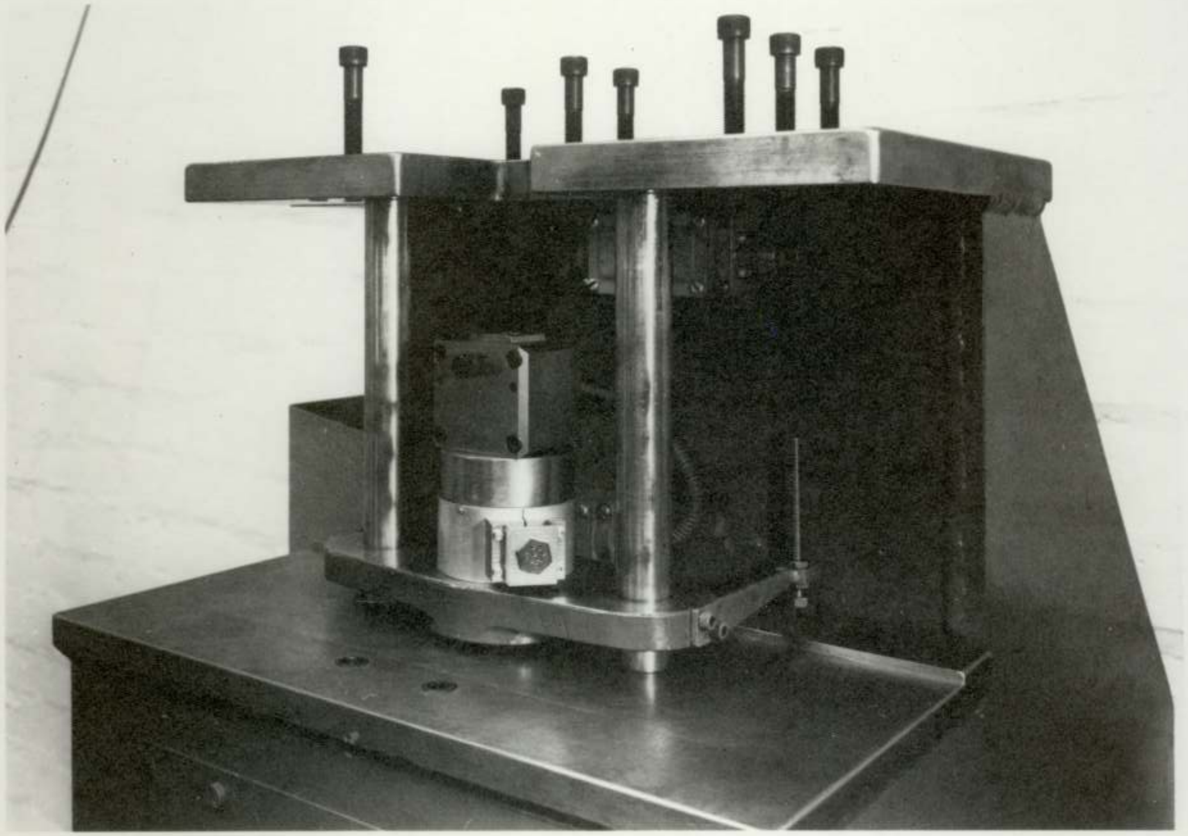

FIG. 47 VIEW OF TESTING MACHINE SHOWING LOCATION OF REDRAW LOAD-CELL BENEATH DOG.

6. 3. Principal dog load-cell data.

(a) Description.

The load cell was designed in alloy steel for an elastic strain of 0.15% at a maximum tensile load of 2 Tonf. These controls dictated the cross-sectional area of the body in the region of strain-gauge attachment, and it became clear that a tubular shape was most suitable. The proportions of the load-cell body were then decided on the basis of (a) ease of manufacture, (b) expediency of attaching standard strain-gauges, (c) fitting into the testing machine. The resulting design is shown in FIG. 48. End projections were precision fits in recesses provided in the testing machine crosshead and dog adaptor, whilst the wide flanges, used for securing the load cell, ensured angular alignment with the direction of load application.

Four foil-type linear electric resistance strain gauges each of 120 $\Omega \pm$ 0.2% resistance were bonded to the centrally located gauge area and were wired to form a full Wheatstone bridge with one gauge in each arm of the circuit. The gauges were symmetrically positioned around the circumference such that alternate gauges were mounted parallel and normal to the load-cell axis. Thus under a uniaxial tensile load the 'parallel' gauges experienced the full gauge-length extensional strain e whilst 'normally' mounted gauged experienced a strain $\nu . e$.

Input to the bridge was via an S.E. type 511/S oscillator operating at 5V. - 3 Kc/s. After passing through a carrier amplifier type S.E. 423/1 the bridge output was fed to the galvanometer of a type S.E. 2005 ultra-violet paper-tape recorder.

The completed load-cell together with its protective cover is illustrated in FIG. 49.

Details of the procedure used in attaching and wiring strain-gauges are given in appendix A_2 . 4.

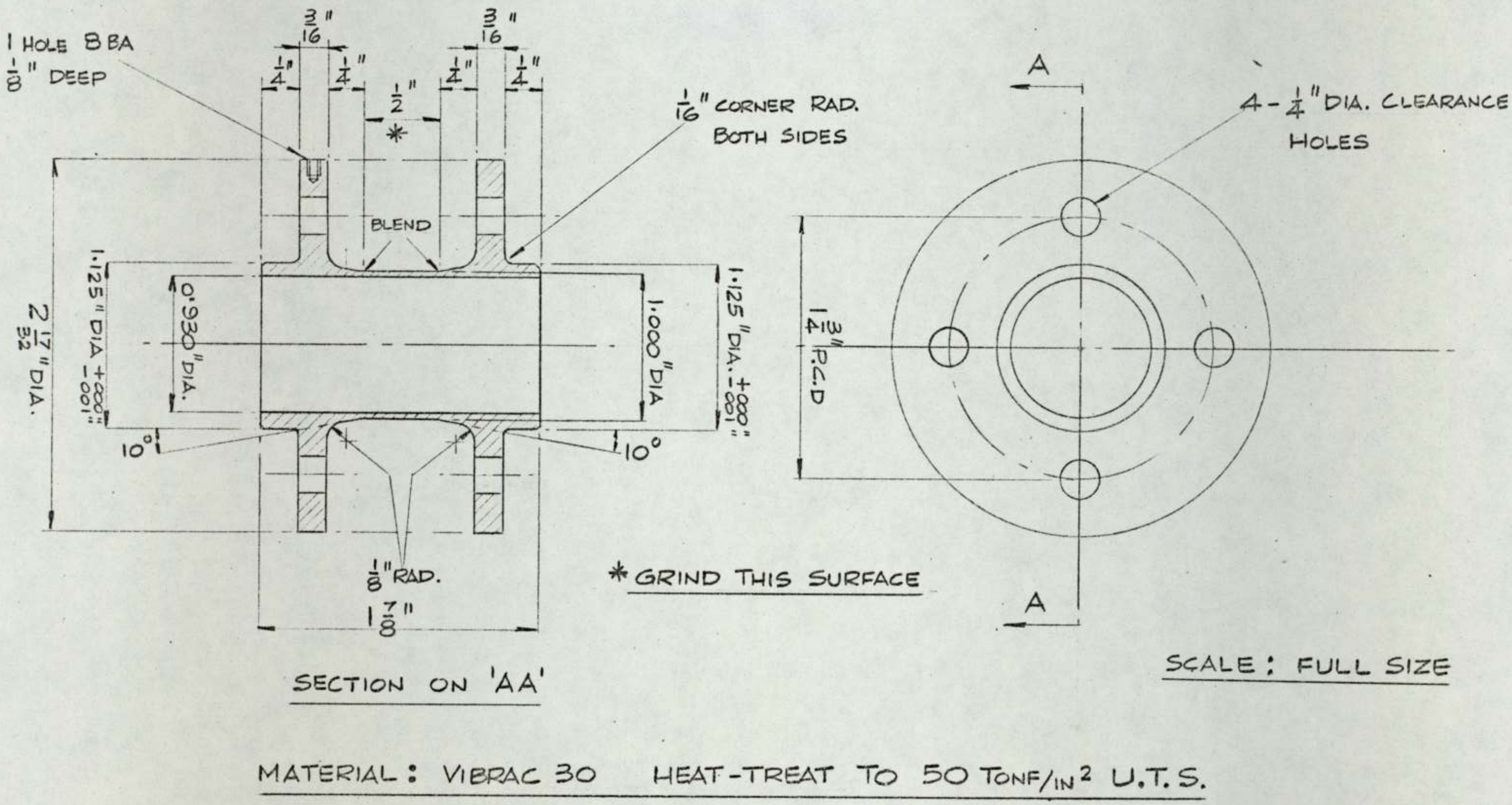

FIG. 48 DETAILS OF DOG LOAD-CELL BODY.

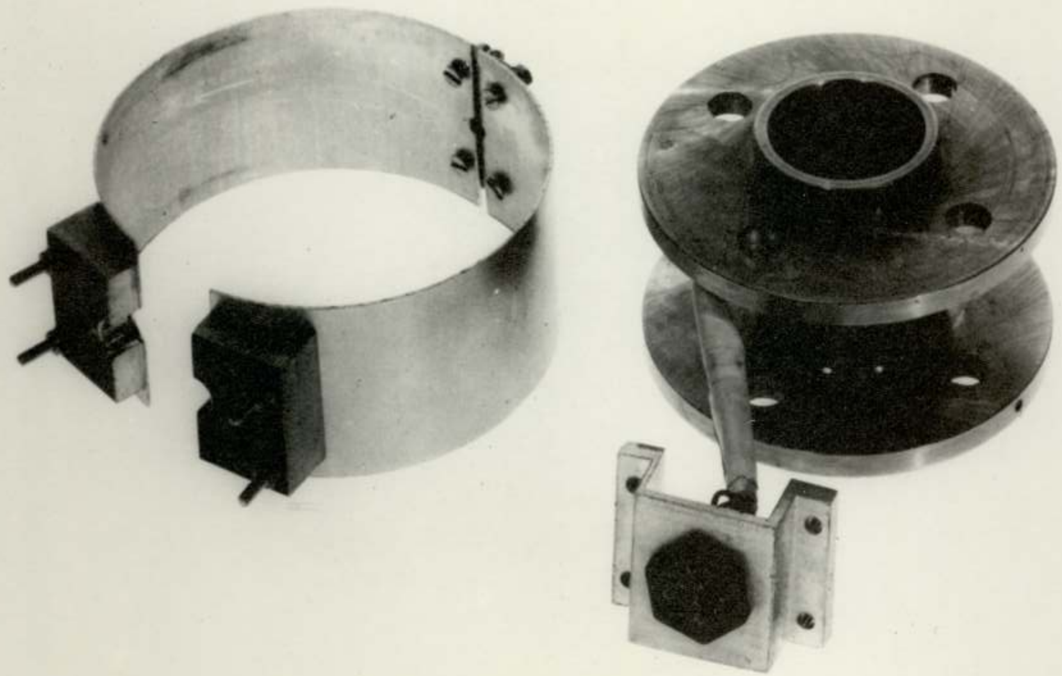

FIG. 49 DOG LOAD-CELL WITH COVER REMOVED.

(b) Calibration.

Before installation in the experimental testing machine the load-cell was calibrated on a regularly inspected 50 Tonf. Denison testing machine, under conditions of loading identical to those during subsequent investigations. This was achieved as shown in FIG. 50, care being taken to ensure that the pulling bars were a precision fit in the central adaptor holes. Recalibration was conducted mid-way through and at the end of the experimental programmes. No signigicant change in load-cell response was detected. Calibration curves for the load-cell are given in FIG. 51.

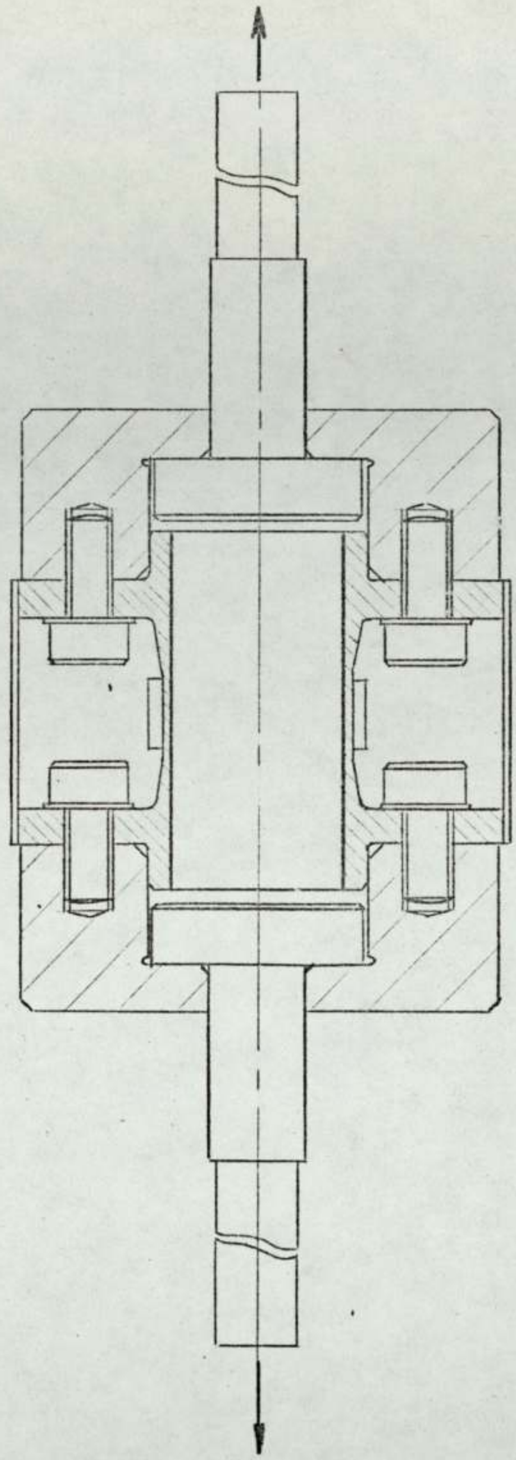

FIG. 50 CALIBRATION OF TESTING MACHINE
DOG LOAD-CELL

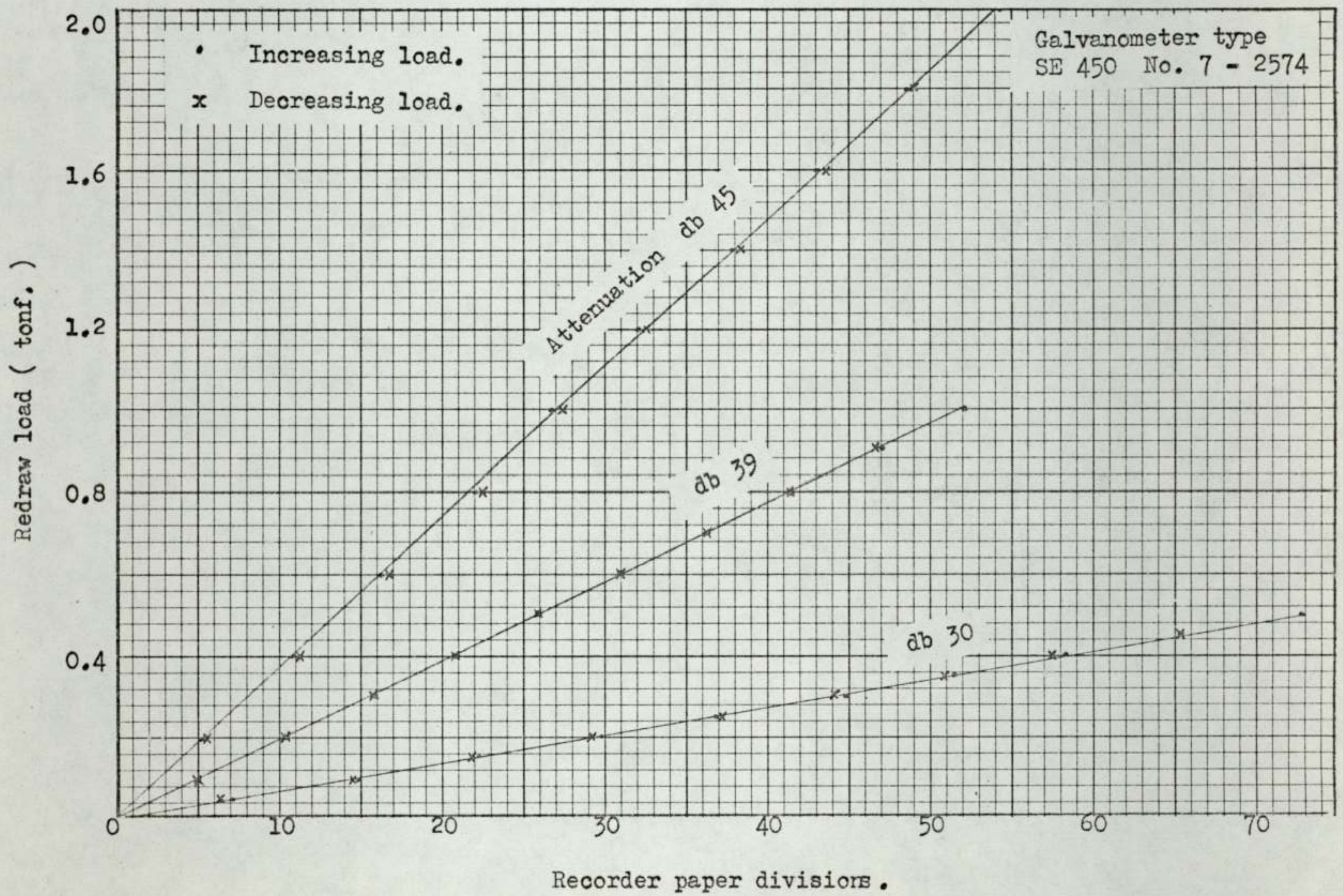

FIG. 51 CALIBRATION CHARACTERISTICS FOR DOG LOAD-CELL USED IN SPLAY-MEASUREMENT PROGRAMME.

7. FIRST EXPERIMENTAL PROGRAMME - SIMULATED REDRAW TESTS.

7. 1. Introductory comments.

FIG. 52 A illustrates a typical constrained redrawing arrangement with the deformation region involved in splaying circumscribed. Preliminary theoretical studies had shown that bending into the zone contributed to splaying whilst unbending at zone exit did not. The contribution of the radial drawing region towards splaying had not been shown by stress analysis of the zone. It was therefore planned to investigate this aspect experimentally.

FIG. 52B. shows the circumscribed region in more detail. In simulating this zone it was considered possible to study the relative contributions of bending and radial drawing towards splaying, by first measuring the moment to prevent splaying for full zone simulation, and then that to prevent splaying with bending only.

The remainder of this section describes the method of simlation, details of tooling, details of test-rig and instrumentation, and experimental results. It transpired that the method of simulation was unsuccessful, since true radial drawing was not achieved. In consequence this part of the research programme contributed nothing positive to an understanding of splaying. Nevertheless the work is reported since it may prove to be enlightening to future investigators.

7. 2. Basis of tool design.

Providing the angle ϕ_2 in FIG. 52 B is small a circumferential cup sliver resembles a flat strip of width W_1 at entry and W_2 at exit. The zone through which the sliver must flow is dictated by redraw tool geometry and constraint of the neighbouring cup wall, and the latter may be simulated by a tool whose boundary planes are mutually inclined at an angle ϕ_2 . The true sliver is drawn through the zone by radial tension transmitted from the redraw punch. This may be simulated by pulling the strip over a curved tool profile radius R, angle of contact α .

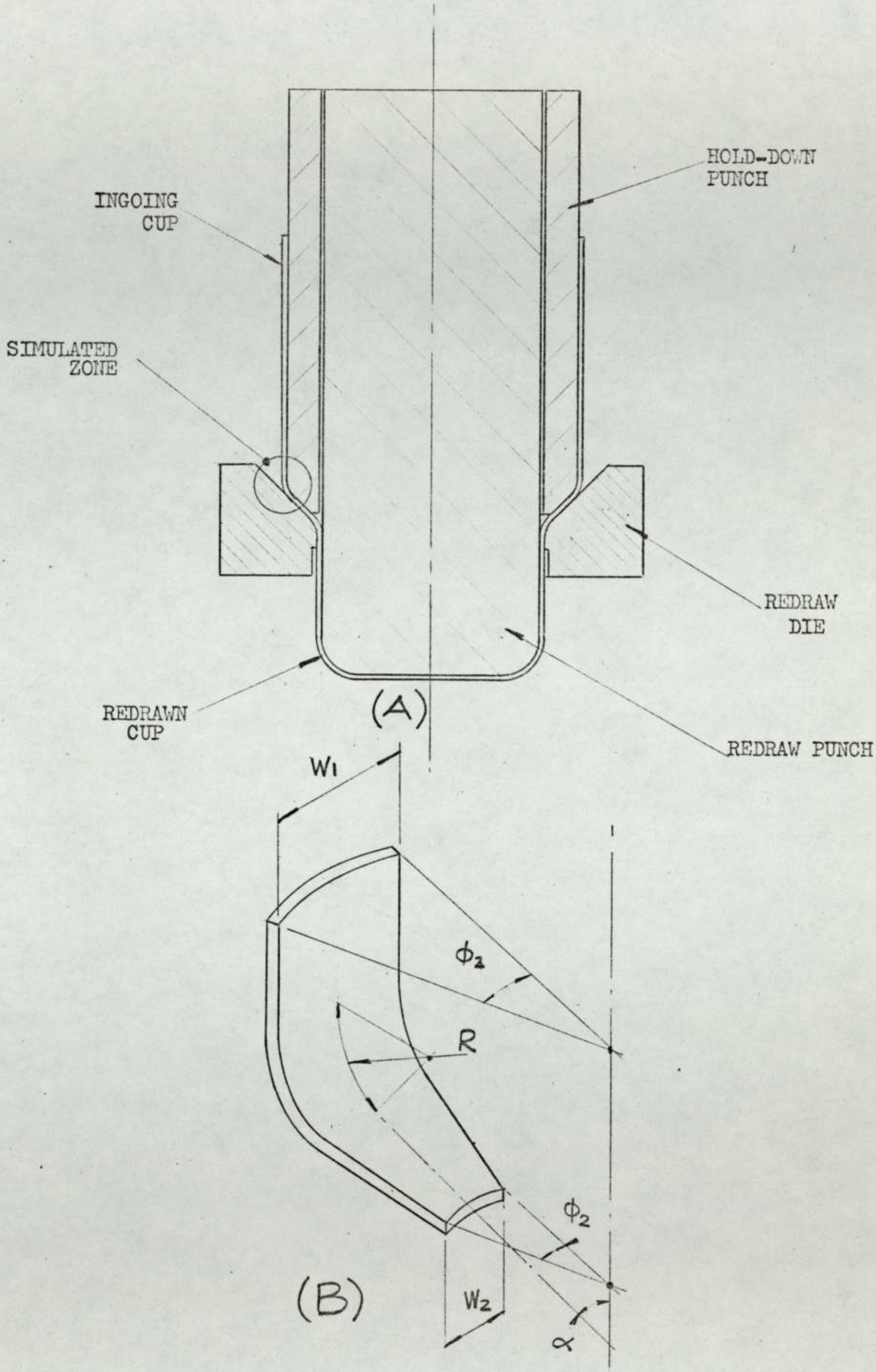

FIG. 52 SIMULATED ZONE OF REDRAWING

In true redrawing the sliver is prevented from splaying by tensile circumferential stresses in the entry region. The simulative strip can by itself offer no such resistance to splaying, but splaying may be suppressed by a tool, the force exerted upon which will be related to splaying.

7. 3. Simulative tool design.

FIG. 53 shows the design of a tool (or die-block) for full zone simulation. Each block comprised three elements, namely, two side pieces and a centre piece, fitting together on a taper ϕ_2 uniform for the die-block length. The elements were precisely located by dowels and clamped by transverse screws. A contour R, α was provided on the central piece, the passage defined by the profile and the side pieces being similar to that around a hold-down punch in constrained redrawing. After an angular contact α, corresponding to the point of die contact in redrawing, simulated drawing terminated, the die-block being relieved to ensure no further deformation.

Die blocks simulating bending only were similar though less complex than those for full zone simulation. A typical block is shown in FIG. 54.

7. 4. Evaluation of test variables.

(a) Test-piece geometry.

In the third experimental programme it was planned to conduct redraw tests on 0.036 in. thick cups. To maintain a degree of similarity between these tests and the simulation tests, test-pieces were made 0.036 in. thick.

Test-piece width was decided on the basis that bending should occur under approximately plane-strain conditions, since this assumption was frequently made in deep-drawing theories. The general rules for plane-strain compression testing recommended by Watts and Ford were then followed to obtain a relationship between width W_1 and thickness t. According to the Watts and Ford test $12 < \frac{W_1}{t} < 24$.

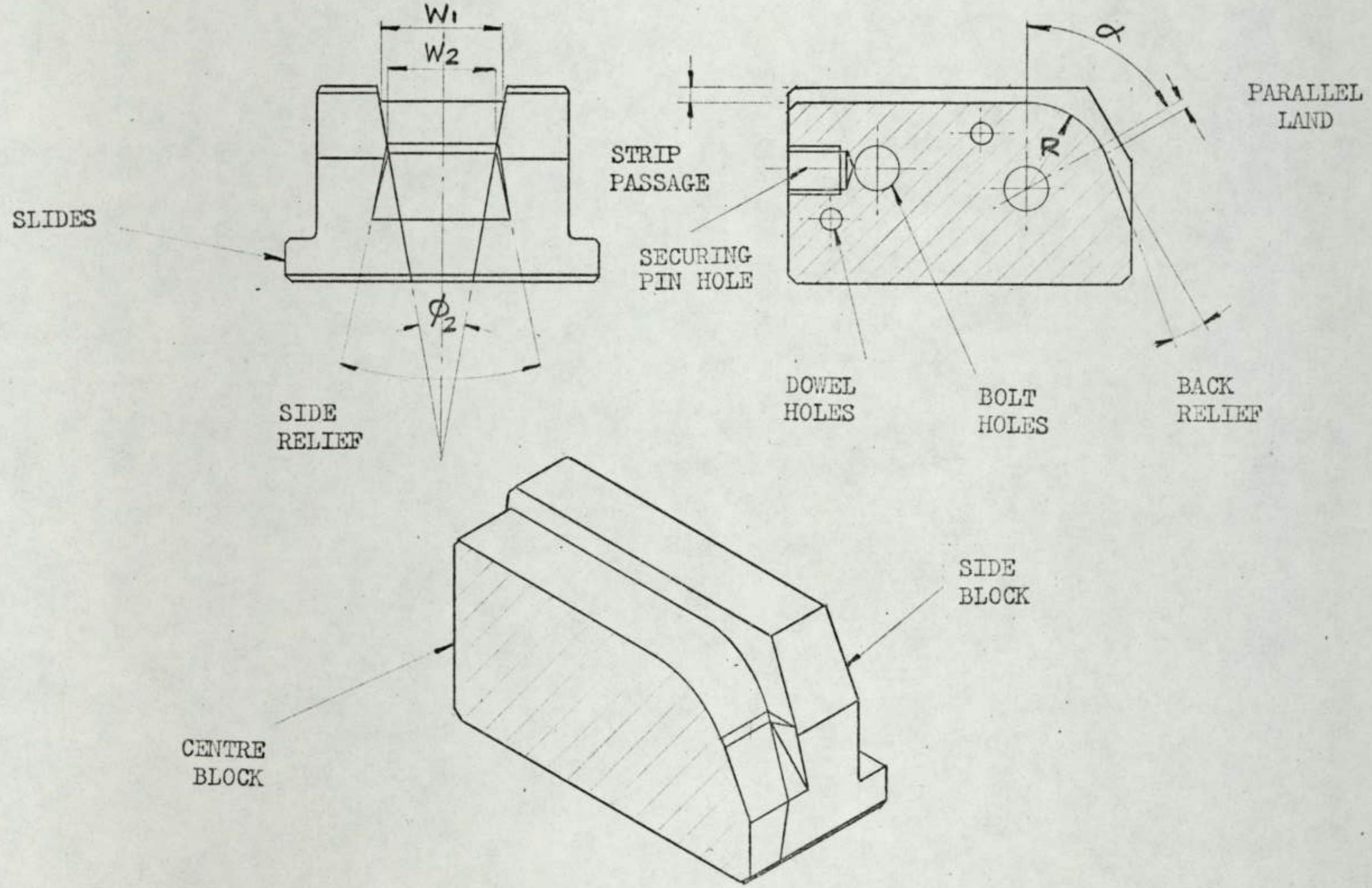

FIG. 53 SIMULATED DIE-BLOCK FOR BENDING AND DRAWING.

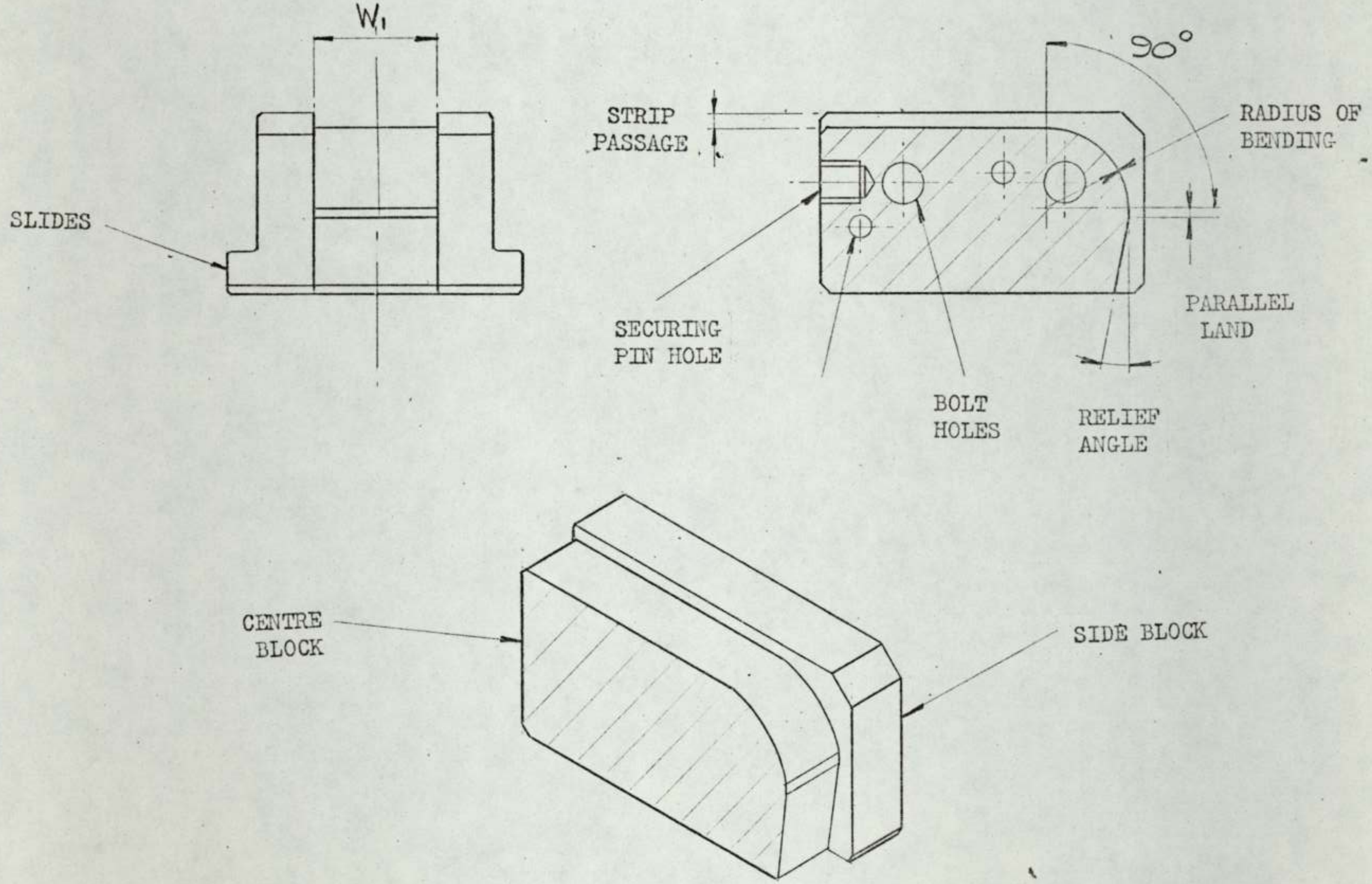

FIG. 54 SIMULATED DIE BLOCK FOR BENDING ONLY

For a strip thickness 0.036 in. the width boundaries were therefore

$0.43 < W_1 < 0.86$. Test-piece width was designated $\frac{3}{4}$ in.

(b) Radius of bending.

Three representative radii of 5, 10 and 15 times cup wall thickness were allocated for the die blocks.

(c) Angle of contact.

The test-rig was designed so that die-blocks for 'bending-only' simulation could be angularly adjusted relative to the direction of movement of the testing-machine draw arm. It was therefore only necessary to manufacture a single 90 degree die-block for each of the three radii. Unfortunately this procedure was not possible with blocks for full-zone simulation, since at zone exit each block required relieving. Angles of 90, 60, and 45 degrees were selected, these being considered representative of actual redrawing.

(d) Wedge angle.

To maintain similarity in die-block design a constant wedge-angle was used throughout. An angle of 20 degrees was adopted, firstly because this angle had been used by Loxley and Swift in their investigation of the somewhat similar wedge-drawing test, and secondly because draw reductions were not excessive when this angle was taken in conjunction with other design parameters.

(e) Reduction of strip width in the die blocks.

The strip width W (FIG. 55) at any point around the die-block profile is given by,

$$\frac{W}{2} = \frac{W_1}{2} - x \operatorname{Tan}\frac{\phi_2}{2} \qquad \text{where} \qquad x = R(1-\cos\theta)$$

The reduction, defined $1 - \dfrac{W_2}{W_1}$ is thus,

$$\frac{2R}{W_1}(1-\cos\theta)\operatorname{Tan}\frac{\phi_2}{2}$$

(f) True deformation profile in die blocks.

At deformation zone entry the die angle was zero whilst

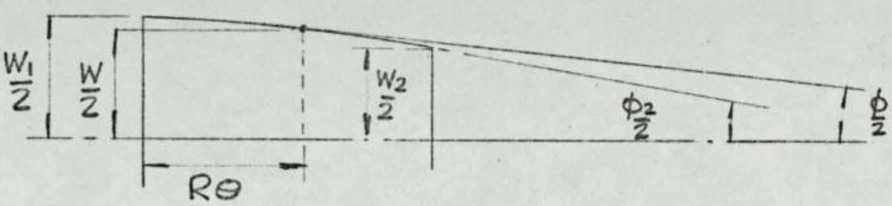

FIG. 56 DEFORMING STRIP GEOMETRY

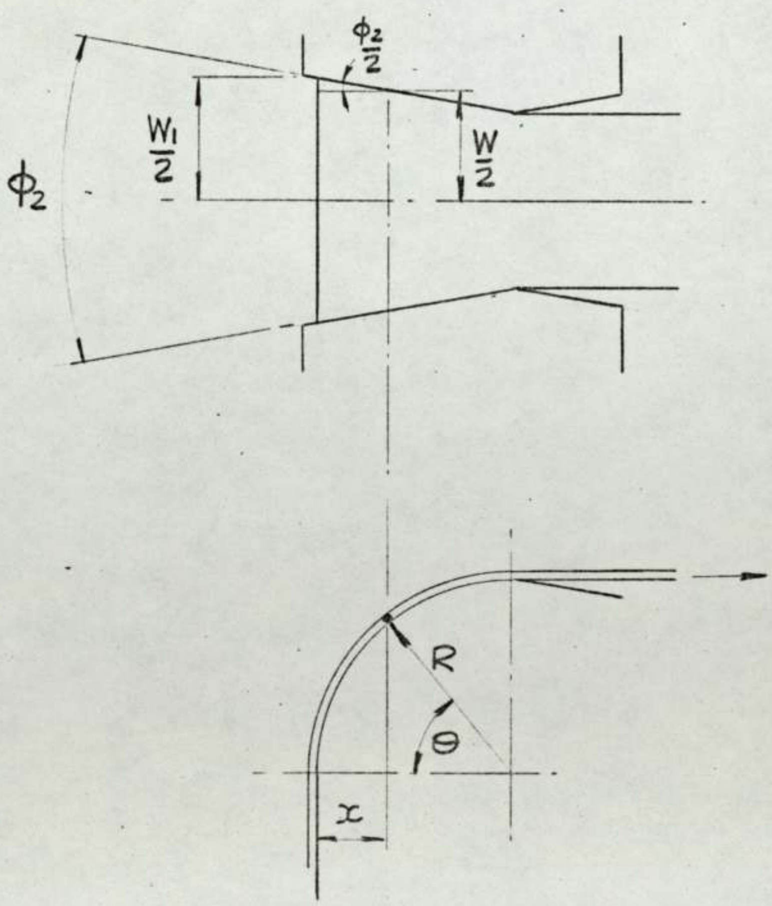

FIG. 55 SIMULATED DIE BLOCK GEOMETRY

after 90 degrees of contact the die angle was ϕ_2 , the wedge angle. The true angle of drawing therefore increased with arc of contact.

FIG. 56 shows the developed zone geometry. At an angle θ the true wedge semi-angle $\frac{\phi}{2}$ is given by,

$$\frac{\phi}{2} = \frac{1}{R} \cdot \frac{d}{d\theta}\left(\frac{W}{2}\right) = -\sin\theta . \tan\frac{\phi_2}{2}$$

The zone profile was thus sinusoidal.

7. 5. Details of simulative die blocks.

Table 6 gives die-block details. The test-plan required nine die-blocks for complete simulation and three die-blocks for 'bending only' simulation.

The die blocks were manufactured in a Vanadium - Molybdenum air hardening tool steel noted for its gauge-holding properties. After heat-treatment to 60 - 62 Rockwell C, the elements of each die block were ground on all external surfaces. The dies were then assembled and diamond-paste polished prior to use.

7. 6. Test-rig for simulated redrawing.

(a) Details of rig.

FIG. 57 shows two elevations of the test rig. The test-piece (1) was drawn around the simulative die-block (2) by a gripping dog coupled through a load-cell to the moving arm of the testing machine. Die blocks were mounted in a housing (3) , being located by shoulders fitting in slots and secured by a single screw. Simulation of draw angle was achieved by rotating the housing relative to the fixed axis of the testing machine arm. This was effected by mounting the housing (3) in a cradle-type structure (4) with two transverse pins, the rear pin being removable and allowing the housing to be rotated into either 90, 60 or 45 degree positions. The cradle (4) also acted as a slide in the slideway (5), and could be adjusted horizontally by the screw wheel (6), so that in any angular configuration the test-piece was always pulled in line with the gripping dog.

TABLE 6 - DESIGN DATA FOR SIMULATED REDRAW DIE BLOCKS.

Design Parameters	$W_1 = 0.75$ in. $t = 0.036$ in.							
	R/t	R in	θ°	$\phi_2{}^\circ$	W_1/t	W_2/t	W_2 in	$1-\frac{W_2}{W_1}$ %
Complete simulation	15	0.540	90	20	20.8	15.5	0.558	25
	15	0.540	60	20	20.8	18.1	0.651	12.7
	15	0.540	45	20	20.8	19.3	0.695	7.41
	10	0.360	90	20	20.8	17.3	0.624	16.9
	10	0.360	60	20	20.8	19.0	0.684	8.45
	10	0.360	45	20	20.8	19.8	0.713	4.95
	5	0.180	90	20	20.8	19.0	0.684	8.45
	5	0.180	60	20	20.8	19.9	0.715	4.23
	5	0.180	45	20	20.8	20.2	0.726	2.47
Bending only simulation	15	0.540	90 60 45	0	20.8	20.8	0.750	0
	10	0.360	90 60 45	0	20.8	20.8	0.750	0
	5	0.180	90 60 45	0	20.8	20.8	0.750	0

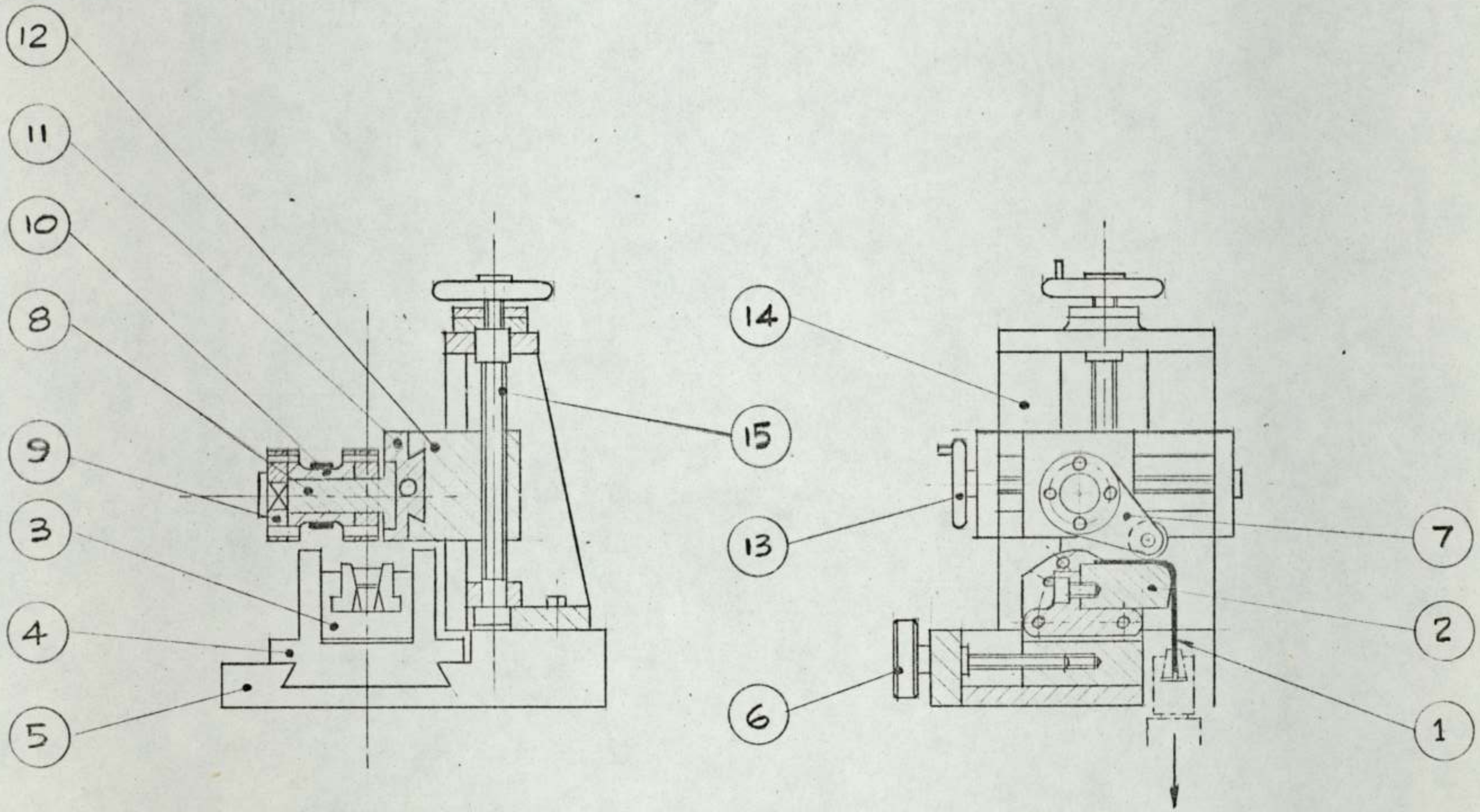

FIG. 57 TEST RIG FOR SIMULATED REDRAWING
(Scale $\frac{1}{4}$ actual size.)

Splaying of the test-piece during deformation was prevented by a roller housed in an arm (7), the arm being a free fit on the shaft (8) which carried a square projection at its outer end. The projection acted as a key for a square hole in plate (9) which was thus prevented from rotating. A strain-gauge torque-cell (10) was rigidly connected between the arm (7) and the plate (9), the bore of the torque-cell being in clearance on the shaft (8). During a test the position of shaft (8) was fixed so that splaying in the test-piece tended to rotate arm (7), inducing elastic torsion in the torque-cell proportional to the splay severity.

The test-rig structure supporting the torque-cell was used to maintain the arm (7) in constant position relative to the die-block for all configurations. To achieve this the arm was capable of horizontal, vertical and rotational movement. Horizontal motion was achieved by securing the shaft (8) in a cross-slide (11) which could be moved in slideway (12) by the wheel (13). The horizontal slideway (12) was itself the vertical slide, and moved in slideway (14) under the action of screw (15). Rotational arm movement was achieved by indexing the torque-cell to either 90, 60 or 45 degree positions where it was locked securely.

Photograph FIG. 58 shows a general view of the test-rig.

(b) Torque-cell.

Owing to the failure of the simulation method the torque-cell could not be used to supply useful information. Its design features are therefore only briefly recorded.

The torque-cell was designed in alloy tool steel for a maximum shear strain of 0.10% corresponding to a shear stress of 12 x 10^3 lbf./in^2. To maintain lift-off at the roller low, a gauge length of ½ in. was selected together with a gauge diameter of 1 in. Maximum torque was envisaged when drawing work-hardened stainless steel, and the maximum fixing moment required for bending only, was calculated to

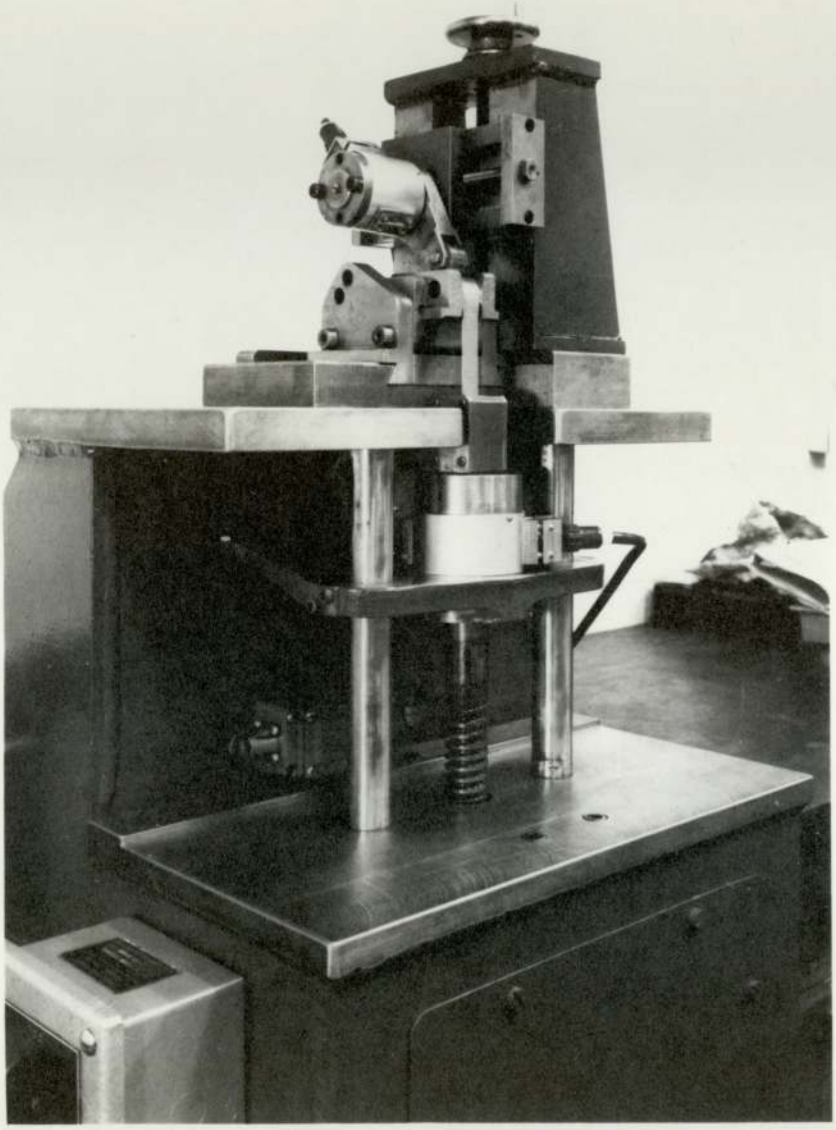

FIG. 58 TEST RIG FOR SIMULATED REDRAW PROGRAMME.

56 lbf. in. It was then possible to compute the torque in the cell in terms of the ratio; length of torque-cell lever arm/distance of roller from point of bending. This ratio was made 2in./$\frac{1}{8}$in. giving a torque of 896 lbf/in^2. Knowing torque, shear stress and gauge diameter the torque-cell wall thickness was calculated to 0.050 in.

Four foil-type torque electric resistance strain gauges each of 200 Ω $\pm$ 0.2 % were bonded to the centrally located gauge area and wired to form a full Wheatstone bridge with one gauge in each arm of the circuit. The gauges were symmetrically positioned around the torque-cell circumference so that adjacent gauges measured the principal strains e_1 , e_2 respectively located at $\pm$ 45 degrees to the torque-cell axis.

The procedure for strain gauge bonding and wiring was similar to that for the dog load-cell already described in appendix A_2. 4.

FIG. 59 is a view of the completed torque-cell with cover removed.

7. 7. Experimental results.

(a) Initial tests.

Tests were carried out initially with the 0.540 in. radius 90 degree angle die-block since this gave the largest reduction in test-piece width and would therefore best reveal any deficiencies in the method of simulation. The tests were conducted with half-hard aluminium. It was found that as the test-piece entered the convergent radial drawing passage its edges commenced to curl upwards, producing a shallow channel section, with the central bulk of the test-piece remaining undeformed. On advancing into the zone the sides of the channel became deeper as illustrated in FIG. 60 a. The curling effect was considered due to the radial component of the die-pressure force, not the transverse component normally associated with wrinkling in deep drawing operations. Although this radial component was small, the

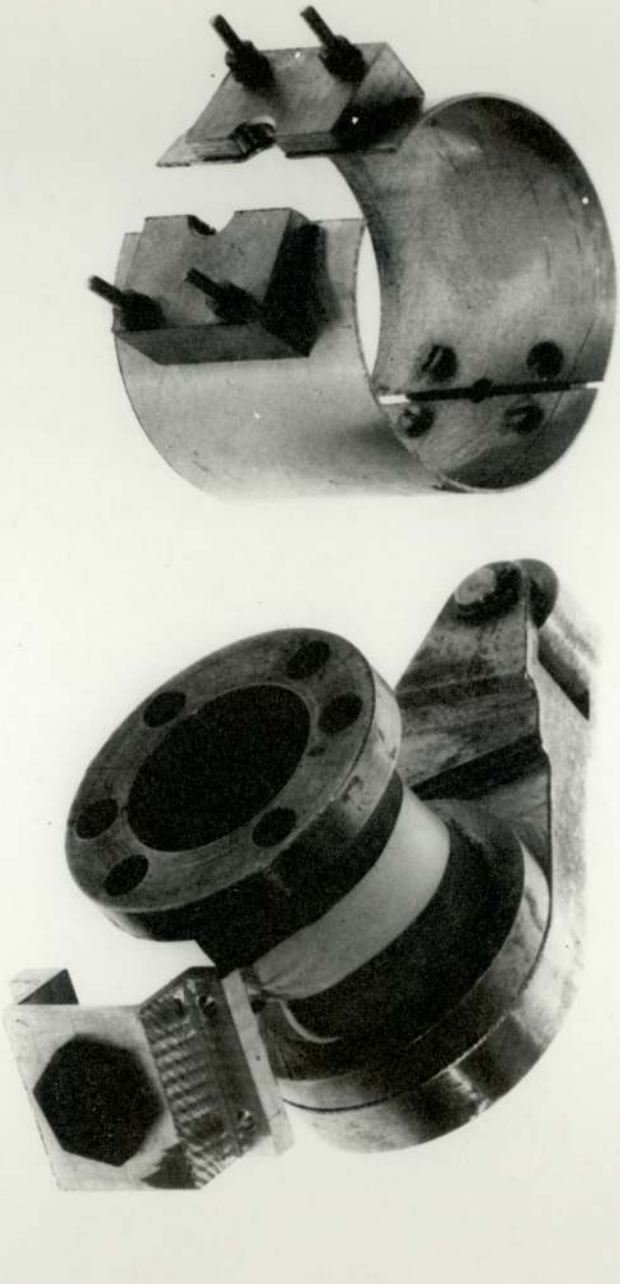

FIG. 59 TORQUE-CELL WITH COVER REMOVED

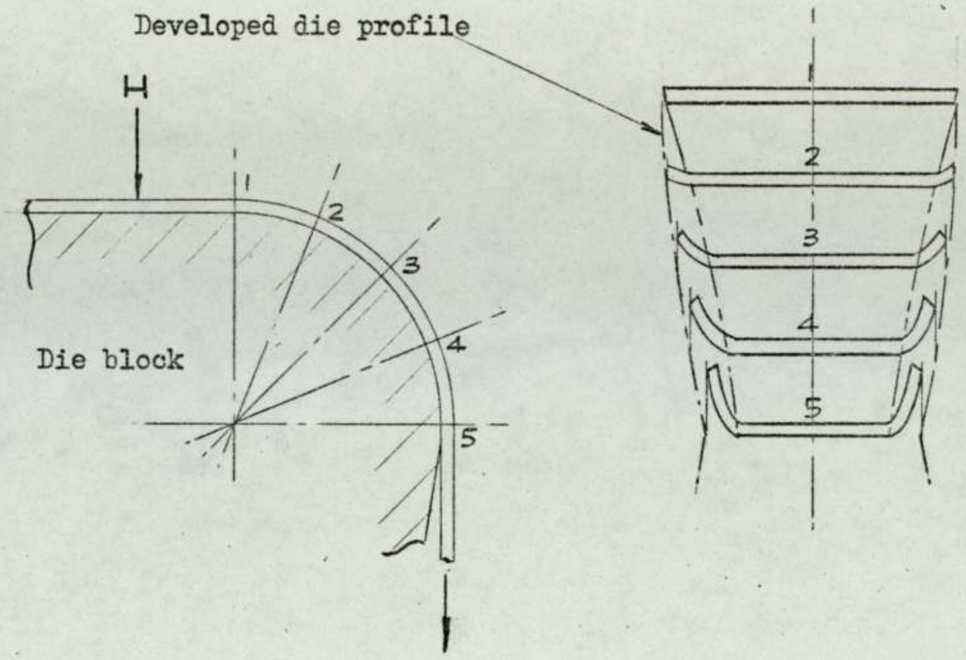

(a) without hold-down

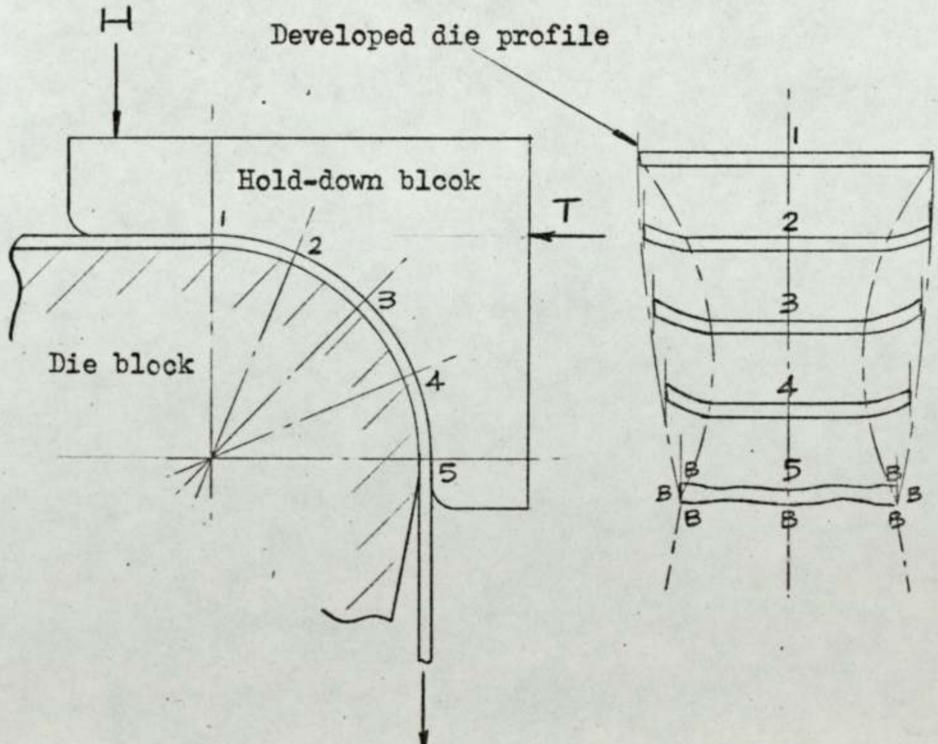

(b) with hold-down

FIG. 60 TYPICAL RESULTS IN SIMULATION TESTS test-piece cross-section was weak from a bending aspect, and once the mechanism commenced and a channel section formed the process became cumulative.

There was nothing in the simulative test to represent die contact at exit from the initial radial drawing zone. To remedy this situation a roller mounted in a cradle was positioned at the point of die-block exit, the radial gap between roller and die-block being just greater than test-piece thickness. With this arrangement it was found that the test-piece edge curled as before and on reaching the roller ironing occurred causing a load which resulted in tag failure.

Test-pieces were prepared with sides angled at 10 degrees so as to accurately fit the entry passage of the die block (previous test-pieces had square edges). Little benefit was gained from this procedure with 0.036 in thick specimens so a test was conducted with an 0.064 in. thick side-angled brass specimen. Curling still occurred.

Test-pieces were drawn on various die-block configurations but results were always similar. Grids marked on test-pieces before drawing clearly showed that no radial drawing occurred. Unless this element could be introduced to the test the simulation was a failure.

(b) Introduction of a hold-down clamp.

A hold-down clamping arrangement was designed with a view to eliminating the edge curling effect and promoting true radial drawing conditions. For preliminary tests a single clamp for use with the 0.540 in. radius - 90 degree angle die block was made, but the clamp support was of adjustable design and capable of accommodating all of the various simulated redraw configurations. FIG. 61 shows this design. The test-piece (1) was drawn over the die-block (2) and prevented from curling by the hold-down clamp(3). Vertical location for the clamp was supplied by the torque-cell lever arm (4), whilst horizontal location was given by the clamp shoe (5). The clamp shoe was pivotted on a pin attached to a slider (6), a needle bearing being included to

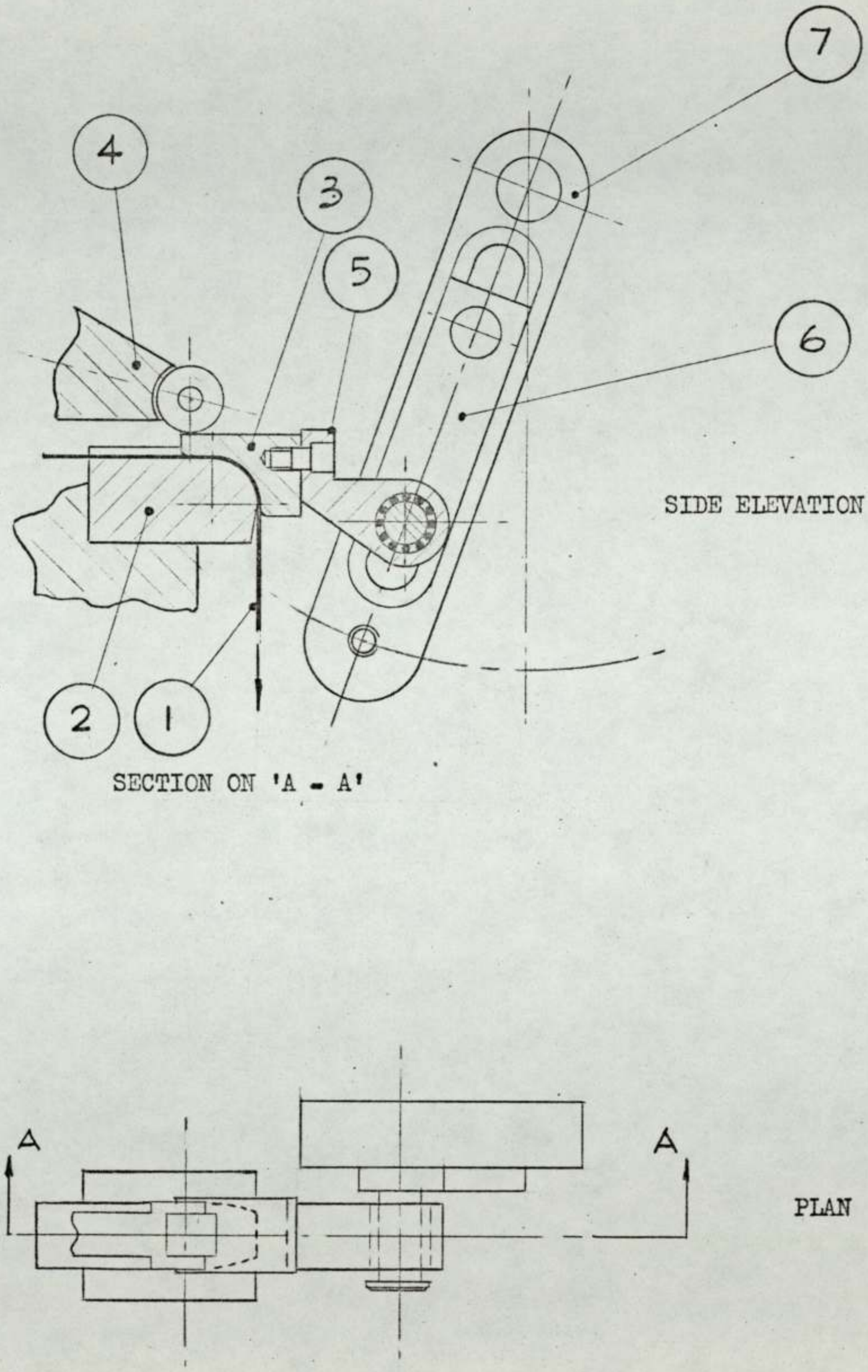

FIG. 61 SIMULATED REDRAWING WITH HOLD-DOWN

reduce friction. The slider was adjustable along a slot in link (7) and could be locked in any required position, whilst the link itself was pivotted at its upper end and was adjustable through an arc. When setting up for drawing the die block exit was aligned with the drawing arm of the testing machine and components (6) and (7) adjusted so that the gap between die-block and clamp at entry and exit was just greater than the test-piece thickness.

At this stage of the investigation it was apparent that simulative test results would be of dubious applicability to splaying, since even if the clamp successfully suppressed edge-curling and promoted true radial drawing conditions it could not with certainty be determined what proportion of torque measured at the torque-cell was due to radial drawing effects and what proportion was due merely to suppressing curling.

(c) Drawing with a hold-down clamp.

Fracture of the test-piece tag always occurred when drawing with the clamp in position. By altering the length of the transition region from $\frac{1}{2}$ in. wide tag to $\frac{3}{4}$ in. wide testpiece it was possible to vary the point at which deformation started. It was found that the failure mode depended upon this point.

When a long transition was used the test-piece first contacted the die-block profile near the exit and it was there that deformation commenced. Due to the geometry of the die-block, the side-angle was negligible at this point and thus no curling occurred. Instead regions of plastic deformation occurred on either side of the testpiece with the central part remaining rigid. This non-uniform deformation caused excessive edge thickening, and a build-up of material at entry to the die throat. The clamping arrangement was rigid at this point, and as the built-up region became ironed between die-block profile and clamp the draw load developed was sufficient to fracture the tag.

When a short transition was used deformation first commenced at the die entry, where the side angle was a maximum and therefore most likely to cause curling. It was found that the slight elastic deflections which occurred in the torque-cell and test rig were sufficient to allow the test-piece to curl slightly but some radial drawing was observed. The curled part moved around the die-block profile and was ironed near the exit, the ironing causing an increase in draw load with ultimate tag fracture. Deformation stages are illustrated in FIG. 60 b, where the letter B indicates burnished areas observed on fractured test-pieces.

7. 8. Termination of simulative test-programme.

The die-blocks did not adequately simulate that region of deformation in a cup involved in splaying, and it was clear that radical changes in die-block design and test-piece width/thickness geometry were required to obtain a reasonable simulation. The extra effort required to achieve this end could not be justified in terms of probable success. Therefore further work in this direction was suspended, and would have been restarted only if difficulties arose in later theoretical studies of splaying. It transpired that this was unnecessary.

8. SECOND EXPERIMENTAL PROGRAMME - SPLAY MEASUREMENT TESTS.

8.1. Introductory comments.

The programme was primarily designed to provide information on the mechanics of splaying in redrawing taking account of all principal process parameters. Experimental information was required on when splaying commenced from steady-state conditions, the splayed cup profile at any stage during the splay phase, and conditions which marked the termination of splaying.

It was also considered important to investigate the precise way in which splaying influenced redraw load.

A literature survey had shown there was a difference of opinion on the effects of using a guide-ring to prevent splaying. It was intended to clarify this situation.

8. 2. Evaluation of test variables.

(a) Test-piece material.

It was proposed to conduct experiments with low carbon steel, austenitic stainless steel, 70/30 brass and aluminium. Low carbon steel was selected because of its extensive use in deep-drawing and also because it exhibited medium work-hardening characteristics. Stainless steel and brass both possessed the property of a high work-hardening rate, and there was some evidence to suggest that both were prone to splaying. No evidence was available on the splaying characteristics of aluminium but this material was noteable for its low work-hardenability.

(b) Prior cold-work in test-piece.

It was considered important to observe the effect of current strain level on splaying since this factor would in all probability be closely related to fracture due to splaying. Three levels of strain were designated; zero (fully annealed), 0.7, and 1.1. A strain of 0.7 corresponded to a cold-reduction of 50 % and was approximately equivalent to the strain in a first-stage cup. A strain of 1.1

corresponded to a reduction of 67 % and was roughly the maximum strain induced by deep-drawing at Tube Investments.

(c) Test-piece geometry and size.

It was required to conduct tests for conditions of constrained and unconstrained redrawing. The single most important parameter governing the need for a hold-down punch was known to be test-piece diameter/thickness ratio although die angle and redraw reduction were also influencial. As a result of previous experience it was considered that constrained redrawing would become necessary in or above the diameter/thickness range 60 -80. The following six levels of diameter/thickness ratio were therefore chosen for investigation;

20, 30, 40, 60, 80, 100.

Preliminary theoretical studies (section 4) had led to the conclusion that splaying would not be influenced by overall redraw reduction. It was however advantageous to make this parameter reasonably large from an aspect of introducing variable tool geometry. A nominal reduction of 30 % was thus selected. Testing procedures were simplified by adopting a standard outside diameter for test pieces. The only remaining consideration for calculating test-piece size was the 2 Tonf. maximum draw load limitation of the testing machine. Maximum loads were envisaged when drawing the stainless steel test-pieces of 67 % cold-work and 20/1 diameter/thickness ratio. As a result of load calculations it was concluded that a test-piece outside diameter of $\frac{3}{4}$ in. would be satisfactory.

(d) Die geometry.

On the basis of a 30 % redraw reduction die throat diameter was fixed at 0.527 in. Previous theoretical work had indicated that die profile might be important in influencing splaying, especially in unconstrained redrawing. The effect of this parameter was studied by selecting die angles of 90, 60, 45 and 30 degrees. By making die throat radius constant, independent of test-piece thickness, only four dies were required for the complete programme. Throat radius was designated 0.110 in. and was a compromise between a large bending radius/wall thickness ratio for the thin-walled test-pieces, and a correspondingly small ratio for the thicker test-pieces. Chung and Swift had shown that this variable could influence drawing stress, but the action taken was considered justified in that experiments were designed to show changes in drawing stress due to splaying within a particular redraw, rather than the effect of tool geometry.

(e) Hold-down punch geometry.

Hold-down punch geometry in constrained redrawing was believed to be an important parameter influencing splaying, since it directly affected deformation in that region where splaying developed. Before geometries for investigation could be specified a fundamental problem required solution: At what level of test-piece diameter/thickness ratio was a hold-down punch necessary? In view of the wide range of variables due for investigation the best way to answer this question was to redraw test-pieces in ascending diameter/thickness order and experimentally determine the particular value of diameter/thickness ($D/_t{}^*$) where wrinkling occurred. Having determined ($D/_t{}^*$), this and every D/t ratio above it, would require hold-down. For each constrained redraw arrangement three levels of bending/wall thickness ratio (Ro/to) were investigated, the largest value of which corresponded to the free-zone condition. This was estimated using a method given in appendix A_3. 1.

8. 3. Test-plan.

The programme was divided into two parts comprising unconstrained and constrained redrawing.

(a) Unconstrained (or free) redrawing programme.

Tests contained within the programme included,

(i) Splay measurement.

(ii) Redraw load measurement for unguided and guided arrangements.

(iii) Measurement of free deformation profiles to provide a comprehensive check on Fogg's theory.

(iv) Determination of diameter/thickness range limitation on free redrawing.

A test plan was designed to include process variables discussed in section 8. 2. In light of subsequent experimental data the plan was modified slightly. The final plan is summarised in table 7 , attention being drawn to the following aspects:

Each letter in the table symbolises a redrawing operation carried out on a separate test-piece, the actual letter denoting the test category.

It was found that wrinkling occurred at a diameter/thickness ratio of 80 with all materials and tempers drawn through the 90 degree semi-angle die. A diameter/thickness ratio of 60 was therefore taken as a maximum for the free-redraw programme.

Only one material (low carbon steel) was drawn through all dies to provide an experimental relationship between splaying and die-angle. It was assumed that similar relationships would hold for the other materials.

Comparisons of the effect of material properties on splaying behaviour were made with the 90 degree die.

It was found that redraw loads had been generally under-estimated, and this put certain tests beyond the rated capacity of the testing machine. The stainless steel programme was mostly affected. To maintain the original level of diameter/thickness ratio stages for steel a ratio of 25/1 was introduced to compensate for the loss of the 20/1 ratio.

Only one test piece failed to draw. This was brass with prior cold-work of 67 %.

(b) <u>Constrained redrawing programme.</u>

The test-plan for constrained redrawing could not be final-

TABLE 7 SPLAY MEASUREMENT TEST PROGRAMME.

TEST-PLAN FOR FREE REDRAWING.

Die semi-angle (deg.)		90			60	45	30
Test-piece material.	Test-piece initial diameter/ thickness ratio.	Prior cold-work (nominal) (%)			Prior cold-work (nominal) (%)	Prior cold-work (nominal) (%)	Prior cold-work (nominal) (%)
		0	50	67	50	50	50
Low carbon steel.	20	A. B. P.	overload	overload	overload	overload	overload
	25	A. B. P.	A. B. G. P.		A. B. P.	A. B. P.	A. B. P.
	30		A. B. G. P.		A. B. P.	A. B. P.	A. B. P.
	40		A. B. G. P.		A. B. P.	A. B. P.	A. B. P.
	60		A. B. G. P.		A. B. P.	A. B. P.	A. B. P.
70/30 brass.	20	A. B. P.	A. B. G. P.	Redraw fracture			
	30		A. B. G. P.				
	40		A. B. G. p.				
	60		A. B. G. P.				
T304 stainless steel.	30	A. B. P.	overload	overload			
	40	A. B. P.	A. B. G. P.				
	60		A. B. G. P.				
Pure aluminium.	20	A. B. P.	A. B. G. P.	A. B. P.			
	30		A. B. G. P.				
	40		A. B. G. P.				
	60		A. B. G. P.				

A = Splay measurement test.

B = Redraw load-travel test. (unguided)

G = Redraw load-travel test. (guided)

P = Deformation profile measurement test.

ised until the 'free' programme was completed and data analysed. It was then possible to calculate hold-down punch profile radii and design punches for the appropriate test-piece diameter/thickness ratio levels. Two basic tests were carried out in the programme;

(i) Splay measurement.

(ii) Redraw load measurement for guided and unguided arrangements.

The final test-plan is summarised in table 8, the only divergence from the original programme being due to difficulties in preparing test-pieces. The actual nature of the difficulties is discussed in section 8. 7.

8. 4. Methods of data collection.

(a) Basis of splay measurement test.

Instrumentation was required to measure the current splayed profile and relate the test-piece rim to a fixed datum (e.g. the die surface) with the test-piece under full draw load conditions. It was concluded that equipment to carry out this function during actual redrawing would be complicated, and that by employing an incremental approach to the problem results would be more easily obtained. By this method the cup would be drawn into the die in stages and splaying recorded between stages with a measuring unit incorporated in the die assembly. The method also showed the advantage that any particular part of the splay phase could be given extra-close scrutiny if required. An objection to the technique was that splaying was not being measured under identical conditions to which it occurred during continuous redrawing. However the self-locking mechanism of the test-machine drive meant that the draw load would be retained even though the machine was static. No serious errors in splay measurement were therefore visualised. It was planned to carry out splay measurement with a single-point stylus which could be adjusted relative to the test piece; radially for splay measurement, circumferentially for mean splay measurement, and axially for distance

TABLE 8 SPLAY MEASUREMENT TEST PROGRAMME

TEST-PLAN FOR CONSTRAINED REDRAWING

Die semi-angle 90 deg.						
Test-piece material.	Test-piece initial diameter/thickness ratio.					
	100				80	
	Bending ratio around hold-down punch profile (R_o/t_o)	Prior cold-work (nominal) (%)			Bending ratio around hold-down punch profile (R_o/t_o)	Prior cold-work nominal (%)
		0	50	67		50
Low carbon steel	4.45		A. B. G.		4.75	A. B.
	5.76	A. B.	A. B. G.	A. B.	5.83	A. B.
	7.07		A. B. G.		6.90	A. B.
70/30 brass	4.45	test-pieces failed to press tag.			4.75	A. B.
	5.76				5.83	A. B.
	7.07				6.90	A. B.
T304 stainless steel	4.45		A. B. G.		4.75	A. B.
	5.76	A. B.	A. B. G.	A. B.	5.83	A. B.
	7.07		A. B. G.		6.90	A. B.
Pure aluminium	4.45		A. B. G.		4.75	test-pieces defective.
	5.76	A. B.	A. B. G.	A. B.	5.83	
	7.07		A. B. G.		6.90	

A = Splay measurement test B = Redraw load-travel test (unguided) G = Redraw load-travel test (guided) location measurement. A high degree of accuracy in the instrument was required to ensure consistent measurements.

(b) Basis of redraw load-measurement test.

Redraw load was measured by a strain-gauge load-cell connected in the testing machine draw arm. Although this load could be monitored before and after a series of splay-measurement readings to check for any load relaxation, it was considered better to obtain load measurements from continuous drawing tests. This meant that to correlate splaying with redraw load for any particular drawing arrangement, tests were necessary on at least two separate test-pieces. However due to their method of manufacture, dissimilarity in test-pieces was considered negligible.

The splay measurement tests provided information on the splayed form in terms of the test-piece rim distance from a fixed datum. Therefore if redraw load could also be measured in terms of test-piece rim position it would be possible to observe variations in redraw load with splaying. It was planned to achieve this result by coupling a displacement transducer to the test-piece rim and recording its output signal simultaneously with that from the load-cell on continuous data recording equipment during a continuous redraw test.

(c) Free-profile test.

The object of the test was to measure the redraw deformation profile. To achieve this the redrawing operation was interrupted during steady-state conditions and the testing machine drive reversed to lift the test-piece deformation zone clear of the die. Measurement of the profile was then made with the instrument used for splay measurement.

8. 5. Form of test-piece.

It was considered an advantage for test-pieces to possess uniform mechanical properties and dimensions throughout their length for it would then be possible to study splaying in terms of basic process parameters without the added complications that variations in these factors would bring. On the question of uniformity a redrawn cup is not outstanding. Due to its manufacturing route different strain histories exist along its length resulting in variations in wall thickness and yield strength, which conspire to produce a rising redraw load/punch travel characteristic. This type of load curve is not conducive to a ready appreciation of the effect of splaying on redraw load, and it was considered better to draw test-pieces which achieved steady redraw load conditions prior to the commencement of splaying, since then it would be far easier to discern the effect of splaying on load. A further complication with redrawn cups was that anisotropy may give rise to variations in wall thickness around the cup circumference and produce distortion in the cup rim. These effects were undesirable from a splay measurement aspect. Attention was therefore turned to the possibility of redrawing specially end-reduced tubular test-pieces by pulling through a die by means of a gripping dog.

It was clear that tubes would fulfil test requirements better than drawn cups on the grounds of, uniformity of wall, uniformity of mechanical properties, and negligible planar anisotropy. There remained however the consideration of whether or not the proposed drawing method truly represented actual cup redrawing conditions, since really tube-sinking was being substituted for redrawing. It was concluded that from a splaying aspect the substitution was valid. FIG. 62 shows free and constrained cup redrawing in diagrams (a) and (c) respectively, whilst the corresponding experimental drawing methods are shown in diagrams (b) and (d). Hill[17] has pointed out that in terms of mechanics of deformation at the die, sinking and redrawing processes are identical. There are practical differences observed between the two processes but these are related to degree rather than type.

8. 6. Test-rig and related instrumentation.

(a) General description.

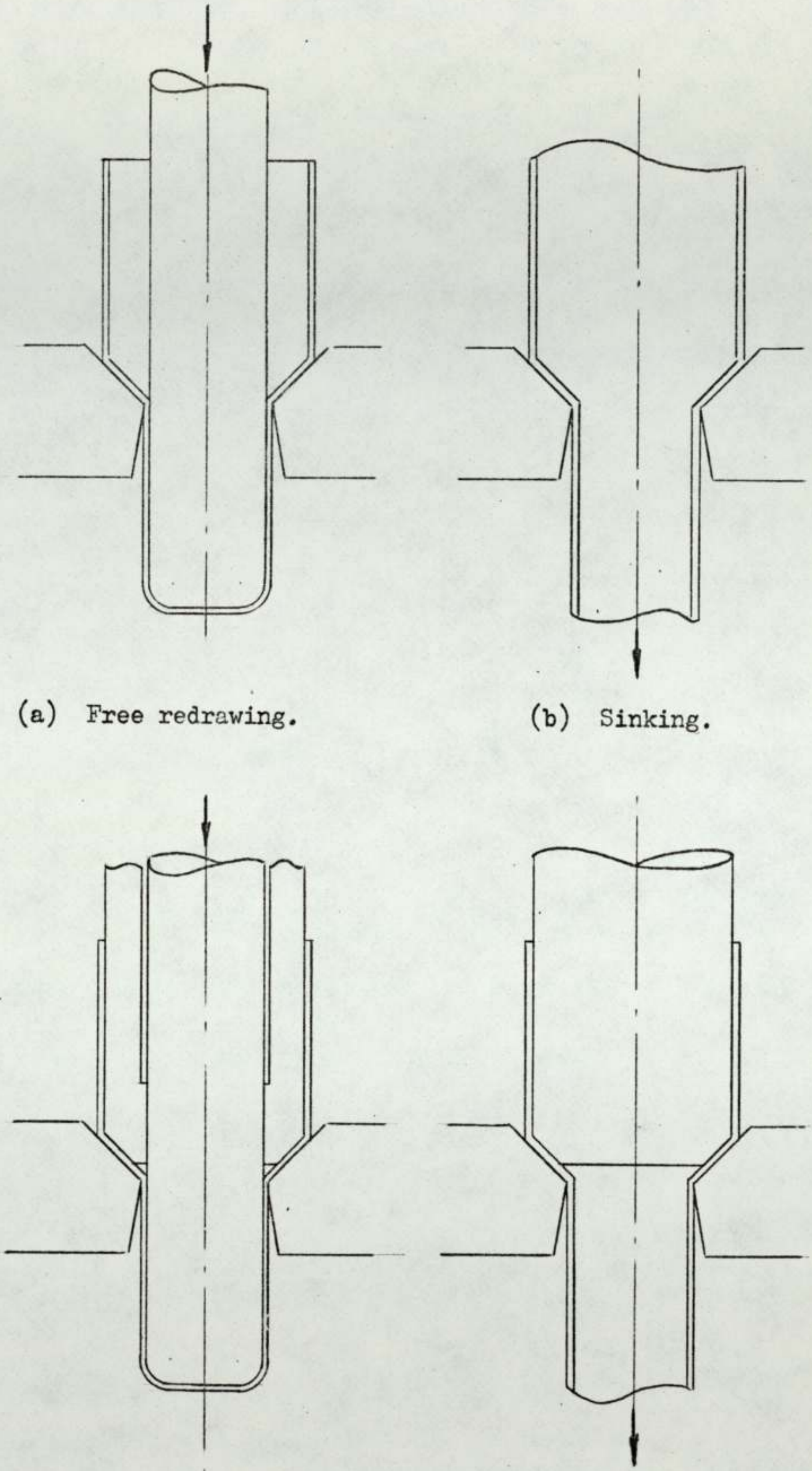

(a) Free redrawing. (b) Sinking.

(c) Constrained redrawing. (d) Constrained sinking.

FIG. 62 SIMULATION OF REDRAWING IN SPLAY-MEASUREMENT TEST PROGRAMME.

FIG. 63 shows a sectional view of the splay measurement test-rig arranged for free redrawing. The rig was mounted on a sturdy base plate (1) which was bolted to the upper platen of the testing machine. A bolster (2), attached to the base plate, was provided with an inner recess for precisely locating the redraw die (3), through which the test-piece (4) was drawn by the dog of the testing machine (5). The bolster was also provided with an outer recess which located an annular ring (6), the ring being in clearance with the die but a precise rotational fit in the bolster. A retaining plate (7) provided axial constraint on the ring, and was graduated in 30 degree intervals around its upper surface to provide angular reference as the ring (6) was rotated. Two vertical columns (8) were mounted, diametrically opposed, from the upper surface of the ring (6). The columns were of identical diameter and length, their parallelism being ensured by precision registers in the ring (6) and upper platen (9). In addition to aligning the columns the upper platen served to support various pieces of test equipment, details of which are given subsequently.

A platen (10) was captive on the vertical columns and carried two micrometers situated 180 degrees apart. Micrometer (11) was vertically mounted, of 0 - 1 in. range and graduated in 0.001 in. divisions. This micrometer was used as a jack to position the platen (10) accurately relative to the die surface, a ball attachment being fitted to the spindle end to reduce friction when the assembly was rotated around the die. A second micrometer (12), graduated in 0.0001 in. divisions with a range of ½ in., was used for splay measurement, and caused a stylus (14) to move into contact with the test-piece via a sensing head (13). The design of this assembly was critical to splay measurement accuracy and its development is discussed separately below.

(b) Splay-measuring head.

(i) Development of design.

The design was aimed at fulfilling two essential

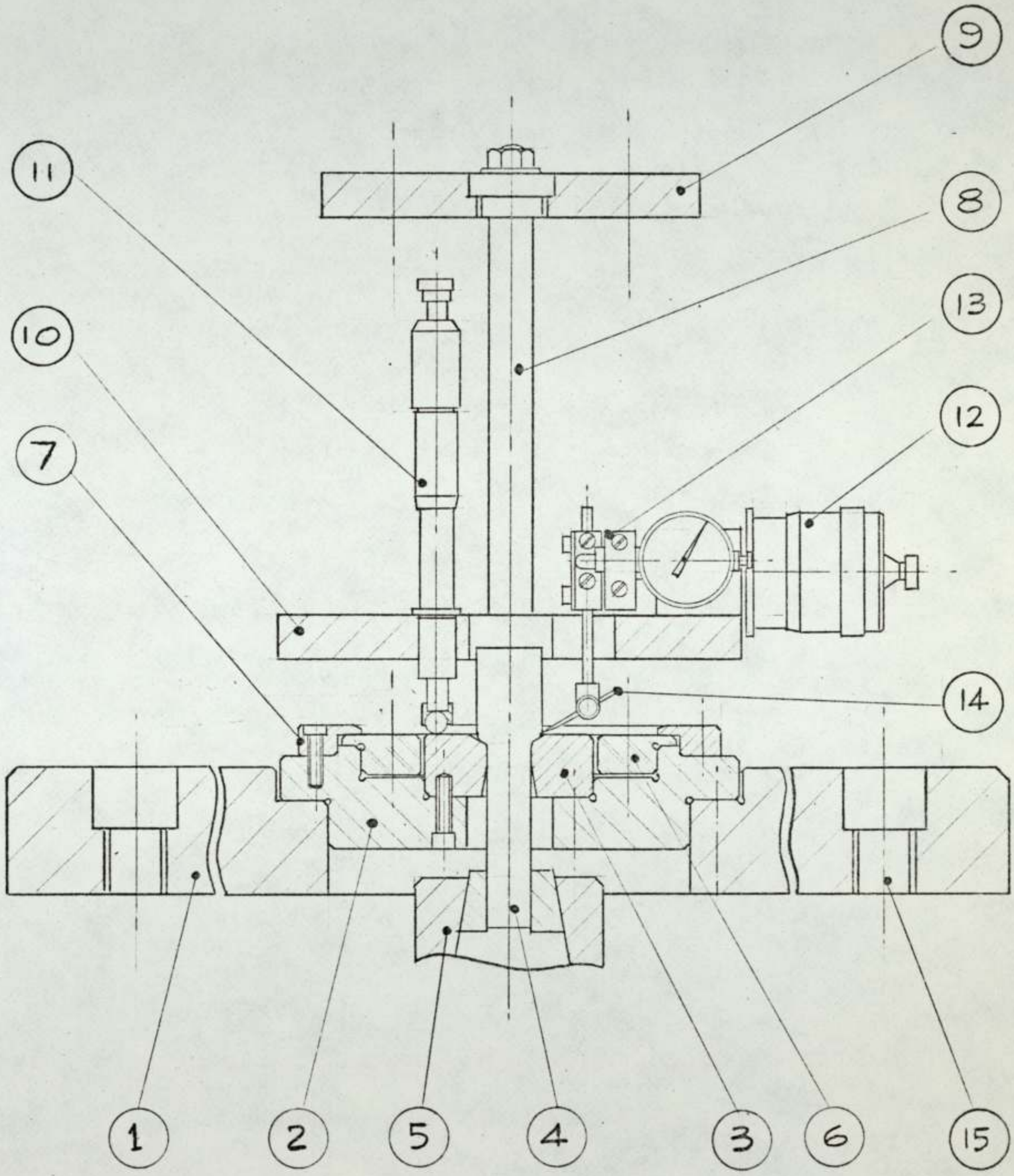

FIG 63 SPLAY MEASUREMENT RIG
(Scale approximately $\frac{1}{2}$ full size)

requirements;

(a) That all movement of the micrometer spindle should be transmitted to the stylus.

(b) That readings of splaying should be taken from the micrometer always when the same light force was applied to the stylus tip by the test-piece.

The original design for achieving these requirements is shown in FIG. 64 where the housing block (1), rigidly pinned to the moving platen of the test-rig, carried the micrometer(2) and a traverse plate (3), the former being a fixture and the latter a sliding fit. The traverse plate was maintained in constant contact with the micrometer spindle (4), and also prevented from rotating, by two spring loaded pins (5). A stylus plate (6) was coupled to the traverse plate (3) by pins (7) which allowed 0.030 in. relative axial movement against the pressure of an internally located spring. The stylus arm (8) was a precise fit in a central hole in the stylus plate (6) and could be locked by means of clamp (9) and locknut (10). The lower end of the stylus arm carried an adjustable holder (11) which clamped the stylus (12) in a variety of angular positions. Pressure sensing at the stylus tip was achieved as follows; When the stylus contacted the testpiece further rotation of the micrometer spindle caused the stylus plate (6) to move towards the traverse plate (3) and relative movement between these members was monitored by a dial gauge (14) operated by a contactor (13). The dial gauge was calibrated in 0.0001 in. divisions and would, it was anticipated, provide a sensitive method of ensuring a constant pressure at the stylus point when taking splay readings.

Unfortunately these expectations proved to be unfounded when tests were carried out, and it was found that reproducibility of readings could not be relied upon closer than 0.0004 in. Also, 0.006 in. travel at the micrometer was required to produce an indication of 0.0001 on the sensing gauge. This adverse ratio explained the poor

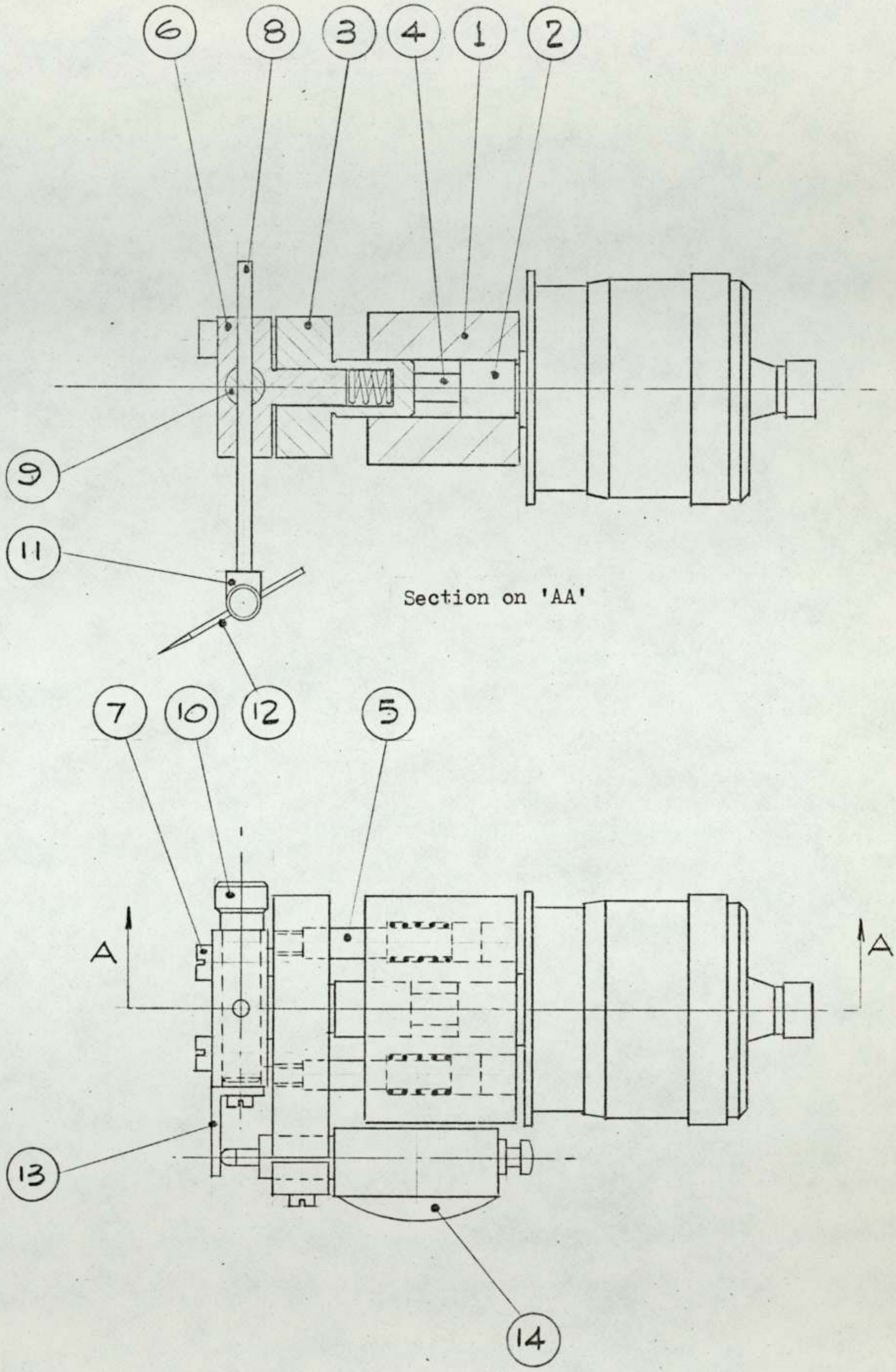

FIG. 64 ORIGINAL SPLAY MEASURING HEAD DESIGN

consistency in readings and was accounted for by deflection in the stylus arm. The source of the problem was that a force at the stylus point tended to rotate item (6) in item (3) causing increased resistance to stylus plate push-back. It was concluded that the design was unsatisfactory.

Little freedom was available for redesign of the measuring head due to limited space and access. The feature of an underslung stylus could not be avoided, and yet it was clear that a rotational tendency would be present with this arrangement. A design was therefore evolved which exploited the tendency. This proved highly successful and is shown in FIG. 65. A new stylus plate (1) was manufactured in duralumin and coupled to the existing traverse plate (2) by a 0.005 in. thick leaf spring,(3) the latter being rigidly clamped to each member, and pre-formed so that on assembly plate (1) lay back against plate (2). Two adjusting (4) screws were then used for setting the stylus arm inclination. Pressure sensing was achieved by the stylus plate rocking forward when the stylus contacted the testpiece, this in turn causing a deflection on the dial gauge. The device proved to be extremely sensitive and reliable over the experimental programme which involved some 18,000 readings. Reproducibility was to within 0.0001 in.

(ii) <u>Calibration</u>.

The splay-measuring head did not give readings of test-piece splaying directly but was a comparative device used in conjunction with standard calibration specimens. After arranging the test-rig for redrawing, a standard piece as shown in FIG. 66 was located in the die and a full set of reading taken with the measuring head at positions of height and angular displacement corresponding to those for the actual subsequent test. The current test-piece diameter during a test was then deduced by comparison. An important feature of the method was that errors in measurement arising from slight manufacturing inaccuracies were committed for both standard and test-piece, and therefore

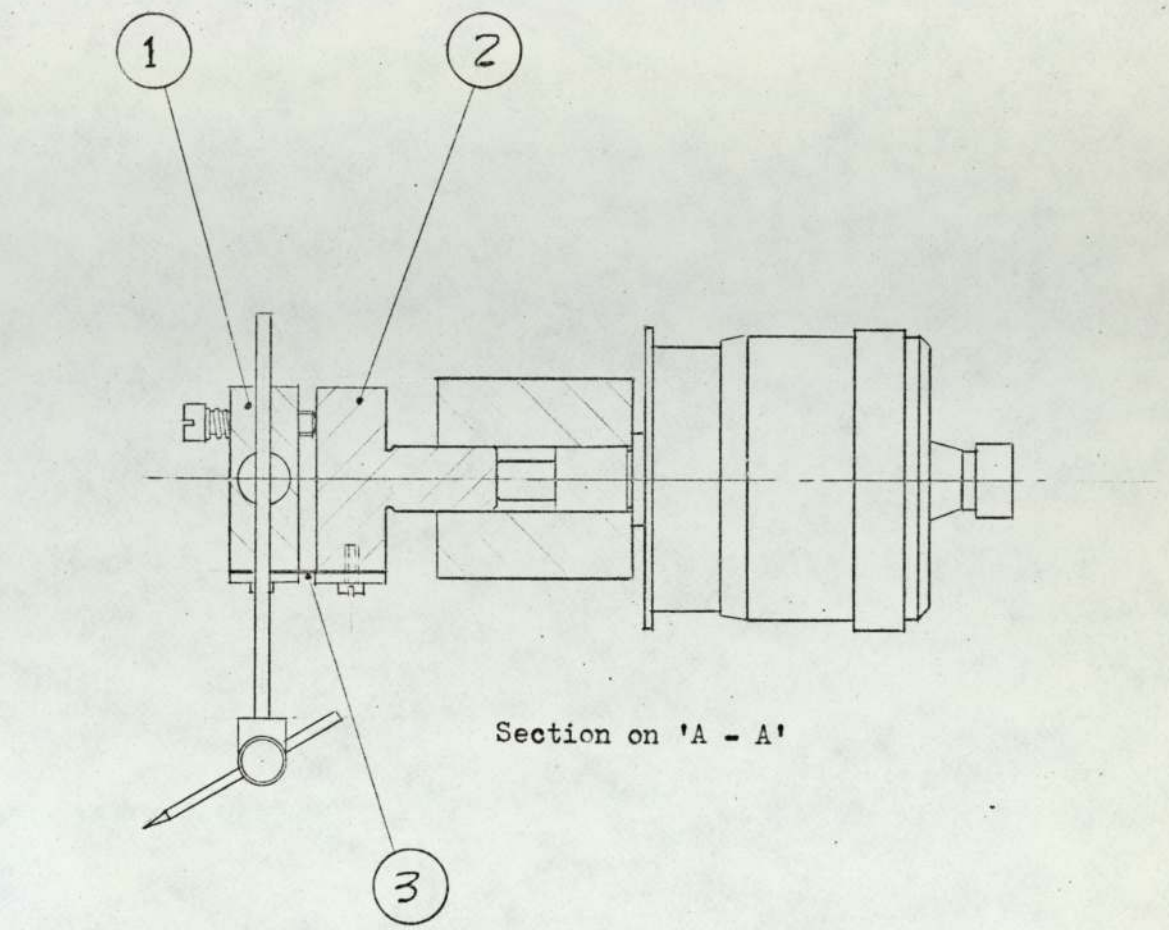

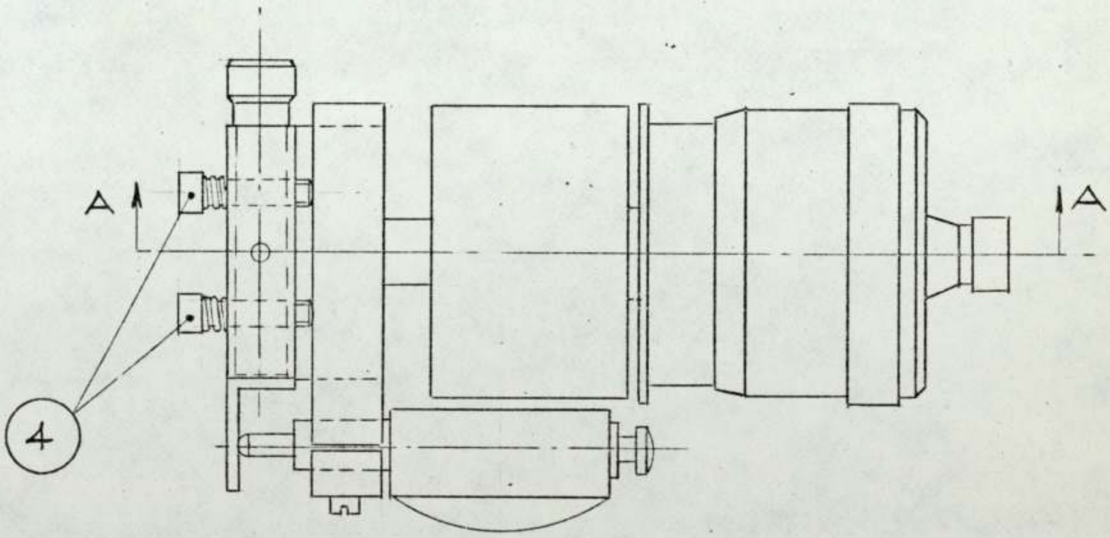

FIG. 65 FINAL SPLAY MEASURING HEAD DESIGN

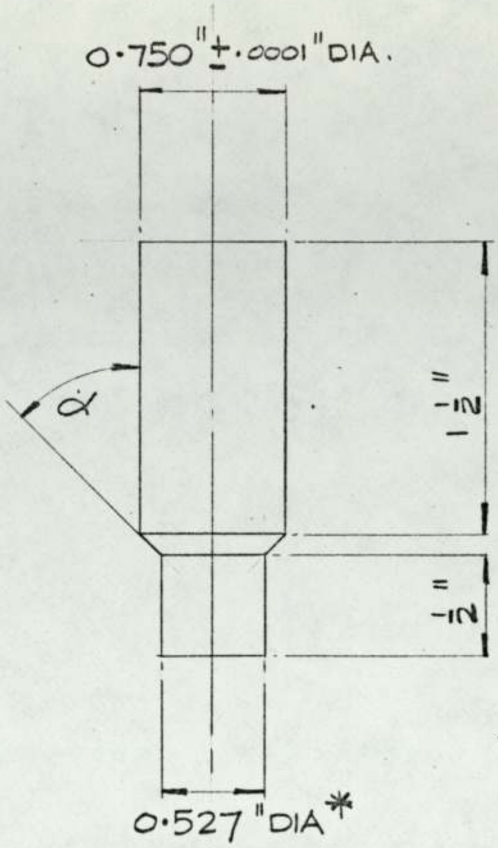

* To be precision fit in die throat

Semi-angle α (degrees)	90	60	45	30

FIG 66 SPLAY MEASUREMENT CALIBRATION STANDARDS

tended to be self cancelling.

(c) Arrangement for constrained and unconstrained redrawing.

FIG. 67 illustrates the test-rig arranged for unconstrained redrawing.

The arrangement for constrained redrawing is shown in FIG.68, with the hold-down assembly comprising an additional framework positioned around the splay measuring unit. Hold-down was of the constant clearance type and was applied by means of a cross-beam carried on two stout pillars, the latter being screwed into the test-rig base. Details of hold-down application are given in FIG. 69. The crossbeam (1) was provided with a centrally located screwed bore which took the nut (2), the lower end of which was attached to a ball. Pressure applied to the nut by a spanner was transmitted through the ball to a hold-down punch extension (3) which acted upon the interchangeable hold-down punch (4). Accurate alignment between punch and extension was ensured by a closely fitting spigot. The extension was aligned by a precision bush (5) located in the upper platen of the test-rig (6).

(d) Redraw load/test-piece rim displacement.

The method used for correlating redraw load with current test-piece rim position is shown in FIG. 70 for unconstrained redrawing. A dummy hold-down punch (1) was axially suspended from the test-rig upper platen (2), its diameter being less than the entering test-piece bore. A follower tube (3) was a loose sliding fit on the dummy punch and in falling freely always maintained contact with the test-piece (4). An arm on the follower tube entered a hole in the end fitting of a potentiometric displacement transducer plunger, the body of the transducer (5) being secured in the upper platen. With the micrometer platen (6) adjusted to its lowest position, and the follower tube resting upon the redraw die (7), the screw (8) was set to just contact the bottom of the plunger end fitting. This corresponded to the datum position for rim height measurement. Calibration of the transducer was then carried

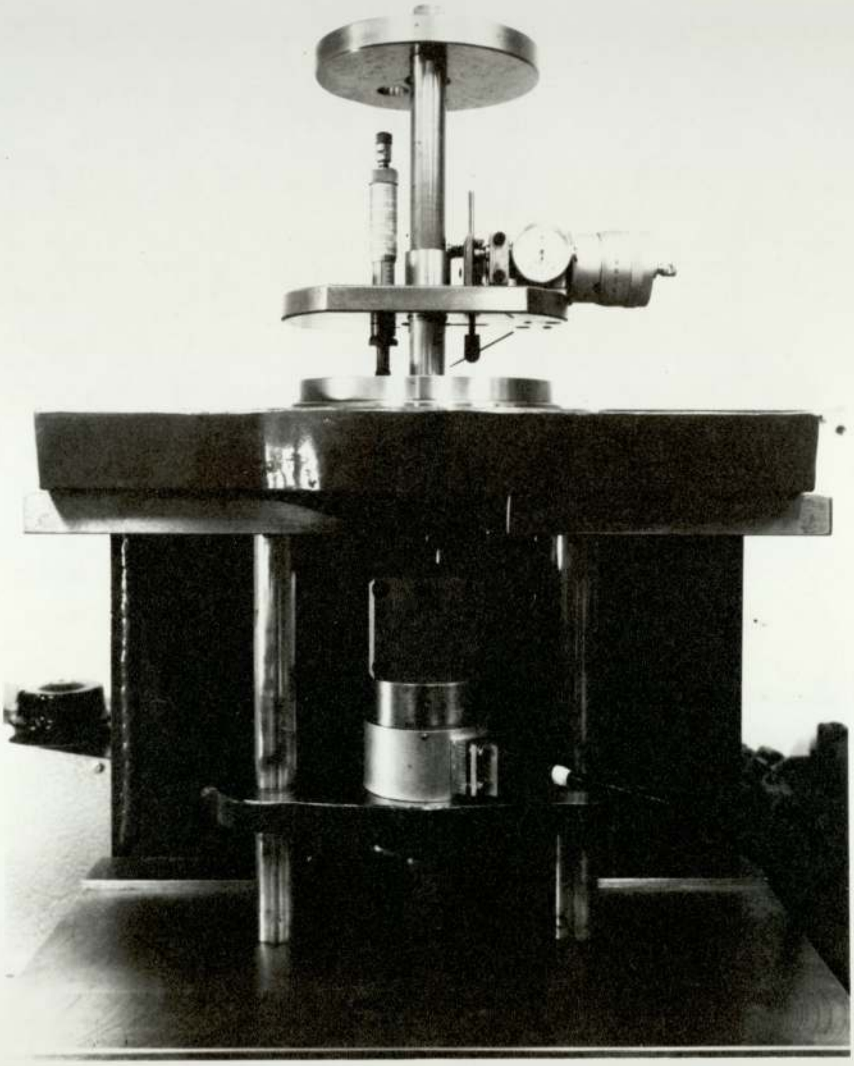

FIG. 67. TEST RIG FOR SPLAY-MEASUREMENT PROGRAMME ARRANGED FOR FREE REDRAWING.

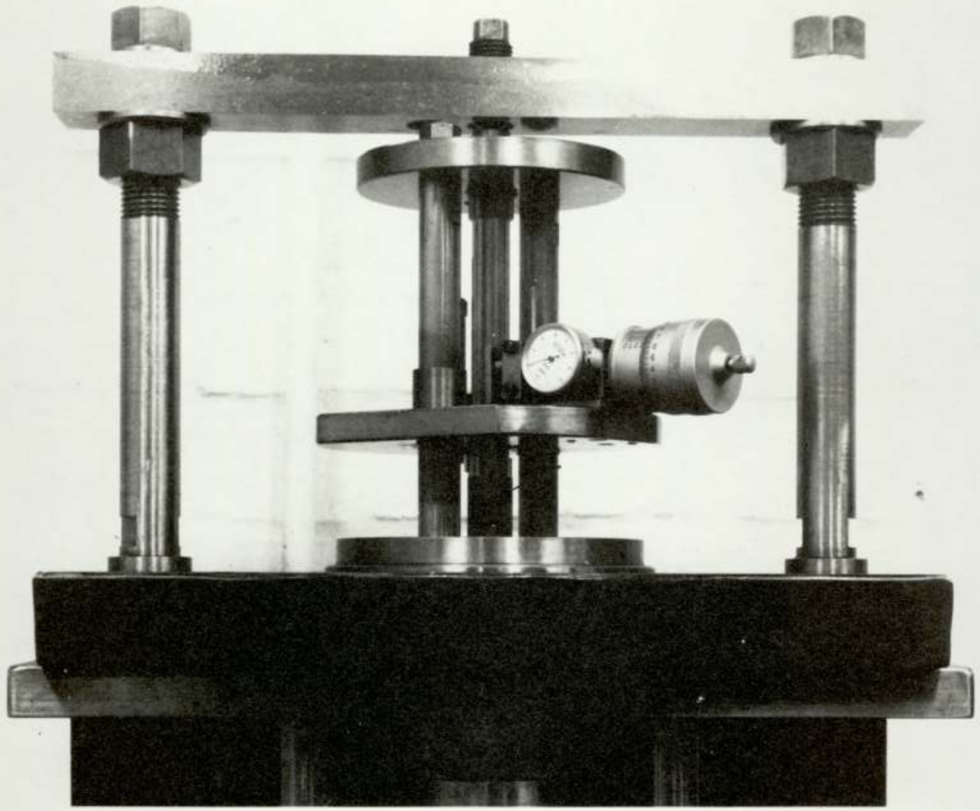

FIG. 68 TEST RIG FOR SPLAY-MEASUREMENT PROGRAMME ARRANGED FOR CONSTRAINED REDRAWING.

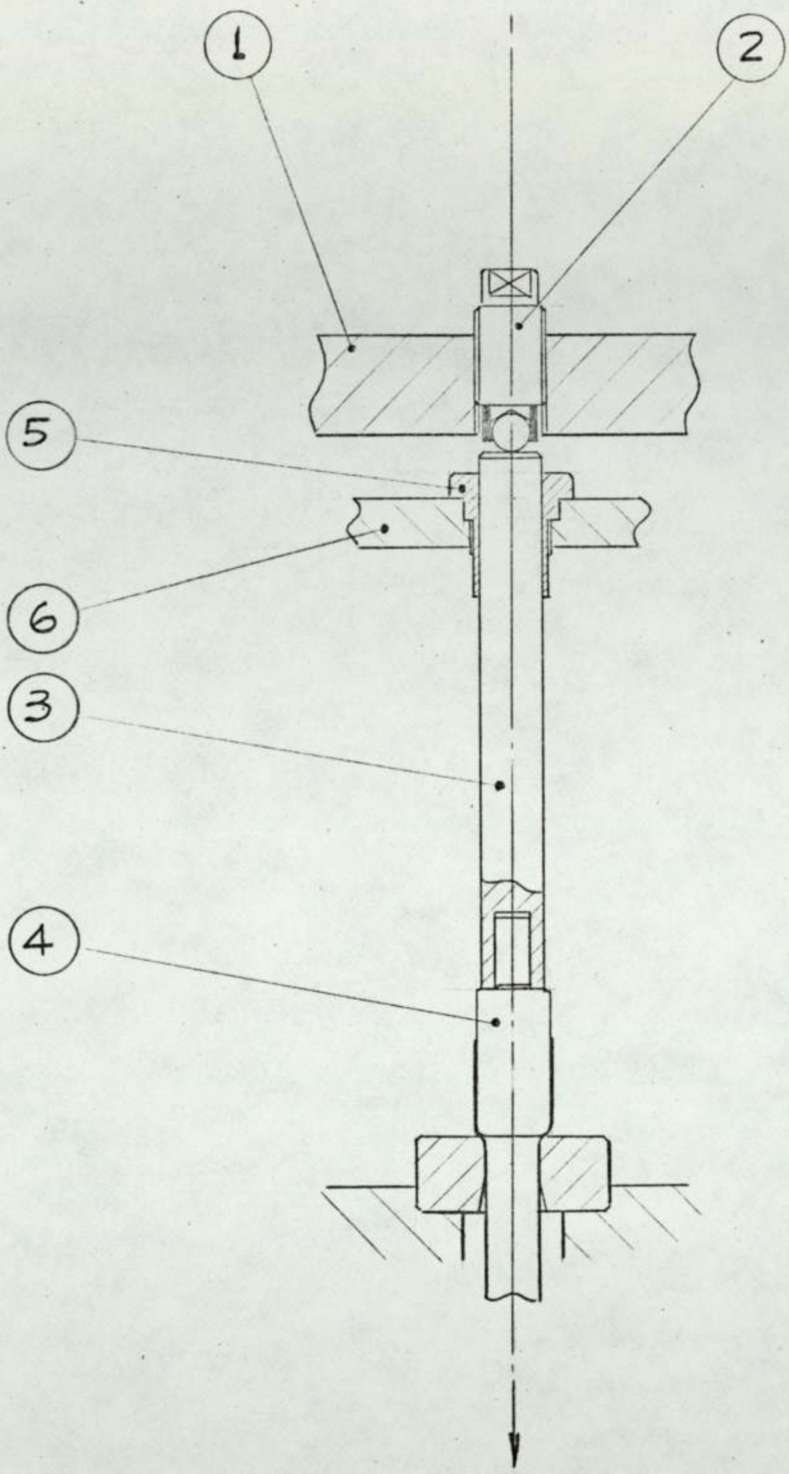

FIG. 69 DETAILS OF HOLD-DOWN APPLICATION

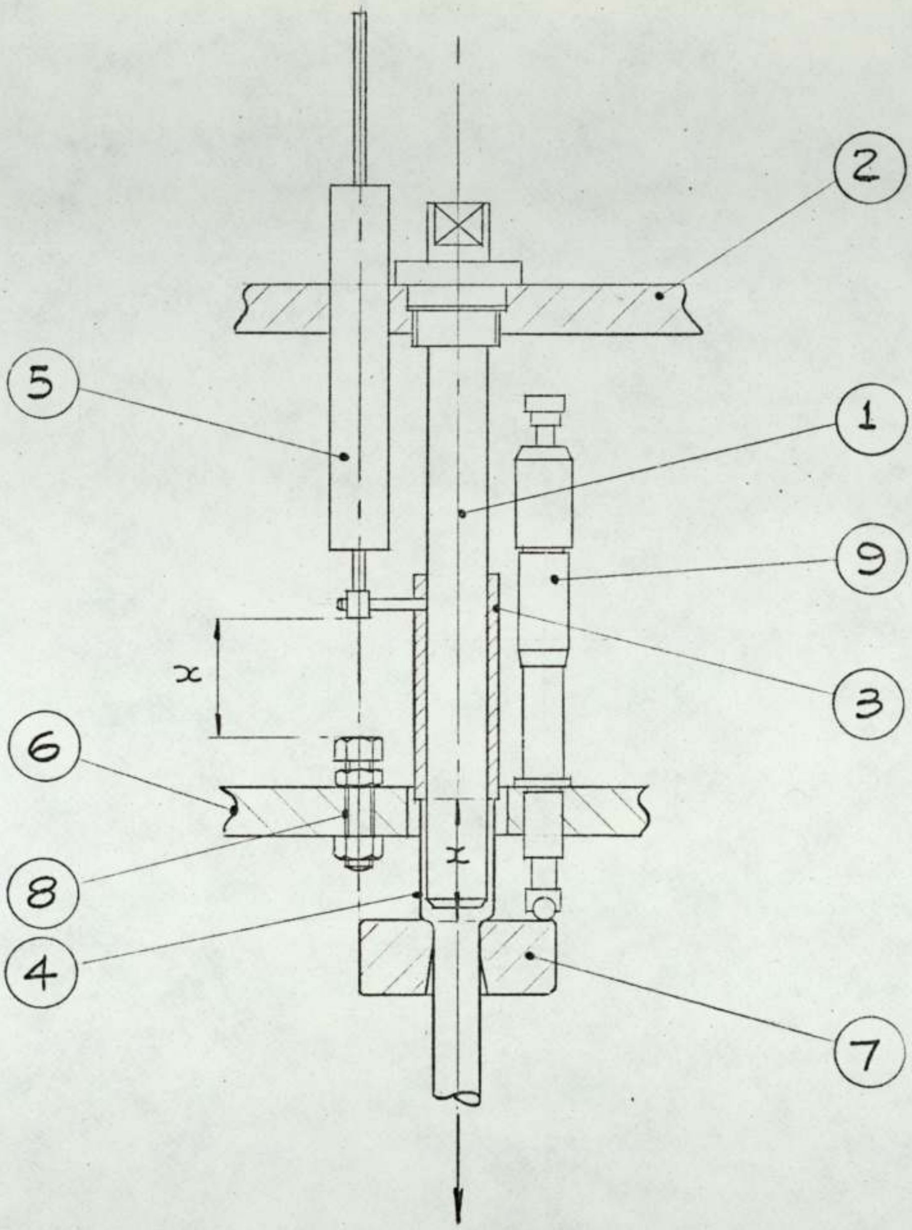

FIG. 70 COUPLING OF DISPLACEMENT TRANSDUCER TO TEST-PIECE RIM.

out by lifting the platen (6) by known amounts using the micrometer (9), and recording transducer output on an ultra-violet trace.

When conducting constrained redraw tests the dummy punch (1) was replaced by the hold-down punch arrangement illustrated in FIG. 71.

During actual tests output from the displacement transducer was recorded simultaneously with that from the dog load-cell.

(e) Guided redrawing.

The method of obtaining the redraw load-rim displacement correlation was essentially as that discussed above. FIG. 72 shows the guiding arrangement. The guide ring (1) was mounted above the redraw die (2) and located by four shoulder pins (3) which allowed the ring 0.005 in. float in a lateral direction but prevented movement along the axis of drawing. In this way the ring provided only diametral constraint to the test-piece, and was made 0.002 in. larger than the test-piece outside diameter.

To track the test-piece rim during its passage through the guide-ring two radial slots were incorporated in the latter, through which passed projections machined onto a special follower tube.

(f) Displacement transducer details.

An 'Ether' rectilinear displacement transducer type PD 13 was used for displacement measurement. The transducer was of 0 - 2 in. range, 0 - 18,000 Ω resistance with a maximum rating of 5 m.A at 150 V. Linearity was $\pm$ 0.5 %.

To obtain the required response the transducer was wired into one arm of a full Wheatstone bridge circuit with the slider as one terminal so that maximum change in output from the bridge when the transducer was operated was,

$$v = \frac{V r}{2(2R + r)}$$

where V = input to bridge from oscillator (5V).

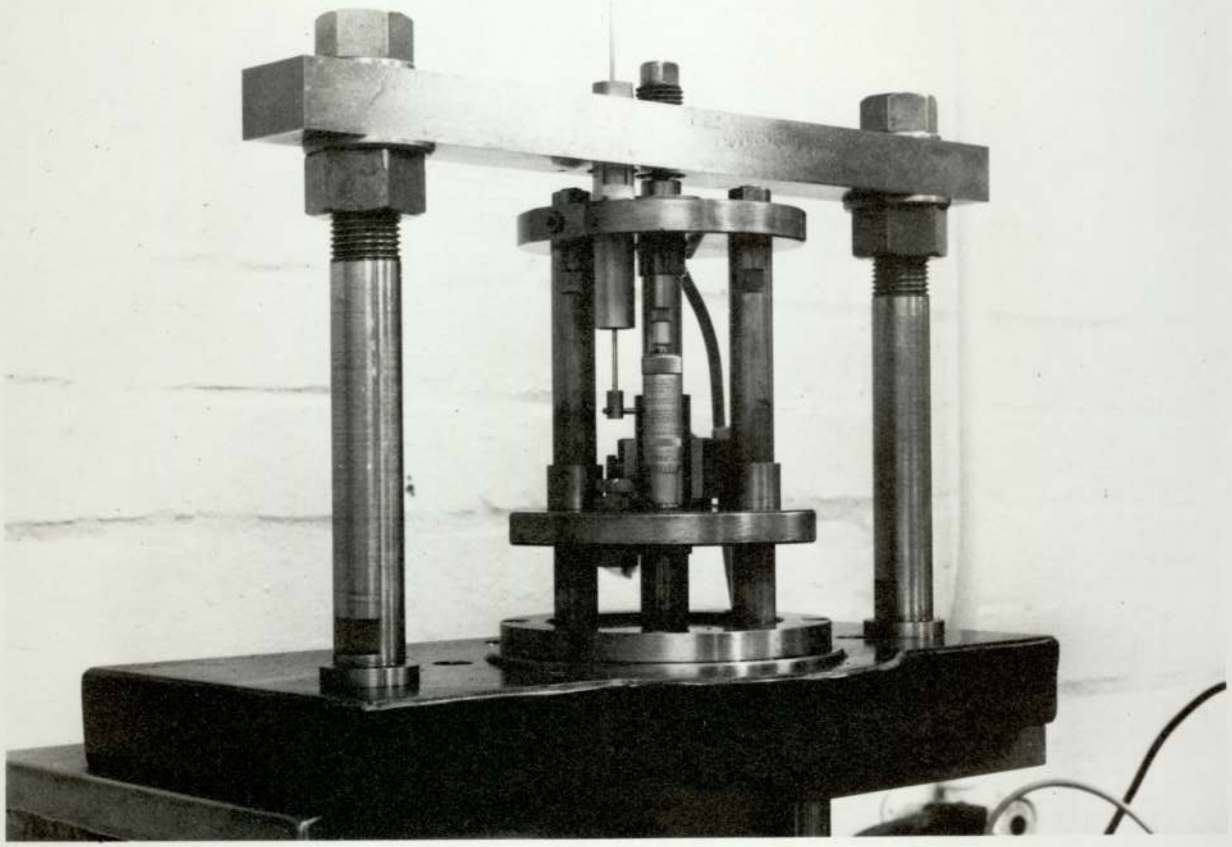

FIG. 71 TEST RIG FOR SPLAY-MEASUREMENT PROGRAMME ARRANGED FOR RIM DISPLACEMENT TEST.

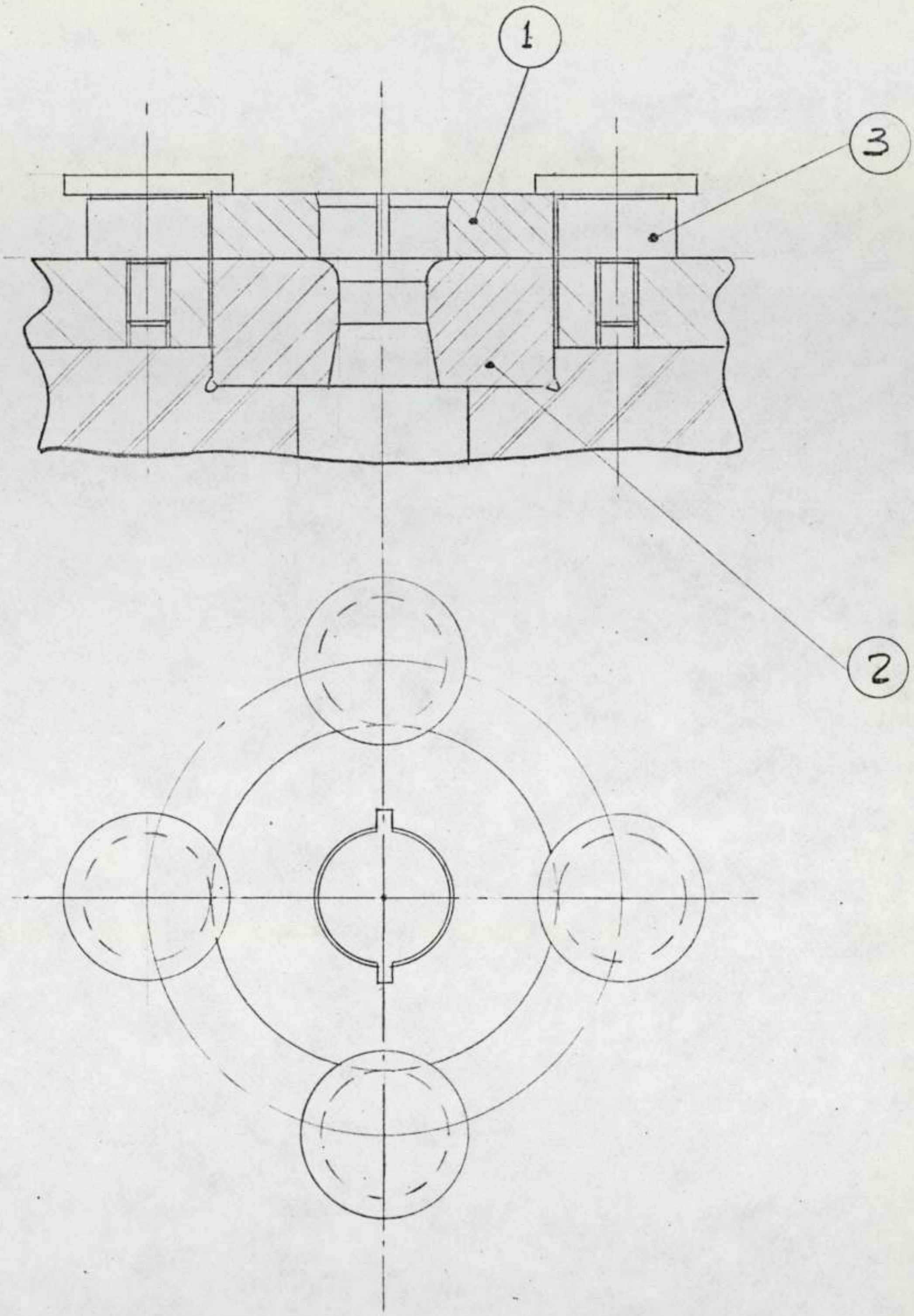

FIG 72 EXTERNAL GUIDE-RING ARRANGEMENT
(Scale - full size)

r = transducer resistance. (18,000 Ω)

R = resistance of each arm of bridge.

R was calculated from the above expression on the basis that maximum current flow through a 120 Ω galvanometer should not exceed $1\frac{1}{2}$ m.A. A resistance of R = 120,000 Ω was found satisfactory for this purpose.

(g) Recording equipment.

Splay measurement test data was obtained and recorded manually, whilst information from redraw load - rim displacement tests was monitored continuously on 'S.E.' recording equipment which included;

(1) Power supply unit type S.E. 427.

(2) Oscillator type S.E. 511/S.

(3) Carrier amplifiers type S.E. 423/1.

(4) Ultra-violet paper-tape recorder S.E. 2005 with B 450 galvanometers.

FIG. 73 illustrates the testing arrangement.

(h) Details of redraw tooling.

Tooling details are included in FIG 74. An extra-long throat was built into all four redrawing dies with a view to ensuring good alignment between test-piece and die axis. The increased frictional drag resulting from this procedure was considered of secondary importance.

Details of hold-down punch geometry were not finalised until the first phase of experiments - the unconstrained redraw programme - was completed. Two hold down punches were used corresponding to test-pieces of 80 and 100 diameter/thickness ratio. The influence of profile radius on splaying was studied by first providing each punch with its smallest radius, and subsequently increasing the radius in stages.

All tooling was manufactured from a high quality tool steel and heat-treated to 60 Rockwell C. Tool profiles were polished before use. Table 9 gives details of tool surface finish readings taken at

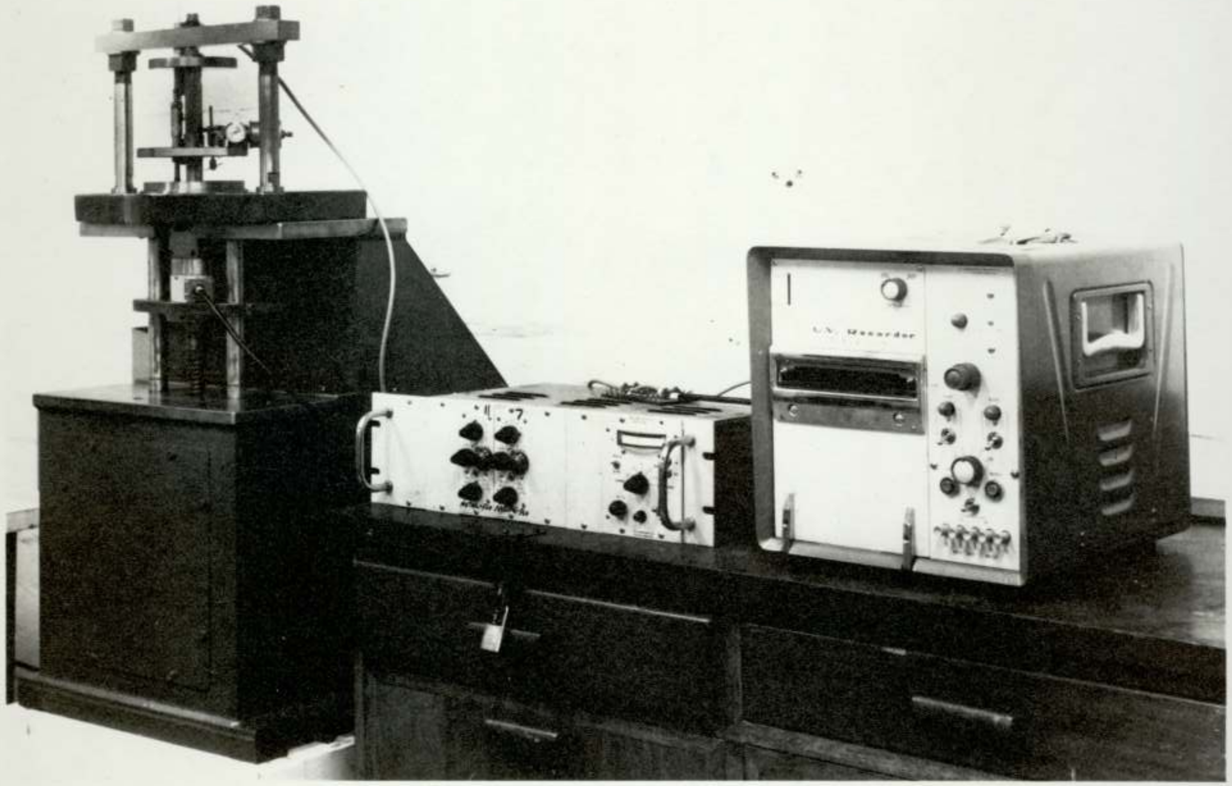

FIG. 73 GENERAL VIEW OF APPARATUS FOR SPLAY-MEASUREMENT PROGRAMME.

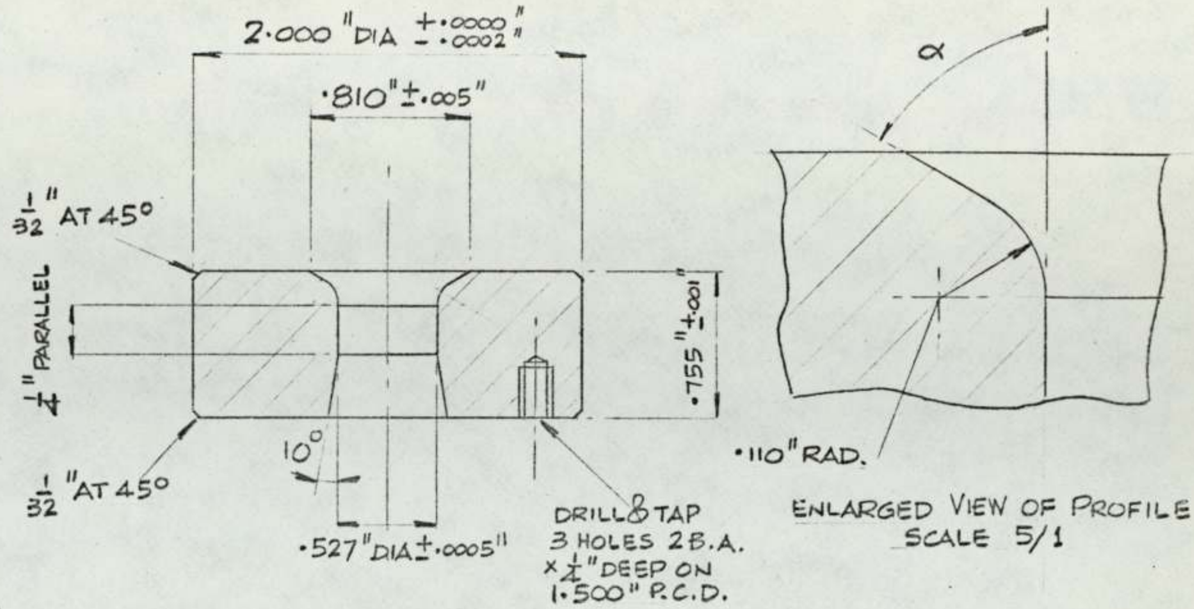

ONE DIE OF EACH ANGLE				
α°	90	60	45	30

GRIND ALL EXTERNAL SURFACES. POLISH PROFILE TO 5 μ" C.L.A.

DETAILS OF REDRAW DIES.

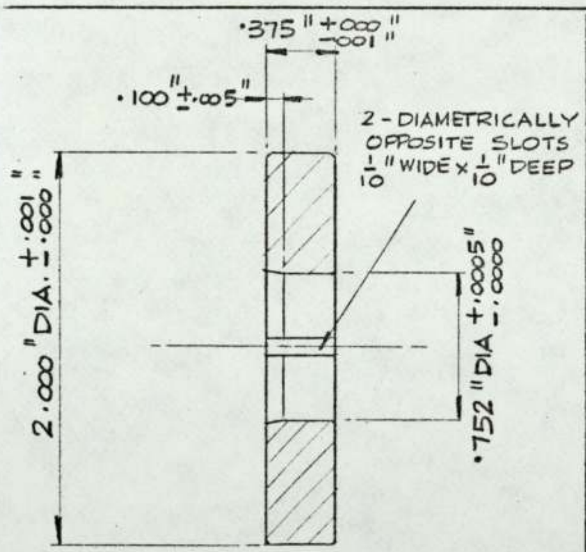

GRIND ALL SURFACES

DETAILS OF GUIDE RING

NOTE

1. SCALE FULL SIZE OR OTHERWISE STATED.
2. MATERIAL FOR ALL TOOLING CHROME - MOLYBDENUM - VANADIUM TOOL - STEEL HEAT - TREATED TO 60 ROCKWELL C.

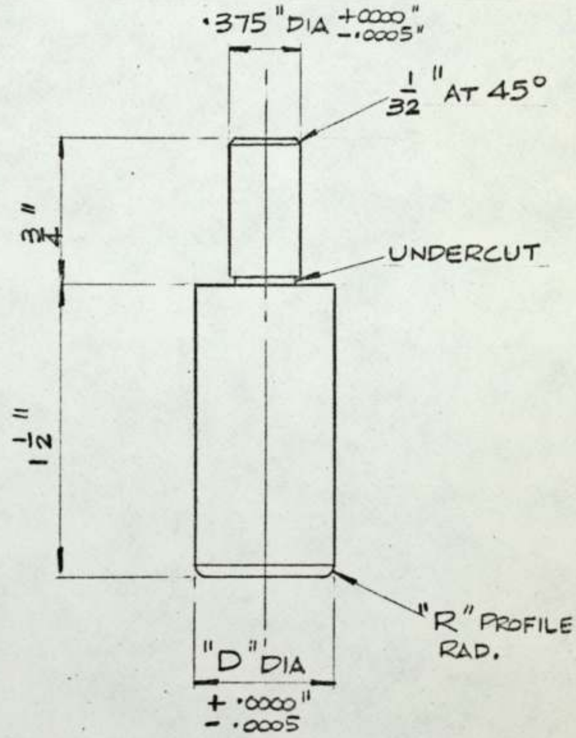

"D" DIA.	"R" PROFILE RAD.		
·733"	·030"	·040"	·050"
·729"	·040"	·050"	·060"

POLISH PROFILE TO 5 μ" C.L.A.

DETAILS OF HOLD-DOWN PUNCHES

FIG. 74 DETAILS OF REDRAW TOOLING FOR SPLAY MEASUREMENT TESTS.

TABLE 9 SURFACE-FINISH OF SPLAY-MEASUREMENT PROGRAMME REDRAW TOOLING.

Tool	Location of surface - finish reading	Surface-finish, micro in. C.L.A.
90^o die	At die throat. Parallel to drawing direction .	2
60^o die	At die throat. Parallel to drawing direction.	$6\frac{1}{2}$
45^o die	At die throat. Parallel to drawing direction.	6 - 7
30^o die	At die throat. Parallel to drawing direction.	4 - 8
Guide ring	In bore. Parallel to drawing direction	6
Hold-down punch for 80 D/t test-pieces.	On full diameter just above nose radius. Parallel to drawing direction.	4
Hold-down punch for 100 D/t test-pieces.	On full diameter just above nose radius. Parallel to drawing direction.	3 - 4

the termination of the test programme, whilst FIG. 75 is a photograph of the tooling. (The 30 and 60 degree dies were incorrectly stamped.)

8. 7. Manufacture of test-pieces.

(a) Geometry of test-piece.

The test-length was dictated by the need to commence redrawing well before the stage where splaying was initiated, since only then would it be possible to observe the complete splay phase. A test-length/diameter ratio of $1\frac{2}{3}$ was used giving a test-length of $1\frac{1}{4}$ in. The length of test-piece tag was governed by the requirement to pass through die and die-bolster and leave sufficient protusion for gripping. A length of 2 in. was found adequate. Tag diameter was designated 0.002 in. smaller than the redraw die size. Test-piece details are shown in FIG. 76.

(b) Plan of manufacture.

Test-pieces were prepared from tubes cold-drawn within a Tube Investments company. To ensure that for each of the four materials investigated test-pieces were from a common origin all tubing for each material was drawn from a single hollow. Details of hollows and problems encountered in drawing down to the test-piece sizes are given in appendix A_3. 2.

Test-pieces were cut to a length of $3\frac{1}{4}$ in. from the tube-lengths using a single-point cutting tool in a lathe, an ample coolant supply being used to prevent test-piece heating.

Tags were formed by pressing the short tube lengths into a series of dies. The possibility of swage tagging was considered at the outset but was rejected on the grounds of lack of precision and the need for a long transition from tag to test-diameter.

(c) Development of tagging procedure.

It was required to reduce the tag diameter to 0.525 in. from a tube diameter of 0.750 in., the diameter reduction involved being 30 %. Work by Swift and others had indicated that even under the most favourable conditions of pressing 30 % reduction would initiate yielding

Top - hold-down punches

Centre - redraw dies

Bottom - guide ring

FIG. 75 TOOLING FOR SPLAY-MEASUREMENT PROGRAMME.

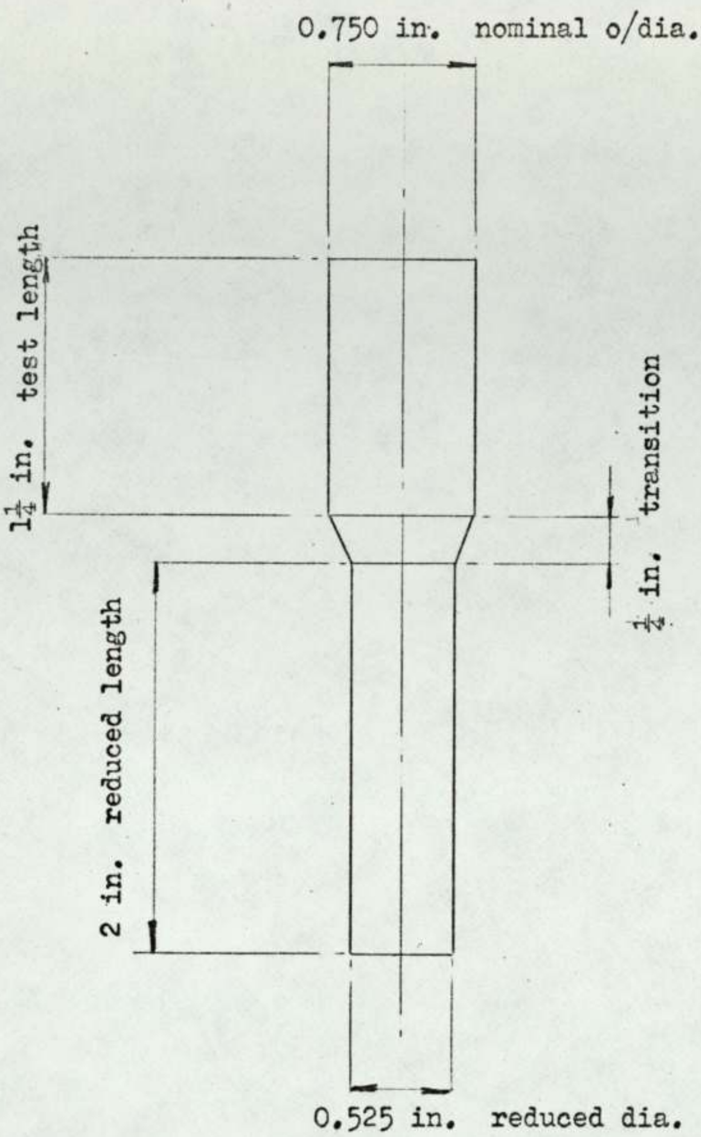

Wall thickness range 0.0075 - 0.040 in.

FIG. 76 DETAILS OF TEST-PIECE FOR SPLAY MEASUREMENT TESTS.

in the section above die entry. Initial tests were therefore carried out using a 2 stage procedure. It was found that buckling occurred at die entry in the first stage. After further experimentation a workable 5 stage procedure, based on approximately equal load per stage, was evolved. It was noticed that the tendency to buckle was most severe with materials that work-hardened rapidly, fully soft stainless-steel and brass were particularly prone. Test-pieces at the higher diameter/thickness ratios gave rise to additional problems.

Full details of the work on press tagging are included in appendix A_3. 3., together with experimental data on strain development plotted from measurements taken whilst tagging. Problems encountered during the work are also discussed.

FIG. 77 illustrates a typical tagged test-piece.

8. 8. Chemical analysis of test-piece materials.

Samples of each hollow were retained for quantitative chemical analysis. Results are given in appendix A_3. 4. The stainless steel hollow, supplied by a Tube Investments company, was originally thought to be a T.316 alloy. However the chemical analysis revealed that the alloy was T304. This did not detract from the scope of the investigation since both alloys were widely cold-formed.

8. 9. Preparation of test-pieces for redrawing.

Care was taken to ensure test-pieces were adequately and consistently lubricated since variations in lubrication throughout the length of a test-piece could cause fluctuations in redraw load and hence adversely affect the correlation between redraw load and splaying.

Tag-formed test-pieces were thoroughly degreased and chemically etched to form a lubricant key . Steel, brass and aluminium test-pieces were then water rinsed, lubricated in textile soap at 60 - 70°C, and allowed to air dry at room temperature. In view of the possibility of pick-up with the work-hardened stainless-steel test-pieces, these test-pieces were immersed in an oxalate solution which provided a

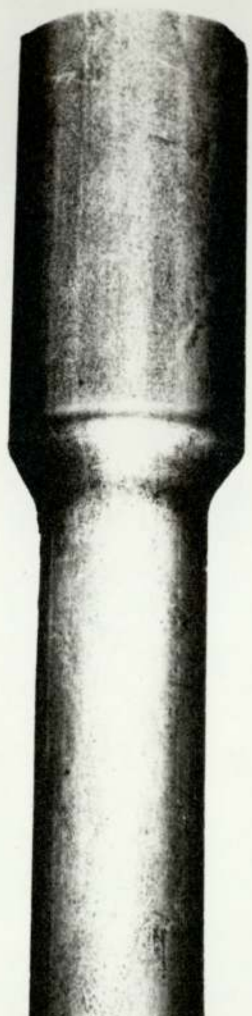

FIG. 77 TYPICAL TEST-PIECE FOR SPLAY-MEASUREMENT PROGRAMME.

good surface key, and the soap film was baked hard in an oven at 120°C.

Full details of etching solutions and lubrication procedures are given in appendix A_3. 5.

8. 10. Experimental techniques.

(a) Free and constrained redrawing.

Free (unconstrained) redrawing was straightforward. The dog was fully retracted with jaws locked open, and the test-piece entered into the die from above. On releasing its jaws the dog gripped the test-piece tag and drawing could commence.

For constrained redrawing the following procedure was developed:

(1) The dog was fully retracted with jaws open.

(2) The hold-down punch was inserted in the test-piece and the latter entered into the die.

(3) The hold-down punch extension was threaded through its guide and located on the hold-down punch spigot.

(4) The hold-down pressure nut was then operated to push the test-piece into the die and fully seat the hold-down punch. This operation was complete when solid resistance to motion was felt. The hold-down screw was then slackened $\frac{1}{8}$ turn.

(5) Drawing commenced after releasing the dog jaws.

To ensure satisfactory gripping by the dog, plugs were inserted in the tags of all test-pieces. The plugs were removeable and re-usable.

(b) Splay measurement tests.

(1) Exploratory tests were made to indicate at which point in the redraw splaying commenced. Tests were then planned so that the bulk of experimental readings were taken during the splaying phase.

(2) The stylus assembly was set so that the vertical 'height' micrometer registered zero when the stylus point just rested on the upper die surface.

(3) The testing procedure is described with the aid of Table 10. The test-piece was drawn until its rim was 1.00in. above the die. Drawing was then interrupted and the test-piece scanned with the measuring head to provide 'splay' readings at 6 circumferential points for each 'height' interval. A 360 degree reading was always taken as a check against stylus movement. The test-piece was then drawn to a height of 0.60 in. and the measurement procedure repeated. The process was continued until the test-piece rim was drawn into the die mouth.

During the latter stages of some tests there was a tendency for the test-piece rim to cant slightly. When this occurred individual readings of rim height were taken at each circumferential position to ensure that splay readings were always taken on the actual rim. An average height was calculated.

(4) After completing a batch of tests on a particular die the measuring head was calibrated by inserting an accurately made 0.750 in. diameter gauge in the die and taking 'splay' readings for each position of height and circumference covered in the tests.

(c) Redraw-load measurement tests.

(1) The displacement transducer calibration screw was set to its datum position with the test-piece follower tube coupled to the transducer and in contact with the die surface. This operation was carried out in the absence of a test-piece.

(2) The recording equipment was switched on and both channels (load-cell and displacement transducer) adjusted to give zero output signal.

(3) The hold-down punch assembly (or dummy hold-down punch for free redrawing) were then removed together with follower-tube, and the testing machine retracted with dog jaws open.

(4) A test-piece was entered in the die as reported in section 8.10(a).

(5) The appropriate follower-tube was placed against the test-piece rim and its arm coupled to the displacement transducer.

(6) The hold-down punch extension (or dummy) were then installed by

TABLE 10 TYPICAL DATA SHEET FOR SPLAY-MEASUREMENT TESTS.

Test-piece rim height above die (in.)	Height micrometer reading (in.)	Splay micrometer readings (in.)						
		0°	60°	120°	180°	240°	300°	360°
1.00	1.00							
	0.60							
	0.30							
	0.20							
	0.15							
	0.10							
	0.05							
	0.00							
0.60	0.60							
	0.30							
	0.20							
	0.15							
	0.10							
	0.05							
	0.00							
0.30	0.30							
	0.20							
	0.15							
	0.10							
	0.05							
	0.00							
0.20	0.20							
	0.15							
	0.10							
	0.05							
	0.00							
0.15	0.15							
	0.10							
	0.05							
	0.00							
0.10	0.10							
	0.05							
	0.00							
0.05	0.05							
	0.00							
0.000	0.00							

threading through the follower-tube.

(7) Recorder channels were checked for zero drift, and the load/rim displacement test carried out at a speed of $2\frac{1}{2}$ - 4 in./minute.

(8) On completion of each test the displacement transducer was calibrated by lifting the micrometer platen with the vertical micrometer and recording the corresponding transducer output signal. A typical calibration curve is shown in FIG. 78.

Testing procedures for guided redrawing were similar, but a special follower tube with end projections was used to track the test-piece rim within the guide-ring.

(d) Measurement of free profiles in unconstrained redrawing.

The redrawing process was interrupted during steady-state conditions, and the testing-machine drive reversed to retract the test-piece deformation profile approximately $\frac{1}{2}$ in. clear of the die. The splay measuring head was then used to obtain readings on the profile from the undeformed entering tube surface to the redrawn tube surface.

8. 11. Methods of test-data interpretation.

(a) Splay measurement tests.

Suppose that circle C_1 (FIG. 79) represents the standard calibration piece, concentric with the die and centre of rotation of the measuring head. Further, suppose the circle C_2 represents the splayed tube whose radius exceeds that of the standard by Δr, and which is slightly eccentric to the die by amount x. The dotted circle represents the standard displaced by x to become concentric with the test-piece.

From FIG. 79, the radial difference between test-piece and standard measured by a stylus at point (1) is, $x \cos\theta + \Delta r$, whilst that measured at (2) is $-x\cos\theta + \Delta r$. Therefore across (1) - (2) the difference in readings on standard and test-piece is $2\Delta r$ or Δd. This result infers that the method of splay measurement used cancels any eccentricity between test-piece and die.

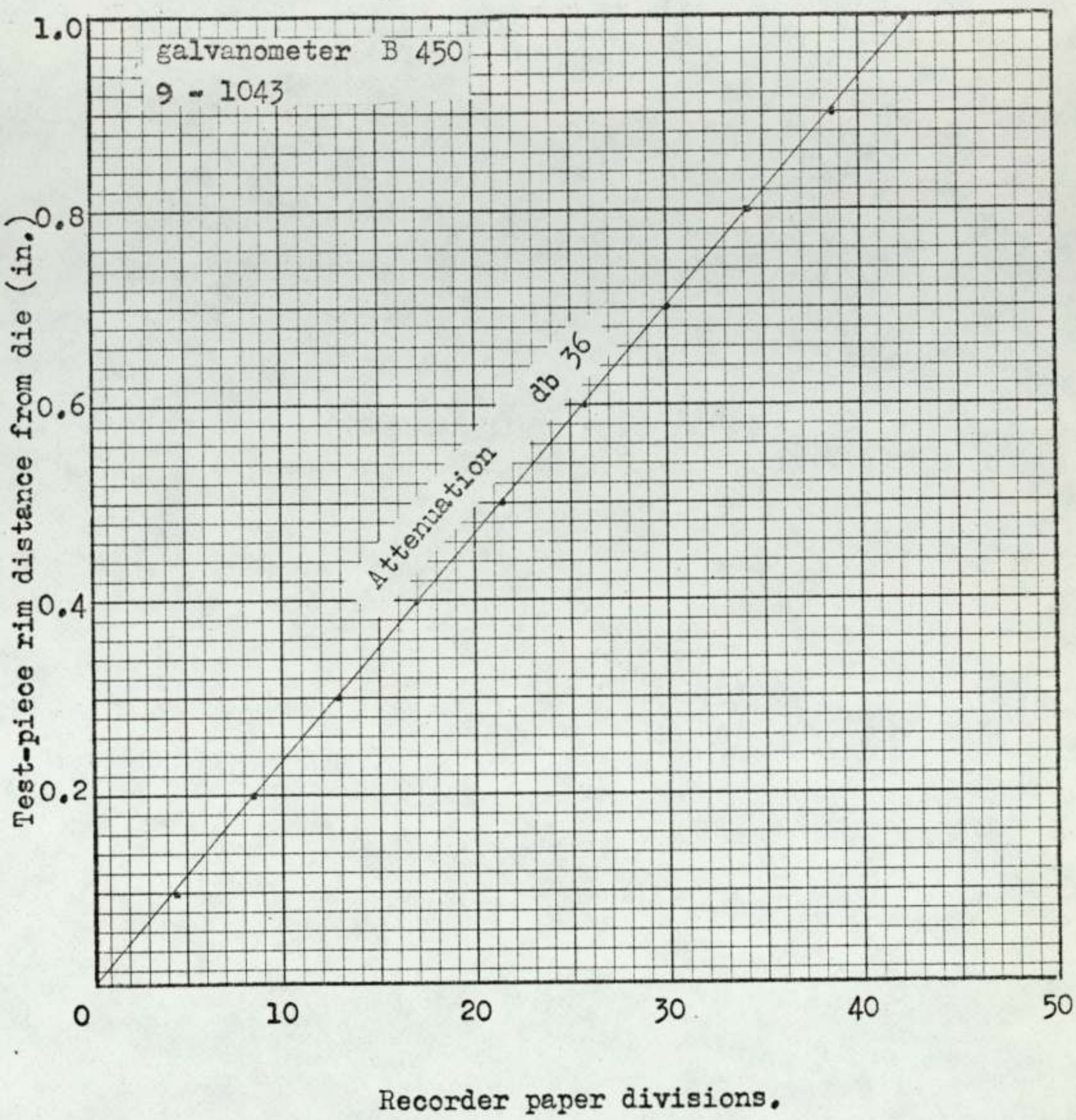

FIG. 78 CALIBRATION CHARACTERISTICS FOR POTENTIOMETRIC DISPLACEMENT TRANSDUCER USED IN SPLAY-MEASUREMENT PROGRAMME.

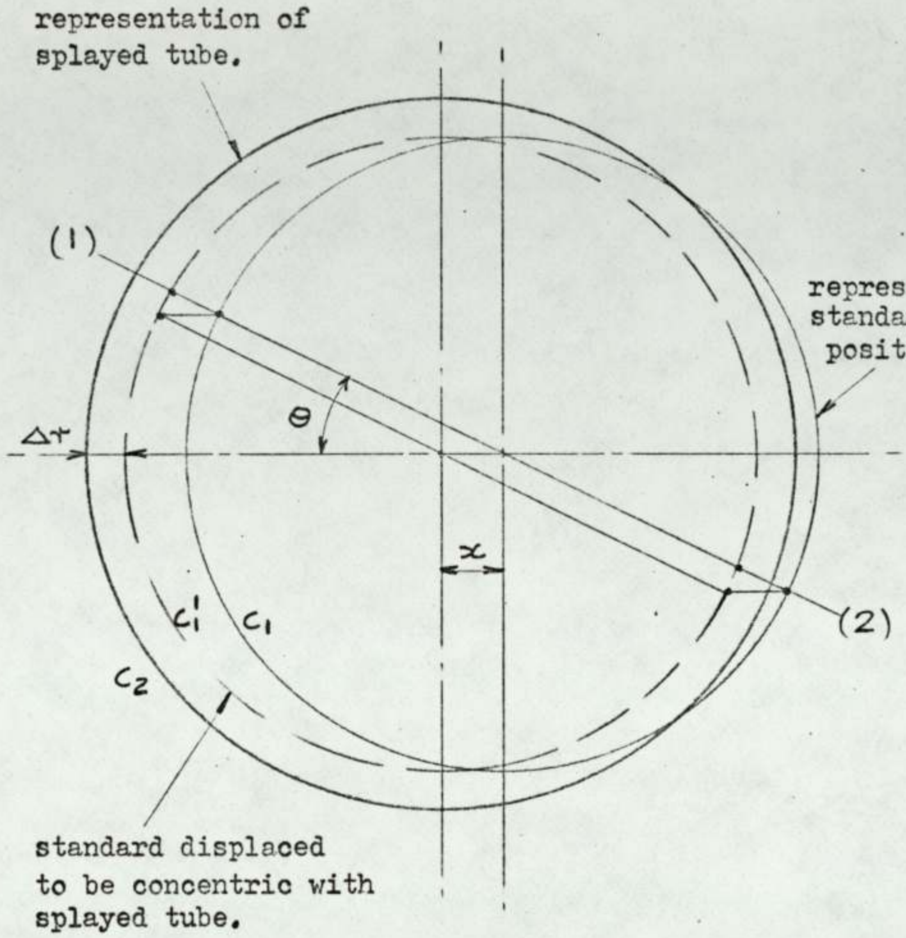

FIG. 79 PRINCIPLE OF SPLAY MEASUREMENT

For stylus readings of T_1, S_1, T_2, S_2 on test-piece and standard at points (1) and (2) respectively the deviation of test-piece from standard is given by,

$$\Delta d = (T_1 - S_1) + (T_2 - S_2) = (T_1 + T_2) - (S_1 + S_2)$$

This expression was used for computing diametral splay in the splay-measurement tests.

(b) Redraw load/test-piece rim displacement tests.

Two concurrent traces were obtained from the ultra-violet recorder, being representative of redraw load and test-piece rim displacement respectively. The 'load' traces were of constant magnitude during the greater part of the redraw, but showed fluctuations during the splaying phase before falling away rapidly at the termination of drawing. A number of transverse lines were drawn across each record linking load and displacement signals, the majority of lines being concentrated at that part of the record corresponding to splaying. The signal magnitudes on each line were then measured, and translated to actual loads and displacements using calibration curves.

(c) Combined splay - redraw load - rim displacement data.

Although splay and load measurement tests were carried out separately, each had current test-piece rim position as a common reference. Moreover the tests were on identical specimens. Graphical results were therefore combined to show not only the development of splaying but also its effect on redraw load.

(d) Free profile tests.

For each of the six circumferential positions of measurement the deformation profile was found taking 'splay' micrometer readings on the drawn test-piece surface as a datum. Results were then averaged around the circumference to provide a mean profile.

This profile was plotted to a scale twenty times full size and the best mean value of 'free' radius drawn through the experimental points. The procedure was straightforward for the 30 and 45 degree dies but not so easily applied to those of 60 and 90 degree semi-angle, where often the true contact angle was less than the semi-angle. When this situation arose the known die radius was first drawn in and the steepest possible tangent consistent with experimental points was fitted. A radial line was then drawn through the point of tangency and extended. The best free radius was then located along this line.

8. 12. Experimental results.

(a) General comments.

It was stated in section 8.3, when discussing test-plan modifications, that redraw loads were generally underestimated. This result was thought to have occurred for two reasons. Firstly, Sachs' tube-sinking expression had been used for calculations and thus the effects of bending, unbending work had been ignored. Secondly, loads were calculated on the basis of estimated material yield-strength properties which were later found to be on the low side.

Quality of lubrication appeared good. No problems with pick-up occurred and generally redraw loads were steady during the steady-state part of the cycle.

Only one test-piece failed in redrawing. This was brass at a diameter/thickness ratio of 20 and 67 % prior cold-work. Failure occurred at the die exit and was of the brittle type.

No test-piece failures occurred due to splaying in any of the combinations of tool geometry, test-piece geometry and prior-cold work investigated.

(b) Main results.

Tables **11** and **12** are indexes to the free and constrained redraw programmes respectively, free tests being depicted by the suffix F and constrained tests by the suffix C. Each basic test number designation was used to describe a particular redraw arrangement of tool geometry, test-piece geometry, test-piece material and prior cold- work. Within each designation at least two tests, splay measurement and redraw-

TABLE 11

INDEX TO SPLAY MEASUREMENT TESTS - FREE

Test number	Test material	Prior cold-work. Nominal. (%)	Nominal test-piece dimensions (in.)		Die semi-angle (deg.)
			O/Dia.	Wall Thk.	
1F	steel	0	0.750	0.0375	90
2F	steel	0	0.750	0.030	90
3F	steel	50	0.750	0.030	90
4F	steel	50	0.750	0.030	60
5F	steel	50	0.750	0.030	45
6F	steel	50	0.750	0.030	30
7F	steel	50	0.750	0.025	90
8F	steel	50	0.750	0.025	60
9F	steel	50	0.750	0.025	45
10F	steel	50	0.750	0.025	30
11F	steel	50	0.750	0.019	90
12F	steel	50	0.750	0.019	60
13F	steel	50	0.750	0.019	45
14F	steel	50	0.750	0.019	30
15F	steel	50	0.750	0.0125	90
16F	steel	50	0.750	0.0125	60
17F	steel	50	0.750	0.0125	45
18F	steel	50	0.750	0.0125	30
19F	brass	0	0.750	0.0375	90
20F	brass	50	0.750	0.0375	90
21F	brass	50	0.750	0.025	90
22F	brass	50	0.750	0.019	90
23F	brass	50	0.750	0.0125	90
24F	stainless	0	0.750	0.025	90
25F	stainless	0	0.750	0.019	90
26F	stainless	50	0.750	0.019	90
27F	stainless	50	0.750	0.0125	90
28F	aluminium	0	0.750	0.0375	90
29F	aluminium	50	0.750	0.0375	90
30F	aluminium	67	0.750	0.0375	90
31F	aluminium	50	0.750	0.025	90
32F	aluminium	50	0.750	0.019	90
33F	aluminium	50	0.750	0.0125	90

TABLE 12

INDEX TO SPLAY MEASUREMENT TESTS - CONSTRAINED.

Test number	Test material	Prior cold work. Nominal (%)	Nominal test-piece dimensions (in.)		Die semi-angle. (deg.)	Hold-down punch nose radius (in.)
			O/Dia.	Wall Thk.		
1C	steel	67	0.750	0.0075	90	0.030
2C	steel	0	0.750	0.0075	90	0.040
3C	steel	50	0.750	0.0075	90	0.040
4C	steel	67	0.750	0.0075	90	0.040
5C	steel	67	0.750	0.0075	90	0.050
6C	steel	50	0.750	0.0095	90	0.040
7C	steel	50	0.750	0.0095	90	0.050
8C	steel	50	0.750	0.0095	90	0.060
9C	brass	50	0.750	0.0095	90	0.040
10C	brass	50	0.750	0.0095	90	0.050
11C	brass	50	0.750	0.0095	90	0.060
12C	stainless	50	0.750	0.0075	90	0.030
13C	stainless	0	0.750	0.0075	90	0.040
14C	stainless	50	0.750	0.0075	90	0.040
15C	stainless	67	0.750	0.0075	90	0.040
16C	stainless	50	0.750	0.0075	90	0.050
17C	stainless	50	0.750	0.0095	90	0.040
18C	stainless	50	0.750	0.0095	90	0.050
19C	stainless	50	0.750	0.0095	90	0.060
20C	aluminium	50	0.750	0.0075	90	0.030
21C	aluminium	0	0.750	0.0075	90	0.040
22C	aluminium	50	0.750	0.0075	90	0.040
23C	aluminium	67	0.750	0.0075	90	0.040
24C	aluminium	50	0.750	0.0075	90	0.050

load measurement, were carried out. Additionally guided redrawing was introduced to some arrangements, whilst for the 'free' programme deformation profile measurements were made for each test number. The following code was used to identify individual tests:

(1) The first number and letter gave the basic test designation as indicated in index tables 11 and 12.

(2) Suffixes (A), (B), (G) and (P) were used to denote splay, redraw load, guided redraw load, and free-profile measurement tests respectively.

Thus, for example, test 5 F(A) was a free redraw splay measurement test on a steel test-piece 0.030 in. thick with 50 % prior cold-work using a 45 degree die; whilst test 12C (G) was a constrained guided-redraw on a stainless-steel test-piece 0.0075 in. thick with 50 % prior cold-work using a 90 degree die and a hold-down punch with 0.030 in. profile radius.

Tabulated results.

All tabulated test data is given in appendix A_3. 6. of the thesis, where:

Tables A_3.3 - A_3.35 provide splay measurement data for the free-redraw programme.

Tables A_3.36 - A_3.82 provide redraw-load measurement data for unguided and guided conditions in the free-redraw programme.

Tables A_3.83 - A_3.87 provide free-profile measurement data for the free-redraw programme.

Tables A_3.88 - A_3.111 provide splay measurement data for the constrained-redraw programme.

Tables A_3.112 - A_3.144 provide redraw-load measurement data for unguided and guided conditions in the constrained redraw programme.

Graphical results.

For each particular test designation splay and redraw load were plotted against current test-piece rim position on a common format.

These results indicated the way in which the cup wall splayed, splaying in the cup rim, and the effect of splaying on redraw load. In tests where guided redrawing was undertaken, unguided and guided load traces were superimposed to study the effect of guiding. Results for free-redrawing are shown in FIGS. 80 -111, and for constrained redrawing in FIGS. 112 - 135. A smooth curve was drawn through experimental rim-splay points and peak rim-splay found by interpolation. The error involved in the procedure was small since most splay measurements had purposely been concentrated in this region. Maximum rim-splay for each test is included on the appropriate graph, and was evaluated as the fractional diametral increase in the test-piece rim from steady-state conditions. This information was later used in experimental correlation with theory. The short vertical dotted line drawn through each rim-splay locus in constrained-programme results has a special significance discussed in a later section. Results from test 10F were not plotted because the test-piece rim canted in the latter stages of redrawing, causing splay readings of doubtful validity.

On plotting test results it was noticed that a number of test-pieces were apparently necked-in slightly at the open end whilst others exhibited a bell-mouth in this region. The effect was magnified by the scales selected for plotting splay results. In retrospect both peculiarities are thought to have occurred during parting-off of test-pieces from the tube-lengths. The 'necking-in' effect was most prevalent in fully soft test-pieces and this is consistent with the proposed cause. Conversely the 'bell-mouth' effect was more common with work-hardened test-pieces and was probably due to the release of residual stress on cutting. However when results were plotted for the test-pieces in question splay development appeared unimpaired. The results were therefore included.

On analysing test results it was found that a definite correlation existed between splaying and prior cold-work. FIGS. 136 and 137 show the development of rim-splay for test-pieces of various work-hardness drawn in the 'free' programme, whilst FIG. 138 shows the same effect with test-pieces in constrained redrawing.

Deformation profiles were plotted for all tests in the free-redraw programme, and best mean free-radii fitted to the zone of deformation prior to die contact. Experimental values of free-radius were later plotted to check the validity of Fogg's theory[11] (Section 10). It was considered superfluous to include all profile plots in the thesis, but four typical results are given in FIGS. 139 - 142 to illustrate the method of measurement used.

8.13 Ancillary tests.

Although nominal amounts of cold-work had been introduced to test-pieces by previous drawing operations, the exact condition of each test-piece was unknown. It was considered important to obtain information on this aspect not only for purposes of correlating experiment and theory in the current work, but also to provide a precise record of materials investigated during the research.

Tests were therefore conducted to determine test-piece yield-stress and prior plastic strain level. Yield-stress values were found from uniaxial tensile tests, the normal procedure being slightly modified for the thinner-walled test-pieces. An equivalent stress-strain curve was developed for each material by plane-strain compression tests carried out over the plastic range of interest. These tests were conducted on strip-like specimens machined from each of the four hollows used to manufacture test-piece tubing.

An estimation of prior test-piece strain was made by fitting uniaxial stress-strain curves to the appropriate plane-strain envelope.

Full details of procedures followed together with test results are included in appendix A_3. 7.

Test number	Test material	Prior cold work Nominal (%)	Nominal test-piece dimensions (in.)		Die semi-angle (deg.)
			O/Dia.	Wall thk.	
1F	Steel	0	0.750	0.0375	90

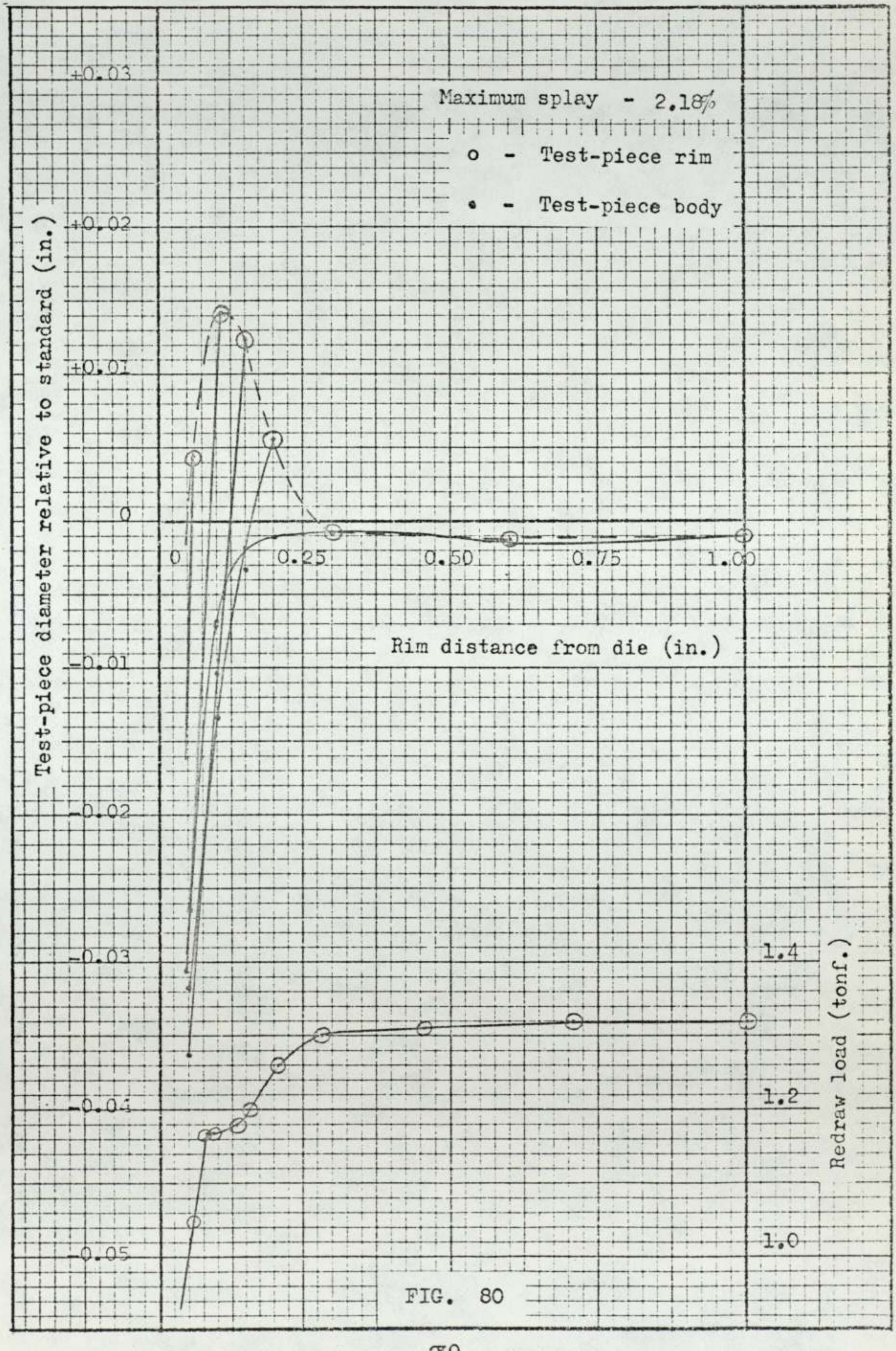

FIG. 80

Test number	Test material	Prior cold work Nominal (%)	Nominal test-piece dimensions (in.)		Die semi-angle (deg.)
			O/Dia.	Wall thk.	
2F	Steel	0	0.750	0.030	90

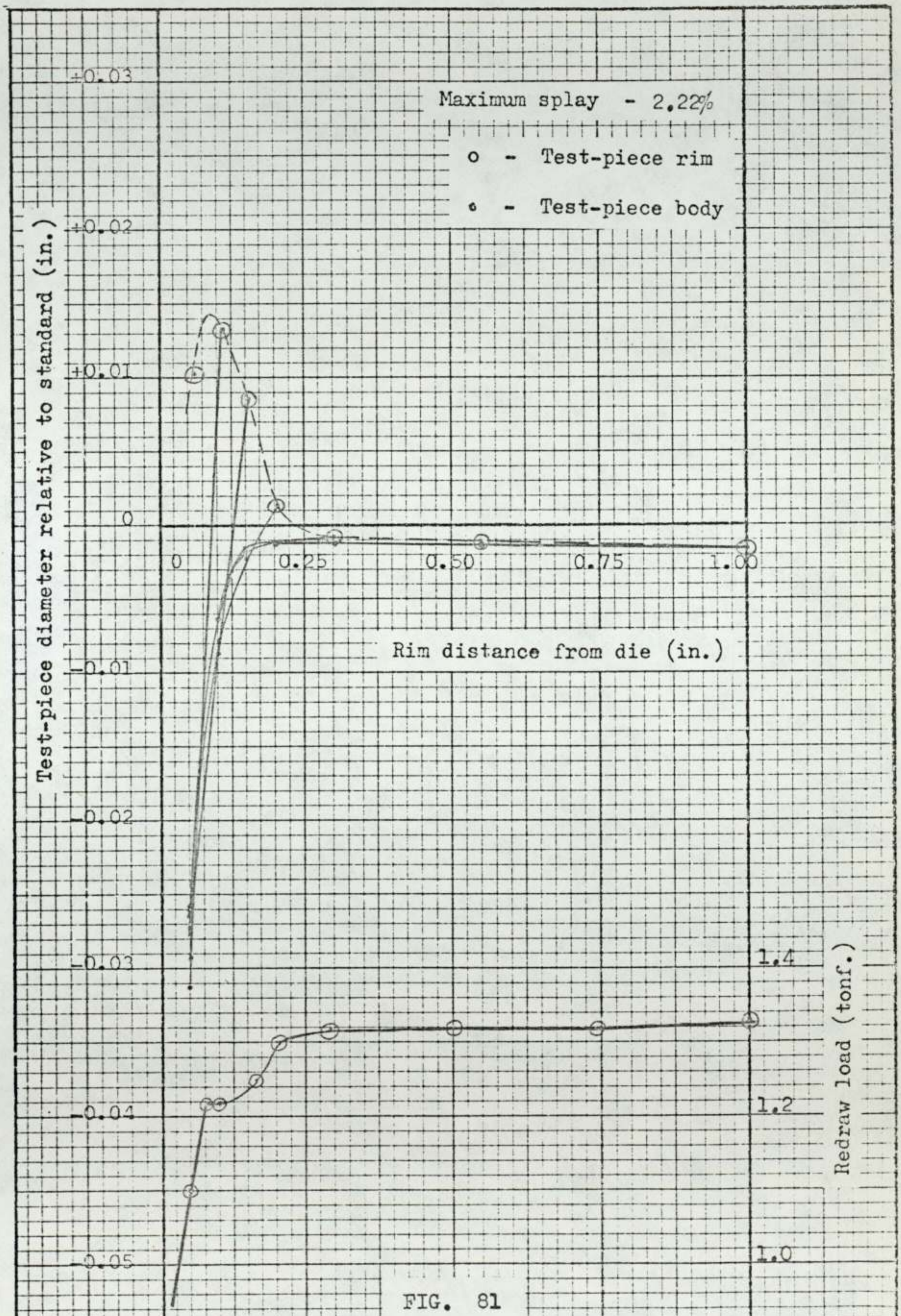

FIG. 81

Test number	Test material	Prior cold work Nominal (%)	Nominal test-piece dimensions (in.)		Die semi-angle (deg.)
			O/Dia.	Wall thk.	
3F	Steel	50	0.750	0.030	90

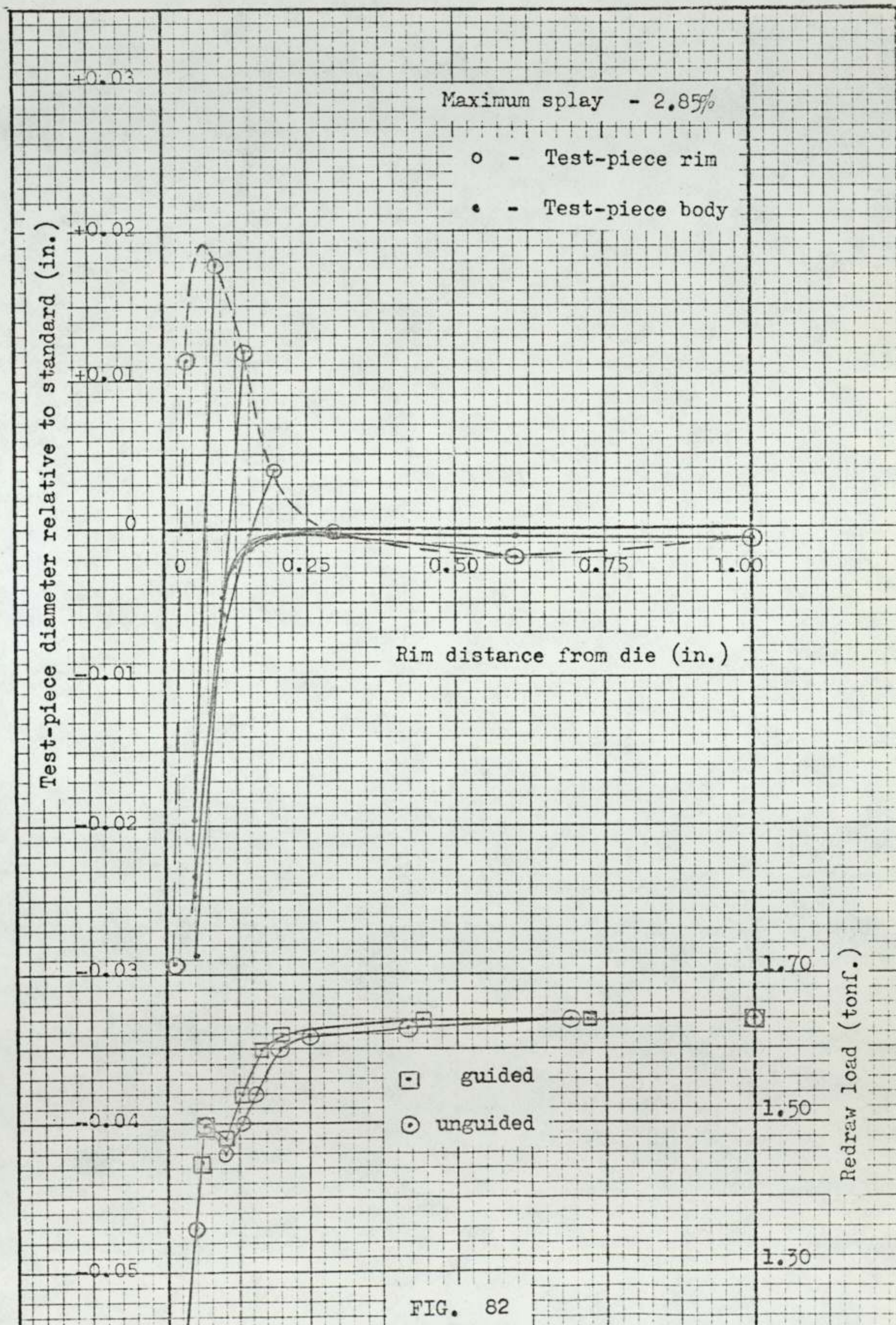

FIG. 82

Test number	Test material	Prior cold work Nominal (%)	Nominal test-piece dimensions (in.)		Die semi-angle (deg.)
			O/Dia.	Wall thk.	
4F	Steel	50	0.750	0.030	60

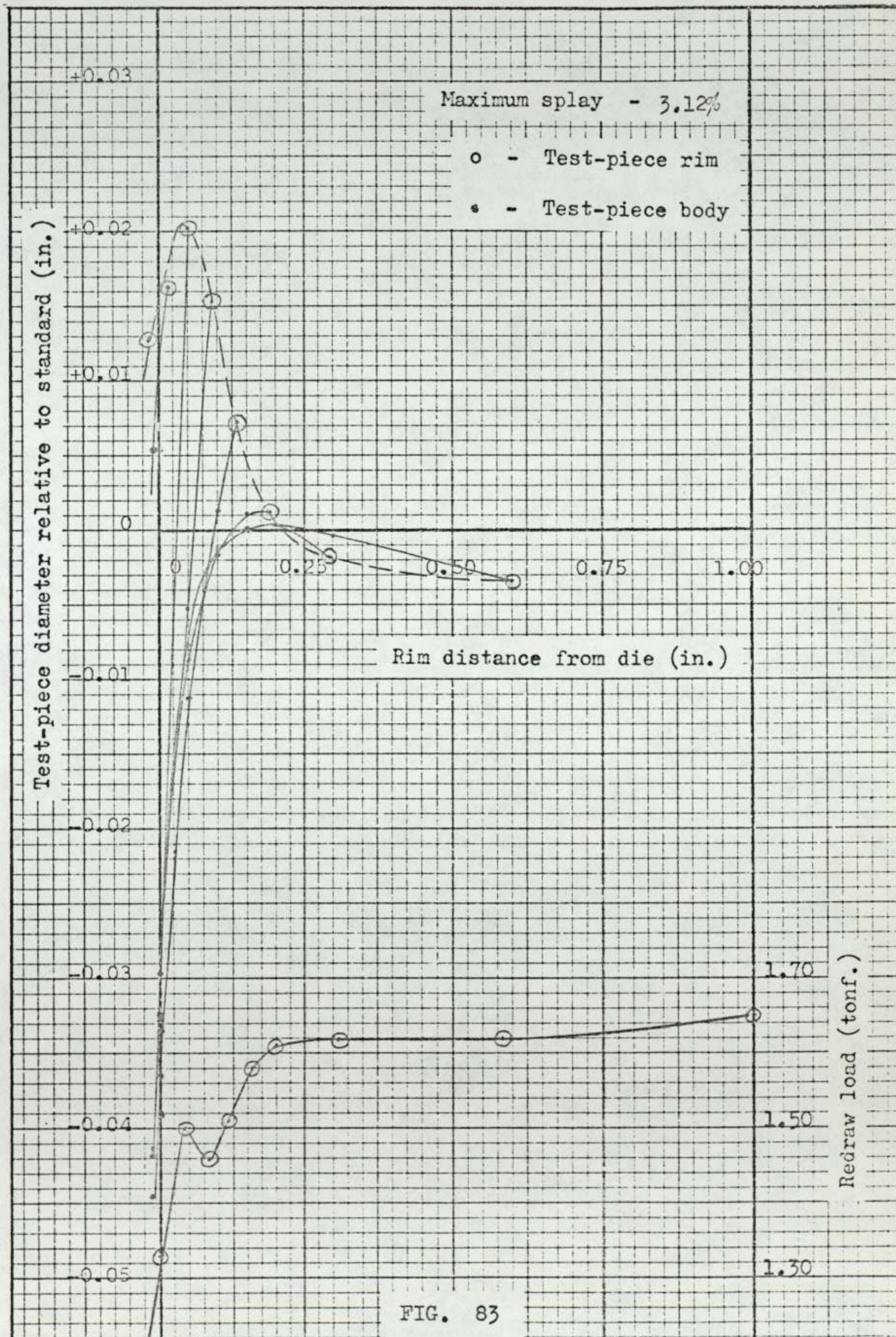

FIG. 83

Test number	Test material	Prior cold work Nominal (%)	Nominal test-piece dimensions (in.)		Die semi-angle (deg.)
			O/Dia.	Wall thk.	
5F	Steel	50	0.750	0.030	45

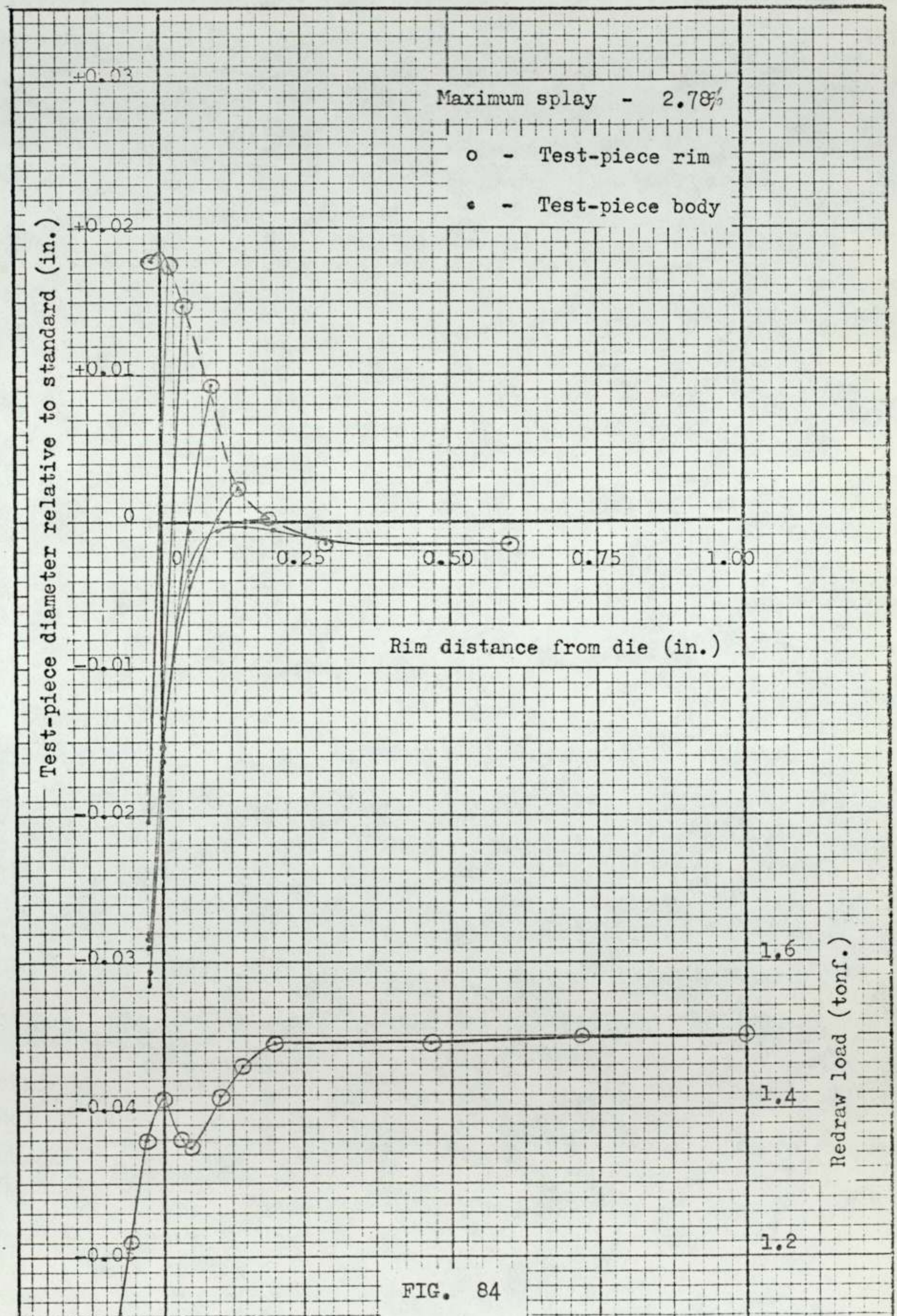

FIG. 84

Test number	Test material	Prior cold work Nominal (%)	Nominal test-piece dimensions (in.)		Die semi-angle (deg.)
			O/Dia.	Wall thk.	
6F	Steel	50	0.750	0.030	30

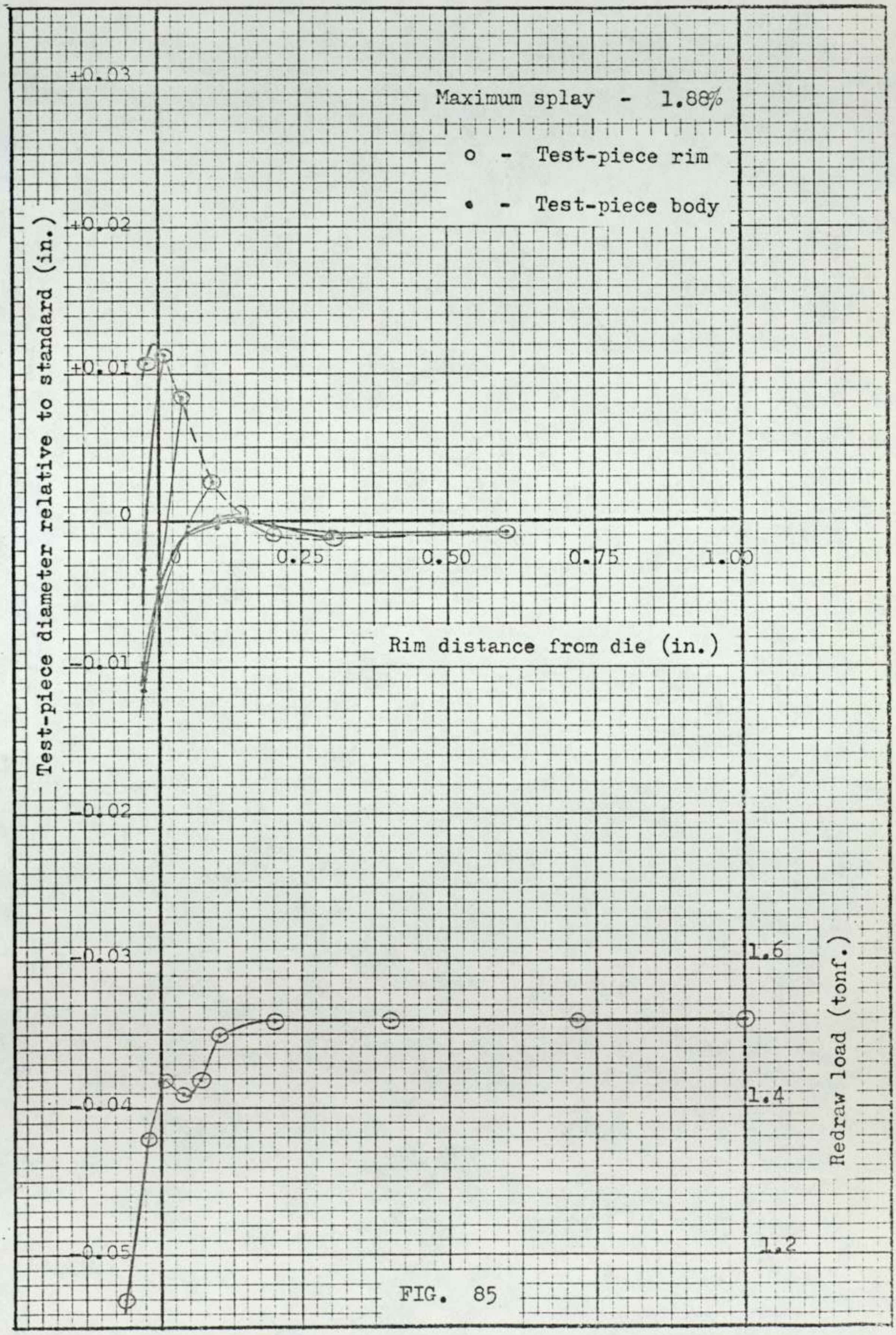

FIG. 85

Test number	Test material	Prior cold work Nominal (%)	Nominal test-piece dimensions (in.)		Die semi-angle (deg.)
			O/Dia.	Wall thk.	
7F	Steel	50	0.750	0.025	90

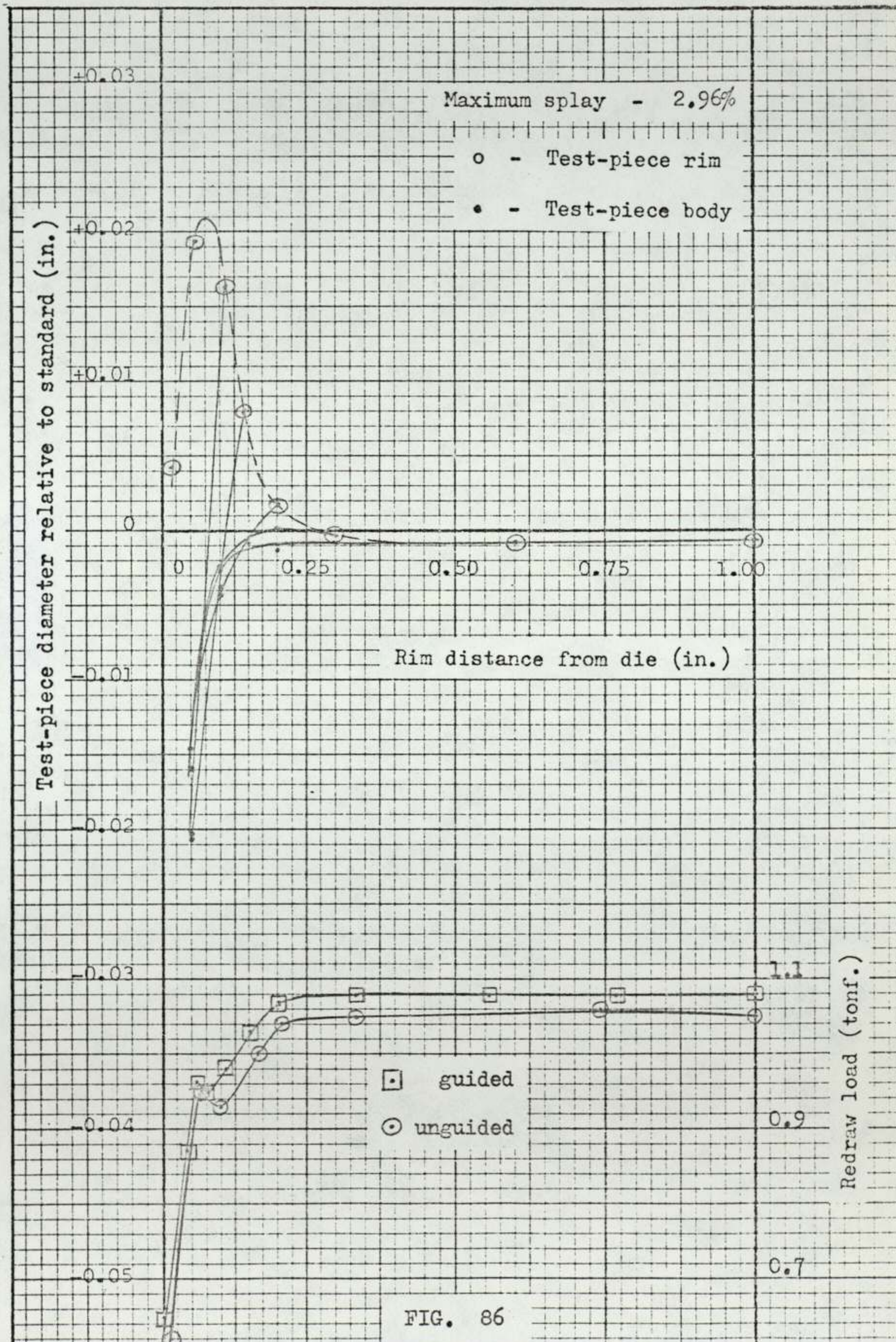

FIG. 86

Test number	Test material	Prior cold work Nominal (%)	Nominal test-piece dimensions (in.)		Die semi-angle (deg.)
			O/Dia.	Wall thk.	
8F	Steel	50	0.750	0.025	60

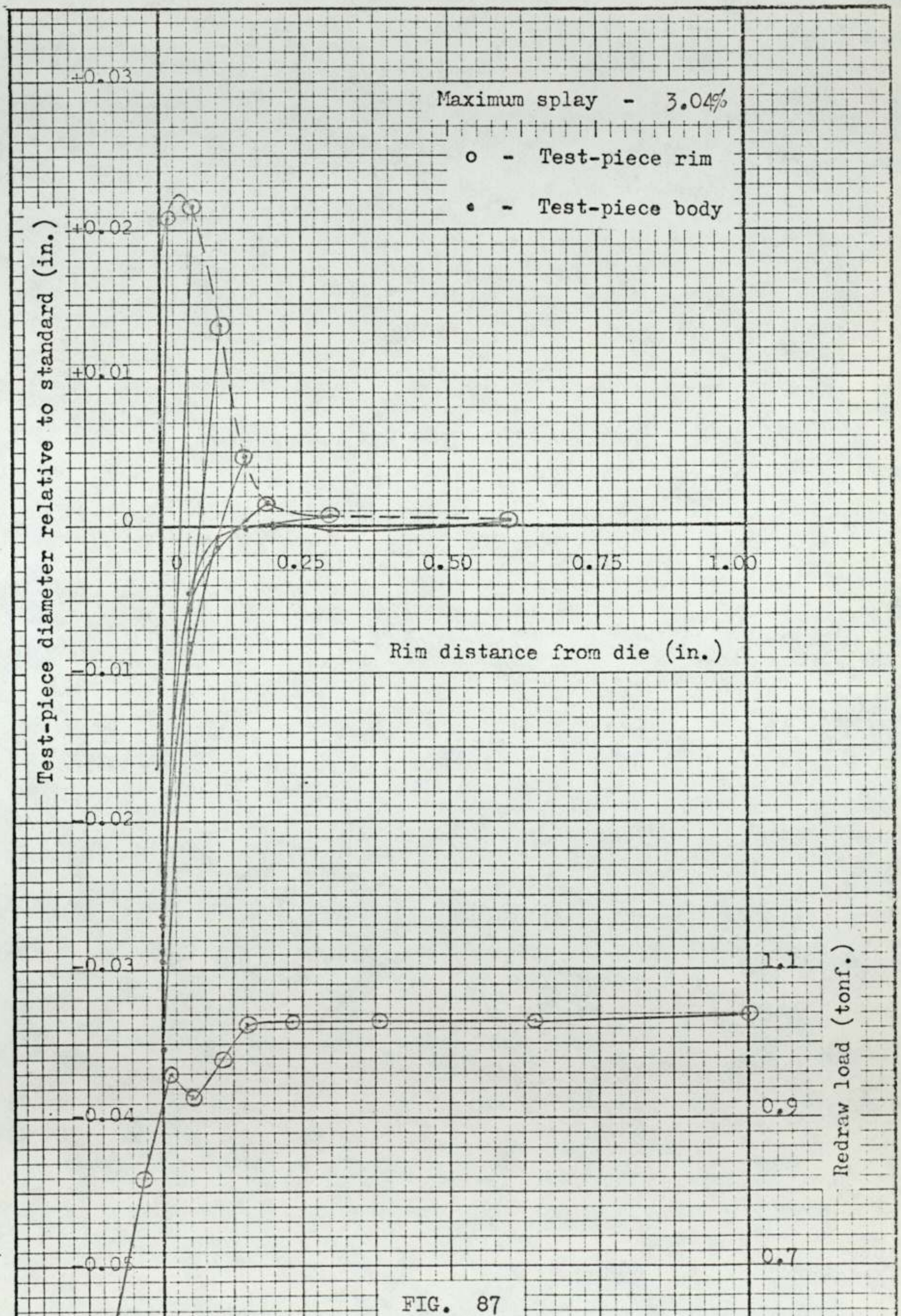

FIG. 87

Test number	Test material	Prior cold work Nominal (%)	Nominal test-piece dimensions (in.)		Die semi-angle (deg.)
			O/Dia.	Wall thk.	
9F	Steel	50	0.750	0.025	45

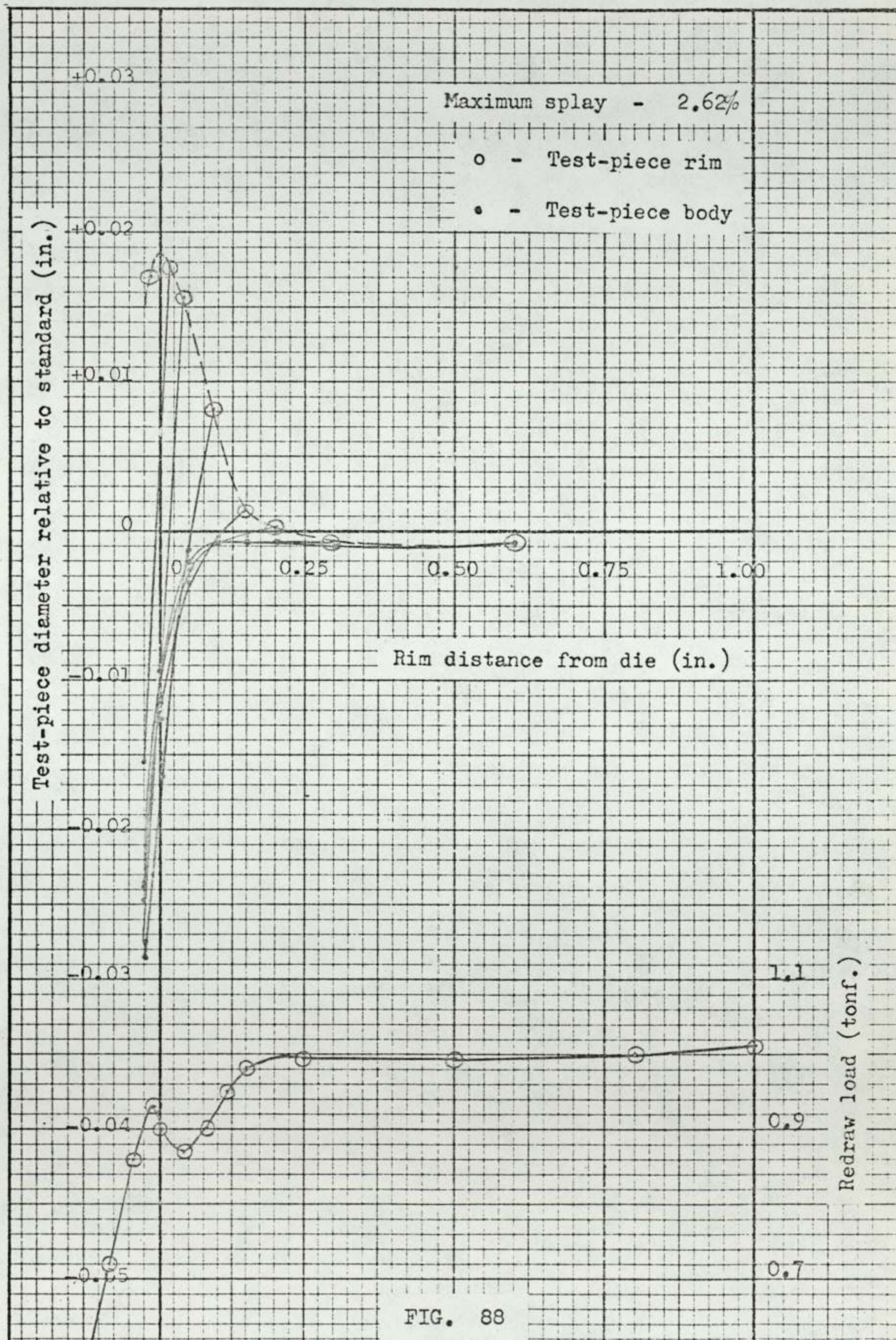

FIG. 88

Test number	Test material	Prior cold work Nominal (%)	Nominal test-piece dimensions (in.)		Die semi-angle (deg.)
			O/Dia.	Wall thk.	
11F	Steel	50	0.750	0.019	90

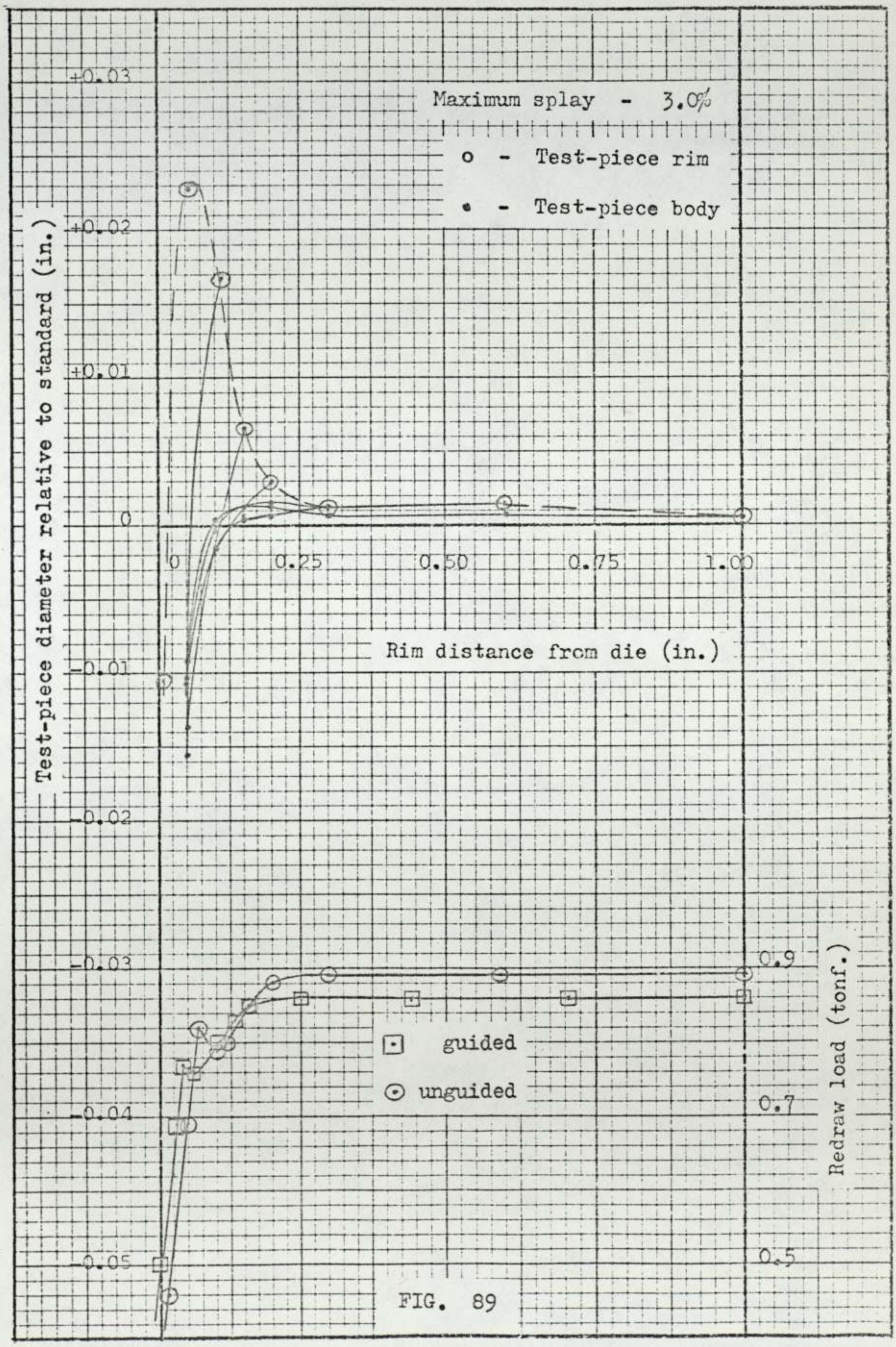

FIG. 89

Test number	Test material	Prior cold work Nominal (%)	Nominal test-piece dimensions (in.)		Die semi-angle (deg.)
			O/Dia.	Wall thk.	
12F	Steel	50	0.750	0.019	60

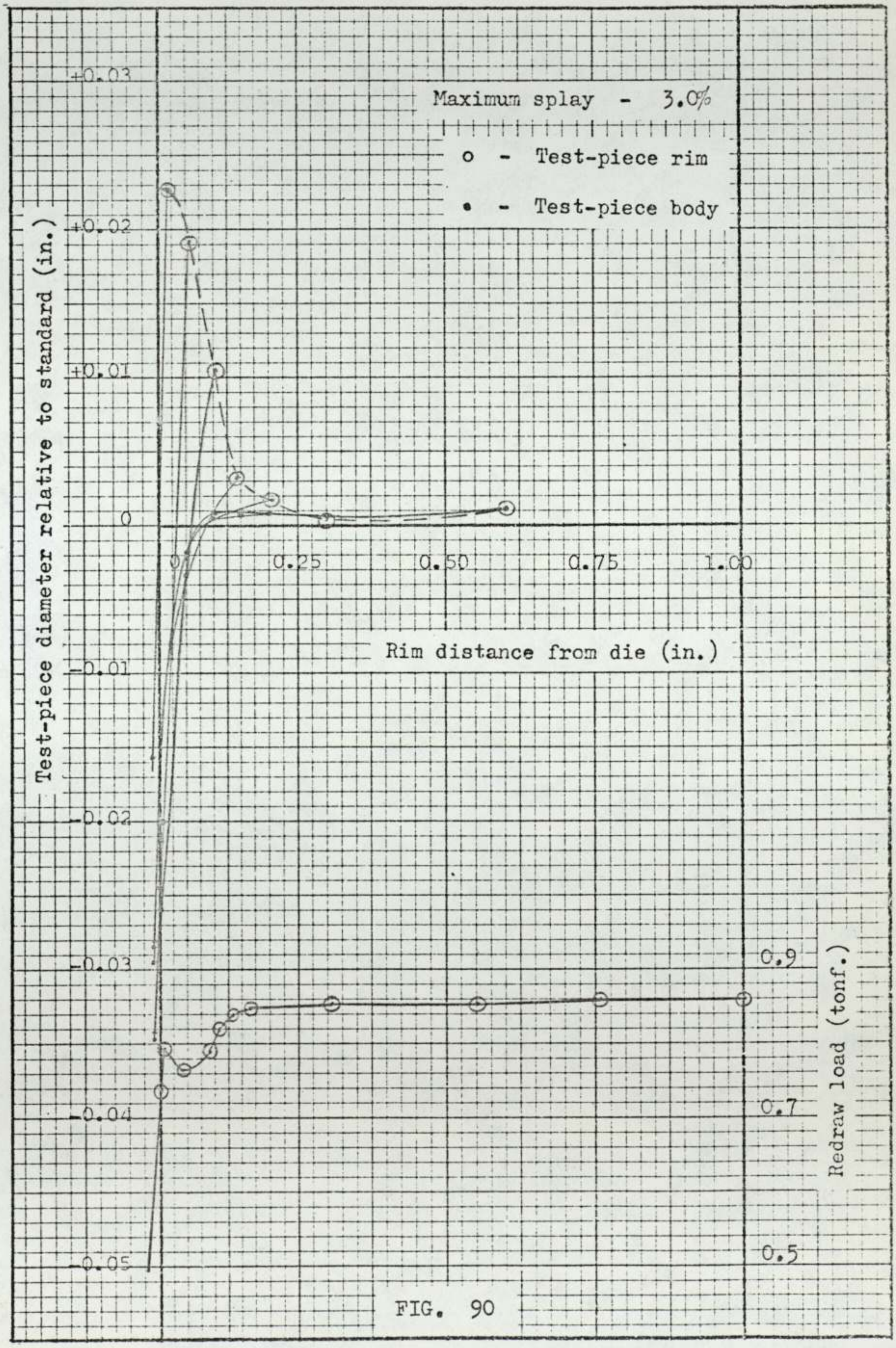

FIG. 90

Test number	Test material	Prior cold work Nominal (%)	Nominal test-piece dimensions (in.)		Die semi-angle (deg.)
			O/Dia.	Wall thk.	
13F	Steel	50	0.750	0.019	45

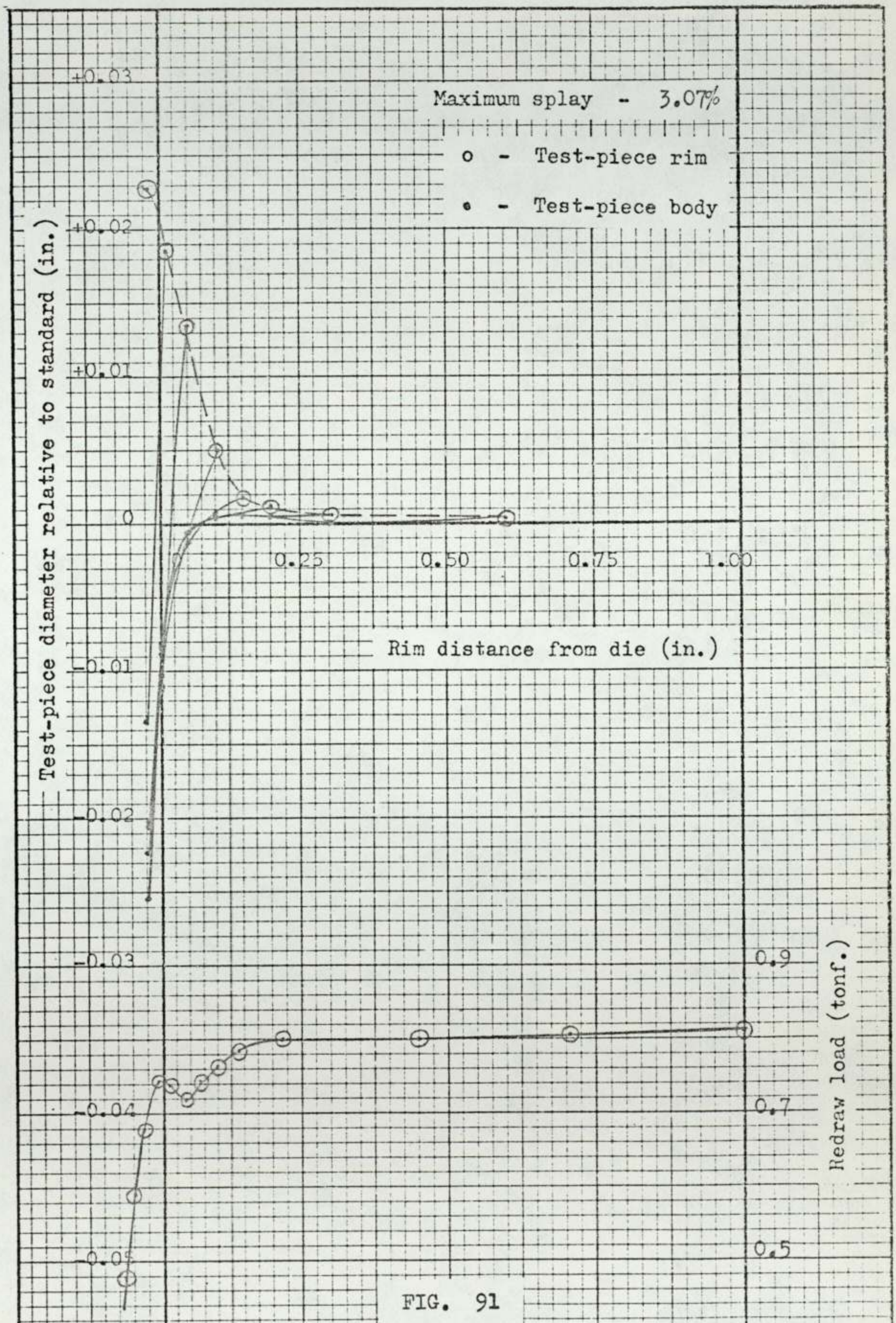

FIG. 91

Test number	Test material	Prior cold work Nominal (%)	Nominal test-piece dimensions (in.)		Die semi-angle (deg.)
			O/Dia.	Wall thk.	
14F	Steel	50	0.750	0.019	30

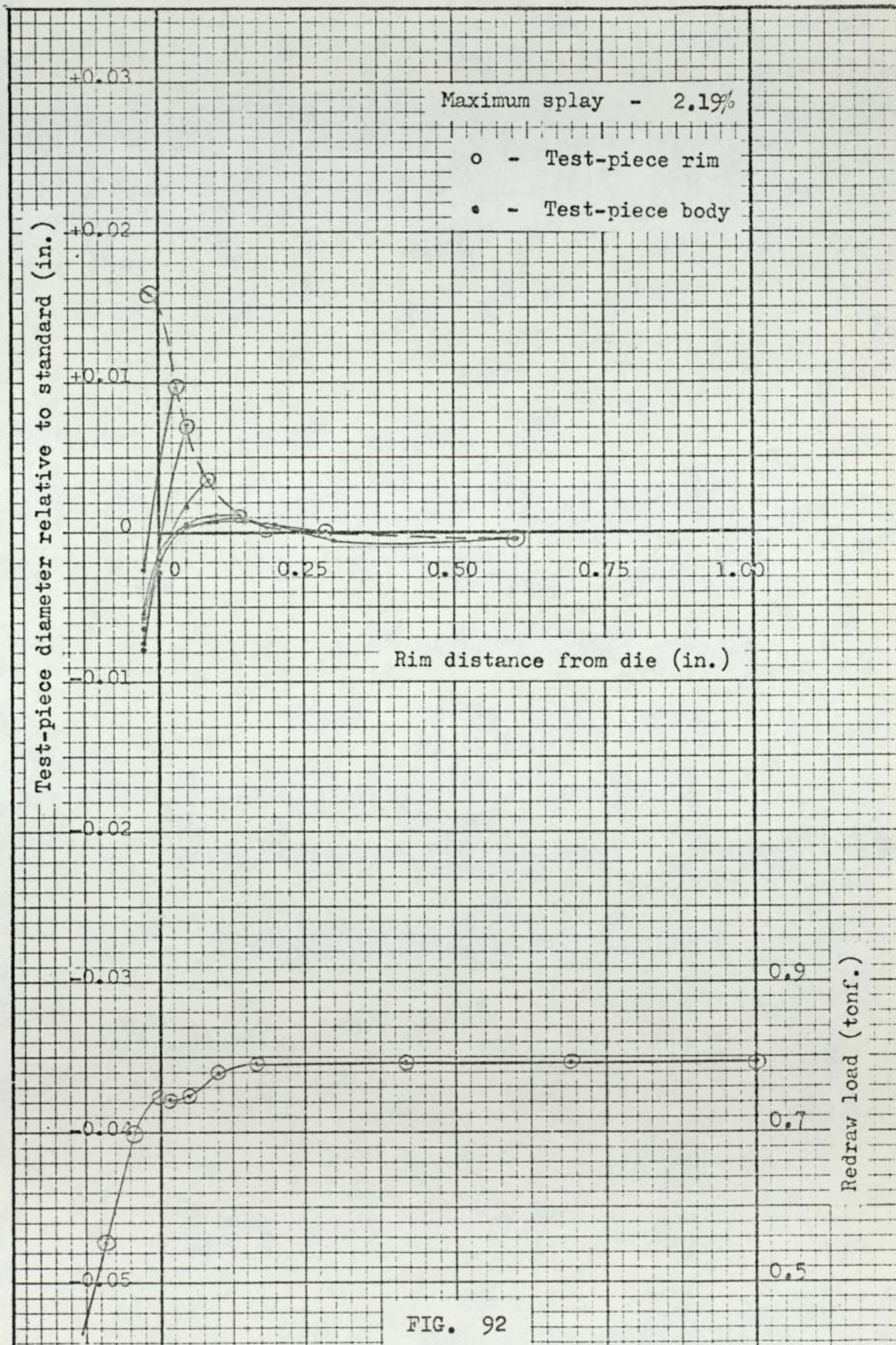

FIG. 92

Test number	Test material	Prior cold work Nominal (%)	Nominal test-piece dimensions (in.)		Die semi-angle (deg.)
			O/Dia.	Wall thk.	
15F	Steel	50	0.750	0.0125	90

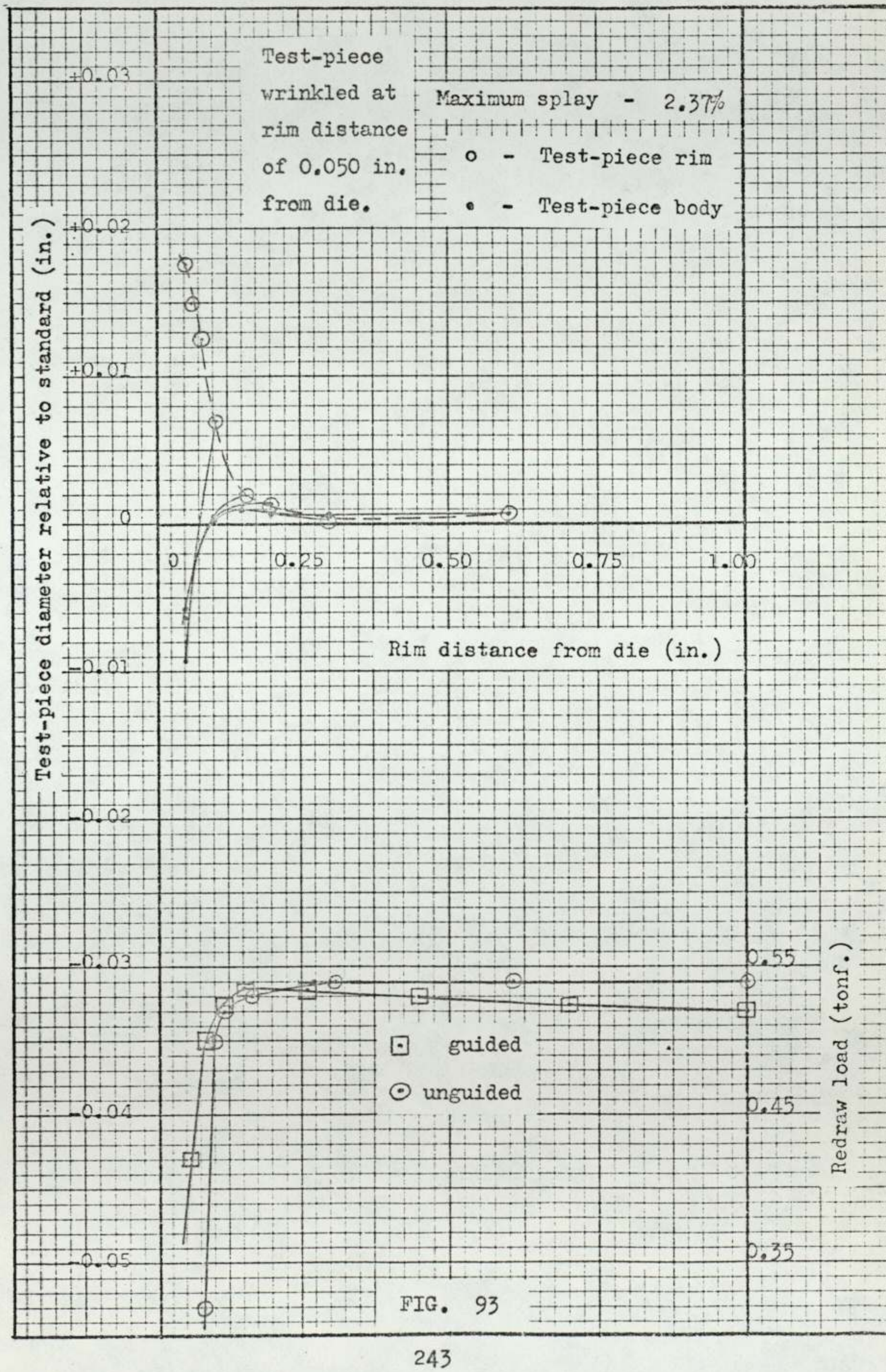

FIG. 93

Test number	Test material	Prior cold work Nominal (%)	Nominal test-piece dimensions (in.)		Die semi-angle (deg.)
			O/Dia.	Wall thk.	
16F	Steel	50	0.750	0.0125	60

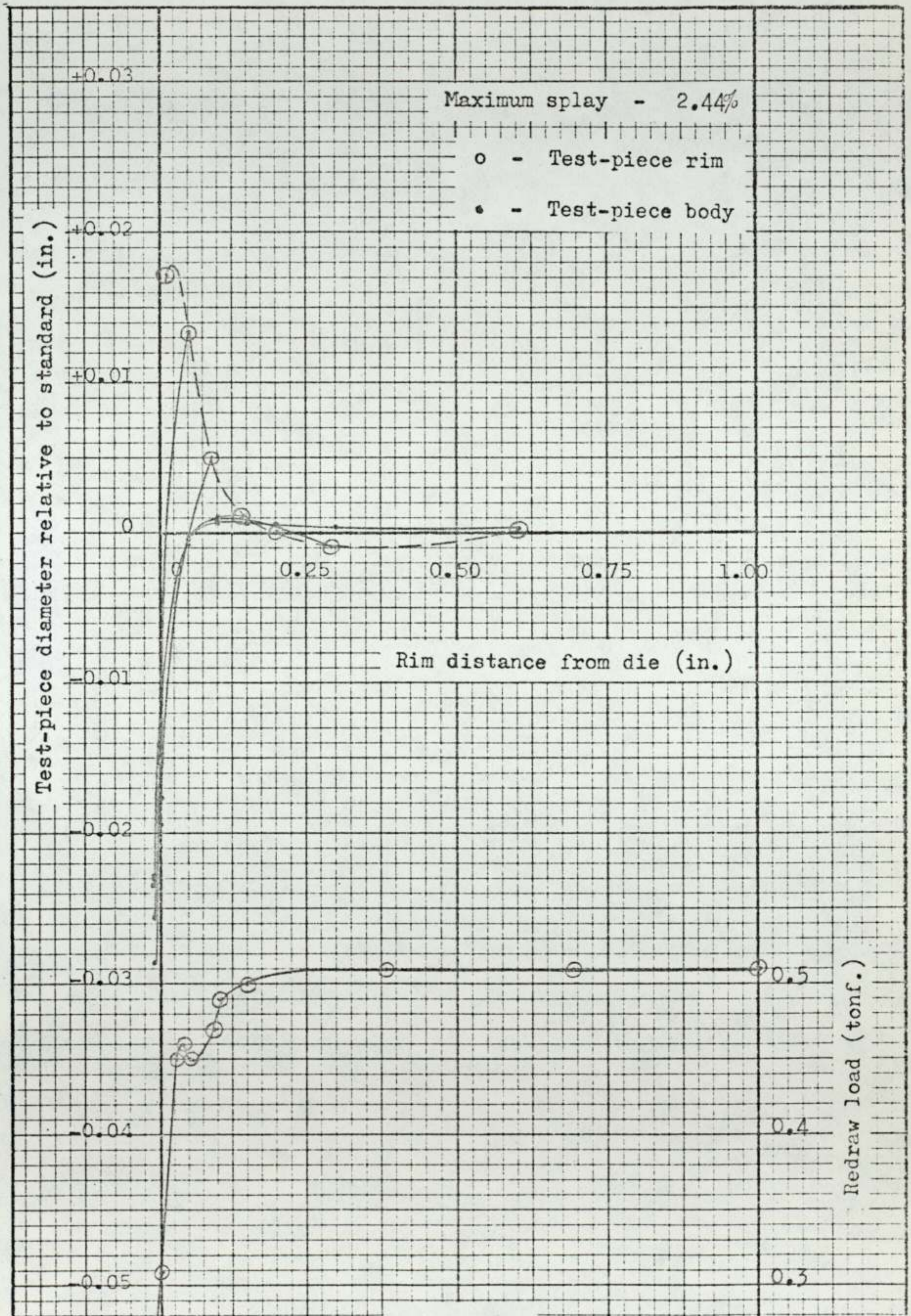

FIG. 94

Test number	Test material	Prior cold work Nominal (%)	Nominal test-piece dimensions (in.)		Die semi-angle (deg.)
			O/Dia.	Wall thk.	
17F	Steel	50	0.750	0.0125	45

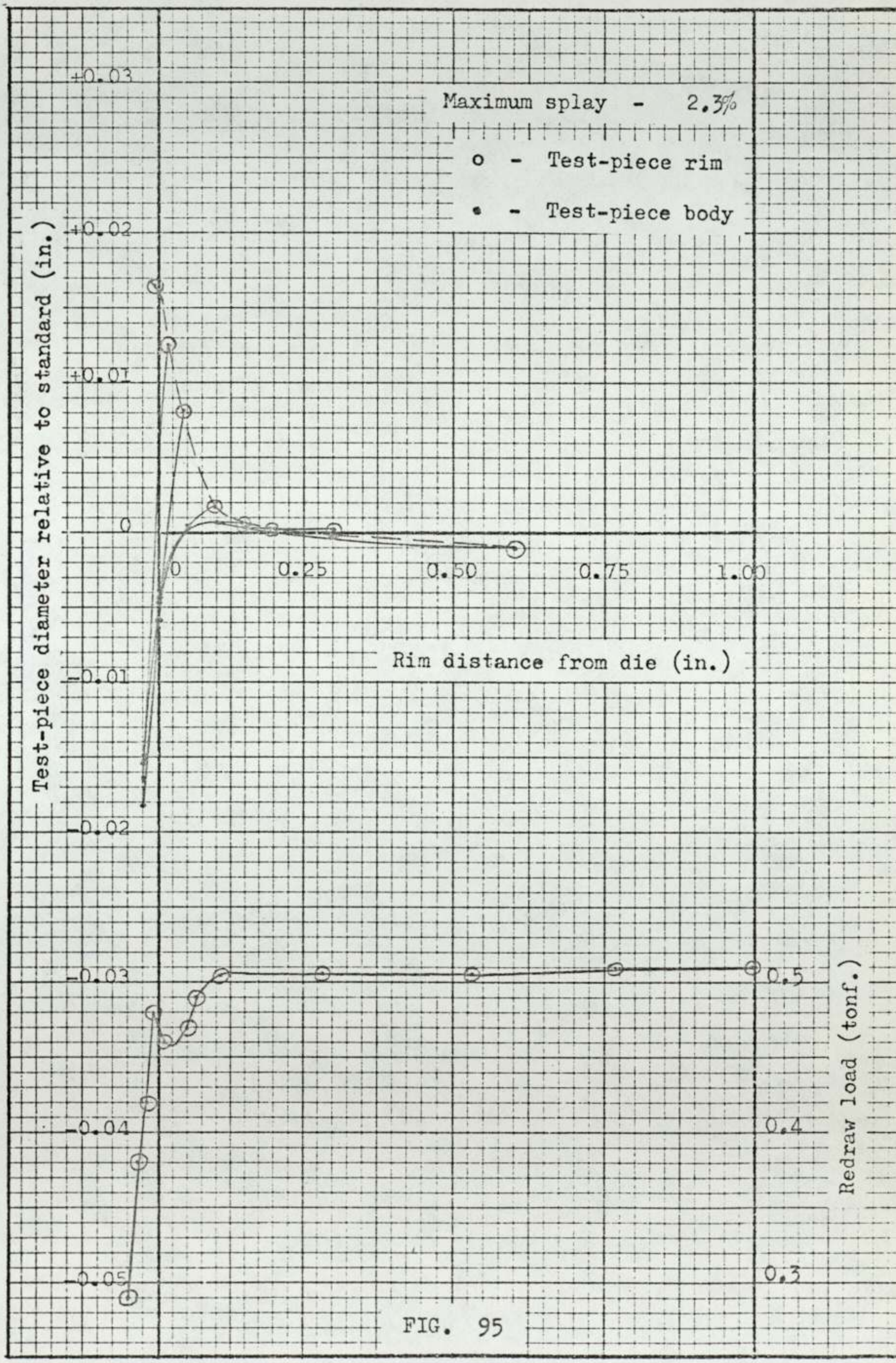

FIG. 95

Test number	Test material	Prior cold work Nominal (%)	Nominal test-piece dimensions (in.)		Die semi-angle (deg.)
			O/Dia.	Wall thk.	
18F	Steel	50	0.750	0.0125	30

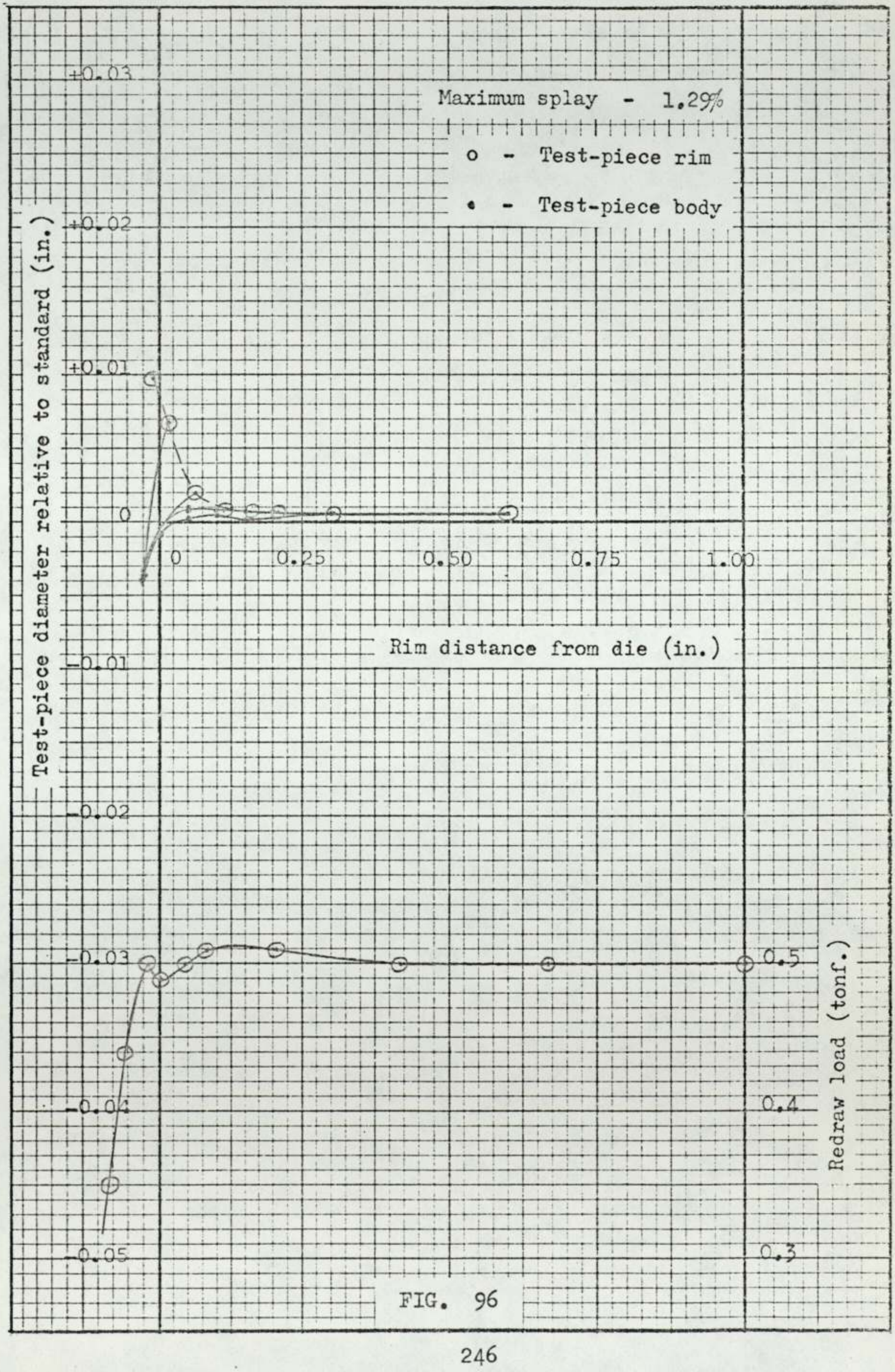

FIG. 96

Test number	Test material	Prior cold work Nominal (%)	Nominal test-piece dimensions (in.)		Die semi-angle (deg.)
			O/Dia.	Wall thk.	
19F	70/30 brass	0	0.750	0.0375	90

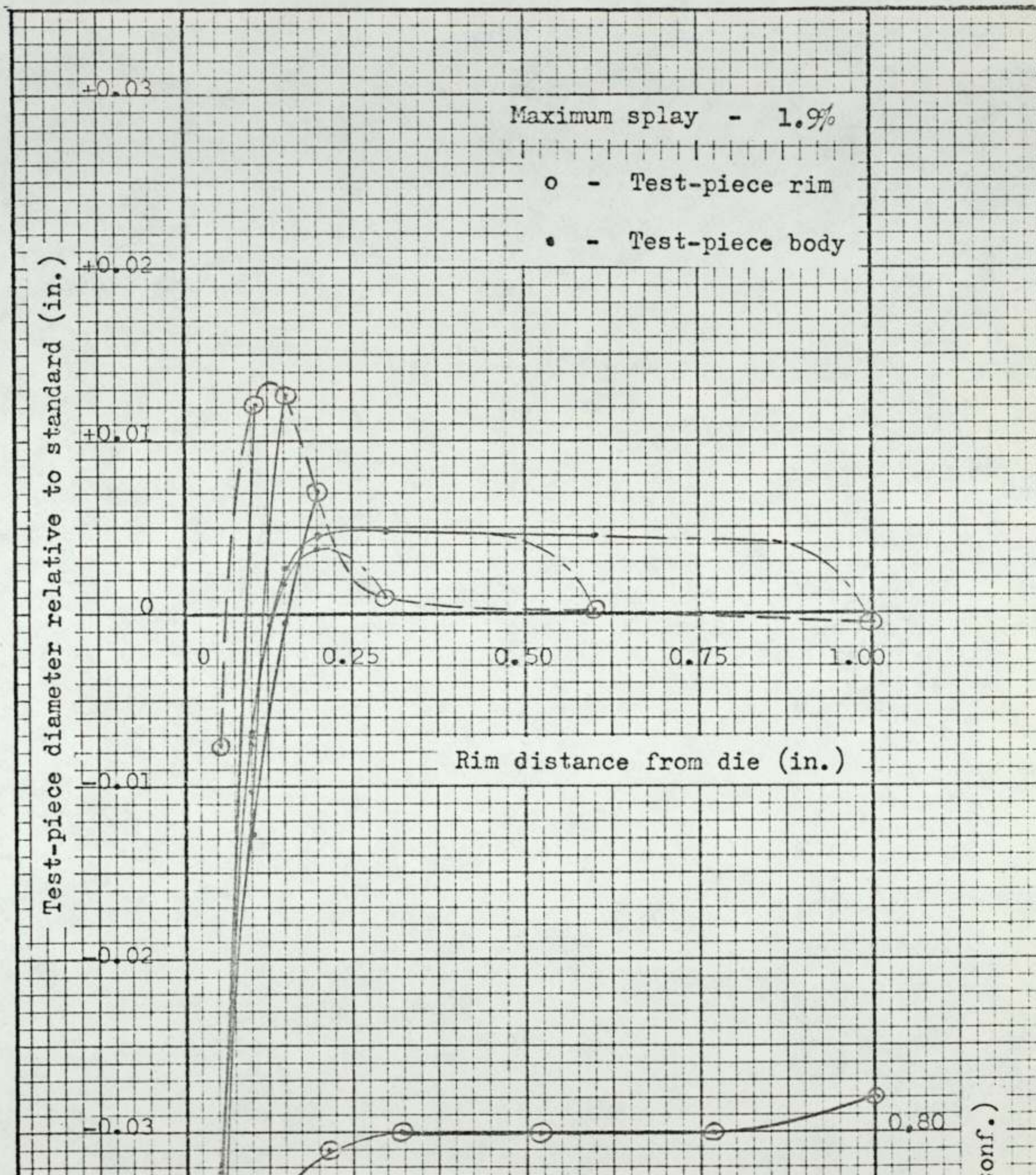

FIG. 97

Test number	Test material	Prior cold work Nominal (%)	Nominal test-piece dimensions (in.)		Die semi-angle (deg.)
			O/Dia.	Wall thk.	
20F	70/30 brass	50	0.750	0.0375	90

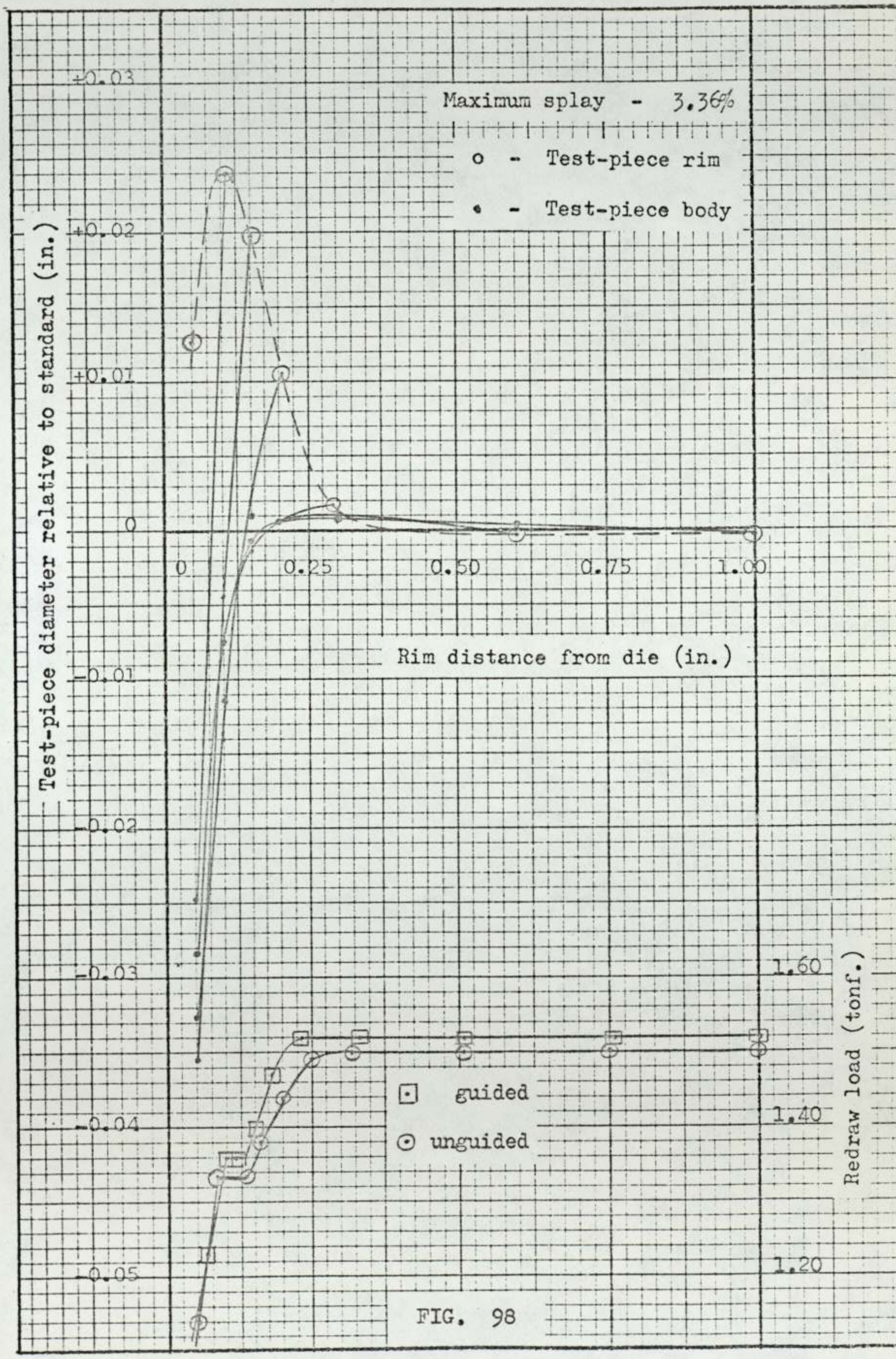

FIG. 98

Test number	Test material	Prior cold work Nominal (%)	Nominal test-piece dimensions (in.)		Die semi-angle (deg.)
			O/Dia.	Wall thk.	
21F	70/30 brass	50	0.750	0.025	90

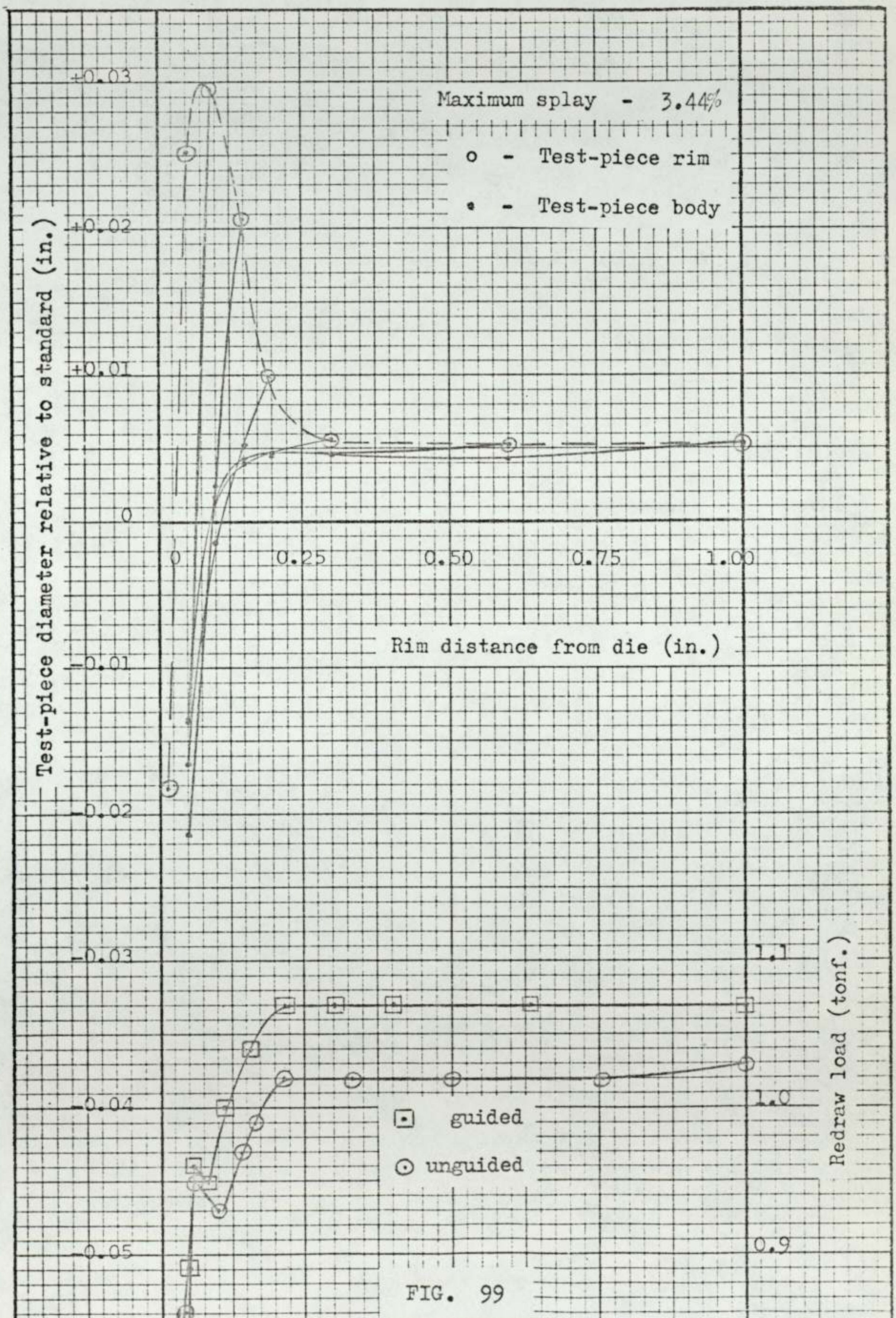

FIG. 99

Test number	Test material	Prior cold work Nominal (%)	Nominal test-piece dimensions (in.)		Die semi-angle (deg.)
			O/Dia.	Wall thk.	
22F	70/30 brass	50	0.750	0.019	90

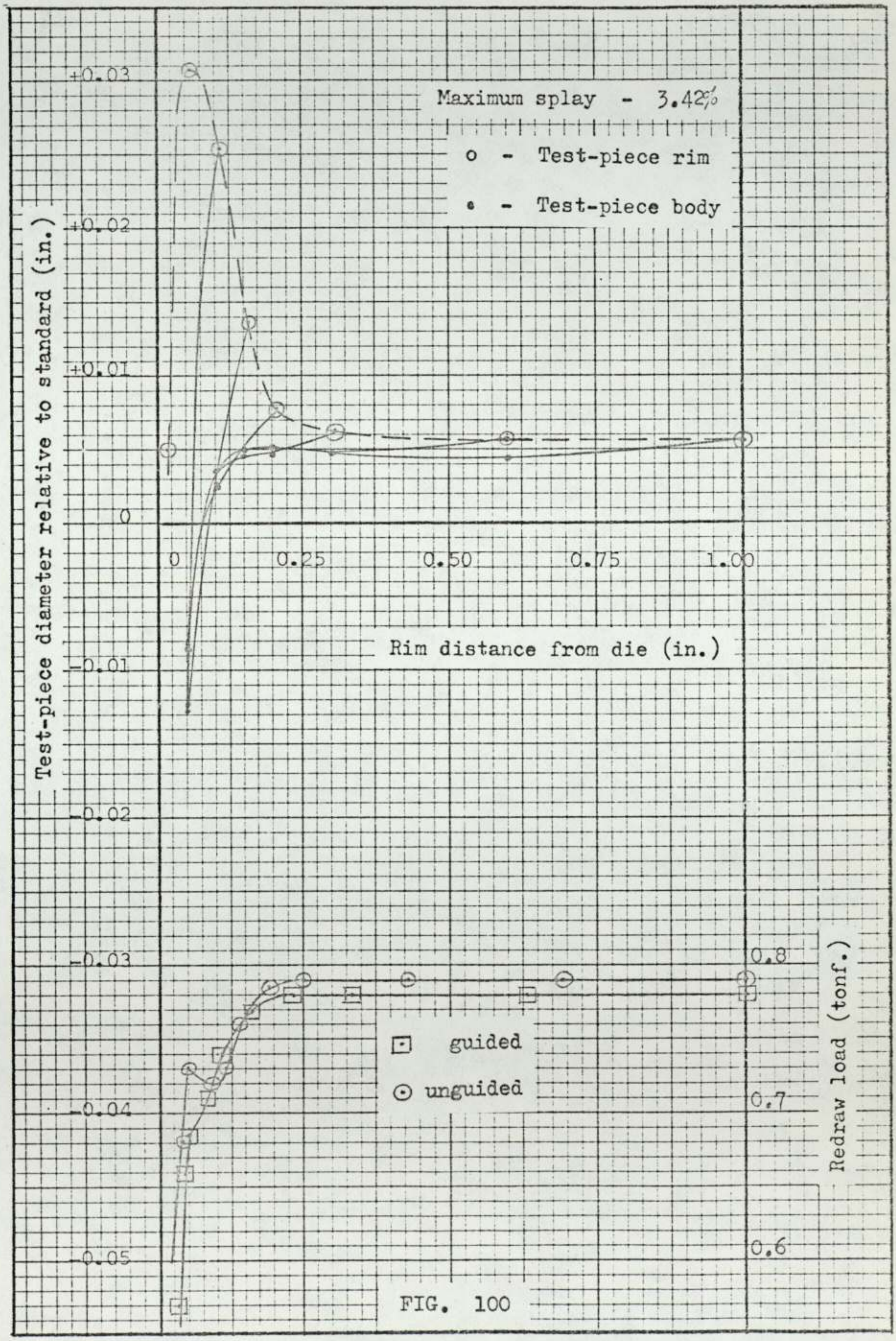

FIG. 100

Test number	Test material	Prior cold work Nominal (%)	Nominal test-piece dimensions (in.)		Die semi-angle (deg.)
			O/Dia.	Wall thk.	
23F	70/30 brass	50	0.750	0.0125	90

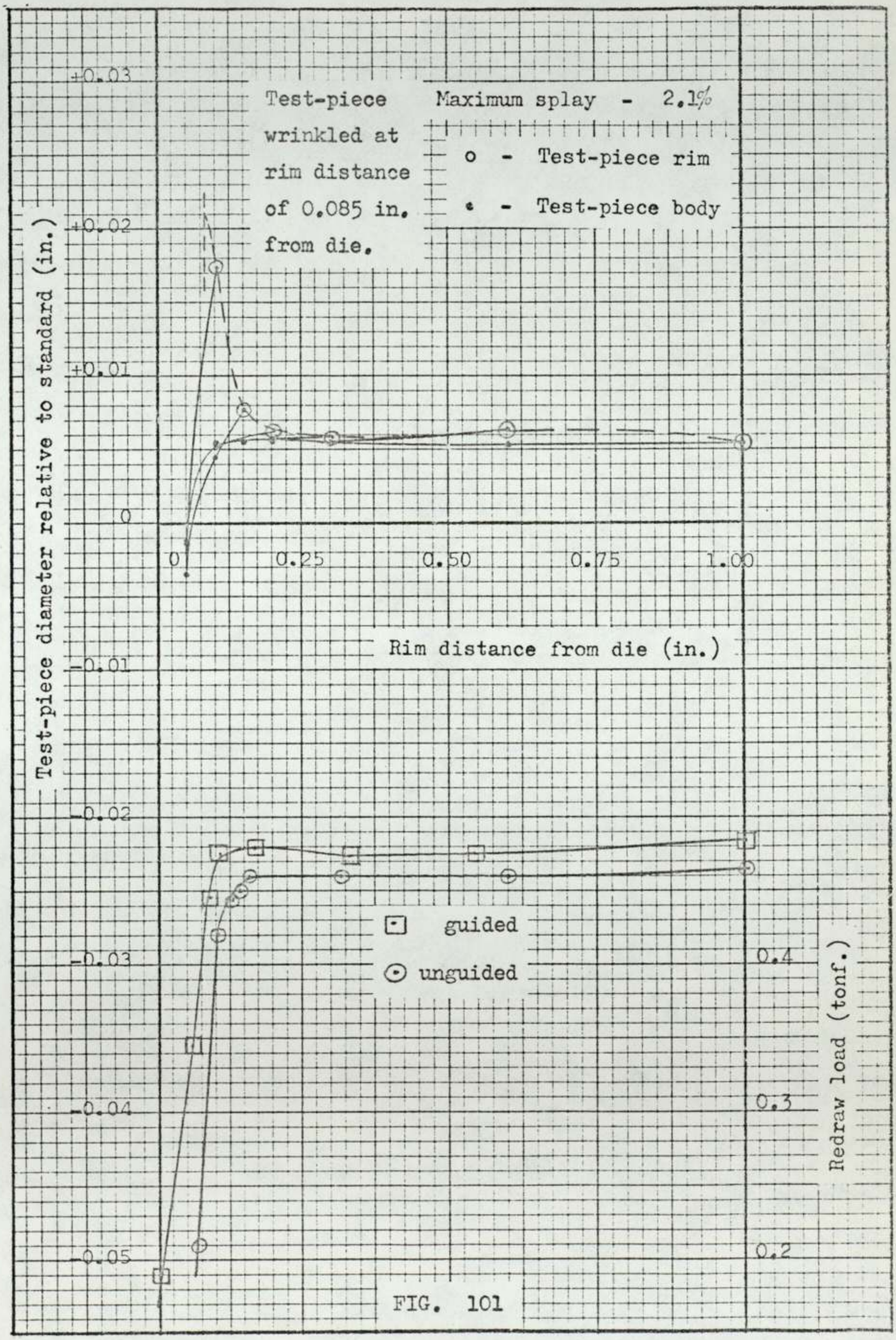

FIG. 101

Test number	Test material	Prior cold work Nominal (%)	Nominal test-piece dimensions (in.)		Die semi-angle (deg.)
			O/Dia.	Wall thk.	
24F	T304 Stainless	0	0.750	0.025	90

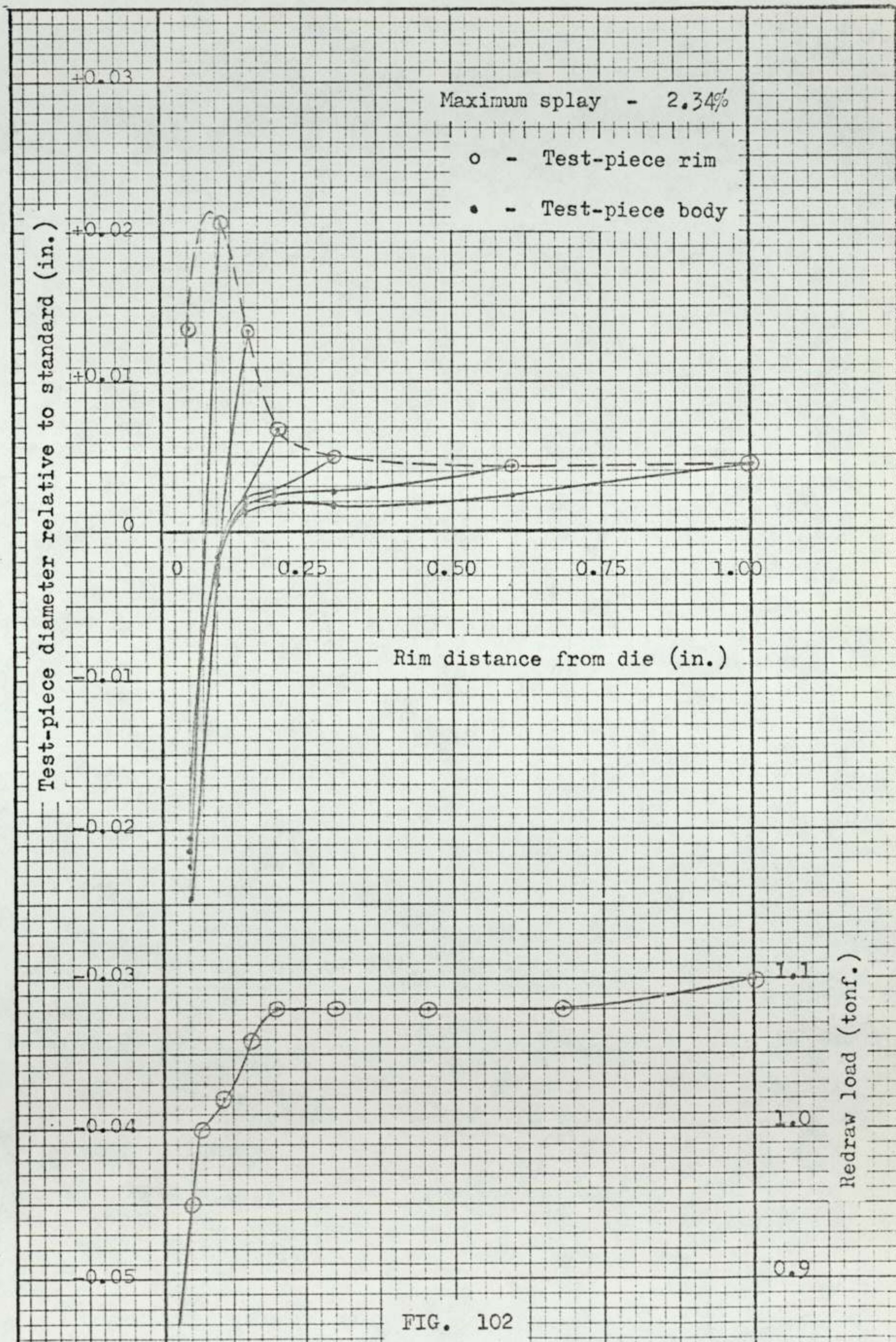

FIG. 102

Test number	Test material	Prior cold work Nominal (%)	Nominal test-piece dimensions (in)		Die semi-angle (deg.)
			O/Dia.	Wall thk.	
25F	T304 Stainless	0	0.750	0.019	90

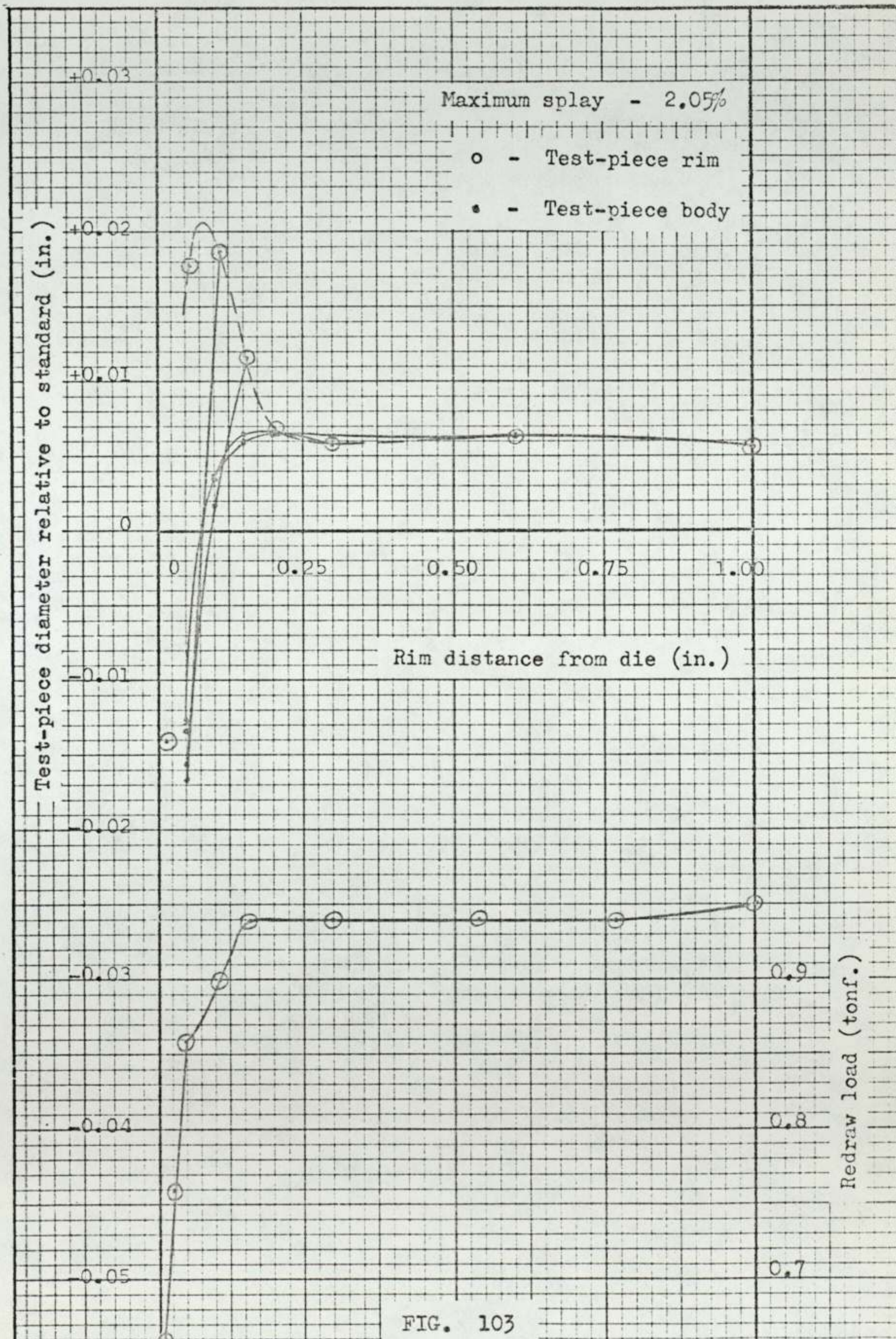

FIG. 103

Test number	Test material	Prior cold work Nominal (%)	Nominal test-piece dimensions (in.)		Die semi-angle (deg.)
			O/Dia.	Wall thk.	
26F	T304 Stainless	50	0.750	0.019	90

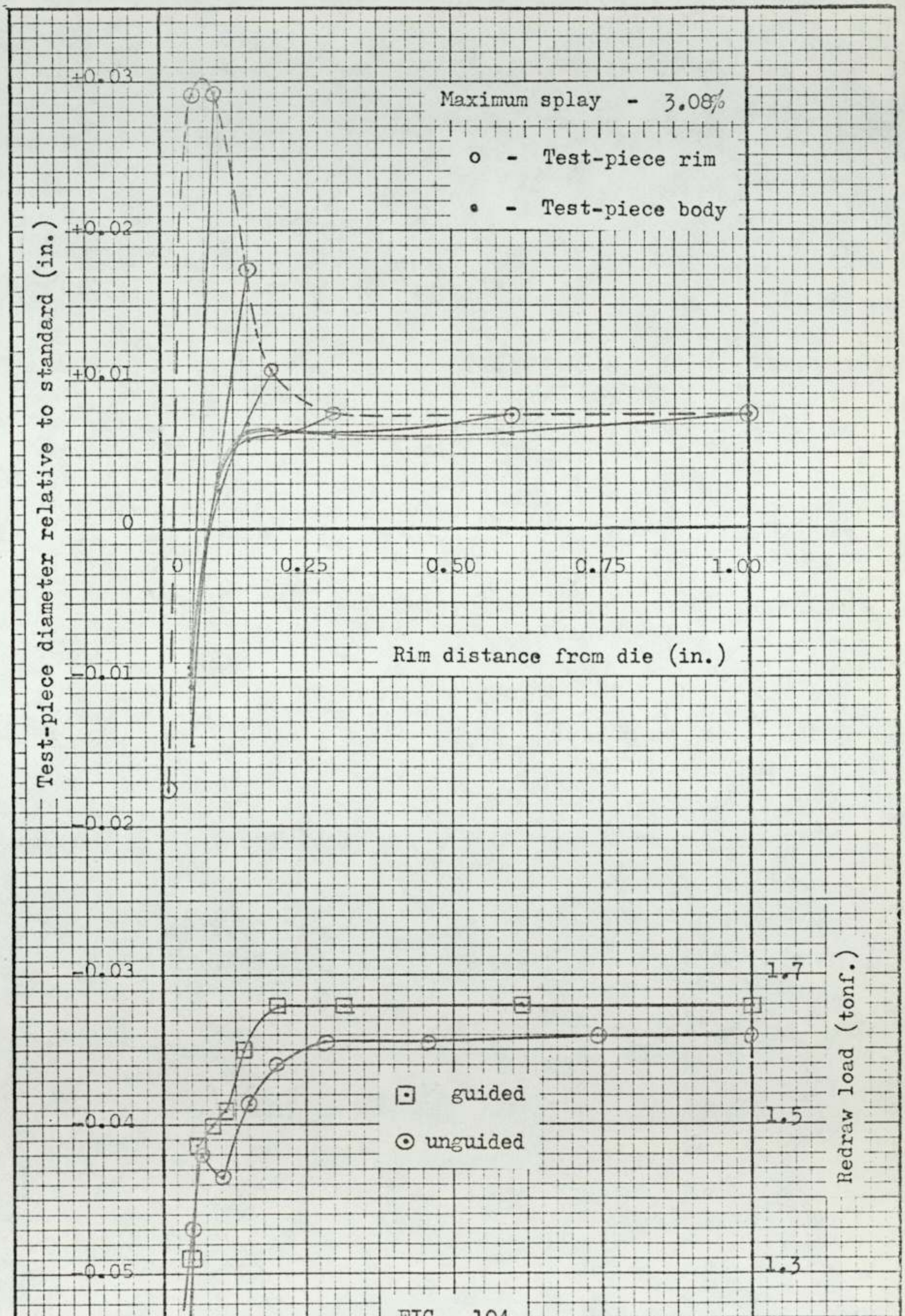

FIG. 104

Test number	Test material	Prior cold work Nominal (%)	Nominal test-piece dimensions (in.)		Die semi-angle (deg.)
			O/Dia.	Wall thk.	
27F	T304 Stainless	50	0.750	0.0125	90

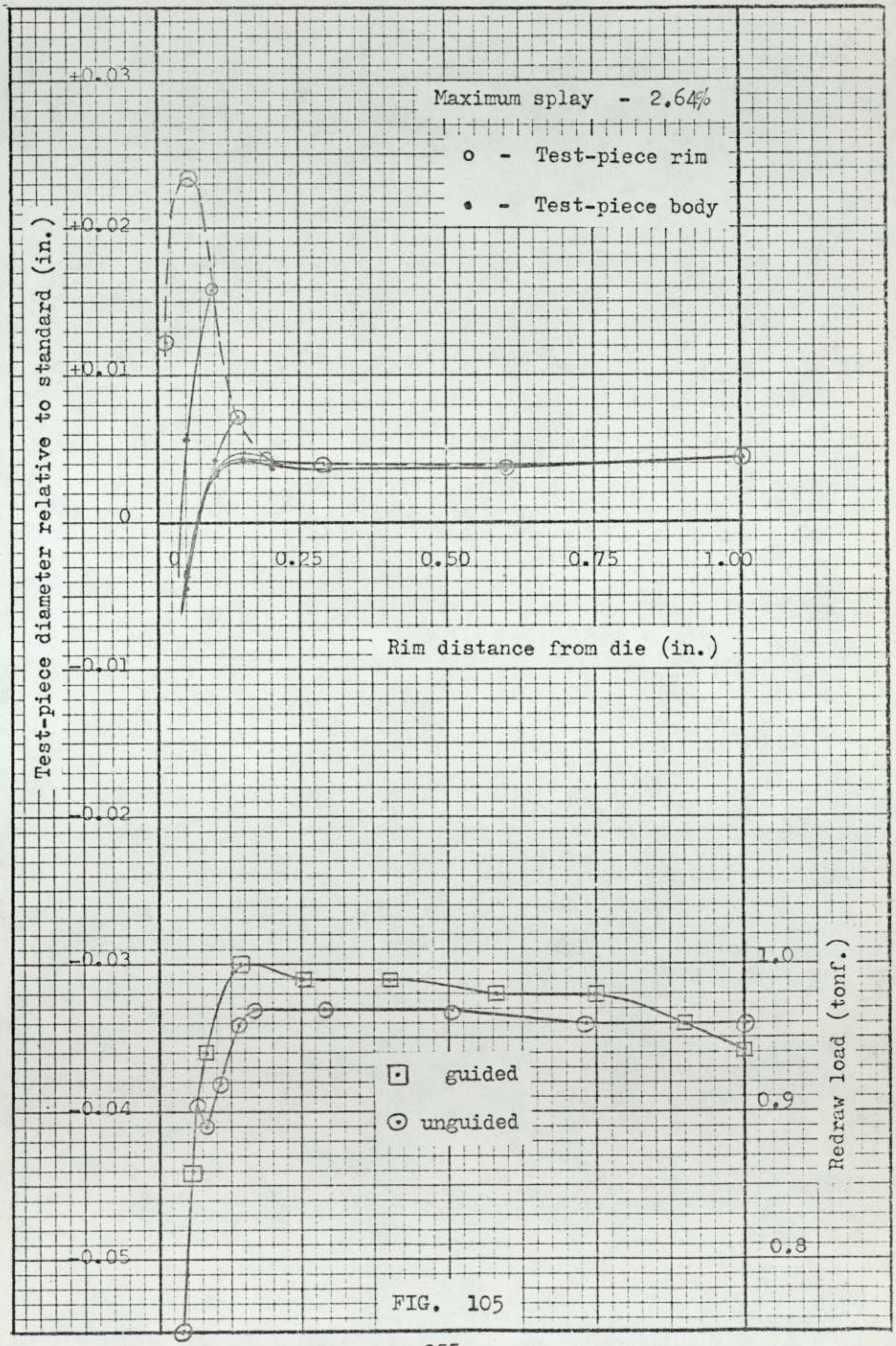

FIG. 105

Test number	Test material	Prior cold work Nominal (%)	Nominal test-piece dimensions (in.)		Die semi-angle (deg.)
			O/Dia.	Wall thk.	
28F	Aluminium	0	0.750	0.0375	90

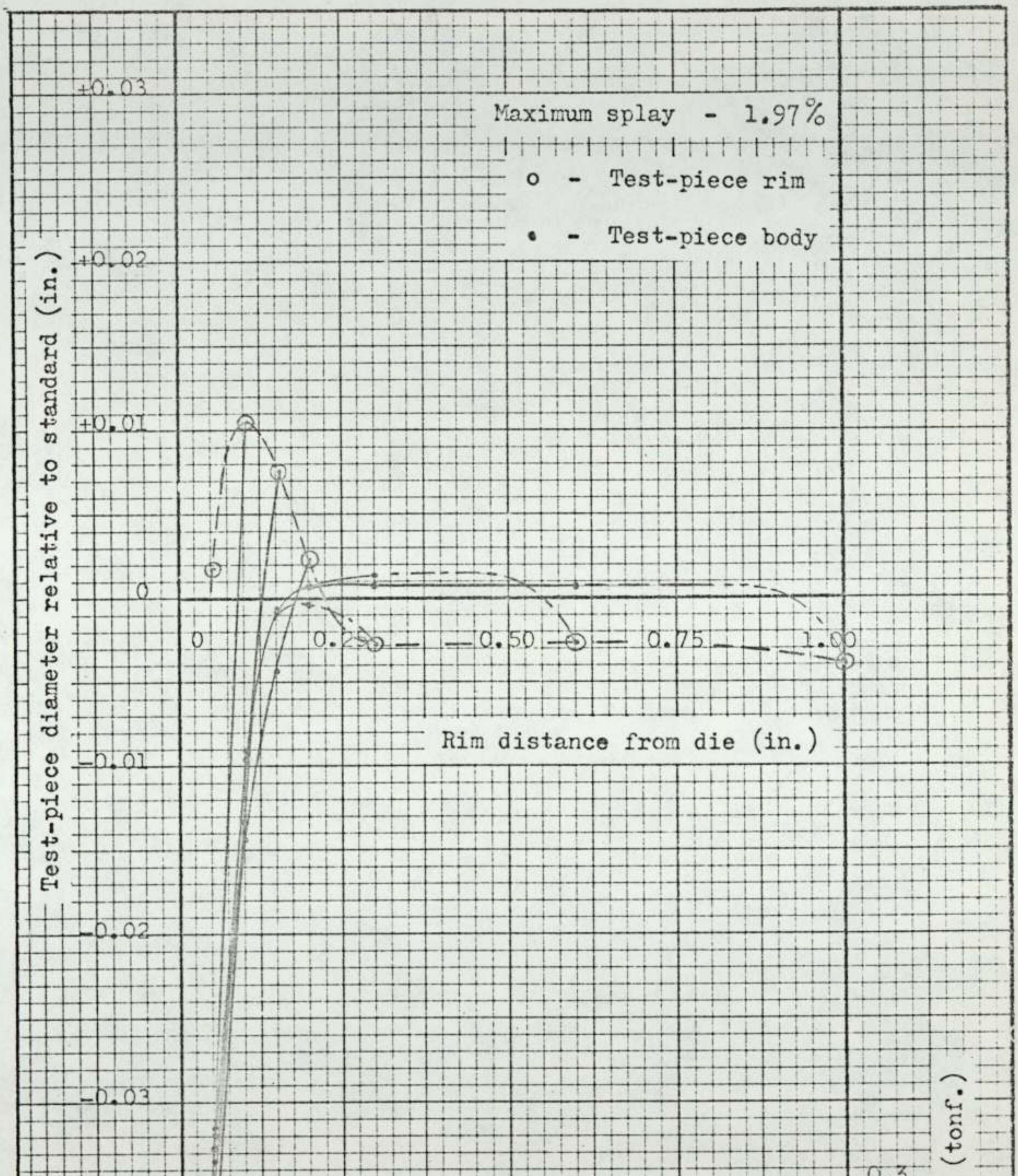

FIG. 106

Test number	Test material	Prior cold work Nominal (%)	Nominal test-piece dimensions (in.)		Die semi-angle (deg.)
			O/Dia.	Wall thk.	
29F	Aluminium	50	0.750	0.0375	90

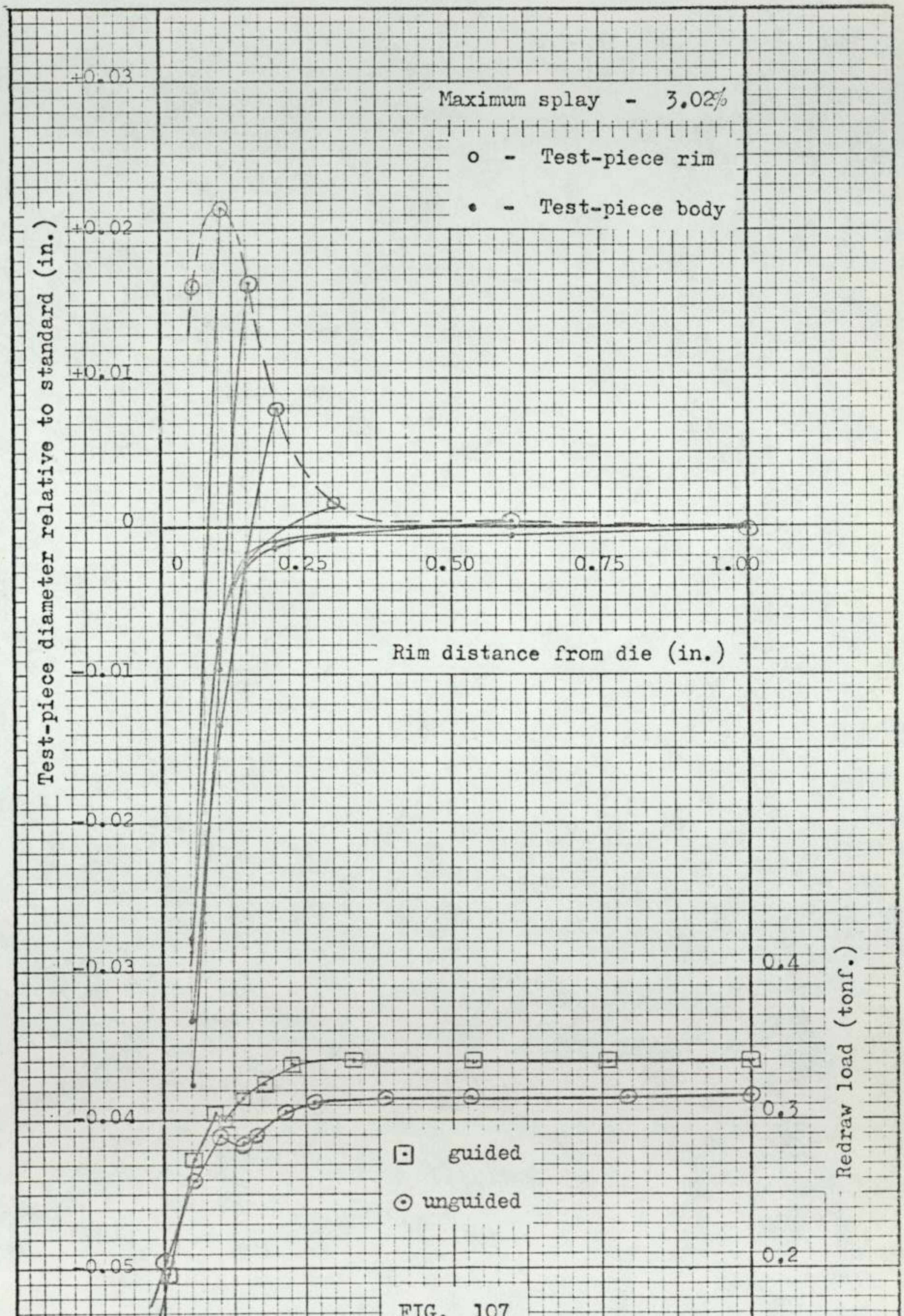

FIG. 107

Test number	Test material	Prior cold work Nominal (%)	Nominal test-piece dimensions (in.)		Die semi-angle (deg.)
			O/Dia.	Wall thk.	
30F	Aluminium	67	0.750	0.0375	90

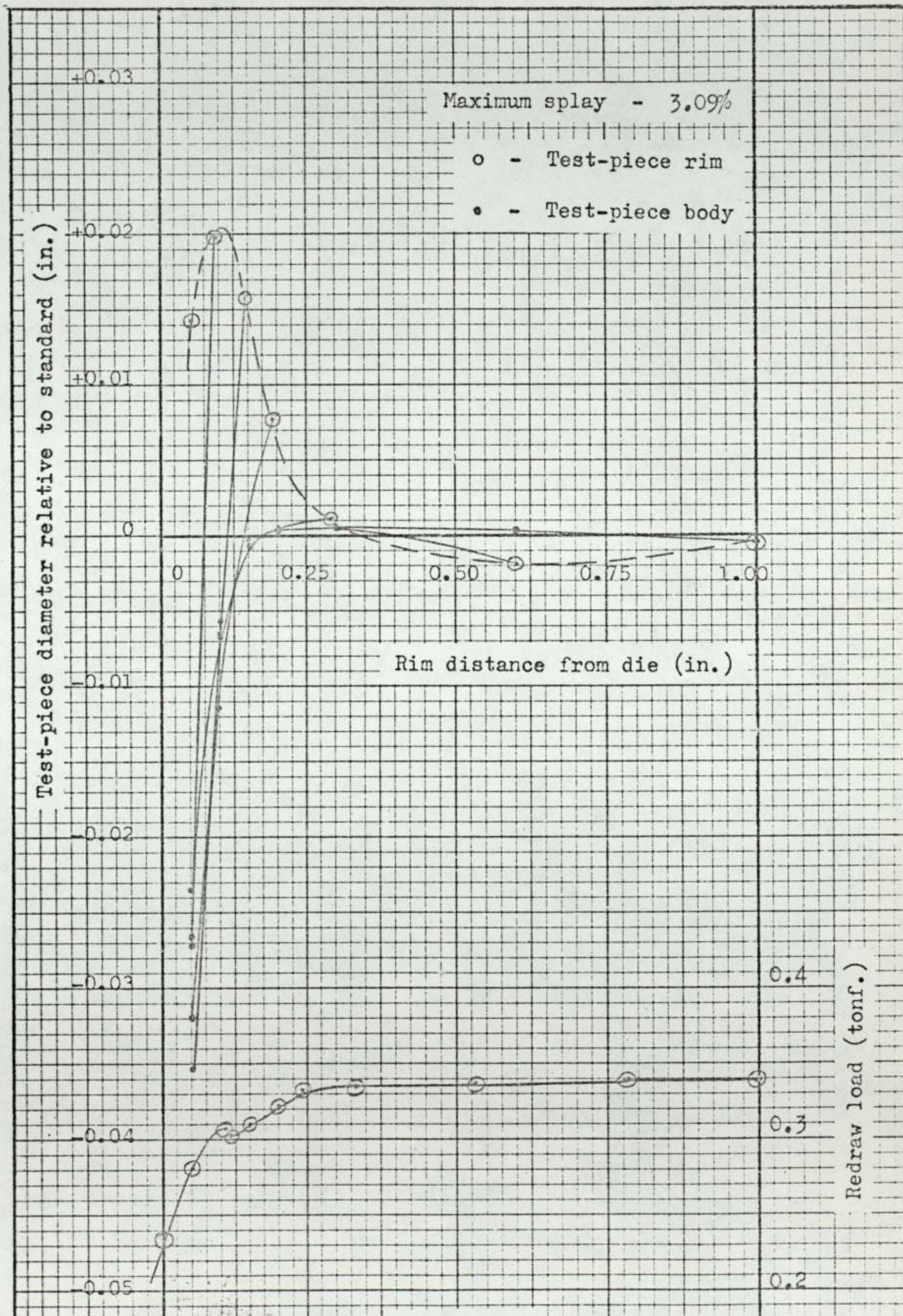

FIG. 108

Test number	Test material	Prior cold work Nominal (%)	Nominal test-piece dimensions (in.)		Die semi-angle (deg.)
			O/Dia.	Wall thk.	
31F	Aluminium	50	0.750	0.025	90

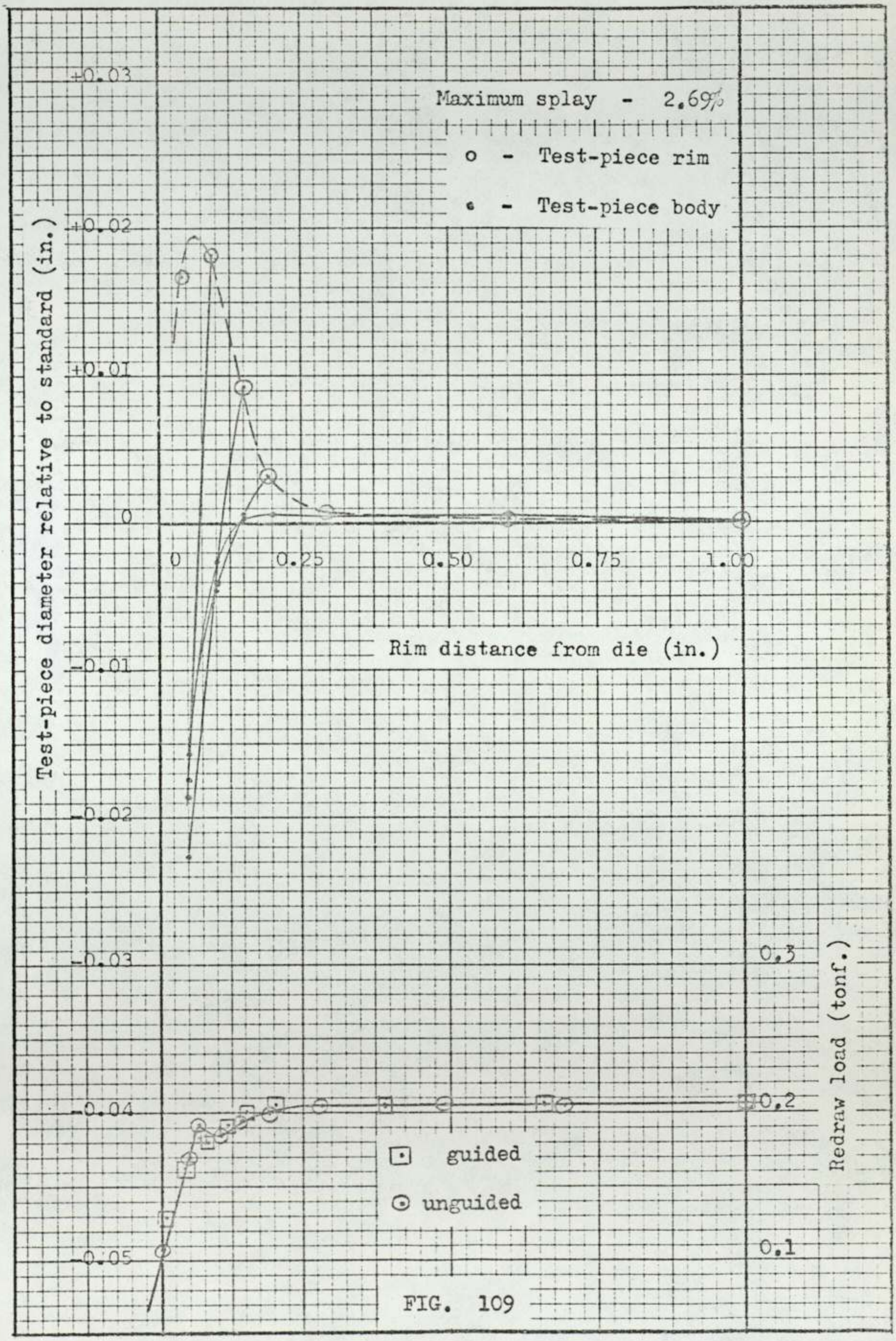

FIG. 109

Test number	Test material	Prior cold work Nominal (%)	Nominal test-piece dimensions (in.)		Die semi-angle (deg.)
			O/Dia.	Wall thk.	
32F	Aluminium	50	0.750	0.019	90

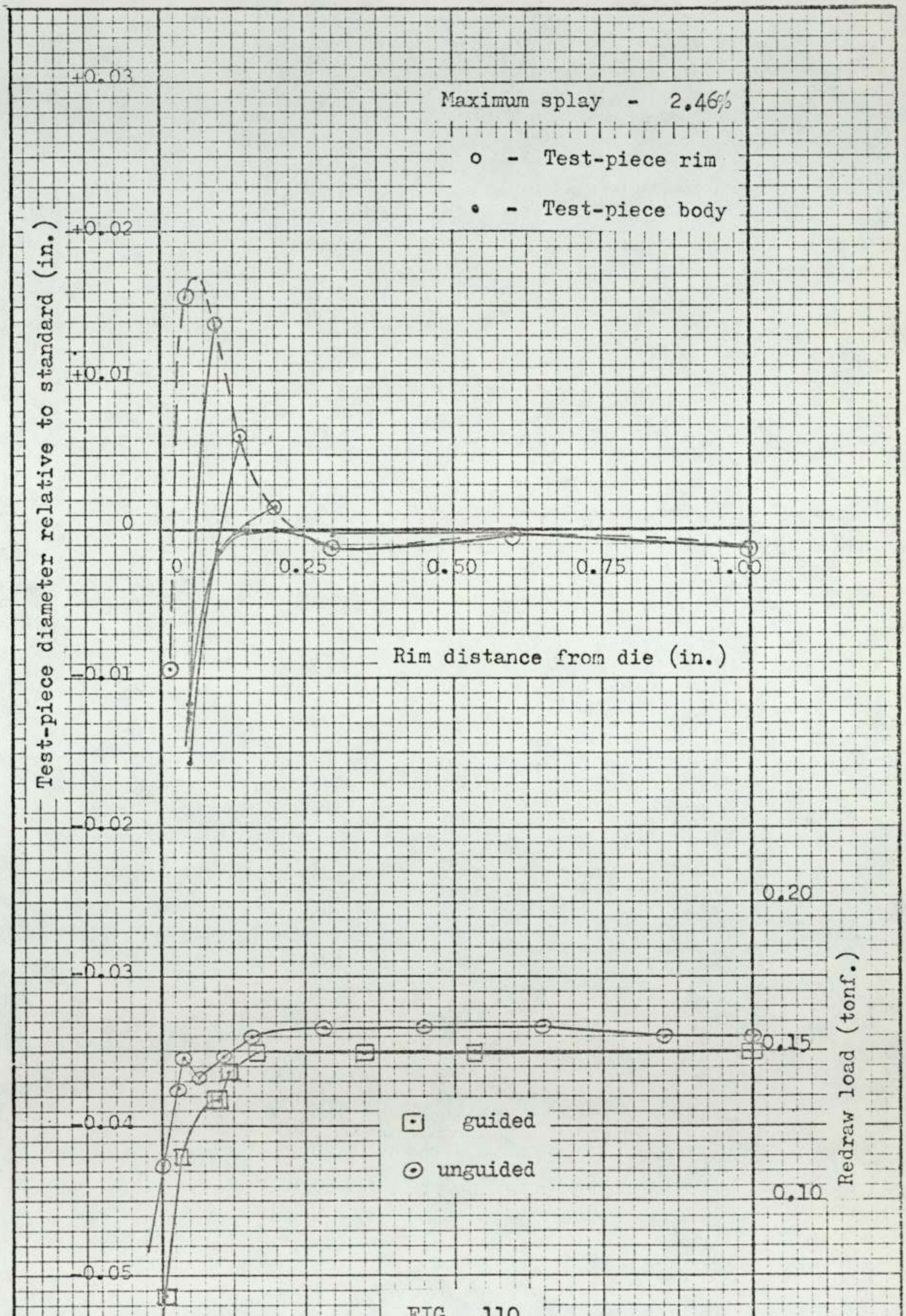

FIG. 110

Test number	Test material	Prior cold work Nominal (%)	Nominal test-piece dimensions (in.)		Die semi-angle (deg.)
			O/Dia.	Wall thk.	
33F	Aluminium	50	0.750	0.0125	90

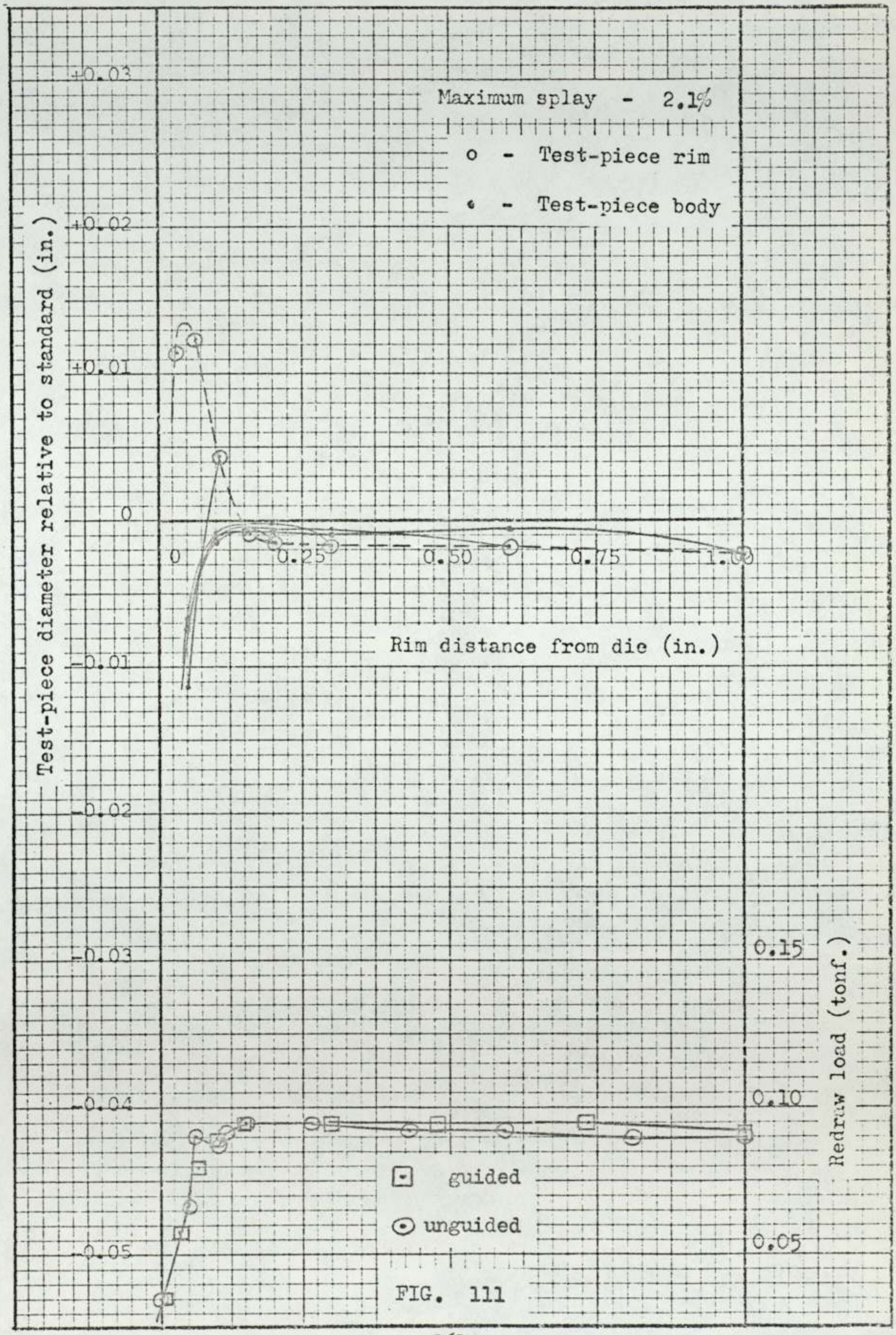

FIG. 111

Test Number	Test Material	Prior cold work. Nominal (%)	Nominal test - piece dimensions (in.)		Die semi-angle (deg.)	Hold-down punch nose radius (in.)
			O/Dia.	Wall thk.		
1C	Steel	67	0.750	0.0075	90	0.030

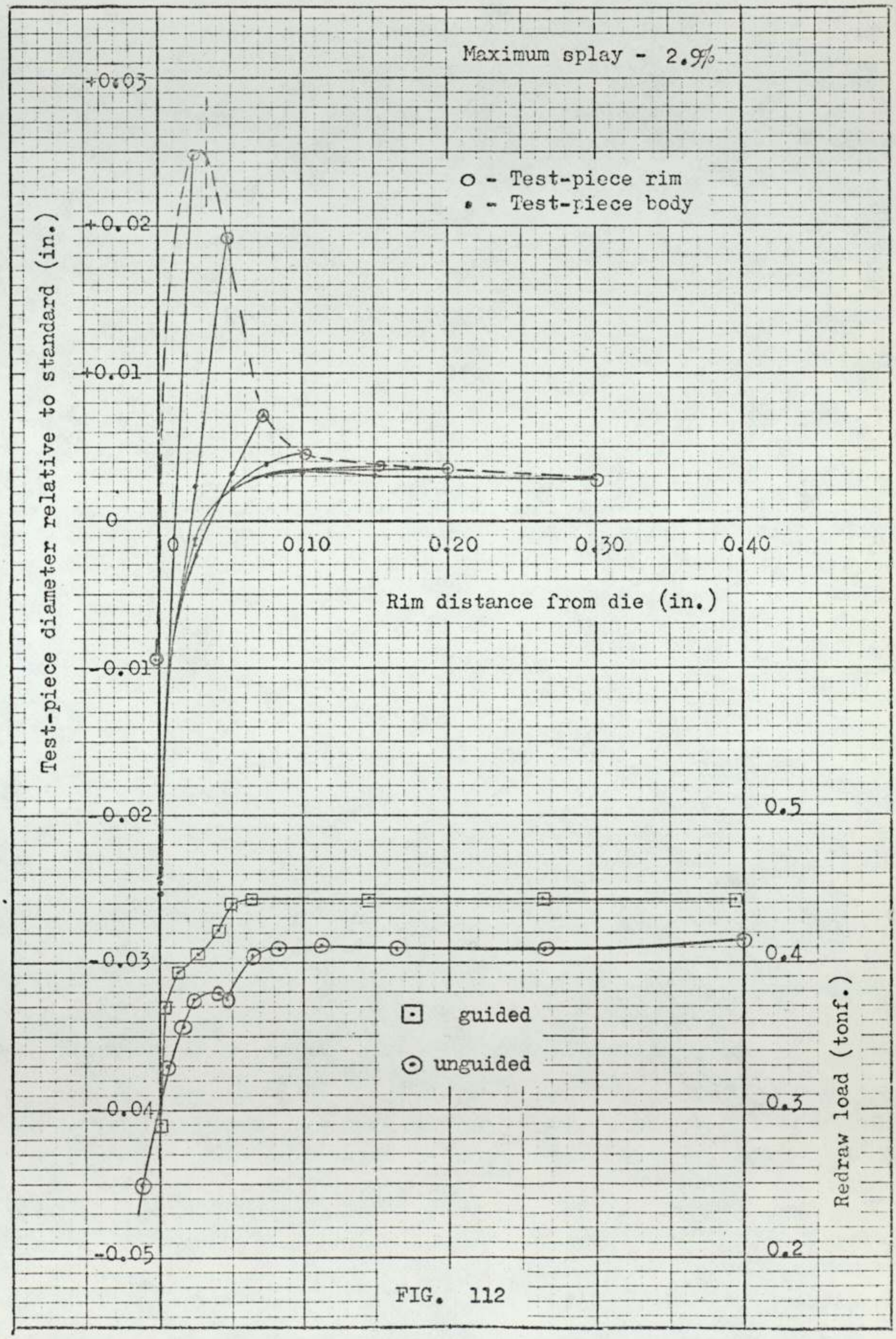

FIG. 112

Test Number	Test Material	Prior cold work. Nominal (%)	Nominal test - piece dimensions (in.)		Die semi-angle (deg.)	Hold-down punch nose radius (in.)
			O/Dia.	Wall thk.		
2C	Steel	0	0.750	0.0075	90	0.040

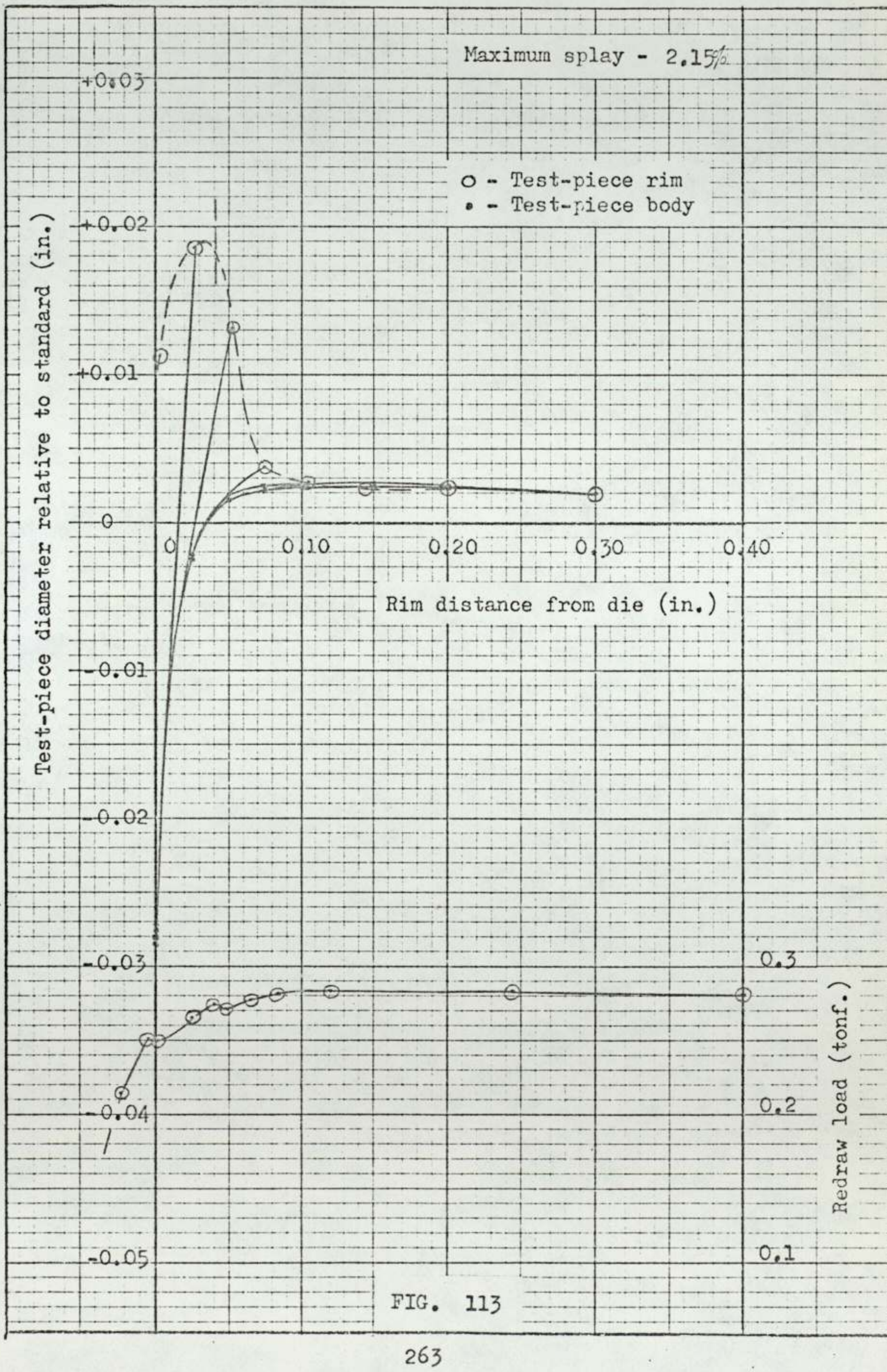

FIG. 113

Test Number	Test Material	Prior cold work. Nominal (%)	Nominal test - piece dimensions (in.)		Die semi-angle (deg.)	Hold-down punch nose radius (in.)
			O/Dia.	Wall thk.		
3C	Steel	50	0.750	0.0075	90	0.040

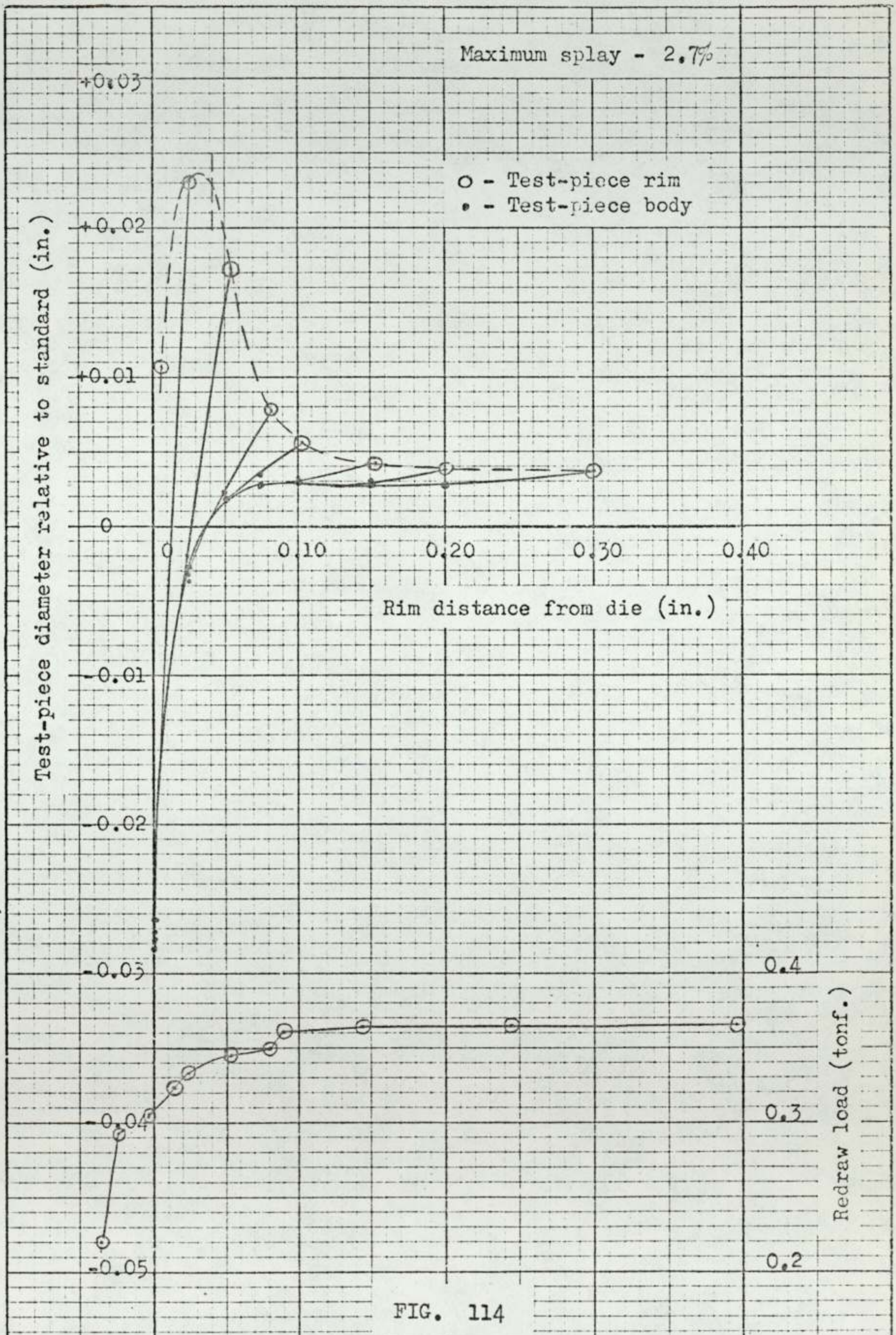

FIG. 114

Test Number	Test Material	Prior cold work. Nominal (%)	Nominal test - piece dimensions (in.)		Die semi-angle (deg.)	Hold-down punch nose radius (in.)
			O/Dia.	Wall thk.		
4C	Steel	67	0.750	0.0075	90	0.040

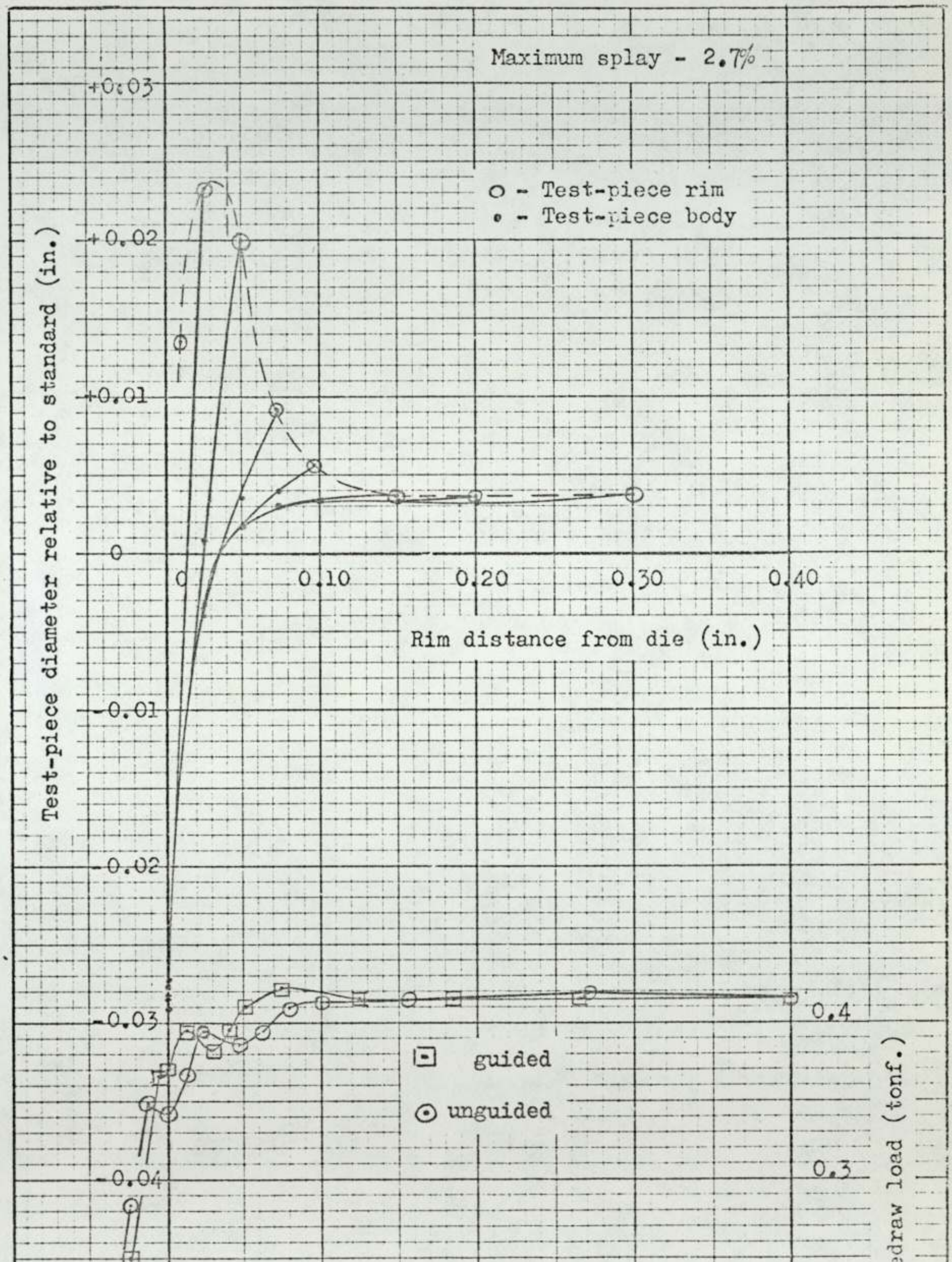

FIG. 115

Test Number	Test Material	Prior cold work. Nominal (%)	Nominal test - piece dimensions (in.)		Die semi-angle (deg.)	Hold-down punch nose radius (in.)
			O/Dia.	Wall thk.		
5C	Steel	67	0.750	0.0075	90	0.050

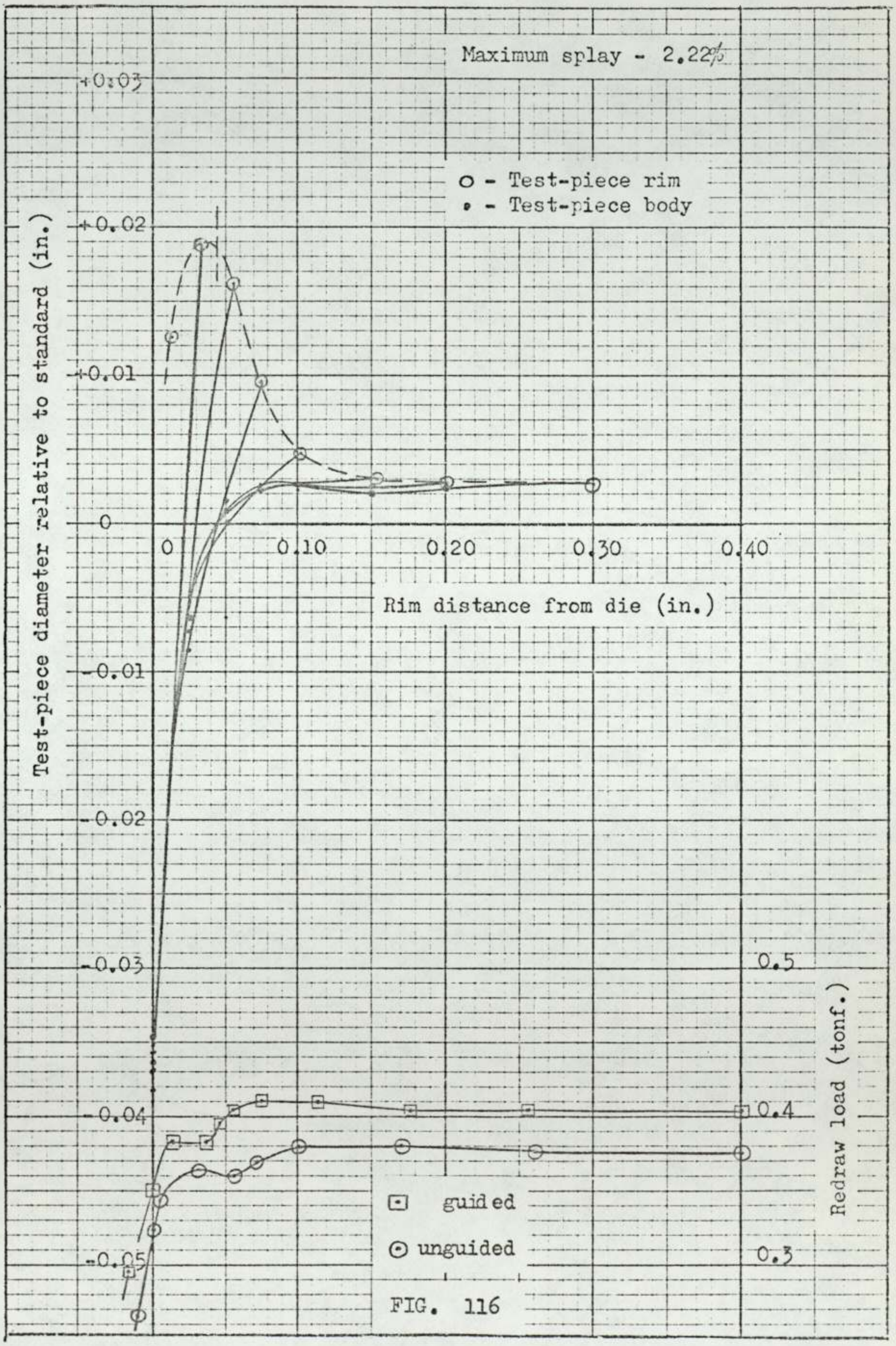

FIG. 116

Test Number	Test Material	Prior cold work. Nominal (%)	Nominal test - piece dimensions (in.)		Die semi-angle (deg.)	Hold-down punch nose radius (in.)
			O/Dia.	Wall thk.		
6C	Steel	50	0.750	0.0095	90	0.040

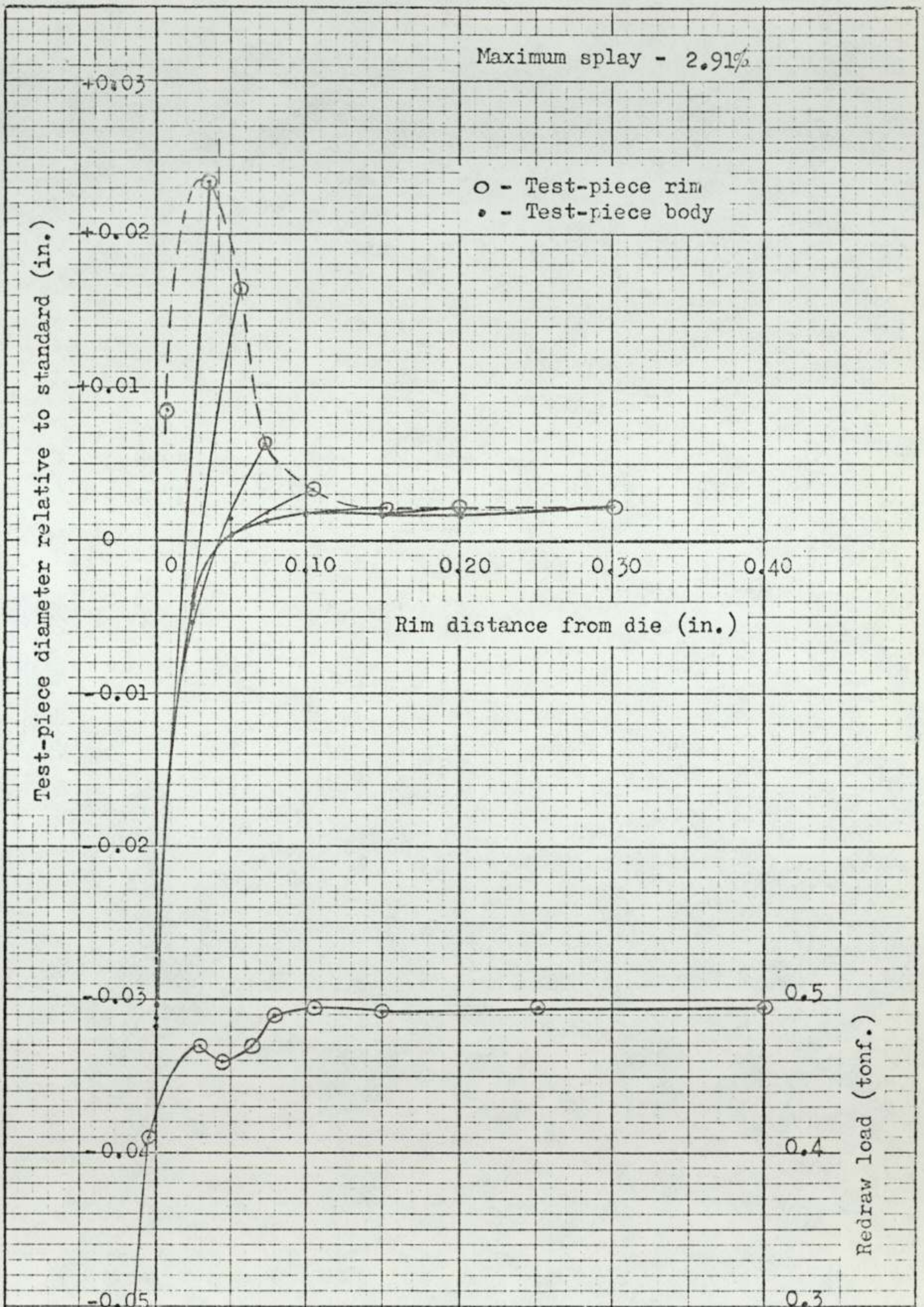

FIG. 117

Test Number	Test Material	Prior cold work. Nominal (%)	Nominal test - piece dimensions (in.)		Die semi-angle (deg.)	Hold-down punch nose radius (in.)
			O/Dia.	Wall thk.		
7C	Steel	50	0.750	0.0095	90	0.050

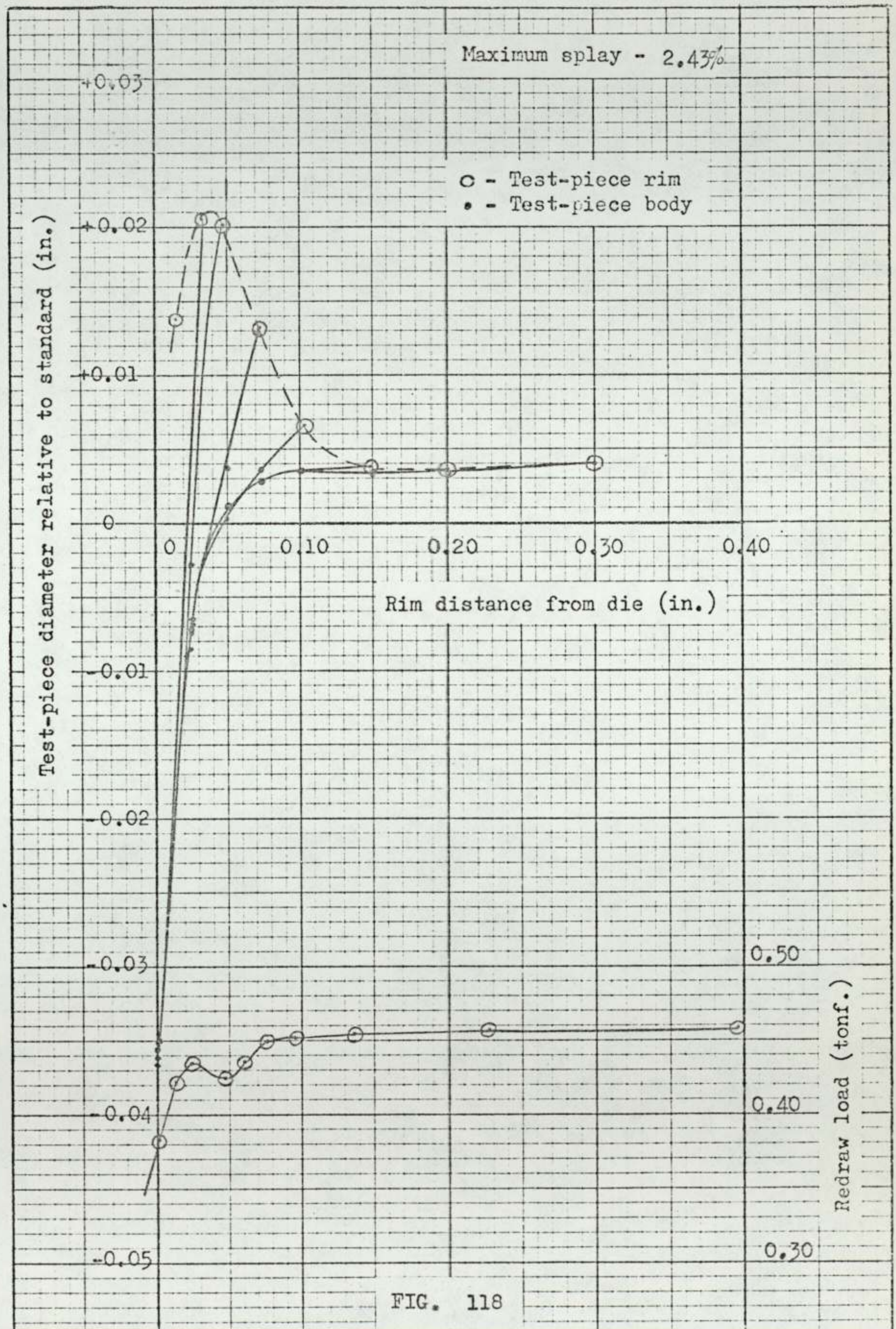

FIG. 118

Test Number	Test Material	Prior cold work. Nominal (%)	Nominal test - piece dimensions (in.)		Die semi-angle (deg.)	Hold-down punch nose radius (in.)
			O/Dia.	Wall thk.		
8C	Steel	50	0.750	0.0095	90	0.060

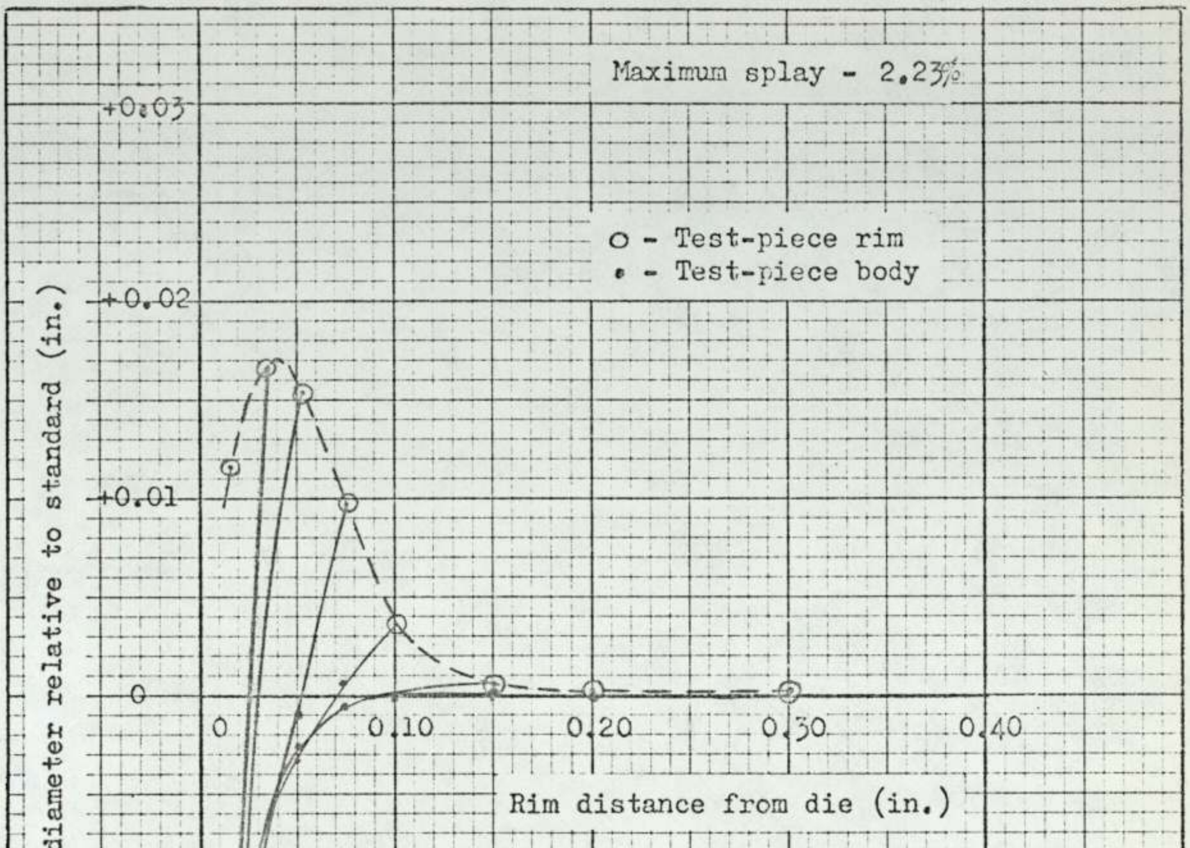

FIG. 119

Test Number	Test Material	Prior cold work. Nominal (%)	Nominal test - piece dimensions (in.)		Die semi-angle (deg.)	Hold-down punch nose radius (in.)
			O/Dia.	Wall thk.		
9C	70/30 brass	50	0.750	0.0095	90	0.040

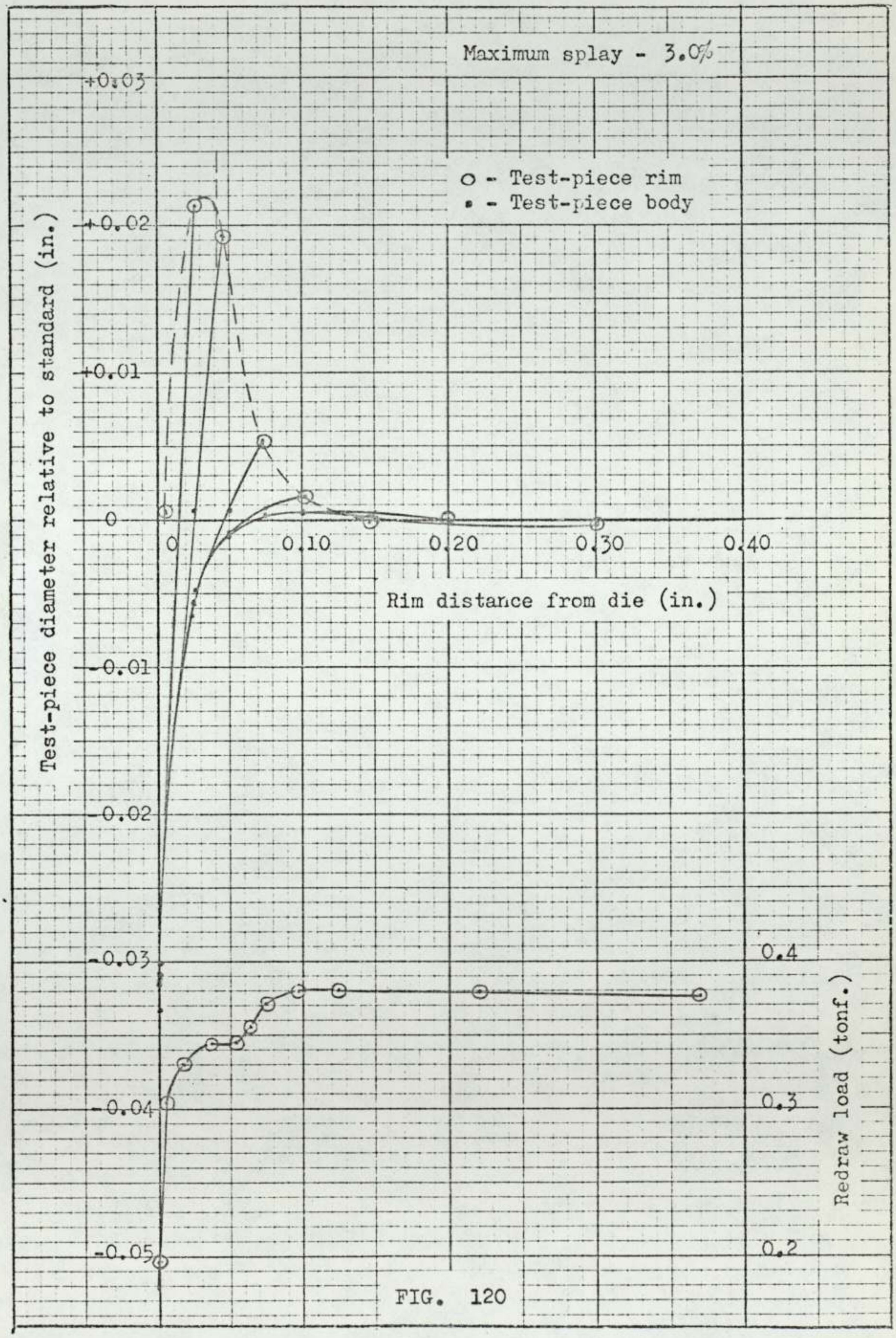

FIG. 120

Test Number	Test Material	Prior cold work. Nominal (%)	Nominal test - piece dimensions (in.)		Die semi-angle (deg.)	Hold-down punch nose radius (in.)
			O/Dia.	Wall thk.		
10C	70/30 brass	50	0.750	0.0095	90	0.050

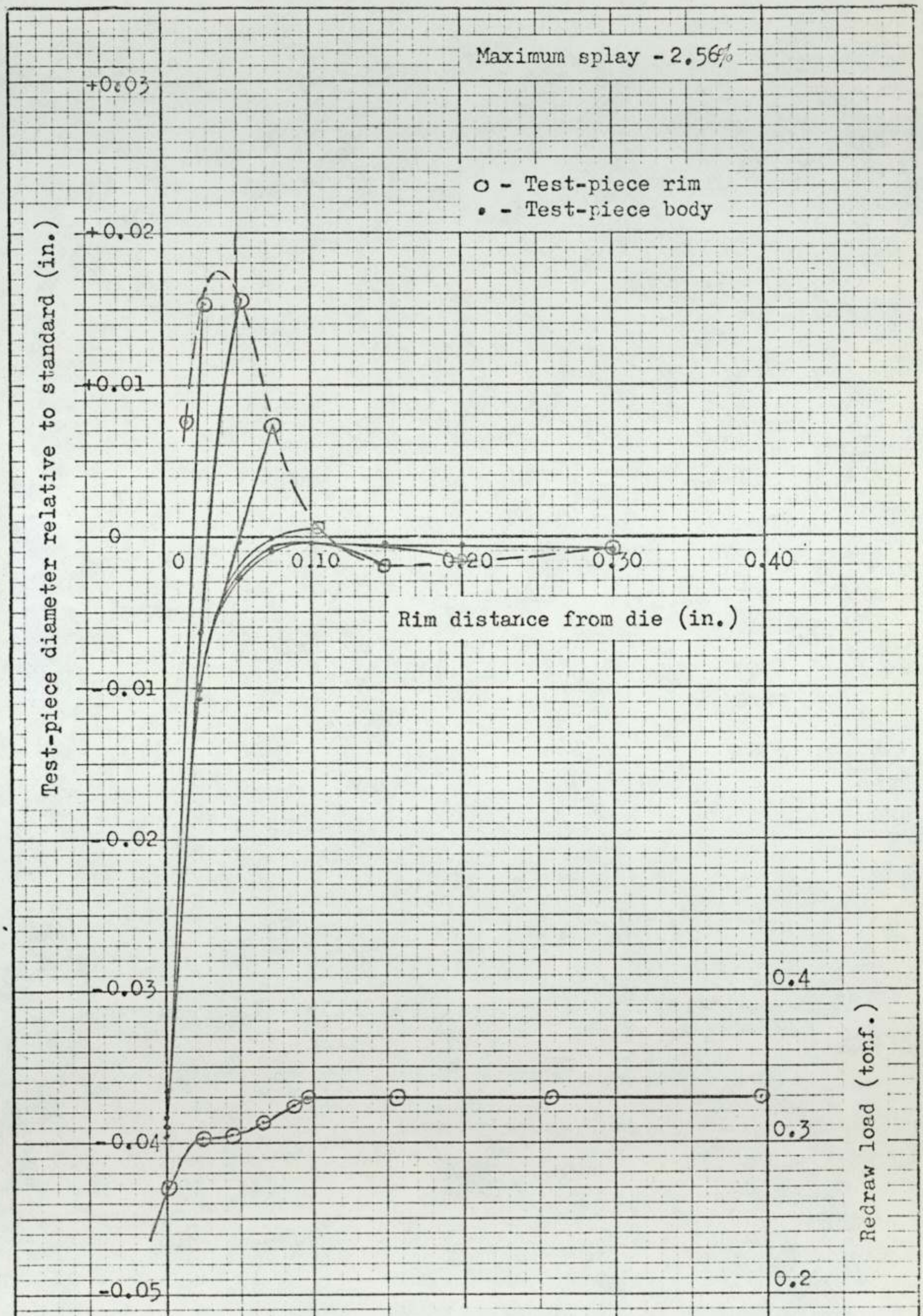

FIG. 121

Test Number	Test Material	Prior cold work. Nominal (%)	Nominal test - piece dimensions (in.)		Die semi-angle (deg.)	Hold-down punch nose radius (in.)
			O/Dia.	Wall thk.		
11C	70/30 brass	50	0.750	0.0095	90	0.060

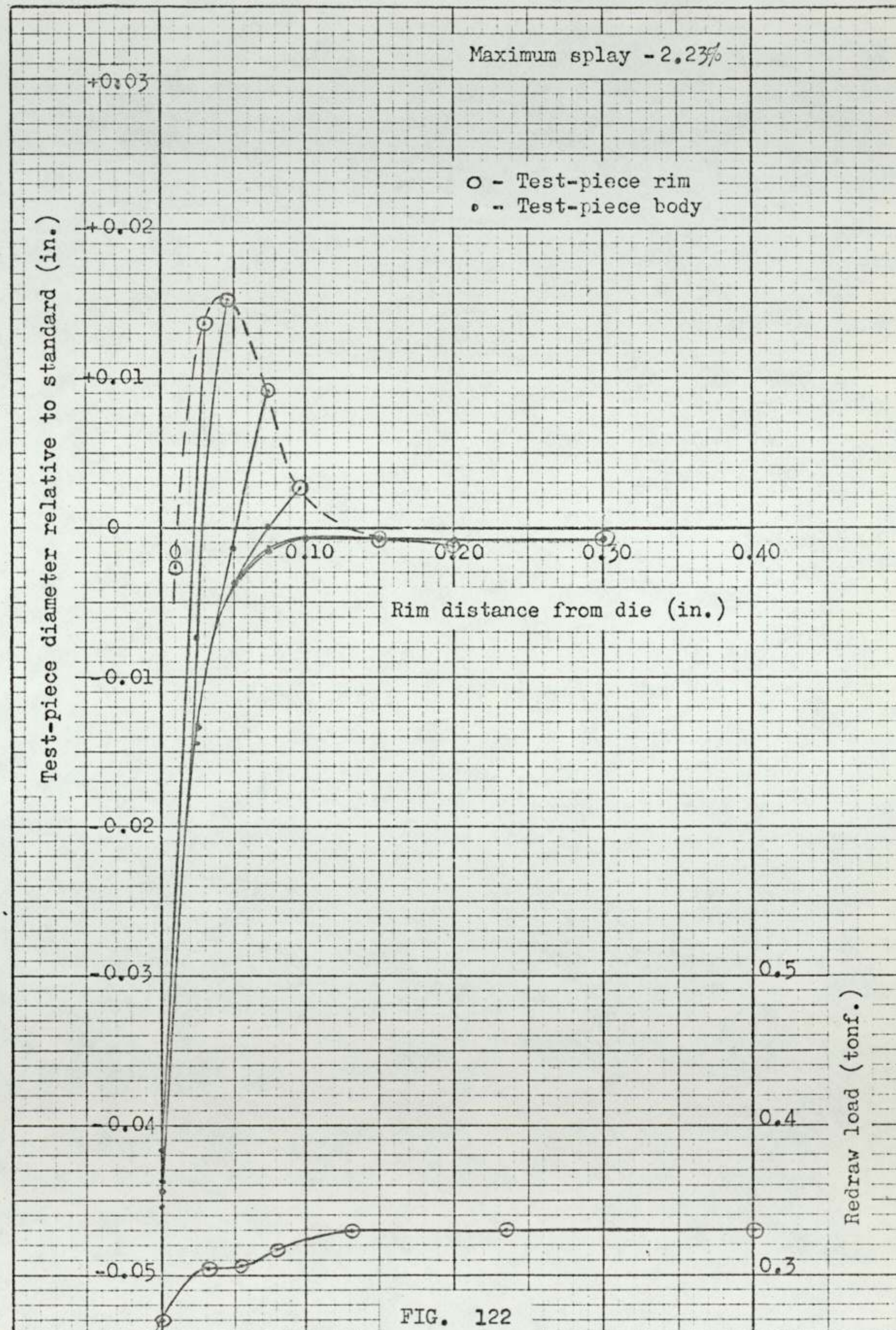

FIG. 122

Test Number	Test Material	Prior cold work. Nominal (%)	Nominal test - piece dimensions (in.)		Die semi-angle (deg.)	Hold-down punch nose radius (in.)
			O/Dia.	Wall thk.		
12C	T304 Stainless	50	0.750	0.0075	90	0.030

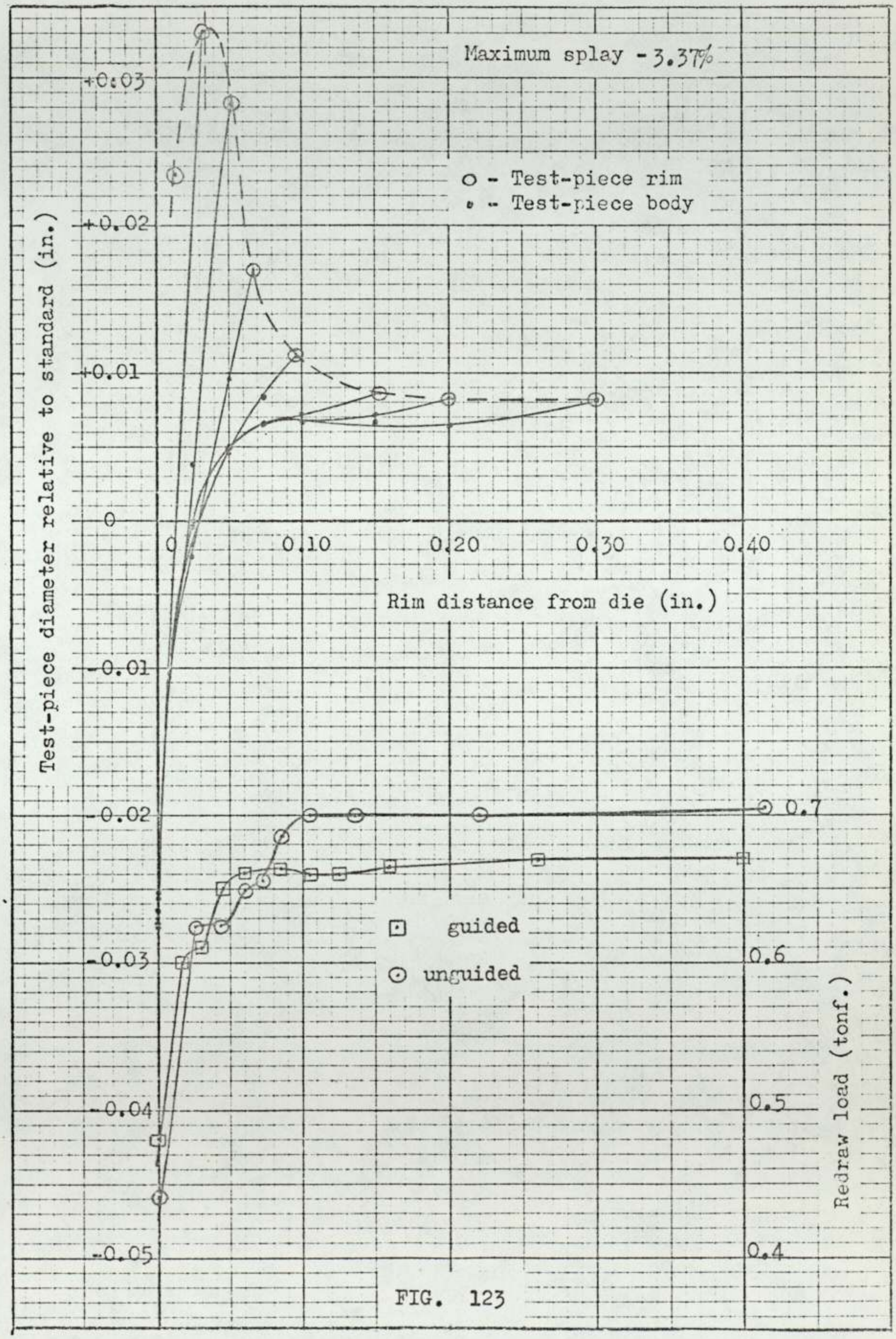

FIG. 123

Test Number	Test Material	Prior cold work. Nominal (%)	Nominal test - piece dimensions (in.)		Die semi-angle (deg.)	Hold-down punch nose radius (in.)
			O/Dia.	Wall thk.		
13C	T304 Stainless	0	0.750	0.0075	90	0.040

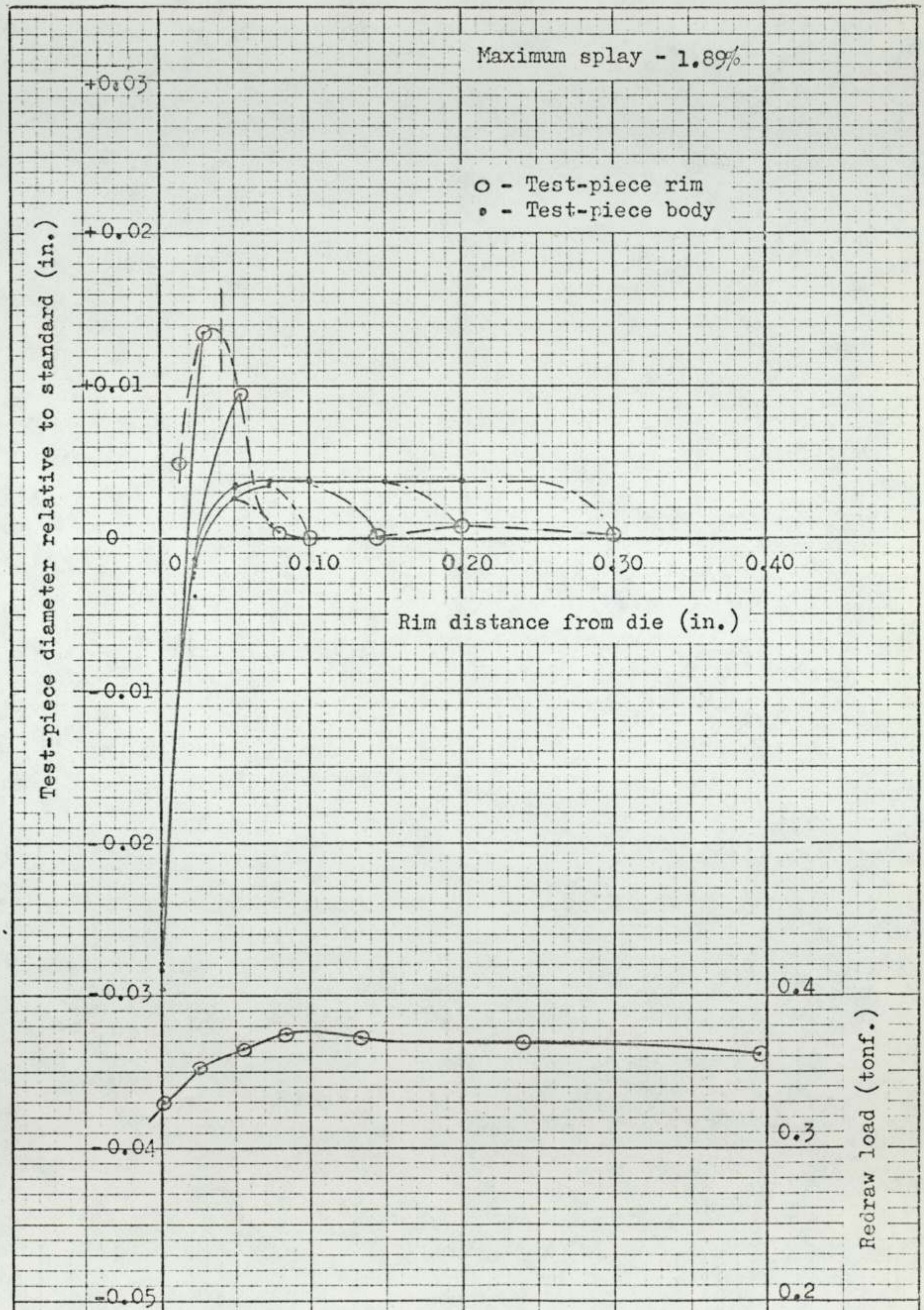

FIG. 124

Test Number	Test Material	Prior cold work. Nominal (%)	Nominal test - piece dimensions (in.)		Die semi-angle (deg.)	Hold-down punch nose radius (in.)
			O/Dia.	Wall thk.		
14C	T304 Stainless	50	0.750	0.0075	90	0.040

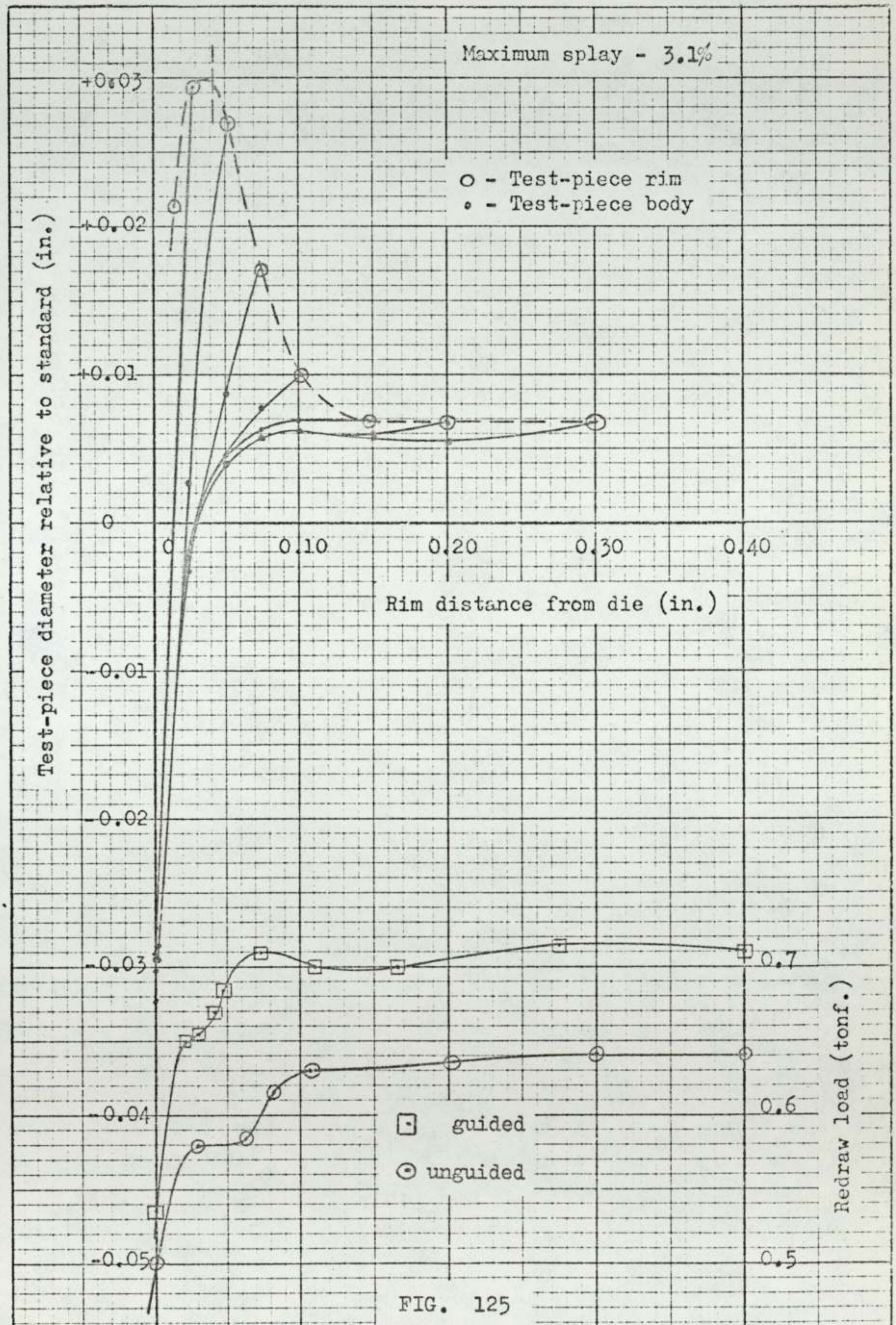

FIG. 125

Test Number	Test Material	Prior cold work. Nominal (%)	Nominal test - piece dimensions (in.)		Die semi-angle (deg.)	Hold-down punch nose radius (in.)
			O/Dia.	Wall thk.		
15C	T304 Stainless	67	0.750	0.0075	90	0.040

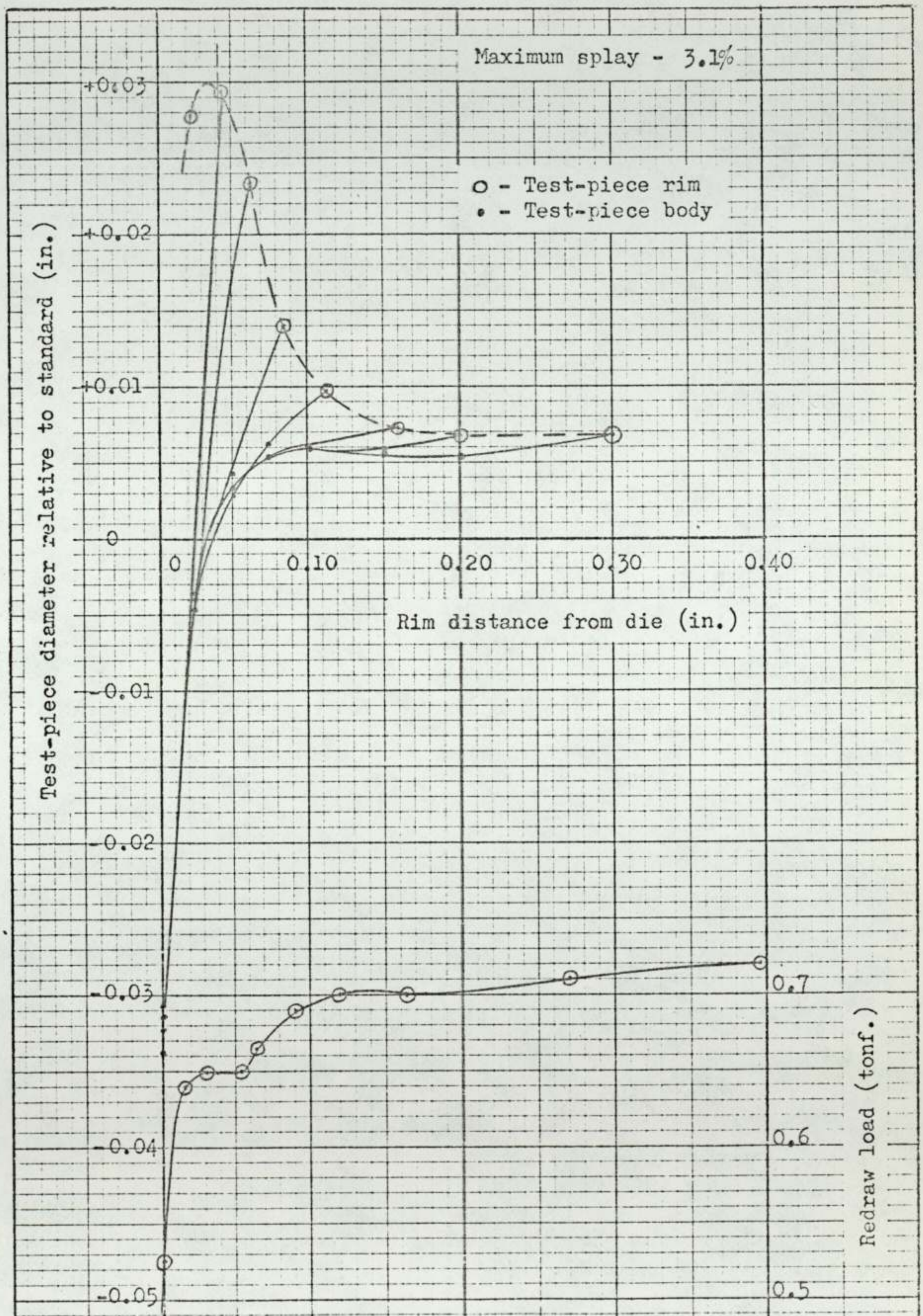

FIG. 126

Test Number	Test Material	Prior cold work. Nominal (%)	Nominal test - piece dimensions (in.)		Die semi-angle (deg.)	Hold-down punch nose radius (in.)
			O/Dia.	Wall thk.		
16C	T304 Stainless	50	0.750	0.0075	90	0.050

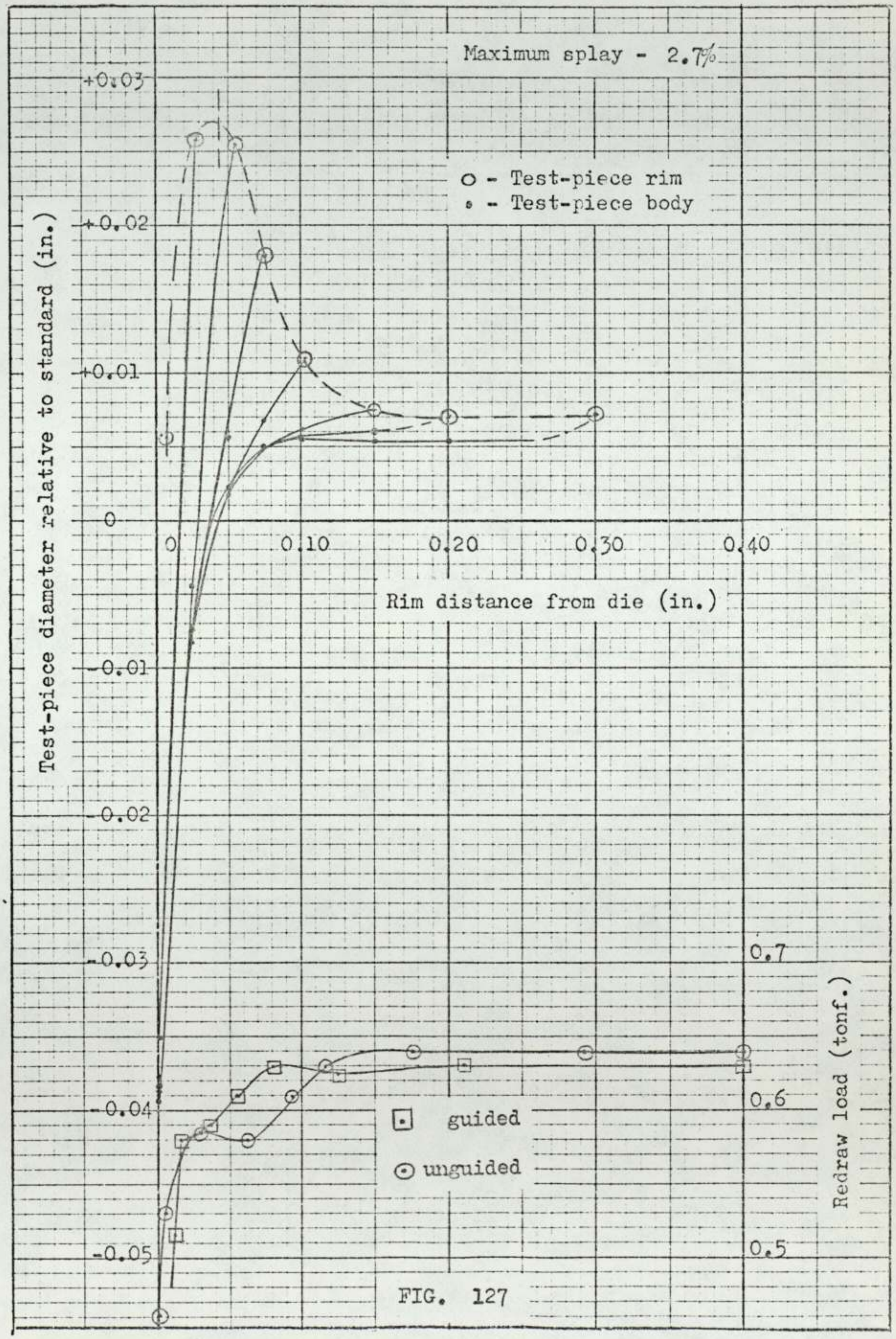

FIG. 127

Test Number	Test Material	Prior cold work. Nominal (%)	Nominal test - piece dimensions (in.)		Die semi-angle (deg.)	Hold-down punch nose radius (in.)
			O/Dia.	Wall thk.		
17C	T304 Stainless	50	0.750	0.0095	90	0.040

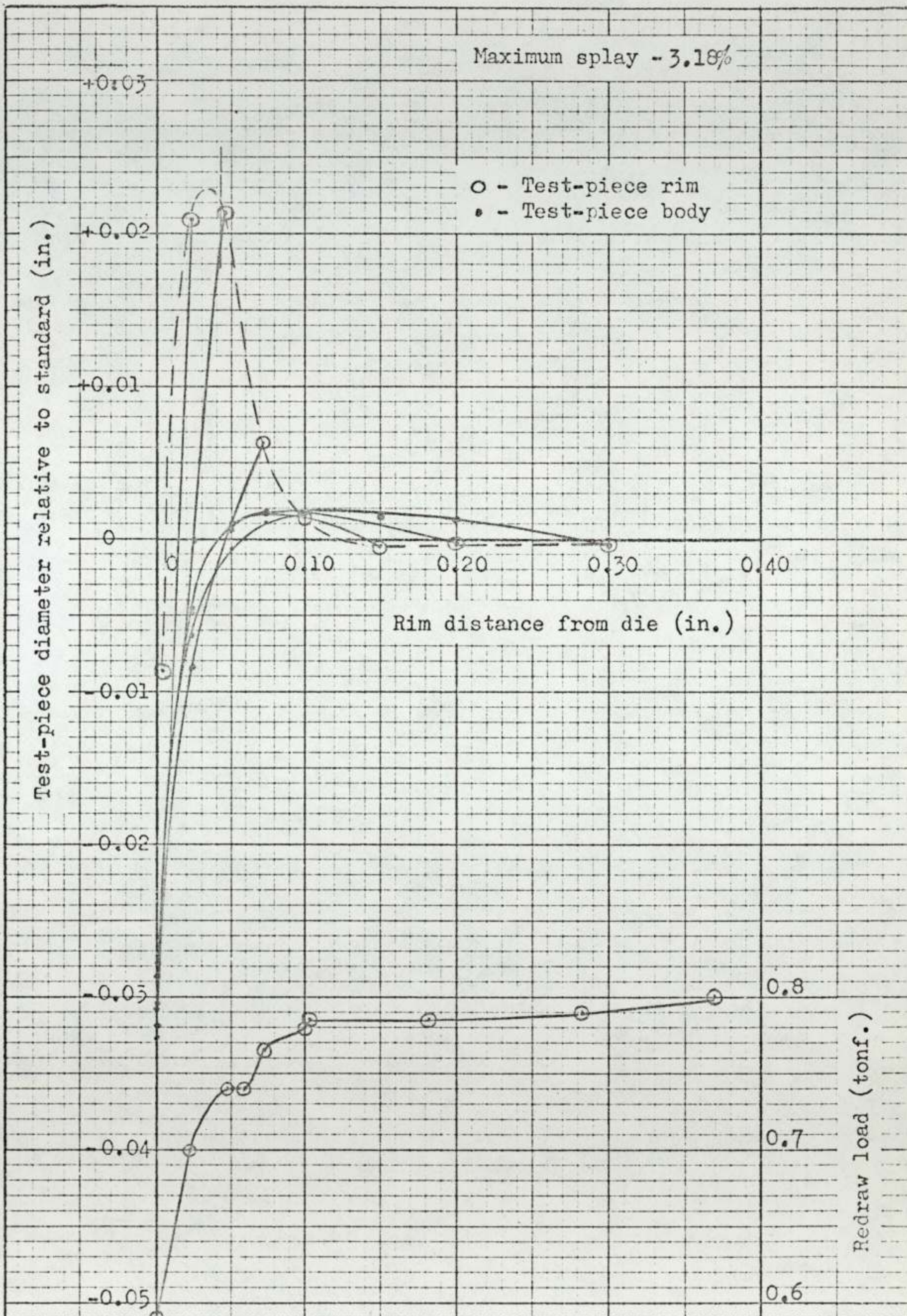

FIG. 128

Test Number	Test Material	Prior cold work. Nominal (%)	Nominal test - piece dimensions (in.)		Die semi-angle (deg.)	Hold-down punch nose radius (in.)
			O/Dia.	Wall thk.		
18C	T304 Stainless	50	0.750	0.0095	90	0.050

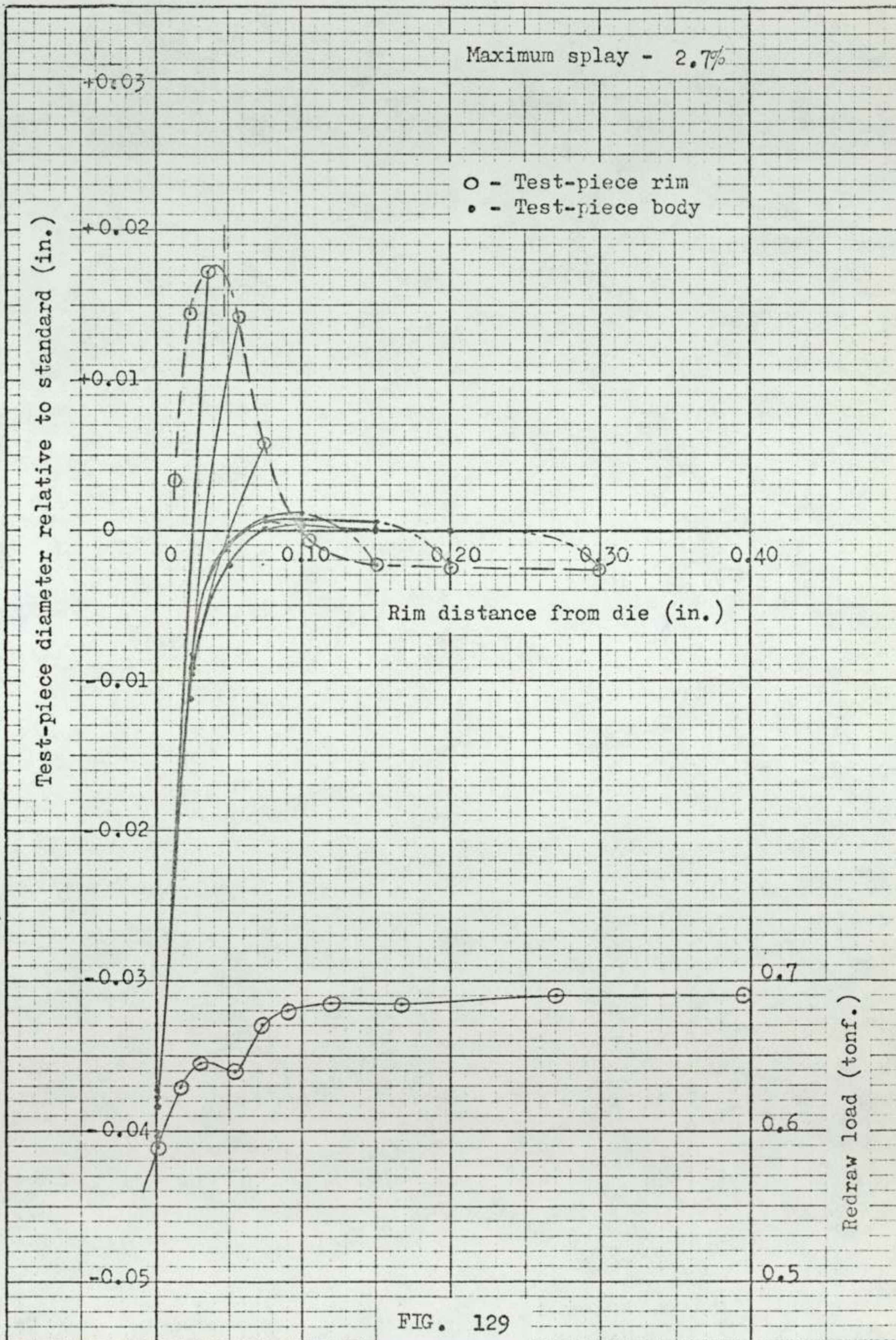

FIG. 129

Test Number	Test Material	Prior cold work. Nominal (%)	Nominal test - piece dimensions (in.)		Die semi-angle (deg.)	Hold-down punch nose radius (in.)
			O/Dia.	Wall thk.		
19C	T304 Stainless	50	0.750	0.0095	90	0.060

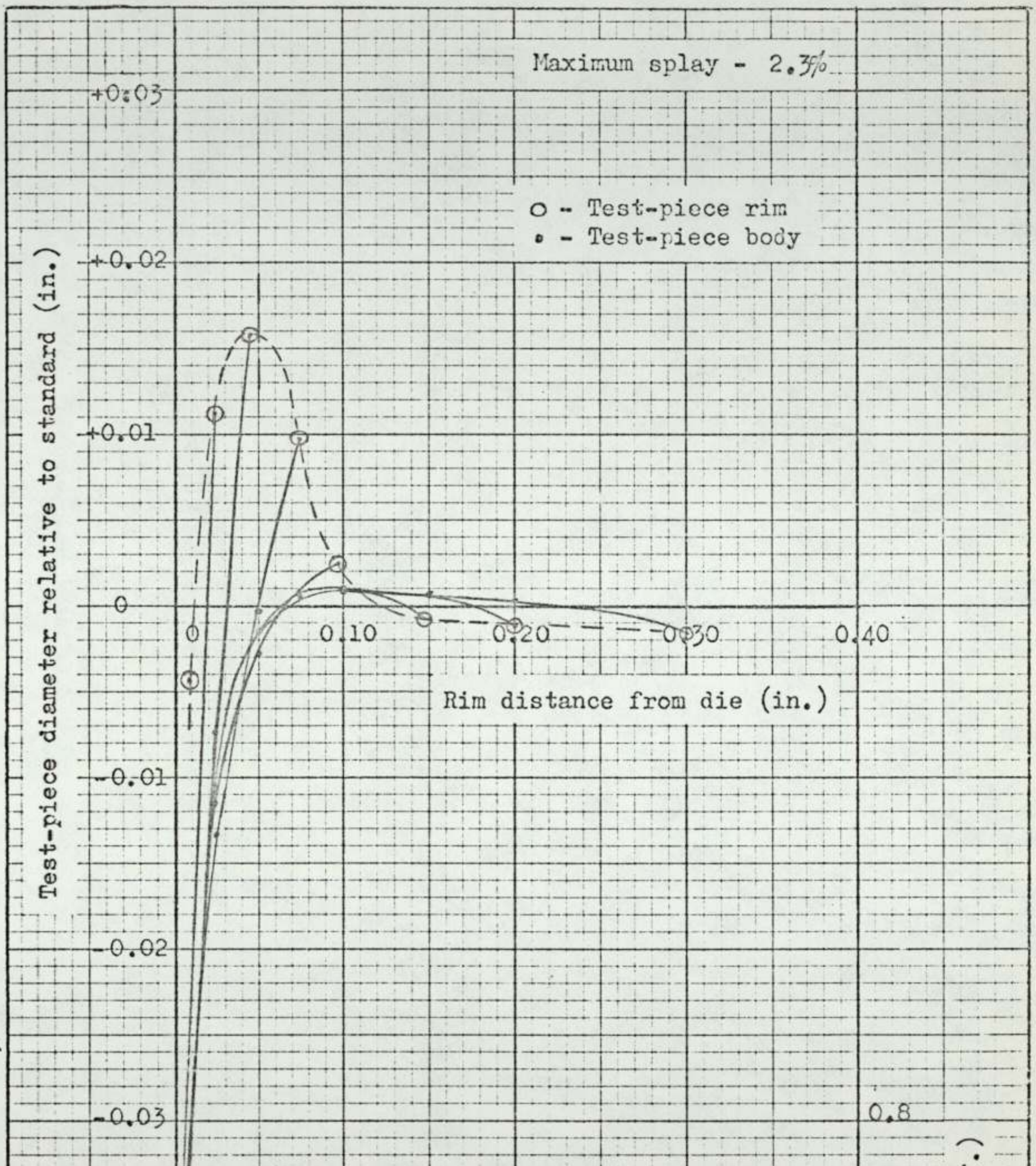

FIG. 130

Test Number	Test Material	Prior cold work. Nominal (%)	Nominal test - piece dimensions (in.)		Die semi-angle (deg.)	Hold-down punch nose radius (in.)
			O/Dia.	Wall thk.		
20C	Alum.	50	0.750	0.0075	90	0.030

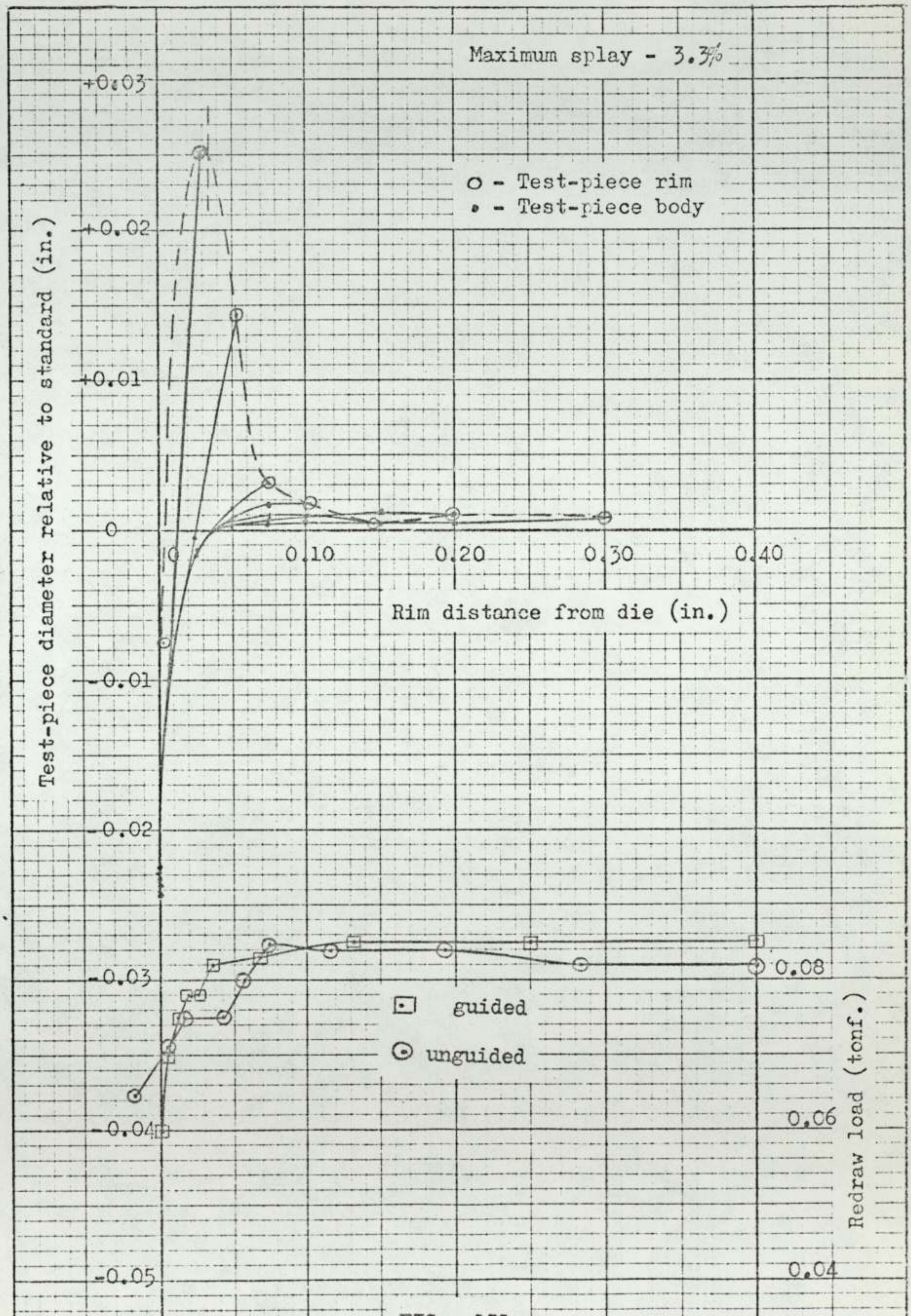

FIG. 131

Test Number	Test Material	Prior cold work. Nominal (%)	Nominal test - piece dimensions (in.)		Die semi-angle (deg.)	Hold-down punch nose radius (in.)
			O/Dia.	Wall thk.		
21C	Alum.	0	0.750	0.0075	90	0.040

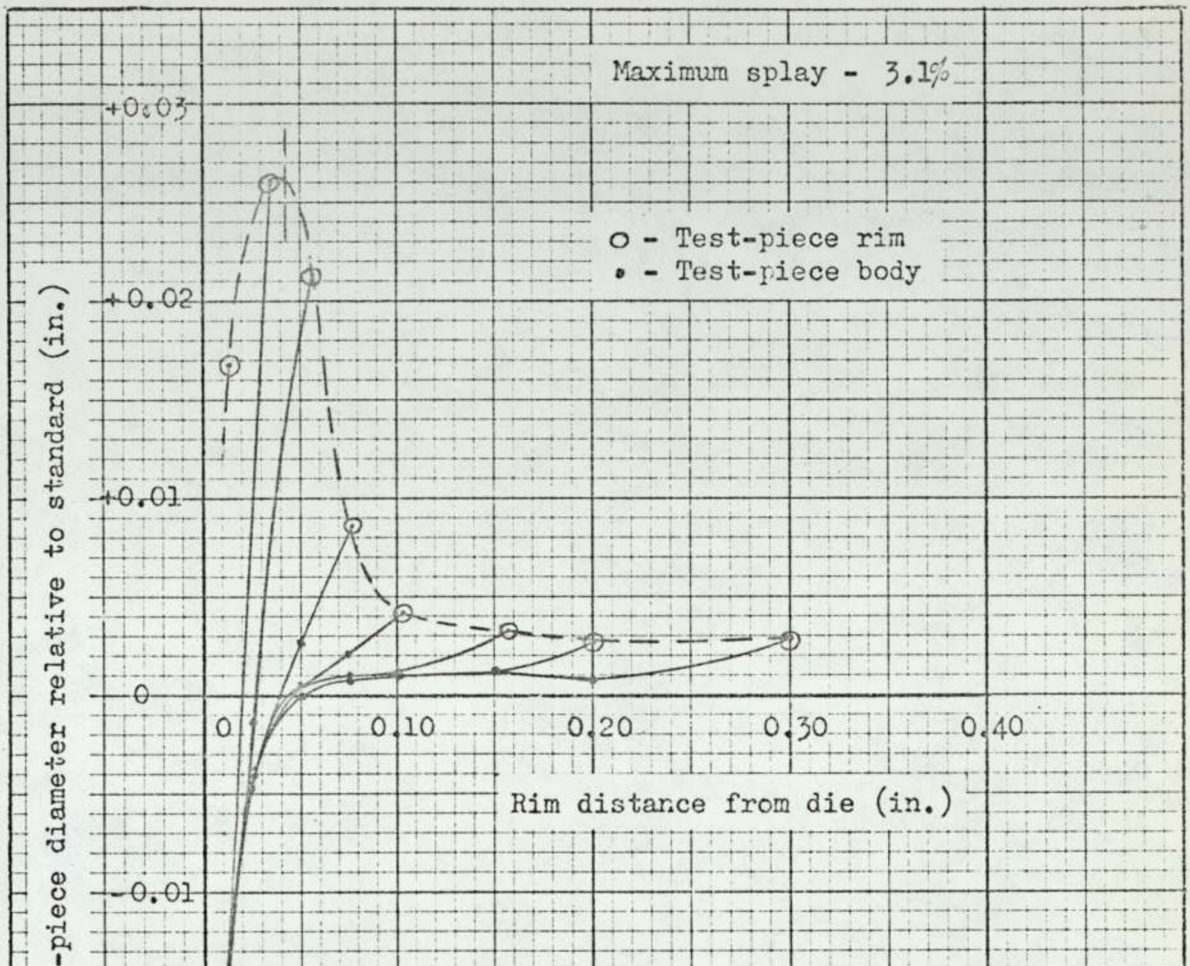

FIG. 132

Test Number	Test Material	Prior cold work. Nominal (%)	Nominal test - piece dimensions (in.)		Die semi-angle (deg.)	Hold-down punch nose radius (in.)
			O/Dia.	Wall thk.		
22C	Alum.	50	0.750	0.0075	90	0.040

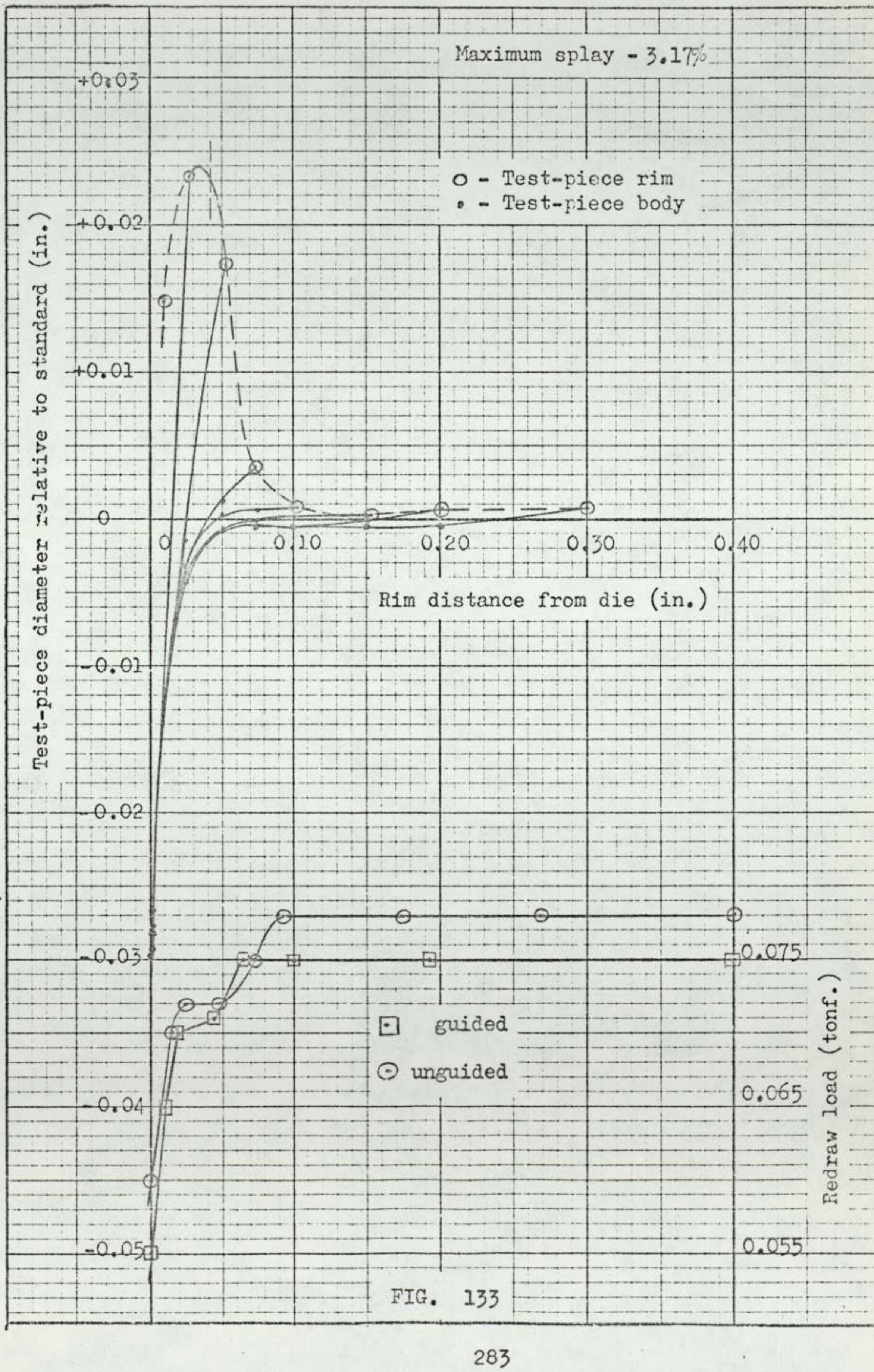

FIG. 133

Test Number	Test Material	Prior cold work. Nominal (%)	Nominal test - piece dimensions (in.)		Die semi-angle (deg.)	Hold-down punch nose radius (in.)
			O/Dia.	Wall thk.		
23C	Alum.	67	0.750	0.0075	90	0.040

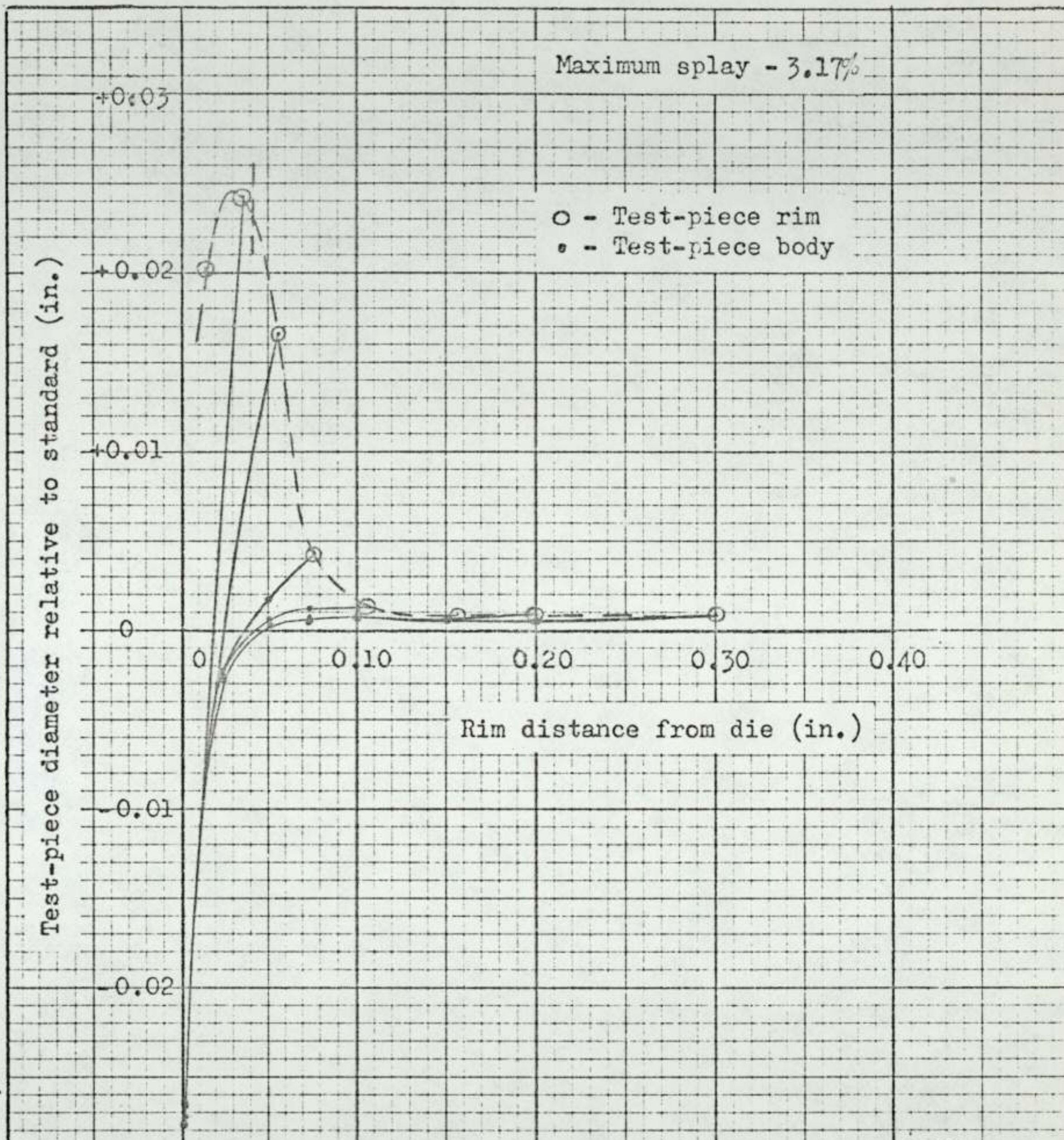

FIG. 134

Test Number	Test Material	Prior cold work. Nominal (%)	Nominal test - piece dimensions (in.)		Die semi-angle (deg.)	Hold-down punch nose radius (in.)
			O/Dia.	Wall thk.		
24C	Alum.	50	0.750	0.0075	90	0.050

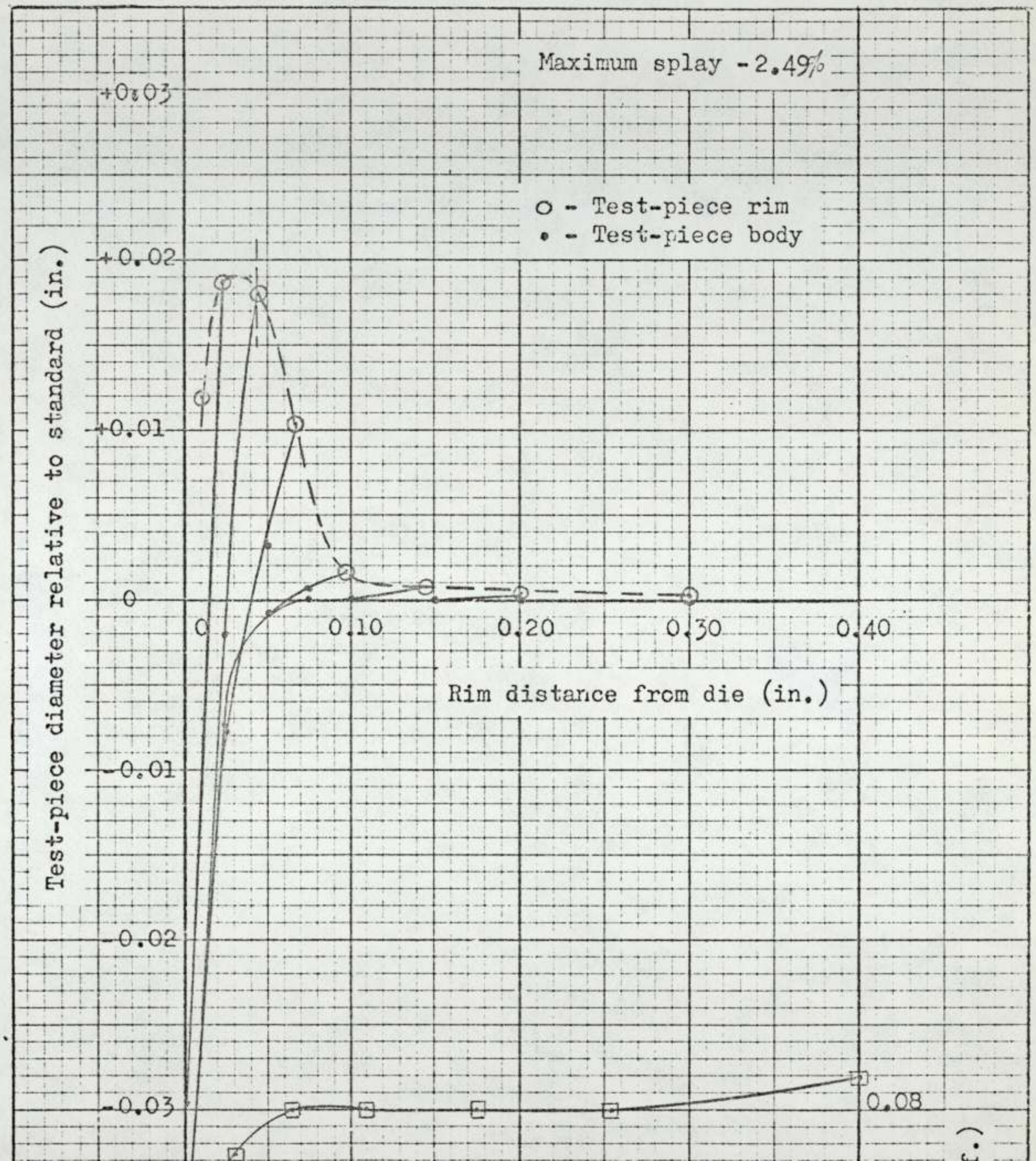

FIG. 135

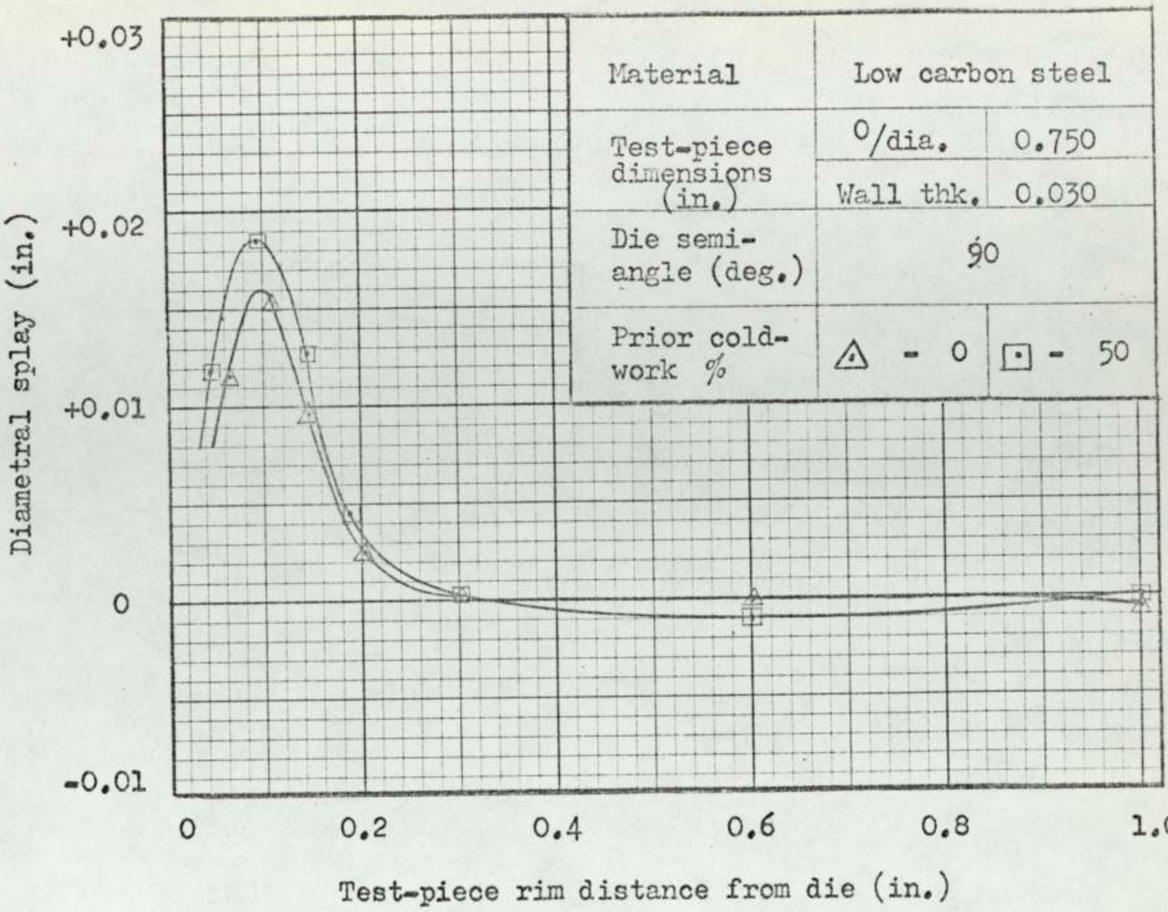

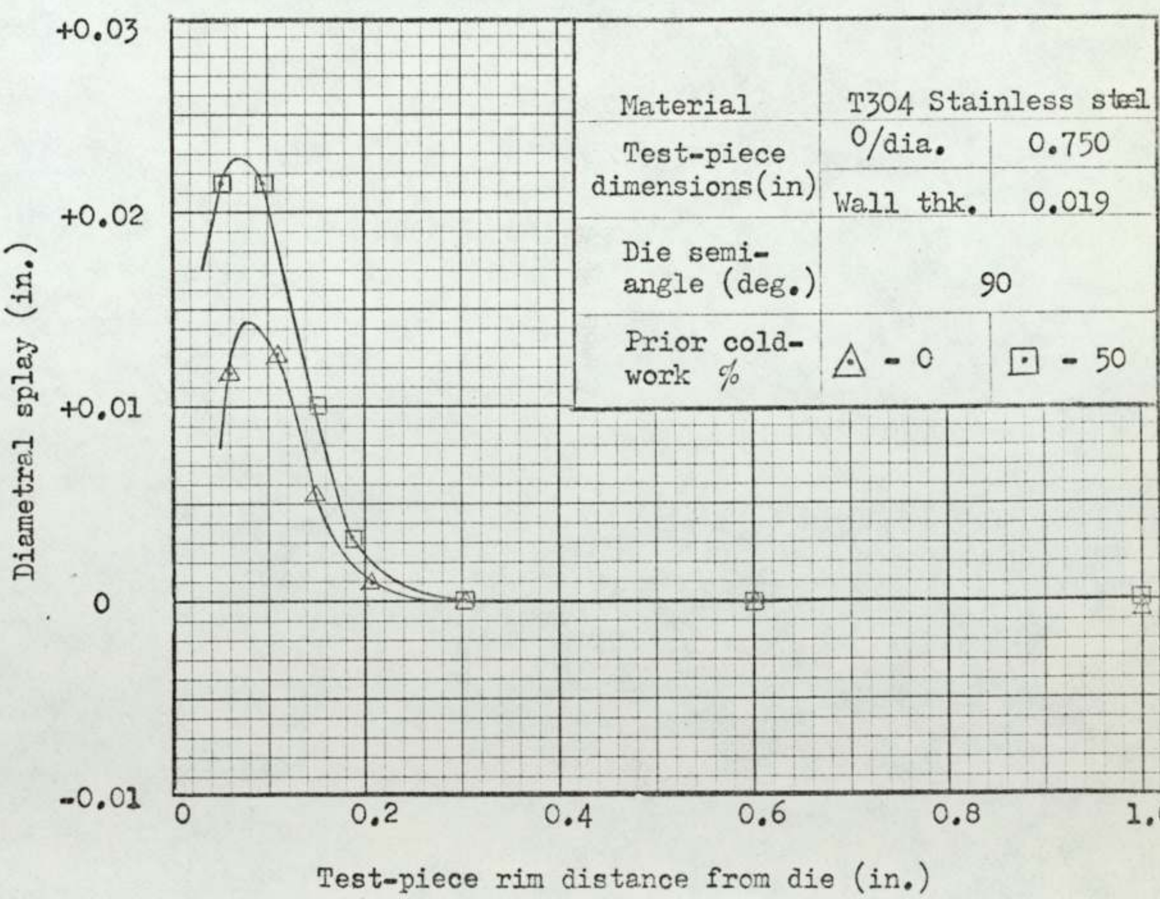

FIG. 136 EFFECT OF PRIOR COLD-WORK ON SPLAYING. FREE REDRAWING.

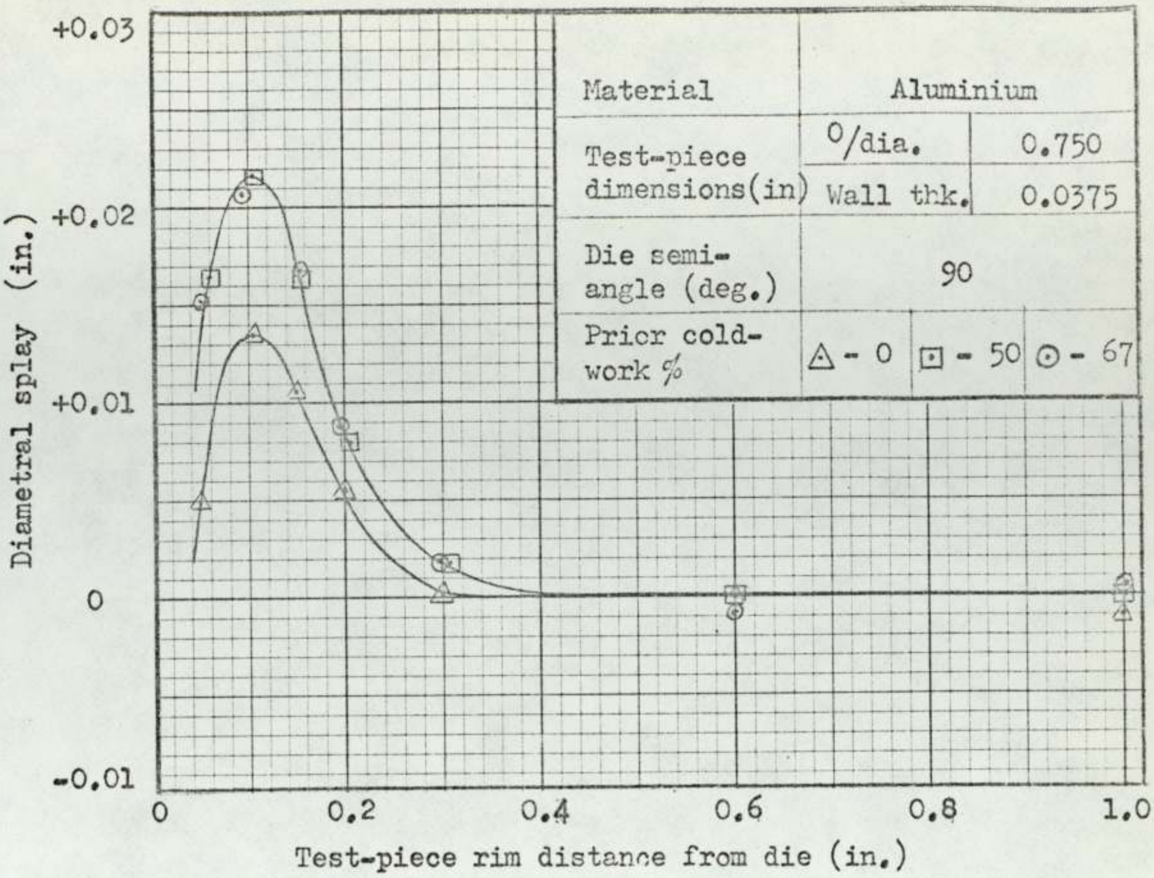

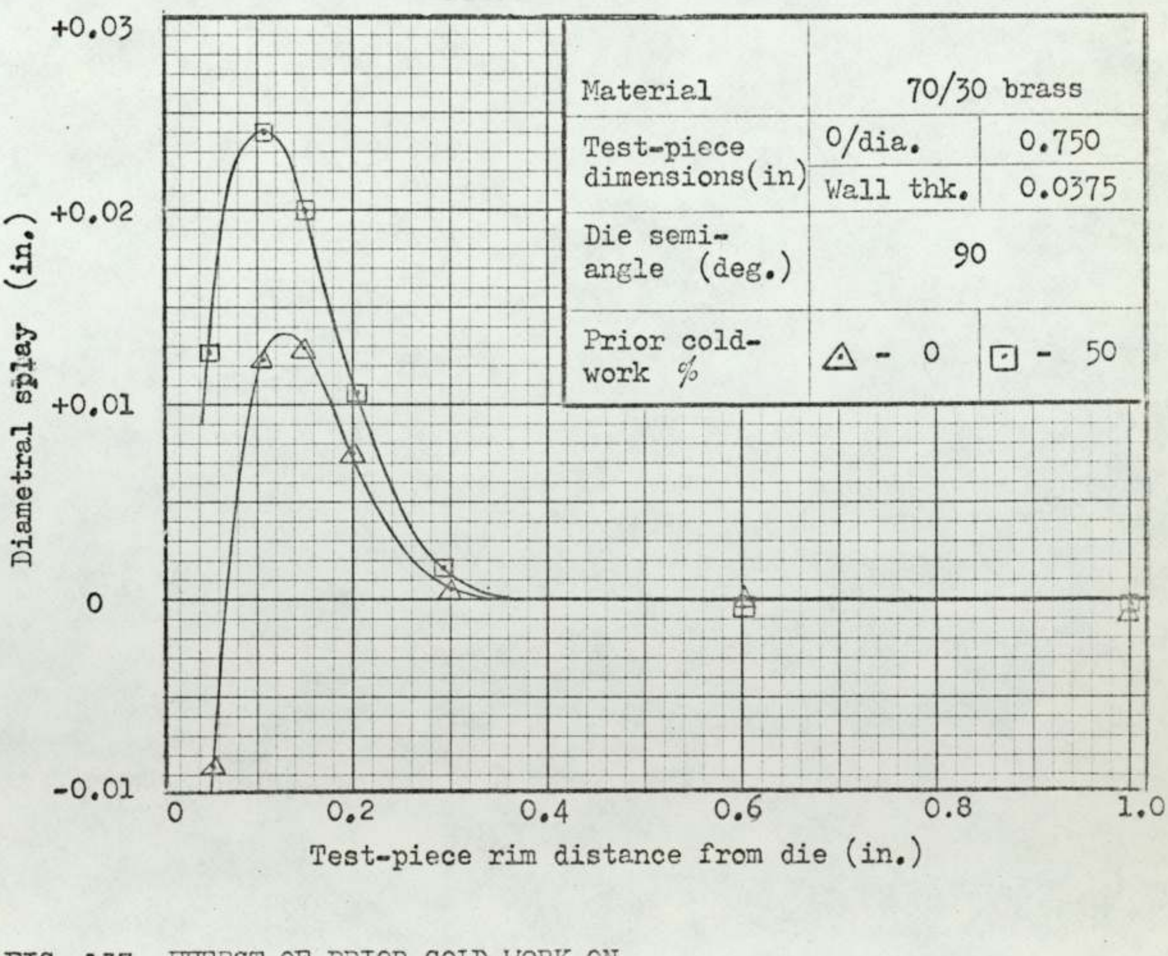

FIG. 137 EFFECT OF PRIOR COLD-WORK ON SPLAYING. FREE REDRAWING.

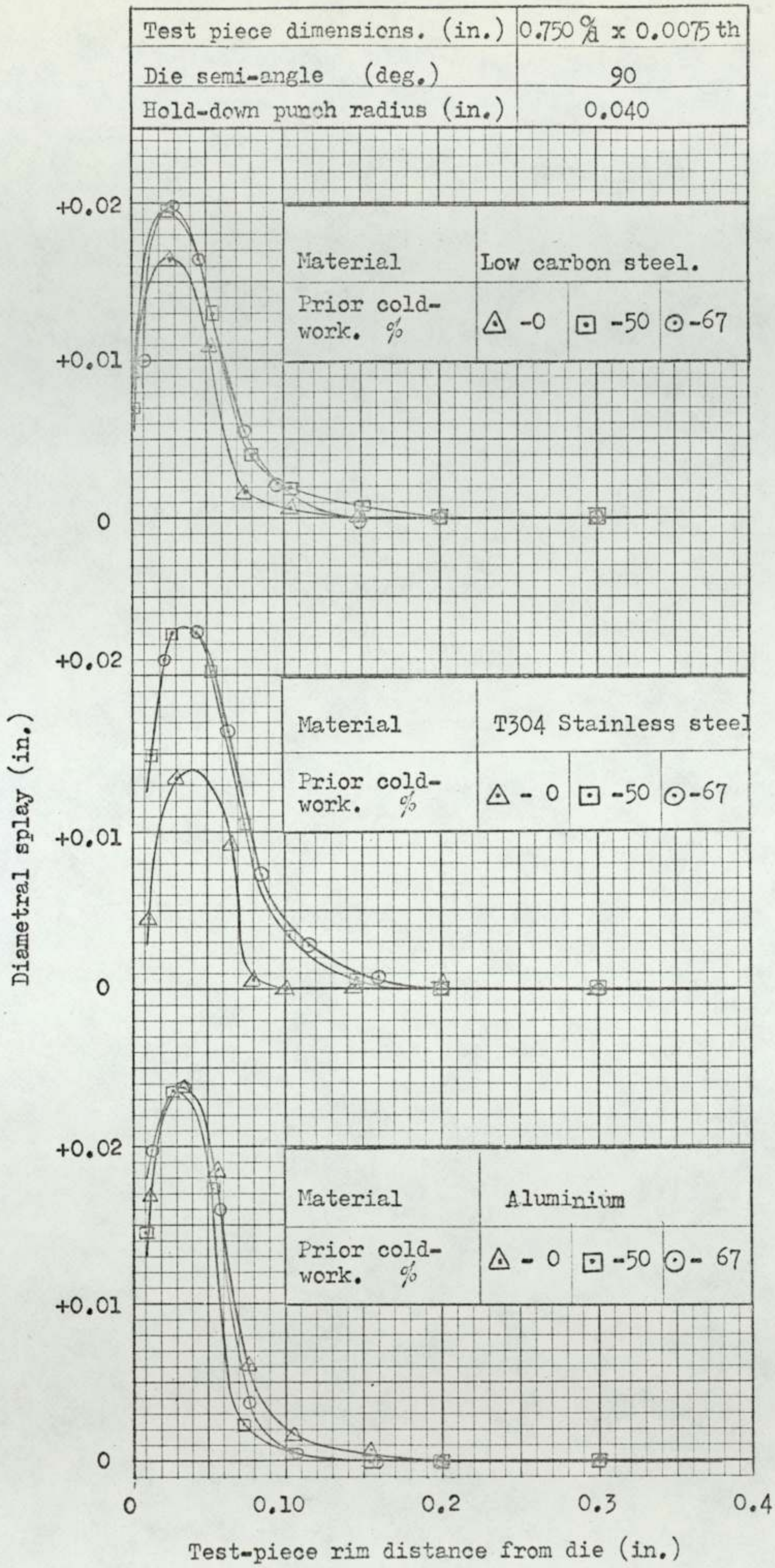

FIG. 138 EFFECT OF PRIOR COLD-WORK ON SPLAYING. CONSTRAINED REDRAWING.

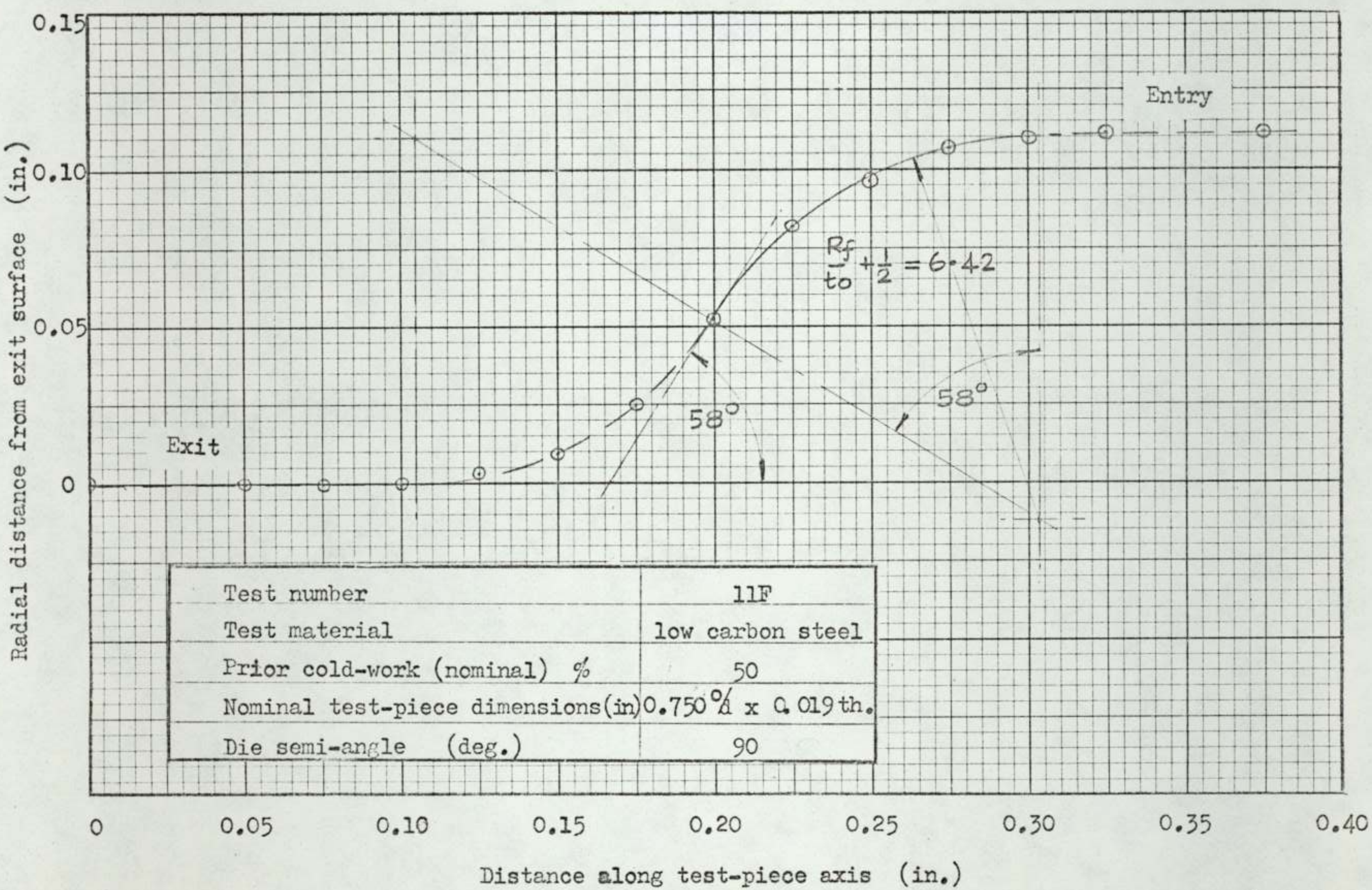

FIG. 139 DEFORMATION PROFILE IN FREE REDRAWING.

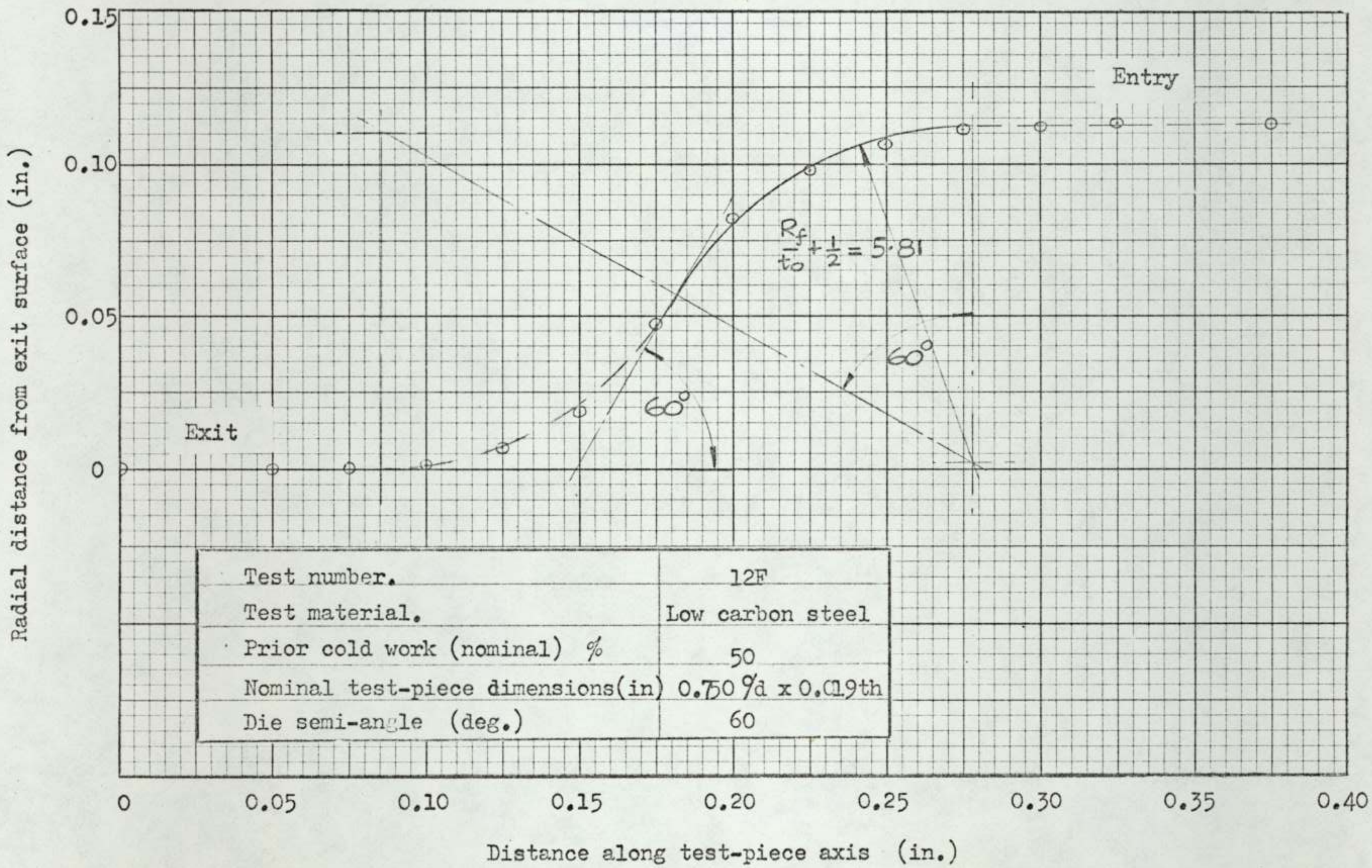

Test number.	12F
Test material.	Low carbon steel
Prior cold work (nominal) %	50
Nominal test-piece dimensions(in)	0.750 ^{o}/d x 0.019th
Die semi-angle (deg.)	60

FIG. 140 DEFORMATION PROFILE IN FREE REDRAWING.

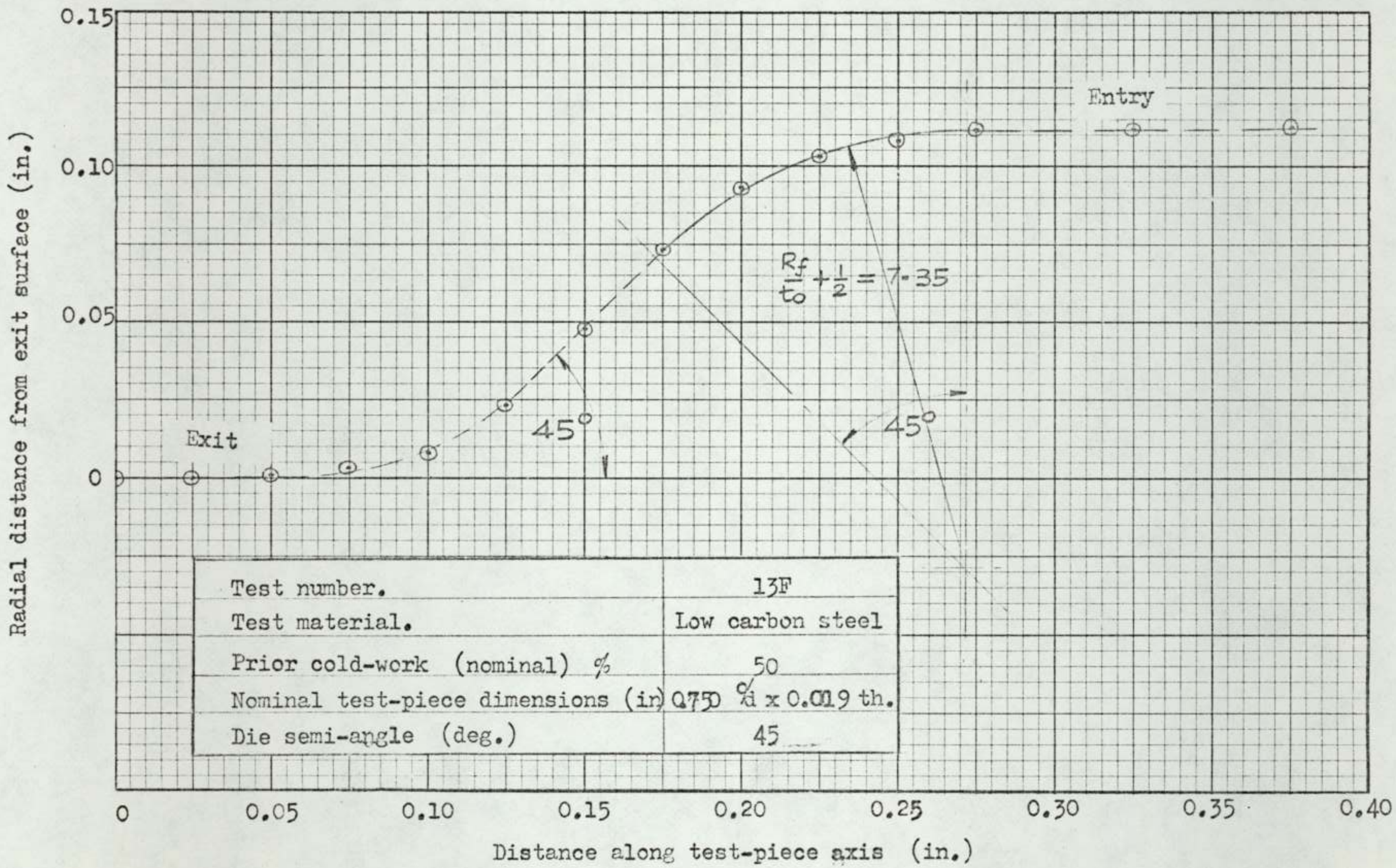

FIG. 141 DEFORMATION PROFILE IN FREE REDRAWING.

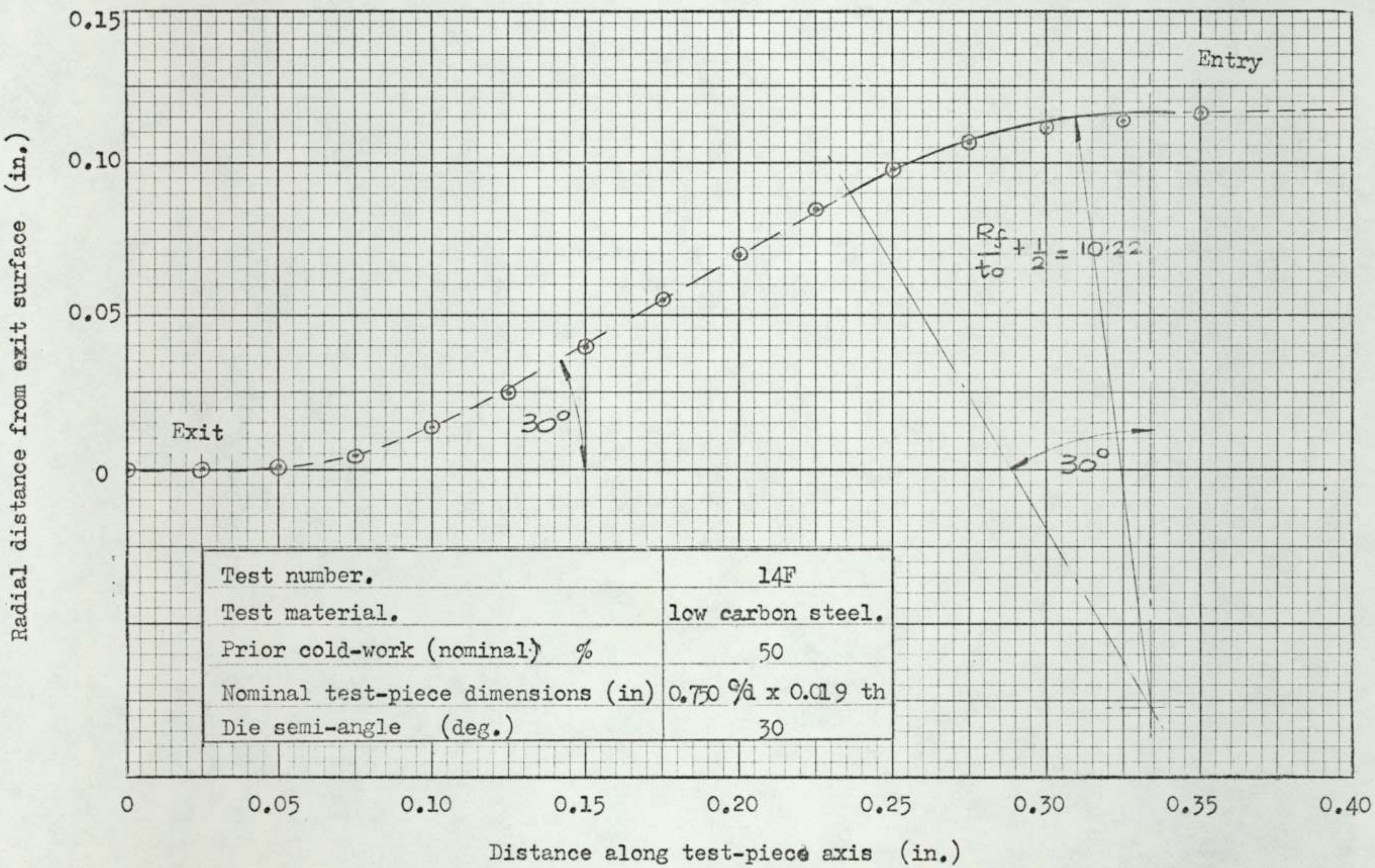

FIG. 142 DEFORMATION PROFILE IN FREE REDRAWING.

9 DEVELOPMENT OF THEORIES OF SPLAYING.

9. 1. Introductory comments.

Preliminary theoretical studies (section 4) had suggested that an 'energy' approach was most suitable for analysing splaying, and that the phenomenon was associated with a decrease in process work such that cup wall elements involved in splaying pass from radius r_O to radius r_B (FIG. 143.) with less work of deformation than those during steady-state conditions.

Within this broad concept two distinctly different modes of splaying may be postulated. In the first, splaying may be considered as a gradual change from steady-state in which the specific work of elements increases in proportion to their distance from the cup rim. Thus splaying may be viewed as a gradual unbending process. In the second mode, splaying may be envisaged as a radical change in steady-state conditions with elements near point A at splaying initiation receiving little subsequent work above that to produce radial drawing from r_O to r_B, whereas elements near the cup rim receive greatest specific work. This mode, in the limit, would be characterised by the complete absence of bending/unbending operations, the cup wall splaying tangentially.

Providing the bulk work of deformation during splaying is always less than that for the steady-state in an equal increment of punch travel, both of the above modes would appear admissible. However, the actual splay mode would be that involving minimum energy of deformation in a true elastic-plastic material, and could only be found by analysing the work involved over small successive stages of splaying for a variety of assumed stage deformations. During steady-state unconstrained redrawing free-zone geometry is dictated by process constraint and gives a minimum energy condition for that situation. Splaying may be viewed as a gradual release of constraint such that over any small splay increment work is a minimum for the instantaneous constraint exercised.

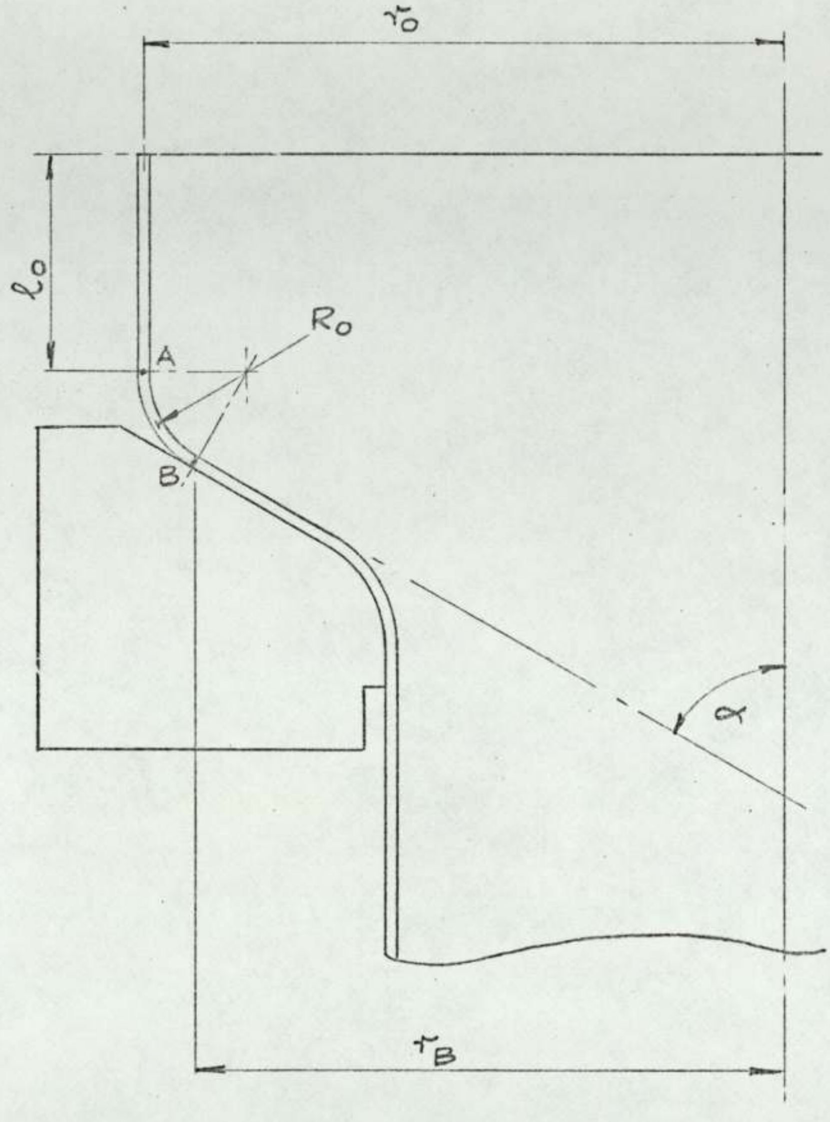

FIG. 143 CUP AT ONSET OF SPLAYING.

9. 2. General concepts.

It was shown in section (4) that the specific work for an element traversing zone A - B (FIG. 143) during steady-state redrawing is,

$$w_0 = w_{b_0} + w_{r_0} + w_{u_0} \doteq 2\,w_{b_0} + w_{r_0}$$

where the suffix 0 denotes steady-state.

The specific work w to transmit any wall element to point B during splaying comprises;

(1) That for splaying from the original cup radius

(2) That for radial drawing from the point of maximum splay to the radius r_B at B.

(3) That for bending to and unbending from some radius at which the element passes through the zone.

It was assumed, as for steady-state conditions, that unbending work w_u is equal to bending work w_b. Work component (3) is thus $2\,w_b$. If work component (1) is designated w_s then component (2) is $w_s + w_{r_0}$. For a decrease in process work with splaying the inequality may be written;

$$w = 2\left(w_s + w_b\right) + w_{r_0} < 2\,w_{b_0} + w_{r_0}$$

The term w_{r_0} is common to both sides of the inequality and represents the absolute minimum specific energy input to transport any element from A to B. Thus,

$$w_s + w_b < w_{b_0} \qquad (9.1.)$$

Equation 9.1 implies that for splaying to occur in any element the combined splay and bending work must be less than the steady-state bending work.

This approach to splaying provides an insight into the character of deformation in the splayed cup before contact with the die at point B. During splaying, that part of the cup between cup-rim and die is simultaneously undergoing two different deformations. The region near the rim will be splaying and carrying a tensile circumferential stress, whereas the region near the die is being radially drawn inwards with an associated compressive circumferential stress. Between these two extremes there is, at any instant, a particular element in neither of the above mentioned regions. This element has previously moved through the splay zone, attained its maximum tensile circumferential strain, and is now just about to enter the radial drawing zone. The element may be regarded as neutral for an instant and be at a neutral point in the overall zone.

The analysis indicates that although an element may currently be at a radius $r > r_0$ it does not follow that it is splaying. If the length of current unbent cup wall involved in splaying is ℓ, then true splaying is only occurring in those elements for which $\frac{dr}{d\ell}$ is negative, whilst radial drawing is occurring in elements where $\frac{dr}{d\ell}$ is positive.

9. 3. Experimental support for theory.

(1) The splay-measurement programme results indicated conclusively that the splay-phase corresponded to a decrease in drawing load. Since apart from splaying all other process parameters remained unchanged, this could only mean that splaying produced a reduction in process work. The original concept was therefore verified.

(2) Observations on test-piece profiles during splaying indicated that early in the splay-phase the radius of bending increased rapidly from R_0 such that the region near the cup rim appeared to splay almost tangentially and receive little bending.

(3) There was some doubt about the validity of an expression derived for the onset of splaying (Equation 4.17 a, b and c). However experimental results showed that the theoretical prediction was reasonable, although slightly under-estimating the length of cup wall involved in splaying.

(4) During unconstrained redraw tests with the highest test-piece

diameter/thickness ratio (60/1) and 90 degree semi-angle die, it was found that splaying developed up to a point where the test-piece rim suddenly wrinkled. This was taken as an indication that circumferential stresses in the rim region had changed from tensile to compressive i.e. rim elements had passed through the neutral state.

9.4. Major theoretical assumptions. (See also appendix A5)

Assumptions peculiar to various aspects of theoretical work are stated under the appropriate section. Additionally the following general assumptions were made :

(1) A rigid-plastic material was assumed enabling problems involved with elastic spring-back effects, as the constraint of the entering cup wall diminished, to be avoided.

(2) Yield-stress in tension was considered to be equal to that in compression.

(3) Residual stresses from previous cold-drawing operations were negligibly small.

(4) That the cup material was homogeneous and isotropic, both normal and planar anisotropy was ignored.

(5) All bending operations, during steady-state and splay phases, were assumed plane-strain with $\varepsilon_3 = 0$.

(6) Fogg's theory for deducing free-zone geometry in unconstrained redrawing was adopted.

(7) Radial, circumferential and through-thickness stresses and strains in the splayed cup were taken to be principal values.

(8) Throughout the splaying phase the cup wall thickness was assumed constant and equal to that of the entering cup.

9.5. Simple upper-bound theory of splaying.

The specific energy ω required to transmit any element of the splayed cup wall to point B (FIG. 143) is given by the condition,

$$\omega_{r_0} < \omega < \omega_0$$

ω_{r_0} is an ideal lower bound, whilst ω_0 is an upper bound set by the steady-state redrawing conditions. $w \not> w_o$ and hence from equation 9.1.,

$$w_s + w_b \not> w_{bo}$$

for any splayed element. In the limit,

$$w_s + w_b = w_{bo}$$

Now an element situated at the cup rim cannot bend since it cannot support a bending moment. Therefore for this particular element an upper bound is given by $w_s = w_{bo}$. Splaying represented by w_s is then a maximum and cannot be exceeded.

If the cup rim splays to radius r_s, then for a rigid - perfectly plastic material,

$$w_s = Y . \ln \frac{r_s}{r_o}$$

and since $w_{bo} = \frac{2}{\sqrt{3}} . \frac{Y.t_o}{4 R_o}$,

$$\frac{r_s}{r_o} = e^{\frac{t_o}{2\sqrt{3} R_o}}$$

The fractional increase in the cup rim on splaying is,

$$\Delta s_o = \frac{r_s - r_o}{r_o}$$

therefore $\Delta s_o = e^{\frac{t_o}{2\sqrt{3} R_o}} - 1 \simeq \frac{t_o}{2\sqrt{3} R_o}$ ———— (9.2.)

since $\frac{t_o}{2\sqrt{3} R_o}$ is small, never exceeding about 0.07.

The term R_o in equation 9.2. is the radius of bending during steady-state conditions. It may be the free-radius in unconstrained redrawing or the mean radius of bending around the hold-down punch in constrained redrawing.

Equation 9.2. suggests;

(1) The tendency to splay will increase as the ratio $\frac{R_o}{t_o}$ becomes smaller.

(2) Splaying is not a direct function of the entering cup radius r_o

or die semi-angle α . (These factors influence R_o in unconstrained redrawing but not in constrained redrawing.)

(3) According to Fogg's free-zone theory,[11] splaying in unconstrained redrawing will be most severe for low $\frac{r_o}{t_o}$ cups redrawn through dies of large semi-angles.

FIG. 144 shows the upper bound splay ΔS_o — R_o/t_o relationship, valid for unconstrained or constrained redrawing. There is a single curve since theory predicts splaying is only a function of R_o/t_o . In the unconstrained condition R_o $(= R_f)$ is not known immediately but may be found from equation 2.34. Substitution of $R_o = R_f$ in equation 9.2. provides,

$$\Delta s_o \simeq \frac{1}{2(3)^{1/4}} \sqrt{\frac{1 - \cos\alpha}{r_o/t_o}}$$

A plot of ΔS_o against r_o/t_o gives a family of curves of similar form to FIG. 144, splaying increasing with increases in die angle.

Results from the simple upper-bound theory were considered important since the theory did provide an over-estimate of splaying, the actual magnitude of over-estimation being about 100 % on the basis of splay-measurement programme results. This indicated that an energy approach was useful, and that splaying was wholly accountable in terms of bending work of zone entry during steady-state conditions. It was no longer necessary to pursue investigations into the possibility of a splaying contribution from the complex radial drawing zone prior to die contact.

An objection to the theory was that it failed to take account of the splayed zone as a whole. That is, rim elements were treated in isolation and constraint exercised by neighbouring elements lower down the wall ignored. Further theoretical studies were aimed at eliminating this objection.

9.6. Tangential theory of splaying.

(a) Basis of theory.

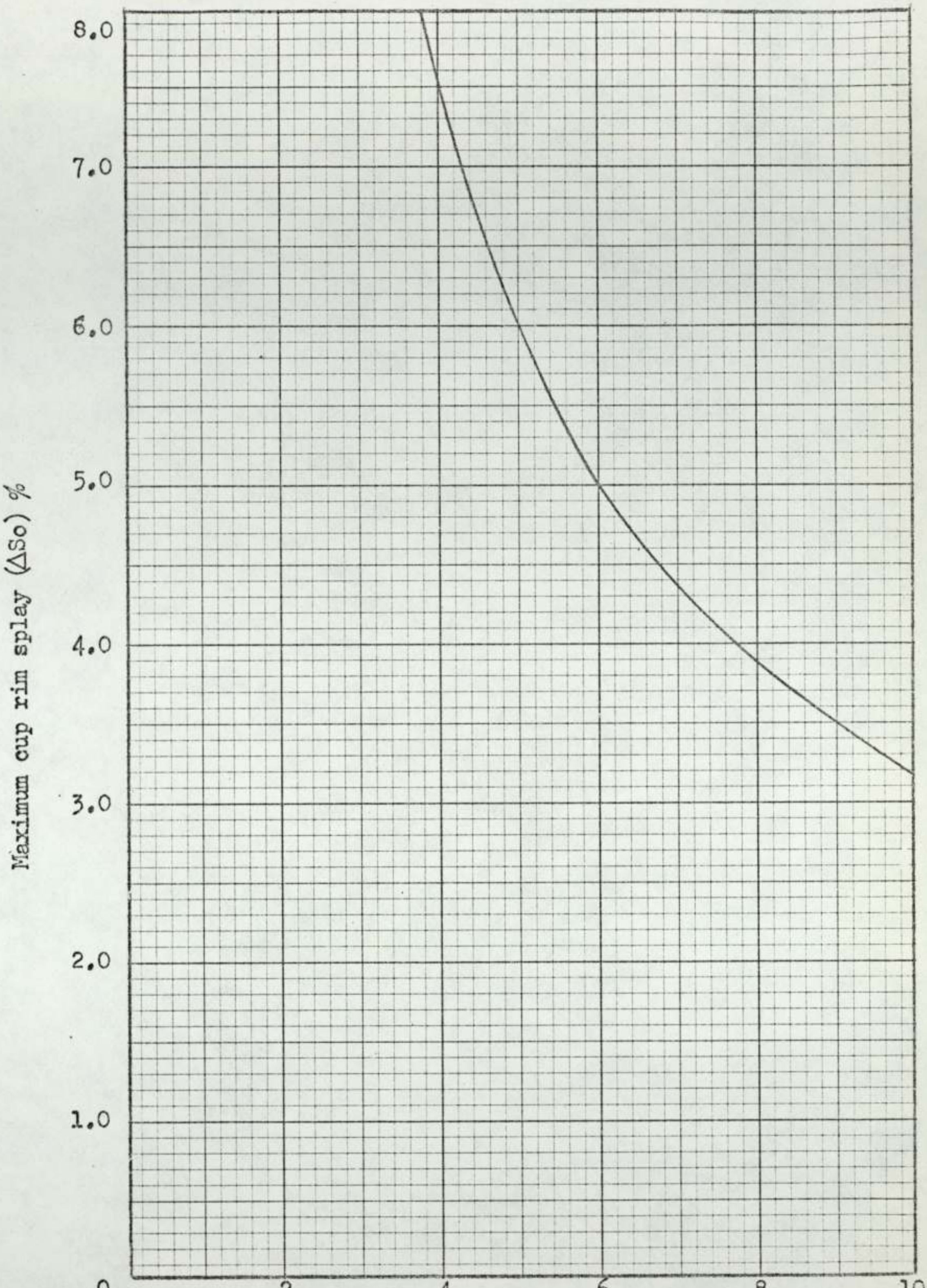

FIG. 144 MAXIMUM SPLAYING AS A FUNCTION OF STEADY-STATE BENDING RATIO ($^{Ro}/_{to}$) SIMPLE UPPER-BOUND THEORY.

It is postulated that during the terminal stages of redrawing a stage is reached when the entering cup wall can no longer provide the bending moment to maintain steady-state conditions, and then the previously undeformed cup wall ℓ_0 (FIG. 143) splays out tangentially as the element originally at point A (already bent to radius R_0) moves towards the die at B.

Experimental evidence from the splay-measurement programme suggested that some bending occurred in ℓ_0 during the splay phase. Therefore, provided the value of ℓ_0 is reasonably predicted, the tangential theory should provide an upper limit to splaying since any bending in ℓ_0 must tend to reduce its magnitude.

(b) Maximum splaying.

FIG. 145 shows the splayed configuration when an element, originally at A when splaying commenced, has travelled an angular distance θ into the radial drawing zone.

The radial splay S in an element at x is given by,

$$S = x \sin\theta - R_0\left(1 - \cos\theta\right) \qquad (9.3.)$$

maximum splay condition is reached when,

$$\frac{dS}{d\theta} = 0 \quad , \text{ or,}$$

$$x \cos\theta - R_0 . \sin\theta = 0$$

Therefore at maximum splaying, $\tan\theta = \dfrac{x}{R_0}$.

It follows,

$$\sin\theta = \frac{x}{\sqrt{R_0^2 + x^2}} \quad , \quad \cos\theta = \frac{R_0}{\sqrt{R_0^2 + x^2}}$$

substitution for $\sin\theta$, $\cos\theta$ in equation 9.3. gives

$$\hat{S} = \sqrt{R_0^2 + x^2} - R_0$$

The maximum radial splay at the cup rim is thus,

$$\hat{S}_0 = \sqrt{R_0^2 + \ell_0^2} - R_0$$

and the fractional rim splay,

$$\Delta S_0 = \frac{\hat{S}_0}{r_0} = \sqrt{\frac{R_0^2 + \ell_0^2}{r_0^2}} - \frac{R_0}{r_0} \qquad (9.4.)$$

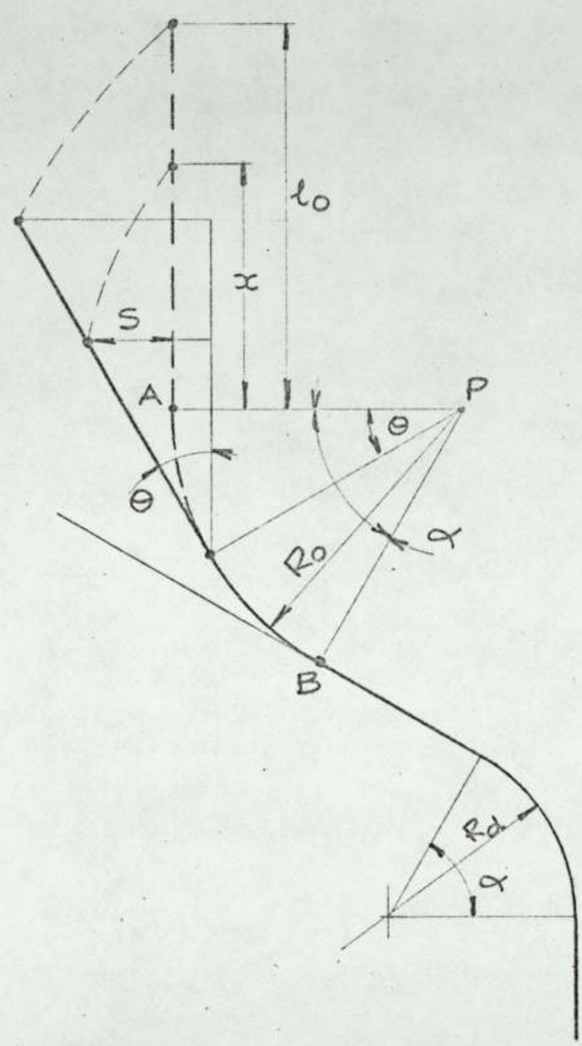

FIG. 145. TANGENTIAL SPLAYING.

For a rigid - perfectly plastic material it was earlier found that,

$$l_o = 0{\cdot}76\sqrt{r_o . t_o}$$

This expression when combined with equation 9.4. gives rim splaying in terms of known process parameters. FIG. 146 expresses the relationship graphically over the range of cup radius/thickness ratios covered in the splay-measurement programme.

The tangential theory gives lower values of splaying than the simple upper-bound theory, which lends support to the admissibility of the former. Unlike the upper-bound theory, the tangential theory implies that cup geometry r_o/t_o influences splaying.

(c) Locus of maximum splay for wall elements.

All elements within the wall length l_o (FIG. 145) attain a maximum splay value when,

$$\tan\theta = \frac{x}{R_o}$$

If the horizontal and vertical co-ordinates of the element at x are a, b measured from P then,

$$\begin{aligned} a &= R_o.\cos\theta + x\sin\theta \\ &= R_o.\cos\theta + R_o.\tan\theta.\sin\theta = R_o\sec\theta. \\ b &= x\cos\theta - R_o\sin\theta \\ &= R_o.\tan\theta.\cos\theta - R_o\sin\theta = 0 \end{aligned}$$

Since x was a general element, the maximum splay locus of all splayed elements is therefore a horizontal line drawn outwards from point A. On reaching this line all elements commence to radially draw inwards.

(d) Bulk work in splayed and steady-state modes.

The fundamental postulate was that splaying occurs because the work of deformation in the splayed mode was less than that in the steady state. Therefore for the assumed tangential mode to be admissible, work of deformation in the length l_o (FIG. 145) when point A moves through angular displacement θ, must be less than

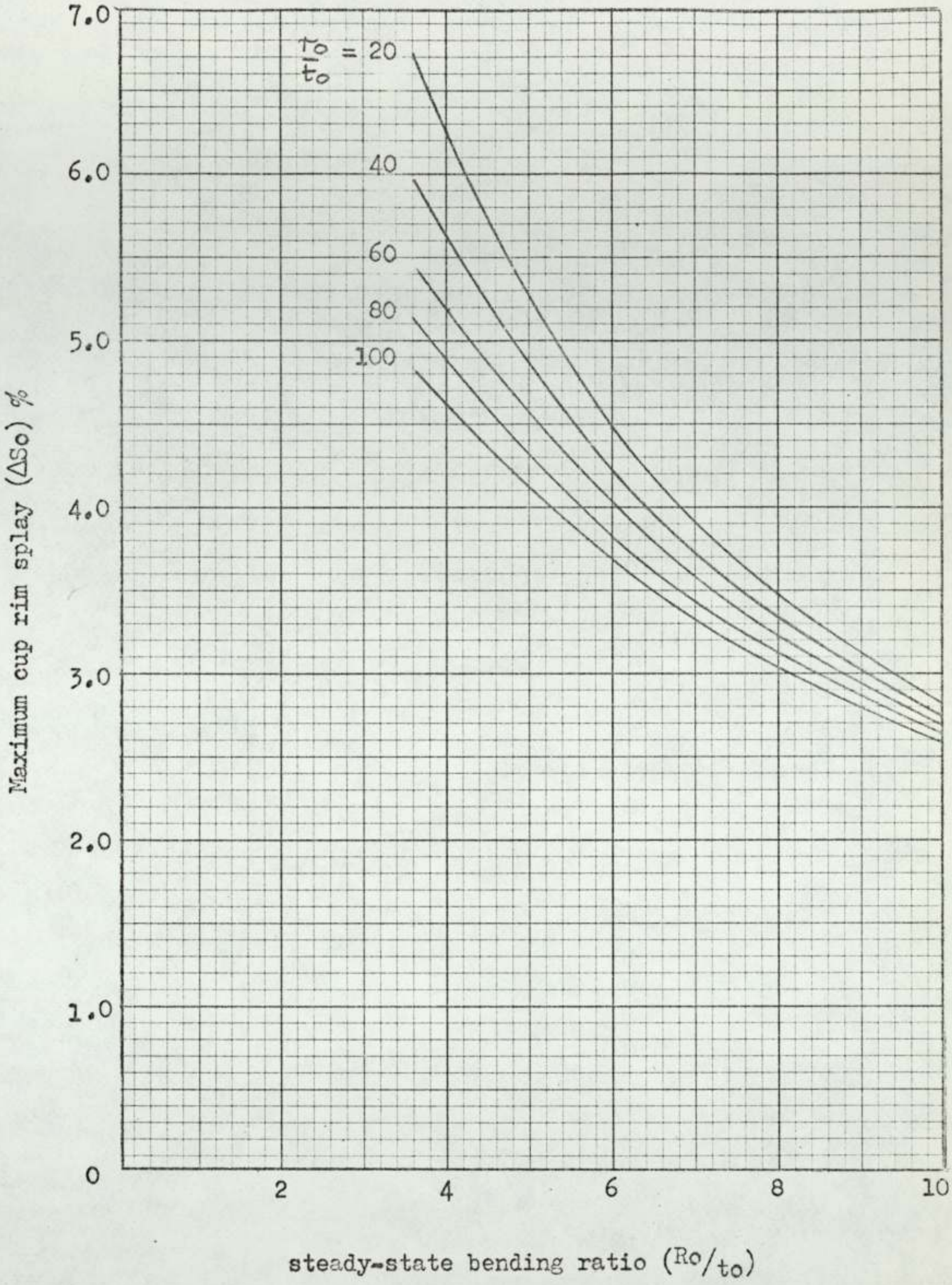

FIG.146 MAXIMUM SPLAYING AS A FUNCTION OF STEADY-STATE BENDING RATIO ($^{Ro}/_{to}$) TANGENTIAL THEORY.

the corresponding steady-state work in deforming length $R_O.\Theta$. The following analysis investigates this situation. A rigid - perfectly plastic material was assumed throughout.

(i) Splayed mode.

Suppose at an angle Θ in FIG. 147 a particular element, originally at distance x_n above A when splaying started, has reached its neutral point, ie. it has passed through the splay zone and is now just about to commence radial drawing. The total work in splaying to Θ is the sum of;

(1) That to splay elements $x_n < x < l_o$

(2) That in previously splaying elements $0 < x < x_n$

(3) That to radially draw elements $0 < x < x_n$

(1) Consider an element at $x_n < x < l_o$, length δx, circumferential width unity. The elemental work of splaying,

$$\delta W_{S_1} = Y \ln \frac{r_s}{r_o} . \delta V = Y \ln\left(1+\frac{s}{r_o}\right)\delta x . t_o$$

$$\simeq Y . \frac{s}{r_o} . \delta x . t_o$$

Hence the total splay work for all elements $x_n < x < l_o$ is,

$$W_{S_1} = Y\frac{t_o}{r_o}\int_{x_n}^{l_o} s . dx \qquad (9.5.)$$

From equation 9.3. , $s = x\sin\Theta - R_o(1-\cos\Theta)$.

Also, $x_n = R_o \tan\Theta$. Substituting these values in equation 9.5. gives,

$$W_{S_1} = Y.\frac{t_o}{r_o}\int_{R_o\tan\Theta}^{l_o}\left[x\sin\Theta - R_o(1-\cos\Theta)\right]dx$$

Integrating,

$$W_{S_1} = Y\frac{t_o}{r_o}\left[\frac{\sin\Theta}{2}\left(l_o^2 - R_o^2\tan^2\Theta\right) - (1-\cos\Theta)R_o(l_o - R_o\tan\Theta)\right] \qquad (9.6.)$$

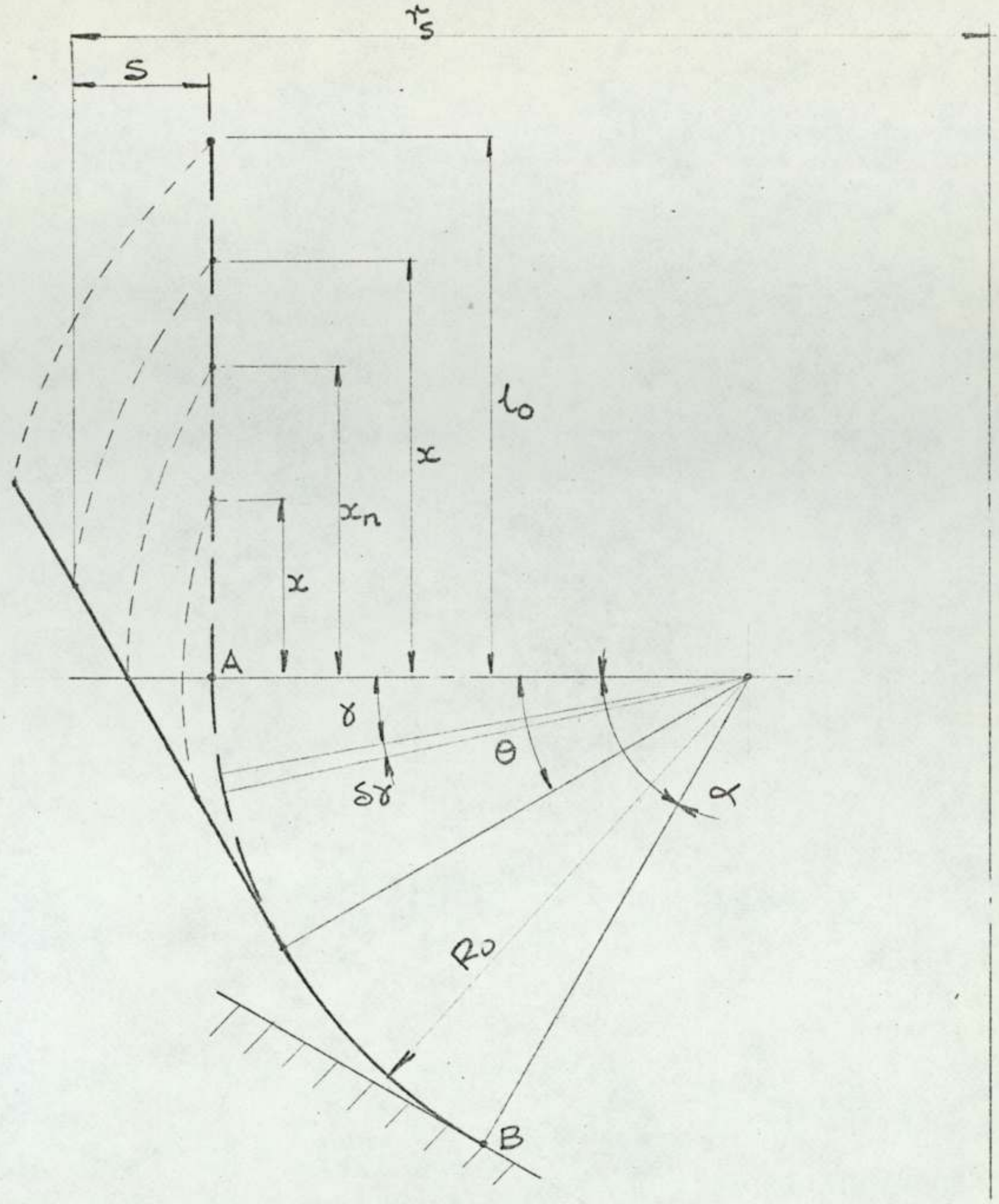

FIG. 147. NOMENCLATURE FOR BULK WORK IN TANGENTIAL SPLAYING.

(2) Consider an element at $0 < x < x_n$. Work of previous splaying $\delta W s_2$ is given by,

$$\delta W s_2 = Y \ln \frac{\hat{r}_s}{r_0} . t_0 . \delta x$$
$$\simeq Y . \frac{t_0}{r_0} . \hat{S} . \delta x$$

where $\hat{S}$ is the greatest radial splay attained by the element.

From section 9.6 b,

$$\hat{S} = \sqrt{R_0^2 + x^2} - R_0$$

Therefore $\delta W s_2 = Y \frac{t_0}{r_0} \left(\sqrt{R_0^2 + x^2} - R_0 \right) \delta x$

The total previous splay work for all elements $0 < x < x_n$ is,

$$W s_2 = Y \frac{t_0}{r_0} \int_0^{x_n} \left(\sqrt{R_0^2 + x^2} - R_0 \right) dx$$

Integrating, and putting $x_n = R_0 . \tan\theta$,

$$W s_2 = \frac{Y . t_0}{2 r_0} R_0^2 \left[\tan\theta (\sec\theta - 2) + \ln(\sec\theta + \tan\theta) \right] \text{——— } (9.7.)$$

(3) For an element at $0 < x < x_n$ work of radial drawing is,

$$\delta W_r = Y . \ln \frac{\hat{r}_s}{r} . t_0 . \delta x .$$

where $\hat{r}_s$ is the maximum radius attained during the splay-phase and r is its current radius.

Now $\hat{r}_s = r_0 + \hat{S}$, and $r = r_0 + S$. (Where S takes a negative value when $R_0(1 - \cos\theta) > x \sin\theta$). Therefore,

$$\ln \frac{\hat{r}_s}{r} = \ln \frac{r_0 + \hat{S}}{r_0 + S} = \ln\left(1 + \frac{\hat{S}}{r_0}\right) - \ln\left(1 + \frac{S}{r_0}\right)$$
$$\simeq \frac{\hat{S} - S}{r_0}$$

But $\hat{S} = \sqrt{R_0^2 + x^2} - R_0$ and $S = x \sin\theta - R_0(1 - \cos\theta)$

Therefore,

$$\delta W_r = Y.\frac{t_o}{r_o}\left[\sqrt{R_o^2+x^2} - x\sin\theta - R_o.\cos\theta\right]\delta x$$

and $$W_r = Y\frac{t_o}{r_o}\int_0^{x_n}\left[\sqrt{R_o^2+x^2} - x\sin\theta - R_o.\cos\theta\right]dx$$

Integrating and putting $x_n = R_o.\tan\theta$,

$$W_r = \frac{Y.t_o.R_o^2}{2r_o}\left[\ln(\sec\theta+\tan\theta) - \sin\theta\right] \text{ ——— } (9.8.)$$

The total work in the splayed mode after drawing to θ is given by the sum,

$$W_{S_1} + W_{S_2} + W_r$$

as given by equations 9.6, 9.7 and 9.8 respectively.

(ii) Steady-state mode.

Consider an element at an angular position $0 < \gamma < \theta$ as shown in FIG. 147. The elemental work comprises;

(1) That due to bending to zone radius R_o

(2) That for radial drawing from cup radius r_o to current radius r .

For an element length $R_o.\delta\gamma$, circumferential width unity, the work is given by

$$\delta W_{s.s.} = R_o.\delta\gamma.t_o\left(\frac{2}{\sqrt{3}}.\frac{Y.t_o}{4\,R_o} + Y\ln\frac{r_o}{r}\right)$$

$$\ln\frac{r_o}{r} = \ln\frac{r_o}{r_o - R_o(1-\cos\gamma)} \simeq \ln\left[1+\frac{R_o}{r_o}(1-\cos\gamma)\right]$$

which may be approximated by $\frac{R_o}{r_o}(1-\cos\gamma)$

Therefore,

$$\delta W_{s.s.} = R_o.Y.t_o.\delta\gamma\left[\frac{2}{\sqrt{3}}.\frac{t_o}{4.R_o} + \frac{R_o}{r_o}(1-\cos\gamma)\right]$$

The total work in drawing to θ is thus

$$W_{s.s.} = R_o . Y . t_o \int_0^{\theta} \left[\frac{2}{\sqrt{3}} \cdot \frac{t_o}{4 R_o} + \frac{R_o}{r_o}(1 - \cos\gamma) \right] d\gamma$$

$$= \frac{Y . t_o . R_o^2}{2 r_o} \left[\left(\frac{t_o . r_o}{\sqrt{3} . R_o^2} + 2 \right) \theta - 2 \sin\theta \right] \quad \text{——— (9.9.)}$$

(iii) <u>Deducing length of cup wall involved in splaying.</u>

The length of cup wall l_o at the start of splaying was derived in section 4 using an equilibrium approach. It is possible to check this result with the aid of equations 9.6, 9.7, 9.8 and 9.9. in the following way;

on an energy basis splaying can only occur if at the onset of splaying,

$$\frac{d}{d\theta}\left(W_{s_1} + W_{s_2} + W_r \right) \leq \frac{d}{d\theta}\left(W_{s.s} \right)$$

The left-hand term will attain a maximum possible value when l_o is greatest, and then

$$\frac{d}{d\theta}\left(W_{s_1} + W_{s_2} + W_r \right) = \frac{d}{d\theta}\left(W_{s.s} \right)$$

Differentiating equations 9.6, 9.7, 9.8, and putting $\theta = 0$,

$$\frac{d}{d\theta}\left(W_{s_1} + W_{s_2} + W_r \right) = \left(\frac{l_o}{R_o} \right)^2 \left(\frac{Y . t_o . R_o^2}{2 r_o} \right)$$

A similar procedure for equation 9.9 gives,

$$\frac{d}{d\theta}\left(W_{s.s} \right) = \frac{1}{\sqrt{3}} \cdot \frac{t_o . r_o}{R_o^2} \left(\frac{Y . t_o . R_o^2}{2 r_o} \right)$$

Equating the two differentials,

$$\left(\frac{l_o}{R_o} \right)^2 = \frac{1}{\sqrt{3}} \cdot \frac{t_o . r_o}{R_o^2}$$

or $$l_o = \sqrt{\frac{r_o . t_o}{\sqrt{3}}} = 0.76 \sqrt{r_o . t_o}$$

This was the expression developed in section 4.

(iv) Interpretation of bulk-splay results.

Unfortunately the number of independent variables involved in the work terms make a comprehensive graphical coverage difficult. However to observe predictions of theory, process work of the splayed and steady-state modes was compared for a particular redraw with $r_o/t_o = 50$, $R_o/t_o \approx 4$. A severe bending ratio was purposely selected since theory suggested this parameter greatly influences splaying. Results are plotted in FIG. 148. The splay-mode work terms totalling W are associated with equations 9.6., 9.7., 9.8., the splaying phase being completed when $\theta = 53$ degrees. Theory predicts that the tangential mode is admissible from a work aspect.

9.7. Hyperbolic theory of splaying.

(a) Basis of theory.

The theory takes account of the bending which was observed to occur in the splayed cup wall during the splay-measurement programme, and postulates that the total specific work of elements undergoing splaying is proportional totheir distance from the cup rim. This is in contrast with the 'tangential' theory where elements near the rim receive more work of deformation than those lower down the wall. A key assumption made in developing the theory is that a hyperbolic relationship exists between the radius of bending of an element in the splay-zone and its position relative to the cup rim. Elements involved in splaying are assumed to splay outwards, bend to a radius on attaining their neutral point, and pass through the radially drawing zone at this curvature before unbending on contact with the die.

(b) Maximum splaying of cup rim.

A rigid - perfectly plastic material is assumed for the present, but later the effect of work-hardening is analysed. Bending and unbending work for any element were considered equal.

An element located at point A (FIG. 143) when splaying

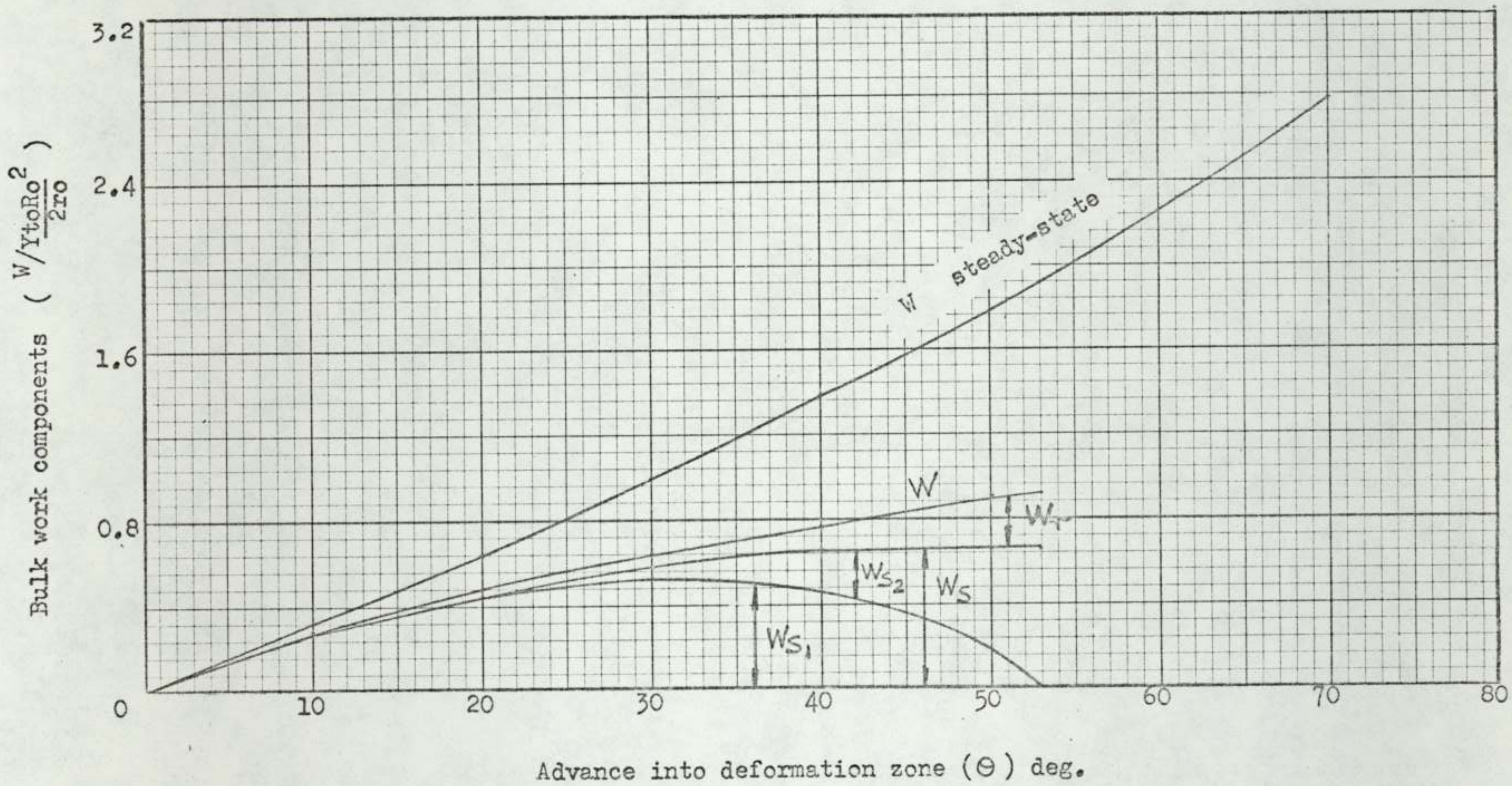

FIG. 148 BULK PLASTIC WORK COMPONENTS DURING SPLAYING PHASE

TANGENTIAL THEORY.

commences bends to the steady-state radius R_o , whereas an element at the cup rim can receive no bending. It was assumed that bending work was proportional to distance from the cup rim, i.e.

$$\omega_b = \frac{l}{l_o} \cdot \omega b_o \qquad \text{———————} \qquad (9.10.)$$

where the suffix 0 denotes steady-state.

On reaching its neutral point an element was considered to bend instantaneously, implying plane-strain conditions with $\varepsilon_3 = 0$. If the radius of bending of an element in the splay-zone is R , equation 9.10 may be written,

$$\frac{2}{\sqrt{3}} \cdot \frac{Y t_o}{4R} = \frac{l}{l_o} \cdot \frac{2}{\sqrt{3}} \frac{Y.t_o}{4R_o}$$

whence,

$$R = R_o . \frac{l_o}{l} \qquad \text{———————} \qquad (9.11.)$$

providing a hyperbolic $R-l$ relationship.

The total specific work for any element $0 \leq l \leq l_o$ in reaching the die is,

$$\omega = 2(\omega s + \omega_b) + \omega t_o \quad ,$$

and for the postulated deformation mode $\frac{d\omega}{dl}$ cannot be negative i.e. the work in elements decrease as l decreases. From equation 9.11,

$$\omega_b = \frac{l}{l_o} \frac{2}{\sqrt{3}} \cdot \frac{Y t_o}{4 R_o}$$

Therefore, $$\frac{d\omega}{dl} = 2\left(\frac{d\omega s}{dl} + \frac{1}{l_o} \cdot \frac{2}{\sqrt{3}} \cdot \frac{Y t_o}{4 R_o}\right)$$

Now splaying will continue provided $\frac{d\omega}{dl} > 0$, but must end when $\frac{d\omega}{dl} = 0$. The condition for maximum splaying is therefore,

$$\frac{d\omega s}{dl} = -\frac{1}{l_o} \cdot \frac{2}{\sqrt{3}} \cdot \frac{Y.t_o}{4 R_o} \qquad \text{———————} \qquad (9.12.)$$

and this can only be true at the cup rim where $l = 0$.

The specific work of splaying is,

$$w_s = Y.\mathcal{E}_s = Y \ln \frac{r_s}{r_o} = Y \ln\left(1+\frac{s}{r_o}\right) \simeq Y.\frac{s}{r_o}$$

Therefore

$$\frac{dw_s}{dl} = \frac{Y}{r_o}.\frac{ds}{dl} \quad \text{, and when} \quad l = 0 \quad ,$$

$$\frac{Y}{r_o}\cdot\left(\frac{ds}{dl}\right)_{l=0} = -\frac{1}{l_o}\cdot\frac{2}{\sqrt{3}}\cdot\frac{Y t_o}{4 R_o}$$

or,

$$\left(\frac{ds}{dl}\right)_{l=0} = -\frac{r_o}{l_o}\cdot\frac{2}{\sqrt{3}}\cdot\frac{t_o}{4R_o} \quad \text{———————} \quad (9.13.)$$

The negative sign informs that splaying increases as l decreases.

At the start of the splay-phase $(l = l_o)$, splaying is instantaneously tangential to radius R_o , and from equation 9.3.,

$$s = (l_o - l)\sin\theta - R_o(1-\cos\theta)$$

or $\quad \frac{ds}{dl} = -\sin\theta$

Now when $l = l_o$, $\theta = 0$, and therefore $\left(\frac{ds}{dl}\right)_{l=l_o} = 0$.

Splaying may now be found by assuming a relationship between s and l which satisfies the conditions,

$$\left(\frac{ds}{dl}\right)_{l=l_o} = 0$$

$$\left(\frac{ds}{dl}\right)_{l=0} = \frac{r_o}{l_o}\cdot\frac{2}{\sqrt{3}}\cdot\frac{t_o}{4R_o}$$

If this is a circular arc as shown in FIG. 149, then,

$$S_o = \rho(1-\cos\beta) = \frac{l_o}{\sin\beta}(1-\cos\beta) \quad \text{——————} \quad (9.14.)$$

where, $\tan\beta = \left(\frac{ds}{dl}\right)_{l=0}$

Putting $\quad \tan\beta = x, \ \sin\beta = \frac{x}{\sqrt{1+x^2}}, \ \cos\beta = \frac{1}{\sqrt{1+x^2}}$

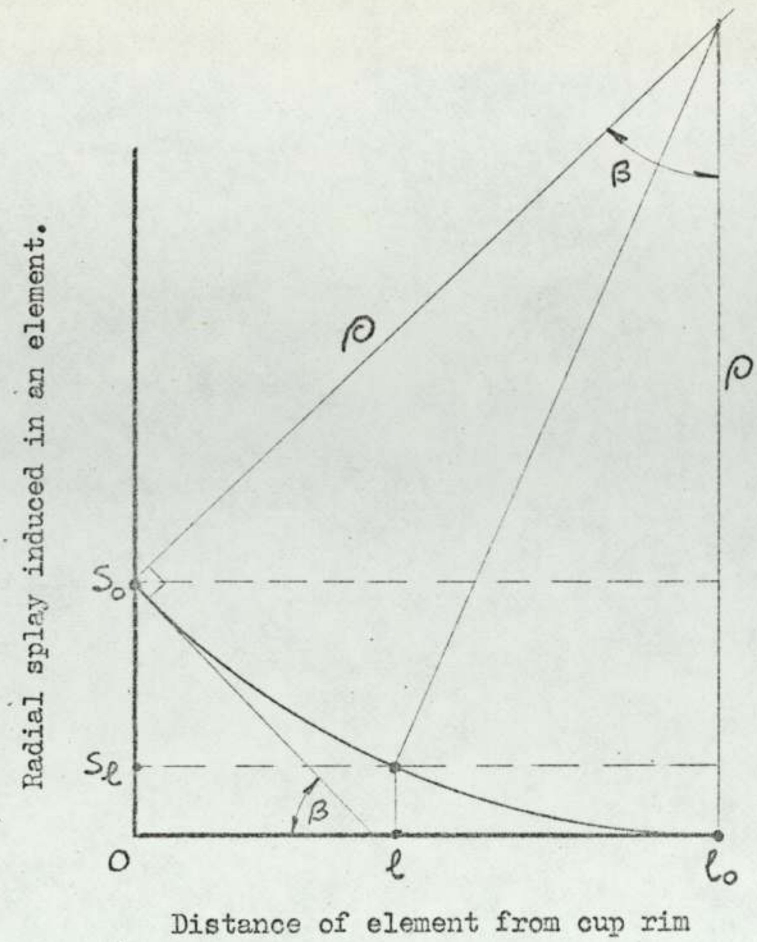

FIG. 149. RELATIONSHIP BETWEEN MAXIMUM SPLAYING AND DISTANCE FROM CUP RIM. HYPERBOLIC THEORY.

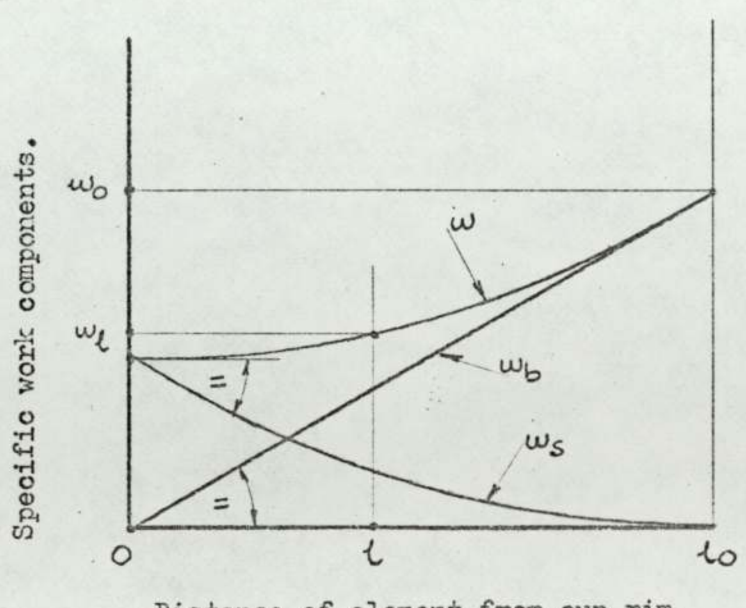

FIG. 150 DISTRIBUTION OF SPECIFIC WORK COMPONENTS IN HYPERBOLIC THEORY.

Substitution for $\sin\beta$, $\cos\beta$ in equation 9.14. gives,

$$S_o = l_o\left(\frac{\sqrt{1+x^2} - 1}{x}\right) \qquad (9.15.)$$

and
$$\Delta S_o = \frac{S_o}{r_o} = \frac{l_o}{r_o}\left(\frac{\sqrt{1+x^2} - 1}{x}\right) \qquad (9.16.)$$

where $l_o = 0{\cdot}76\sqrt{r_o . t_o}$

According to theory the specific work distribution will be as shown in FIG. 150.

The expression for maximum splaying at the cup rim (equation 9.16.) may be simplified by putting $\sqrt{1+x^2} \simeq 1 + \frac{1}{2}x^2$

Then,

$$\Delta S_o = \frac{1}{2}\left(\frac{2}{\sqrt{3}} \cdot \frac{t}{4R_o}\right) \qquad (9.16.a)$$

Thus the hyperbolic theory states that maximum cup rim splay is about one-half of that given by the upper-bound theory (equation 9.2.) .

FIG. 151 shows maximum rim splay as a function of steady-state bending ratio. The full curves were plotted from equation 9.16 whilst the dotted line was from equation 9.16a. The influence of cup geometry on splaying is not strong when (R_o/t_o) is an independent parameter.

Maximum rim splay in unconstrained redrawing may be deduced from equation 9.16. using Fogg's[11] expression for free-zone geometry,

$$\frac{R_o}{t_o} = \sqrt{\frac{r_o/t_o}{\sqrt{3}(1-\cos\alpha)}}$$

x then becomes $\frac{1}{2}\sqrt{1-\cos\alpha}$, and equation 9.16 may be rewritten,

$$\Delta S_o = \frac{0{\cdot}76}{\sqrt{r_o/t_o}}\left[\frac{\sqrt{1+\frac{1}{4}(1-\cos\alpha)} - 1}{\frac{1}{2}\sqrt{1-\cos\alpha}}\right] \qquad (9.16b)$$

Equation 9.18 is graphically represented by FIG. 152.

(c) Maximum splaying of a general element $0 < l < l_o$

Returning to FIG. 149, it is readily shown that the maximum

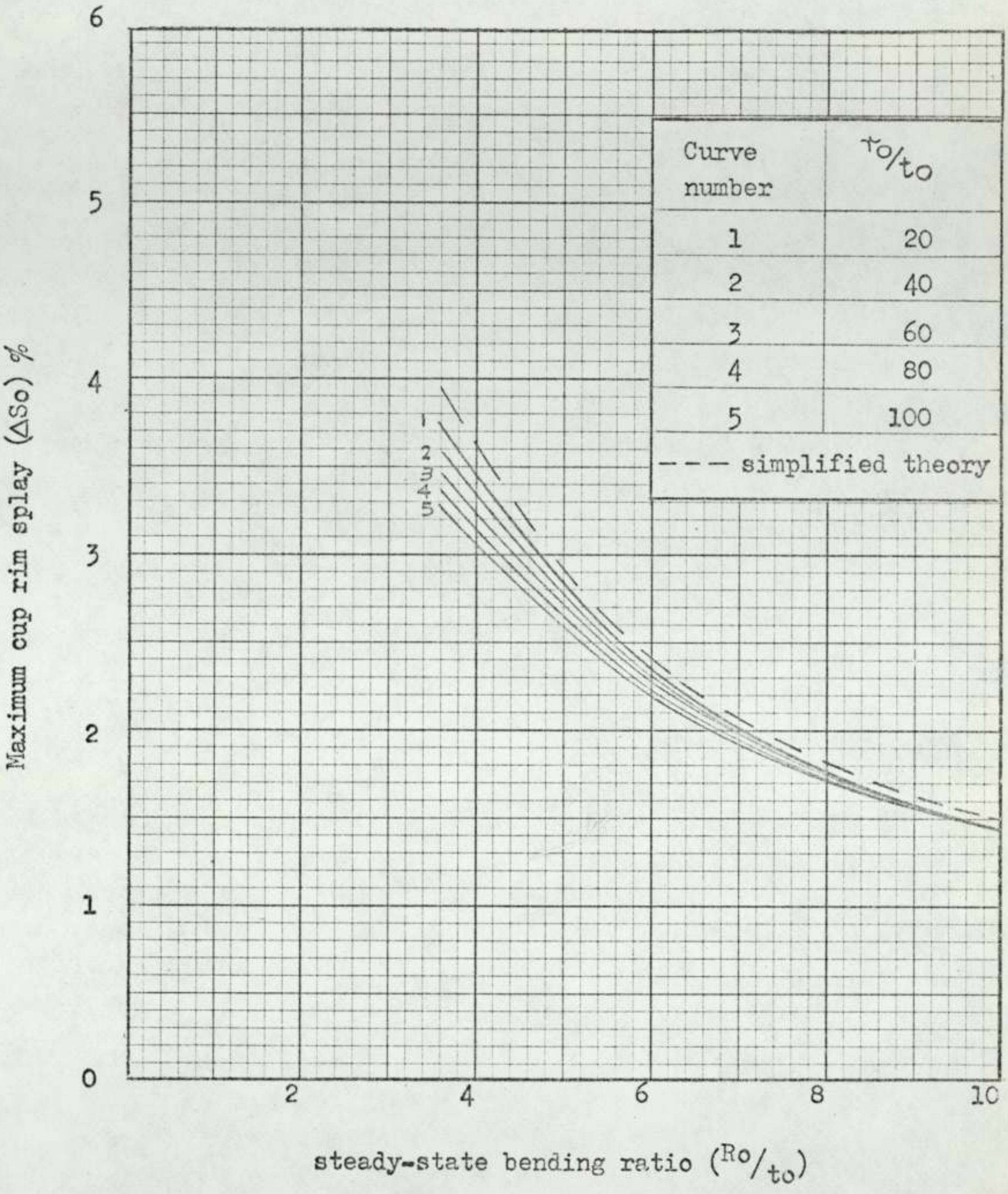

FIG. 151 MAXIMUM SPLAYING AS A FUNCTION OF STEADY-STATE BENDING RATIO ($^{Ro}/_{to}$) HYPERBOLIC THEORY.

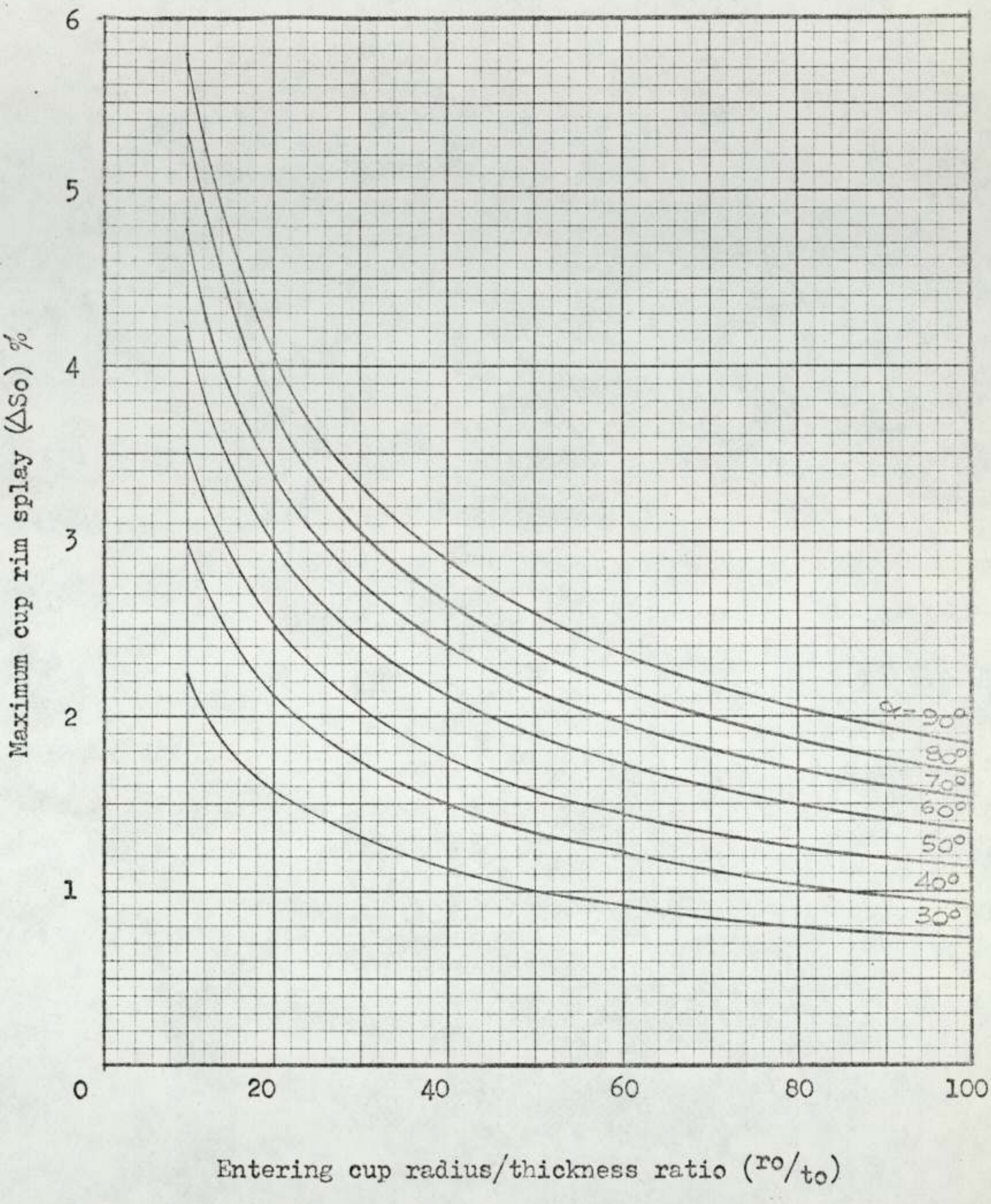

FIG. 152 MAXIMUM SPLAYING AS A FUNCTION OF ENTERING CUP RADIUS/THICKNESS RATIO IN FREE REDRAWING. (HYPERBOLIC THEORY)

radial splay S_l induced in an element distance l from the cup rim is,

$$S_l = \frac{l_o\sqrt{1+x^2}}{x}\left[1 - \sqrt{1 - \left(\frac{l_o - l}{l_o}\right)^2 \cdot \frac{x^2}{1+x^2}}\right] \qquad (9.17.)$$

(d) Locus of maximum splay for wall elements.

The locus could not be established a priori since the expression for maximum splay (equation 9.16.) was not in terms of θ, and therefore $dS/d\theta$ was unknown. Although the current radius of bending R was known in terms of l, values could not be given to l unless the splay locus was known. The locus must start at point A (FIG. 153) since at $l = l_o$, $R = R_o$. To establish the end point, experimental evidence of the constrained splay-measurement programme was examined, where R_o was positively fixed by the hold-down punch nose radius. Each of the experimental splay curves was marked with a short vertical line corresponding to point A in FIG. 153. It was found that in all cases the line intersected the splay curve at or near the point of maximum splay. This result was used to establish point E in FIG. 153. Since maximum radial splay represented by A - E is small compared with r_o, the splay locus cannot vary widely from a straight line joining A to E.

(e) Geometry of splaying.

To compare bulk work of the postulated splay mode with that for steady-state conditions it was necessary to establish splayed geometry in terms of current angular position θ of an element situated at point A when splaying commenced.

The bent cup wall below A - E in FIG. 153. is given by $\int R\,d\psi'$ which may be approximated by $R_o.\theta$. Therefore the unbent length of wall above A - E, is, $l = l_o - R_o.\theta$, and equation 9.11 becomes,

$$R = \frac{R_o.l_o}{l_o - R_o.\theta} \qquad (9.18.)$$

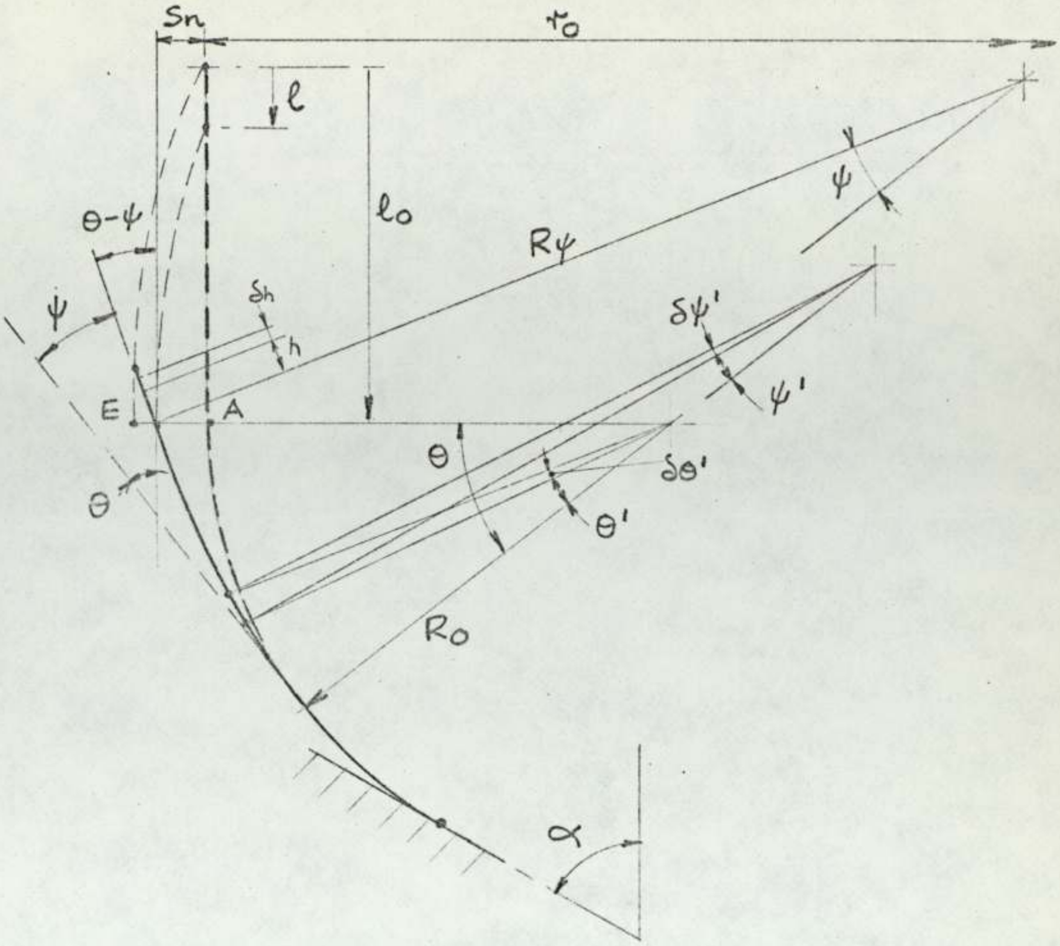

FIG. 153 HYPERBOLIC SPLAYING.

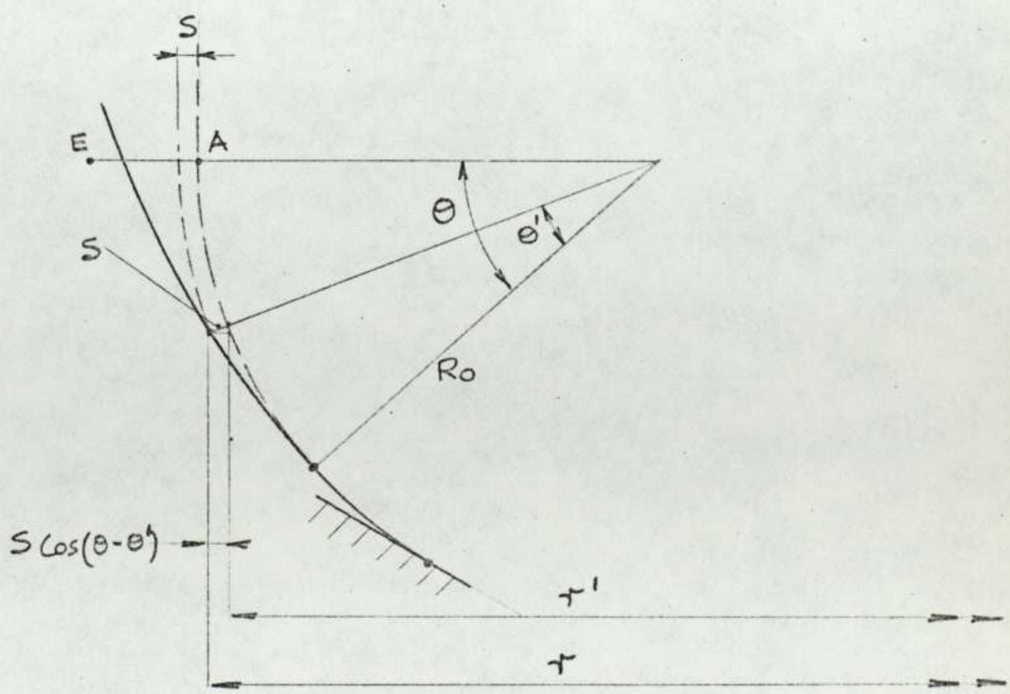

FIG. 154 CURRENT RADIUS OF AN ELEMENT IN RADIAL DRAWING REGION.

For an element length δ situated at θ' from the plane of bending $R = R_o$,

$$\delta = R\,\delta\psi' \simeq R_o . \delta\theta'$$

where R at θ' is given by equation 9.18.

Therefore,

$$\delta\psi' = \frac{l_o - R_o\theta'}{l_o} . \delta\theta'$$

$$\psi' = \frac{1}{l_o}\left(l_o.\theta' - \frac{R_o.\theta'^2}{2}\right) \qquad \text{———————— (9.19.)}$$

When $\theta' = \theta$, $\psi' = \psi$. To establish maximum rim splay at any intermediate stage the angle $(\theta - \psi)$ is required. From equation 9.19.,

$$\theta - \psi = \frac{1}{2} . \frac{R_o}{l_o} . \theta^2 \qquad \text{———————— (9.20.)}$$

(f) Bulk work in splayed and steady-state modes.

A similar approach to that for tangential splaying was used to develop equations representing work done in deforming the cup wall length l_o according to the postulated splay mode. This work was then compared with that for steady-state deformation. A rigid-perfectly plastic material was assumed throughout.

(i) Splayed mode.

Suppose at an angle θ in FIG. 153 a particular element distance l from the cup rim has attained its neutral point, having passed through the splay zone and being just about to bend to radius R before commencing to radial draw inwards. The total work in splaying to θ is the sum of:

(1) That to splay elements in the wall length l

(2) That to bend elements in the wall length $l_o - l$

(3) That in previously splaying elements in the wall length $l_o - l$

(4) That to radially draw elements in the wall length $l_o - l$

(1) Consider an element distance h above the current neutral

point, length δh , unit circumferential width. The elemental work of splaying is,

$$\delta W s_1 = Y . \delta \varepsilon . to . \delta h$$

$$= Y \ln \frac{r_s}{r_o} . to . \delta h$$

where $\quad r_s = r_o + s = r_o + s_n + h \sin(\theta - \psi)$

Therefore,

$$\ln . \frac{r_s}{r_o} = \ln \left[1 + \frac{s_n + h \sin(\theta - \psi)}{r_o} \right] \simeq \frac{s_n + h \sin(\theta - \psi)}{r_o}$$

and $$W s_1 = \frac{Y to}{r_o} \int_0^l \left[s_n + h \sin(\theta - \psi) \right] dh$$

Integrating,

$$W s_1 = \frac{Y . to}{r_o} \left[s_n . l + \frac{l^2}{2} . \sin(\theta - \psi) \right] \qquad (9.21.)$$

where, equation 9.17 gives s_n

equation 9.20 gives $(\theta - \psi)$

and $l = l_o - R_o . \theta .$

(2) Consider an element of length $R \delta \psi \simeq R_o . \delta \theta'$ currently within the radial drawing region i.e. below A - E FIG. 153. For unit circumferential width the elemental work of bending is approximately,

$$\delta W_b = \frac{2}{\sqrt{3}} . \frac{Y . to}{4 R} . R_o . \delta \theta' to$$

Substituting for R from equation 9.18.,

$$\delta W_b = \frac{2}{\sqrt{3}} . \frac{Y . to^2}{4} \left(\frac{l_o - R_o . \theta'}{l_o} \right) . \delta \theta'$$

and $$W_b = \frac{2}{\sqrt{3}} . \frac{Y . to^2}{4 l_o} \int_0^\theta (l_o - R_o . \theta') \, d\theta'$$

Integrating,

$$W_b = \frac{2}{\sqrt{3}} . \frac{Y . to^2}{4 l_o} \left(l_o . \theta - \frac{R_o . \theta^2}{2} \right) \qquad (9.22.)$$

(3) The previous splay work of the element in (2) above is,

$$\delta W_2 = Y \ln.\frac{r_s}{r_0} . R_0 . \delta\theta' . t_0$$

where $$\ln\frac{r_s}{r_0} = \ln\frac{r_0+S}{r_0} \simeq \frac{S}{r_0}$$

Maximum splaying occurred in this element when $l = l_0 - R_0.\theta'$.
Substituting for l in equation 9.17.,

$$S = \frac{l_0\sqrt{1+x^2}}{x}\left[1-\sqrt{1-\left(\frac{R_0.\theta'}{l_0}\right)^2.\frac{x^2}{1+x^2}}\right]$$

Therefore the elemental work may be written,

$$\delta Ws_2 = Y.t_0.\frac{l_0}{r_0}\frac{\sqrt{1+x^2}}{x}.\left[1-\sqrt{1-\left(\frac{R_0.\theta'}{l_0}\right)^2.\frac{x^2}{1+x^2}}\right]R_0.\delta\theta'$$

and the total previous splay work for all elements currently below A - E is thus,

$$Ws_2 = Y.t_0.\frac{l_0}{r_0}\frac{\sqrt{1+x^2}}{x}.R_0\int_0^{\theta}\left[1-\sqrt{1-\left(\frac{R_0}{l_0}\right)^2\frac{x^2}{1+x^2}.\theta'^2}\right]d\theta'$$

Putting $\left(\frac{R_0}{l_0}\right)^2.\frac{x^2}{1+x^2} = M$ and integrating,

$$Ws_2 = \frac{1}{2}\frac{Y.t_0}{r_0}.\frac{R_0^2}{\sqrt{M}}\left[\theta\left(2-\sqrt{1-M\theta^2}\right)-\frac{1}{\sqrt{M}}.\sin^{-1}\sqrt{M}\,\theta\right] \text{—— (9.23.)}$$

(4) Consider the radial drawing work of an element currently located at θ' from the plane of R_0 , as shown in FIG. 153. (This is the same element as that considered for work components 2 and 3). Suppose the elemental length $\delta \simeq R_0.\delta\theta'$, and the circumferential width is unity.

On attaining its maximum radial splay S at θ' the element was assumed to bend to radius R , and pass through the radial drawing zone at this curvature as shown in FIG. 154. Its current radius r in the cup wall may be written,

$$r = r' + S\cos(\theta-\theta')$$

or $$r = r_0 - R_0\left[1-\cos(\theta-\theta')\right] + S\cos(\theta-\theta')$$

The radius of the element at the start of radial drawing was $r_0 + S$

where,

$$S = l_0 \frac{\sqrt{1+x^2}}{x}\left[1 - \sqrt{1 - \left(\frac{R_0}{l_0}\right)^2 \cdot \frac{x^2}{1+x^2} \cdot \theta'^2}\right]$$

$$= l_0 \frac{\sqrt{1+x^2}}{x}\left[1 - \sqrt{1 - M\theta'^2}\right]$$

Radial strain in the element $\quad \varepsilon_r = \ln \dfrac{r_0+S}{r}$

$$= \ln. \frac{r_0 + S}{r_0 - \left[R_0 - (R_0+S)\cos(\theta-\theta')\right]}$$

$$= \ln.\left(1 + \frac{S}{r_0}\right) - \ln\left[1 - \frac{\{R_0 - (R_0+S)\cos(\theta-\theta')\}}{r_0}\right]$$

$$\simeq \frac{S}{r_0} + \frac{R_0 - (R_0+S)\cos(\theta-\theta')}{r_0}$$

Radial drawing work for the element is,

$$\delta W_r = Y.\varepsilon_r.R_0.\delta\theta'.t_0$$

$$\simeq \frac{S}{r_0}.Y.R_0.\delta\theta' t_0 \qquad + \frac{\left[R_0 - (R_0+S)\cos(\theta-\theta')\right]Y.R_0.\delta\theta' t_0}{r_0}$$

= work to draw back to radius r_0 + work to draw from r_0 to current radius r

The total radial drawing work for all elements currently below A - E (FIG. 153) is therefore,

$$W_r = \int_{\theta'=0}^{\theta} \frac{S}{r_0}.Y.R_0.t_0.d\theta' + \int_{\theta'=0}^{\theta} \frac{R_0^2}{r_0}.Y.t_0.d\theta' - \int_{\theta'=0}^{\theta} \frac{(R_0+S)}{r_0}\cos(\theta-\theta')Y.R_0.t_0.d\theta'$$

$$= I_1 + I_2 - I_3$$

The integrated form of I_1 is given by equation 9.23. I_2 may be integrated directly to give,

$$I_2 = \frac{R_0^2.Y.t_0\,\theta}{r_0}$$

$$I_3 = \frac{Y.R_o.t_o}{r_o}\left[\int_0^{\theta} R_o \cos(\theta-\theta')\,d\theta' + \int_0^{\theta} S\cos(\theta-\theta')\,d\theta'\right]$$

$$= \frac{Y.R_o.t_o}{r_o}\left[I_{3_1} + I_{3_2}\right]$$

$I_{3_1} = R_o.\sin\theta$ in integrated form.

$$I_{3_2} = l_o\frac{\sqrt{1+x^2}}{x}\left[\int_0^{\theta}\cos(\theta-\theta')\,d\theta' - \int_0^{\theta}\sqrt{1-M\theta'^2}.\cos(\theta-\theta')\,d\theta'\right]$$

$$= l_o\frac{\sqrt{1+x^2}}{x}\left[\sin\theta - \int_0^{\theta}\sqrt{1-M\theta'^2}.\cos(\theta-\theta').\,d\theta'\right]$$

Now over the range $0 < \theta' < \frac{\pi}{2}$, $4 < \frac{R_o}{t_o} < 8$, $16 < \frac{r_o}{t_o} < 100$ the maximum error involved in approximating $\sqrt{1-M\theta'^2}$ by the first three terms of the series,

$$1 - \frac{1}{2}.M.\theta'^2 - \frac{1}{8}(M\theta'^2)^2 - \ldots.$$

is only about 3 %, the average error being less than this. Making this substitution and integrating gives,

$$I_{3_2} = l_o\frac{\sqrt{1+x^2}}{x}\left[M(\theta - \sin\theta) + \frac{M^2}{2}\left\{\theta^3 - 6(\theta-\sin\theta)\right\}\right]$$

The summation of I_1, I_2 and I_3 gives

$$\frac{W_r}{\frac{Y.t_o.R_o^2}{2r_o}} = \frac{1}{\sqrt{M}}\left[\theta\left(2-\sqrt{1-M\theta^2}\right) - \frac{1}{\sqrt{M}}.\sin^{-1}\sqrt{M}.\theta\right] + 2\theta$$
$$- \frac{2}{R_o}\left[R_o.\sin\theta + l_o\frac{\sqrt{1+x^2}}{x}\left\{M(\theta-\sin\theta) + \frac{M^2}{2}\left\langle\theta^3 - 6(\theta-\sin\theta)\right\rangle\right\}\right]$$

(9.24.)

The total work after drawing to θ is given by the sum,

$$W_{S_1} + W_b + W_{S_2} + W_r = W,$$

as given by equations 9.21, 9.22, 9.23 and 9.24 respectively where $l_o = 0.76\sqrt{r_o.t_o}$.

(ii) Steady-state mode.

The total work in drawing to θ is given by equation 9.9.

(iv) Interpretation of bulk-work results.

As for tangential theory the number of independent variables involved in the work terms made a comprehensive graphical coverage impracticable without the aid of computation facilities. However to observe theoretical predictions, splay work according to the hyperbolic mode was compared with steady-state work for the particular redraw $R_o/t_o = 4$, $r_o/t_o = 50$. Since these parameters had also been selected for the 'tangential' theory comparison (FIG. 148) , it was possible to compare work in hyperbolic and tangential modes. Results are plotted in FIG. 155, where total splay work is represented by the curve W . Splaying was complete when $\theta \simeq 76$ degrees, i.e. when $W_{S_1} = 0$. Although the hyperbolic theory is admissible from a work aspect $W < W_{s.s.}$, the bending work component W_b makes the total work at any stage θ greater than that for the tangential theory, even though splay work is less.

9.8. The effect of work-hardening on splaying.

Theory and experimental evidence suggested that maximum plastic strain induced by splaying would be of the order 4 - 5 %. Strains due to bending would usually be less than 12% . Over such intervals the equivalent stress-strain curve may be considered approximately linear. A relationship,

$$\sigma = \bar{\sigma}_0 + a\,\bar{\varepsilon}$$

was therefore assumed for the analysis, where $\bar{\sigma}_0$ is the equivalent stress of the cup wall preceding the splaying phase.

According to the hyperbolic theory the maximum splay condition at the cup rim is given by,

$$\frac{d}{dl}(w_s) + \frac{d}{dl}(w_b) = 0 \qquad \text{———} \qquad (9.25.)$$

(a) Specific work of splaying (w_s)

Fundamentally,

$$w_s = \int_0^{\bar{\varepsilon}} \bar{\sigma}\, d\bar{\varepsilon} \qquad \text{———} \qquad (9.26.)$$

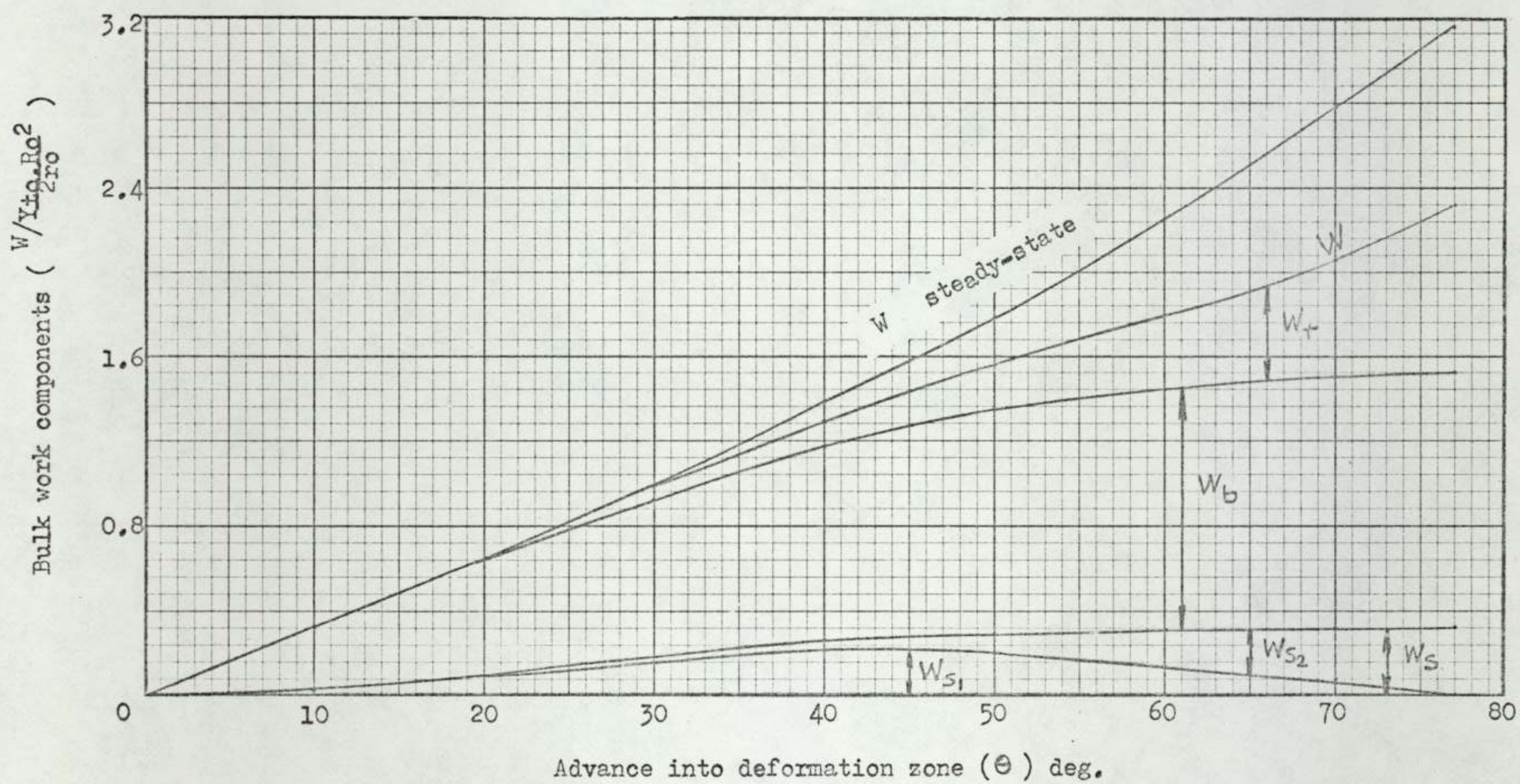

FIG. 155 BULK PLASTIC WORK COMPONENTS DURING SPLAYING PHASE. HYPERBOLIC THEORY.

It was assumed that splaying produces a uniaxial circumferential stress σ_3. Therefore yielding occurs when $\sigma_3 = \bar{\sigma}$, and the strain induced by splaying $\varepsilon_3 = \bar{\varepsilon}$.

$$\text{Now} \quad \varepsilon_3 = \ln \frac{r_s}{r_0} = \ln\left(1 + \frac{S}{r_0}\right) \doteq \frac{S}{r_0}$$

$$\text{Therefore} \quad d\varepsilon_3 = \frac{dS}{r_0}$$

Equation 9.26 may be re-written,

$$w_S = \frac{1}{r_0}\int_0^S \left(\bar{\sigma}_0 + a\frac{S}{r_0}\right) dS$$

Integrating, $$w_S = \frac{S}{r_0}\left(\bar{\sigma}_0 + \frac{aS}{2r_0}\right) \qquad (9.27.)$$

(b) Specific work of bending

Bending was assumed to occur instantaneously at the neutral point between splaying and radial drawing, implying plane strain conditions with $\varepsilon_3 = 0$.

Any splayed element has undergone plastic strain before reaching its neutral point. Strictly this strain should be taken into account when computing $\bar{\sigma}_0'$ immediately before bending. However this is not possible since the degree of splaying is unknown. A similar problem exists when computing the work of unbending at the die, where account should be taken of strain increments induced in previous splaying, bending and radial drawing operations. The present theory ignores these factors and considers bending and unbending work equal.

The longitudinal strain ε_1 induced in an elemental layer δy, distance y from the neutral surface of bending, is given by,

$$\varepsilon = \ln\left(1 + \frac{y}{R}\right) \doteq \frac{y}{R}$$

$$\text{since generally} \quad \frac{y}{R} < \frac{1}{10}$$

Corresponding equivalent strain $\bar{\varepsilon} = \frac{2}{\sqrt{3}} \cdot \frac{y}{R}$. If the elemental length is $(R+y)\,\delta\theta$, and the circumferential width unity, work of bending is,

$$\delta W_b = \bar{\sigma}.\delta\bar{\varepsilon}(R+y).\delta\theta.\delta y$$
$$= \left(\bar{\sigma}_0 + \frac{2}{\sqrt{3}}\cdot\frac{y}{R}.a\right)\frac{2}{\sqrt{3}}\cdot\frac{y}{R}(R+y)\,\delta\theta.\delta y$$

Bending work for the whole cup wall is therefore

$$W_b = \frac{4}{\sqrt{3}}\cdot\frac{\delta\theta}{R}\int_0^{\frac{t_0}{2}}\left[\bar{\sigma}_0(R.y+y^2)+\frac{2}{\sqrt{3}}\cdot\frac{a}{R}(R.y^2+y^3)\right]dy$$

Integrating,

$$W_b = \frac{t_0^2\,\delta\theta}{2\sqrt{3}}\left[\bar{\sigma}_0\left(1+\frac{1}{3}\cdot\frac{t_0}{R}\right)+\frac{2a}{3\sqrt{3}}\cdot\frac{t_0}{R}\left(1+\frac{3}{8}\cdot\frac{t_0}{R}\right)\right]$$

The specific work of bending $\omega_b = W_b/R.\delta\theta.t_0$ or

$$\omega_b = \frac{1}{2\sqrt{3}}\cdot\frac{t_0}{R}\left[\bar{\sigma}_0\left(1+\frac{1}{3}\cdot\frac{t_0}{R}\right)+\frac{2a}{3\sqrt{3}}\cdot\frac{t_0}{R}\left(1+\frac{3}{8}\cdot\frac{t_0}{R}\right)\right] \quad\text{———}\quad (9.28.)$$

where, from equation 9.11., $R = R_0.\frac{l_0}{l}$

(c) <u>Maximum splaying at the cup rim</u>

Differentiating equation 9.27,

$$\frac{d}{dl}(\omega_s) = \frac{1}{\tau_0}\left(\bar{\sigma}_0 + a\frac{S}{\tau_0}\right)\frac{dS}{dl} \quad\text{———}\quad (9.29.)$$

Differentiating equation 9.28,

$$\frac{d}{dl}(\omega_b) = \frac{1}{2\sqrt{3}}\cdot\frac{t_0}{R_0.l_0}\left[\bar{\sigma}_0\left(1+\frac{2}{3}\frac{t_0.l}{R_0.l_0}\right)+\frac{4a}{3\sqrt{3}}\cdot\frac{t_0.l}{R_0 l_0}\left(1+\frac{9}{16}\cdot\frac{t_0.l}{R_0 l_0}\right)\right] \text{——} (9.30.)$$

Substituting for $\frac{d}{dl}(\omega_s)$, $\frac{d}{dl}(\omega_b)$ in equation 9.25 and putting $l=0$ for the maximum rim splay condition,

$$\left(\frac{dS}{dl}\right)_{l=0} = \frac{-\frac{1}{2\sqrt{3}}\cdot\frac{\tau_0.t_0}{l_0.R_0}}{1+\frac{a}{\bar{\sigma}_0}\cdot\frac{S_0}{\tau_0}} \quad\text{———}\quad (9.31.)$$

Equation 9.31. was solved for S_0 using the procedure developed in section 9.7.(b). Thus,

$$S_o = l_o\left(\frac{\sqrt{1+x^2}-1}{x}\right) \quad \text{where} \quad \left(\frac{dS}{dl}\right)_{l=0} = x$$

FIG. 151 indicates that a reasonable approximation to S_o may be found by putting $\sqrt{1+x^2} = 1+\frac{1}{2}x^2$. Then,

$$S_o = \frac{1}{2} l_o . x$$

$$= \frac{\frac{1}{4}\frac{\tau_o}{\sqrt{3}}.\frac{t_o}{R_o}}{1+\frac{a}{\bar{\sigma}_o}.\frac{S_o}{\tau_o}}$$ (dropping the negative sign in equation 9.31.)

Hence,

$$\Delta S_o = \frac{\frac{1}{\sqrt{3}}.\frac{t_o}{4R_o}}{1+\frac{a}{\bar{\sigma}_o}.\Delta S_o} \qquad (9.32.)$$

Equation 9.32 is a quadratic in ΔS_o and may be solved to give,

$$\Delta S_o = \frac{1}{2}\frac{\bar{\sigma}_o}{a}\left[\sqrt{1+\frac{1}{\sqrt{3}}\frac{t_o.a}{R_o.\bar{\sigma}_o}} - 1\right] \qquad (9.33.)$$

FIG. 156 shows a graphical plot of ΔS_o against the work-hardening parameter $\frac{a}{\bar{\sigma}_o}$. According to theory splaying diminishes as work-hardening rate increases.

9.9. Limitations on splay theories.

According to both tangential and hyperbolic theories maximum rim splay occurs after the plane of steady-state bending has rotated an angle θ towards the die. For tangential splaying $\theta = \tan^{-1} l_o/R_o$ whilst for hyperbolic splaying $\theta \triangleq l_o/R_o$ (Truthfully θ would be less than this.) In either case the situation may arise where the die angle $\alpha < \theta$, and splaying cannot then achieve its maximum value as predicted by equations 9.4 and 9.16. Therefore for constrained redrawing, although die angle does not influence the splaying potential, it nevertheless may interrupt its development. For free redrawing die angle influences the steady-state

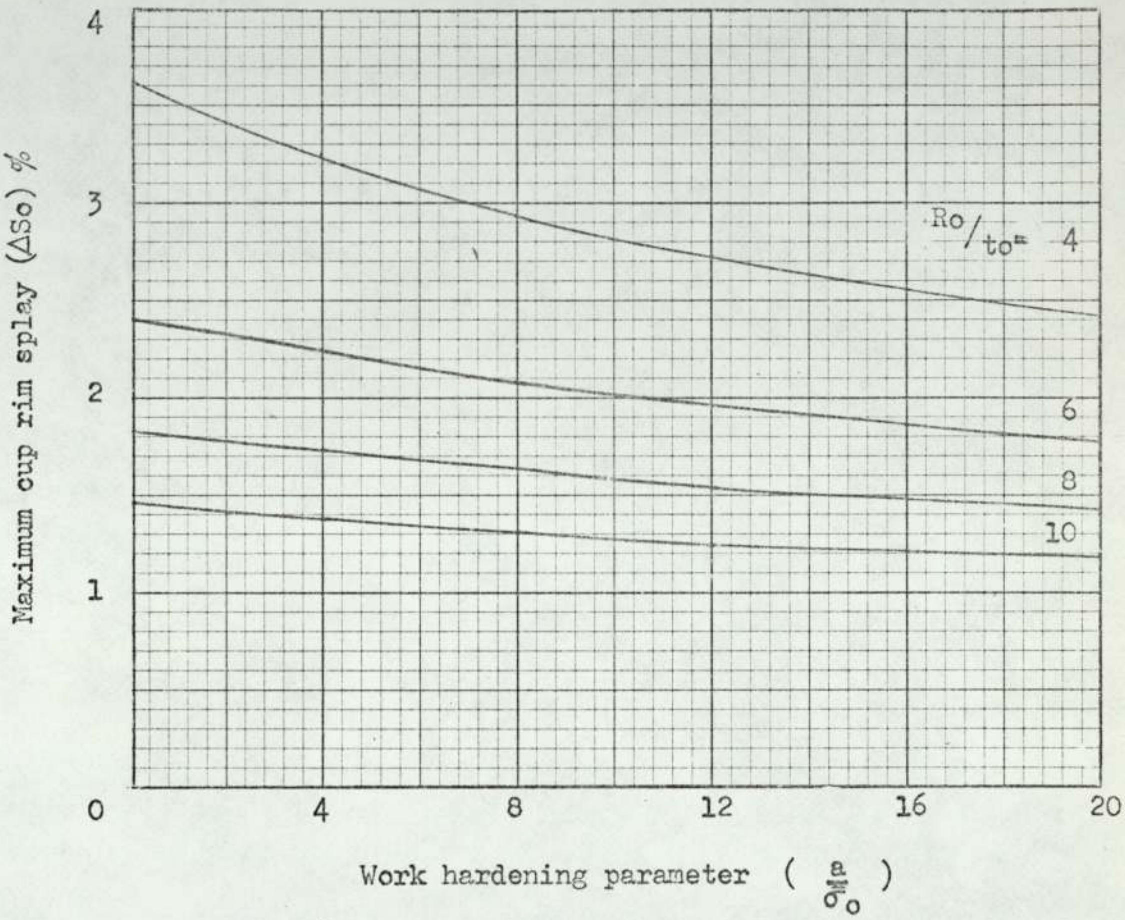

FIG. 156 MAXIMUM SPLAYING AS A FUNCTION OF CURRENT PLASTIC STRESS-STRAIN CHARACTERISTICS.

bending radius R_o and so directly affects the splay potential. It may also restrict the development of splaying. Generally, therefore, splaying will be most severe with wide-angled dies for both constrained and unconstrained (free) redraw configurations.

10. CORRELATION OF THEORY AND SPLAY-MEASUREMENT PROGRAMME RESULTS.

10.1. Fogg's theory of free-zone geometry.

For each basic test in the unconstrained programme the free-zone profile was measured and the best mean radius fitted to the experimental points. Corresponding values of R_f/t_o were computed.

FIG. 157 shows these values plotted on a $t_o/t_o - \alpha$ field. The curved lines were drawn from Fogg's expression,

$$\frac{R_f}{t_o} = \sqrt{\frac{t_o/t_o}{\sqrt{3}(1-\cos\alpha)}}$$

For all materials and states of prior cold-work the theory over-estimated the severity of bending for a given combination of cup geometry t_o/t_o and die geometry α by about 10 - 20 %.

10.2. Maximum splaying at the test-piece rim.

After 50 % prior cold-work the effect of strain hardening over the strain range of splaying was found to be very small for all four materials. This was not true however for the fully annealed test-pieces. Theoretical-experimental correlations were only made for 50 % and 67 % cold-worked test-pieces.

(a) Constrained redrawing.

Results are shown in FIG. 158. The general qualitative relationship between maximum splay ΔS_o and steady-state bending ratio R_o/t_o was correctly predicted by all three theories, but the upper-bound theory over-estimated splaying (as-expected) by almost 100 %. Experimental points fell between the 'tangential' and 'hyperbolic' curves and were closer to the latter. The chain-dotted hyperbolic curve represents the simplified expression for splaying as given by equation 9.16.a.

(b) Unconstrained (free) redrawing.

FIG. 159 shows maximum rim splay ΔS_o versus cup geometry t_o/t_o. The constant die angle curves were constructed from

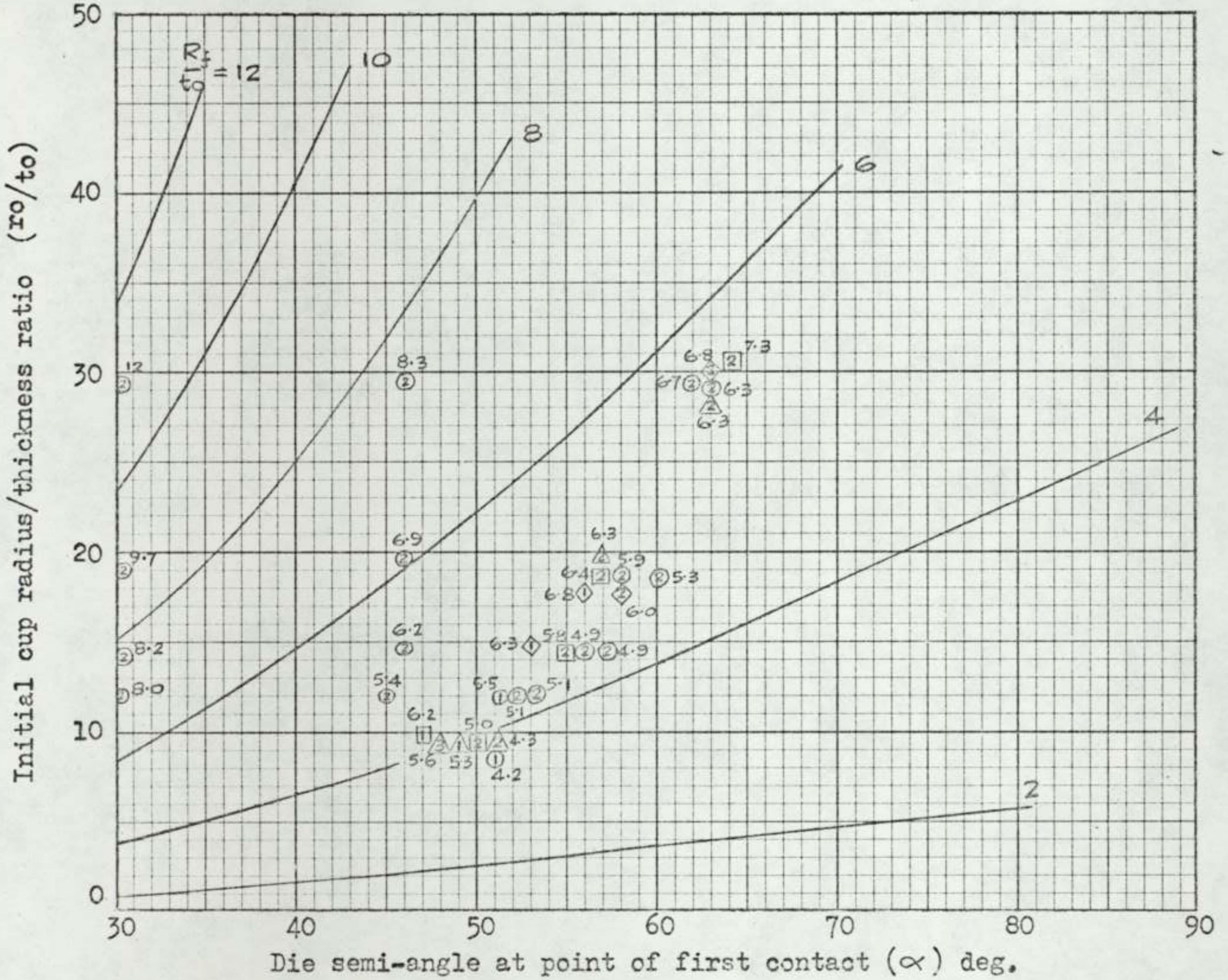

FIG. 157 EXPERIMENTAL CORRELATION WITH FOGG'S THEORY FOR FREE-ZONE GEOMETRY IN UNCONSTRAINED REDRAWING.

Symbol	Material
⊙	Low carbon steel
⊡	70/30 brass
◇	T304 Stainless steel
△	Aluminium

Note 1.

Numbers adjacent to symbols are measured values of (R_f/t_o)

Note 2.

Numbers inside symbols refer to test-piece prior cold-work.

1. - annealed.
2. - 50% cold work.
3. - 67% cold work.

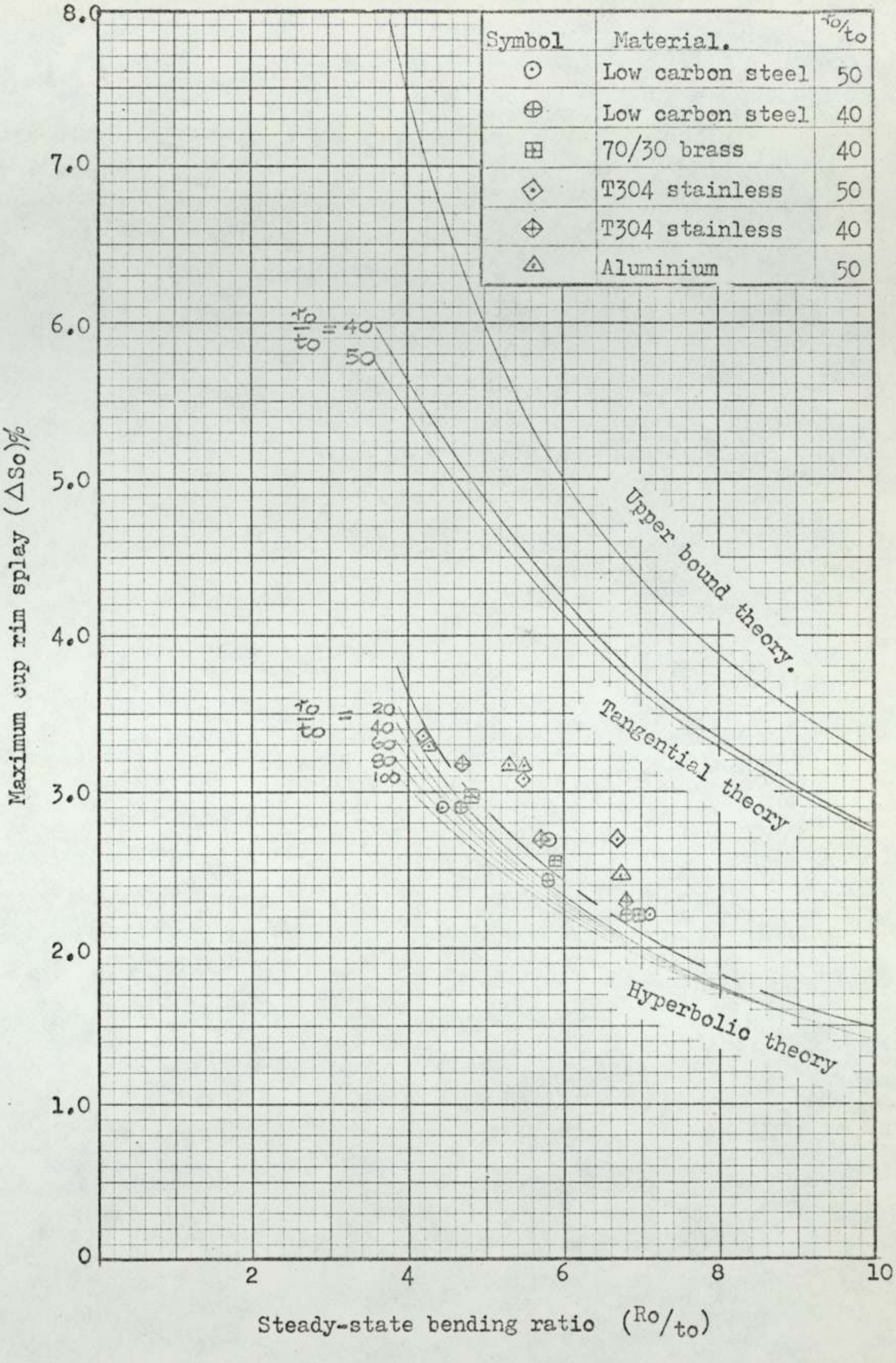

FIG. 158 EXPERIMENTAL/THEORETICAL CORRELATION FOR MAXIMUM SPLAYING. SPLAY-MEASUREMENT TESTS - CONSTRAINED REDRAWING.

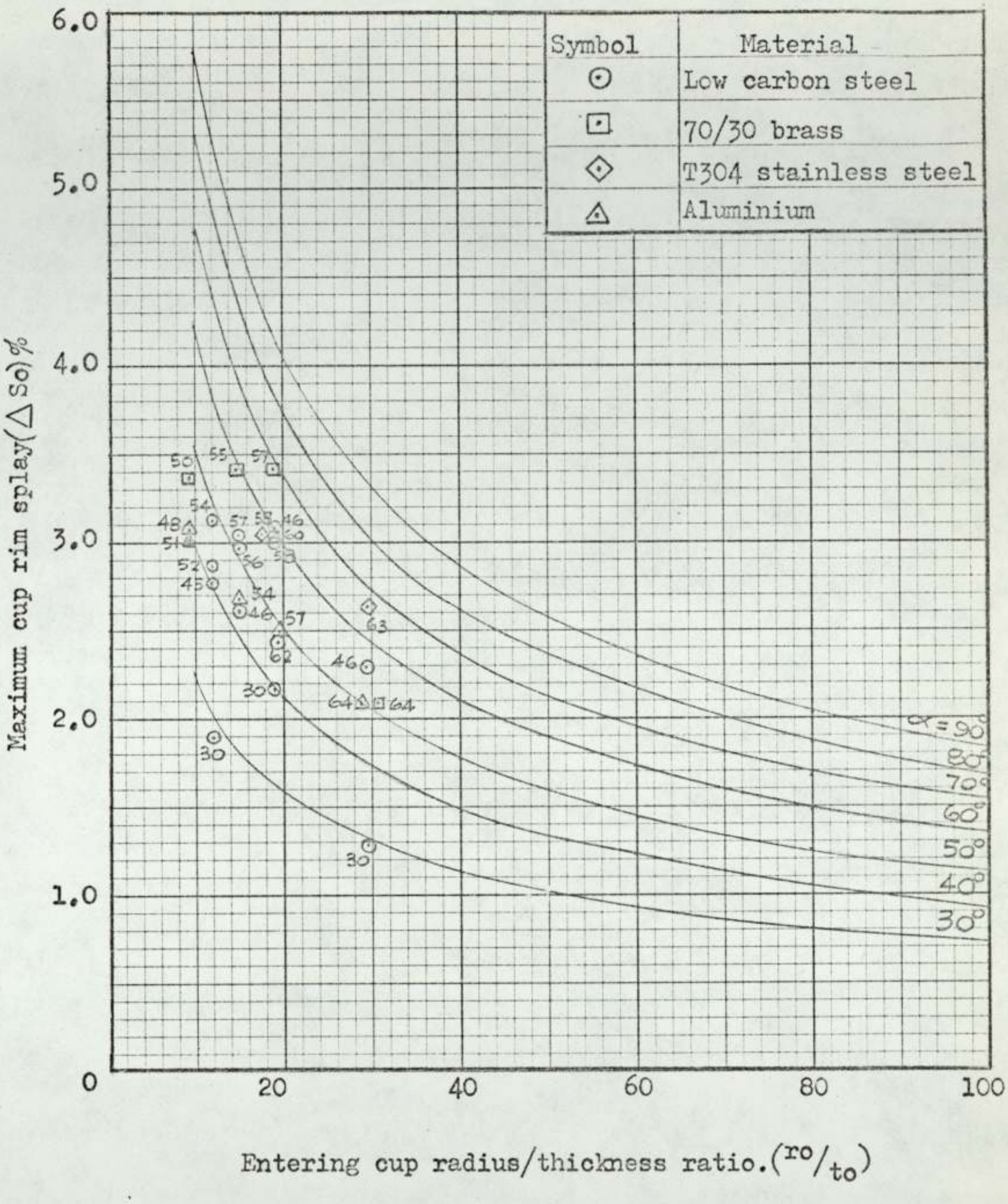

Note - Figures on graph are measured die contact angles.

FIG. 159 EXPERIMENTAL/THEORETICAL CORRELATION FOR MAXIMUM SPLAYING. SPLAY MEASUREMENT TESTS - FREE REDRAWING. (HYPERBOLIC THEORY.)

equation 9.16b. The die-angles included beside experimental points were those at which the test-piece first contacted the die. For the wider angled dies the contact angle did not necessary coincide with the die semi-angle.

Scatter in experimental points was greater than in the constrained programme, but overall theory predicted the level of splaying reasonably well.

10.3. Splay locus of test-piece rim.

Results from test number 20C are replotted in FIG. 160 with the plane of steady-state bending included as a line of reference. The redraw load curve is also included to show the effect of splaying on process work. This particular test was selected because work-hardened aluminium closely approached the theoretical rigid - perfectly plastic material, and also splaying was greatest with the smallest hold-down punch nose radius used.

The graphical scales selected emphasise the difference between the abrupt start of rim splaying predicted by theory and the gradual build-up which actually occurred. Theory ignored elastic splaying.

The relationship between the location of maximum splaying and the plane of steady-state bending is well illustrated.

As generally found in the constrained programme (FIG. 158.), the hyperbolic theory gave closer correlation with experiment than the tangential theory.

10.4. Effect of work-hardening.

Insufficient tests were conducted for a quantitative assessment of experimental trends, but it was found that less splaying occurred in fully annealed test-pieces, particularly with brass and stainless steel. Such a trend was theoretically predicted in terms of rate of work-hardening.

Test number.	20C
Test-piece material.	Aluminium
Prior cold work (nominal)	50%
Test-piece dimensions (in.)	0.750 Ød x 0.0075 th
Die semi-angle (deg.)	90
Hold-down punch radius (in.)	0.030

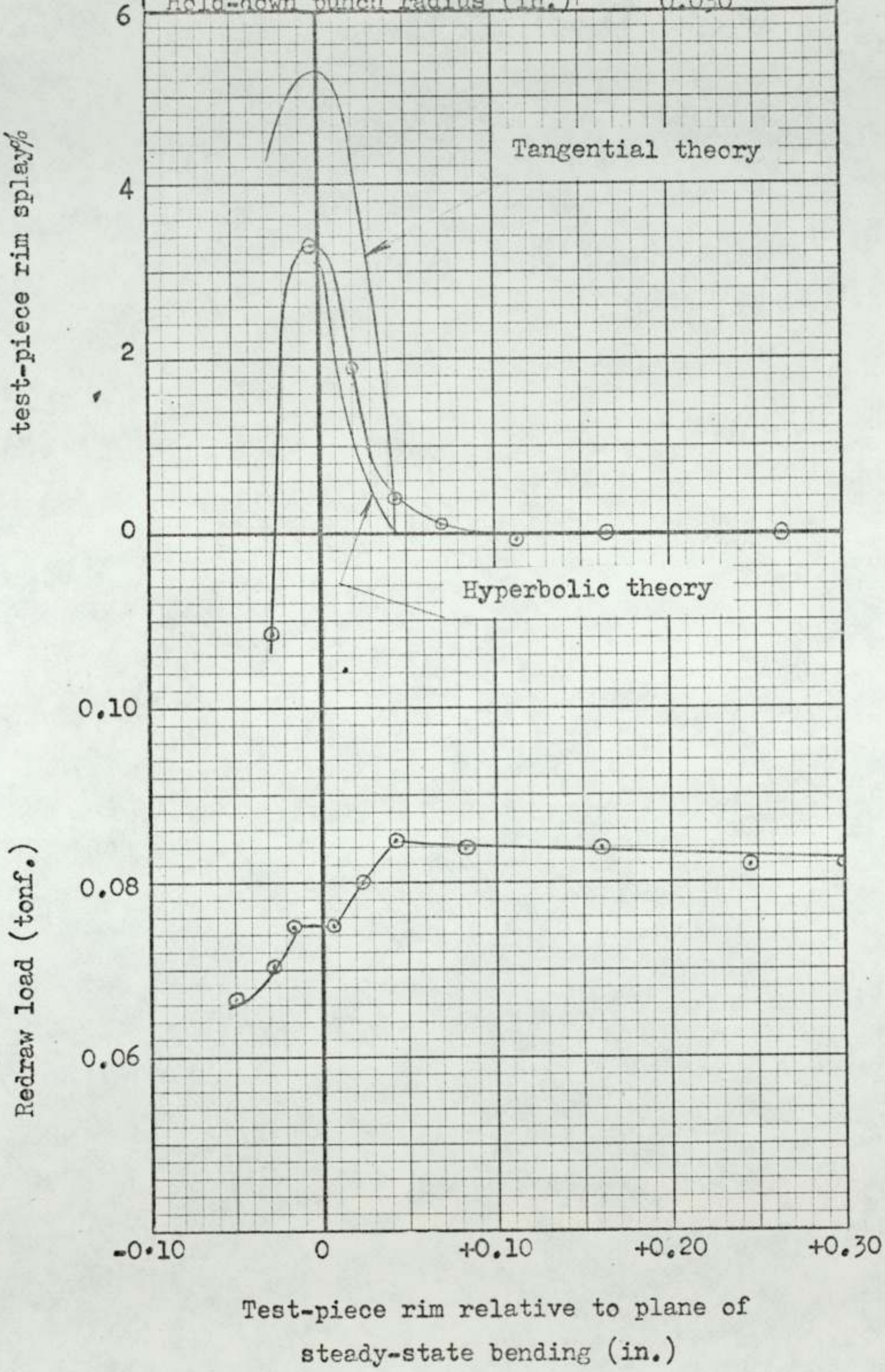

FIG. 160 SPLAY LOCUS OF TEST-PIECE RIM
EXPERIMENTAL/THEORETICAL CORRELATION

11. THIRD EXPERIMENTAL PROGRAMME - PROVING TESTS.

11.1. Introduction.

To complete the experimental programme redraw tests were carried out on cups under conditions similar to those in redrawing at Tube Investments Limited, the object being to verify theories of splaying behaviour.

Cups for redrawing were limited to two sizes, and were taken from a process route comprising four sequential draw stages which had previously been developed within the company for drawing stainless steel and other high work-hardening rate materials. From each cup size one basic redraw reduction was given, and tool geometry varied to observe its effect on splaying and redraw load. For convenience the redraws are here-after referred to as redraw I and redraw 2. Redraw I was given from a second stage cup in the four-draw schedule and was specially designed to achieve certain tool configurations. Redraw 2 was the same reduction as the last stage of the schedule and was selected on the grounds that it had been observed to promote splaying.

Redraw tests were conducted on a 12 Tonf. hydraulic press modified to provide a constant pressure hold-down facility.

11.2. Evaluation of test variables.

(a) Cup material.

Tests were conducted on low carbon steel, 70/30 brass and commercially pure aluminium with a view to comparing results with those from the 'splay-measurement' programme. It was initially intended to include stainless-steel but previously obtained load measurements indicated that press overload problems may have been encountered. Also it was not possible to achieve the reduction of redraw I with as-drawn stainless cups.

(b) Prior cold-work.

Cups for redrawing were produced from annealed sheet stock and were cold-worked by an amount corresponding to the preparatory draw stages. Nominal cold-work in the region of the cup rim, based on pure radial drawing, was 51 % for redraw I and 61 % for redraw 2. For comparison purposes a few cups in steel and aluminium were fully annealed before redrawing.

(c) Cup geometry.

Table 13 gives details of cup sizes before and after proving-test redraws 1 and 2. Cups were produced from 0.036 - 0.037 in. thick blanks. The initial cup wall thickness t_o shown in the table is for the region near the cup rim where it was assumed that thickening in the preparatory draw stages would cause ironing to the die-draw punch radial clearance. Similarly the thickness after redrawing t_e was taken to be that of clearance in the test tools.

Cup length was limited principally by clearance available in the redrawing press. This meant that smaller blanks were used than originally planned for the four-draw schedule. Cups for redraw 1 and 2 measured $2\frac{1}{2}$ and $3\frac{1}{2}$ in. long respectively after manufacture, but for the majority of tests about $\frac{1}{2}$ in. was trimmed from the cup rim to remove ears which would have adversely influenced test readings.

(d) Die geometry.

In its original form in the four-draw schedule redraw 2 used a 90 degree semi-angle die. This angle was retained for the proving tests, but on analysing the redraw geometry it became clear that the actual angle at which the cup first contacted the die was only about 60 degrees, all deformation at the die occurring around the profile radius. To observe the effect of die angle on splaying a die of 45 degree semi-angle was also used for the same reduction.

The geometry of redraw I was designed to provide a true die contact angle approaching 90 degrees, since this was not possible with redraw 2. All tests were carried out using a single die of 90 degrees semi-angle.

A die throat radius six times blank thickness was designated

TABLE 13 - CUP GEOMETRY IN "PROVING" REDRAWS.

REDRAW	2	I
Mean cup radius at entry (r_o) in.	1.271	1.603
Cup thickness at entry (t_o) in.	0.046	0.045
Mean cup radius at exit (r_e) in.	1.042	1.177
Cup thickness at exit (t_e) in.	0.044	0.044
Redraw reduction $(1-\frac{r_e}{r_o})$ percent.	18	26.7

for all dies.

(e) Hold-down punch geometry.

Positive hold-down was used in both redraws to observe the effect of hold-down punch profile radius on splaying. For each of the three cup-die geometry combinations the free-zone radius was calculated using the method outlined in appendix A_3.1 with cup wall thickness as shown in table 13. Two profile radii were then specified for each combination, the first being based on R_f i.e. $R_f - t_0/2$, and the second being 60 - 70 % of this value.

11.3. Test plan.

Steel and aluminium were drawn with redraw 1, and steel and brass with redraw 2. Two basic tests were conducted for each redraw arangement;

(1) Measurement of splaying (at cup rim only.)

(2) Measurement of redraw load.

A guide ring was introduced for some tests on redraw 1 to provide further information about the effect of guiding on redraw load. The test plan is summarised in table 14, where the code letters A, B and G represent separate tests on identical tooling and cups. Most cups were trimmed before redrawing to remove earing from preparatory draw stages since it was thought that the presence of ears would introduce problems in interpreting splay-measurement results and also influence redraw load characteristics during the splaying phase. A few cups were redrawn in the untrimmed state for comparison purposes.

Whilst conducting proving tests it was found that cups could be drawn on redraw 2 with no hold-down without wrinkling, apart from a slight rim puckering at termination of the splaying phase. Therefore it was of interest to compare results from the unconstrained condition with those when redrawing with the largest hold-down punch radius (which was based on Fogg's predicted free-zone radius).

TABLE 14. PROVING TEST PROGRAMME

TEST-PLAN

	Test code	Cup details (before redrawing.)			Tooling details.		
		Material.	Hardness condition	Rim condition	Hold-down punch Ro/to ratio*	Redraw semi-angle (deg.) die	Redraw semi-angle (deg.) actual**
Redraw 1	A.B.G.	steel	as-drawn	trimmed	4.5	90	88.5
	A.B.G.	alum.	as-drawn	trimmed	4.5	90	88.5
	A.B.G.	steel	as-drawn	trimmed	6.0	90	88.2
	A.B.G.	alum.	as-drawn	trimmed	6.0	90	88.2
	A.B.	steel	annealed	trimmed	4.5	90	88.5
	A.B.	alum.	annealed	trimmed	4.5	90	88.5
	A.B.	steel	annealed	trimmed	6.0	90	88.2
	A.B.	alum.	annealed	trimmed	6.0	90	88.2
	A.B.	steel	as-drawn	untrimmed	4.5	90	88.5
	A.B.	alum.	as-drawn	untrimmed	4.5	90	88.5
Redraw 2	A.B.	steel	as-drawn	trimmed	4.5	90	61.2
	A.B.	brass	as-drawn	trimmed	4.5	90	61.2
	A.B.	steel	as-drawn	trimmed	6.1	90	56.1
	A.B.	brass	as-drawn	trimmed	6.1	90	56.1
	A.B.	steel	as-drawn	trimmed	4.5	45	45
	A.B.	brass	as-drawn	trimmed	4.5	45	45
	A.B.	steel	as-drawn	trimmed	7.5	45	45
	A.B.	brass	as-drawn	trimmed	7.5	45	45
	A.B.	steel	as-drawn	untrimmed	4.5	90	61.2
	A.B.	brass	as-drawn	untrimmed	4.5	90	61.2
	A.B.	steel	as-drawn	trimmed	free	90	-
	A.B.	brass	as-drawn	trimmed	free	90	-

A = splay measurement test. B = redraw load-travel test (unguided)

G = redraw load-travel test (guided)

* based on estimated thickness of upper cup wall.

** calculated angle of cup contact with die.

11.4. Methods of data collection.

The proving tests were designed to provide information on maximum rim splaying and its correlation to redraw load, and were not concerned with splay profile development. This aspect was investigated in the 'splay-measurement' programme.

(a) Maximum rim-splay measurement.

A procedure similar to, though less elaborate than that of the 'splay-measurement' programme was followed. The cup was drawn into the die in stages and between each stage, whilst the cup was statically under load, measurements were made of rim diameter and current rim distance from the die.

(b) Redraw load measurement.

A load-cell situated beneath the die measured the combined redraw and hold-down load, whilst a pressure transducer coupled in the hold-down system provide a means of measuring hold-down load separately. Redraw load was taken as the difference between load given by the load-cell and that provided by the pressure transducer.

Redraw load was measured during an un-interrupted test on a cup identical to that used for splay-measurement. Load data was recorded continuously with respect to time on an ultra-violet paper trace. To correlate load with rim splay it was necessary to obtain the former in relation to current rim distance from the die. This was achieved by marking the paper trace at pre-selected positions of the cup rim.

11.5 Test-rig and related instrumentation.

(a) General description.

A Hi-Ton single acting vertical hydraulic press of 12 Tonf capacity was used for the proving tests. The machine had a 14 in. stroke and $18\frac{3}{4}$ in. clearance between the work table and ram, with the latter fully retracted. FIG. 161 shows the press before test-rig installation.

The test-rig was designed to fulfil two functions, to

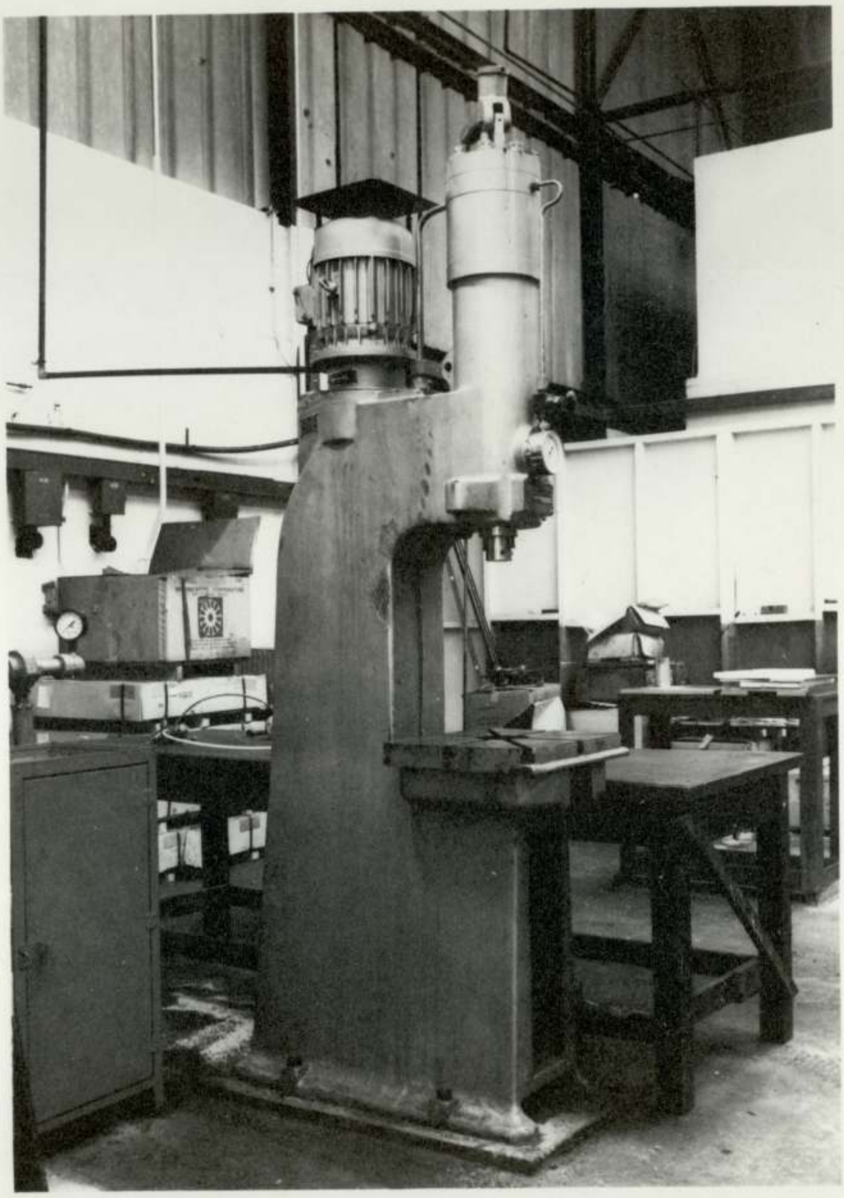

FIG. 161 GENERAL VIEW OF HI-TON PRESS BEFORE INSTALLATION OF PROVING TEST-RIG.

transmit the press ram force to the redraw punch, and to supply an adjustable force to the static hold-down punch. The unit comprised a combined redraw punch/hold-down punch assembly connected to the press ram, and a die assembly. To take full advantage of available press clearance the die assembly extended below the work table surface. Principal statistics of the test rig were:

Maximum redraw load	-	$6\frac{1}{2}$ Tonf
Maximum hold-down load	-	$5\frac{1}{2}$ Tonf
Maximum length of entering cup	-	$3\frac{1}{2}$ in.
Maximum length of redrawn cup	-	$4\frac{1}{2}$ in.

(b) Details of test-rig design and operation.

The test-rig is described with the aid of FIG. 162.

The press cylinder, mounted in the press frame (1) contained the ram (2). An adaptor (3) was coupled to the ram and carried a piston (4), the lower end of which was attached to the redraw punch (5). The piston was arranged to move within a cylinder (6) , coupled to a secondary hydraulic circuit by a flexible pipe (7). An adaptor (8), secured to the underside of the cylinder, housed the hold-down punch (9). The cylinder was single acting, fluid only being present in the volume below the piston. An end cap (10) mounted at the cylinder top prevented escape of the piston.

With the press ram fully retracted, low pressure fluid acting on the underside of the piston caused the cylinder to assume a position such that adaptor(3) contacted the end cap. This corresponded to the retracted position of the test-rig with the nose of the redraw punch (5) then being located about $\frac{1}{4}$ in. inside the hold-down punch (9) , the latter being well clear of the die (11) to enable feeding of a cup (12). When the press ram was advanced redraw and hold-down punches moved forward in unison, the latter entering the cup and continuing to move forwards until reaching the die. At this point, resistance to motion of the press ram was exerted by a pressure developed

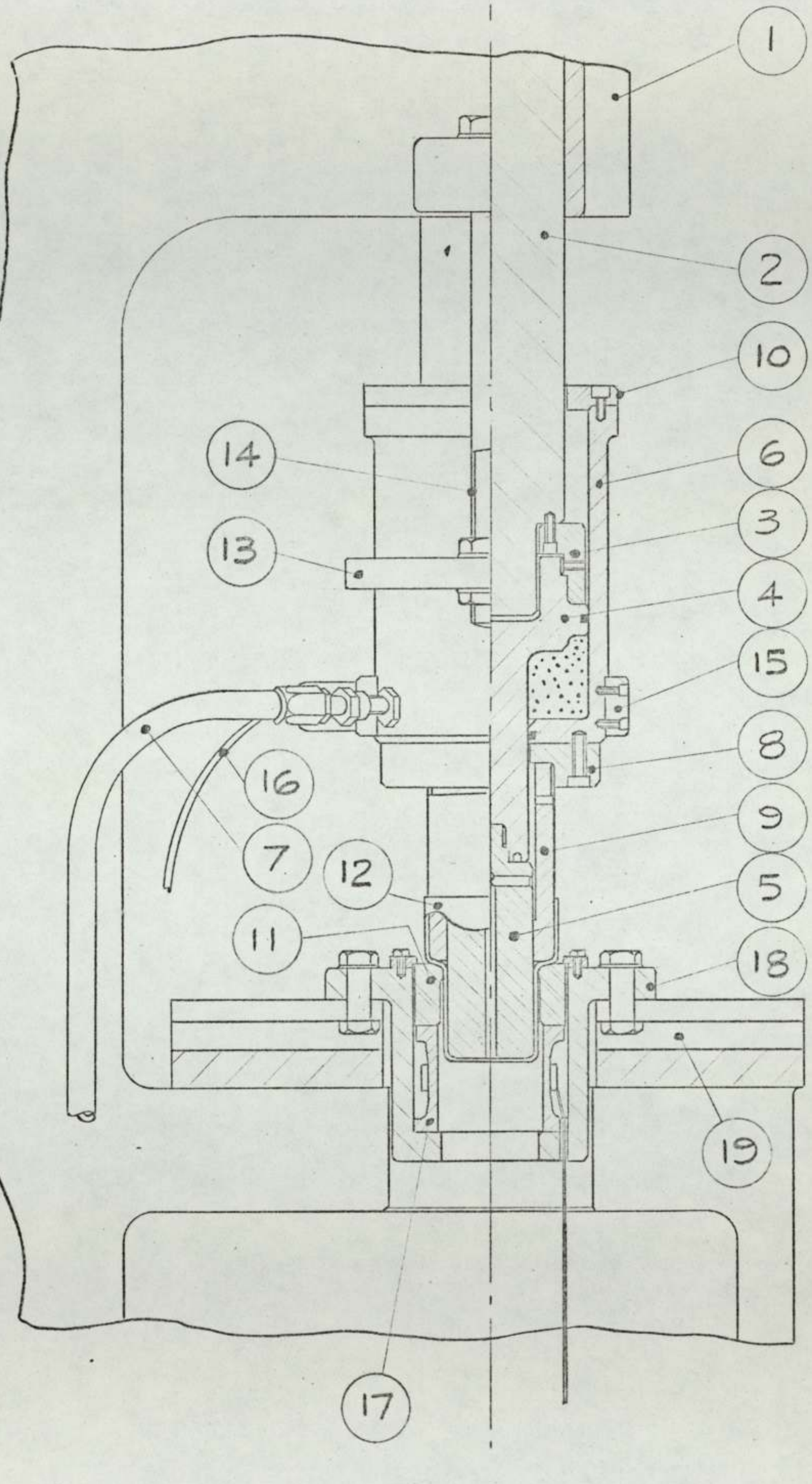

FIG. 162. DETAILS OF TEST-RIG FOR PROVING TESTS.
($\frac{1}{4}$ full size.)

in the cylinder (6). (The pressure could be regulated by a relief valve in the secondary hydraulic circuit and set to provide optimum hold-down force.). Load on the press ram then built up, overcame the hydraulic force in cylinder (6), and with the latter applying a steady hold-down force to the cup, the redraw punch advanced and completed the redrawing operation.

A plate (13.) carried on two arms (14) was mounted around the cylinder (6). The plate acted primarily as a guide for the cylinder, preventing any rotation, but could also be used as a stop to prematurely arrest the hold-down punch in the event of hold-down being unnecessary. Two striker blocks (15) attached to the cylinder were safety features, and precluded any possibility of the hydraulic connection (7) or a pressure transducer (16) being fouled by plate (13) when the press retracted. The arms (14) could slide freely upwards in bosses on the press frame.

The redraw die (11) was mounted above a load-cell (17), both being contained in a housing (18) secured to the press work-table (19). Die and load-cell were designed so that elastic hoop expansion under load would not cause interference with the housing bore.

FIG. 162 shows the arrangement for unguided redrawing. The die retaining plate (situated above the die) could be replaced by a guide-ring for guided redraw tests.

(c) Test-rig hydraulic circuit.

The circuit is shown schematically in FIG. 163. During the forward stroke of the press, fluid was displaced from the cylinder, and returned to a reservoir via an adjustable pressure relief valve set to give optimum hold-down force. When the press retracted, air pressure in the reservoir caused fluid to flow back into the cylinder via a non-return valve. A pressure gauge connected between cylinder and relief valve registered hold-down pressure, and was used for setting-up purposes. During a redraw test cylinder pressure was

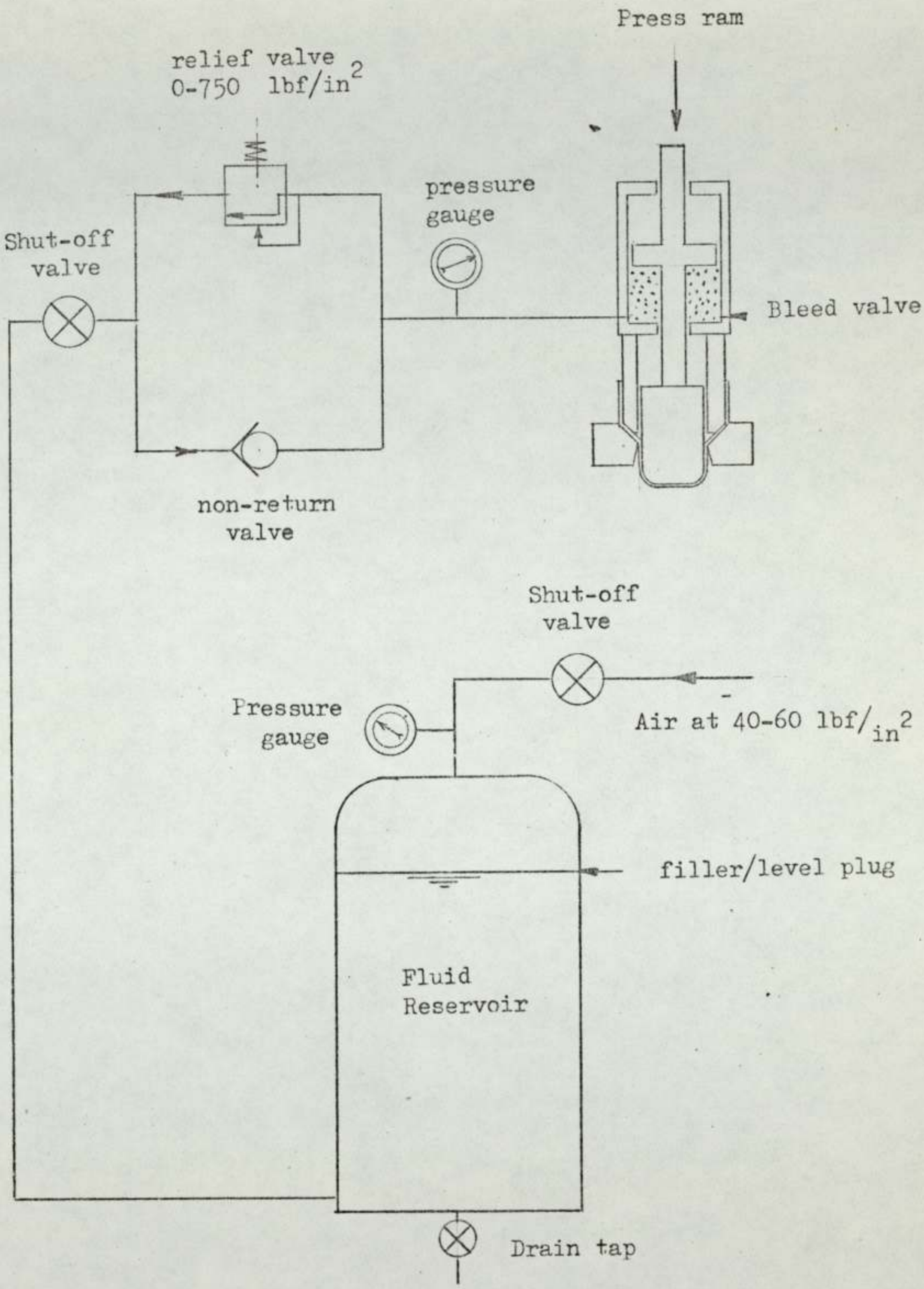

FIG. 163 HYDRAULIC SCHEMATIC FOR TEST-RIG.

monitored continuously by a transducer.

FIG. 164 illustrates the test-rig and hydraulic circuit whilst FIG. 165 shows redraw 2 with the redrawing punch extended. This photograph was obtained by preventing fluid from flowing back into the cylinder when the press was retracted.

(d) <u>Instrumentation.</u>

(i) <u>Load-cell construction details.</u>

The load-cell was designed in alloy steel for an elastic strain of 0.05 % at a compressive load of 12 Tonf. This information enabled the cross sectional area of the body in the region of strain-gauge attachment to be calculated. The bore of the load cell was dictated by the need to be in clearance with redrawn cups. FIG. 166 gives details of the load-cell body. End flanges, ground flat and square to the axis, ensured that the load-cell experienced the full die load during redrawing. Pins screwed into the lower flange were used to secure the load-cell to the die housing.

Four foil-type Tinsley SGD 12/2/CN/E linear electric resistance strain gauges, each of 250 $\pm$ 0.2 % resistance, were bonded to the centrally located gauge area and were wired to form a full Wheatstone bridge with one gauge in each arm of the circuit. The gauges were symmetrically positioned around the circumference with adjacent gauges mounted parallel and normal to the load-cell axis.

Input to the bridge was via an S.E. type 511/S oscillator operating at 5 V - 3 Kc/s. After passing through a carrier amplifier type S.E. 423/1 the bridge output was fed to the galvanometer of a type S.E. 2005 ultra-violet paper-tape recorder.

The procedure used in attaching and wiring strain-gauges was similar to that for the load-cell described in appendix A_2.4.

After wiring, the load-cell was permanently secured in the die housing, and terminal wires taken from the gauge area through a slot in the lower load-cell flange and an aligned hole in the die

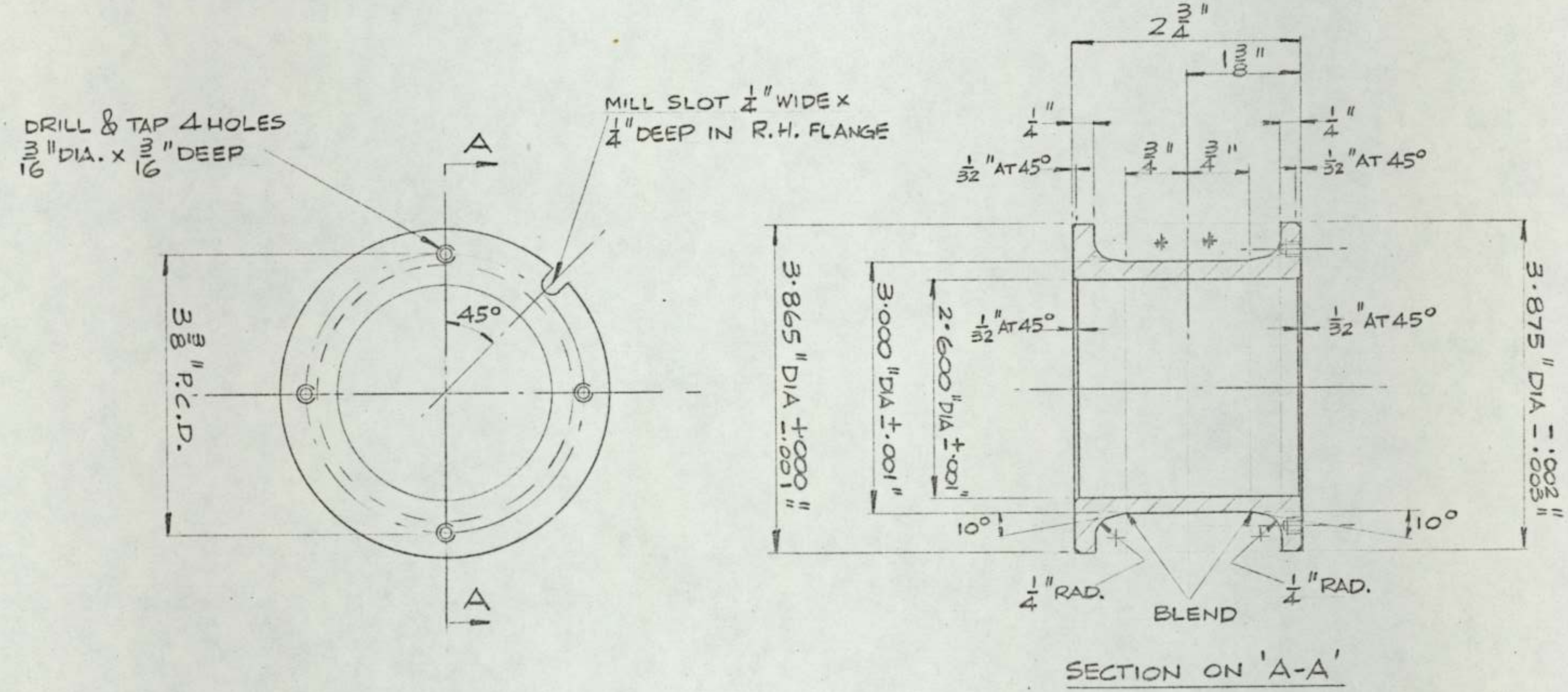

SCALE : 1/2 FULL SIZE

** GRIND OVER THIS LENGTH

MATERIAL : VIBRAC 30

HEAT TREAT TO 50 TONF/IN^2 U.T.S.

FIG. 166. DETAILS OF DIE LOAD-CELL FOR PROVING TESTS.

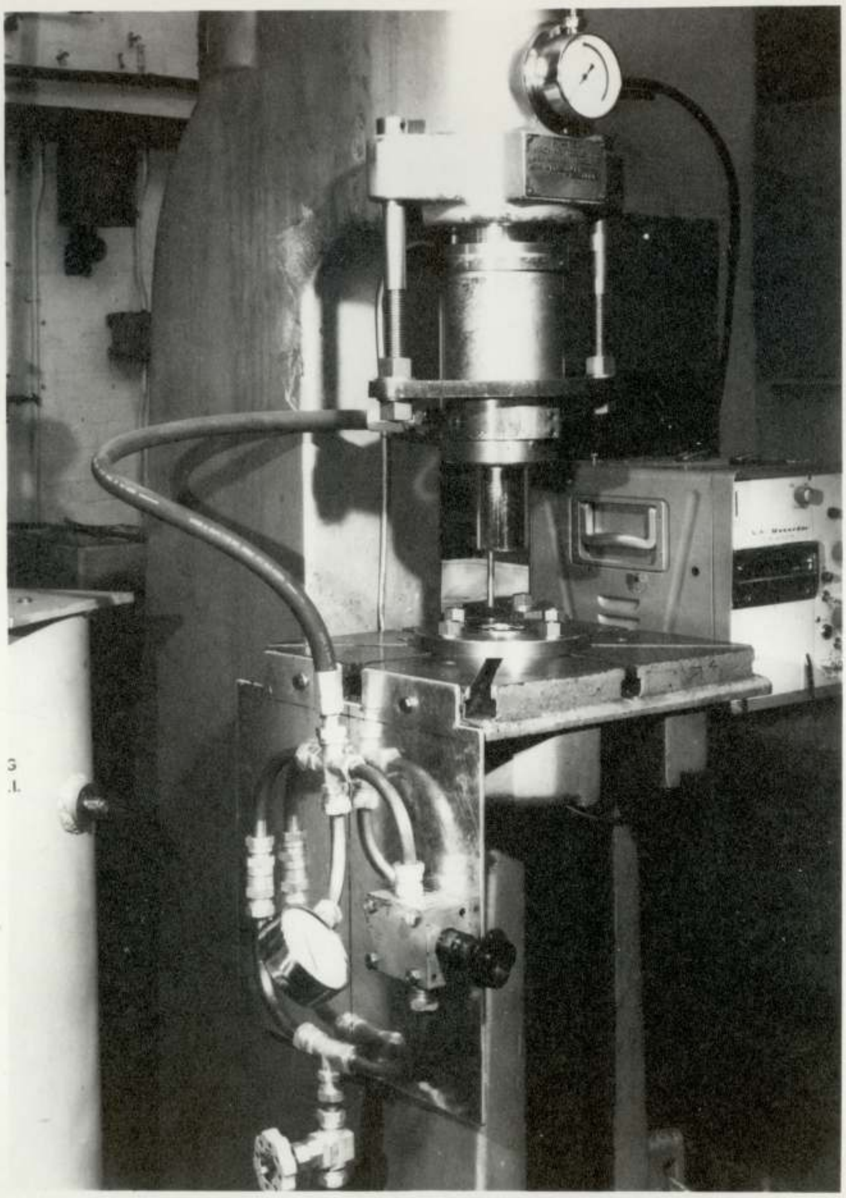

FIG. 164 PROVING TEST-RIG WITH HYDRAULIC CIRCUIT.

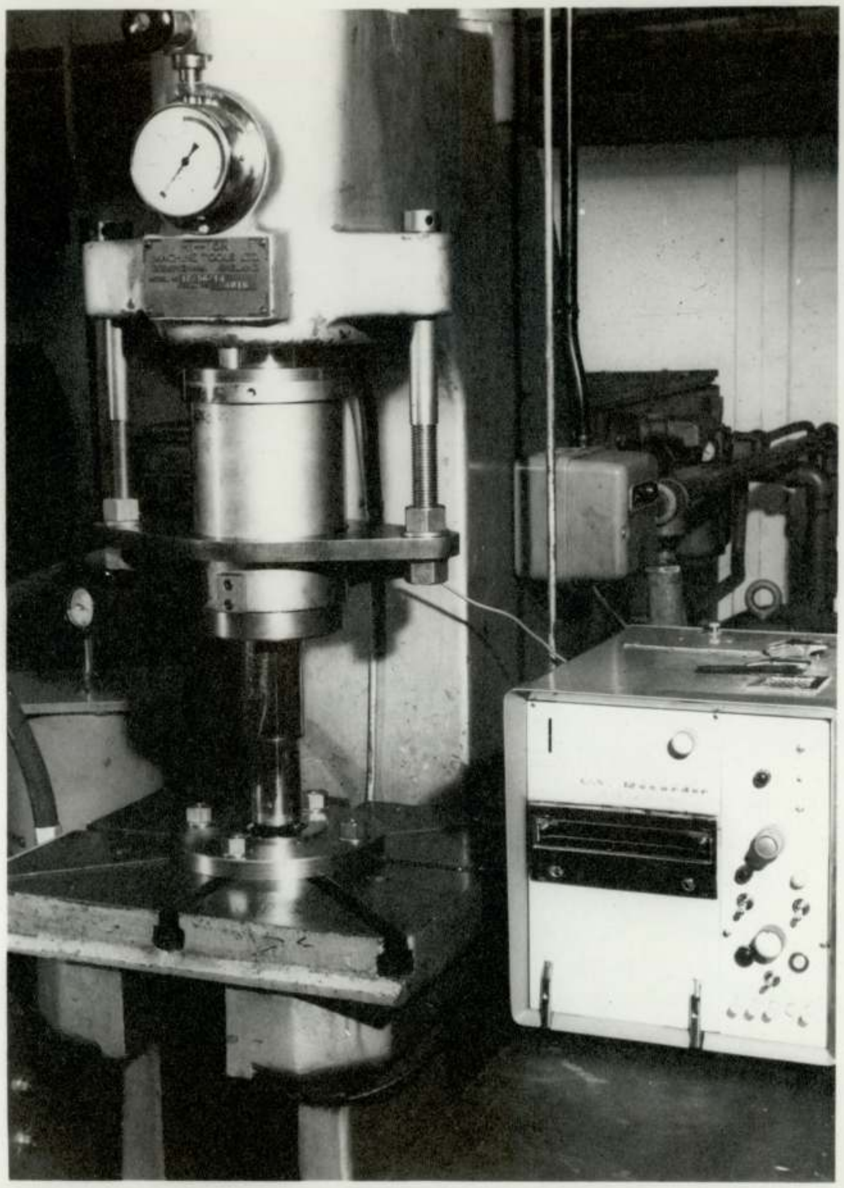

FIG. 165 PROVING TEST-RIG SHOWING REDRAW PUNCH EXTENDED.

housing to an adaptor socket. The final arrangement is shown in FIG. 167.

(ii) Load-cell calibration.

Before installation in the Hi-Ton press the load-cell was calibrated on a regularly inspected 50 Tonf. Denison testing machine. Recalibration was carried out at the end of the programme as a check on any change in load-cell response. No change was detected. Calibration curves for the load-cell are given in FIG. 168.

(iii) Pressure transducer details and calibration.

The transducer was a standard item produced by Intersonde Limited and could be inserted directly into the pressure line. It was used in conjunction with the same recording equipment as the die load-cell.

Transducer details are given below;

Type:	PR 15 - 350
Range:	0 - 10,000 lbf/in^2 (gauge)
Serial number:	611

Calibration was carried out using a Budenburg dead-weight tester serial number 3699. With this instrument an accurately known pressure may be generated in a hydraulic circuit by applying calibrated weights to a piston.

Typical calibration curves are shown in FIG. 169. The 'pressure' curves were obtained from the Budenburg tester, and were converted to hold-down load curves knowing the cross-sectional dimensions of the experimental test-rig cylinder and piston.

(iv) Recording equipment.

Splaying of the cup rim was measured and recorded manually, whilst redraw load information was monitored continuously on S.E. recording equipment which included:

(1) Power supply unit type S.E. 427

(2) Oscillator type S.E. 511/S

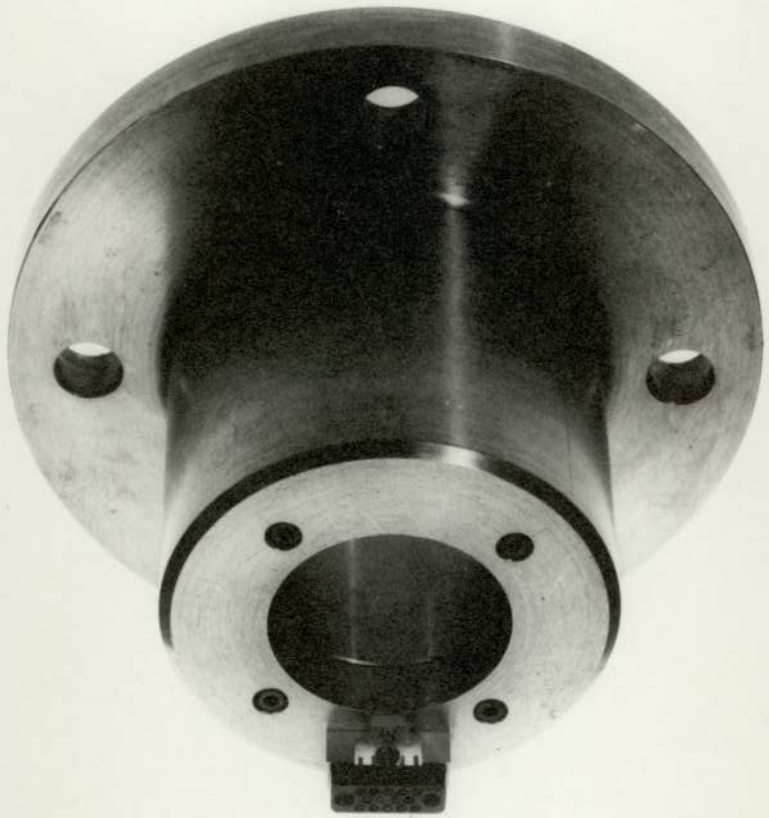

FIG. 167 PROVING TEST DIE HOUSING WITH LOAD-CELL INSERTED.

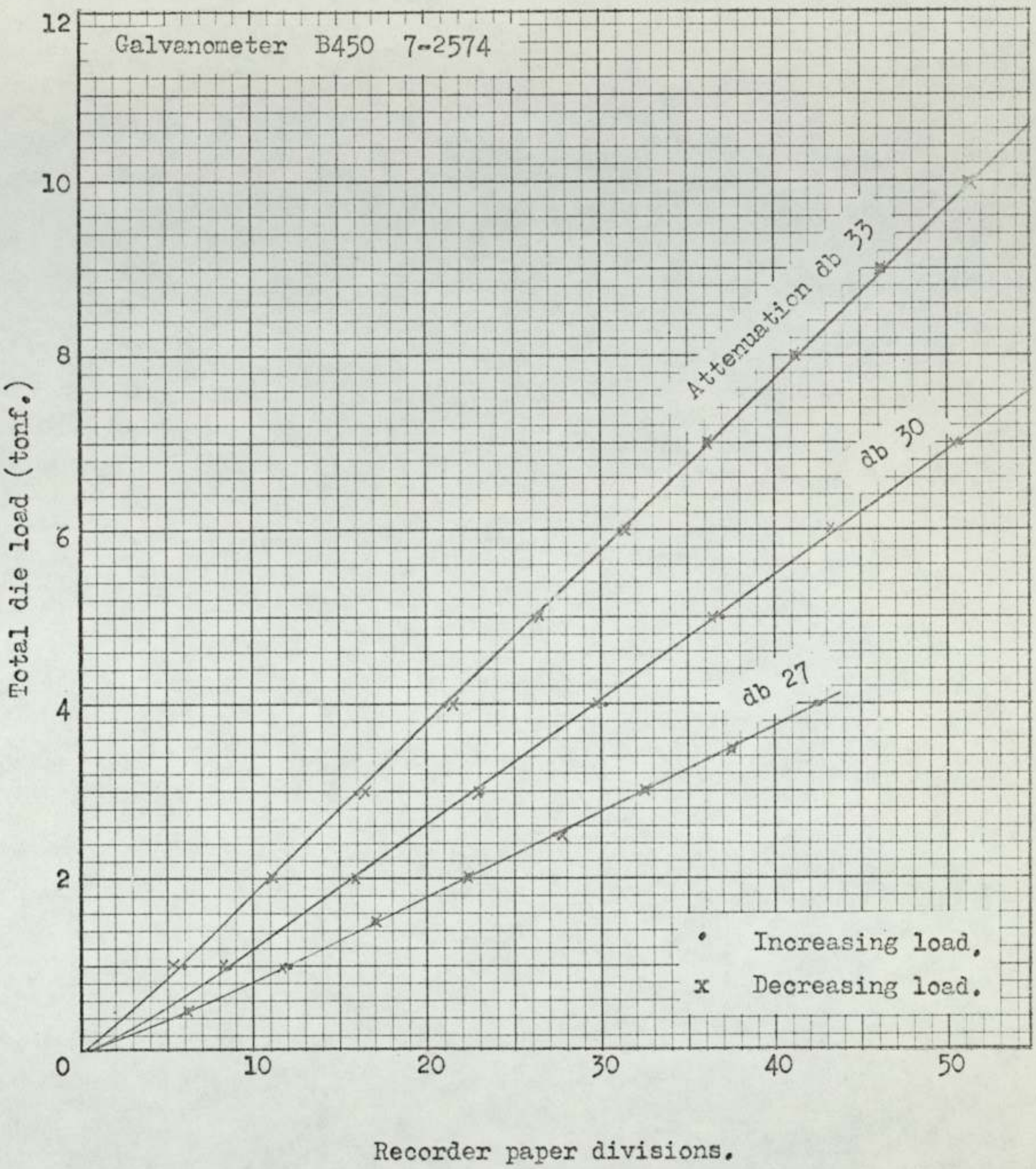

FIG. 168 CALIBRATION CHARACTERISTICS FOR DIE LOAD-CELL USED IN PROVING-TEST PROGRAMME.

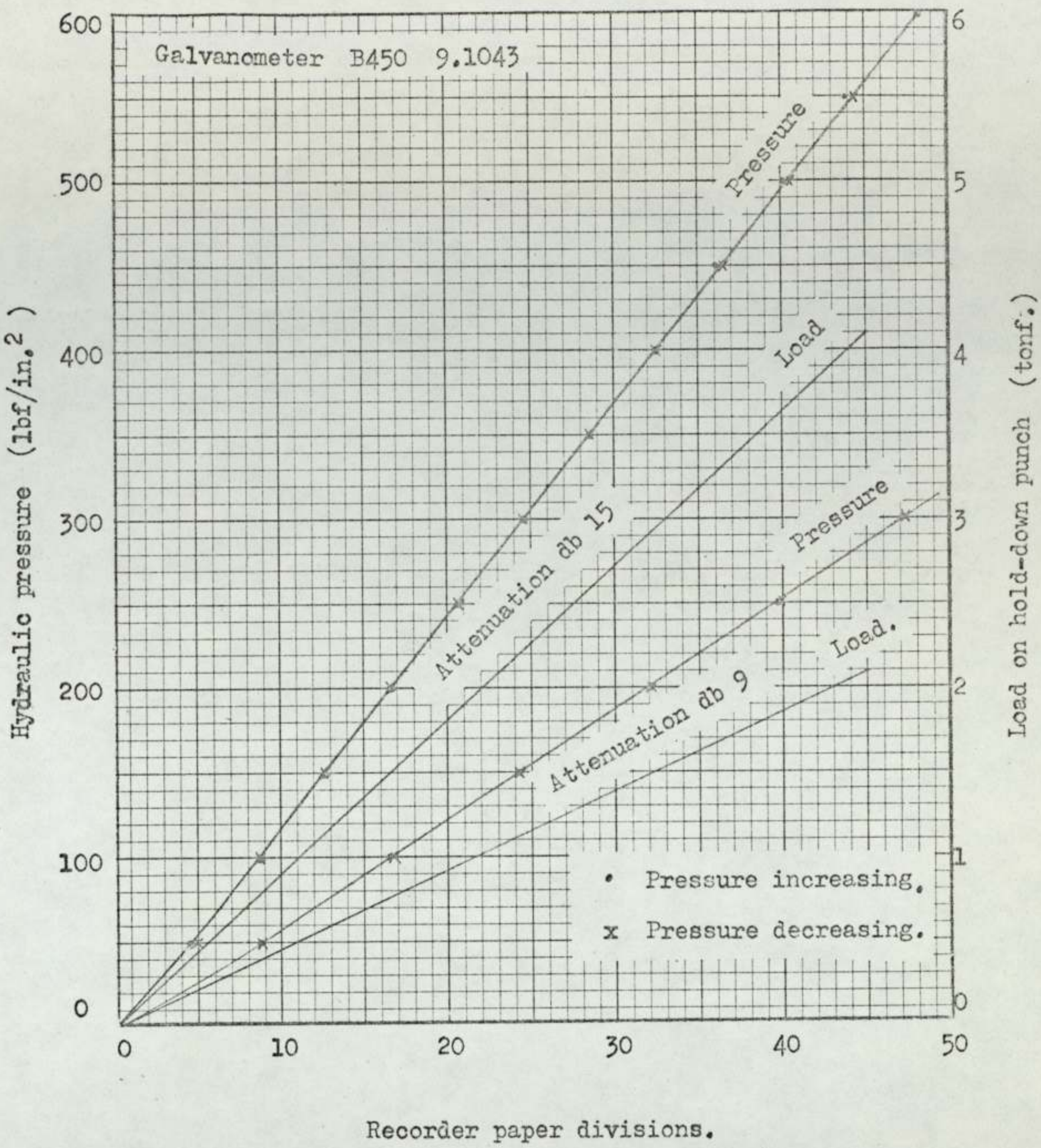

FIG. 169 CALIBRATION CHARACTERISTICS FOR PRESSURE TRANSDUCER.USED IN PROVING - TEST PROGRAMME.

(3) Carrier amplifiers type S.E. 423/1

(4) Ultra-violet paper-tape recorder S.E. 2005 with B 450 galvanometers.

(e) Details of redraw tooling.

Tooling details are provided in FIG. 170 and accompanying table 15.

Hold-down punches were also used in the role of draw punches during the final cup preparatory draw stage, ensuring a close cup fit for the redraw. This was achieved by attaching the hollow punches to specially made adaptors using the internal thread designated D_8. The adaptors fitted existing tooling of the four-draw schedule discussed in section 11.1. Hold-down punches were located in the test-rig with external screw thread D_6. Initially punches were made with the smallest profile radius R, which was later increased according to table 15 during the test programme.

Redraw punches were provided with a small central hole connecting with a vent which allowed air to escape from the cup during feeding, and prevented a vacuum when stripping the cup from the punch after redrawing.

FIG. 171 gives details of the guide ring used in selected tests on redraw I. The guiding section diameter was designed to give 0.005 in. diametral clearance with the thickest cup section. A shallow recess on the underside of the ring located over the redraw die and was in 0.010 in. diametral clearance with the latter. This arrangement enabled the ring to float laterally, thereby only supplying diametral constraint on the splayed cup.

All tools were made from a high quality tool steel and heat treated to 60 Rockwell C. Tools were polished before use to give surface finishes as recorded in table 16.

FIG. 172 is a photograph of the complete proving-test tooling.

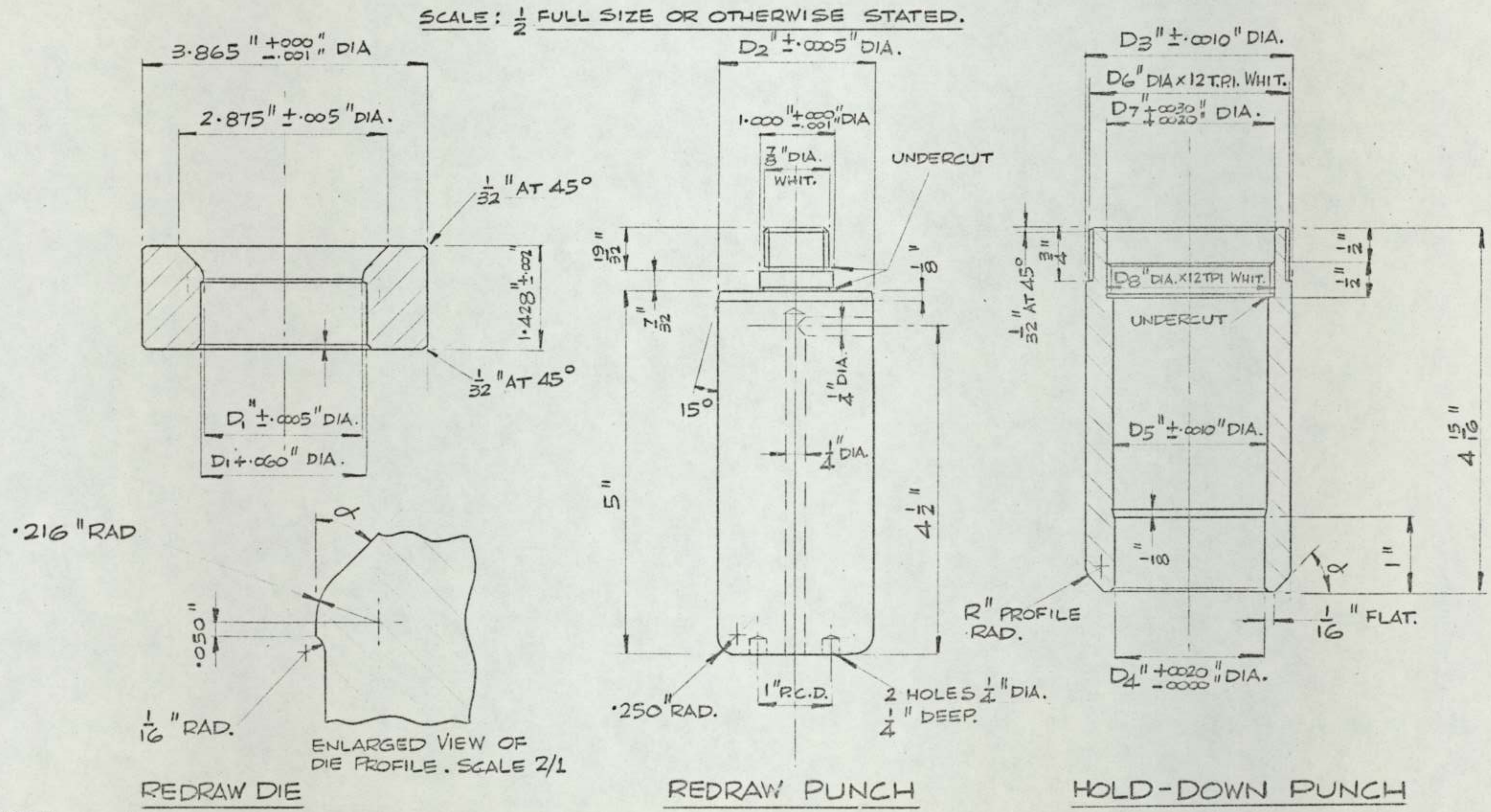

NOTE

1. MATERIAL FOR ALL TOOLING CHROME-MOLYBDENUM-VANADIUM TOOL STEEL HEAT TREATED TO 60 ROCKWELL C.
2. POLISH DIE AND HOLD-DOWN PUNCH PROFILE RADII TO 5 μ" C.L.A.

FIG. 170. DETAILS OF REDRAW TOOLING FOR PROVING-TEST PROGRAMME.

Redraw	Die semi-angle deg.	Hold-down punch profile radius R in.		Diameters (referred to Fig 170) in.							
				D1	D2	D3	D4	D5	D6	D7	D8
1	90	.180	.250	2.398	2.310	3.160	2.313	2.340	3.3/32	2.500	$2\frac{1}{2}$
2	90	.180	.253	2..28	2.040	2.496	2.043	2.063	2.15/32	2.187	2.3/16
2	45	.180	.317	2.128	2.040	2.496	2.043	2.063	2.15/32	2.187	2.3/16

TABLE. 15. PROVING TEST TOOLING DATA.

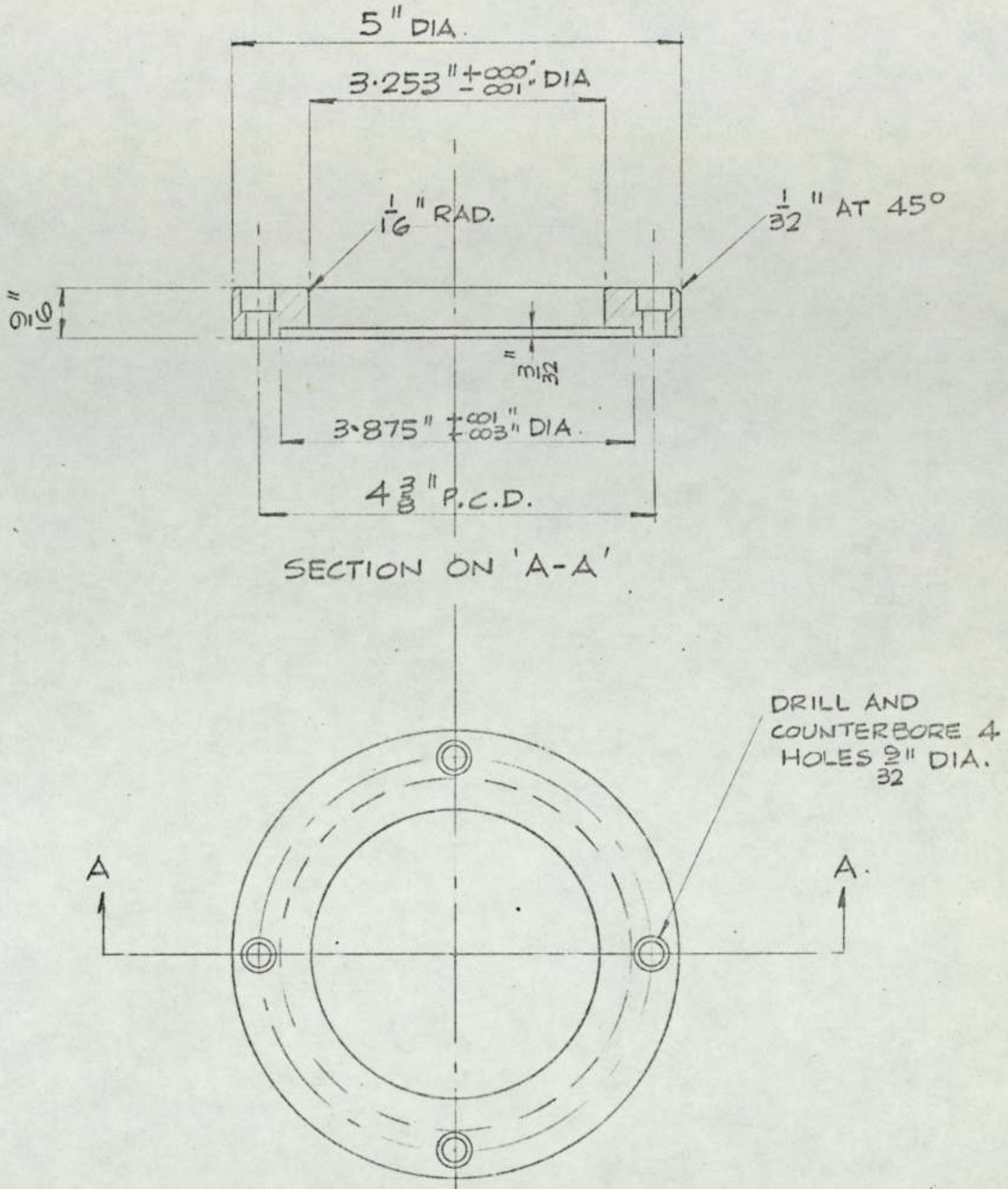

BORE AND BOTTOM FACE TO BE GROUND SQUARE

MATERIAL: CHROME-MOLYBDENUM-VANADIUM TOOL STEEL HEAT-TREATED TO 60 ROCKWELL C.

SCALE: 1/2 FULL SIZE

FIG. 171. DETAILS OF GUIDE RING FOR PROVING-TEST PROGRAMME.

TABLE 16. SURFACE FINISH OF PROVING-TEST PROGRAMME REDRAW TOOLING.

Redraw	Tool	Location of surface-finish reading.	Surface-finish, micro in. C.L.A.
1	90° die	Die mouth: Radial Tangential	½ - 1 ½ - 1
	90° hold-down punch	On full diameter just above nose radius. Parallel to drawing direction	2 - 4
	Redraw punch	On full diameter just above nose radius. Parallel to drawing direction.	1 - 1
	Guide ring.	In bore. Parallel to drawing direction	4 - 6
2	90° die	Die mouth: Radial. Tangential.	2 - 4 ½ - 1
	45° die	Die mouth: Radial	1 - 1
	90° hold-down punch	On full diameter just above nose radius. Parallel to drawing direction.	3 - 3½
	45° hold-down punch.	On full diameter just above nose radius. Parallel to drawing direction.	1 - 2
	Redraw punch.	On full diameter just above nose radius. Parallel to drawing direction.	¾ - 1½

Top left	-	redraw 2 die
Centre left	-	redraw 2 punch
Bottom left	-	redraw 2 hold-down punch
Top right	-	redraw 1 die
Centre right	-	redraw 1 punch
Bottom right	-	redraw 1 hold-down punch
Centre	-	guide ring

FIG. 172 TOOLING FOR PROVING-TEST PROGRAMME.

11.6. Manufacture and preparation of cups for redrawing.

Blanks were sheared $\frac{1}{8}$ in. over-size and lathe machined to 6.500 $\pm$ 0.005 in. diameter using a jig similar to that described by Willis.[7] This procedure gave a clean burr-free edge and removed material work-hardened from shearing. The blanks were then drawn through two and three stages to produce cups for redraws I and 2 respectively. Steel blanks were made from sheet pre-lubricated with a phosphate - stearate treatment and no further lubrication was necessary for preparatory drawing. Brass and aluminium blanks were drawn using a chlorinated mineral oil. All cups were thoroughly degreased after drawing.

The three materials exhibited quite different planar anisotropy or earing characteristics as shown in FIG. 173. Steel showed four pronounced symmetrically distributed ears, whilst the pattern was similar, though far less marked with aluminium. Brass exhibited no noticeable rim undulations.

Before redrawing in the experimental test-rig the majority of cups in each material were trimmed to facilitate splay measurement. Trimming was conducted in a lathe using specially made mandrels, and a plentiful supply of coolant to prevent excessive heating of the cup rim.

Six redraw I cups in steel and aluminium were fully annealed before redrawing for splay comparisons with as-drawn cups.

Aluminium and brass cups were chemically etched before lubricating for redrawing. Cups in all three materials were then lubricated in a textile soap at 60 - 70°C and allowed to air-dry at room temperature. Details of etching and lubricating procedures are given in appendix A_4.1.

Measurements of cup diameter and wall thickness in the rim vicinity were taken for subsequent experimental-theoretical splay correlations. The information is recorded in table A_4.1.

Top left	-	low carbon steel redraw 1
Top right	-	aluminium redraw 1
Bottom left	-	low carbon steel redraw 2
Bottom right	-	70/30 brass redraw 2

FIG. 173 AS-DRAWN UNTRIMMED CUPS PRIOR TO REDRAWING.

11.7. Experimental techniques.

Exploratory tests were carried out to determine suitable hold-down forces for each redraw configuration. A pressure of 200 lbf/in.^{2} in the hold-down cylinder gave satisfactory results in all cases. This pressure was set at the hold-down circuit relief valve and maintained throughout the test programme.

Forward motion of the press ram was controlled by a single two-position (open-shut) valve mounted above the press cylinder and operated by a foot pedal. With the press idling the valve was open, allowing hydraulic fluid to circulate freely from pump to reservoir. When the valve was closed, load developed under the ram depended upon the setting of an adjustable relief valve. This control system was therefore one of load rather than speed and proved to be a source of difficulty throughout the experimental programme. The best method of achieving reasonable speed control was as follows; with the relief valve fully open a cup was located on the hold-down punch, and the flow control valve fully closed to bring the punch assembly into contact with the die, where insufficient ram force was available to initiate drawing. The linkage connecting foot pedal and control valve actuator was now locked by a clamp, maintaining the valve closed. The relief valve was then gradually closed until drawing took place at about 6 in/min.

On completion of drawing cups were stripped from the redraw punch by a lip below the die throat . (FIG. 170.)

(a) Splay-measurement.

(1) When the cup rim was 2 in. above the die, drawing was interrupted by slightly opening the press flow control valve to produce a ram load just less than that necessary for drawing. Measurements of cup rim diameter were then made with a micrometer at three angular positions mutually 60 degrees apart.

(2) Using a procedure similar to (1) above, the cup was drawn into the die in stages with the rim consecutively 1, 1/2, 7/16,

3/8, 5/16, 1/4, 3/16, 1/8, 1/16 in. above the die. At each stage rim diameter was measured.

Variations to procedure.

When using the 45 degree die splaying continued within the die mouth. To measure this splaying the punch assembly was partially retracted and the cup rim lifted clear of the die. Thus measurements were made under zero load conditions.

Splay measurement on untrimmed (eared) cups was basically as described for trimmed cups, but diameters and distances from the die were measured both at the roots and crests of ears.

(b) Redraw-load measurement.

(1) Air supply to the hold-down circuit was cut-off and pressure in the hold-down cylinder reduced to zero by means of a bleed vent. The recording equipment was switched on and the pressure transducer set to a datum. The hold-down circuit was then returned to working order.

(2) The load-cell was adjusted for gain and datum settings and the recorder switched on.

(3) Using the procedure for approximate speed control the cup was redrawn without interruption. When its rim reached pre-selected distances from the die (as used for splay-measurement) event marks were made on the recorder paper trace.

11.8. Methods of test data interpretation.

(a) Splay-measurement test.

For each cup rim position the three diameter measurements were averaged to give a mean. Fractional splay was determined taking the initial readings of diameter at the 2 in. rim position as a datum. (It was known that splaying did not commence until the rim was about $\frac{1}{2}$ in. from the die.)

(b) Redraw load/cup rim displacement tests.

At each event mark made on the recorder trace output signals from load-cell and pressure transducer were measured and converted to total die load and hold-down load respectively using the calibration curves. Redraw load was computed as the difference between die and hold-down loads. The cup rim position coinciding with any additional point of interest on the recorder trace was found by interpolation.

(c) Combined splay - redraw load-rim displacement data.

Both splay and redraw load tests were conducted on identical cups and had current cup rim position as a common reference. Graphical results were therefore combined to show not only the development of splaying but also its effect upon redraw load.

11.9. Experimental results.

(a) General comments.

Throughout the programme lubrication appeared good. No pick-up or scoring of the tools occurred and redrawn cups were free from wrinkling. As anticipated there were indications of ironing in the upper regions of final cups. FIG. 174 illustrates typical cups before and after the two redraws.

No cups failed due to splaying in any of the tool and material combinations investigated.

A number of cups fractured in redrawing, details of which are given below.

Table 17 is an index to the proving-test programme. For each basic test number designation, e.g. 1CP, at least two separate tests were conducted, splay-measurement and unguided redraw-load measurement. Additionally a few load measurement tests were carried out on redraw I with a guide ring installed. Splay measurement tests were identified with the suffix (A), whilst unguided and guided load tests were given the suffix (B) and (G) respectively. The actual test-plan is given in table 14.

(b) Special comments.

(1) When conducting tests 2P it was found that cups were

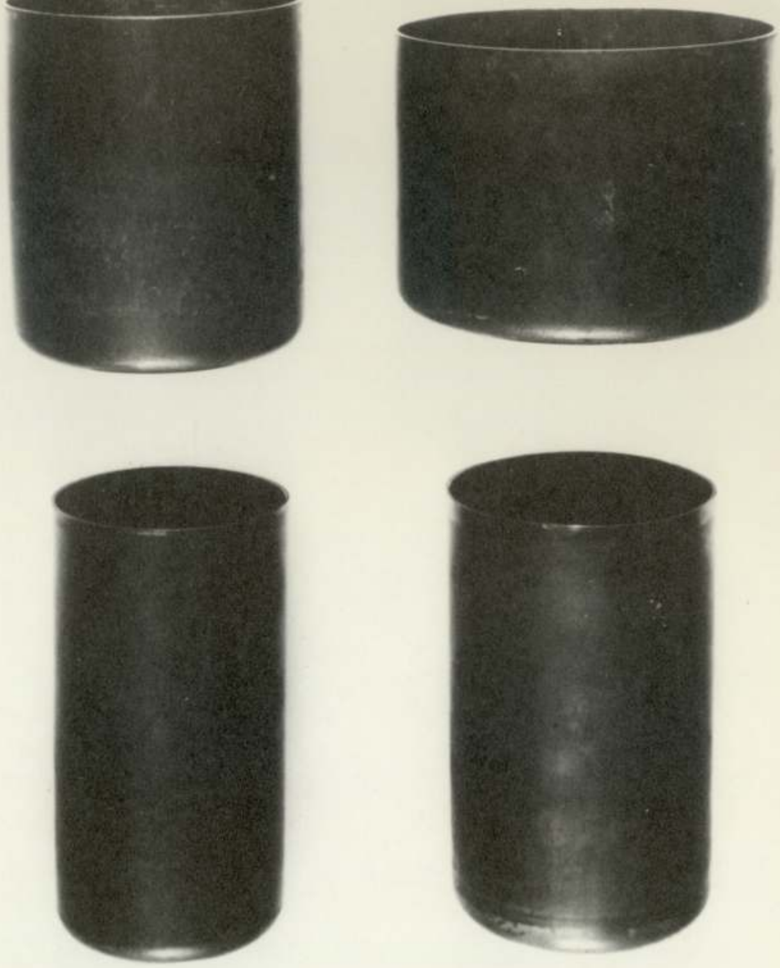

left - redraw 2
top - before redrawing
bottom - after redrawing

right - redraw 1
top - before redrawing
bottom - after redrawing

FIG. 174 CUPS BEFORE AND AFTER EACH OF TWO PROVING-TEST REDRAWS.

TABLE- 17

INDEX TO PROVING TESTS.

Test number	Test material	Cup condition	Nominal cup dimensions (in.)		Die Semi-angle (deg.)	Hold-down Punch nose radius (in.)
			O/Dia	Wall Thk.		
1P	steel	as-drawn/ trimmed.	3.250	0.036	90	0.180
2P	aluminium	as-drawn/ trimmed.	3.250	0.036	90	0.180
3P	steel	as-drawn/ trimmed.	3.250	0.036	90	0.250
4P	aluminium	as-drawn/ trimmed.	3.250	0.036	90	0.250
5P	steel	annealed/ trimmed	3.250	0.036	90	0.180
6P	aluminium	annealed/ trimmed.	3.250	0.036	90	0.180
7P	steel	annealed/ trimmed.	3.250	0.036	90	0.250
8P	aluminium	annealed/ trimmed.	3.250	0.036	90	0.250
9P	steel	as-drawn/ untrimmed.	3.250	0.036	90	0.180
10P	aluminium	as-drawn/ untrimmed.	3.250	0.036	90	0.180
11P	steel	as-drawn/ trimmed.	2.587	0.036	90	0.180
12P	brass	as-drawn/ trimmed.	2.587	0.036	90	0.180
13P	steel	as-drawn/ trimmed	2.587	0.036	90	0.253
14P	brass	as-drawn/ trimmed.	2.587	0.036	90	0.253
15P	steel	as-drawn/ trimmed.	2.587	0.036	45	0.180
16P	brass	as-drawn/ trimmed.	2.587	0.036	45	0.180
17P	steel	as-drawn/ trimmed.	2.587	0.036	45	0.317
18P	brass	as-drawn/ trimmed.	2.587	0.036	45	0.317
19P	steel	as-drawn/ untrimmed.	2.587	0.036	90	0.180
20P	brass	as-drawn/ untrimmed.	2.587	0.036	90	0.180
21P	steel	as-drawn/ trimmed.	2.587	0.036	90	free
22P	brass	as-drawn/ trimmed.	2.587	0.036	90	free

drawn successfully without the guide but failed consistently with the guide installed , failure occurring when the cup rim entered the guide. The radial clearance between hold-down punch and guide was 0.046 in., whilst the measured cup rim thickness was 0.043 in. Unguided and guided redraws were successfully accomplished in tests 4P, i.e. when a larger hold-down punch nose radius was used.

(2) The continuous redraw-load measurement test of tests 12P was conducted successfully, but failure occurred in the interrupted splay-measurement test. To obtain splay-measurement data standard 3 in. cups were shortened to $2\frac{1}{2}$ in. (removing the severely cold-worked rim region). Corresponding load tests were also made with the shorter cups.

Similar results to tests 12P were obtained when conducting tests 16P, but it was possible to redraw 3 in. cups in tests 14P and 18P. Tests 20P were unsuccessful.

(3) Tests 21P and 22P were carried out 'free' with the hold-down punch raised clear of the die. After the splay-phase was complete the cup rim wrinkled during the final drawing-in period.

(c) Main results.

Tabulated.

Test data is tabulated in appendix $A_4.2$. Tables $A_4.2$ - $A_4.8$ give rim splay/redraw load/rim position results. Table $A_4.9$ provides hold-down load information.

Graphical.

For each particular drawing arrangement rim-splay and redraw load were plotted against current cup rim position on a common format. Results are shown in FIG. 175 - 195. Test 20P results are absent since no cups were successfully redrawn with that arrangement. For tests on untrimmed steel cups two rim-splay curves were shown, one for the ear crests and one for the ear valleys. The former curve was labelled 'apparent splay' since the ears did not experience true circumferential constraint.

(d) Sequence of splaying.

A redraw 2 steel cup drawn through the 90 degree semi-angle die was photographed at various stages during the splay-phase. Results are illustrated in FIG. 196. The light coloured residue on die and hold-down punch is lubricant.

11.10 Ancillary tests.

Tensile tests were conducted on ½ in. wide strip specimens taken from blanks, to provide information on the initial yield-stress of materials from which proving-test cups were made. The information was not put to direct use in the research programme but may be useful in future work.

For aluminium and 70/30 brass two specimens were taken at 0, 45 and 90 degrees to the rolling direction. It was not possible to observe the rolling direction with steel blanks due to their lubricant coating so six specimens were taken in random directions.

Tests were carried out on a Hounsfield Tensometer, and stress-strain curves plotted to determine 0.2 % proof stress. Results are summarised in table A_4.10.

Test Number	Test Material	Cup condition	Nominal cup dimensions (in.)		Die semi-angle (deg.)	Hold-down punch nose radius (in.)
			O/Dia.	Wall Thk.		
1P	Steel	as-drawn/ trimmed.	3.250	0.037	90	0.180

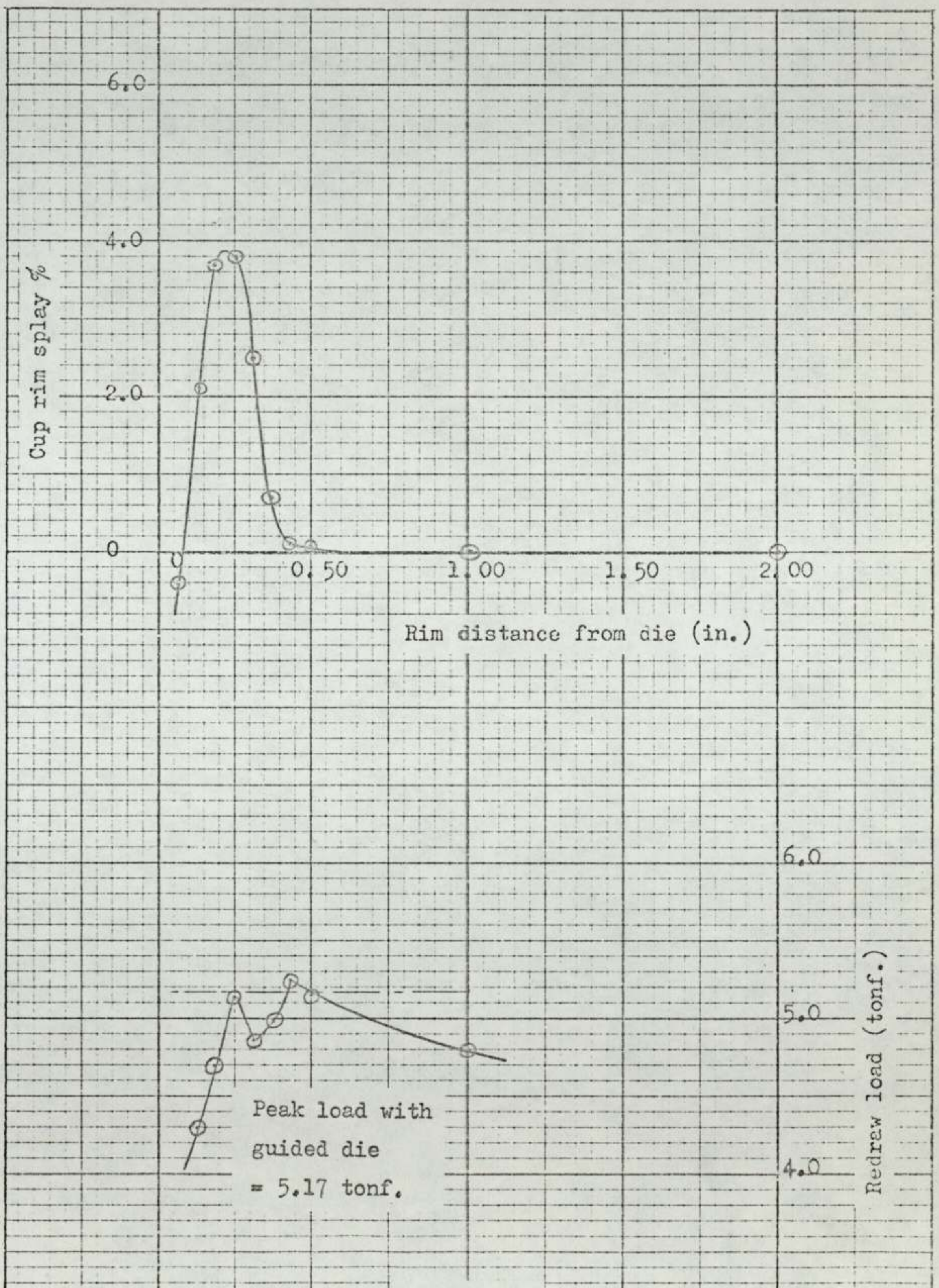

FIG. 175.

Test Number	Test Material	Cup condition	Nominal cup dimensions (in.)		Die semi-angle (deg.)	Hold-down punch nose radius (in.)
			O/Dia.	Wall Thk.		
2P	alum.	as-drawn/ trimmed	3.250	0.036	90	0.180

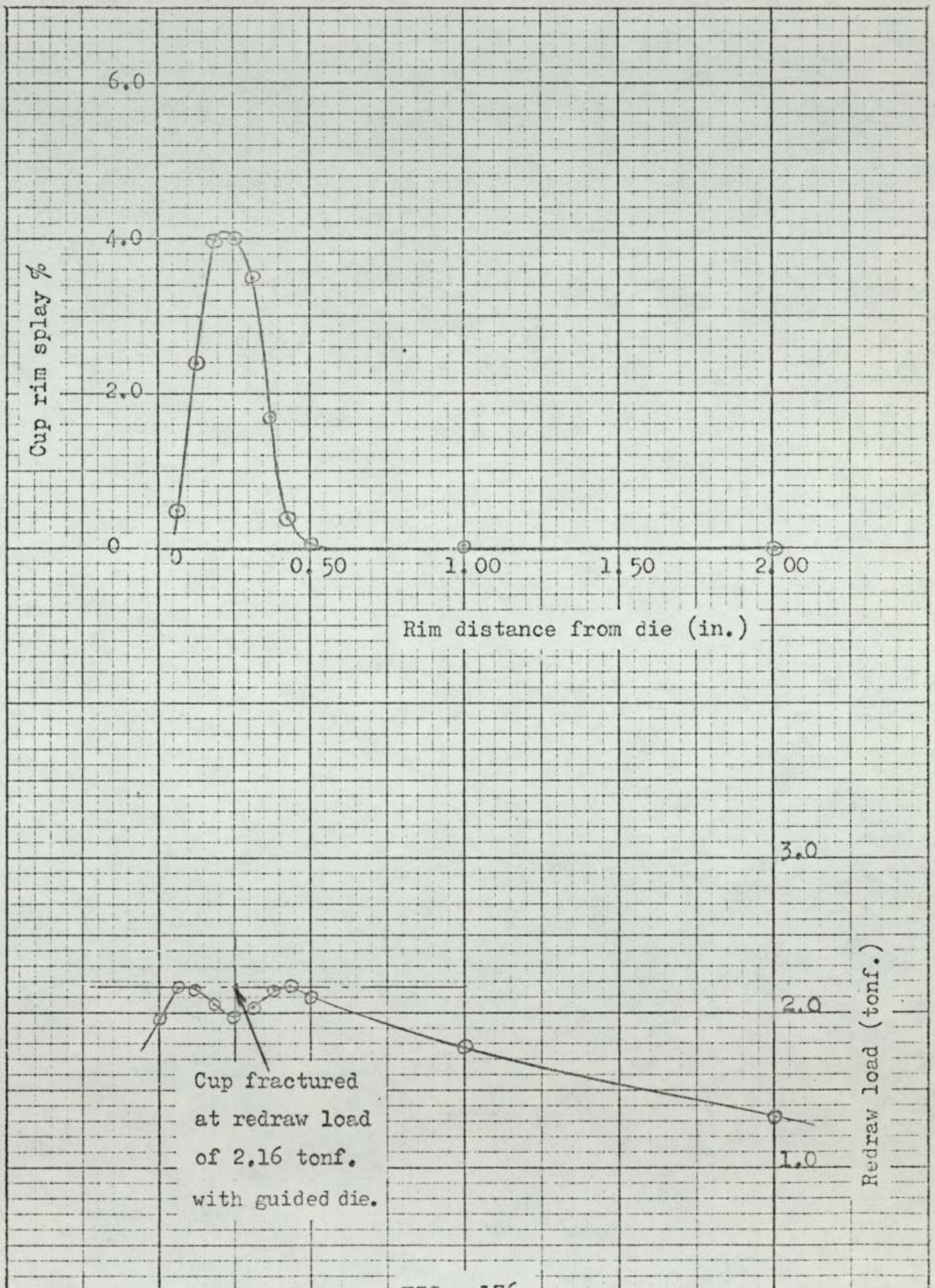

FIG. 176.

Test Number	Test Material	Cup condition	Nominal cup dimensions (in.)		Die semi-angle (deg.)	Hold-down punch nose radius (in.)
			O/Dia.	Wall Thk.		
3P	Steel	as-drawn/ trimmed	3.250	0.037	90	0.250

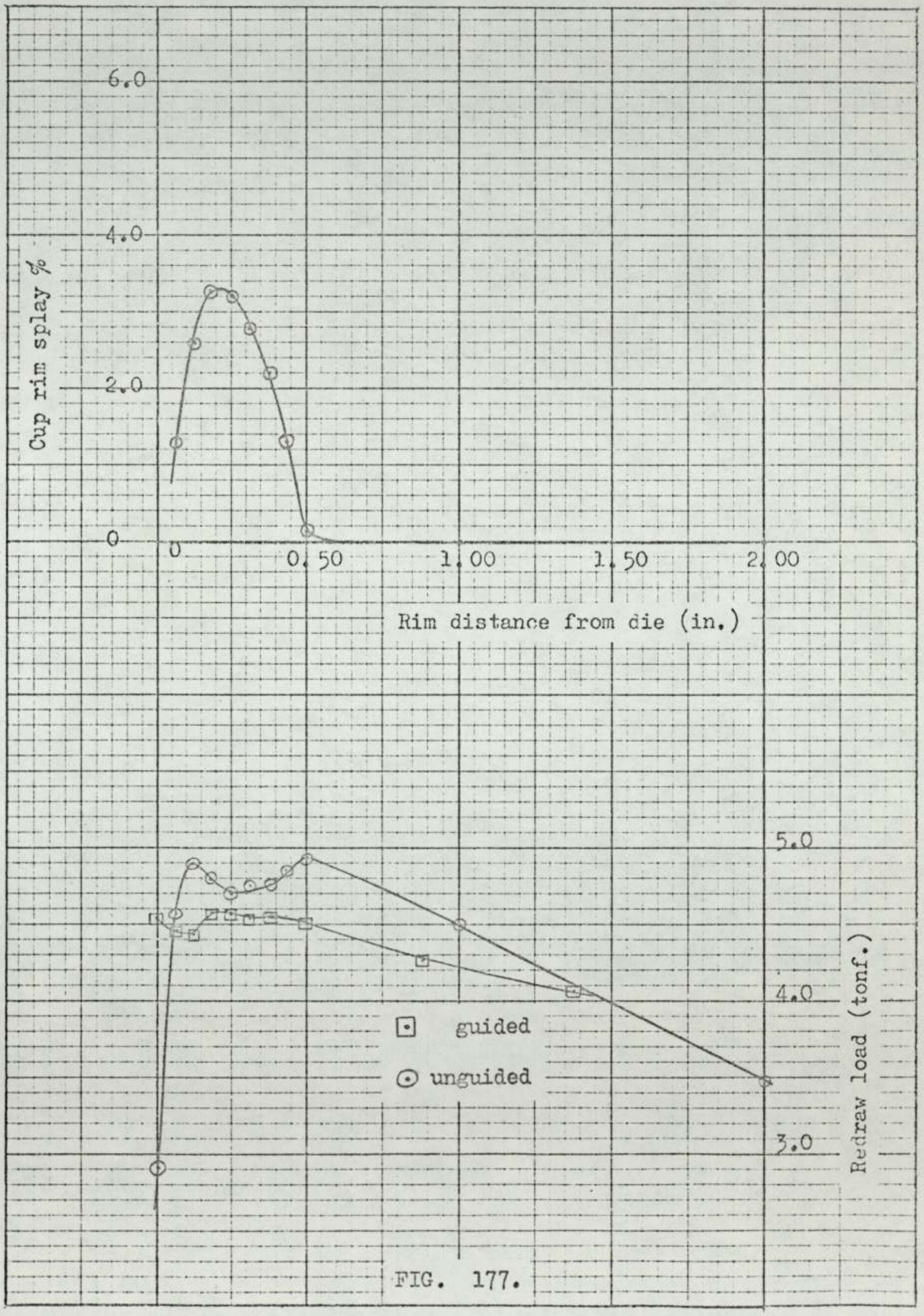

FIG. 177.

Test Number	Test Material	Cup condition	Nominal cup dimensions (in.)		Die semi-angle (deg.)	Hold-down punch nose radius (in.)
			O/Dia.	Wall Thk.		
4P	alum.	as-drawn/ trimmed.	3.250	0.036	90	0.250

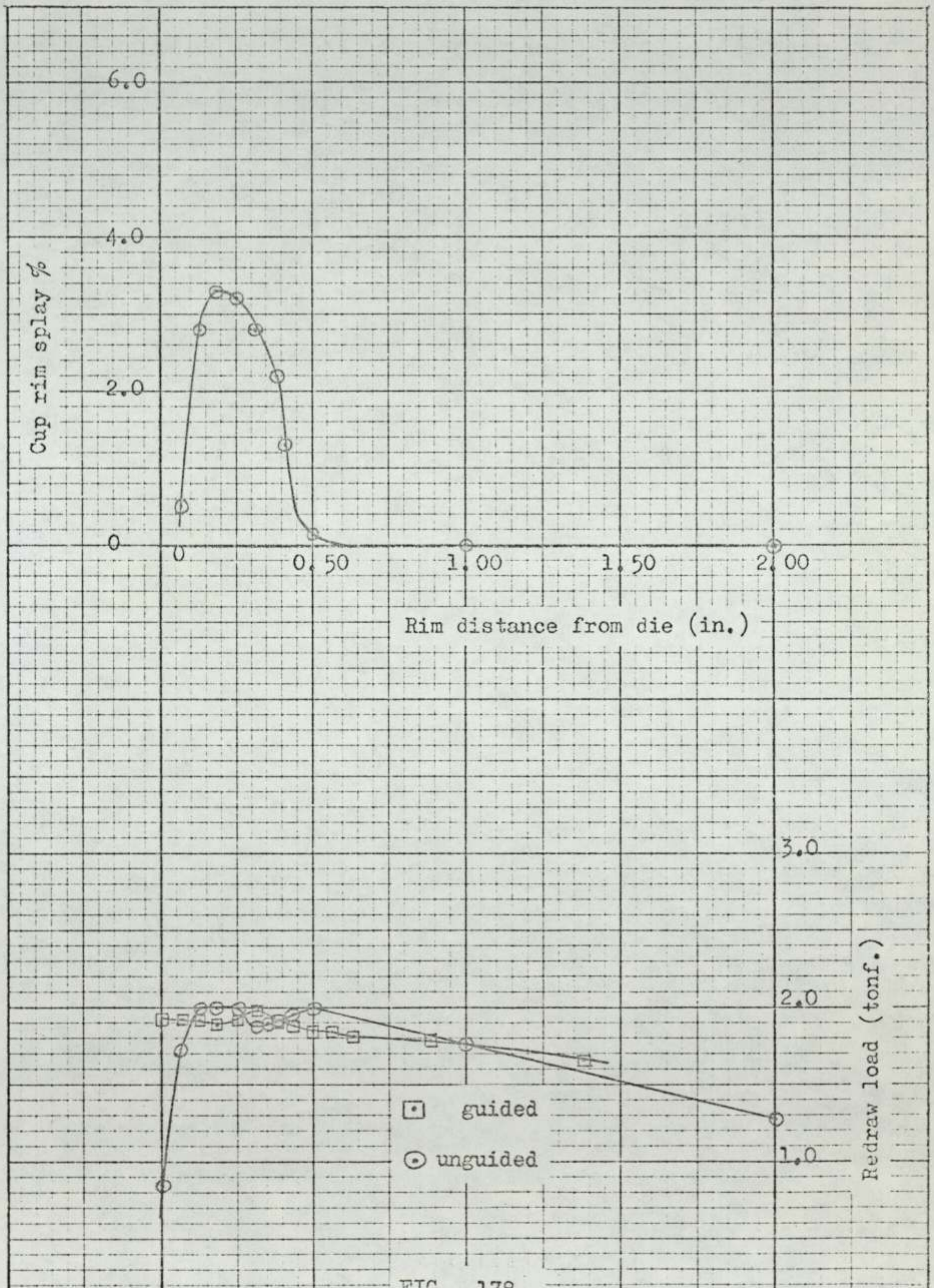

FIG. 178.

Test Number	Test Material	Cup condition	Nominal cup dimensions (in.)		Die semi-angle (deg.)	Hold-down punch nose radius (in.)
			O/Dia.	Wall Thk.		
5P	Steel	annealed/ trimmed.	3.250	0.037	90	0.180

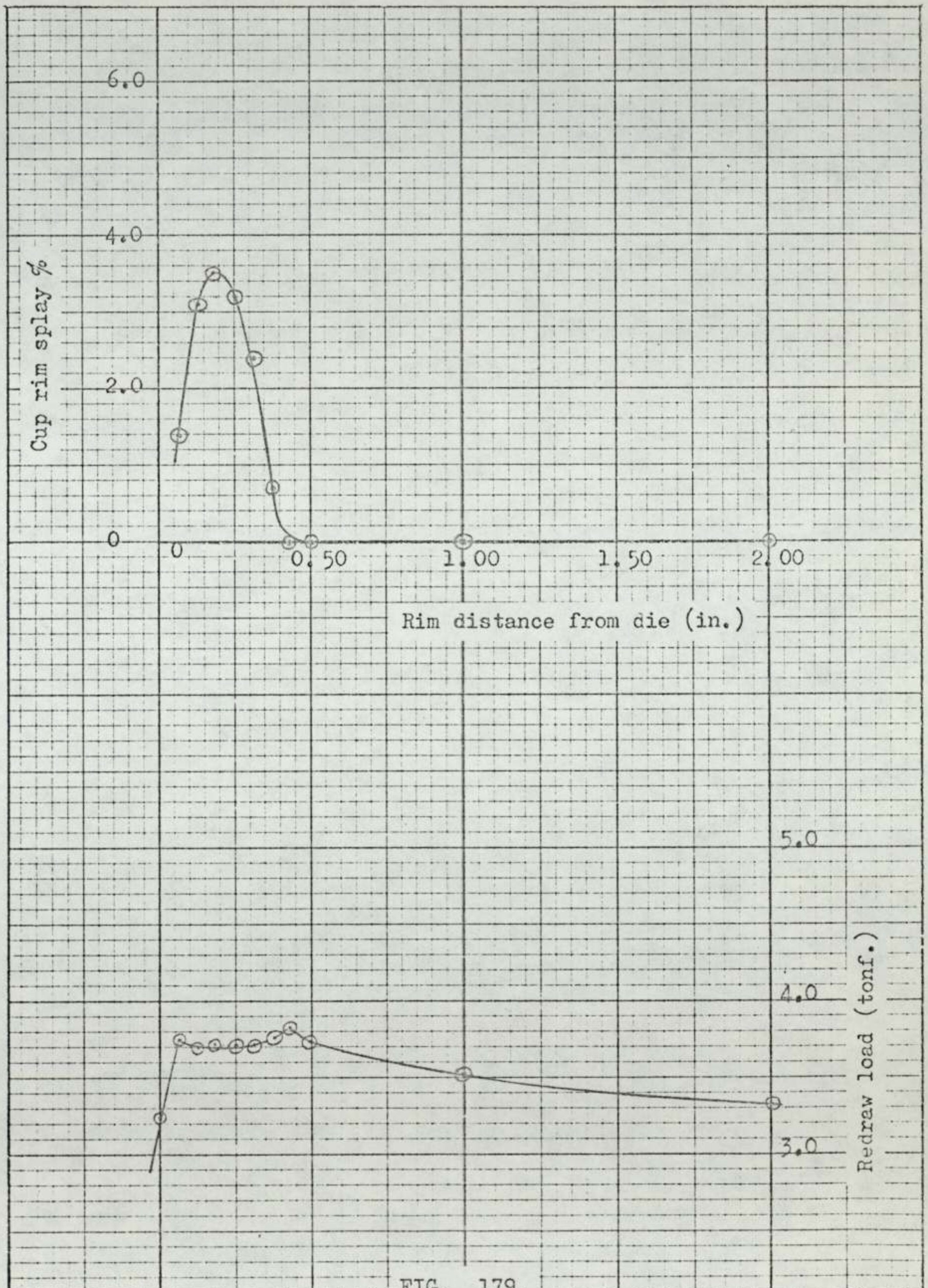

FIG. 179.

Test Number	Test Material	Cup condition	Nominal cup dimensions (in.)		Die semi-angle (deg.)	Hold-down punch nose radius (in.)
			O/Dia.	Wall Thk.		
6P	alum.	annealed/ trimmed.	3.250	0.036	90	0.180

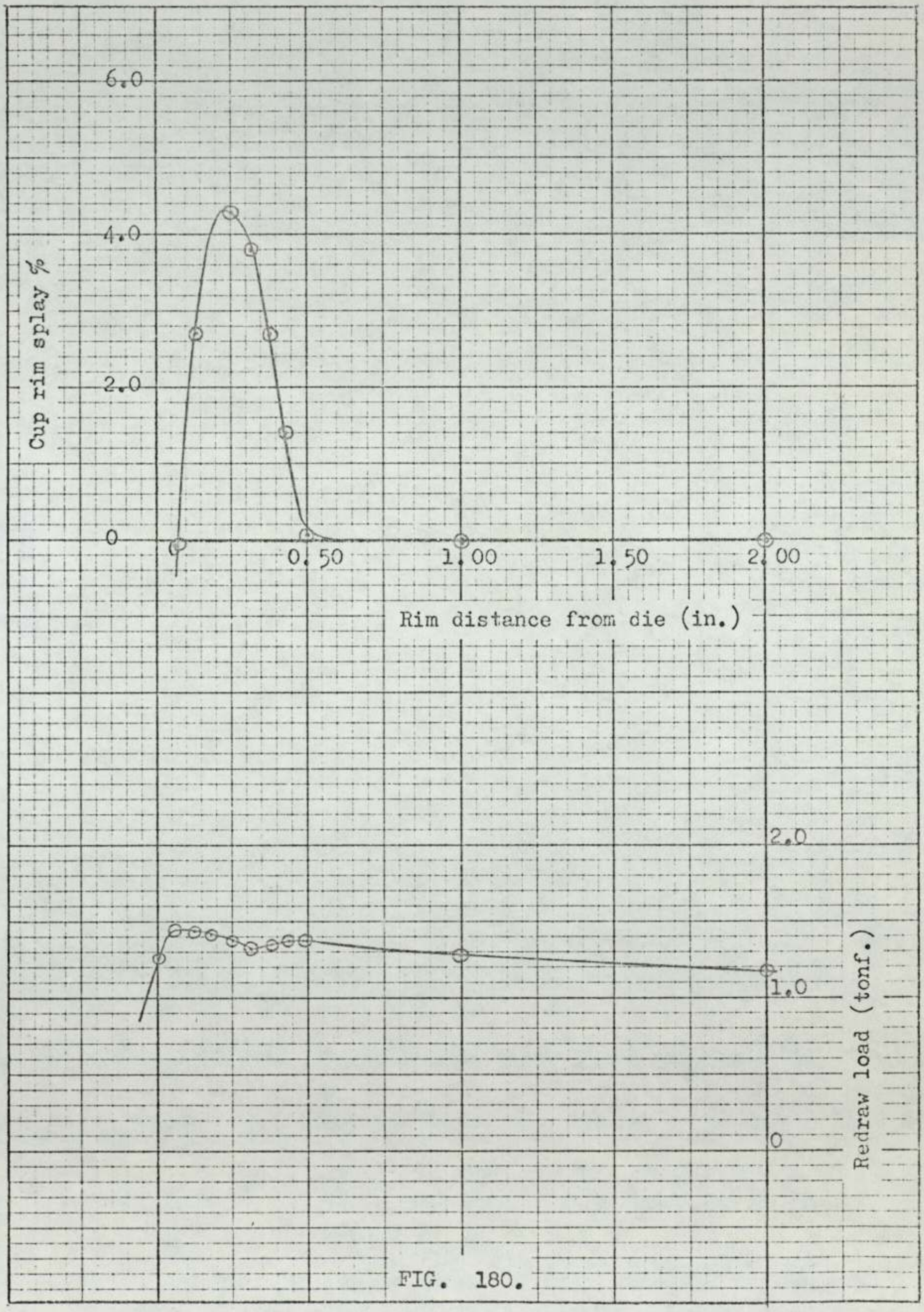

FIG. 180.

Test Number	Test Material	Cup condition	Nominal cup dimensions (in.)		Die semi-angle (deg.)	Hold-down punch nose radius (in.)
			O/Dia.	Wall Thk.		
7P	Steel	annealed/ trimmed.	3.250	0.037	90	0.250

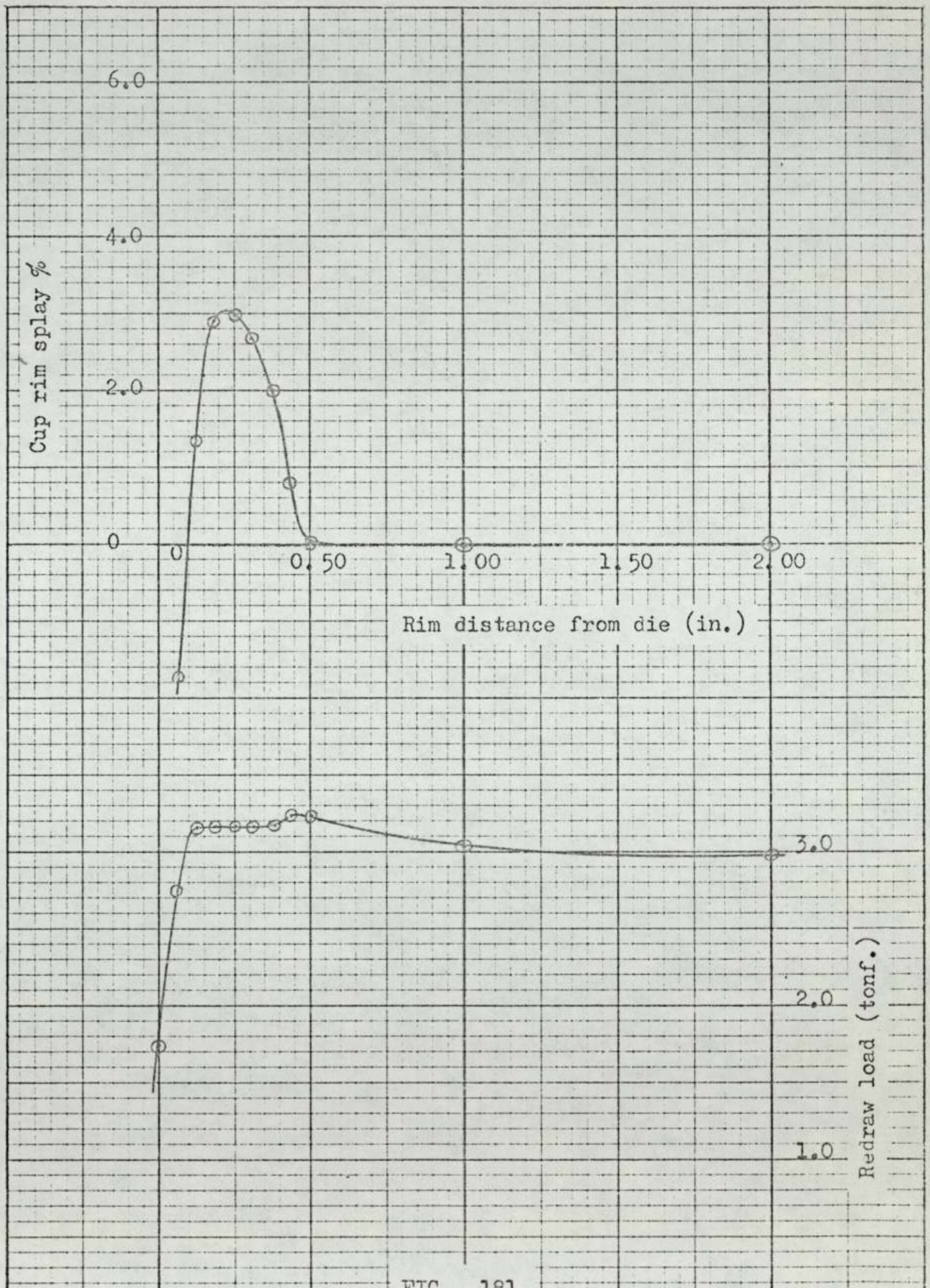

FIG. 181.

Test Number	Test Material	Cup condition	Nominal cup dimensions (in.)		Die semi-angle (deg.)	Hold-down punch nose radius (in.)
			O/Dia.	Wall Thk.		
8P	alum.	annealed/ trimmed	3.250	0.036	90	0.250

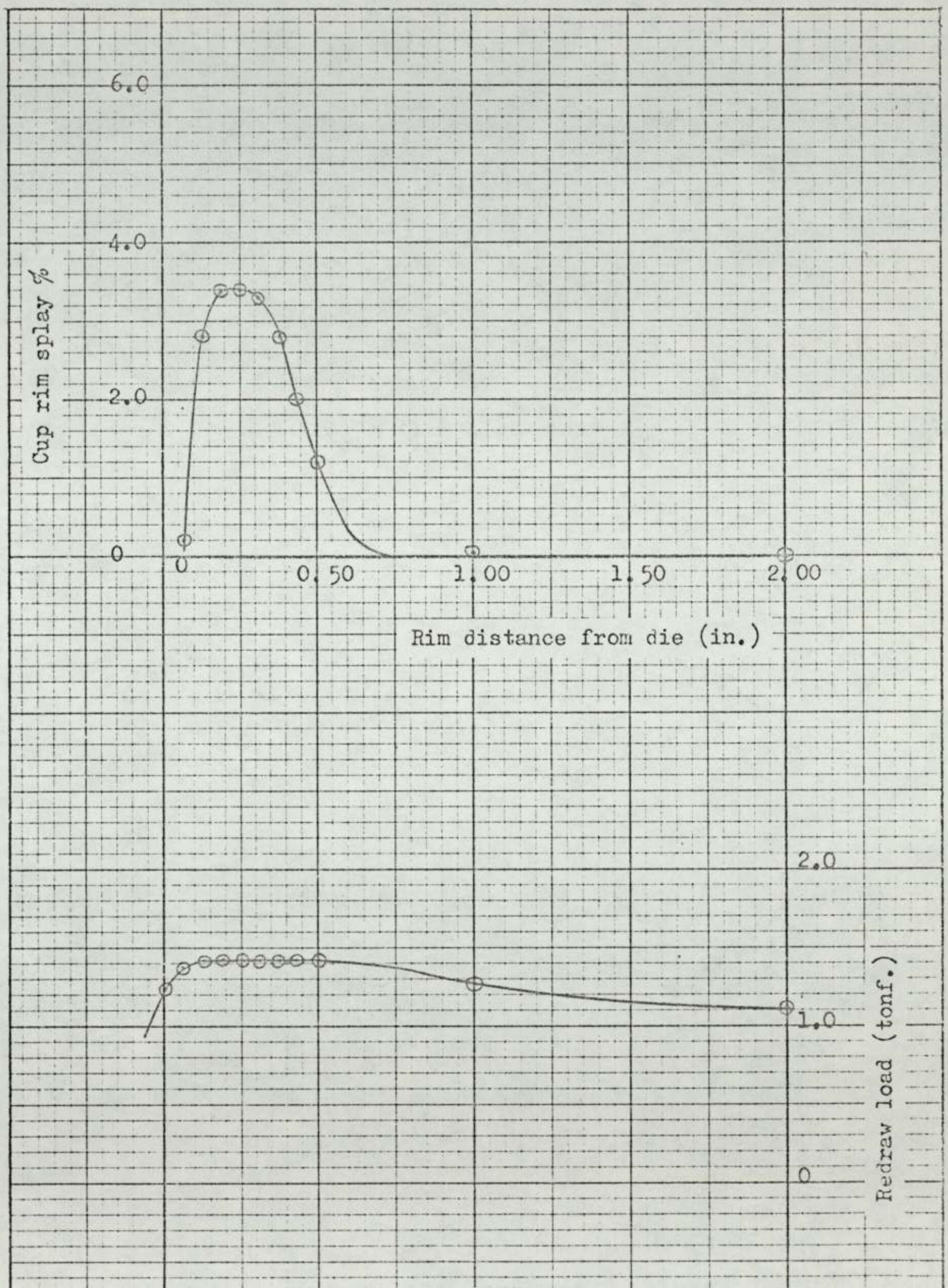

FIG. 182.

Test Number	Test Material	Cup condition	Nominal cup dimensions (in.)		Die semi-angle (deg.)	Hold-down punch nose radius (in.)
			O/Dia.	Wall Thk.		
9P	Steel	as-drawn/ untrimmed.	3.250	0.037	90	0.180

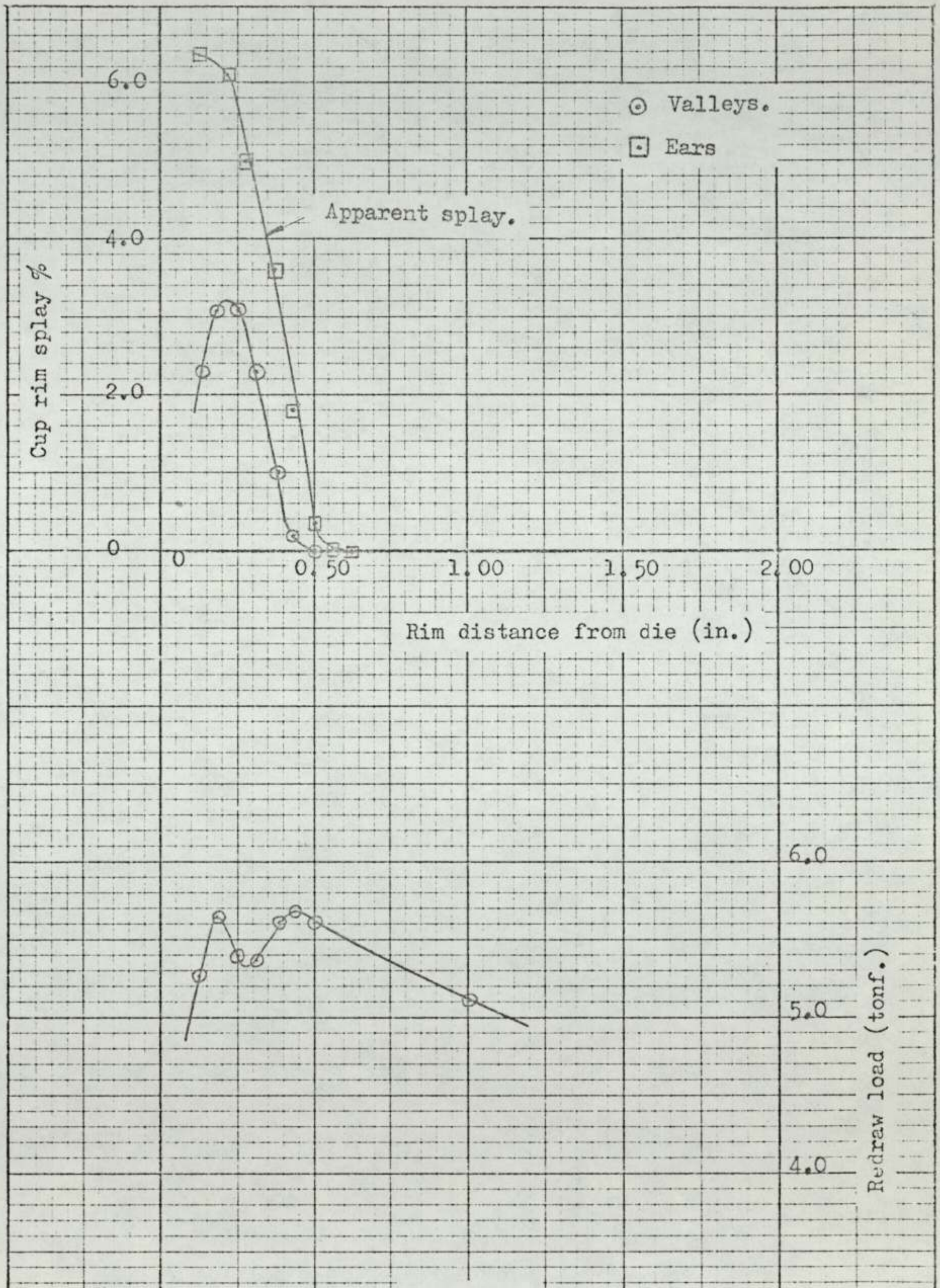

FIG. 183.

Test Number	Test Material	Cup condition	Nominal cup dimensions (in.)		Die semi-angle (deg.)	Hold-down punch nose radius (in.)
			O/Dia.	Wall Thk.		
10P	alum.	as-drawn/ untrimmed.	3.250	0.036	90	0.180

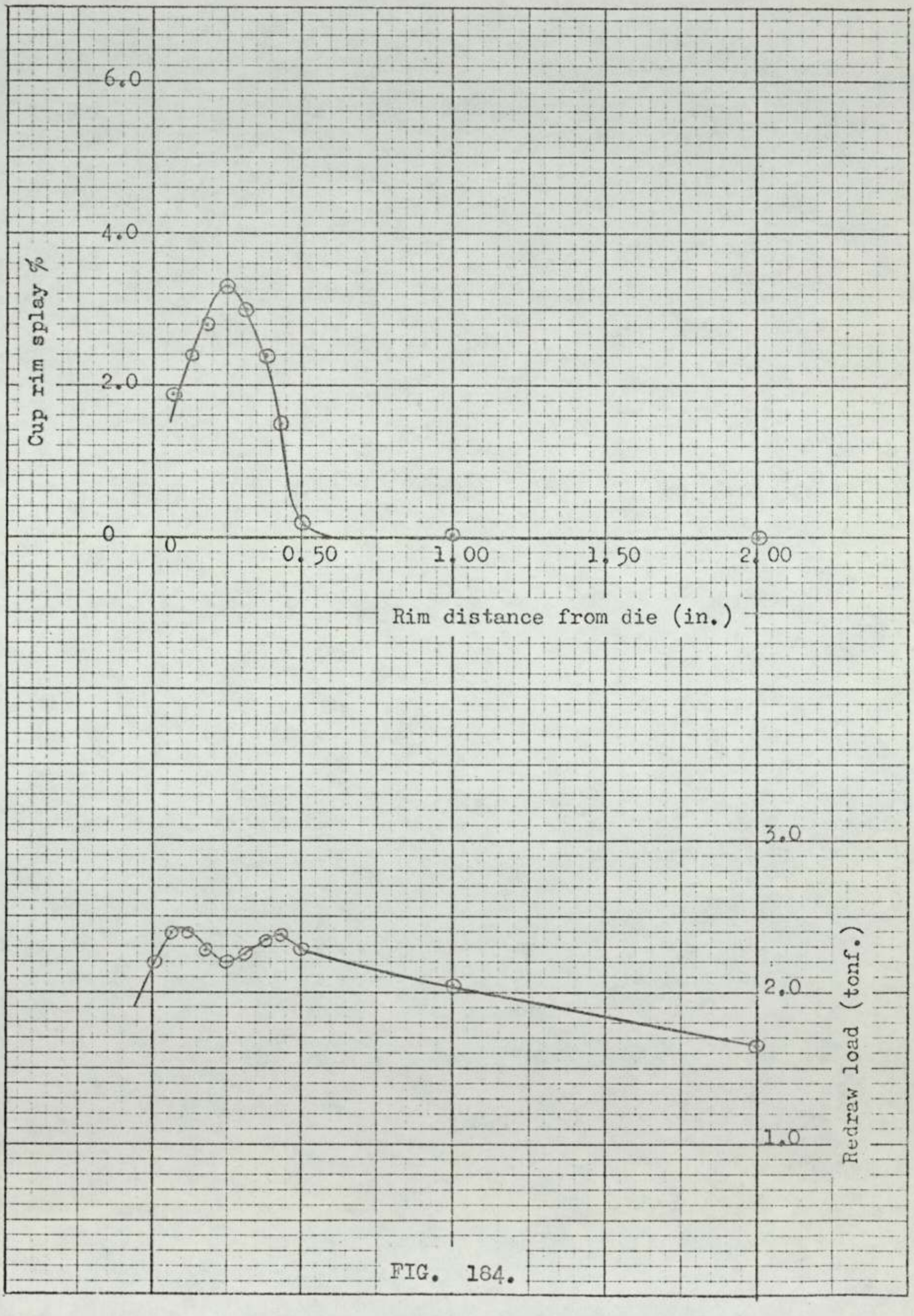

FIG. 184.

Test Number	Test Material	Cup condition	Nominal cup dimensions (in.)		Die semi-angle (deg.)	Hold-down punch nose radius (in.)
			O/Dia.	Wall Thk.		
11P	Steel	as-drawn/ trimmed.	2.587	0.037	90	0.180

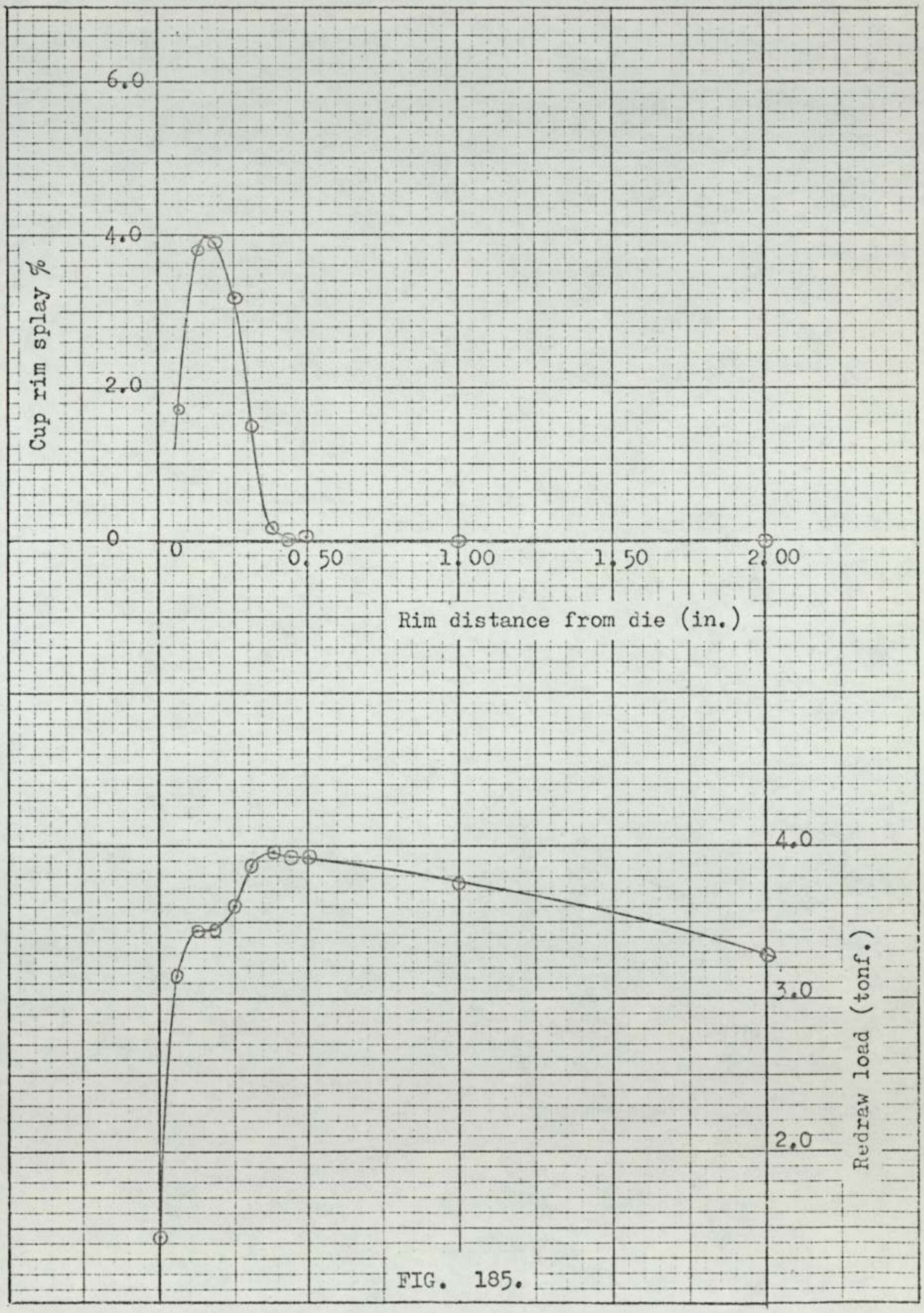

FIG. 185.

Test Number	Test Material	Cup condition	Nominal cup dimensions (in.)		Die semi-angle (deg.)	Hold-down punch nose radius (in.)
			O/Dia.	Wall Thk		
12P	70/30 brass	as-drawn/ trimmed.*	2.587	0.037	90	0.180

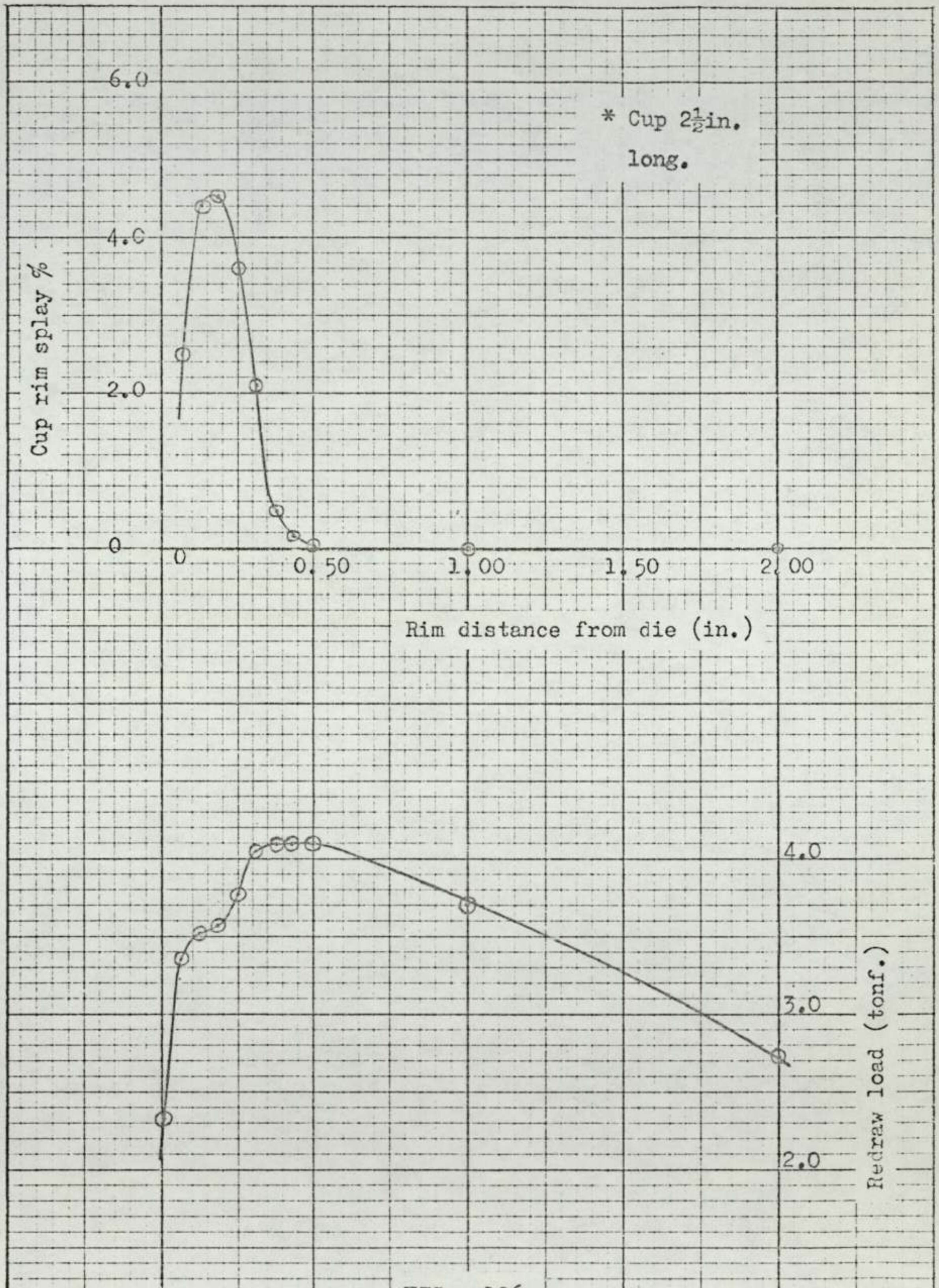

FIG. 186.

Test Number	Test Material	Cup condition	Nominal cup dimensions (in.)		Die semi-angle (deg.)	Hold-down punch nose radius (in.)
			O/Dia.	Wall Thk.		
13P	Steel	as-drawn/ trimmed.	2.587	0.037	90	0.253

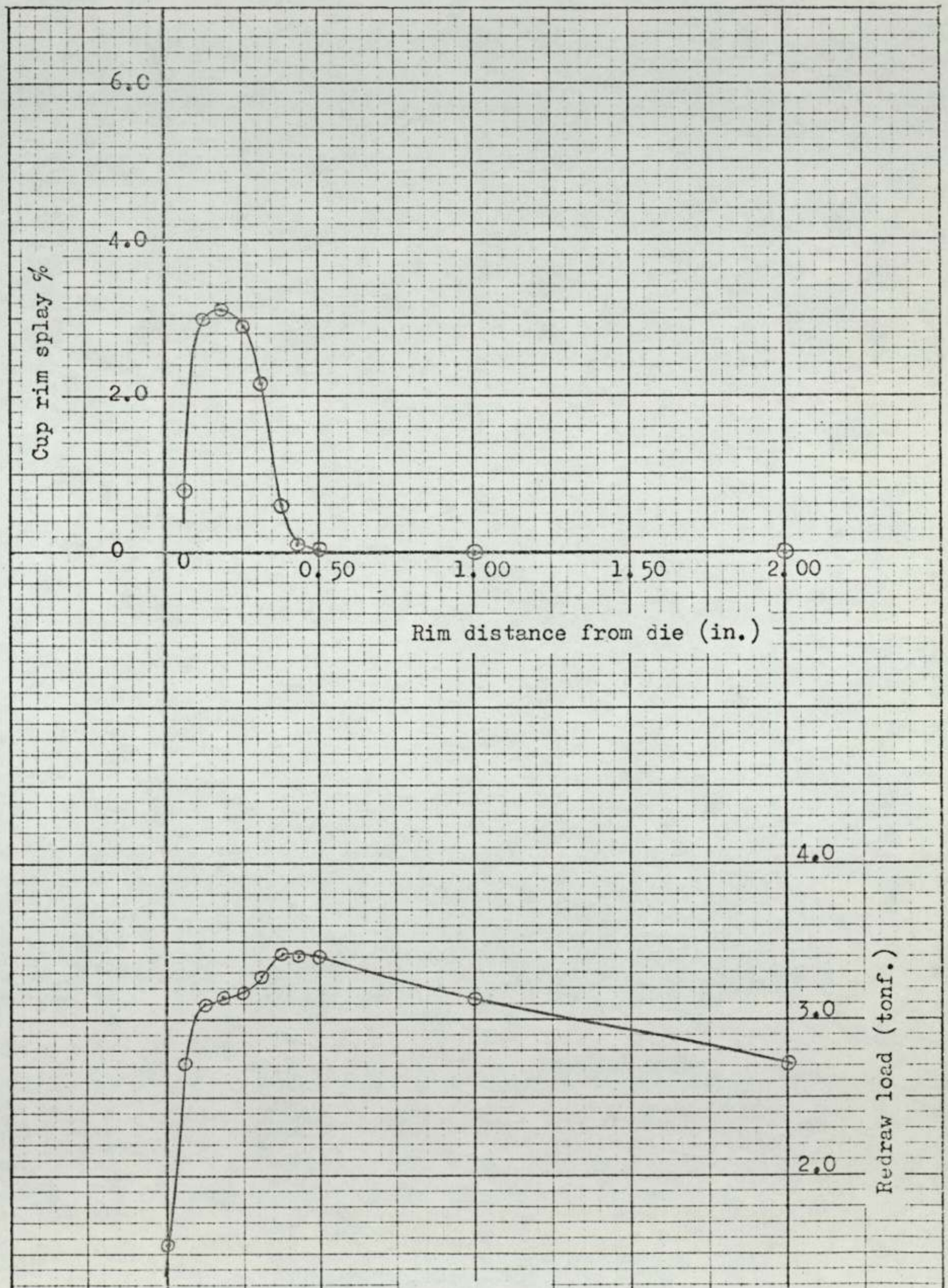

FIG. 187.

Test Number	Test Material	Cup condition	Nominal cup dimensions (in.)		Die semi-angle (deg.)	Hold-down punch nose radius (in.)
			O/Dia.	Wall Thk.		
14P	70/30 brass	as-drawn/ trimmed.	2.587	0.037	90	0.253

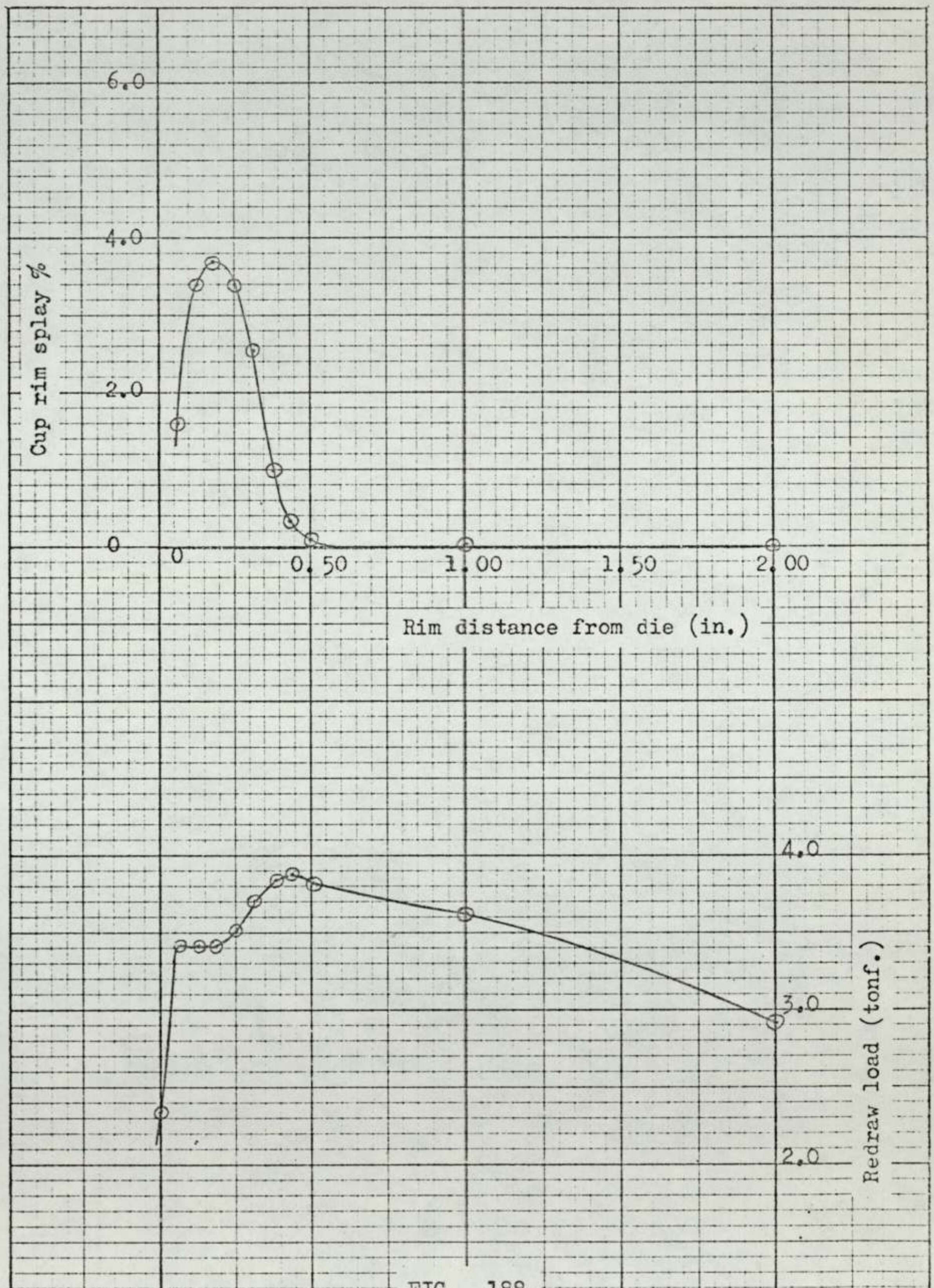

FIG. 188.

Test Number	Test Material	Cup condition	Nominal cup dimensions (in.)		Die semi-angle (deg.)	Hold-down punch nose radius (in.)
			O/Dia.	Wall Thk.		
15P	Steel	as-drawn/ trimmed.	2.587	0.037	45	0.180

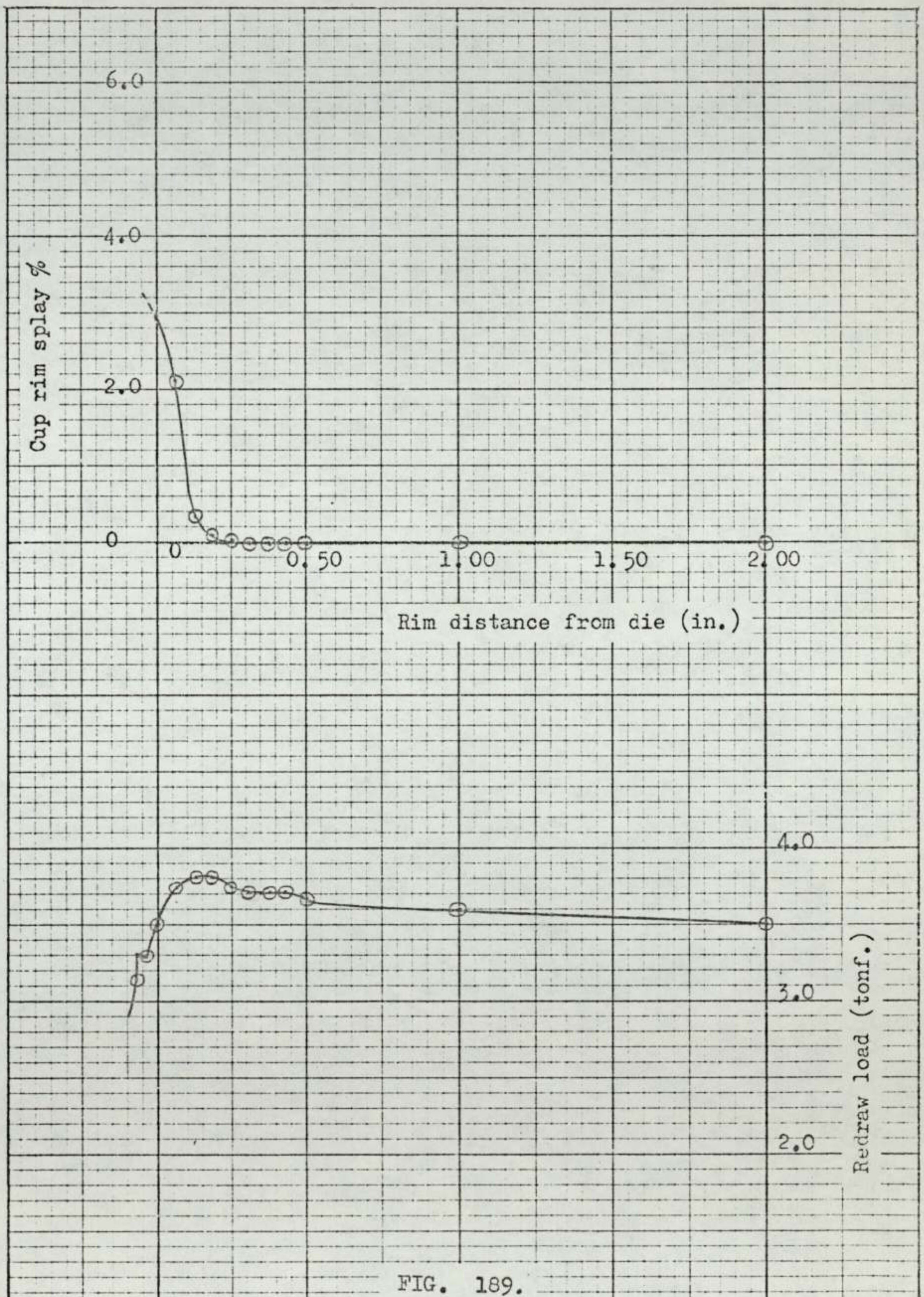

FIG. 189.

Test Number	Test Material	Cup condition	Nominal cup dimensions (in.)		Die semi-angle (deg.)	Hold-down punch nose radius (in.)
			O/Dia.	Wall Thk.		
16P	70/30 brass	as-drawn/ trimmed.*	2.587	0.037	45	0.180

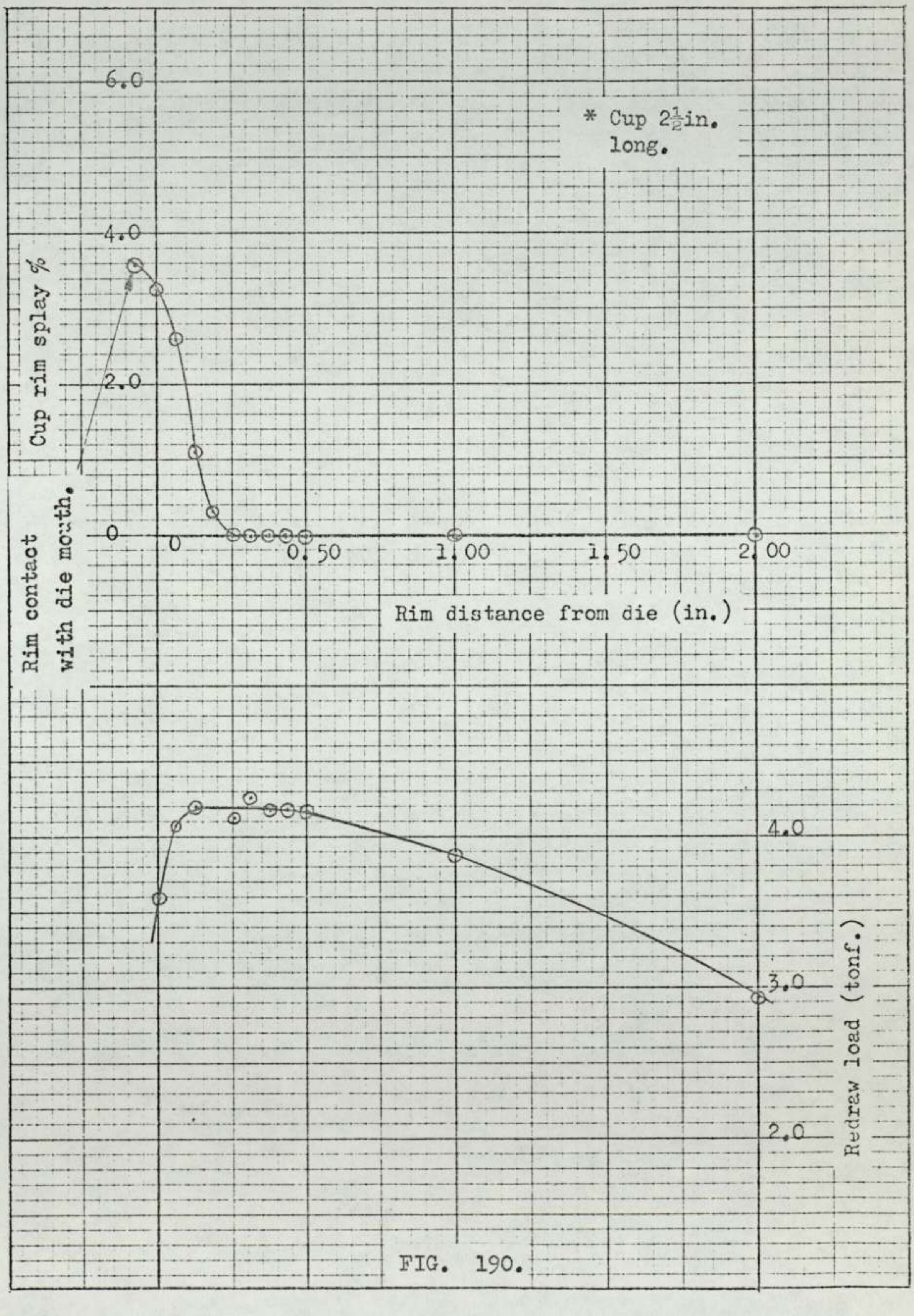

FIG. 190.

Test Number	Test Material	Cup condition	Nominal cup dimensions (in.)		Die semi-angle (deg.)	Hold-down punch nose radius (in.)
			O/Dia.	Wall Thk.		
17P	Steel	as-drawn/ trimmed.	2.587	0.037	45	0.317

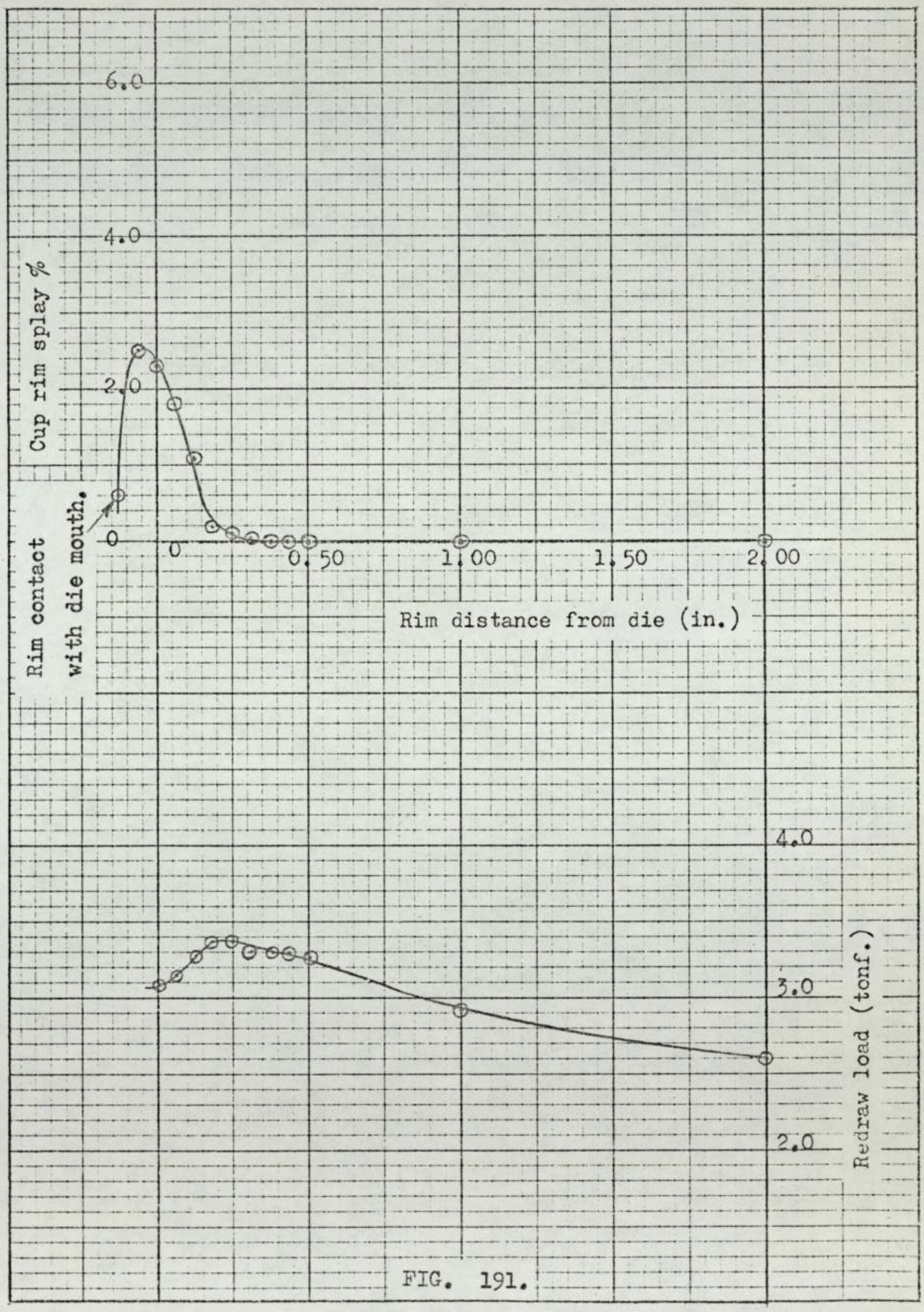

FIG. 191.

Test Number	Test Material	Cup condition	Nominal cup dimensions (in.)		Die semi-angle (deg.)	Hold-down punch nose radius (in.)
			O/Dia.	Wall Thk.		
18P	70/30 brass	as-drawn trimmed.	2.587	0.037	45	0.317

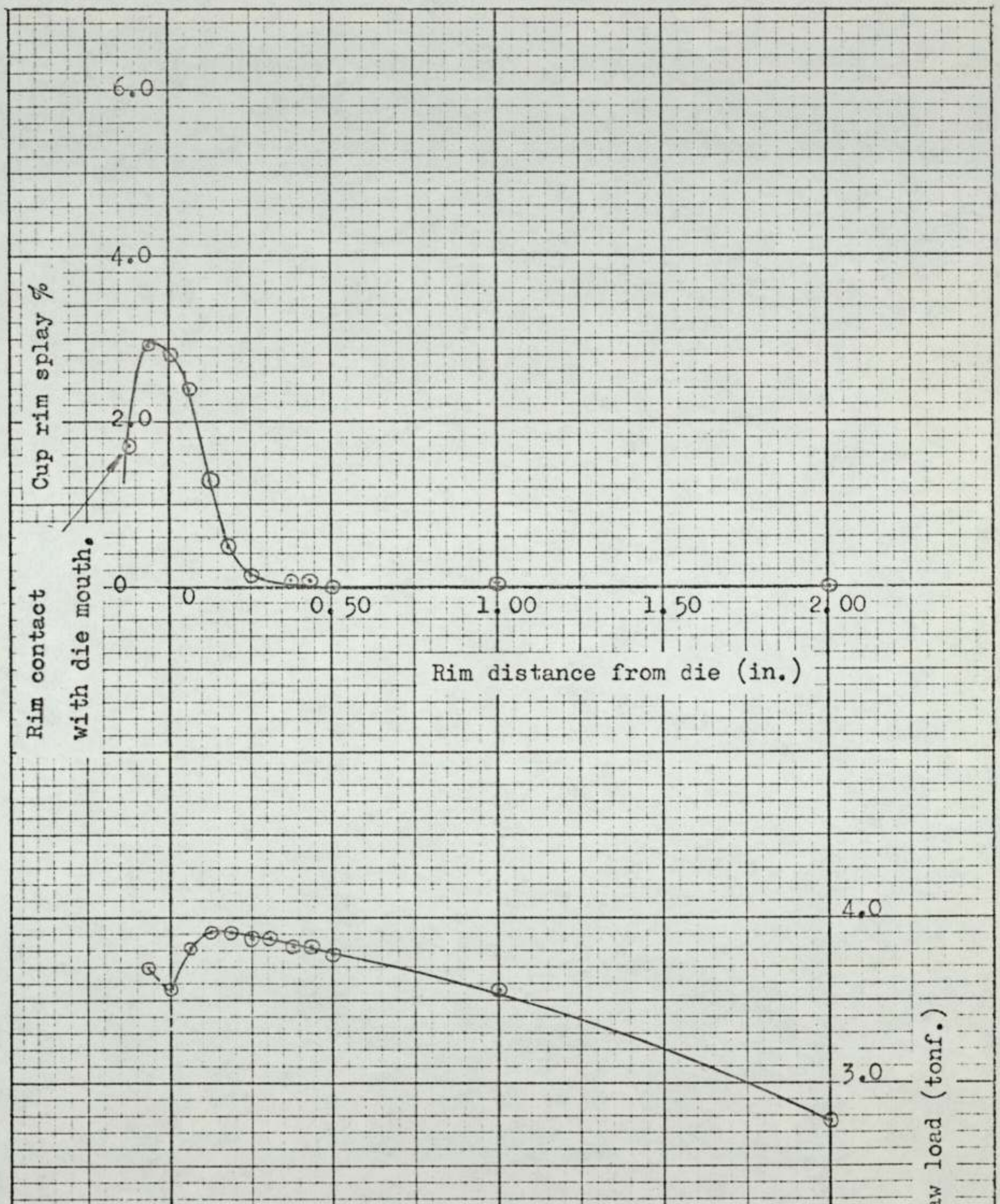

FIG. 192.

Test Number	Test Material	Cup condition	Nominal cup dimensions (in.)		Die semi-angle (deg.)	Hold-down punch nose radius (in.)
			O/Dia.	Wall Thk.		
19P	Steel	as-drawn/ untrimmed.	2.587	0.037	90	0.180

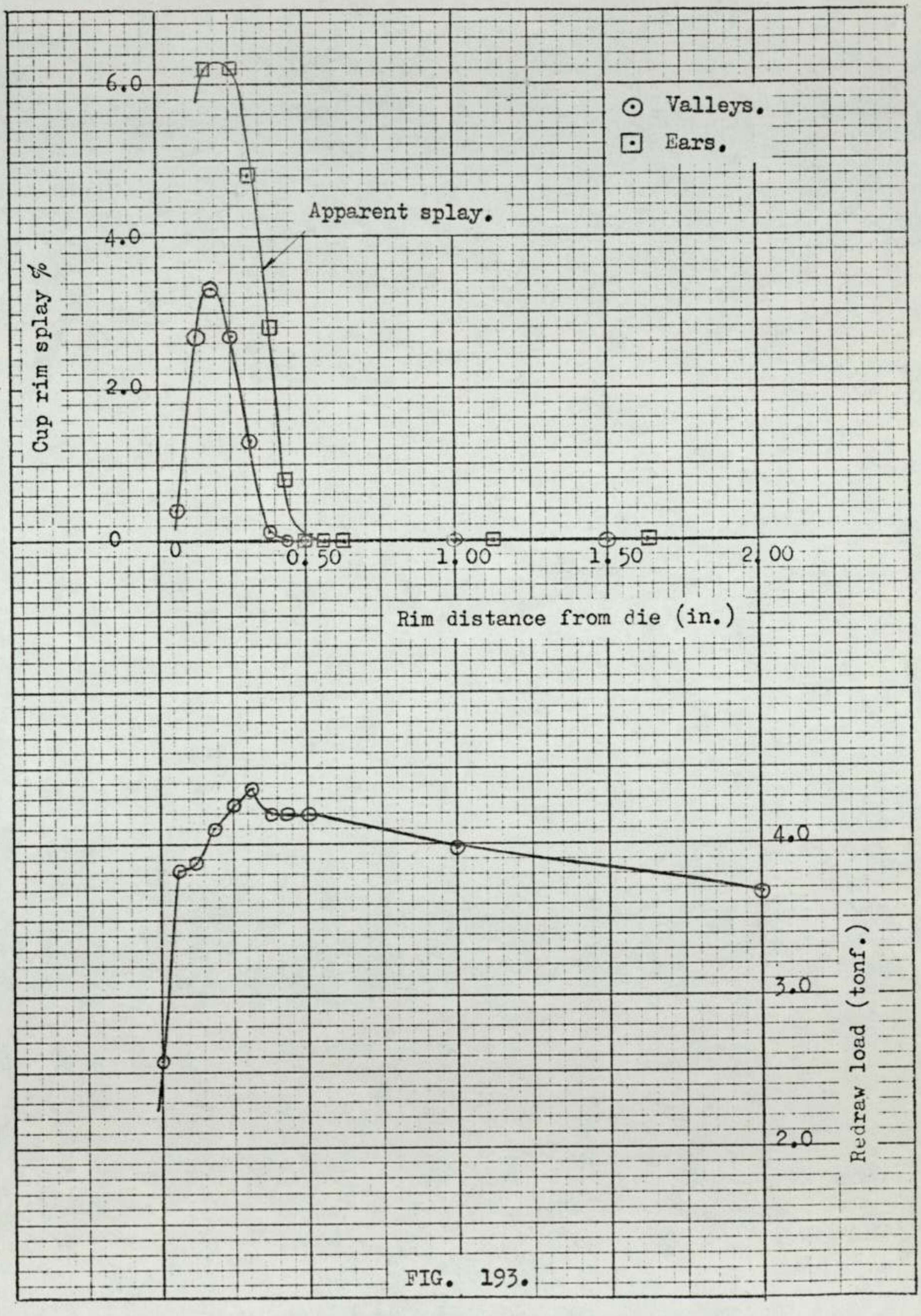

FIG. 193.

Test Number	Test Material	Cup condition	Nominal cup dimensions (in.)		Die semi-angle (deg.)	Hold-down punch nose radius (in.)
			O/Dia.	Wall Thk.		
21P	Steel	as-drawn/ trimmed.	2.587	0.037	90	free

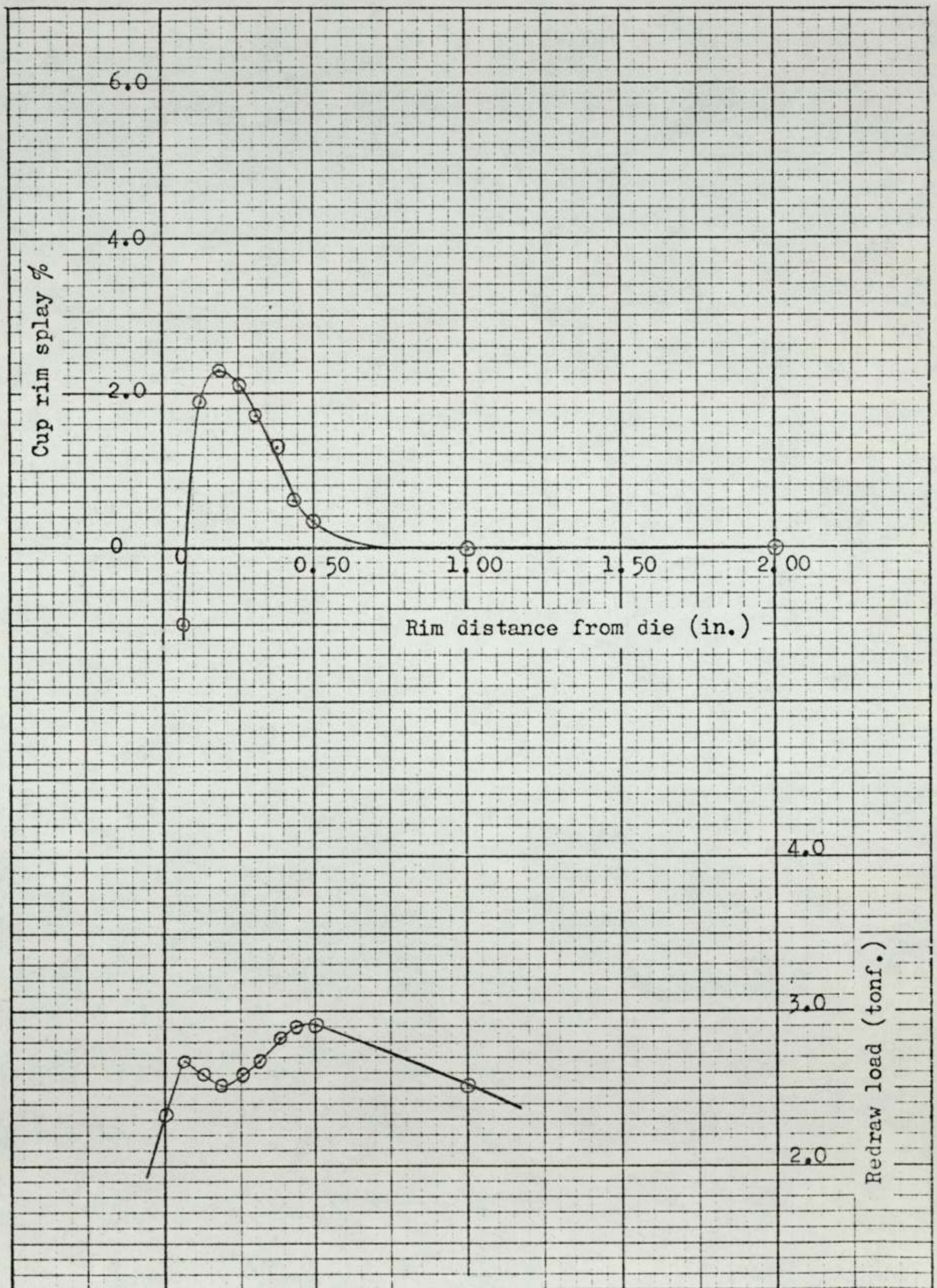

FIG. 194.

Test Number	Test Material	Cup condition	Nominal cup dimensions (in.)		Die semi-angle (deg.)	Hold-down punch nose radius (in.)
			O/Dia.	Wall Thk.		
22P	70/30 brass	as-drawn/ trimmed	2.587	0.037	90	free.

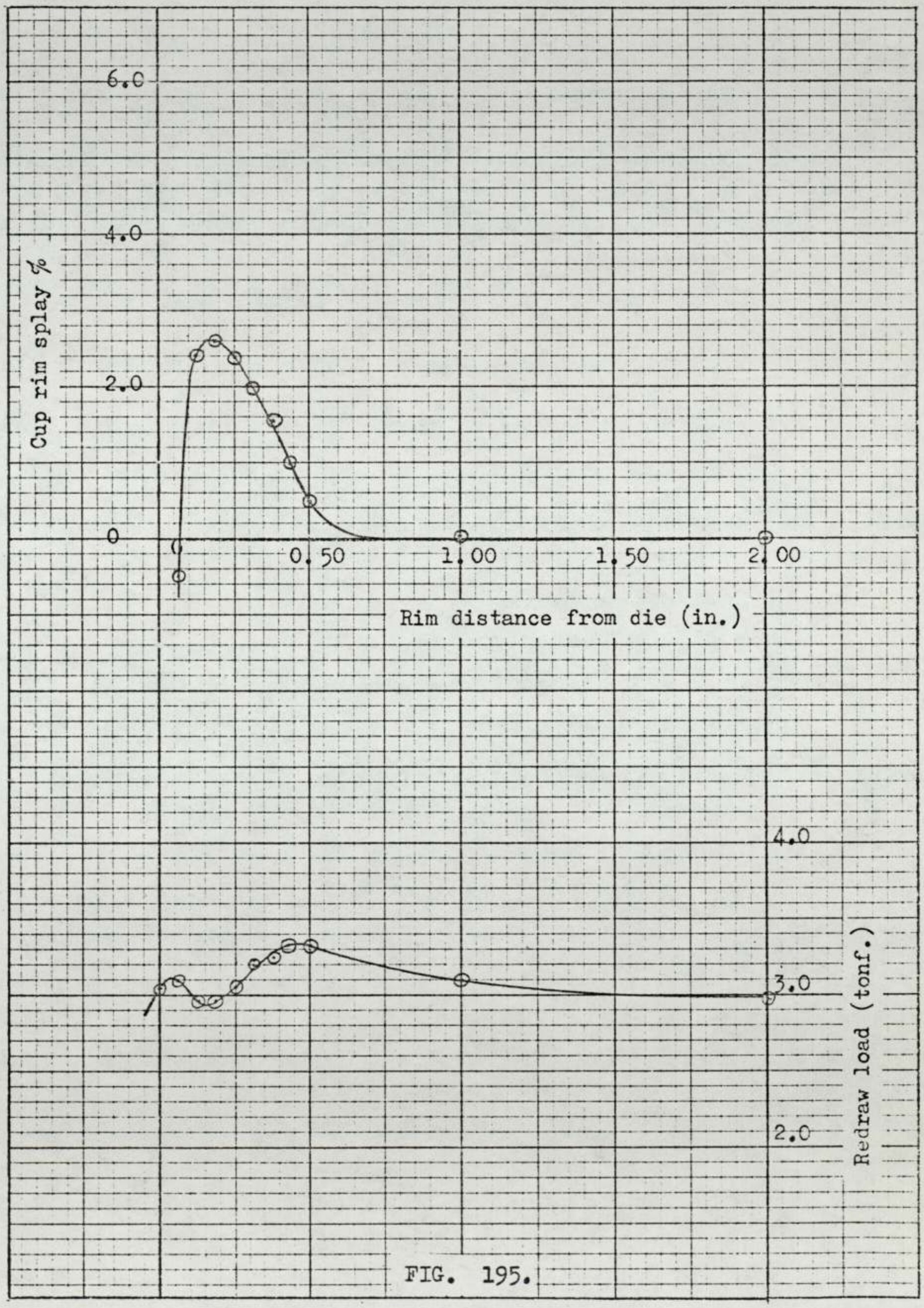

FIG. 195.

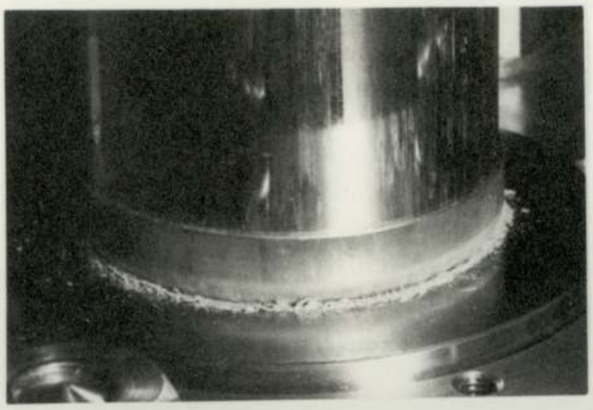

Rim 7/16 in. from die.

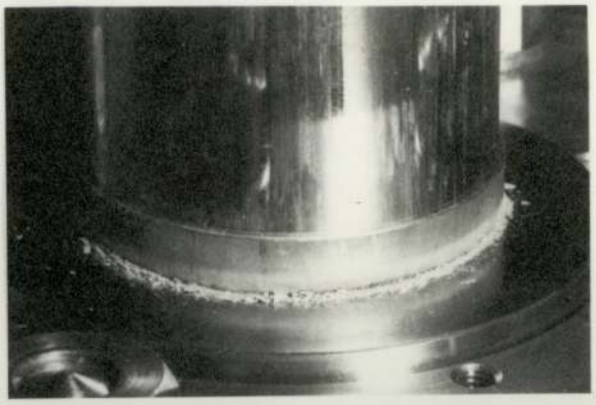

Rim 3/8 in. from die.

Rim 5/16 in. from die.

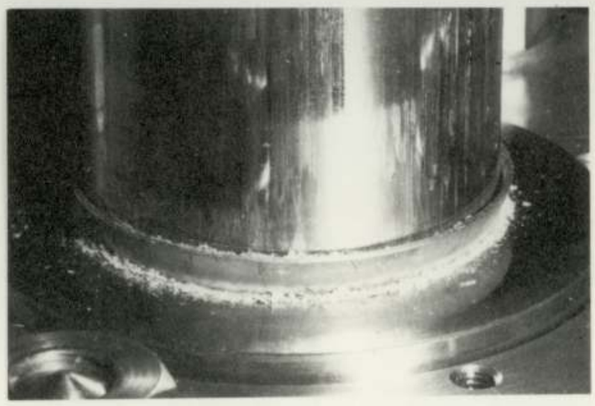

Rim 1/4 in. from die.

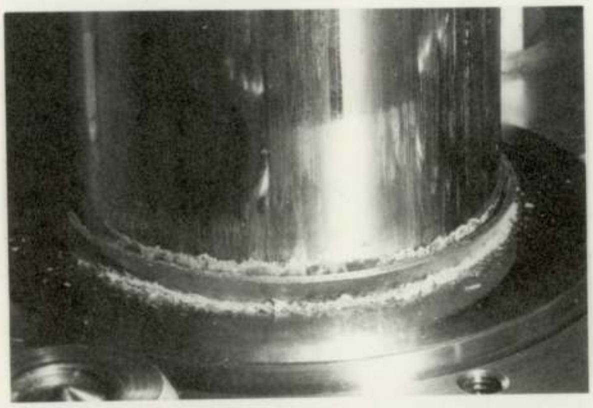

Rim 3/16 in. from die.

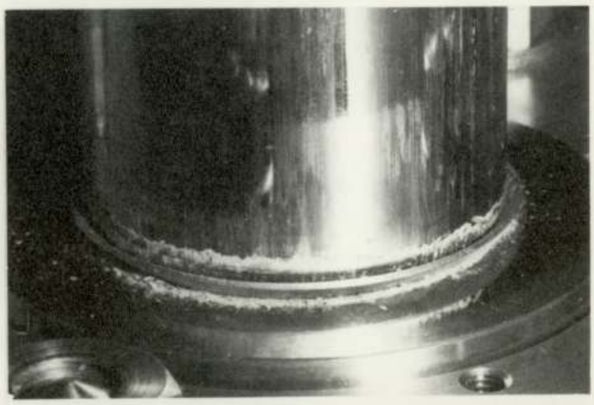

Rim 1/8 in. from die.

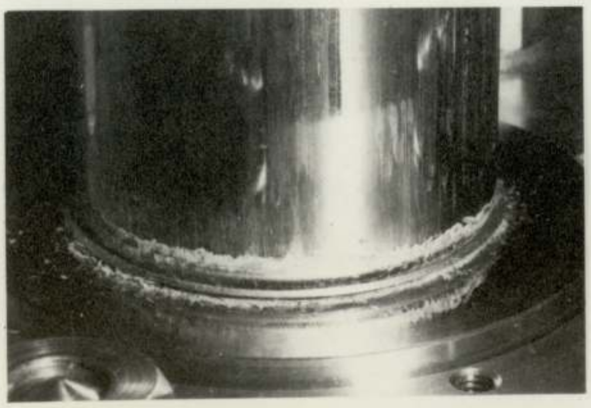

Rim 1/16 in. from die.

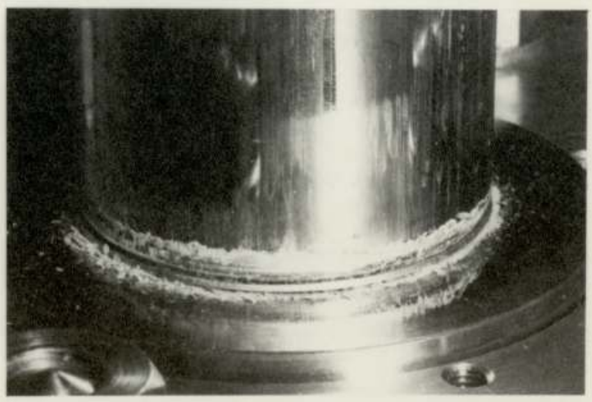

Rim at die.

FIG. 196 SPLAYING SEQUENCE WITH LOW CARBON STEEL. REDRAW NUMBER 2.

12. CORRELATION OF THEORY AND PROVING-TEST PROGRAMME RESULTS.

12.1. Maximum splaying at the cup rim.

The bulk of theoretical studies were made for an ideal non work-hardening material. As-drawn cups approached this condition in the rim region whereas annealed cups did not. Quantitative theoretical/experimental correlations were therefore only considered for as-drawn cups, although qualitative comparisons were made with results for the few annealed cups.

FIG. 197 shows results for as-drawn cups. The stated r_o/t_o values are nominal, being based on the original blank thickness, but the more important R_o/t_o values were calculated in terms of actual cup wall thickness as given in table $A_4.1$. Splaying results from tests 15P and 16P were not plotted since the 45 degree semi-angle clearly limited maximum splaying (FIGS. 189 and 190). The dotted lines labelled 1, 2 represent rim splaying in 'free' tests 21P and 22P, where the hold-down punch was raised. According to Fogg's theory the free radius ratio R_f/t_o should have been about 7.6, and yet splaying measured for constrained R_o/t_o values of 7.6 was greater than in free cases, implying that the hold-down punch was actively influencing the shape of the deformation zone whose true R_f/t_o value was therefore greater than 7.6. The hyperbolic theory was represented by a single curve obtained from the simplified expression equation 9.16a.

Experimental points fell within the bounds of the two theoretical curves with the 'brass' points tending towards the tangential splay mode.

12.2. Splay locus of cup rim.

Results from test 2P are replotted in FIG. 198 with the plane of steady-state bending included as a line of reference. According to theory the splay-phase ended at this point.

The redraw load curve is included to show the effect of splaying on process work. Test 2P was selected because work-hardened

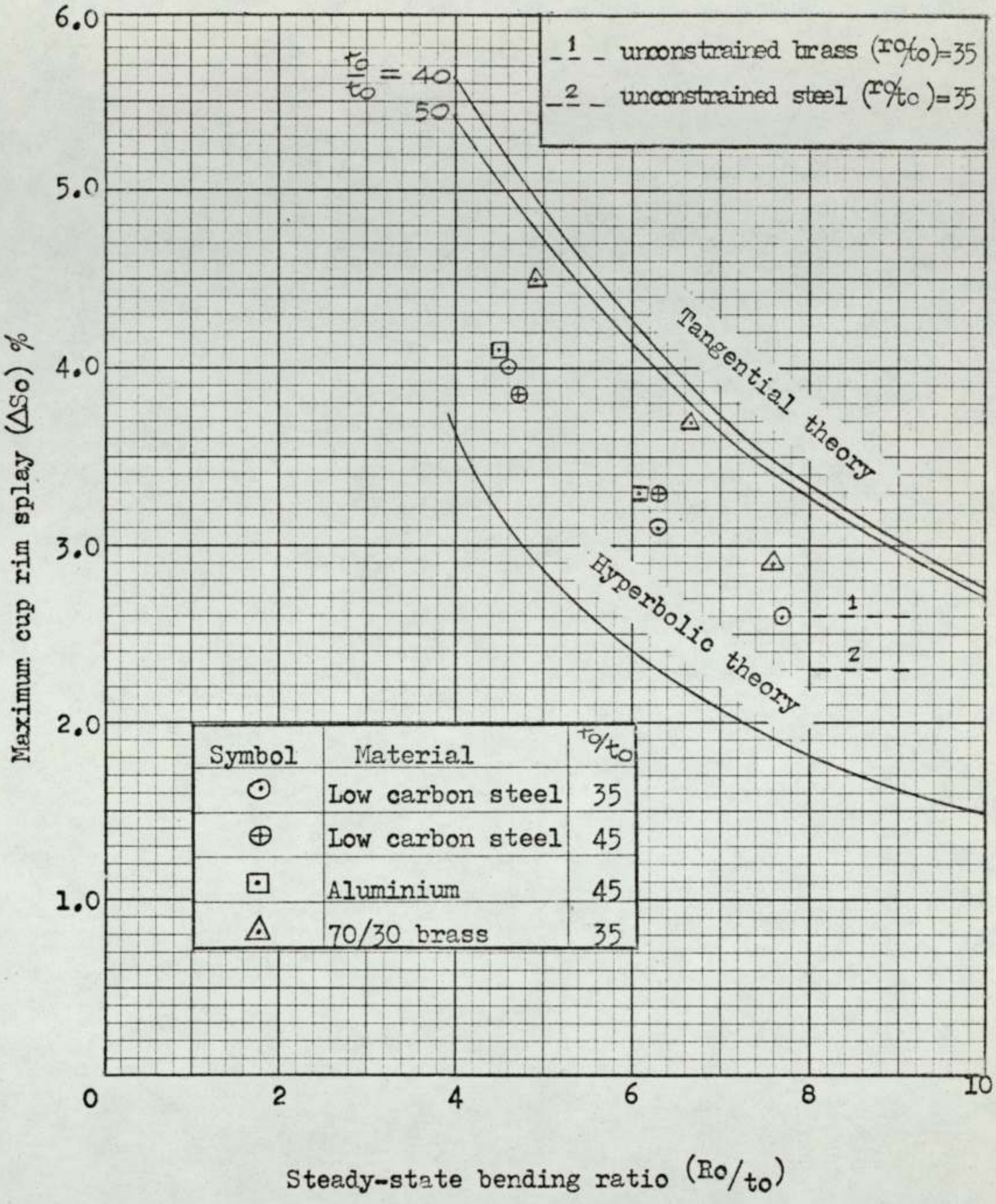

FIG. 197 EXPERIMENTAL/THEORETICAL CORRELATION FOR MAXIMUM SPLAYING. PROVING TESTS - AS-DRAWN CUPS.

Test number	2P
Cup material	Aluminium
Cup condition	As-drawn
Cup dimensions (in.)	3.250 $^{o}/_{d}$ x 0.036th.
Die semi-angle (deg.)	90
Hold - down punch radius (in.)	0.180

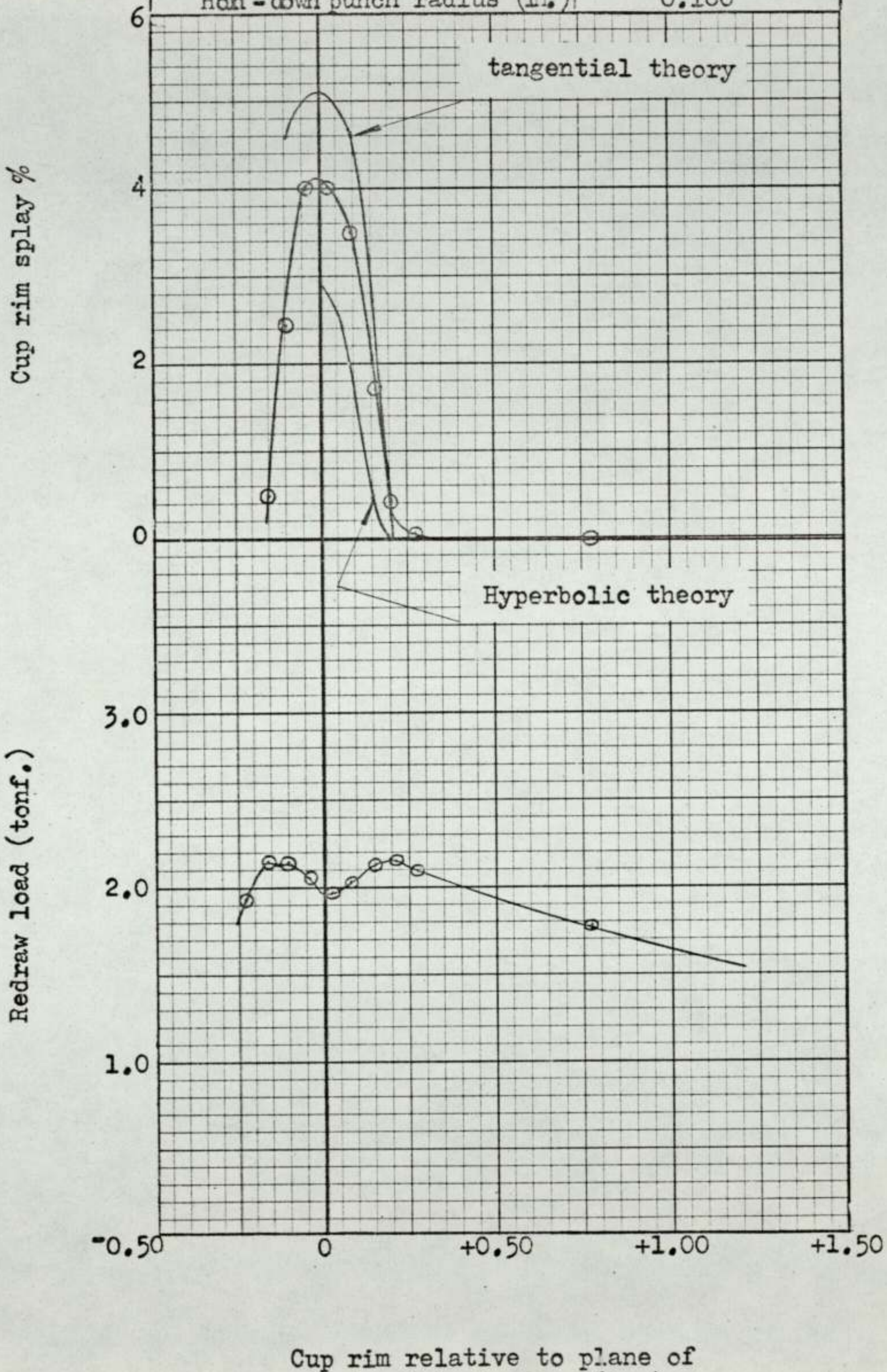

FIG. 198 SPLAY LOCUS OF CUP RIM
EXPERIMENTAL/THEORETICAL CORRELATION

aluminium more closely approached the theoretical perfectly plastic condition than either of the other two proving-test materials. Even so the load curve rose steadily throughout the redraw although this was no doubt partly due to the increase in wall thickness near the cup rim.

The general form of the locus predicted by theory was reasonable, particularly for the position of the maximum splay point. With test 2P the experimental locus lay mid-way between the theoretical hyperbolic and tangential loci.

12.3. Effect of work-hardening.

Experimental results are given in FIGS. 175 - 182. Steel showed the theoretically predicted trend that splaying increased as the rate of work-hardening diminished. With the 0.180 and 0.250 in. hold-down punch nose radii splaying in annealed and as-drawn cups was 3.5 %, 3.9 % and 3.0 %, 3.3 % respectively. The trend with aluminium (which had a lower rate of work-hardening) was less marked, and in fact splaying was marginally greater with annealed cups, 4.3 % against 4.1 % and 3.4 % against 3.3 % for the 0.180 and 0.250 in. radius hold-down punches.

13. DISCUSSION OF RESULTS OF RESEARCH

13.1. Experimental test programmes

(a) Simulated redraw tests.

The tests were designed to show whether or not radial drawing prior to die contact during steady-state redrawing conditions could contribute to subsequent splaying behaviour. Although the tests failed to supply the required information the failure was, in retrospect, considered due to deficiencies in zone simulation rather than the test concept being fundamentally wrong. Problems of simulating true metal flow were encountered by Swift[41] in the wedge drawing test, and in some respects the attempted redraw simulation was a more complex version of this test.

The only immediately obvious deficiency in simulated die-block design was that flat test-pieces were drawn whereas a true circumferential segment of the cup wall is curved. As a result of this design feature the side pressure exerted on the test-piece by the deformation passage had an associated component tending to promote bending over the test-piece cross-section. This caused the side curling effect observed in test-pieces drawn in the absence of the hold-down clamp. The situation was aggrevated by the width/thickness ratio of the test-pieces and would probably have been less severe with a lower ratio. However such a step would have violated the required plane-strain bending/unbending condition. Theoretically there could have been no 'curling' component if the central element of the die-block had been curved. Unfortunately such a design introduces manufacturing problems.

Later theoretical studies indicated that splaying could be wholly accounted for in terms of bending work, implying that the radial drawing zone contributed nothing to the splaying effect.

(b) Splay-measurement tests.

An outstanding feature of the programme was that tubular test-pieces were pulled through the die by an external gripping mechanism, in contrast to cups being redrawn with an internal punch. This divergence from the popular concept of redrawing in no way affected the fundamental deformation mode, and therefore splaying occurred under truly representative conditions. From an experimental aspect the adopted procedure had definite advantages both in test-rig design simplification and interpretation of test data. The test-piece properties of uniform geometry, uniform condition of prior cold-work, and absence of planar anisotropy, enabled the effects of splaying on redraw load to be readily observed.

The precise speed and positional control features designed into the testing machine made it well suited for incrementally drawing the test-piece into the die during splay-measurement tests, but the method devised for measuring splay profile development proved tedious, each test being of three hours duration and involving some 250 individual readings. Throughout the programme about 18,000 readings were taken with the splay-measuring head, which remained reliable to an accuracy of 0.0001 in. Originally it was intended to operate the redraw load-cell at a maximum strain of 0.1%, but due to a general under-estimation of redraw loads the unit was actually used at 0.15% strain in some tests. This did not adversely affect its reliability. The displacement transducer used for monitoring the test-piece rim position and its method of coupling both gave satisfactory performance during redraw load/test-piece rim displacement tests. Recalibration was straightforward and readily carried out with the transducer in its normal operating position. The hold-down punch assembly used the 'constant clearance' system for simplicity, and did not incorporate a means of measuring hold-down force. Effectiveness of hold-down was judged by the condition of the redrawn test-piece. Although this may appear to be a somewhat crude method, the object of the exercise was to observe the effect of splaying on redraw load, not the effect of hold-down load. Providing the latter remained constant throughout a redraw and gave freedom from wrinkling its precise magnitude was considered relatively unimportant.

The splay measurement programme was designed to provide ;

Information on (1) The mechanics of splaying.

(2) The relationship between splaying and process variables.

(3) The effect of splaying on redraw load.

(4) The effect of a guide-ring on redraw load.

(5) The validity of Fogg's free-zone theory.

and (6) A basis for theoretical studies.

To a large extent all of these objectives were realised. Experimental findings are discussed below.

(1) <u>The mechanics of splaying</u>

A range of test-piece $^{t_0}/_{t_0}$ values were covered in the unconstrained programme and the general trend emerged that splaying occurred earlier in a redraw as the $^{t_0}/_{t_0}$ ratio diminished. Also, a similar trend existed between the maximum splay point and $^{t_0}/_{t_0}$ ratio. A further, less marked, trend was that splaying appeared to occur slightly earlier with cold-worked test-pieces than with annealed ones.

In the constrained redraw programme, where the test-piece deformation geometry prior to die contact was fixed, the position of maximum rim splay always closely approached or coincided with the plane in which the test-piece first bent to the hold-down punch nose radius during previous steady-state redrawing. A similar situation was anticipated, though not investigated, for the unconstrained programme where the true position of the plane of steady-state bending was less certain.

During the early stages of splaying the splayed profile comprised a curve, with curvature decreasing rapidly towards the test-piece rim. As splaying progressed the curvature became less and the profile at maximum splay appeared very nearly of conical form.

For the thinnest walled test-pieces redrawn in the unconstrained programme splaying continued as the rim approached the die until, in a further small increment of travel, the rim suddenly wrinkled. Whilst the rim was splaying it carried a tensile circumferential stress which could not induce wrinkling. It was therefore surmised that the point of wrinkling coincided with the termination of the splay-phase when the test-piece rim commenced to radially draw inwards.

(2) Relationship between splaying and process variables

Fogg's theory of free-zone geometry[11] assumed that a cup deformed to a circular arc prior to die contact when redrawing without hold-down, the radius of the arc being a function of cup geometry, die geometry and cup wall thickness. Since the magnitude of this radius was considered important to splaying, tests in the 'unconstrained' programme were aimed at investigating the separate effects of test-piece radius/thickness ratio r_o/t_o and die semi-angle α . The former was varied over the range 10 - 30 (five levels), and the latter over the range 30 - 90 degrees (four levels). For the two lower die angles, 30 and 45 degrees, the true angle of die contact was that of the conical die mouth for all levels of r_o/t_o investigated. It was found however that for die angles above 45 degrees the true angle at which test-piece first contacted the die was less than the die angle, and never exceeded about 60 degrees. The true contact angle depended upon test-piece r_o/t_o ratio, being largest for the thinnest test-pieces. This situation not only limited the experimental range, but also meant that true die angle could not be studied as an independent function. (It was obviously meaningless and wrong to analyse results in terms of the manufactured die angle.) Experimental results of maximum splaying at the test-piece rim are plotted against test-piece geometry r_o/t_o in FIG. 159. (The family of curves are drawn from theory and should for the present be ignored.) The inter-relation of true die-angle and test-piece radius/thickness ratio made clear-cut trends difficult to establish. It was apparent however that generally splaying increased as r_o/t_o decreased, and as true die angle α increased. According to Fogg's free-zone theory this is equivalent to stating that splaying increased as the free bending ratio R_f/t_o decreased. Maximum splaying measured was about 3½% and occurred with brass. FIG. 159. was plotted for test-pieces with nominally 50 and 67% prior cold work.

In the constrained programme splaying was studied as a function of the bending ratio R_o/t_o around the hold-down punch nose profile radius. Only two levels of test-piece r_o/t_o were investigated, nominally 40/1 and 50/1. A 90 degree semi-angle die was used throughout but calculated angles of true die contact were in the range 70 - 75 degrees, depending upon the value of the hold-down punch nose radius. Test results are shown in FIG. 158, where for the present the theoretical curves are ignored. For all four materials investigated splaying increased as R_o/t_o decreased, reaching a maximum of about $3\frac{1}{2}$%. Results were therefore qualitatively in agreement with those in the unconstrained programme. It is interesting to compare results from the two programmes (FIGs. 158 and 159) and note that by increasing bending severity with a hold-down punch, splaying in a test-piece $r_o/t_o = 50$ could be substantially increased above that predicted by extrapolating unconstrained results. The parameter r_o/t_o did not appear influential in the constrained programme results, but only two levels were investigated giving a restricted range.

Results from both constrained and unconstrained programmes showed that splaying was more severe in test-pieces with prior cold-work than in those annealed before redrawing. The effect was most pronounced in stainless-steel and brass and was apparently related to the materials work-hardening characteristics. After 50% prior cold-work all materials splayed about the same amount for the same redrawing conditions. (FIG. 138). The likelihood of failures in splaying must increase as the prior cold-work content increases (due to limited material ductility). Experimental evidence suggests that in such conditions splaying will attain a maximum value.

(3) <u>Effect of splaying on redraw load</u>

The variation in redraw load accompanying splaying was thoroughly investigated for two reasons. Firstly, the load directly affects process limits and press requirements. Secondly, but even more important in the current research, it provided a valuable guide to any changes in process work. Swift[1] concluded that splaying caused an increase in redraw load, implying an increase in process work, but preliminary theoretical studies by the writer had led to the belief that splaying was associated with a decrease in process work. It was therefore vital to establish the effect of splaying on redraw load early in the research programme.

Results from the unconstrained programme are shown in FIGs. 80 - 111. For all 32 tests conducted the onset of splaying occurred simultaneously with a reduction in redraw load. The trend was unmistakable for up to that point redraw load was steady, a tribute to the uniform test-piece qualities. As the splaying phase progressed, the redraw load continued to fall, until at or very near the maximum rim splay point there was an abrupt change in the load characteristic for 91% of test-pieces redrawn. With 28% of these there was a short dwell where load remained constant before again reducing as the rim commenced to draw inwards. With the other 72% the load curve showed a small secondary peak, the crest of which was always below the steady-state load. Reduction in redraw load during splaying was of the order 8 - 10% whilst the peak (where present) was on average 1/5 - 1/3 of this value. The position of the load point immediately before the dwell or secondary peak was compared with the maximum splay point. For 62% of the tests the two points coincided, for 34% the load point just preceded the splay point, and for 4% it occurred immediately afterwards. The 9% of tests which did not show a load irregularity mainly comprised 0.0125 in. wall test-pieces drawn through 60 and 90 degree dies. With these, the thinnest drawable in the programme, there was a tendency for the rim to wrinkle following the splay-phase. This was accompanied by a rapid fall in the load curve.

Results for the constrained programme are shown in FIGs. 112 - 135. Again, for all 24 tests, the onset of splaying accompanied a fall in redraw load which continued throughout the splay phase. At or very near the maximum splay point 92% of the tests showed an irregularity in the load curve. For 67% of these tests the irregularity took the form of a short dwell, whilst for 25% a small secondary peak was present. This peak was generally small and little more than a dwell. 8% of test-pieces drawn showed neither dwell or peak. A comparison was made between the position of the maximum splay point and that of the minimum load attained immediately before dwell or secondary peak. For 87% of the tests the two points co-incided, with 9% the minimum load occurred just before the maximum splay point, and for 4% it was just after. Since splaying was clearly associated with a fall in redraw load an attempt was made to correlate the two effects on a quantitative basis. It was found that minimum splay values coincided with minimum load reduction and maximum splaying values were accompanied by the largest reductions in redraw load. Intermediate results showed considerable scatter.

Throughout any test in the splay-measurement programme drawing speed was constant. The fall in load measured at the test-piece tag can therefore be viewed as a fall in external (testing-machine) work, which must be equal to a fall in deformation work within the test-piece. It was clearly demonstrated in the tests that a definite correlation existed between redraw load reduction and splaying. Therefore it follows that splaying was associated with a fall in process work. This finding marked an important stage in the overall research programme since it confirmed initial ideas on splaying (whilst refuting contrary claims of other investigators) and provided a sound basis for the development of splaying theory. The majority of tests drawn in both unconstrained and constrained programmes showed a load irregularity at or very close to the maximum splay point. At this point the splay phase must end, and circumferential stresses near the test-piece (or cup) rim must suddenly change from tensile to compressive. The load irregularity was viewed as a manifestation of this change.

(4) The effect of a guide-ring on redraw load

Experimental results from this part of the programme were not so informative as expected. A testing problem arose because test-piece diameter varied with different materials and diameter/thickness ratio (table A_3.2). This lead to a variation in the constraint exercised by the guide and the point in the redraw cycle at which it became operative. Originally the guide was made with a 0.7525 in. diameter bore and gave 0.0040 in. maximum, 0.0025 in. minimum diametral clearance on aluminium and steel test-pieces, but was in interference with some stainless-steel and brass test-pieces. To overcome the problem, steel and aluminium were drawn in the unconstrained programme with the original guide bore, which was afterwards increased to 0.755 in. diameter to accommodate stainless-steel and brass. Clearances for these materials were then 0.0035 in. maximum, zero minimum respectively. The 0.755 in. guide was later used for all guided tests in the constrained programme.

In the unconstrained programme 14 unguided-guided test comparisons were made. Of these, during steady-state redrawing, in 8 tests the guided load was higher, in 3 tests guided-unguided loads were equal, and in the other 3 tests the unguided load was slightly higher. This last result is difficult to explain and can only be accounted for in terms of a variation in lubrication between guided and unguided specimens, although this seems unlikely. During the terminal stages of redrawing, when the guide became effective, certain differences between the characteristics of guided and unguided load curves were observed. In suppressing splaying the guide deferred the point in the redraw at which the load commenced to fall. However once initiated a load reduction comparable to that in unguided tests occurred, and was an indication that some relaxation of the steady-state constraint was occuring within the guide.

A further problem was encountered in assessing results from the constrained redraw programme since it could not be guaranteed that equal hold-down loads were applied in guided and unguided tests. This explained why in some tests steady-state redraw loads were highest in the unguided condition. The deferring effect of the guide on load reduction was even more clearly demonstrated in the constrained tests. Also, there was evidence of a slight bulge in the guided load curve corresponding to a point in the redraw where splaying would normally have commenced. This was taken to be an indication that the guide had become operative, and was exerting a frictional resistance to drawing of the test-piece into the die.

On theoretical grounds it was anticipated that the use of a guide would increase maximum redraw load. Theoretically, if splaying is completely prevented the redraw load cannot be less than the steady-state unguided load, and due to friction in the guide it will probably be higher. The guided tests were insufficiently conclusive to firmly support this theory but alternatively there was even less evidence to support Swift's claim that guiding reduced redraw load.

(5) Free-profile measurement

Test-piece deformation profiles were measured in the unconstrained programme to check the validity of Fogg's theory.[11] The work was important because free-zone geometry predicted by Fogg had direct theoretical implications to splaying. Fogg assumed that free-zone deformation would occur along a circular arc. Experimental evidence suggested that free-zone curvature is not truly constant, although this was very nearly so with test-piece $^{r_o}/_{t_o}$ values of 20 and 30. Below 20 a mean radius drawn through the experimental points was above points at die entry but below points at die exit, suggesting that curvature increases progressively throughout the zone. Qualitative predictions of Fogg's theory were found to be correct; for a constant die angle the free radius ratio $^{R_f}/_{t_o}$ increased as $^{r_o}/_{t_o}$ increased, and for a constant $^{r_o}/_{t_o}$ ratio $^{R_f}/_{t_o}$ decreased as the die semi-angle increased.

The exact theoretical/experimental correlation is discussed later in the section.

(c) Proving tests

The simple, open-type construction of the Hi-Ton press proved well suited for installation and operation of the experimental test-rig. However a problem, already discussed at some length in section 11.7, existed in controlling press ram speed, and occurred because primarily the press was designed for load control rather than speed control. To maintain a smooth, reasonably constant drawing speed the main flow control valve was held fully open during a test and the speed of ram advance finely adjusted by a pressure relief valve. This procedure was straightforward with annealed and as-drawn aluminium cups, but gave problems when redrawing as-drawn steel and brass cups (especially the latter), where redraw load increased sharply in relation to length of cup redrawn. It was found possible, after experimentation, to set the initial ram speed so that the press did not stall mid-way through a redraw. Even then ram speed dropped to about one half its initial value just prior to splaying. When splaying commenced the fall in redraw load was apparent from the increase in ram speed. Although variations in speed were undesirable, splay-measurement was conducted while the cup was static. For this test therefore redraw speed was of little consequence. The variation in speed during a continuous load-measurement test was about 6 - 2 in./min. overall, but during the actual splay-phase speed variation was much less than this.

The test-rig performed satisfactorily throughout the programme and gave ready access for tool changes and experimental observations. It was found however that hold-down pressure, as monitored by the pressure transducer, was rather sensitive to the rate at which fluid was expelled from the hold-down cylinder, and therefore to the press ram speed. During tests on as-drawn cups hold-down pressure gradually decreased as press speed of advance decreased, and then increased again as the ram accelerated during splaying and final drawing-in stages. For this reason hold-down data given in table $A_4.9$ comprises a range rather than a single figure. The load-cell and pressure-transducer functioned without complications throughout the programme.

The proving-test programme was designed to check that 'splay-measurement' programme results were applicable to real cups and that theories of splaying were valid for conventional cup redrawing arrangements. Experimental results from the proving-tests are discussed below in comparison with those from the earlier 'splay-measurement' programme, but first the major differences between the two programmes are recapitulated.

(i) The splay-measurement programme was conducted on tubular test-pieces pulled through the die by an external gripping device situated below the die, whereas proving tests were carried out on real cups drawn through the die by an internal punch with drawing force applied above the die. Apart from the difference in draw force application the two processes were identical from a metal deformation aspect and splaying behaviour should therefore also have been the same.

(ii) There was an appreciable difference in scale between test-pieces drawn in the two programmes. Splay-measurement programme tests were conducted on test-pieces 0.750 in. diameter and 0.0075 - 0.0375 in. wall thickness, whereas proving tests were on cups roughly 3.2 and 2.5 in. diameter and 0.044 in. thick. However test-piece and tooling variables were investigated in terms of non-dimensional parameters, i.e. $^{r_0}/_{t_0}$, $^{R_0}/_{t_0}$, ΔS_0 , and therefore no scale effect was anticipated.

(iii) Splay-measurement test-pieces were of uniform prior cold-work and wall thickness throughout their length, but in proving-test cups prior cold-work and wall thickness increased with distance from cup base. In consequence the test-pieces gave a constant steady-state redraw load whereas with cups the load increased steadily throughout the redraw.

(iv) The method of hold-down application was different in the two test programmes. For splay-measurement tests the 'constant clearance' method was used, but in proving tests 'constant pressure' hold-down was adopted. Provided hold-down was effective with both types there was no reason to believe that splaying behaviour should be different.

(1) Relationship between splaying and process variables.

In the proving-test programme splaying was studied primarily as a function of hold-down punch nose radius bending ratio R_o/t_o . The experimental correlation is shown in FIG. 197. For all three materials tested the previous 'splay-measurement' programme trend was confirmed in that splaying increased as R_o/t_o diminished, that is as the bending ratio became more severe. Maximum splaying with brass was greater than that with steel or aluminium. A ready explanation for this is that the elastic component of splaying was highest with brass. However in such an instance similar results would be expected in the 'splay-measurement' tests but there brass exhibited no more splaying than the other materials tested, (FIG. 158). Another possible explanation for the high brass points is that the lower r_o/t_o used for brass influenced splaying, but this argument is nullified by results with steel where no appreciable splaying difference existed for cups of nominal r_o/t_o = 35 and 45. Generally splaying measured in the proving-tests was $\frac{1}{2}$% greater than that in the 'splay-measurement' programme, even discounting the results with brass. Although this discrepancy is small in absolute terms it represents a significant proportion of splaying (10 - 20%) and therefore warrants explanation. A possible cause is that the true proving-test r_o/t_o values measured near the cup rim were lower than those in 'splay-measurement' tests, 37 and 29 against 50 and 40, (theory predicted this type of trend), but in view of the small influence of r_o/t_o within the proving-test programme this explanation, by itself, appears doubtful. There is reason to believe that at the very rim of a redrawncup prior cold-work is less than at points just lower down the wall, because in previous drawing operations the rim has undergone no bending,and although it may have splayed the work of splaying is less than that of steady-state bending/unbending. If the splaying in such a cup were compared with that in a uniformly cold-worked test-piece (for example a drawn tube), it might be expected that splaying would be greater in the former. However this argument is not really justifiable for the proving tests because the true cup rim was removed by trimming before redrawing. It would seem that the differences in splaying observed over the two programmes must be partly due to differences in experimental techniques but it is not obvious why this should be so. Greater accuracy of splay measurement might be expected with the larger cup diameters but there was no reason to doubt the accuracy of readings from the splay-measuring head. In any event inaccuracies in readings would produce experimental scatter rather than the unilateral effect observed.

The proving tests demonstrated that when splaying was allowed to reach its maximum value freely, die angle was not an influencial parameter in deciding the extent of the splaying. True die contact angle with redraw I was almost 90 degrees with a 90 degree die, whereas the true angle on redraw 2 with a 90 degree die was only about 60 degrees. This difference in true contact angle was not reflected in maximum splay values. However when the 45 degree redraw 2 die was used in conjunction with the smallest hold-down punch radius, maximum splaying was clearly prematurely interrupted by the die mouth, (FIGs. 189 and 190). When this die was used with the larger hold-down punch radius the cup rim did not contact the die mouth, until after maximum splaying occurred. Thus a small die angle will always tend to limit maximum splaying even though it does not directly influence the potential for splaying.

The effect of prior cold-work on splaying was not conclusively demonstrated in the proving-tests. Steel followed the 'splay-measurement' programme trend.that splaying increased with prior cold work, but for aluminium, annealed cups splayed marginally more than as-drawn ones. However the difference was slight, 4.3% against 4.1% and 3.4% against 3.3% for the two hold-down punch radii investigated in redraw I. A great variation between annealed and as-drawn results would not be anticipated for aluminium due to its low work-hardening rate. When proving-test results are taken in conjunction with those from the 'splay-measurement' programme the balance of evidence suggests that splaying increases with degree of prior cold-work.

As-drawn cups in each of the three proving-test materials were redrawn in the untrimmed condition and results compared with those for trimmed cups. Unfortunately full length brass cups could not be redrawn successfully, but the degree of earing with brass was negligible and therefore results similar to trimmed cup results would be expected. Aluminium exhibited a slight earing pattern, whilst steel cups showed four pronounced ears. Splay measurements on aluminium cups were made as for trimmed cups since the earing pattern was not diametrically symmetrical. Steel cups exhibited almost perfect earing symmetry and splay measurements were made across diameters corresponding to ears and valleys. For aluminium, splaying in untrimmed cups was less than that in trimmed cups, 3.3% against 4.1%, but the start of splaying and position of maximum splay point were similar for both cups, (FIGs. 176 and 184). Results with steel cups were more complicated but strikingly alike for both sizes of cups drawn. Splaying over the ears was above 6%, whilst that measured in valleys was about 3.2%. By comparison splaying for both trimmed cup sizes was 4%. Apart from maximum splaying attained, trimmed cup splay loci showed close resemblance to those measured in the valleys of eared cups (compare FIGs. 175 with 183, and 185 with 193). If splaying is defined as an increase in circumference then clearly that measured at ear crests (6%) cannot be regarded as true splaying, but conversely the ears do appear to exert a constraining influence on splaying in intermediate valleys. Otherwise, splaying in these valleys would be equal to that in trimmed cups, not less. If the ears do offer additional constraint it follows that in part (near the root) they must experience a true splaying strain greater than that measured in the valleys.

(2) Effect of splaying on redraw load

As anticipated the inherent rising redraw load characteristic complicated a study of the effects of splaying. Even so results were sufficiently informative to elucidate important trends and confirm 'splay-measurement' programme findings. For 20 out of 21 tests conducted the start of splaying was associated with a fall in redraw load. In the other test the load remained constant. Load characteristics were similar to those in the 'splay-measurement' programme but where present the secondary peak was higher, reflecting the non-uniformity of wall thickness and prior cold work. However the maximum redraw load was in no case higher than that given by extrapolating the steady-state load curve over the splay range. Experimental evidence suggested that the point of maximum splaying occurred at or very near the point of minimum redraw load, and that during splaying the load fell continuously.

The presence of ears on cups did not affect the splay-redraw load correlation.

(3) Effect of hold-down punch profile on redraw load

Not only did the hold-down punch nose radius have a significant effect on splaying, it also influenced redraw load considerably. The effect of this parameter on load was similar to that of die profile radius (Chung and Swift)[5]. Although the general trend of results were as expected, the actual load variation which could be brought about by varying the hold-down punch nose radius was greater than anticipated. By increasing its magnitude from 0.180 in. to 0.250 in. on redraw I (90 degree die), the redraw load fell by 7% for both steel and aluminium cups. On redraw 2 the effect was even more pronounced; when the nose radius was increased from 0.180 in. to 0.253 in. (90 degree die) the load with steel fell by 14% while when the redraw was conducted free the load reduced by 26%. However this last result was also partly attributable to the removal of hold-down force. With the 45 degree die a load reduction of 12% was recorded when the nose radius increased from 0.180 in. to 0.317 in. Results with brass on redraw 2 were even more dramatic; cups 3 in. long could not be redrawn without fracture at the cup base using the 0.180 in. nose radius, but were redrawn successfully with the 0.253 in. radius.

(4) Effect of using a guide ring on redraw load

Results were generally similar to those in the 'splay-measurement' programme. The guide removed the falling load characteristic which would otherwise have accompanied splaying, but results for maximum redraw loads with and without the guide were not altogether conclusive. In three of the four unguided-guided comparisons made there was little difference in redraw load, while in the other comparison (FIG 177), the 'guided' load was lower. However in tests on aluminium cups, failure occurred consistently with the guide installed but successful redrawing was achieved in the unguided condition. No measurable difference in maximum load recorded with the two arrangements could be detected. This last result was interpreted that even in unguided conditions the redraw was very close to failure, and by introducing the guide extra friction, although slight, was sufficient to tip the balance.

Proving-test results when taken in conjunction with those from the 'splay-measurement' programme indicate that a simple guide ring of the type used in research will not greatly influence redraw load. There was no firm evidence to support Swift's claim[1] that guiding provided a load reduction, and indeed it seems that the reverse may be true. However any load increase due to guiding was small, and the positive advantage of preventing splaying renders its use desirable in redraws where splaying proves troublesome. On a practical basis it could be argued that redraws in which a correctly designed guide ring promotes failure are too close to critical conditions even for unguided redraws.

13.2. Theoretical results

The concept that splaying was associated with a reduction in process work was used throughout theoretical studies, either directly in deriving expressions for splaying or indirectly to check that any proposed splay mode was admissible. In analysing splaying the investigator is confronted by two major problems. Firstly the process is essentially one of non steady-state where the deformation zone geometry is continuously changing (as in cupping) and secondly, the geometry at any instant is unknown (unlike cupping). Analysis is further complicated by the fact that bending plays a major role in splaying and elastic spring-back must occur as constraint of the entering cup gradually diminishes. To overcome these obstacles certain assumptions were made in developing theory, the justification of which may only be found in correlations with experimental evidence. The theories provide an insight into the way in which process parameters influence splaying, and enable its magnitude to be predicted for a given set of conditions. In this respect they are considered valuable.

The three theories of splaying proposed, simple upper-bound, tangential and hyperbolic represent the development of ideas on the problem. As a result the last theory is most rigorous and attempts to account for all individual deformations which describe splaying.

Throughout the work a rigid-plastic material was assumed to avoid problems of elastic deformation. This assumption is frequently made in plasticity studies but usually plastic strains are large compared with elastic strains. In splaying the assumption is less valid, and this criticism may certainly be levelled at the theory. However errors involved are probably no greater than in other assumptions. For example that in work-hardened steel would be about 5%. Furthermore, if required, allowances can easily be made for the elastic component of splaying.

(a) Simple upper-bound theory

The theory was developed primarily to test the validity of an 'energy' approach to the splaying problem, rather than to supply quantitative information relating the phenomenon to process parameters. By examining work terms in steady-state and splayed modes it was possible to predict, very simply, an upper limit for splaying, and avoid the complications earlier encountered when following an 'equilibrium' approach. The theory also indicated which process parameters were likely to most influence splaying.

An objection to the theory is that rim elements were considered in isolation from the remainder of the splayed cup wall. In truth deformation lower down the wall would, by constraint, set a limit on rim splaying.

(b) Tangential theory

For a rigid-plastic material no bending can theoretically occur unless the applied moment is sufficient to make the whole section plastic. The tangential theory was based on this concept. It was assumed that when the entering cup wall diminished below its shortest length capable of supplying the fully plastic bending moment no further bending would occur. Instead the cup would splay tangential outwards. Knowing the length of cup wall involved, expressions relating splaying to process parameters were derived. Maximum rim splaying was less than that given by the simple upper-bound theory, in other words the work involved by rim elements in splaying according to the assumed tangential mode was less than that in steady-state cup wall elements. With tangential splaying the rim must receive greater work of deformation than splayed elements lower down the wall. It therefore follows that these elements also receive less work than steady-state ones. The theory implies that the cup geometry ratio $^{r_o}/_{t_o}$ influences splaying even when the pre-die contact zone is independently fixed (FIG 146).

For a given cup there is reason to anticipate that the tangential theory provides an upper limit to splaying, since if any bending occurs in elements passing through the splay-zone its effect must be to reduce their splaying. This does not necessary mean that the total work undergone by the elements would also be reduced. Experimental observations lead to the belief that during the early part of the splay-phase some bending did in fact take place.

The admissibility of the tangential theory was investigated by comparing work of deformation with that in steady-state redrawing for the same increment of punch travel. Results for the particular redraw arrangement $^{r_o}/_{t_o} = 50$, $^{R_o}/_{t_o} = 4$ are presented in FIG 148, and demonstrate clearly that tangential splaying requires less work. The upward curving trend of the steady-state work is due to an increase in the specific radial-drawing work component, the specific bending component at die entry being constant. Bulk work of splaying W_s approaches a maximum level before maximum rim splay is attained, (i.e. when $W_{s_1} = 0$). This situation arises because the bulk work is a product of splaying in individual elements and the amount of cup wall currently splaying. Elements not currently splaying must by definition be radially drawing inwards. Consequently the bulk radial-work component W_r increases gradually throughout the splay phase.

The work curves of FIG. 148 provide a useful guide to the effect of splaying on redraw load. Suppose, for example, that a particular curve was of constant gradient $\frac{dW}{d\theta}$. This would mean that work only increased with the volume of material which has undergone deformation (represented by θ) and that drawing stress was constant with θ. A good example of this is the work component of steady-state bending at zone entry. By a similar argument it follows that if $\frac{dW}{d\theta}$ decreases as θ increases the drawing stress at θ must be also decreasing. Since this situation is true for total work of tangential splaying a reduction in punch load would be expected to accompany splaying. This was found to be the case in experiments.

(c) Hyperbolic theory

The theory takes account of bending observed to occur in the early stages of splaying, and which was ignored in the tangential theory. In developing the theory it was assumed that a hyperbolic relationship existed between the current radius of bending of an element in the splay-zone and its distance from the cup rim. Furthermore, unlike the tangential theory, it was proposed that the specific work of elements would increase proportionally to their distance from the cup rim. Expressions for maximum rim splay were then deduced for the special condition that at the rim, rate of change of specific work with respect to splayed wall length was zero. The theory used a more fundamental approach to the problem than the tangential theory but a number of unavoidable assumptions are open to criticism. There is good reason to believe that bending work was over-estimated in elements near the cup rim due to the rigid-plastic material assumption. This is strictly only valid when the radius of bending is sufficient to produce fully plastic strain across most of the bent section. Such a situation would occur when the current radius of bending R was close to that of steady-state bending R_o, but inaccuracies would arise when R increased towards infinity at the cup rim. The arbitrary assumption made in deducing radial rim splay S_o from its derivitive $\left(\frac{dS}{dl}\right)_{l=0}$ could only be justified by a subsequent investigation of process work, and by correlation with experimental evidence.

Splaying predicted by the hyperbolic theory (FIG. 151) was less than that given by the tangential theory, but general trends regarding process parameters were similar. This result was not unexpected as the latter theory represented maximum splaying possible for the predetermined cup wall length involved. Hyperbolic splaying was approximately one-half of that predicted by the simple upper-bound theory.

Bulk work analysis for the hyperbolic mode was complicated by the curved non steady-state nature of the post-splay radial drawing zone. By making certain geometrical approximations work expressions were derived for each associated deformation component. These are shown graphically in FIG. 155 for the particular arrangement $^{r_o}/_{t_o} = 50$, $^{R_o}/_{t_o} = 4$, where the theory is seen to be admissible from a work aspect. The bending component W_b predominates and makes total work W greater than that in tangential splaying even though the actual splaying work is less. During the splay-phase redraw load (represented by $\frac{dW}{d\theta}$) falls slightly as θ increases but just before termination of splaying it appears to increase. It would be imprudent to draw general conclusions from a single result, but this type of load trend (i.e. a secondary peak) was observed in a number of experiments.

Since the tangential theory gave lower work of deformation than the hyperbolic theory it might, on first impressions, be concluded that the former more closely approaches true splaying behaviour. Throughout the splay-phase the principal of minimum work of deformation must be upheld. However the true splay profile at any stage will be such that for over each small increment of strain work is minimal. Any theory is only as good as its assumptions, and the rigid-plastic assumption almost certainly introduces less potential error with the tangential mode where bending was completely absent. It is possible that for a true elastic-plastic material a deformation mode including bending would provide less splaying and less bulk work than the tangential mode.

(d) Effect of work hardening

The hyperbolic theory was used to investigate the effect of work-hardening on splaying for an idealised linearly work-hardening material. Over the strain range associated with splaying this provides a reasonable approximation to materials with non-linear characteristics. At high strain levels the approximation becomes even better.

It was found that as the ratio, work-hardening rate/current yield stress increased, splaying diminished (FIG. 156). Theory therefore suggests that for normal engineering metals splaying will increase as the material becomes work hardened.

13.3 Correlation of theory and experiment

(a) Unconstrained redrawing

Splay theory indicated that bending geometry in the pre die-contact zone during steady-state redrawing was a potent factor affecting splaying behaviour. In unconstrained redrawing the zone geometry is not immediately known but may be found from an expression deduced by Fogg.[11] At the time of developing splay theory no comprehensive data were available to support Fogg's theory, and therefore tests were conducted. The results of these tests are compared with theory in FIG. 157, where the curved lines represent Fogg's free-zone expression. Generally theory over-estimated bending severity by about 10 - 20%.

All three splay theories predicted that splaying increased as the pre-die contact bending ratio $\frac{R_o}{t_o}$ reduced. By adopting Fogg's expression an over-estimate of splaying in unconstrained redrawing would therefore be anticipated. However the general level of splaying given by theory and experiment was reasonably in agreement (FIG. 159). Within experimental scatter no trend of a theoretical over-estimate could be distinguished, but this may have been partially obscured by the elastic component present in experimental results which would amount to about 0.1 - 0.2%. Even allowing for this the correlation lends support to the validity of theory.

(b) Constrained redrawing

Maximum rim splay results in the 'splay-measurement' programme for tubular test-pieces are given in FIG. 158, whilst results with cups in the 'proving-test' programme are shown in FIG. 197. Both sets of results were obtained for as-drawn material.

As anticipated the simple upper-bound theory over-estimated splaying. It did however predict the correct trend between splaying and steady-state bending ratio R_o/t_o .

Experimental points from both test programmes fell between hyperbolic and tangential theory curves. (The general trend for 'proving-test' points to be higher has been discussed earlier, and can only be attributed to the different experimental techniques used.) There were good grounds for believing that the tangential theory would over-estimate splaying, and this proved to be the case. However it appears that the hyperbolic theory under-estimates splaying. This could well be due to the high bending work component present in the latter. It would seem that actual splaying lies roughly mid-way between the two theories. Even so the bound provided is useful for predicting least and greatest splaying likely to be encountered in a given redraw arrangement.

(c) Locus of cup rim during splay-phase

When developing expressions for bulk work in tangential and hyperbolic splay modes it was first necessary to determine how the splayed cup wall deformed during its passage towards the die. Theoretical and experimental cup rim loci are compared in FIG. 160 and 198 for the two experimental programmes. The expression for predicting splaying onset was common to both tangential and hyperbolic theories. Consequently theoretical loci start from a common point, which is slighly retarded from the actual (experimental) start due to the assumption of a rigid-plastic material. Splaying ends and radial drawing commences when the plane of steady-state bending is reached. Experimental/theoretical correlation for the form of the splay locus is reasonable, particularly for the point of maximum splaying.

(d) Effect of work-hardening

In both experimental programmes the trend was observed that splaying was greater with prior cold-worked test-pieces (or cups) than with annealed ones. The effect was most noticeable with materials of a high work-hardening rate, and therefore could at least be partly attributed to the elastic component of splaying. To investigate if plastic material properties influenced splaying,theoretical studies were made by modifying the hyperbolic theory to include a linear work-hardening term. Theory predicted that even for a rigid-plastic material splaying would reduce as the parameter work-hardening rate/current yield stress increased (FIG. 156). This parameter reduces as prior cold-work increases for most common materials, including those used in the experimental programmes, and therefore theory explained the observed trends.

13.4. Fracture arising from splaying

The test programmes were deliberately planned to provoke a high degree of splaying in cups with a substantial prior cold-work content. It was anticipated, in view of earlier experience, that fracture was likely in some of the tool/work-piece combinations investigated. However no such results were attained. Maximum splaying was in the region of 4% and all cups redrawn were apparently capable of withstanding this circumferential tensile strain level.

A prime factor influencing splaying failure in actual production processes may well be the condition of the cup rim. It is not uncommon for wrinkling to occur in this region as the cup leaves the constraint of the blank-holder (in cupping) or hold-down punch (in redrawing) during the terminal stages of deep drawing operations. The wrinkles are frequently ironed out between draw punch and die-throat and so are not visible in the drawn product, but the additional strain introduced in the rim by first wrinkling and then ironing may weaken its resistance to splaying failure in following redrawing operations. Similarly any microscopic cracks present in ear valleys of anisotropic cups may form fracture sites when splaying occurs. By using tubular test-pieces in the 'splay-measurement' programme a uniform, defect-free rim was ensured, whilst in 'proving-tests' the trimming of cups to facilitate splay measurement may have unintentionally lessened the probability of splay fracture.

The research programme was concerned primarily with providing information on splaying behaviour. A considerable amount of knowledge, both experimental and theoretical, is now available for predicting levels of splaying likely to be encountered with various tool geometry combinations and cup properties. It now remains to develop failure criteria and so establish when splaying will attain a critical level in a given material.

Levels of splaying found in research were less than those expected after surveying what little previous information was available on the subject. It seems to the writer that if a cup or cup material is incapable of withstanding splaying strains it is generally in an unsuitable condition for redrawing.

14. CONCLUSIONS

1. The splaying phenomenon is associated with a reduction in process work and a corresponding decrease in redraw load from that of steady-state conditions.

2. Splaying behaviour can be explained in terms of conditions prevalent during steady-state redrawing prior to the commencement of splaying.

3. Splaying may be encountered in redraws of both the constrained and unconstrained type, although severe splaying is most likely to occur in the former.

4. The most influential parameter affecting the severity of splaying is the curvature of the cup prior to die contact during steady-state conditions.

5. Following from conclusion 4, when redraws are of the unconstrained type curvature is a function of cup and die geometry, (cup diameter/thickness ratio and die-angle). When redraws are of the constrained type, provided the mean radius of bending around the hold-down punch is less than the equivalent free radius, splaying is not strongly influenced by the cup diameter/thickness ratio.

6. Die geometry performs a complex role in influencing the magnitude of splaying.
With constrained redraws die angle does not affect the splay potential, that is the amount of splaying which would occur if splaying could progress unimpeded. If the die angle is small however it may physically restrict the development of

splaying. On this basis greatest splaying would be expected with dies of large angle.

With unconstrained redraws die angle may affect splaying two ways. Firstly it influences free-zone curvature and hence the splaying potential. Secondly, as for constrained redraws the die-angle may cause interruption of the splay-phase. On both counts splaying is likely to be greatest with large die angles.

7. Since splaying is associated with a reduction in redraw load, the use of a guide ring to prevent splaying cannot produce redraw loads less than those under splaying conditions. This premise was confirmed by redraw load measurements with and without a guide ring where it was found that the guide maintained the general redraw load trend to a later stage of the process.

8. Experiments with fully-soft and work-hardened materials have indicated that for similar conditions of redrawing the work-hardened materials splay most. Materials in this condition are also more likely to fracture as a result of splaying.

9. Within the range of process variables covered by the investigation maximum measured splaying has been of the order 4 - 4.5%.

10. Splaying is most severe with :

    (a) A small hold-down punch nose radius

    (b) A large die angle

    (c) Fully work-hardened materials

11. For redraws of the constrained type the hold-down punch nose radius/cup wall thickness ratio should be sufficiently large to prevent excessive splaying and unduly high redraw loads, but conversely if this ratio is too large there is a danger of the cup rim wrinkling during the final drawing-in stage. A reasonable compromise between these two extremes is a ratio of 5 - 6.

12. Theoretical studies of splaying behaviour have been carried out using an energy approach. Reasonable agreement was shown with experimental evidence.

13. Two theories are proposed for predicting splaying in fully work-hardened materials. The first or 'tangential' theory will always slightly over-estimate splaying whilst the second or 'hyperbolic' theory is closer to the majority of experimental evidence but appears to give a slight under-estimate. Experimental points in constrained redraw tests were found to lie within the bounds of the two theories.

14. An expression for splaying in unconstrained redrawing was obtained by combining the 'hyperbolic' theory with Fogg's theory of free-zone geometry. Correlation with experimental evidence is reasonable although Fogg's theory appears to over-estimate bending severity by 10 - 20%.

15. A theoretical study was made into the effects of work-hardening on splaying. Theory suggests that splaying increases as the ratio rate of work-hardening/current yield strength decreases, and is therefore qualitatively in agreement with experimental evidence (conclusion 8).

15. FUTURE WORK

The highest cup radius/wall thickness ratio redrawn in the experimental programmes was 50, whilst the actual range covered in constrained redraws was also limited (30 - 50). In industry it is common to redraw cups with a ratio up to 250. Additional work to extend the cup radius/wall thickness ratio range would be of value both in supplying further experimental data and checking theoretical predictions.

Research was confined to direct redrawing arrangements. There is however no reason to believe that splay results will not apply equally well to indirect redrawing arrangements. Tests are required to confirm this proposition.

Research has provided information on splaying behaviour. It was demonstrated conclusively that the phenomenon is associated with a reduction in redraw load. Therefore the only potentially detrimental effect of splaying is fracture at the cup rim. To determine when this situation will arise work is needed on fracture criteria. The circumferential stress system in the cup rim when splaying is one of uniaxial tension. It should be possible to arrange fairly simple tests on work-hardened cups to investigate their ability to withstand splay strains. Tensile tests on peripheral rim slivers may provide the necessary information or an even more straightforward test may be to flare actual cups with a well lubricated tapered plug.

16. ACKNOWLEDGEMENTS

The author wishes to make the following acknowledgements :

(1) To the board of directors of Tube Investments Limited for sponsoring the research, and to directors of the Steel Tube Division Development Engineering Department, especially Mr. G. R. Hall, for their assistance in launching the project and making available necessary facilities and equipment.

(2) To personnel of the development department of Accles and Pollock Limited, who found time to manufacture the tubing used in experimental work.

(3) To personnel of S.T.D. Services Limited Workshop who arranged for equipment manufacture, and whose willing assistance was appreciated throughout the project.

(4) To Dr. D. H. Sansome of the University of Aston in Birmingham for his efforts in getting the work started and for acting as project supervisor.

17. REFERENCES.

1. H. W. Swift and others "Deep drawing Research." Fifth progress report to Inst. Auto. Engs. 1940.

2. E. V. Crane. "Plastic working of metals and power press operations." John Wilay, 1938.

3. J. D. Jevons. "The metallurgy of deep drawing and pressing." Chapman and Hill Ltd. 1940.

4. G. Sachs. "Principles and methods of sheet metal fabricating." Reinhold Publishing Corporation, 1951.

5. S. Y. Chung and H. W. Swift. "Cup-drawing from a flat blank. Part I experimental investigation. Part II analytical investigation." Inst. Mech. Eng., January 1951.

6. D. A. Barlow. "The formability of aluminium alloys." Engineering, May 11, 1956.

7. J. Willis. "Deep drawing." Butterworths Scientific Publications 1954.

8. J. M. Alexander. "An appraisal of the theory of deep-drawing." Metallurgical reviews, 1960, Vol. 5, No. 19.

9. S. Y. Chung and H. W. Swift. "An experimental investigation into the redrawing of cylindrical shells." Inst. Mech. Eng., January, 1952.

10. S. Y. Chung. "Stress analysis of reverse redrawing of cylindrical chells." Sheet Metal Industries, May, 1951.

11. B. Fogg. "Theoretical analysis for the redrawing of cylindrical cups through conical dies without pressure-sleeves." Journal Mech. Eng. Science, Vol. 10. No. 2. 1968.

12. W. Prager. "Introduction to plasticity." Addison-Wesley, 1959.

13. W. M. Baldwin and T. W. Howald. "Folding in the cupping operation." Trans. A.S.M., 1947, Vol. 38, p. 757.

14. B. W. Senior. "Flange wrinkling in deep-drawing operations." Journal Mech. Physics Solids, 1956 Vol. 4. p. 235.

15. E. Siebel. "Hold-down force in deep drawing." Stahl und Eisen, January, 1954, p. 155.

16. W. Johnson and P. B. Mellor. "Plasticity for Mechanical Engineers." D. Van Nostrand Company Ltd., 1962.

17. R. Hill. "The mathematical theory of plasticity." Oxford, 1950. p. 317.

18. R. L. Whiteley. "The importance of directionality in drawing - quality sheet steel." Trans. A.S.M., 1960. Vol. 24, p. 154.

19. M. Atkinson and I. M. Maclean. "The measurement of normal plastic anisotropy in sheet steel." Sheet Metal Industries, April, 1965, p. 290.

20. R. T. Holcomb and W. A. Backofen, "An evaluation of anisotropy for drawability control by plane strain compression testing." Inst. Sheet Metal Eng. Int. Deep Drawing Research Group. Colloquium, London, 3rd. June, 1964.

21. G. G. Moore and J. F. Wallace. "The effect of anisotropy on drawability in sheet metal forming." Inst. Sheet Metal Eng. Int. Deep Drawing Research Group. Colloquium, London 3rd. June, 1964.

22. D. V. Wilson. "Plastic anisotropy in sheet metals." Journal Inst. Metals, 1966, Vol. 94. p. 84.

23. L. Lilet and M Wybo. "An investigation into the effect of plastic anisotropy and rate of work-hardening in deep drawing," Sheet Metal Industries, October 1964. p. 783.

24. B. Fogg. "The relationship between the blank and product surface finish and lubrication in deep-drawing and stretching operations." Sheet Metal Industries, February, 1967, p.95.

25. E. M. Loxley and P. Freeman. "Some lubrication effects in deep-drawing operations." Journal Inst. Petroleum, No.370, October, 1954, p.299.

26. J. F. Wallace. "Improvements in punches for cylindrical deep drawing." Sheet Metal Industries. December, 1960.

27. P. W. Whitton and D. R. Mear. "An investigation of Swift cupping test correlation and the influence of tool and material surface finish on the test results." Sheet Metal Industries, October, 1960. p. 743.

28. O. H. Kemmis. "The assessment of the drawing and forming qualities of sheet metal by the Swift cup-forming test." Sheet Metal Industries, March, 1957, p. 203.

29. S. Fukui and others, "The effect of surface roughness of sheet and tools on deep-drawability." Sheet Metal Industries, October, 1963, p. 739.

30. E. A. Evans, H. Silman and H. W. Swift, "Lubrication in drawing operations." Sheet Metal Industries, October 1947, p. 1995.

31. D. H. Lloyd. "Lubrication for press forming - 2." Sheet Metal Industries, July, 1963, p. 477.

32. D. R. Mear, H. H. Topper, and D. A. Ford. "The use of organic polymers as lubricants in deep drawing." Sheet Metal Industries, July, 1963. p. 477.

33. H. T. Coupland and W. Holyman. "Laboratory and press-shop examination of some dry-film lubricants." Sheet Metal Industries, January, 1965, p. 7.

34. H. T. Coupland and D. V. Wilson. "Speed effects in deep drawing." Sheet Metal Industries, February, 1958, p. 85.

35. G. Sachs and G. Espey. "The measurement of residual stresses in metal - Part I." The Iron Age, September 18, 1941.

36. A. A. Denton. "Determination of residual stresses." Metallurgical Reviews 1966, Vol. 11.

37. G. Sachs and G. Espey. "The measurement of residual stresses in metal - part II." The Iron Age, September 25, 1941.

38. H. W. Swift. "An experimental study of the drawing of a cylindrical cup." Third progress report No. 9110 B. Class 81,51 to Inst. Auto. Engs. November, 1938.

39. J. R. Wallace. "An assessment of simulative testing for presswork." Journal. Inst. Metals. 1962-3, Vol. 91, p. 19.

40. L. R. Hawtin. "Recommended procedure for performing the Swift cupping test." Sheet Metal Industries, May 1969, p. 418 - 421 .

41. E. M. Loxley and H. W. Swift. "The wedge drawing test." Ninth progress report No. 194415. to Inst. Auto. Engs. 1944.

42. H. W. Swift and others "Deep drawing Research." Fourth progress report to Inst. Auto. Engs. 1939.

43. R. Norman. "The effect of guiding on punch load in redrawing." Internal Tube Investments report. Hinxton Hall research on the Metal Flo process, Job Report No. 2. January, 1968.

44. W. H. Busby and B. Fogg. "The deep drawing of High Speed steel and low Tungsten tool steel thin-walled cups." Inst. Sheet Metal Eng. British Deep Drawing Research Group, Colloquium on Heat Treatment and Metallurgy in Metal Forming at Aston University, Birmingham, March, 1969.

45. H. W. Swift. "Stresses and strains in tube-drawing." Phil. Mag. Serial 7. Vol. 40, No.308. - Sept. 1949.

18. APPENDICES

A_1 MEASUREMENT OF FREE-ZONE PROFILES IN SUNK TUBING.

Bethel's sinking tests were conducted with low carbon steel tube , $1\frac{1}{2}$ in. outside diameter, 0.048 and 0.064 in. wall thickness. Two die sizes were used $1\frac{1}{4}$, and 1 in. diameter, each with semi-angles of 15, 25, 35 and 45 degrees. Diameter and wall thickness dimensions for partially drawn samples are given in Table A_1. I. Deformation profiles were measured using a profilometer and are reproduced in FIGS. A_1. 1 to A_1. 16. For each sample the observed point of contact with the die is indicated.

Theoretical values of the free radius R_f to the tube outer surface were calculated using equation 4.27 with die-angles measured from the experimental profiles. For tube numbers 10, 11, 12, 14, 15, 16 drawn through the $1\frac{1}{4}$ in. diameter die the true contact angle was less than the die-angle, contact occurring at a point on the profile radius. Theoretical values of R_f (outside) as given in Table A_1. 2 were superimposed on the plotted profiles.

TABLE A_1.1 - DIAMETER AND WALL THICKNESS MEASUREMENTS OF LOW CARBON STEEL TUBES PARTIALLY SUNK THROUGH DIES OF VARIOUS ANGLES.

Tube Number	Die semi-angle (degrees)	Entering tube				Exit tube			
		Outside diameter (in)		Wall thickness (in)		Outside diameter (in)		Wall thickness (in)	
		Range	Average	Range	Average	Range	Average	Range	Average
1	15	1.497 1.499	1.498	.047 .050	.049	.994 .995	.995	.052 .054	.053
2	25	1.498	1.498	.048 .049	.049	.996 .998	.997	.052 .053	.053
3	35	1.498	1.498	.047 .050	.049	1.002	1.002	.051 .054	.053
4	45	1.497 1.499	1.498	.046 .049	.048	1.002 1.003	1.003	.049 .051	.050
5	15	1.498 1.499	1.499	.062 .065	.064	.992 .993	.993	.067 .070	.069
6	25	1.497 1.500	1.499	.062 .065	.064	.996 .999	.998	068 069	.069
7	35	1.498 1.499	1.499	.062 .065	.064	1.001 1.002	1.002	.067 .069	.068
8	45	1.498 1.499	1.499	.062 .066	.064	1.003 1.004	1.004	.065 .069	.067
9	15	1.490 1.504	1.497	.046 .050	.048	1.250 1.249	1.250	.049 .053	.051
10	25	1.497 1.498	1.498	.047 .049	.048	1.243 1.247	1.245	.051 .052	.052
11	35	1.498 1.499	1.499	.047 .049	.048	1.247 1.249	1.248	.051 .052	.052
12	45	1.495 1.501	1.498	.047 .050	.049	1.246 1.249	1.248	.050 .052	.051
13	15	1.496 1.501	1.499	.061 .066	.064	1.241 1.243	1.242	.065 .069	.067
14	25	1.495 1.502	1.499	.063 .065	.064	1.249 1.250	1.250	.067 .068	.068
15	35	1.497 1.500	1.499	.063 .065	.064	1.248 1.249	1.249	.066 .068	.067
16	45	1.498 1.499	.1499	.061 .066	.064	1.246 1.247	1.247	.064 .069	.067

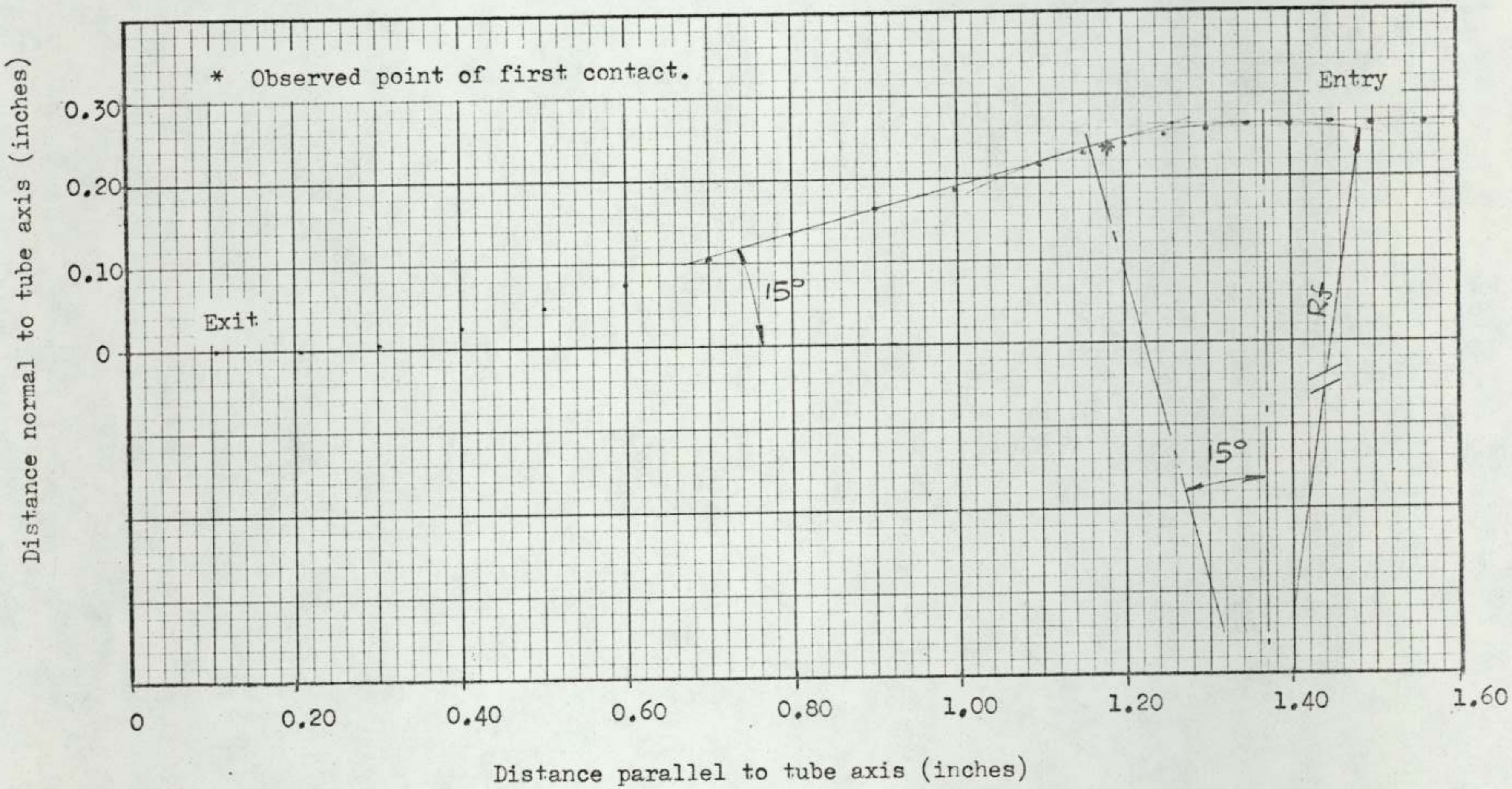

FIG. A_1.1 SUNK TUBE PROFILE SAMPLE 1.

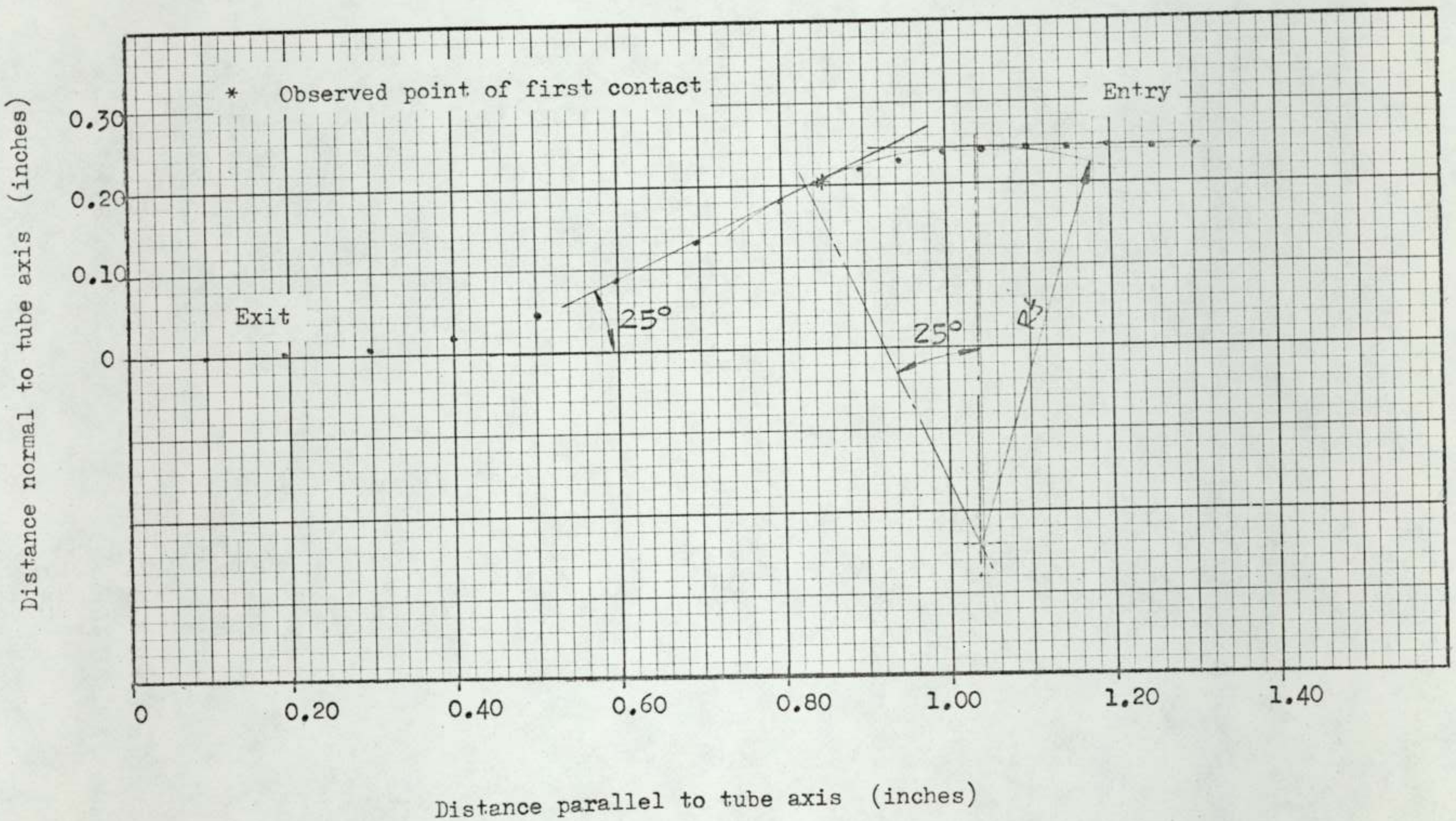

FIG. A_1.2 SUNK TUBE PROFILE SAMPLE 2.

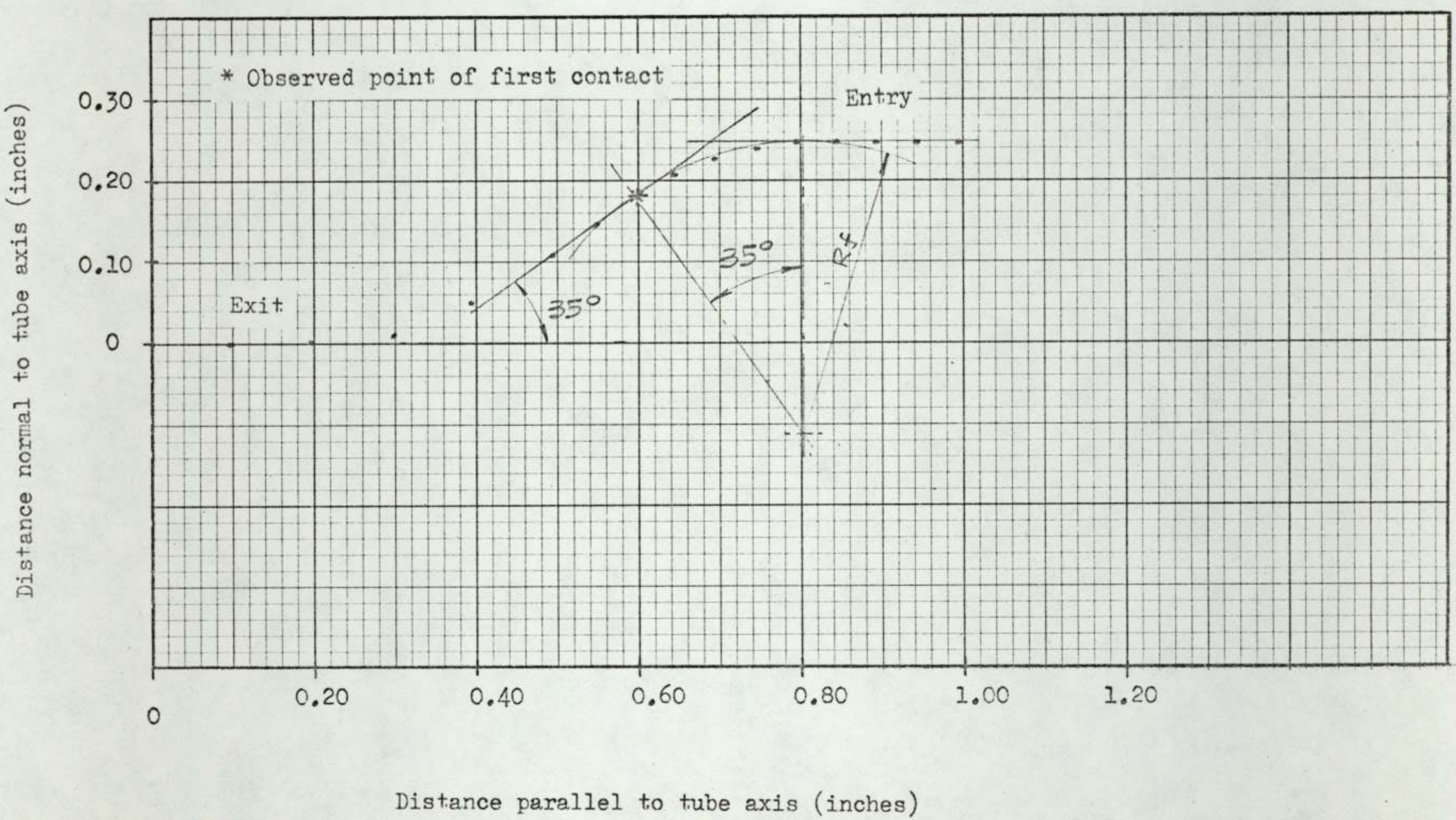

FIG. A_1.3 SUNK TUBE PROFILE SAMPLE 3.

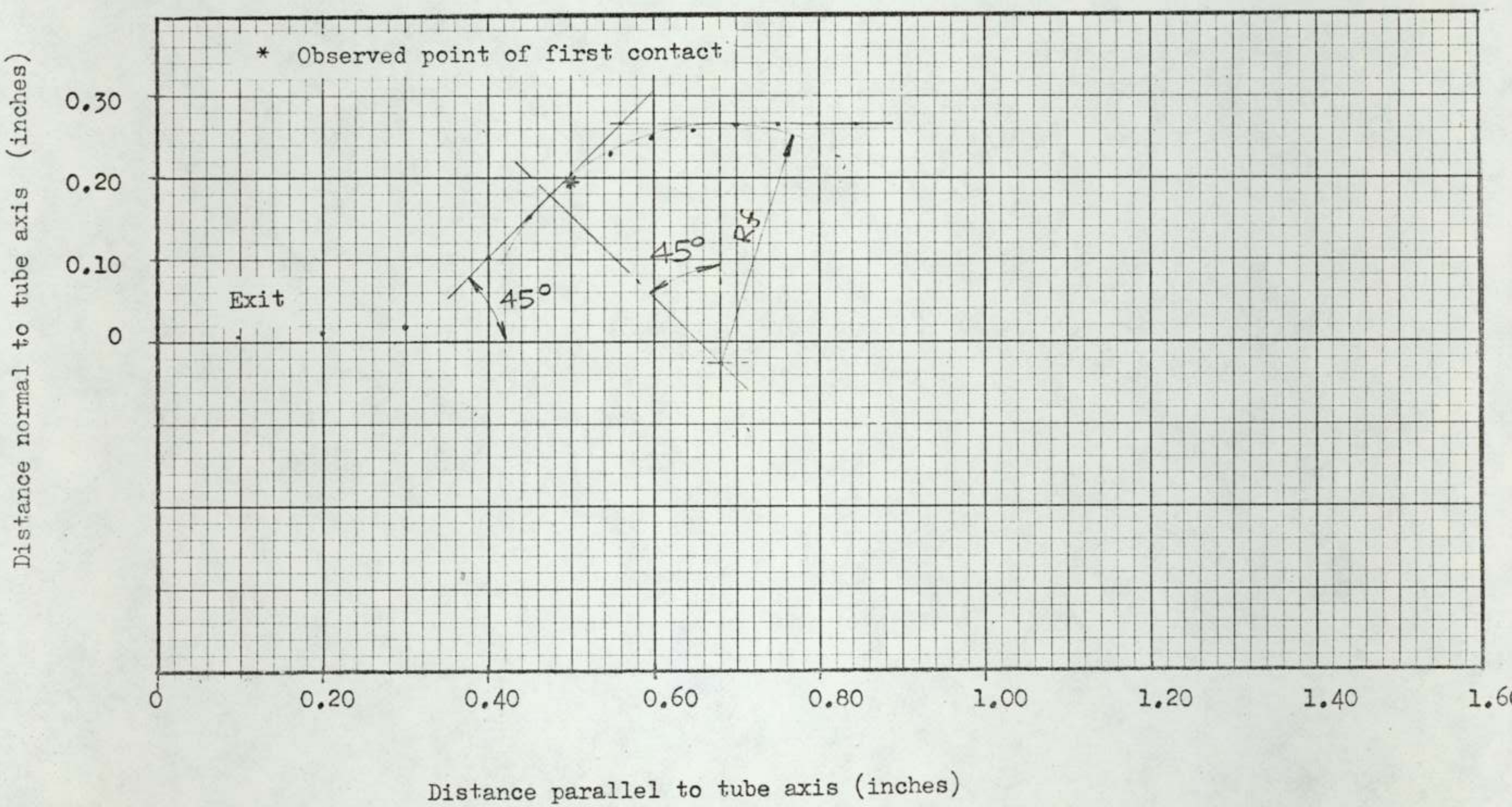

FIG A_1.4 SUNK TUBE PROFILE SAMPLE 4

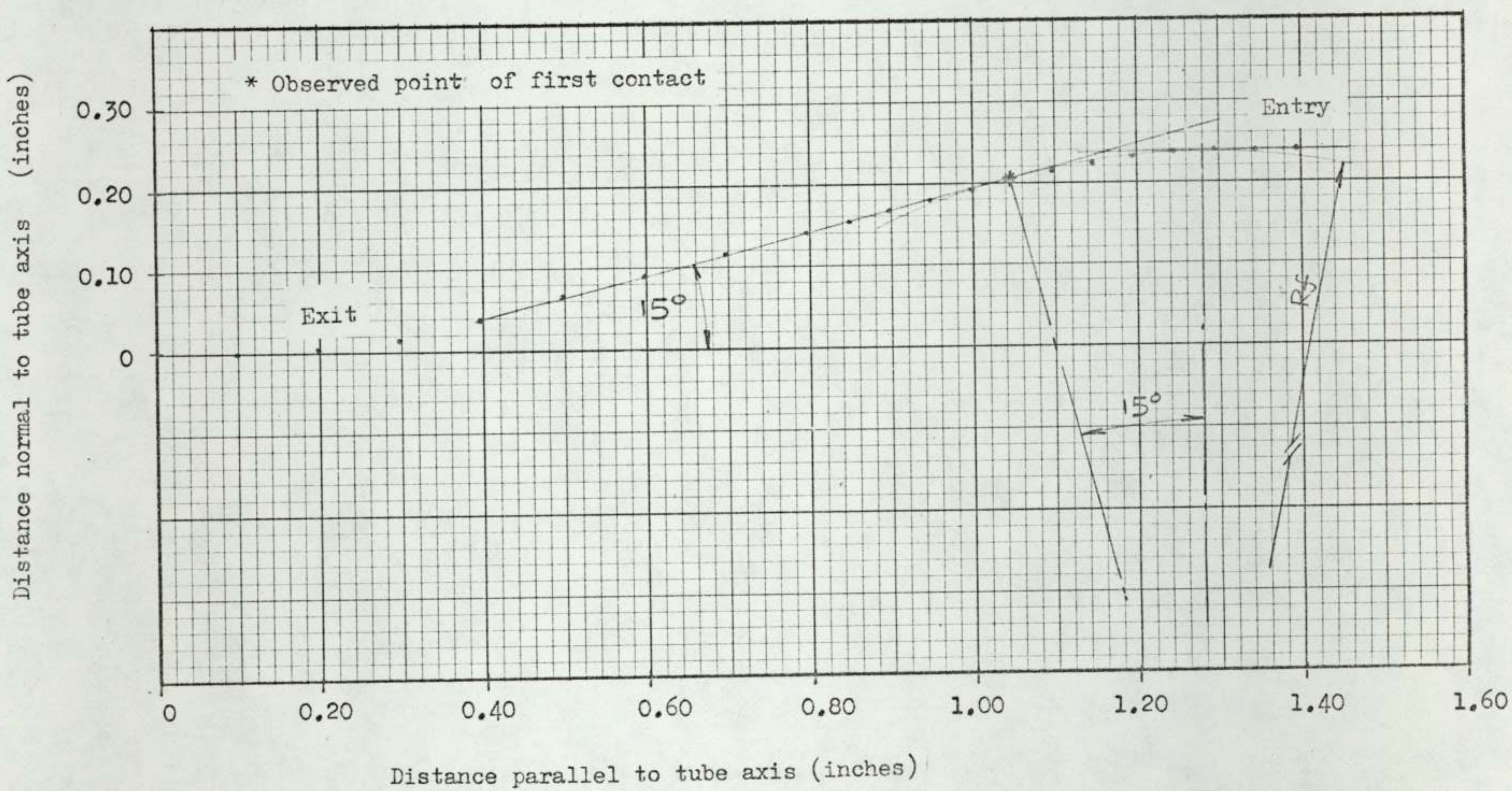

FIG A_1.5 SUNK TUBE PROFILE SAMPLE 5

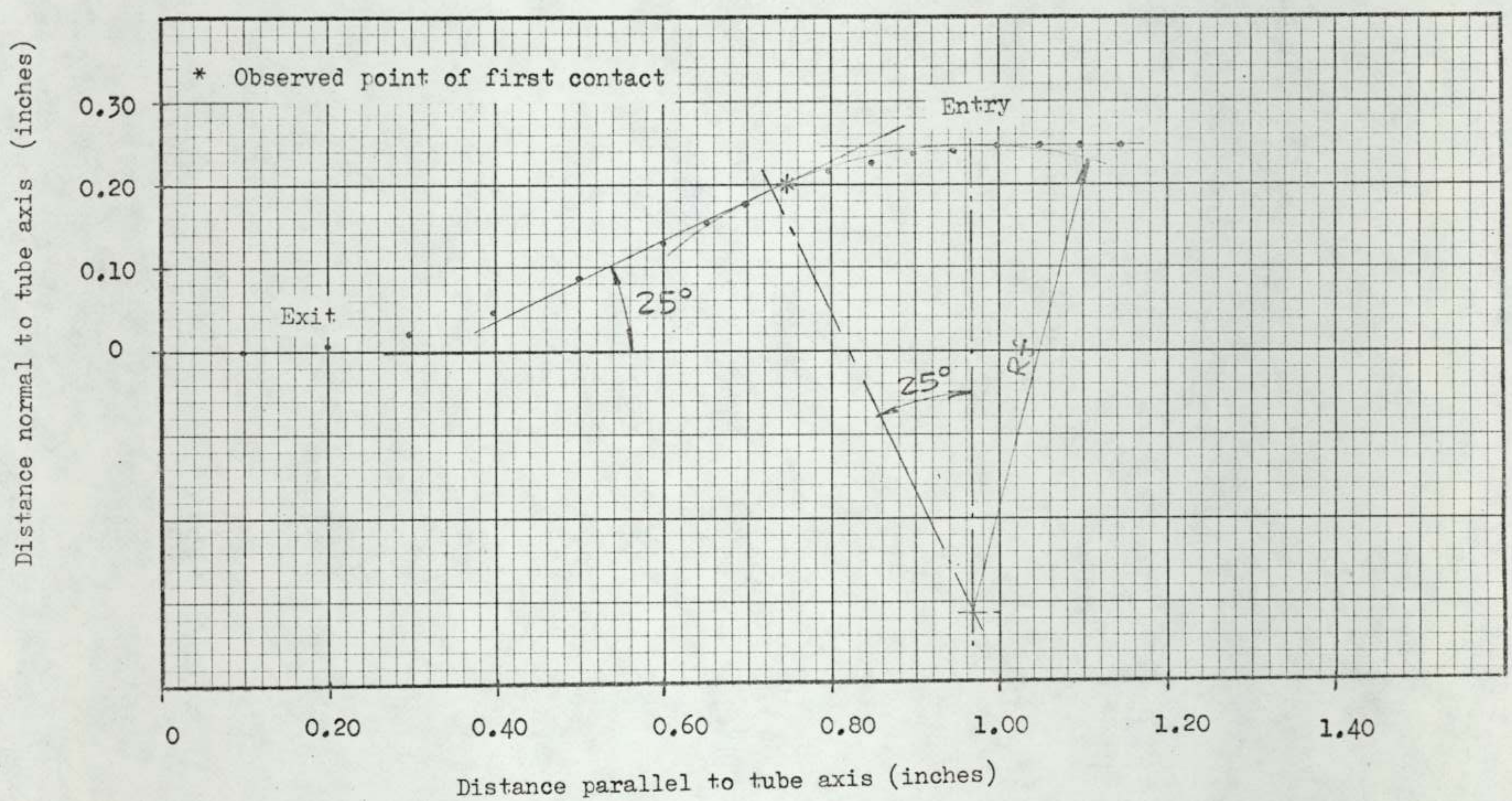

FIG A_1.6 SUNK TUBE PROFILE SAMPLE 6

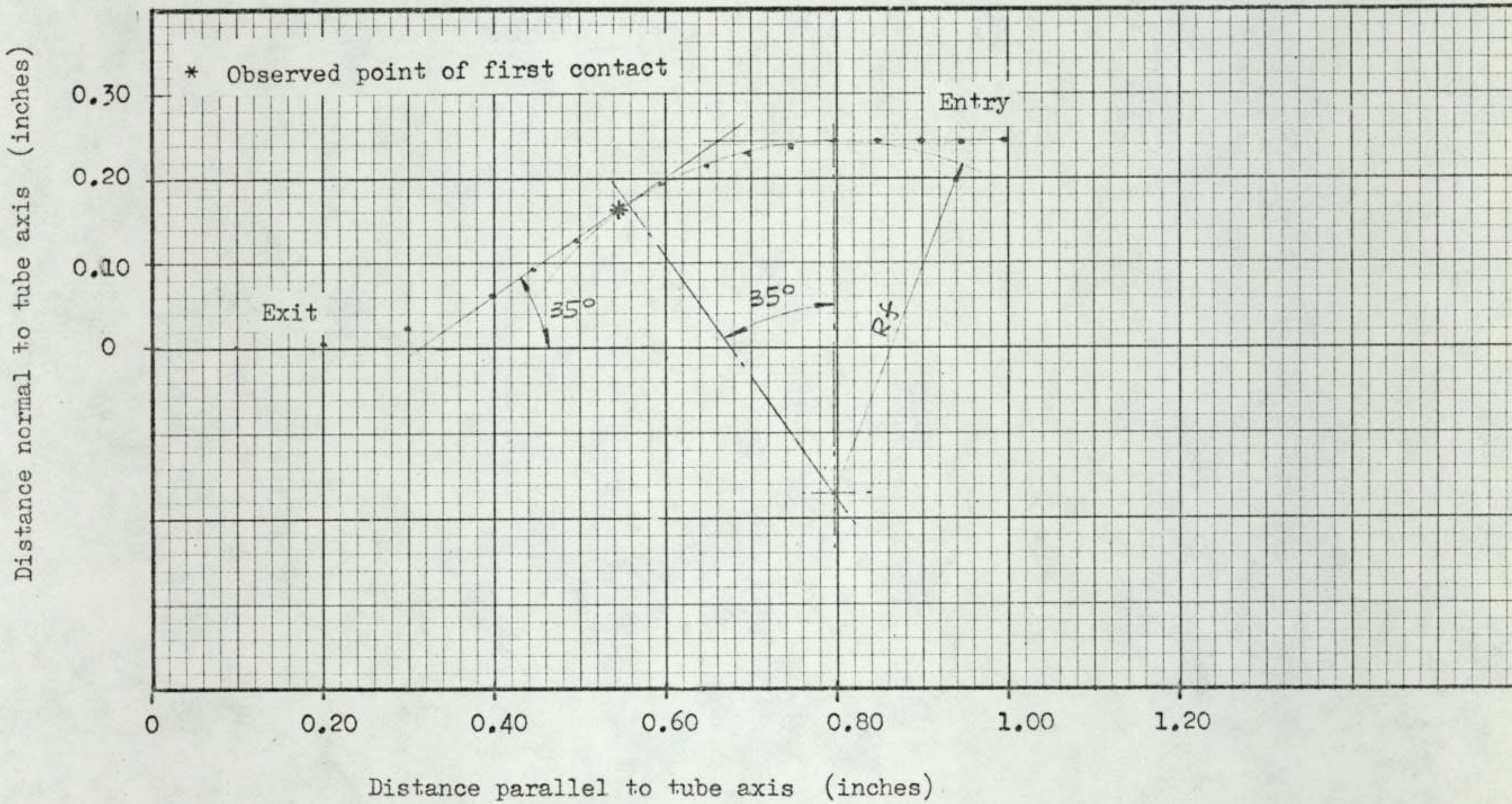

FIG $A_1.7$ SUNK TUBE PROFILE SAMPLE 7

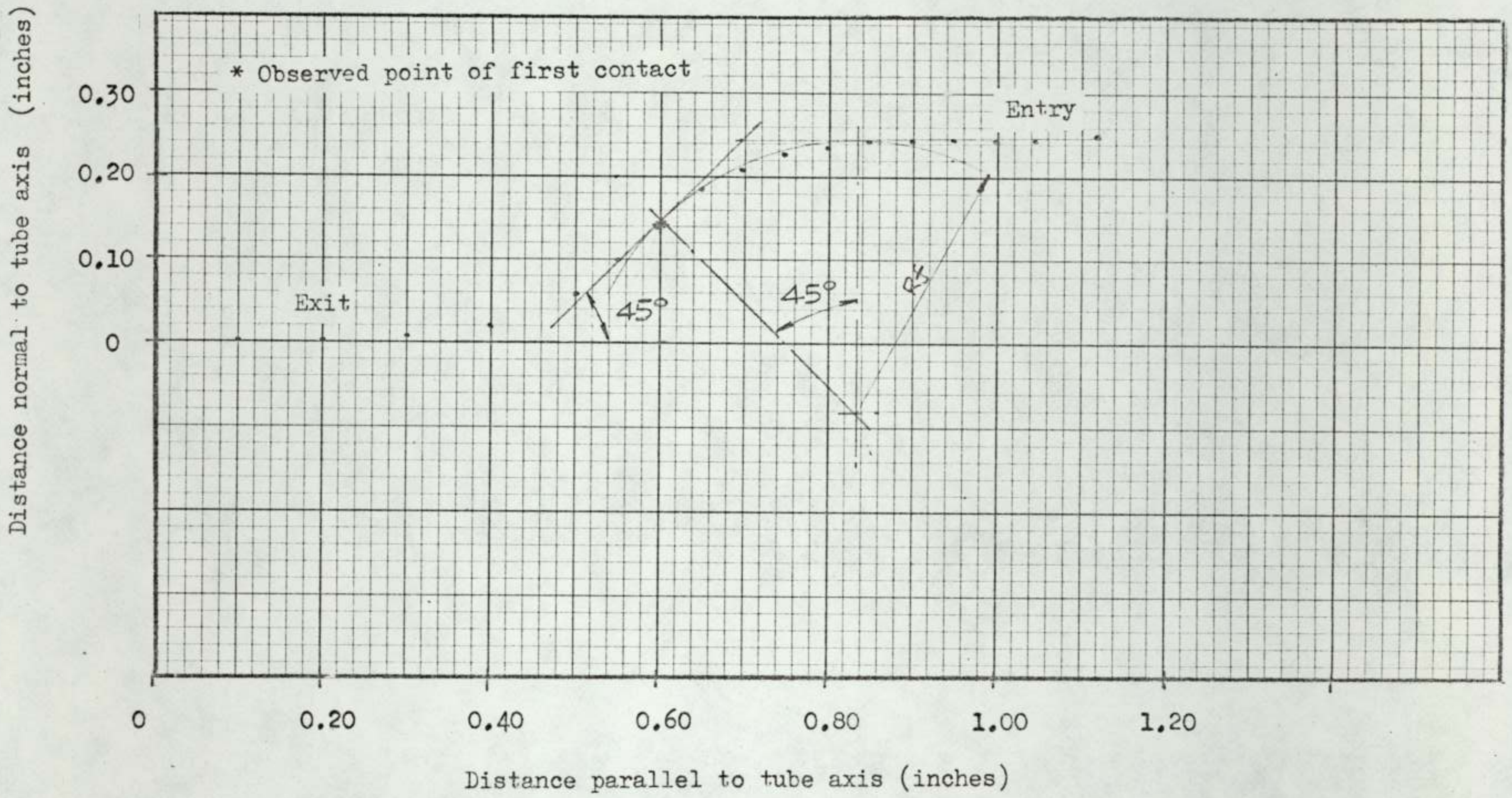

FIG A_1.8 SUNK TUBE PROFILE SAMPLE 8

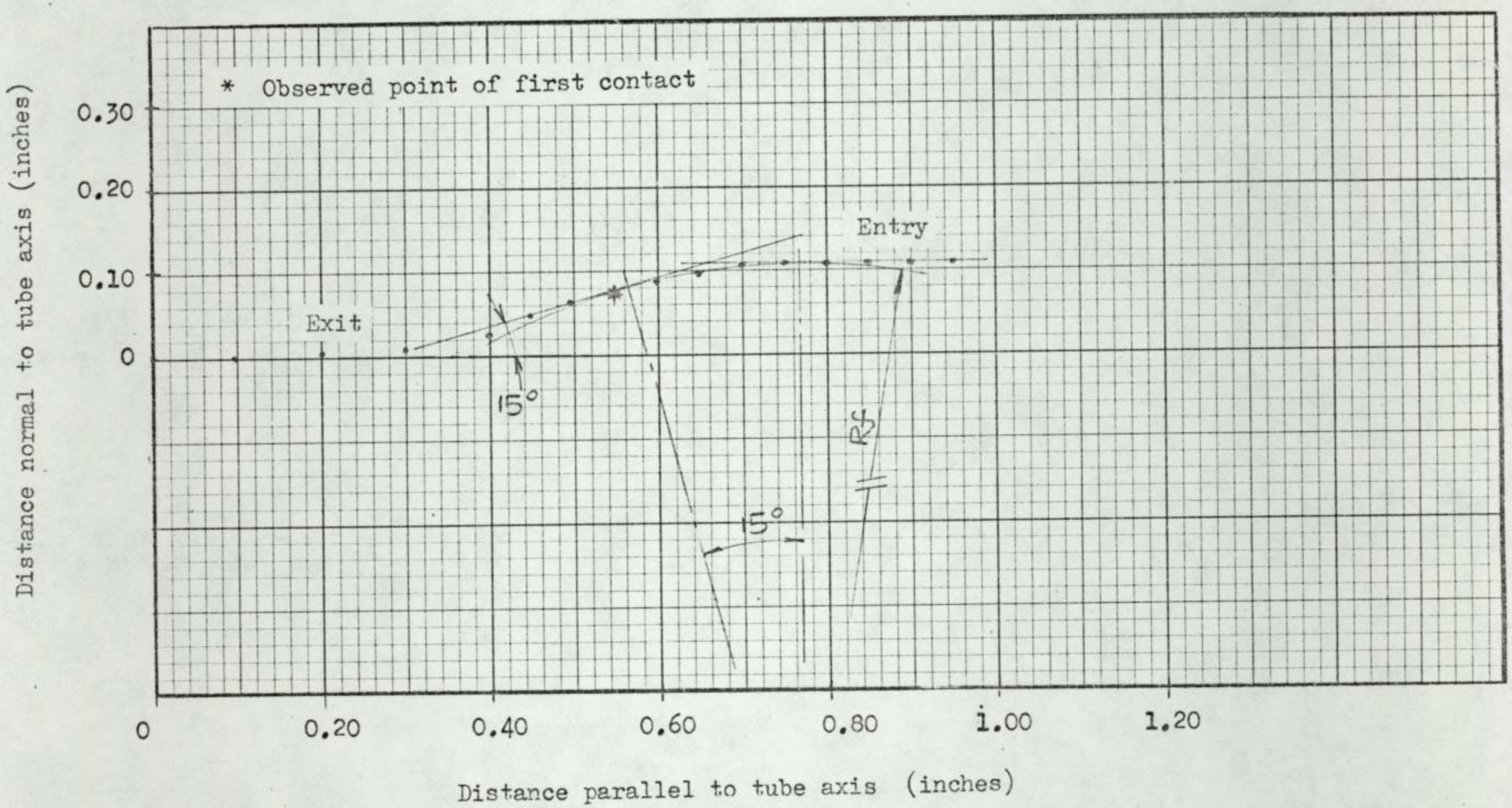

FIG A_1.9 SUNK TUBE PROFILE SAMPLE 9

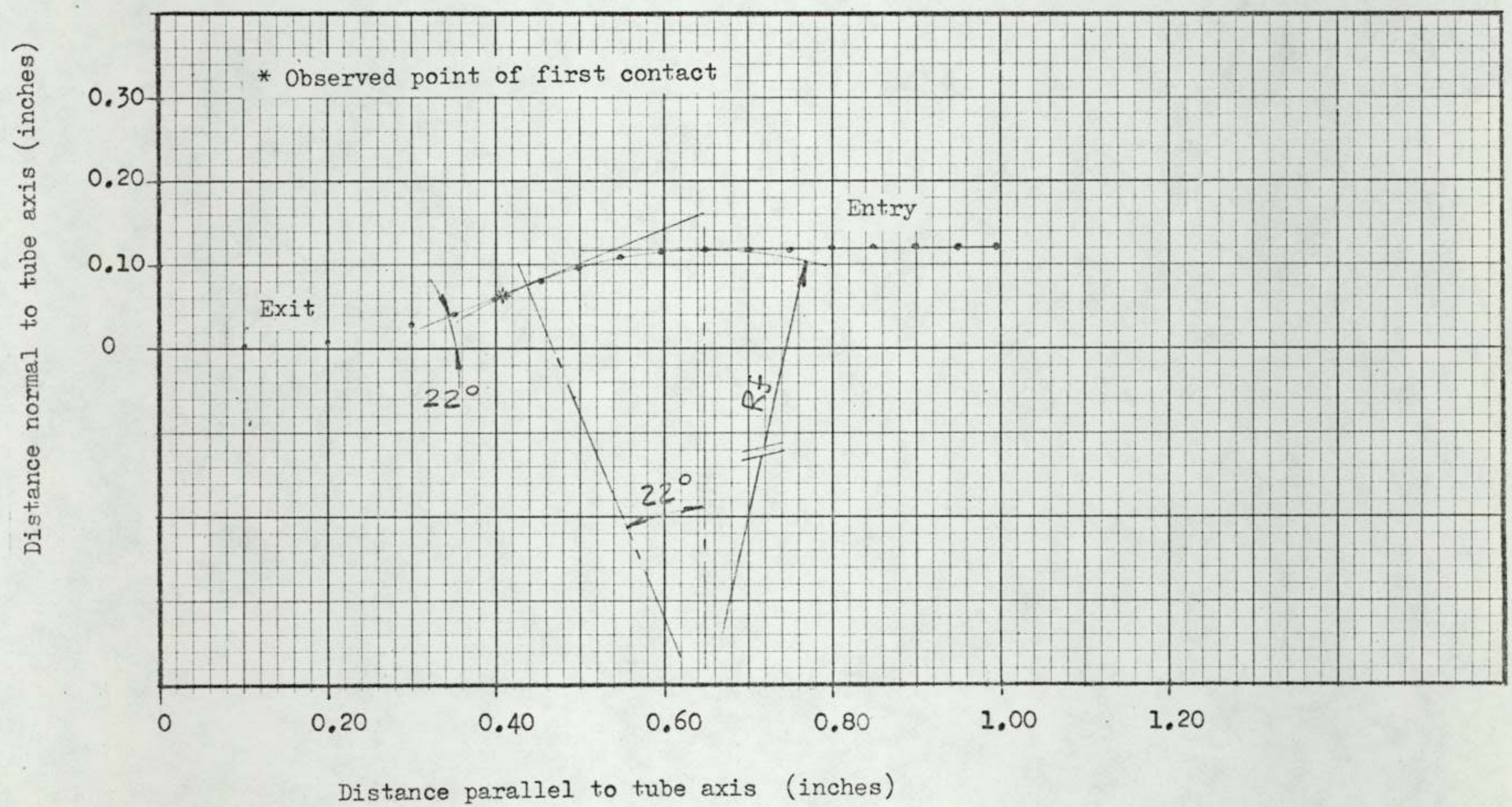

FIG A3.10 SUNK TUBE PROFILE SAMPLE 10

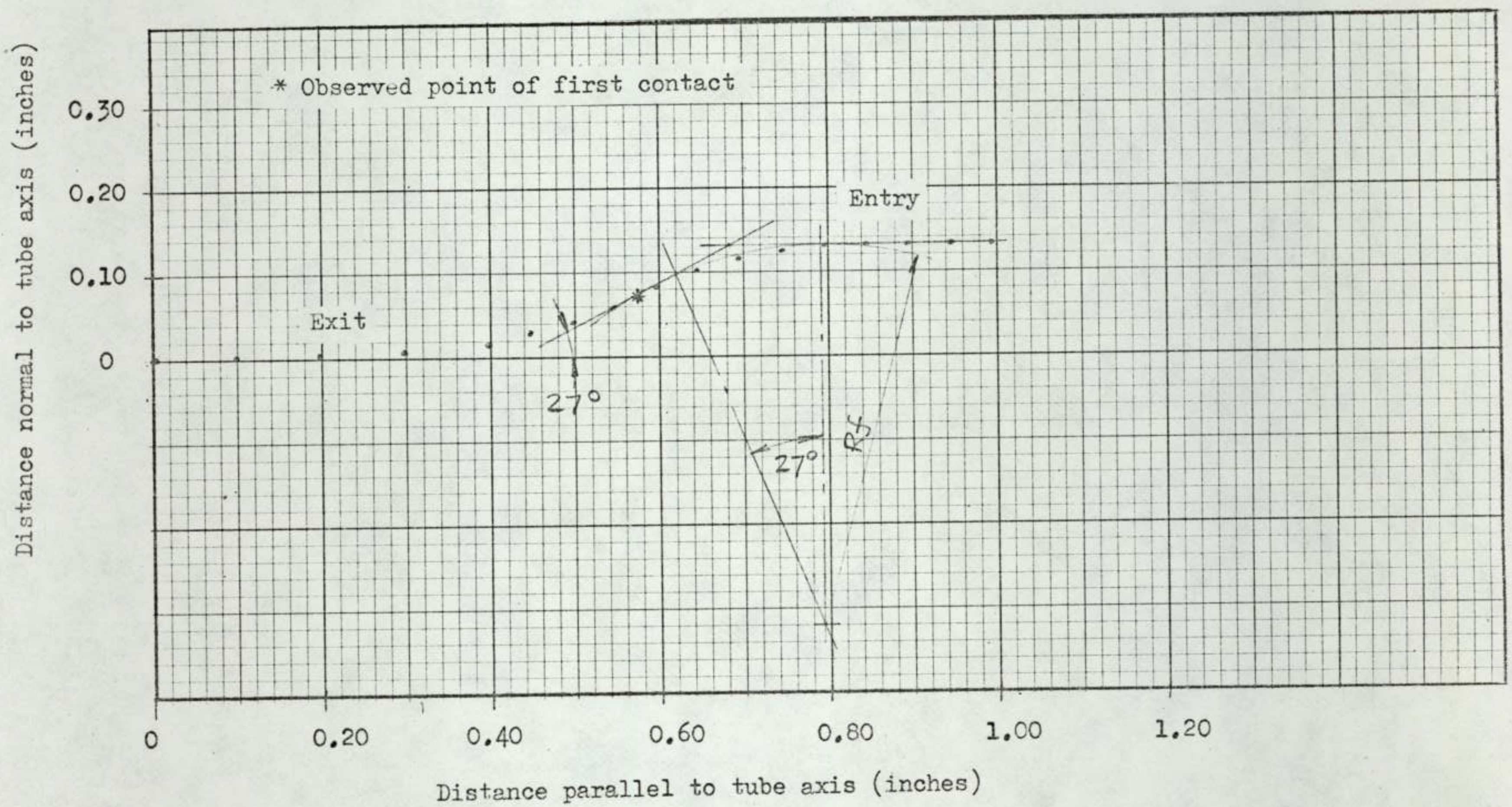

FIG A_1. 11 SUNK TUBE PROFILE SAMPLE 11

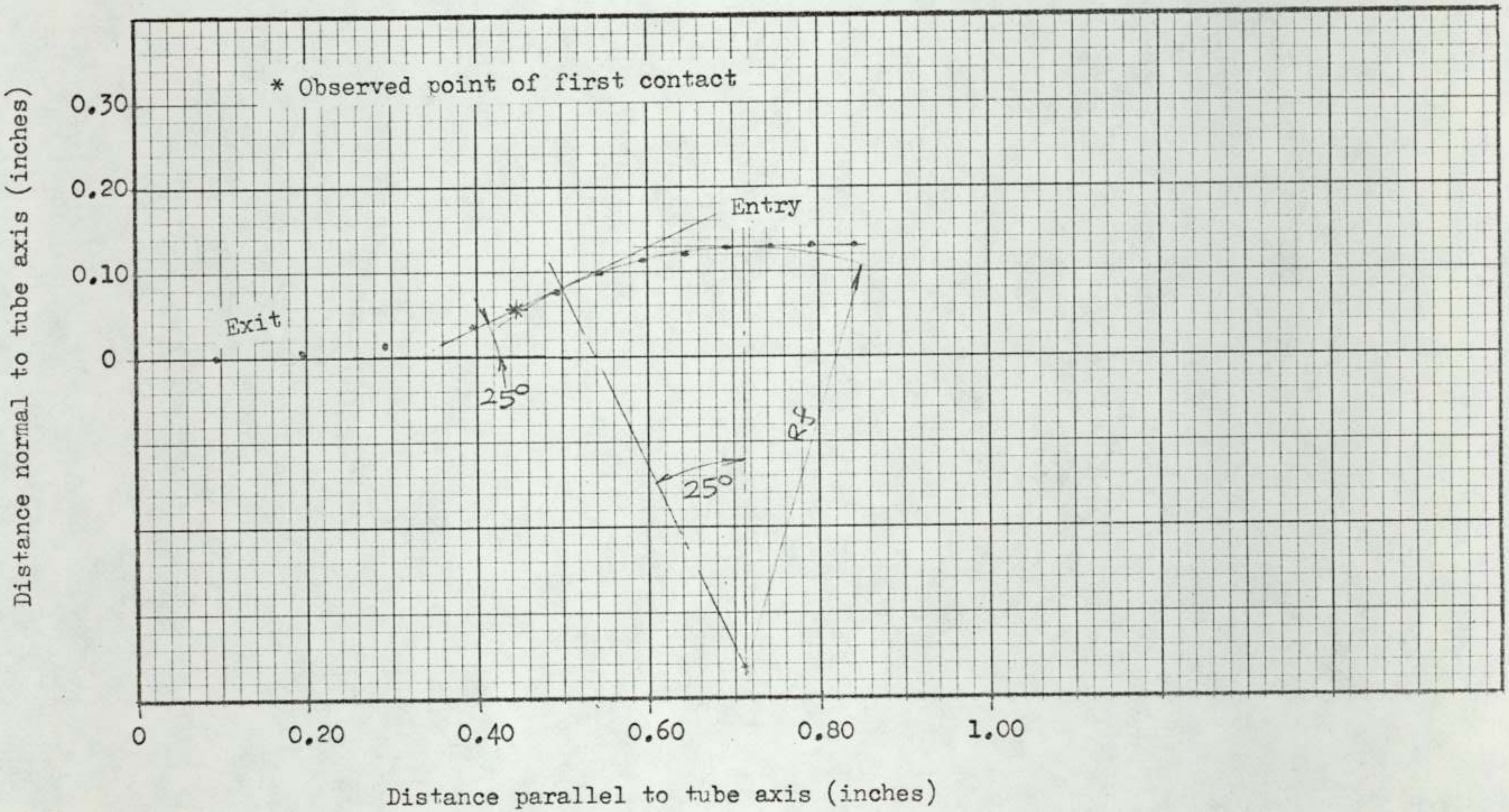

FIG A_1. 12 SUNK TUBE PROFILE SAMPLE 12

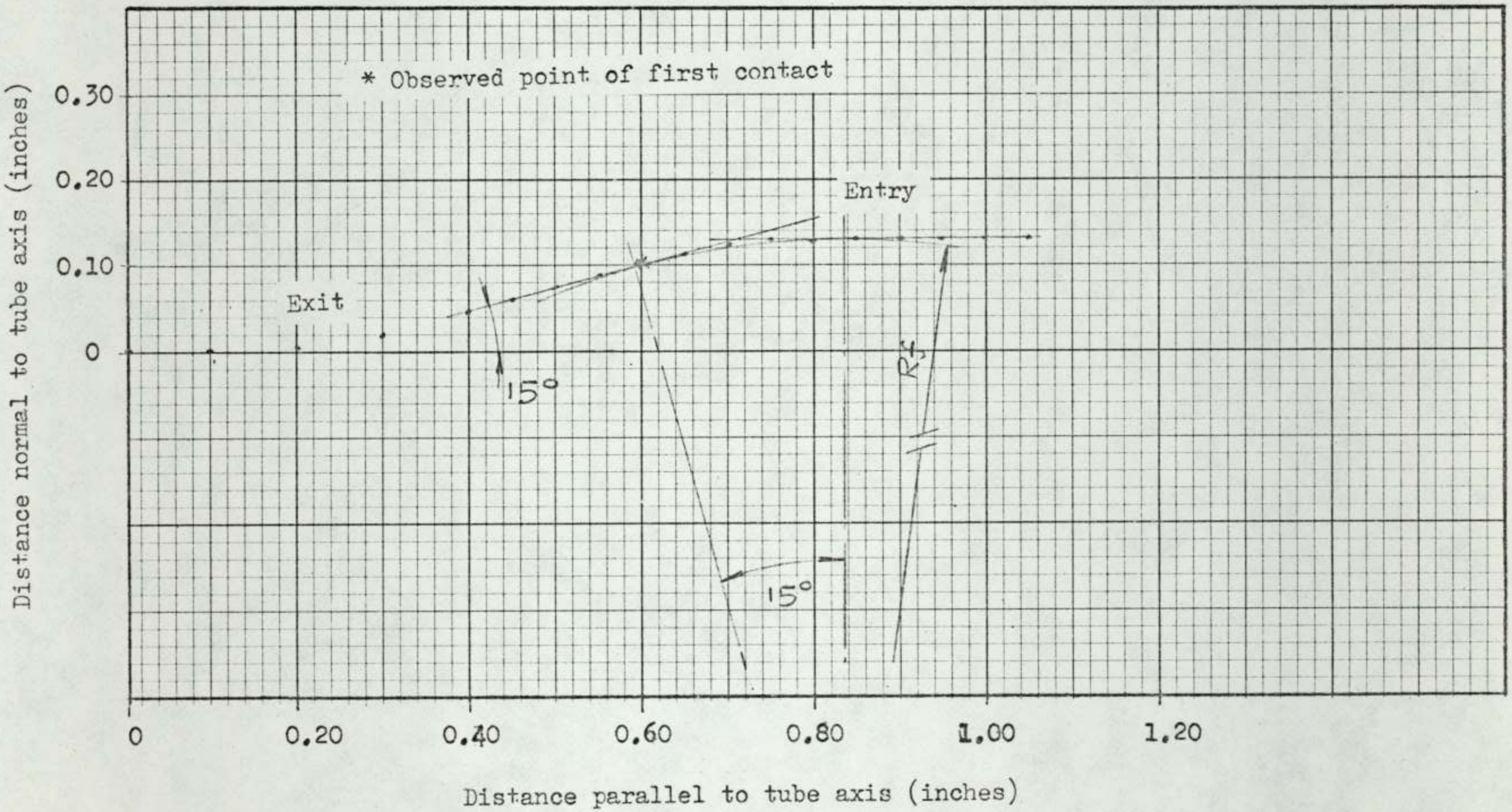

FIG A_1.13 SUNK TUBE PROFILE SAMPLE 13

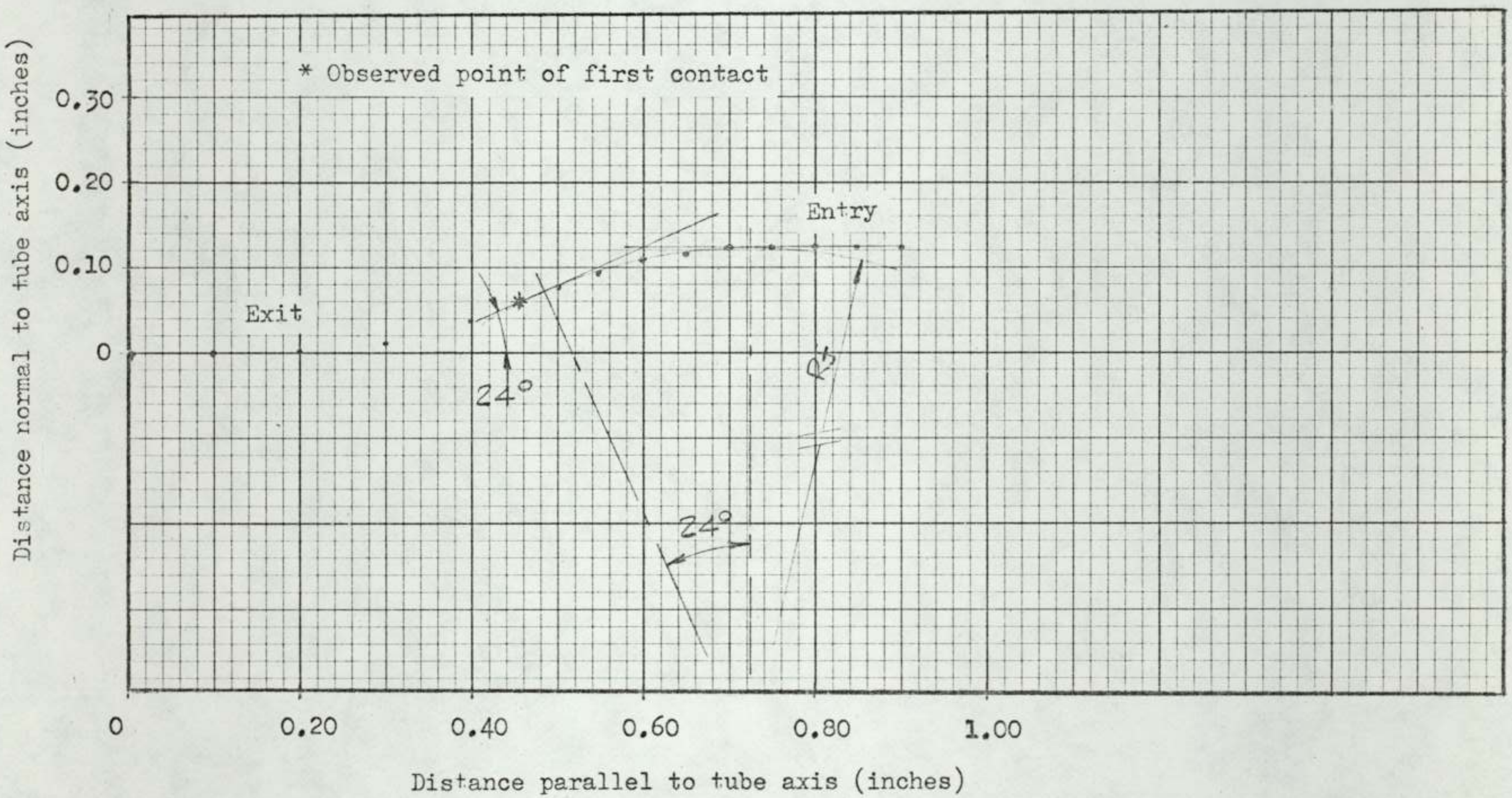

FIG A_1.14 SUNK TUBE PROFILE SAMPLE 14

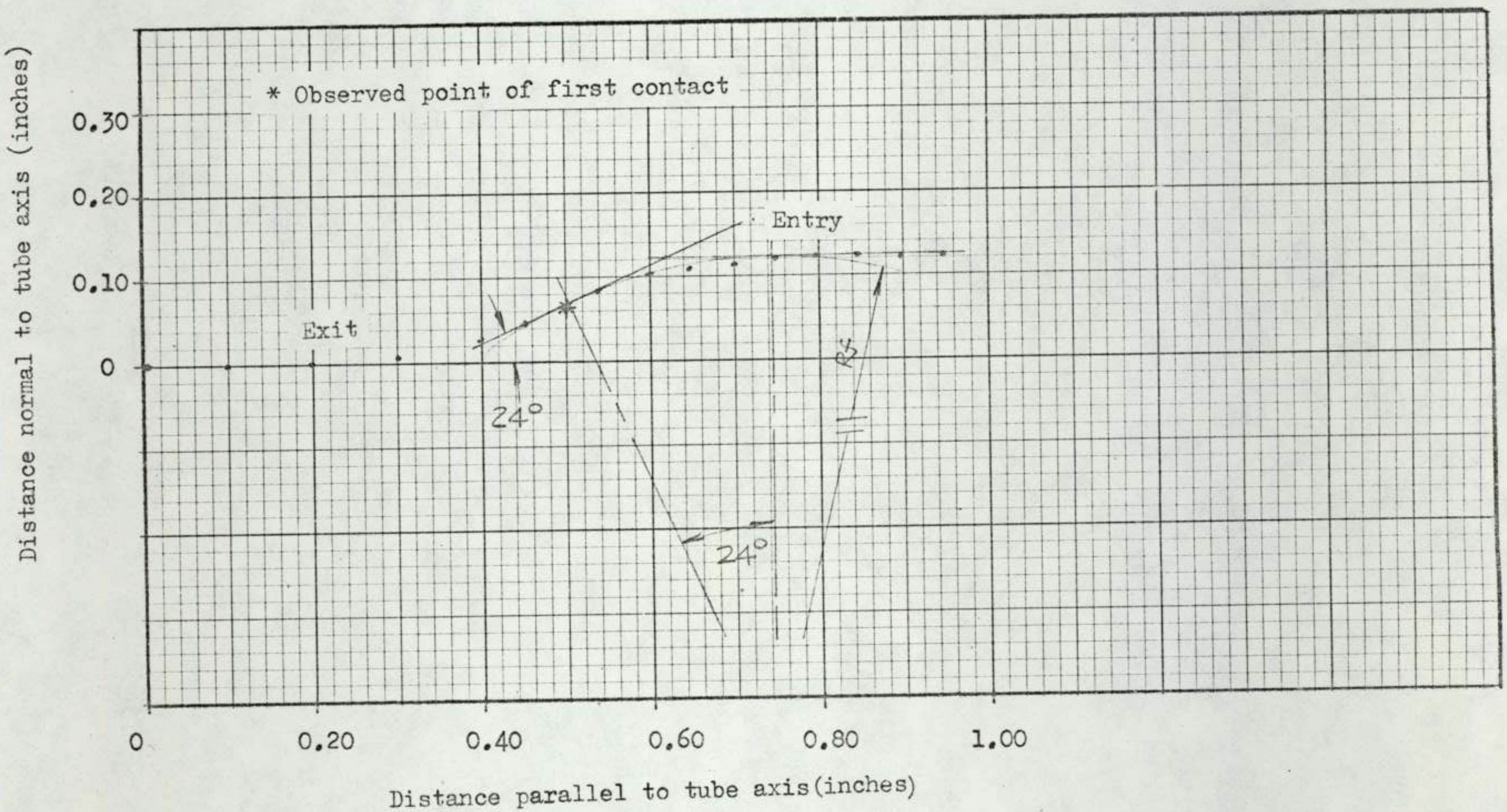

FIG A_1. 15 SUNK TUBE PROFILE SAMPLE 15

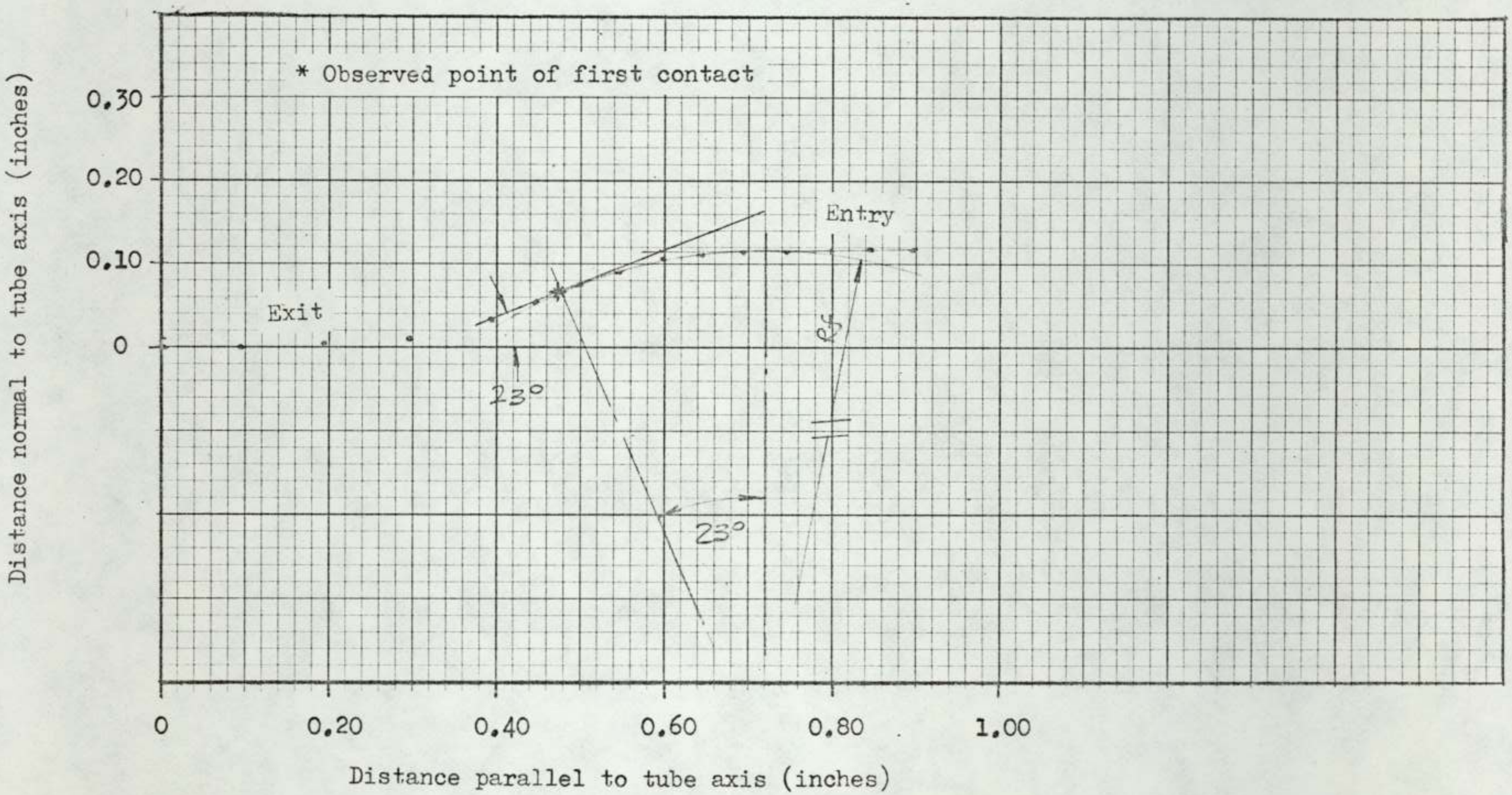

FIGA_1.16 SUNK TUBE PROFILE SAMPLE 16

TABLE A_1.2. FREE OUTER RADIUS Rf CALCULATED FROM

EQUATION 4.27

Tube Number	Die semi-angle at first point of tube contact (deg.)	Tube free outer radius Rf (in.)
1	15	0.810
2	25	0.487
3	35	0.362
4	45	0.290
5	15	0.915
6	25	0.564
7	35	0.415
8	45	0.334
9	15	0.792
10	22	0.548
11	27	0.454
12	25	0.493
13	15	0.884
14	24	0.588
15	24	0.588
16	23	0.612

A_2. DETAILS OF TESTING MACHINE FOR FIRST AND SECOND EXPERIMENTAL PROGRAMMES.

A_2. 1. Testing machine general arrangement.

Two views of the machine are shown in FIG. A_2. 1. The machine frame was a rigid box-like welded fabrication designed to provide a vertical drawing action. Apart from two horizontal platens (1), (2) which were $\frac{3}{4}$ in. thick the remainder of the frame was built in $\frac{1}{2}$ in. plate. The two platens, both machined flat and parallel on upper and lower surfaces were tied by bolts passing through spacer tubes (3) which also acted as load bearing columns. The upper surface of platen (1) was used for mounting experimental test rigs, whilst the lower surface of platen (2) carried a rotary/linear drive converter (4), the latter being accessible via apertures in the front and base panels of the machine frame. Drive to the motion converter (4) was supplied by an electric motor (5) through transmission (6). A journal bearing (7) was mounted in the bulkhead panel dividing motor and converter compartments.

The moving arm of the converter (4) was coupled to a crosshead (8) constrained to move vertically along the two spacer tubes (3). A strain-gauge transducer (9) for measuring draw-load was attached to the crosshead, alignment being ensured by a projection on the transducer fitting a recess in the crosshead. The upper part of the transducer was a similar fit in an adaptor (10) which carried the test-piece gripping dog (11). The dog could pass freely through a recess in the platen (1).

A_2. 2. Rotary/linear drive converter.

A standard Duff-Norton inverted 'jactuator' converted rotary drive from the motor into linear motion of the drawing arm. The unit was an accurately manufactured worm-gear jack with a self-locking facility. The manufacturer claimed that loads could be held indefinitely without creep, and due to its inherent accuracy the

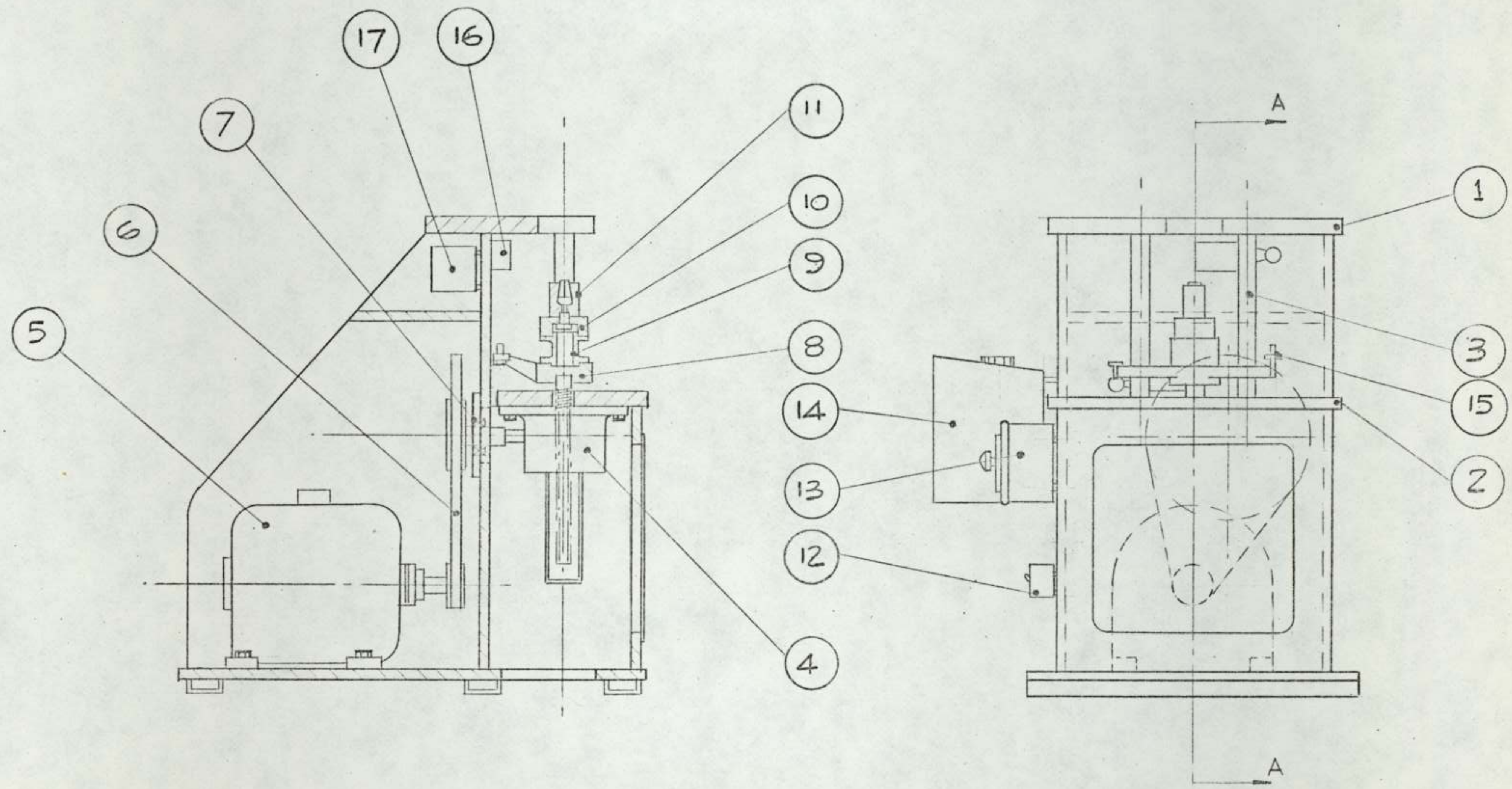

FIG. A_2.1 ARRANGEMENT OF TESTING MACHINE (Scale $\frac{1}{8}$ full size) unit was ideally suited for positional control.

The 'jactuator used in the testing machine was of 2 Tonf. capacity with a maximum stroke of 6 in., and was capable of transmitting $\frac{1}{2}$ horse-power at 500 revs/min. This corresponded to a linear jack speed of 20.8 in/min.

A_2. 3. Drive and speed control.

To achieve the speed control required by the experimental programmes the 'Neco' drive system was employed. This system uses a d.c. motor controlled by an electronic unit supplied with an a.c. input. In conjunction with the speed control unit a $\frac{3}{4}$ horse-power motor operating at 2000 revs/min. was sufficiently robust to cover all loading conditions expected in the experimental programmes.

The 'Neco' system provided smooth infinitely variable speed control at constant torque throughout a motor speed range, the control unit comprising an auto-transformer, and silicon field and armature rectifiers. The auto-transformer controlled armature voltage which in turn controlled speed. Reversing was carried out manually, using a double-pole switch incorporating a device for dynamically braking the machine.

Automatic adjustable cut-out devices were included to stop the machine at termination of forward and return strokes. This was achieved by strikers on the moving crosshead operating electrical limit switches which energised relays carrying the armature current.

FIG. A_2. 2. shows the testing machine electrical circuit. During the forward stroke the armature circuit was completed via reversing switch terminals A_4, B_4., and during the return stroke by terminals A_2, B_2. Dynamic braking was effected by a resistance connected across the armature when the reversing switch was operated to the 'off' position (terminals A_1, B_1 or A_3, B_3)

The physical arrangement of electrical controls is shown by FIG A_1. 1. An isolator switch (12), reversing switch (13), and speed control unit (14) were mounted on the left side of the machine.

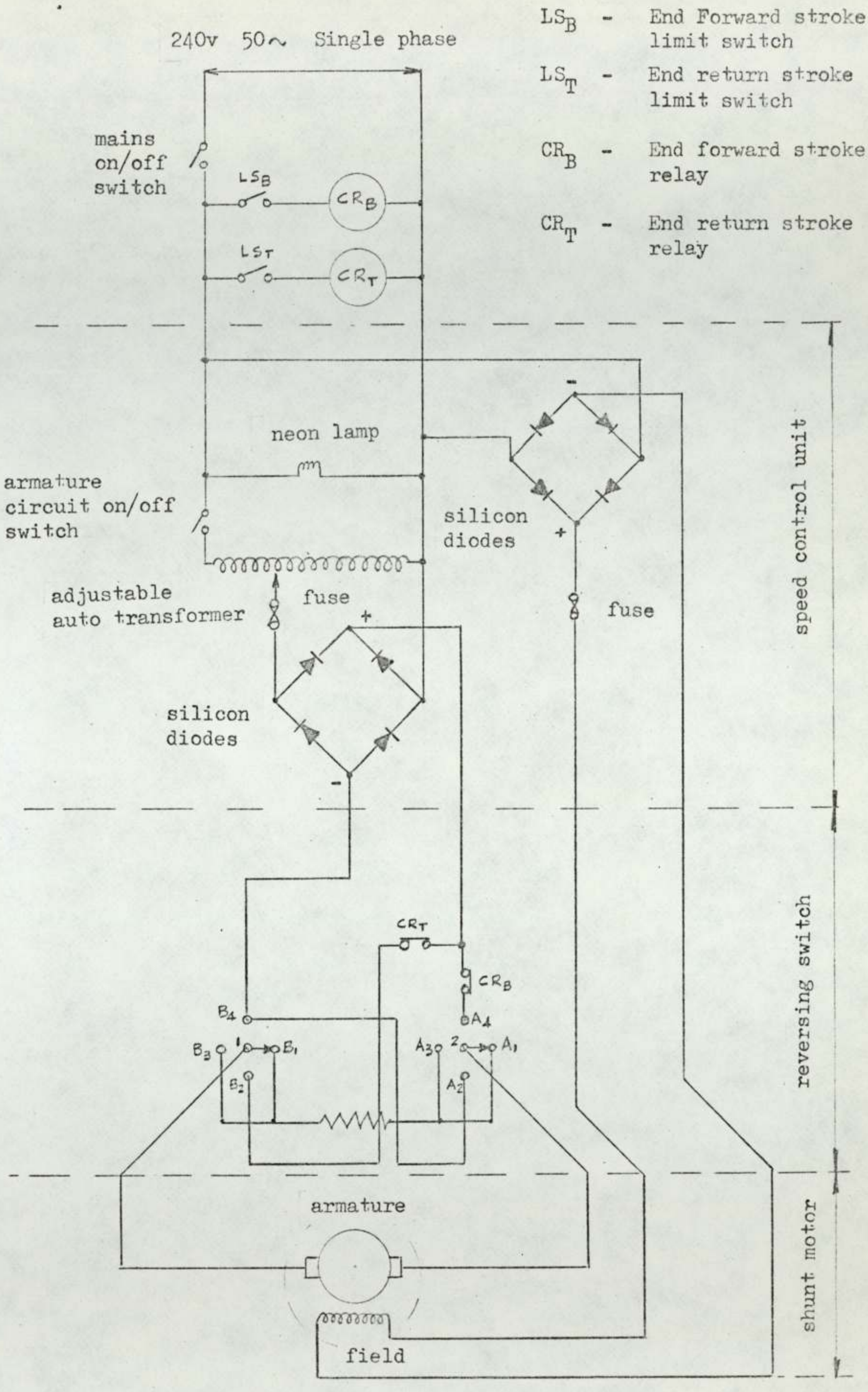

FIG. A_2.2 ELECTRICAL SCHEMATIC FOR TESTING MACHINE

The striker arms (15) contacted limit switches (16) attached to the bulkhead panel. Relays (17) were housed in a separate compartment.

A_2. 4. Construction of dog load-cell.

(a) Strain gauge attachment to load-cell body.

Tinsley epoxy backed linear foil strain gauges type LSG9A/2/CN/E were used. The procedure for attaching gauges was as follows,

(1) The backing on each gauge was cut down to suit the load-cell gauge area, corners being removed to reduce the possibility of subsequent lift-off.

(2) The load-cell gauge area was degreased, roughened with 400C grade silicon carbide paper and further degreased.

(3) Gauges were positioned on the load cell, held in place by a band of soft rubber, and left for two days at $100^{\circ}F$. to pre-form to the load-cell curvature.

(4) Araldite strain-gauge cement with hardener HY956 was used for bonding mixed in the proportions 100/8 - 10. by weight. A thin film of cement was applied to gauge back and load-cell body. Each gauge was positioned and retained by a soft rubber pad, the latter being held by adhesive tape. After the cement had cured for four days at 60 - 70 $^{\circ}F$. the quality of bonding was checked and found to be satisfactory.

(b) Strain-gauge wiring.

(1) Tabs on the bonded gauges were cleaned with 600 silicon paper and degreased. Continuity and insulation checks were then made on each gauge with an Avometer.

(2) Terminal strips on insulated backing were attached to the load-cell body between adjacent gauges, using an impact adhesive. Miniature p.v.c. coated 7/40 wires were then taken from strain gauge tabs to the terminal strips, and out to a socket located in the load-

cell cover. After wiring each gauge, continuity and insulation checks were made. This procedure was repeated before and after wires were taken to the socket.

(3) On completion of wiring all gauges and terminal strips were coated in Di-Jell 171 strain-gauge waterproofing, and to provide additional protection a rubber sheath was arranged around the mid-section of the load-cell.

A_3. SECOND EXPERIMENTAL PROGRAMME - SPLAY MEASUREMENT TESTS.

A_3. 1. Calculation of hold-down punch geometry using Fogg's[11] expression.

Providing the constrained radius of bending R_c is less than the corresponding free radius R_f the hold-down punch will be effective in controlling deformation prior to die contact. Before designating values of R_c it was therefore necessary to compute values of R_f.

Fogg's expression is,

$$\frac{R_f}{t_o} = \sqrt{\frac{\tau_o/t_o}{\sqrt{3}\,(1 - \cos\alpha_f)}} \qquad \text{———————} \qquad (a)$$

where α_f is the die semi-angle at point of cup/die contact.

The situation frequently occurs where α_f is less than the die semi-angle α, contact occurring around the die profile radius. A check for this may be made by comparing R_f from equation (a) putting $\alpha_f = \alpha$, with R_f' calculated from the orthogonal situation,

$$R_f' = \frac{\gamma - 1}{\gamma} \cdot \frac{t_o}{(1 - \cos\alpha)} - R_d$$

Provided $R_f < R_f'$ contact occurs along the conical die-face and equation (a) is valid with $\alpha_f = \alpha$. If $R_f > R_f'$ however, α_f is not immediately known in equation (a). The free radius R_f is then given by,

$$R_f = \frac{\gamma . t_o}{2\sqrt{3}(\gamma - 1)} \left[1 + \sqrt{1 + \frac{4\sqrt{3}(\gamma - 1) R_d}{\gamma . t_o}} \right]$$

If required the corresponding die semi-angle at contact may be found from,

$$\cos\alpha_f = 1 - \frac{\tau_o(\gamma - 1)}{\gamma\,(R_d + R_f)}$$

A_3. 2. Manufacture of tubing for splay-measurement test-pieces.

Table A_3. 1. gives details of measurements taken on each of the four hollows before drawing.

All drawing was carried out using soap as a lubricant, but in addition low carbon steel and stainless steel tubes were bonderised. Interpass annealing, where necessary, was conducted in a controlled atmosphere furnace.

For intermediate 'breaking-down' passes captive plugs were used, but to achieve some similarity with the cold-worked state of a redrawn cup it was planned to complete each tube with a 25% sink. This procedure was problem-free with diameter/thickness ratios below and including 40/1 (0.019 in. wall thickness). However above 40/1 , and particularly at 100/1, a number of processing problems were encountered. To sink-finish to a diameter/thickness ratio of 100/1 meant that the tube after the final plug pass exceeded 100/1. This pass gave problems, especially with those tubes at a high level of prior cold-work. It was found that a slight variation in reduction of area around the tube caused a build-up of transverse waves at die-entry. In passing through the die the waves became ironed to produce crescent shaped laps in the drawn tube. A further problem was encountered in wrinkling when sinking from the final plug pass size to finished tube size. Problems were relieved by ommitting the 25 % sink from test-piece tube sizes above a diameter/thickness ratio of 40/1, and plug drawing to the final size.

Only one of the 38 tube size/cold-work combinations was found to be defective after drawing. This was aluminium at a diameter/thickness ratio of 80/1 with 50 % prior cold-work. The tubing exhibited gross longitudingal fissuring, the cause of the defect being unidentified. FIG. A_3. 1. illustrates a typical fissure to a magnification of 10/1.

Table A_3. 2. gives mean dimensions of all test-piece tubing

TABLE A_3.1. DIMENSIONS OF HOLLOWS FOR MANUFACTURING SPIAY-MEASUREMENT TEST-PIECES.

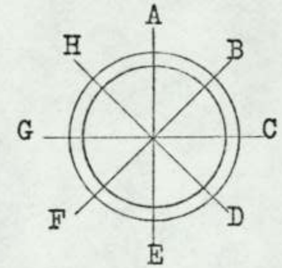

Material	Outside diameter (in.)	Wall thickness (in.)								eccentricity
		A	B	C	D	E	F	G	H	%
Low carbon steel	1.403 1.404	0.116	0.117	0.118	0.117	0.116	0.115	0.115	0.116	2.5
T304 stainless steel.	1.763 1.764	0.110	0.110	0.110	0.109	0.108	0.109	0.109	0.109	1.8
70/30 brass	1.499 1.501	0.127	0.127	0.128	0.128	0.129	0.129	0.129	0.128	1.6
Pure aluminium	1.503 1.504	0.131	0.127	0.125	0.125	0.130	0.133	0.135	0.134	7.4

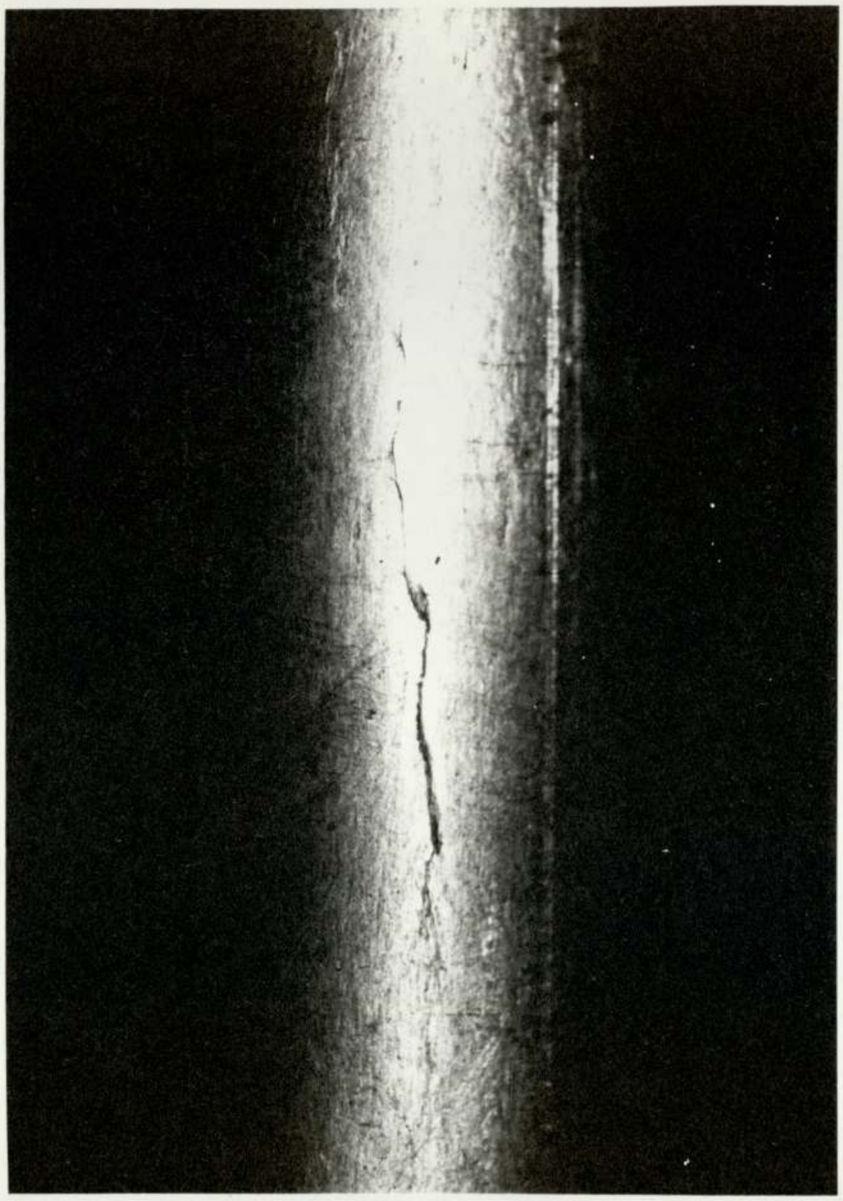

FIG. A_3.1. FISSURES IN 0.750 in. OUTSIDE DIAMETER x 0.0095 in. WALL THICKNESS ALUMINIUM TUBING AFTER 50 % COLD-WORK BY DRAWING.

TABLE A_3.2. DIMENSIONS OF TEST-PIECES IN SPLAY - MEASUREMENT TESTS.

Nominal O/dia wall thk.	Nominal o/dia. and wall thk. (in.)	Actual mean o/dia. (in.)	Actual mean wall thk. (in.)	Degree of prior cold work %	Material
20	0.750 x 0.0375	0.749	0.0399	0	steel
		0.750	0.0365	0	brass
		0.750	0.0368	50	brass
		0.750	0.0366	67	brass
		0.749	0.0374	0	alum.
		0.749	0.0378	50	alum.
		0.750	0.0378	67	alum.
25	0.750 x 0.030	0.748	0.0299	0	steel
		0.749	0.0299	50	steel
30	0.750 x 0.025	0.749	0.0253	50	steel
		0.753	0.0253	50	brass
		0.751	0.0241	0	stainless
		0.749	0.0243	50	alum.
40	0.750 x 0.019	0.750	0.0193	50	steel
		0.752	0.0194	50	brass
		0.755	0.0205	0	stainless
		0.755	0.0205	50	stainless
		0.749	0.0186	50	alum.
60	0.750 x 0.0125	0.749	0.0124	50	steel
		0.753	0.0121	50	brass
		0.752	0.0126	50	stainless
		0.749	0.0129	50	alum.
80	0.750 x 0.0095	0.752	0.0095	50	steel
		0.747	0.0093	50	brass
		0.750	0.0095	50	stainless
100	0.750 x 0.0075	0.751	0.0076	0	steel
		0.752	0.0076	50	steel
		0.752	0.0076	67	steel
		0.750	0.0078	0	stainless
		0.756	0.0081	50	stainless
		0.755	0.0081	67	stainless
		0.750	0.008	0	alum.
		0.748	0.008	50	alum.
		0.749	0.0082	67	alum.

which was subsequently redrawn in the splay-measurement programme.

A_3. 3. Tagging of splay-measurement test-pieces.

(a) Development of procedure.

Initial trials were carried out on a hydraulic press with the arrangement shown in FIG. A_3. 2a, the length of the adaptor bore L being equal to the test-piece test length. To maintain the transition from tag diameter to test-piece diameter short, single curvature dies of 3/16 in. profile radius were used throughout.

In a first series of tests attempts were made to tag-form 0.750 in. diameter, 0.025 in. thick tubes in various materials and states of hardness, using a two die procedure. It was planned to reduce tubes to 0.630 in. diameter in the first die, but this reduction proved unsuccessful, the tube wall collapsing into a bulge at die entry. The conclusion was drawn that reductions on a two die procedure were excessive.

Equilibrium of an element during frictionless pressing is given by,

$$(\sigma_1 - \sigma_3)\,dr + r\,d\sigma_1 = 0$$

The greatest algebraic principal stress is σ_2 which is small for thin-walled tubes. i.e. $\sigma_2 \simeq 0$. The radial stress σ_1 takes a maximum numerical value at die entry where it must not exceed Y for satisfactory pressing. Therefore according to Tresca's criterion the yield condition may be written,

$$0 - \sigma_3 = Y$$

Substitution in the equilibrium equation and integrating gives,

$$\sigma_1 = -Y\left(1 - \frac{r_e}{r_o}\right)$$

and the pressing force is thus $P = 2\pi t_o . Y\,(r_o - r_e)$. This expression was used to calculate a four-stage reducing procedure in which forming loads were approximately balanced;

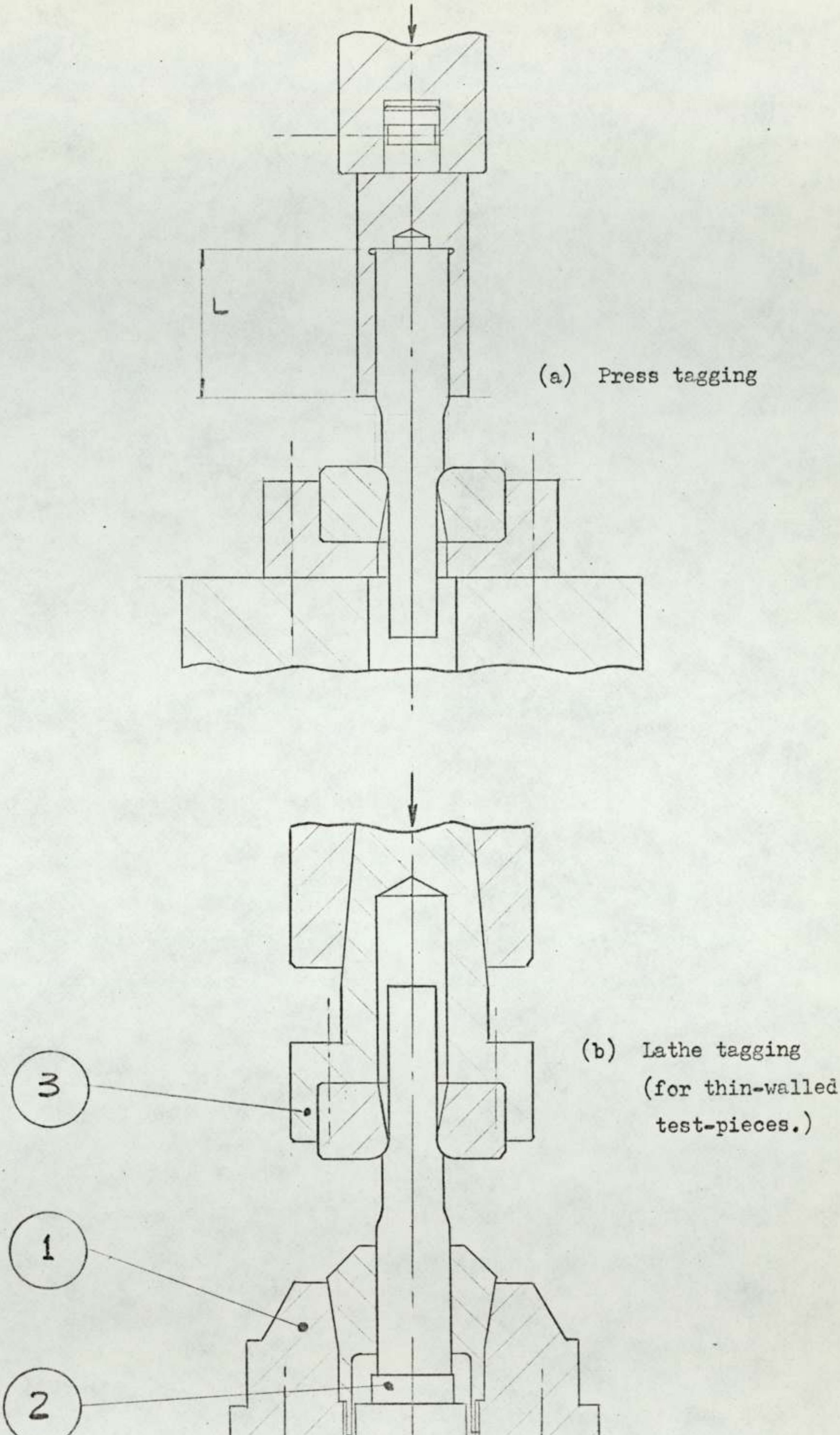

FIG. A_3.2. METHODS OF TAGGING SPLAY-MEASUREMENT TEST-PIECES.

Stage	tag diameter (in.)	diameter reduction %
0	0.750	-
1	0.655	12½
2	0.600	8½
3	0.559	7
4	0.525	6

In further tagging tests it was found that 0.750 in. diameter, 0.025 in. thick tubes could be reduced without the tube collapsing, but final tags were slightly bent. The problem commenced in the first stage and became accentuated in later stages. It was overcome by inserting a further light reduction stage in the procedure, as indicated;

Stage	tag diameter (in.)	diameter reduction %
0	0.750	-
1	0.700	6½
2	0.655	6½
3	0.600	8½
4	0.559	7
5	0.525	6

This procedure was followed throughout the remainder of the programme. Chlorinated mineral oil was used as the forming lubricant.

(b) Additional problems.

A problem was encountered in extracting test-pieces from dies after stages were completed due to the formation of a bell mouth at the open end of each tag, the 'bell' being of larger diameter than the die throat. With the thicker walled test-pieces (above 0.0125 in. thick) it was possible to remove the test-piece by reversing the die in its holder and using a knock-out piece. This procedure proved unsatisfactory with the thinner test-pieces (which tended to spring most), since any damage to the tag-end frequently led to failures in following stages where folding of the tag occurred in regions of previous damage. To circumvent the problem a different reducing arrangement was adopted for the thinner walled tubing and is illustrated in FIG. A_3. 2b. The test-piece was loaded into a collet (1) attached to the spindle of a centre-lathe, and abutted a stop (2). The stop served a dual purpose, it acted as a positioning device for the testpiece, and also carried most of the axial forming load when the die assembly (3), fitted in the tailstock, was advanced. Grip supplied by the collet was sufficient to retain the test-piece when the die assembly was retracted over the bell-mouth.

Although the above procedure enabled thin-walled test-pieces to be produced, the scrap rate was higher than with thicker ones. The main reason for this was folding at the tag mouth. Usually if this region was passed successfully there was little danger of buckling further along the tag. It was originally thought that folding problems for any particular tube would be most severe in the initial reducing stages, when the diameter/thickness ratio was largest. However this did not prove to be the case and the likelyhood of folding generally increased with overall reduction. A prime reason for this was a gradual deterioration of surface finish, particularly with brass where surface fissuring and pitting occurred. For the 0.0075 in. thick brass test-pieces fissures developed of sufficient magnitude to cause folding. FIG. A_3. 3 illustrates the condition. Due to this defect it was not possible to produce any test-pieces in 0.0075 in. thick brass.

Another failure mode with thinner tubing was that of bulge formation at the transition from tube diameter. This result was common with fully soft materials, especially stainless and brass, but was absent in highly work-hardened test-pieces.

(c) Data derived from tagging tests.

Information was obtained upon the variation of tube wall thickness with diameter reduction, and the deviation of final tag diameter from die diameter, for the various combinations of tube geometry and hardness covered in the splay measurement investigation.

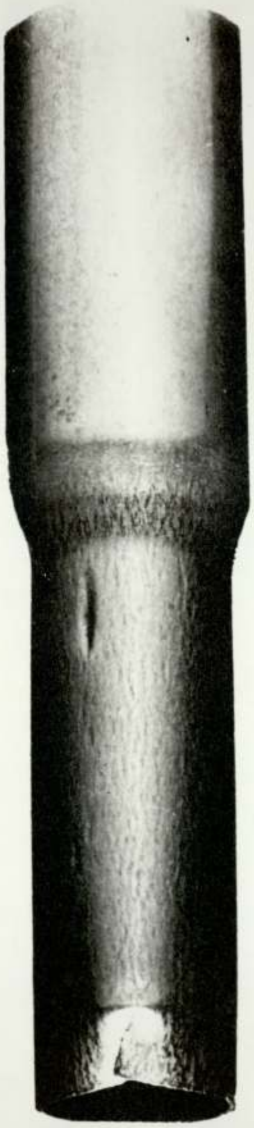

FIG. A_3.3. SURFACE DETERIORATION AND FOLDING IN 70/30 BRASS TUBING DURING MANUFACTURE OF TEST-PIECE FOR SPLAY-MEASUREMENT PROGRAMME.

Results of wall thickness changes with diameter reduction are shown for the four materials in FIGS. A_3. 4, A_3. 5, A_3. 6 and A_3. 7. Within the experimental scatter it was not possible to distinguish any positive trend related to prior cold work or tube diameter/thickness ratio. For this reason tabulated data is also included. Steel, brass and stainless gave an average thickening some 90 % of the overall diameter reduction, whilst aluminium appeared to have thickened slightly more than the corresponding diameter reduction, inferring a shortening of the test-piece.

Deviation of tag diameter from the final die size is shown in FIGS. A_3. 8 and A_3. 9. A correlation existed between diameter deviation and original tube diameter/thickness ratio, but again the influence of prior cold-work was not strong. Deviation was apparently a function of the materials elastic properties, brass and stainless springing more than aluminium or steel.

A_3.4. Chemical analysis of splay-measurement test-piece material.

Low carbon steel.

Carbon	-	0.098 %
Silicon	-	0.26 %
Manganese	-	0.46 %
Sulphur	-	0.034 %
Phosphorus	-	0.013 %

Stainless steel (T304)

Carbon	-	0.066 %
Silicon	-	0.51 %
Manganese	-	1.46%
Nickel	-	9.60 %
Chromium	-	17.20 %
Molybdenum	-	0.63 %
Sulphur	-	0.007 %
Phosphorus	-	0.023 %
Titanium	-	None found.

70/30 brass

Copper	-	71 %
Zinc	-	28 %

Aluminium (99.5 % pure)

Iron	-	0.29 %
Silicon	-	0.16 %

FIG. A_3.4 INCREASE IN WALL THICKNESS WITH DIAMETER REDUCTION FOR PRESSING. MATERIAL LOW CARBON STEEL.

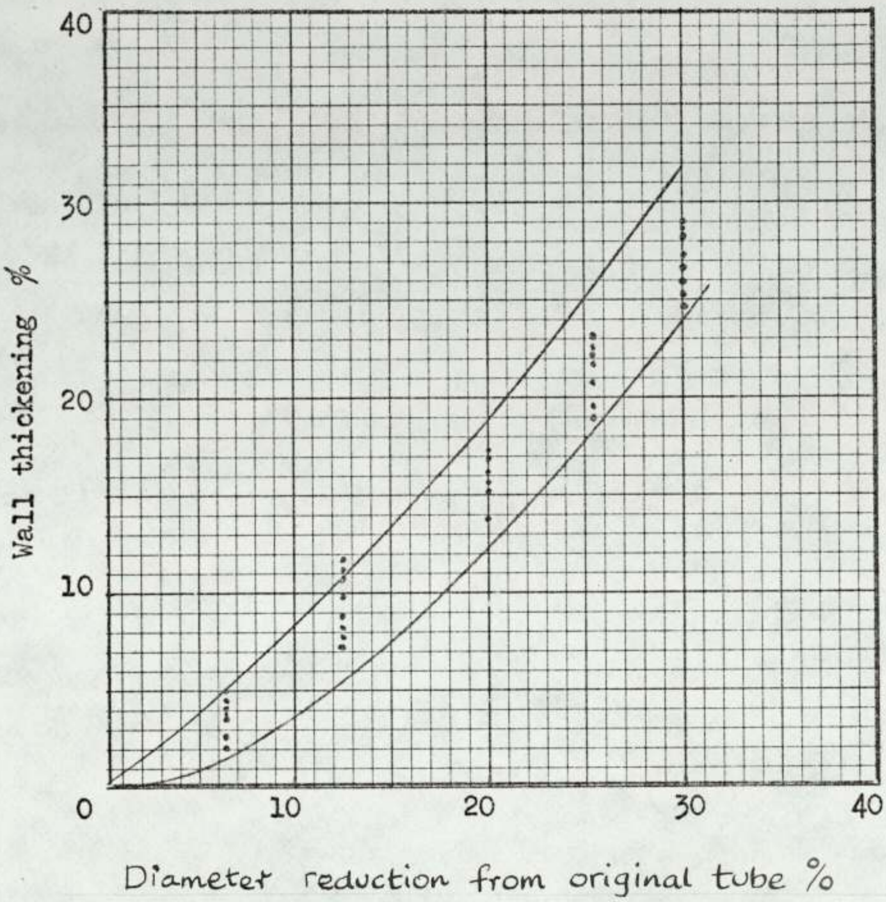

Diameter reduction %	Wall thickening %									
6.6	5.0	4.5	3.7	4.4	3.7	3.6	4.0	2.0	2.53	3.9
12.6	11.7	10.8	10.8	11.2	9.8	8.3	8.9	7.2	8.9	7.8
20.0	17.2	17.0	16.2	17.3	15.1	13.9	16.1	15.5	15.2	15.6
25.5	22.2	22.5	20.5	23.1	19.5	19.6	21.8	19.6	19.0	22.1
30.0	26.0	27.4	29.0	28.8	25.2	24.8	27.4	26.8	26.6	28.6
Original wall thickness (in.)	0.0401	0.0400	0.0297	0.0295	0.0246	0.0194	0.0124	0.0097	0.0079	0.0077
Prior cold-work (nominal)%	0	50	0	50	50	50	50	50	0	67

FIG.A_3.5 INCREASE IN WALL THICKNESS WITH DIAMETER REDUCTION FOR PRESSING. MATERIAL 70/30 BRASS.

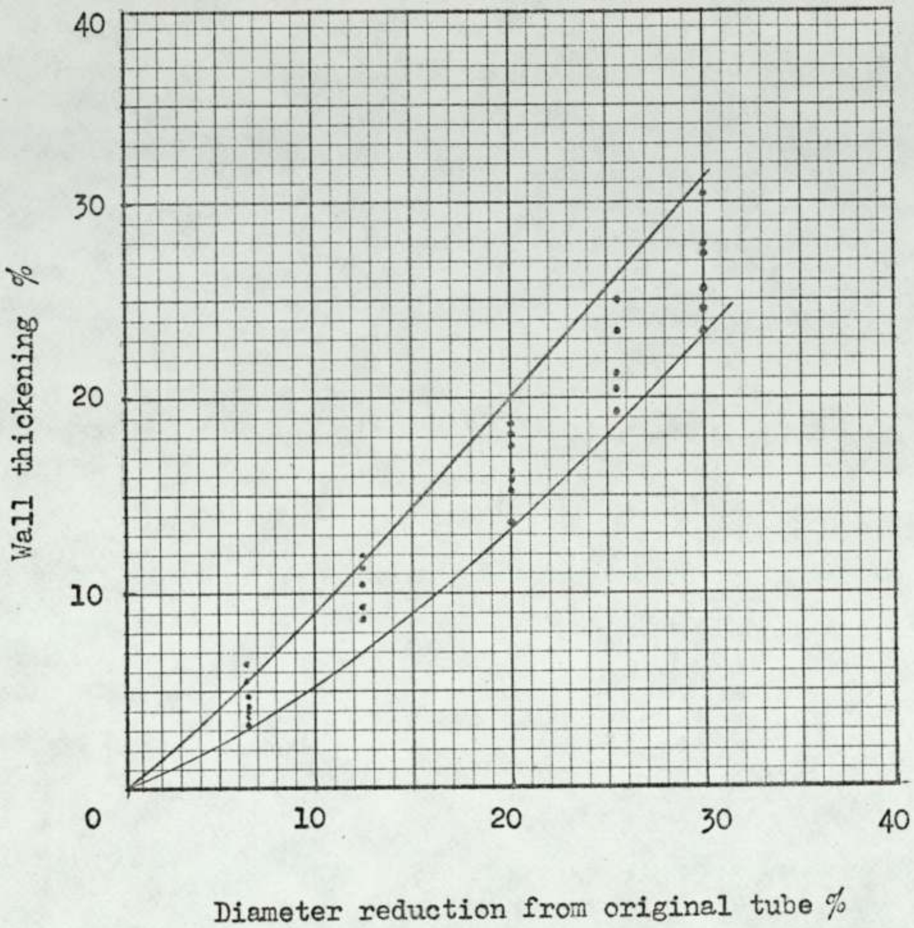

Diameter reduction %	Wall thickening %						
6.6	5.5	4.7	3.8	4.0	6.3	4.2	3.3
12.6	12.0	11.4	8.9	9.1	10.4	10.2	8.7
20.0	18.2	16.1	13.7	15.4	15.7	17.5	18.5
25.5	23.4	21.3	19.4	20.6	21.4	25.0	25.0
30	27.8	25.5	23.4	24.5	27.6	-	30.4
Original wall thickness (in.)	0.0368	0.0361	0.0371	0.0253	0.0192	0.0120	0.0092
Prior cold-work (nominal) %	0	50	67	50	50	50	50

FIG. A_3.6 INCREASE IN WALL THICKNESS WITH DIAMETER REDUCTION FOR PRESSING. MATERIAL T304 STAINLESS STEEL.

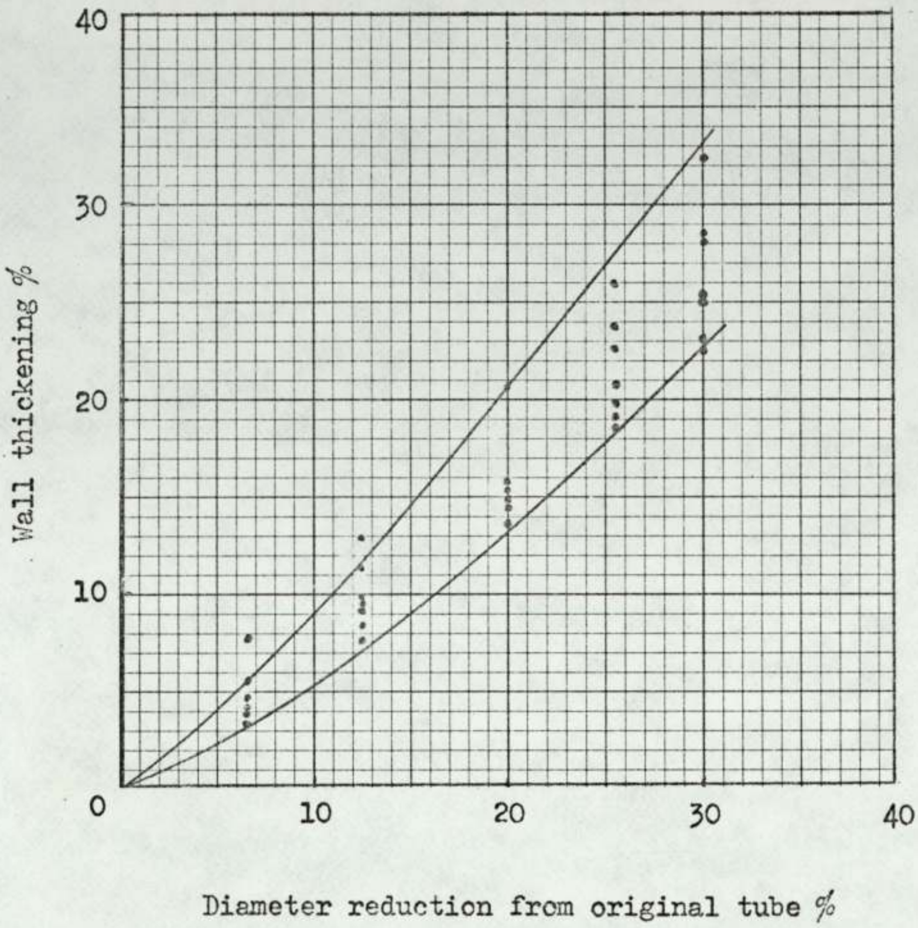

Diameter Reduction %	Wall thickening %								
6.6	4.14	4.16	4.41	5.41	3.2	3.2	7.8	3.8	3.8
12.6	9.9	8.33	11.3	9.9	9.6	8.4	13.0	7.5	7.5
20.0	15.7	14.6	17.7	14.3	15.4	15.8	20.8	13.8	15.0
25.5	19.0	18.8	22.6	19.7	20.8	18.9	26.0	18.8	18.8
30.0	28.1	23.0	28.4	22.6	-	25.2	32.2	25	25
Original wall thickness (in.)	0.0242	0.0240	0.0204	0.0203	0.0125	0.0095	0.0077	0.0080	0.0080
Prior cold-work (nominal)%	0	50	0	50	50	50	0	50	67

FIG. A_3.7 INCREASE IN WALL THICKNESS WITH DIAMETER REDUCTION FOR PRESSING. MATERIAL PURE ALUMINIUM.

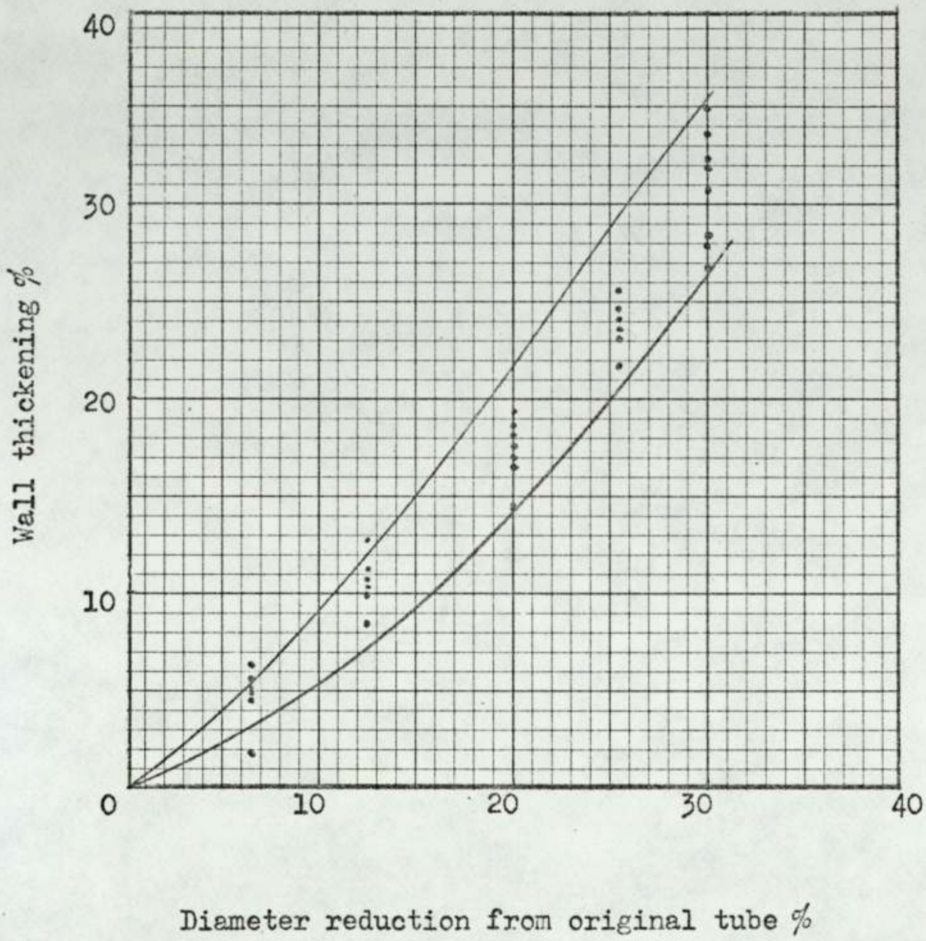

Diameter reduction %	Wall thickening %								
6.6	4.6	5.4	4.84	4.6	4.9	1.7	6.4	5.1	6.3
12.6	11.1	10.0	10.2	10.0	10.9	8.4	12.8	10.2	8.9
20.0	17.6	18.1	18.6	17.0	17.5	14.3	19.2	16.6	19
25.5	24.2	24.5	23.2	23.7	21.8	23.6	25.6	21.8	24
30.0	32.2	32.0	35.0	27.8	28.4	33.6	30.8	26.8	30.4
Original wall thickness (in.)	0.0369	0.0371	0.0372	0.0241	0.0183	0.0119	0.0078	0.0078	0.0079
Prior cold-work (nominal) %	0	50	67	50	50	50	0	50	67

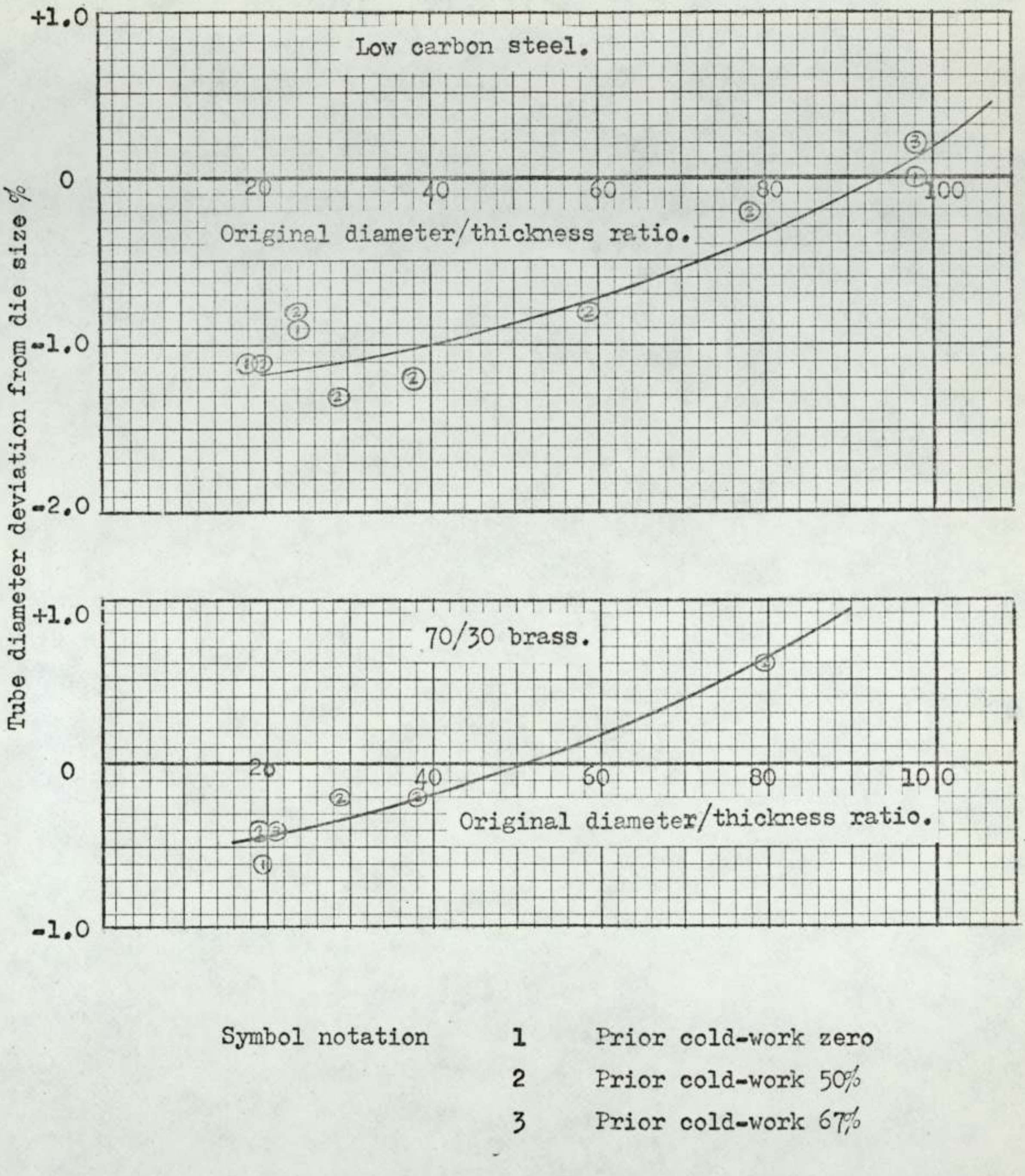

Symbol notation	1	Prior cold-work zero
	2	Prior cold-work 50%
	3	Prior cold-work 67%

FIG. A_3.8 TUBE DIAMETER DEVIATION FROM DIE SIZE AS A FUNCTION OF ORIGINAL DIAMETER/THICKNESS RATIO. TUBE PRESSED THROUGH 30% DIAMETER REDUCTION.

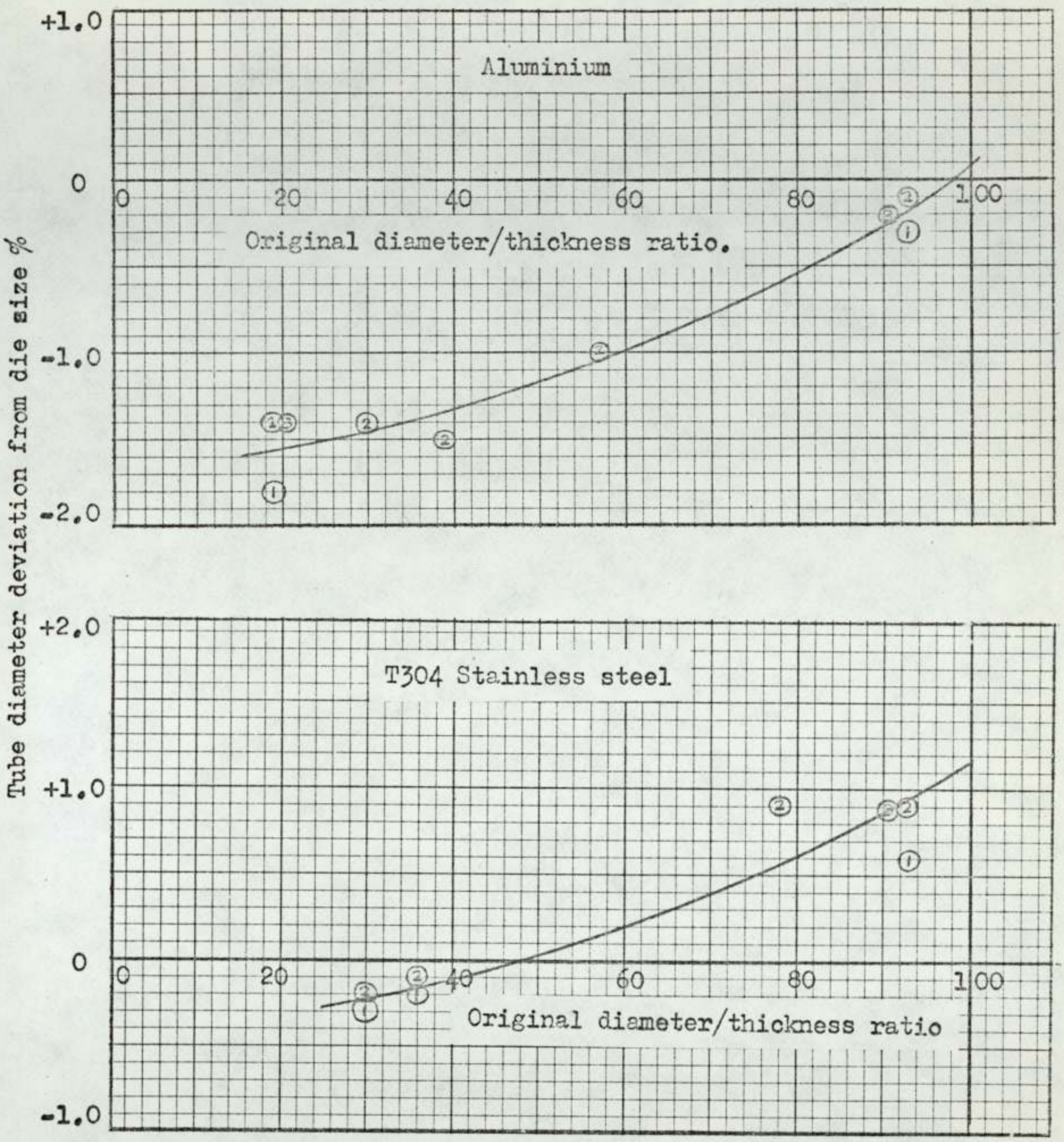

Symbol notation

Symbol notation	1	Prior cold-work zero
	2	Prior cold-work 50%
	3	Prior cold-work 67%

FIG. A_3.9 TUBE DIAMETER DEVIATION FROM DIE SIZE AS A FUNCTION OF ORIGINAL DIAMETER/THICKNESS RATIO. TUBE PRESSED THROUGH 30% DIAMETER REDUCTION.

A_3. 5. Preparation of splay-measurement test-pieces for redrawing.

(a) Etching solutions.

Low carbon steel:	50 % solution of hydrochloric acid at room temperature with added 0.1 % Armohib 28 inhibitor. Time of immersion 2 minutes.
70/30 brass:	10 % solution of sulphuric acid at 50 - 70°C. Time of immersion 5 minutes.
99.5 % pure aluminium:	20 - 21 gm./litre of caustic soda at room temperature. Time of immersion 2 minutes.
T304 stainless steel:	20 % nitric, 5 % hydrofluoric acid by volume at room temperature. Time of immersion 5 minutes. Followed by immersion in 'titox' oxalate solution for 10 minutes at 40°C.

(b) Lubricant.

Textile soap, comprising stearates and oleates, at 60 - 70°C. Steel, brass and aluminium test-pieces allowed to air dry. Stainless test-pieces heated for half-hour in an oven at 120°C to bake on soap film.

A_3. 6. Tabulated experimental results.

SPLAY MEASURMENT DATA - FREE REDRAWING

Table number $A_3.3$	Test number 1F(A)	
Mean test-piece rim distance from die (in.)	Distance along test-piece from die (in.)	Mean test-piece diameter relative to standard (in.)
1.000	1.000	-0.0010
	0.600	-0.0015
	0.300	-0.0009
	0.200	-0.0010
	0.150	-0.0018
	0.100	-0.0068
	0.050	-0.0263
	0.000	-0.0745
0.600	0.600	-0.0013
	0.300	-0.0009
	0.200	-0.0010
	0.150	-0.0019
	0.100	-0.0069
	0.050	-0.0263
	0.000	-0.0738
0.300	0.300	-0.0008
	0.200	-0.0010
	0.150	-0.0018
	0.100	-0.0070
	0.050	-0.0265
	0.000	-0.0739
0.200	0.200	+0.0056
	0.150	-0.0032
	0.100	-0.0133
	0.050	-0.0319
	0.000	-0.0777
0.150	0.150	+0.0125
	0.100	-0.0102
	0.050	-0.0364
	0.000	-0.0823
0.105	0.105	+0.0141
	0.050	-0.0306
	0.000	-0.0840
0.057	0.057	+0.0044
	0.000	-0.0752
0.008	0.008	-0.0733

Table number $A_3.4$	Test number 2F(A)	
Mean test-piece rim distance from die (in.)	Distance along test-piece from die (in.)	Mean test-piece diameter relative to standard (in.)
1.000	1.000	-0.0016
	0.600	-0.0013
	0.300	-0.0012
	0.200	-0.0013
	0.150	-0.0018
	0.100	-0.0063
	0.050	-0.0262
	0.000	-0.0804
0.600	0.600	-0.0011
	0.300	-0.0011
	0.200	-0.0012
	0.150	-0.0016
	0.100	-0.0062
	0.050	-0.0259
	0.000	-0.0777
0.300	0.300	-0.0008
	0.200	-0.0011
	0.150	-0.0016
	0.100	-0.0061
	0.050	-0.0260
	0.000	-0.0775
0.204	0.204	+0.0014
	0.150	-0.0021
	0.100	-0.0079
	0.050	-0.0271
	0.000	-0.0779
0.153	0.153	+0.0086
	0.100	-0.0087
	0.050	-0.0312
	0.000	-0.0809
0.113	0.113	+0.0133
	0.050	-0.0291
	0.000	-0.0829
0.063	0.063	+0.0102
	0.000	-0.0773
0.015	0.015	-0.0504

Table number $A_3.5$	Test number 3F(A)	
Mean test-piece rim distance from die. (in.)	Distance along test-piece from die. (in.)	Mean test-piece diameter relative to standard. (in.)
1.000	1.000	-0.0007
	0.600	-0.0004
	0.300	-0.0003
	0.200	-0.0003
	0.150	-0.0011
	0.100	-0.0058
	0.050	-0.0233
	0.000	-0.0733
0.600	0.600	-0.0020
	0.300	-0.0004
	0.200	-0.0001
	0.150	-0.0010
	0.100	-0.0056
	0.050	-0.0231
	0.000	-0.0726
0.296	0.296	-0.0001
	0.200	-0.0001
	0.150	-0.0009
	0.100	-0.0056
	0.050	-0.0229
	0.000	-0.0726
0.196	0.196	+0.0040
	0.150	-0.0004
	0.100	-0.0074
	0.050	-0.0249
	0.000	-0.0739
0.144	0.144	+0.0120
	0.100	-0.0047
	0.050	-0.0287
	0.000	-0.0772
0.096	0.096	+0.0179
	0.050	-0.0196
	0.000	-0.0784
0.045	0.045	+0.0113
	0.000	-0.0636
0.018	0.018	-0.0292

Table number $A_3.6$	Test number 4F(A)	
Mean test-piece rim distance from die. (in.)	Distance along test-piece from die. (in.)	Mean test-piece diameter relative to standard. (in.)
0.600	0.600	-0.0035
	0.300	-0.0002
	0.200	+0.0004
	0.150	+0.0001
	0.100	-0.0013
	0.050	-0.0078
	0.000	-0.0324
	-0.010	-0.0412
0.297	0.297	-0.0018
	0.200	+0.0004
	0.150	+0.0002
	0.100	-0.0011
	0.050	-0.0078
	0.000	-0.0327
	-0.010	-0.0411
0.187	0.187	+0.0012
	0.150	+0.0011
	0.100	-0.0016
	0.050	-0.0087
	0.000	-0.0334
	-0.010	-0.0419
0.137	0.137	+0.0072
	0.100	+0.0013
	0.050	-0.0111
	0.000	-0.0363
	-0.010	-0.0447
0.092	0.092	+0.0153
	0.050	-0.0051
	0.000	-0.0390
	-0.010	-0.0476
0.050	0.050	+0.0201
	0.000	-0.0298
	-0.010	-0.0416
0.017	0.017	+0.0163
	-0.010	+0.0054
-0.018	-0.018	+0.0129

SPLAY MEASUREMENT DATA - FREE REDRAWING

Table number A_3. 7	Test number 5 F(A)	
Mean test-piece rim distance from die. (in.)	Distance along test-piece from die. (in.)	Mean test-piece diameter relative to standard. (in.)
0.600	0.600	-0.0015
	0.300	-0.0012
	0.200	-0.0005
	0.150	-0.0002
	0.100	-0.0005
	0.050	-0.0032
	0.000	-0.0153
	-0.025	-0.0282
0.292	0.292	-0.0015
	0.200	-0.0005
	0.150	-0.0002
	0.100	-0.0006
	0.050	-0.0033
	0.000	-0.0151
	-0.025	-0.0280
0.195	0.195	+0.0001
	0.150	0.0000
	0.100	-0.0006
	0.050	-0.0033
	0.000	-0.0153
	-0.025	-0.0282
0.143	0.143	+0.0023
	0.100	+0.0001
	0.050	-0.0044
	0.000	-0.0163
	-0.025	-0.0290
0.089	0.089	+0.0094
	0.050	-0.0007
	0.000	-0.0189
	-0.025	-0.0317
0.047	0.047	+0.0148
	0.000	-0.0132
	-0.025	-0.0307
0.020	0.020	+0.0175
	-0.025	-0.0204
-0.013	-0.013	+0.0179

Table number A_3.8	Test number 6 F (A)	
Mean test-piece rim distance from die (in.)	Distance along test-piece from die. (in.)	Mean test-piece diameter relative to standard. (in.)
0.600	0.600	-0.0008
	0.300	-0.0009
	0.200	-0.0004
	0.150	+0.0001
	0.100	-0.0002
	0.050	-0.0009
	0.000	-0.0045
	-0.025	-0.0098
0.305	0.305	-0.0011
	0.200	-0.0002
	0.150	0.0000
	0.100	0.0000
	0.050	-0.0008
	0.000	-0.0045
	-0.025	-0.0098
0.198	0.198	-0.0010
	0.150	+0.0001
	0.100	-0.0001
	0.050	-0.0010
	0.000	-0.0046
	-0.025	-0.0098
0.148	0.148	+0.0004
	0.100	+0.0003
	0.050	-0.0010
	0.000	-0.0047
	-0.025	-0.0099
0.098	0.098	+0.0027
	0.050	-0.0003
	0.000	-0.0056
	-0.025	-0.0109
0.047	0.047	+0.0083
	0.000	-0.0036
	-0.025	-0.0115
0.008	0.008	+0.0114
	-0.025	-0.0032
-0.022	-0.022	+0.0109

SPLAY MEASUREMENT DATA - FREE REDRAWING

Table number A_3.9	Test number 7F(A)	
Mean test-piece rim distance from die. (in.)	Distance along test-piece from die. (in.)	Mean test-piece diameter relative to standard. (in.)
1.000	1.000	-0.0006
	0.600	-0.0008
	0.300	-0.0009
	0.200	-0.0013
	0.150	-0.0007
	0.100	-0.0026
	0.050	-0.0146
	0.000	-0.0557
0.600	0.600	-0.0007
	0.300	-0.0002
	0.200	+0.0001
	0.150	-0.0004
	0.100	-0.0024
	0.050	-0.0145
	0.000	-0.0556
0.300	0.300	-0.0003
	0.200	-0.0006
	0.150	-0.0011
	0.100	-0.0029
	0.050	-0.0147
	0.000	-0.0558
0.200	0.200	+0.019
	0.150	-0.0007
	0.100	-0.0039
	0.050	-0.0160
	0.000	-0.0564
0.145	0.145	+0.0080
	0.100	-0.0042
	0.050	-0.0207
	0.000	-0.0607
0.110	0.110	+0.0163
	0.050	-0.0202
	0.000	-0.0651
0.055	0.055	+0.0194
	0.000	-0.0589
0.023	0.023	+0.0042

Table number A_3.10	Test number 8F(A)	
Mean test-piece rim distance from die. (in.)	Distance along test-piece from die. (in.)	Mean test-piece diameter relative to standard. (in.)
0.600	0.600	+0.0003
	0.300	-0.0003
	0.200	+0.0001
	0.150	-0.0001
	0.100	-0.0007
	0.050	-0.0046
	0.000	-0.0263
	-0.010	-0.0354
0.300	0.300	+0.0007
	0.200	0.0000
	0.150	-0.0003
	0.100	-0.0008
	0.050	-0.0047
	0.000	-0.0295
	-0.010	-0.0353
0.193	0.193	+0.0016
	0.150	+0.0004
	0.100	-0.0013
	0.050	-0.0056
	0.000	-0.0269
	-0.010	-0.0358
0.150	0.150	+0.0048
	0.100	-0.0007
	0.050	-0.0080
	0.000	-0.0294
	-0.010	-0.0380
0.101	0.101	+0.0137
	0.050	0.0070
	0.000	-0.0353
	-0.010	-0.0438
0.053	0.053	+0.0217
	0.000	-0.0289
	-0.010	-0.0409
0.016	0.016	+0.0209
	-0.010	-0.0164
-	-	-

SPLAY MEASUREMENT DATA - FREE REDRAWING

Table number A_3.11	Test number 9F(A)	
Mean test-piece rim distance from die. (in.)	Distance along test-piece from die. (in.)	Mean test-piece diameter relative to standard. (in.)
0.600	0.600	-0.0008
	0.300	-0.0010
	0.200	-0.0007
	0.150	-0.0007
	0.100	-0.0007
	0.050	-0.0020
	0.000	-0.0114
	-0.025	-0.0235
0.292	0.292	-0.0007
	0.200	-0.0008
	0.150	-0.0007
	0.100	-0.0008
	0.050	-0.0020
	0.000	-0.0114
	-0.025	-0.0238
0.192	0.192	+0.0002
	0.150	-0.0002
	0.100	-0.0009
	0.050	-0.0024
	0.000	-0.0114
	-0.025	-0.0240
0.148	0.148	+0.0014
	0.100	-0.0004
	0.050	-0.0033
	0.000	-0.0126
	-0.025	-0.0249
0.091	0.091	+0.0081
	0.050	-0.0012
	0.000	-0.0164
	-0.025	-0.0286
0.040	0.040	+0.0157
	0.000	-0.0091
	-0.025	-0.0274
0.018	0.018	+0.0176
	-0.025	-0.0153
-0.010	-0.010	+0.0170

Table number A_3.12	Test number 10F(A)	
Mean test-piece rim distance from die (in.)	Distance along test-piece from die. (in.)	Mean test-piece diameter relative to standard. (in.)
0.600	0.600	
	0.300	
	0.200	
	0.150	
	0.100	
	0.050	
	0.000	
	-0.025	
	0.200	spurious test results. Misalignment developed in test-piece.
	0.150	
	0.100	
	0.050	
	0.000	
	-0.025	
	0.150	
	0.100	
	0.050	
	0.000	
	-0.025	
	0.100	
	0.050	
	0.000	
	-0.025	
	0.050	
	0.000	
	-0.025	
	0.000	
	-0.025	
	-0.025	

SPLAY MEASUREMENT DATA - FREE REDRAWING

Table number A_3.13	Test number 11F(A)	
Mean test-piece rim distance from die. (in.)	Distance along test-piece from die. (in.)	Mean test-piece diameter relative to standard. (in.)
1.000	1.000	+0.0005
	0.600	+0.0008
	0.300	+0.0008
	0.200	+0.0012
	0.150	+0.0012
	0.100	+0.0004
	0.050	-0.0091
	0.000	-0.0486
0.600	0.600	+0.0016
	0.300	+0.0012
	0.200	+0.0014
	0.150	+0.0012
	0.100	-0.0001
	0.050	-0.0091
	0.000	-0.0481
0.300	0.300	+0.0011
	0.200	+0.0006
	0.150	+0.0004
	0.100	-0.0015
	0.050	-0.0101
	0.000	-0.0496
0.200	0.200	+0.0030
	0.150	+0.0005
	0.100	-0.0014
	0.050	-0.0105
	0.000	-0.0499
0.153	0.153	+0.0067
	0.100	-0.0018
	0.050	-0.0138
	0.000	-0.0523
0.112	0.112	+0.0169
	0.050	-0.0156
	0.000	-0.0576
0.054	0.054	+0.0229
	0.000	-0.0529
0.009	0.009	-0.0104

Table number A_3.14	Test number 12F(A)	
Mean test-piece rim distance from die. (in.)	Distance along test-piece from die. (in.)	Mean test-piece diameter relative to standard. (in.)
0.600	0.600	+0.0011
	0.300	+0.0007
	0.200	+0.0010
	0.150	+0.0009
	0.100	+0.0010
	0.050	-0.0018
	0.000	-0.0200
	-0.010	-0.0280
0.300	0.300	+0.0004
	0.200	+0.0010
	0.150	+0.0009
	0.100	+0.0006
	0.050	-0.0019
	0.000	-0.0201
	-0.010	-0.0281
0.203	0.203	+0.0017
	0.150	+0.0010
	0.100	+0.0004
	0.050	-0.0021
	0.000	-0.0201
	-0.010	-0.0284
0.148	0.148	+0.0033
	0.100	+0.0007
	0.050	-0.0033
	0.000	-0.0212
	-0.010	-0.0295
0.101	0.101	+0.0105
	0.050	-0.0033
	0.000	-0.0260
	-0.010	-0.0342
0.054	0.054	+0.0191
	0.000	-0.0244
	-0.010	-0.0349
0.018	0.018	+0.0229
	-0.010	-0.0158
-	-	-

Table number A_3.15	Test number 13F(A)	
Mean test-piece rim distance from die. (in.)	Distance along test-piece from die. (in.)	Mean test-piece diameter relative to standard. (in.)
0.600	0.600	+0.0003
	0.300	0.0000
	0.200	+0.0005
	0.150	+0.0007
	0.100	+0.0006
	0.050	-0.0005
	0.000	-0.0082
	-0.025	-0.0205
0.305	0.305	+0.0005
	0.200	+0.0003
	0.150	+0.0005
	0.100	+0.0004
	0.050	-0.0007
	0.000	-0.0081
	-0.025	-0.0202
0.201	0.201	+0.0011
	0.150	+0.0007
	0.100	+0.0006
	0.050	-0.0008
	0.000	-0.0083
	-0.025	-0.0202
0.150	0.150	+0.0019
	0.100	+0.0009
	0.050	-0.0011
	0.000	-0.0088
	-0.025	-0.0205
0.101	0.101	+0.0050
	0.050	-0.0013
	0.000	-0.0110
	-0.025	-0.0223
0.050	0.050	+0.0135
	0.000	-0.0102
	-0.025	-0.0255
0.011	0.011	+0.0186
	-0.025	-0.0134
-0.022	-0.022	+0.0229

Table number A_3.16	Test number 14F(A)	
Mean test-piece rim distance from die (in.)	Distance along test-piece from die. (in.)	Mean test-piece diameter relative to standard. (in.)
0.600	0.600	-0.0003
	0.300	-0.0006
	0.200	+0.0005
	0.150	+0.0008
	0.100	+0.0008
	0.050	+0.0004
	0.000	-0.0017
	-0.025	-0.0058
0.288	0.288	0.0000
	0.200	+0.0005
	0.150	+0.0007
	0.100	+0.0008
	0.050	+0.0006
	0.000	-0.0014
	-0.025	-0.0055
0.187	0.187	+0.0002
	0.150	+0.0010
	0.100	+0.0007
	0.050	+0.0005
	0.000	-0.0015
	-0.025	-0.0056
0.144	0.144	+0.0011
	0.100	+0.0012
	0.050	+0.0005
	0.000	-0.0020
	-0.025	-0.0064
0.085	0.085	+0.0036
	0.050	+0.0019
	0.000	-0.0028
	-0.025	-0.0075
0.050	0.050	+0.0071
	0.000	-0.0017
	-0.025	-0.0079
0.028	0.028	+0.0098
	-0.025	-0.0025
-0.013	-0.013	+0.0160

SPLAY MEASUREMENT DATA - FREE REDRAWING

Table number A_3.17	Test number 15F(A)	
Mean test-piece rim distance from die. (in.)	Distance along test-piece from die. (in.)	Mean test-piece diameter relative to standard. (in.)
1.000	1.000	-
	0.600	-
	0.300	-
	0.200	-
	0.150	-
	0.100	-
	0.050	-
	0.000	-
0.600	0.600	+0.0009
	0.300	+0.0008
	0.200	+0.0008
	0.150	+0.0010
	0.100	+0.0003
	0.050	-0.0058
	0.000	-0.0512
0.300	0.300	+0.0004
	0.200	+0.0008
	0.150	+0.0011
	0.100	+0.0003
	0.050	-0.0057
	0.000	-0.0513
0.200	0.200	+0.0013
	0.150	+0.0013
	0.100	+0.0004
	0.050	-0.0057
	0.000	-0.0516
0.158	0.158	+0.0020
	0.100	+0.0006
	0.050	-0.0063
	0.000	-0.0522
0.109	0.109	+0.0070
	0.050	-0.0092
	0.000	-0.0542
0.083	0.083	+0.0126
	0.000	-0.0571
0.066	0.066	+0.0150
0.053	0.053	+0.0178

Table number A_3.18	Test number 16F(A)	
Mean test-piece rim distance from die. (in.)	Distance along test-piece from die. (in.)	Mean test-piece diameter relative to standard. (in.)
0.600	0.600	+0.0002
	0.300	+0.0004
	0.200	+0.0006
	0.150	+0.0008
	0.100	+0.0009
	0.050	-0.0003
	0.000	-0.0150
	-0.010	-0.0234
0.297	0.297	-0.0010
	0.200	+0.0007
	0.150	+0.0010
	0.100	+0.0010
	0.050	-0.0003
	0.000	-0.0151
	-0.010	-0.0230
0.202	0.202	+0.0001
	0.150	+0.0009
	0.100	+0.0012
	0.050	-0.0001
	0.000	-0.0149
	-0.010	-0.0229
0.146	0.146	+0.0011
	0.100	+0.0010
	0.050	-0.0006
	0.000	-0.0153
	-0.010	-0.0232
0.091	0.091	+0.0050
	0.050	-0.0008
	0.000	-0.0179
	-0.010	-0.0256
0.050	0.050	+0.0134
	0.000	-0.0194
	-0.010	-0.0286
0.015	0.015	+0.0171
	-	-
	-	-

SPLAY MEASUREMENT DATA - FREE REDRAWING

Table number A_3.19	Test number 17F(A)	
Mean test-piece rim distance from die. (in.)	Distance along test-piece from die. (in.)	Mean test-piece diameter relative to standard. (in.)
0.600	0.600	-0.0010
	0.300	-0.0001
	0.200	0.0000
	0.150	+0.0004
	0.100	+0.0008
	0.050	+0.0002
	0.000	-0.0042
	-0.025	-0.0154
0.292	0.292	+0.0001
	0.200	+0.0001
	0.150	+0.0002
	0.100	+0.0008
	0.050	+0.0004
	0.000	-0.0040
	-0.025	-0.0150
0.192	0.192	+0.0002
	0.150	+0.0005
	0.100	+0.0006
	0.050	+0.0003
	0.000	-0.0040
	-0.025	-0.0149
0.145	0.145	+0.0006
	0.100	+0.0007
	0.050	+0.0001
	0.000	-0.0042
	-0.025	-0.0151
0.099	0.099	+0.0018
	0.050	+0.0004
	0.000	-0.0047
	-0.025	-0.0155
0.047	0.047	+0.0082
	0.000	-0.0060
	-0.025	-0.0181
0.022	0.022	+0.0125
	-0.025	-0.0163
-0.003	-0.003	+0.0166

Table number A_3.20	Test number 18F(A)	
Mean test-piece rim distance from die (in.)	Distance along test-piece from die. (in.)	Mean test-piece diameter relative to standard. (in.)
0.600	0.600	+0.0005
	0.300	+0.0005
	0.200	+0.0002
	0.150	+0.0001
	0.100	+0.0005
	0.050	+0.0001
	0.000	-0.0007
	-0.025	-0.0035
0.305	0.305	+0.0005
	0.200	+0.0006
	0.150	+0.0008
	0.100	+0.0008
	0.050	+0.0010
	0.000	-0.0004
	-0.025	-0.0033
0.212	0.212	+0.0006
	0.150	+0.0007
	0.100	+0.0009
	0.050	+0.0011
	0.000	-0.0002
	-0.025	-0.0033
0.163	0.163	+0.0007
	0.100	+0.0009
	0.050	+0.0008
	0.000	-0.0002
	-0.025	-0.0032
0.114	0.114	+0.0008
	0.050	+0.0010
	0.000	-0.0004
	-0.025	-0.0033
0.065	0.065	+0.0020
	0.000	-0.0002
	-0.025	-0.0039
0.018	0.018	+0.0069
	-0.025	-0.0040
-0.010	-0.010	+0.0098

SPLAY MEASURMENT DATA - FREE REDRAWING

Table number A_3.21	Test number 19F(A)	
Mean test-piece rim distance from die (in.)	Distance along test-piece from die (in.)	Mean test-piece diameter relative to standard (in.)
1.000	1.000	-0.0005
	0.600	+0.0046
	0.300	+0.0049
	0.200	+0.0046
	0.150	+0.0028
	0.100	-0.0070
	0.050	-0.0327
	0.000	-0.0868
0.600	0.600	+0.0001
	0.300	+0.0049
	0.200	+0.0048
	0.150	+0.0026
	0.100	-0.0069
	0.050	-0.0331
	0.000	-0.0871
0.298	0.298	+0.0010
	0.200	+0.0039
	0.150	+0.0018
	0.100	-0.0075
	0.050	-0.0332
	0.000	-0.0869
0.198	0.198	+0.0072
	0.150	-0.0005
	0.100	-0.0129
	0.050	-0.0383
	0.000	-0.0894
0.151	0.151	+0.0127
	0.100	-0.0101
	0.050	-0.0410
	0.000	-0.0920
0.107	0.107	+0.0121
	0.050	-0.0358
	0.000	-0.0931
0.055	0.055	-0.0075
	0.000	-0.0880
0.008	0.008	-0.0859

Table number A_3.22	Test number 20F(A)	
Mean test-piece rim distance from die (in.)	Distance along test-piece from die (in.)	Mean test-piece diameter relative to standard (in.)
1.000	1.000	-0.0003
	0.600	+0.0003
	0.300	+0.0009
	0.200	+0.0007
	0.150	-0.0009
	0.100	-0.0074
	0.050	-0.0282
	0.000	-0.0783
0.600	0.600	-0.0002
	0.300	+0.011
	0.200	+0.0007
	0.150	-0.0007
	0.100	-0.0076
	0.050	-0.0281
	0.000	-0.0784
0.293	0.293	+0.0018
	0.200	+0.0007
	0.150	-0.0012
	0.100	-0.0076
	0.050	-0.0284
	0.000	-0.0788
0.202	0.202	+0.0105
	0.150	+0.0010
	0.100	-0.0113
	0.050	-0.0327
	0.000	-0.0809
0.152	0.152	+0.0199
	0.100	-0.0044
	0.050	-0.0355
	0.000	-0.0843
0.104	0.104	+0.0240
	0.050	-0.0249
	0.000	-0.0846
0.049	0.496	+0.0127
	0.000	-0.0720
0.016	0.016	-0.0543

SPLAY MEASURMENT DATA - FREE REDRAWING

Table number A_3.23	Test number 21F(A)	
Mean test-piece rim distance from die (in.)	Distance along test-piece from die (in.)	Mean test-piece diameter relative to standard (in.)
1.000	1.000	+0.0052
	0.600	+0.0042
	0.300	+0.0046
	0.200	+0.0048
	0.150	+0.0042
	0.100	+0.0018
	0.050	-0.0137
	0.000	-0.0639
0.600	0.600	+0.0052
	0.300	+0.0045
	0.200	+0.0047
	0.150	+0.0042
	0.100	+0.0018
	0.050	-0.0135
	0.000	-0.0637
0.297	0.297	+0.0056
	0.200	+0.0045
	0.150	+0.0040
	0.100	+0.0016
	0.050	-0.0137
	0.000	-0.0639
0.197	0.197	+0.0100
	0.150	+0.0051
	0.100	-0.0014
	0.050	-0.0166
	0.000	-0.0659
0.149	0.149	+0.0207
	0.100	+0.0023
	0.050	-0.0213
	0.000	-0.0705
0.097	0.097	+0.0295
	0.050	-0.0136
	0.000	-0.0732
0.050	0.050	+0.0251
	0.000	-0.0616
0.017	0.017	-0.0182

Table number A_3.24	Test number 22F(A)	
Mean test-piece rim distance from die (in.)	Distance along test-piece from die (in.)	Mean test-piece diameter relative to standard (in.)
1.000	1.000	+0.0056
	0.600	+0.0044
	0.300	+0.0049
	0.200	+0.0052
	0.150	+0.0050
	0.100	+0.0035
	0.050	-0.0085
	0.000	-0.0572
0.600	0.600	+0.0058
	0.300	+0.0046
	0.200	+0.0051
	0.150	+0.0050
	0.100	+0.0036
	0.050	-0.0081
	0.000	-0.0570
0.308	0.308	+0.0062
	0.200	+0.0047
	0.150	+0.0047
	0.100	+0.0035
	0.050	-0.0082
	0.000	-0.0567
0.206	0.206	+0.0078
	0.150	+0.0050
	0.100	+0.0024
	0.050	-0.0086
	0.000	-0.0568
0.156	0.156	+0.0138
	0.100	+0.0026
	0.050	-0.0122
	0.000	-0.0583
0.111	0.111	+0.0254
	0.050	-0.0129
	0.000	-0.0631
0.059	0.059	+0.0309
	0.000	-0.0603
0.021	0.021	+0.0050

SPLAY MEASURMENT DATA - FREE REDRAWING

Table numberA_3.25	Test number 23F(A)	
Mean test-piece rim distance from die (in.)	Distance along test-piece from die (in.)	Mean test-piece diameter relative to standard (in.)
1.000	1.000	+0.0054
	0.600	+0.0053
	0.300	+0.0053
	0.200	+0.0056
	0.150	+0.0055
	0.100	+0.0054
	0.050	-0.0012
	0.000	-0.0467
0.600	0.600	+0.0063
	0.300	+0.0055
	0.200	+0.0057
	0.150	+0.0056
	0.100	+0.0053
	0.050	-0.0016
	0.000	-0.0484
0.305	0.305	+0.0059
	0.200	+0.0058
	0.150	+0.0058
	0.100	+0.0055
	0.050	-0.0011
	0.000	-0.0474
0.205	0.205	+0.0063
	0.150	+0.0056
	0.100	+0.0053
	0.050	-0.0013
	0.000	-0.0470
0.150	0.150	+0.0078
	0.100	+0.0044
	0.050	-0.0035
	0.000	-0.0476
0.103	0.103	+0.0174
	0.050	-0.0015
	0.000	-0.0505
0.084	Test-piece rim became wrinkled.	
-		

Table numberA_3.26	Test number 24F(A)	
Mean test-piece rim distance from die (in.)	Distance along test-piece from die (in.)	Mean test-piece diameter relative to standard (in.)
1.000	1.000	+0.0043
	0.600	+0.0024
	0.300	+0.0019
	0.200	+0.0020
	0.150	+0.0014
	0.100	-0.0024
	0.050	-0.0213
	0.000	-0.0738
0.600	0.600	+0.0043
	0.300	+0.0026
	0.200	+0.0023
	0.150	+0.0018
	0.100	-0.0024
	0.050	-0.0212
	0.000	-0.0742
0.303	0.303	+0.0050
	0.200	+0.0028
	0.150	+0.0024
	0.100	-0.0018
	0.050	-0.0206
	0.000	-0.0738
0.205	0.205	+0.0069
	0.150	+0.0023
	0.100	-0.0029
	0.050	-0.0214
	0.000	-0.0742
0.156	0.156	+0.0134
	0.100	-0.0035
	0.050	-0.0249
	0.000	-0.0760
0.106	0.106	+0.0206
	0.050	-0.0224
	0.000	-0.0789
0.050	0.050	+0.0136
	0.000	-0.0724
0.014	0.014	-0.0401

SPLAY MEASURMENT DATA - FREE REDRAWING

Table number A_3.27	Test number 25F(A)	
Mean test-piece rim distance from die (in.)	Distance along test-piece from die (in.)	Mean test-piece diameter relative to standard (in.)
1.000	1.000	+0.0056
	0.600	+0.0064
	0.300	+0.0061
	0.200	+0.0065
	0.150	+0.0060
	0.100	+0.0035
	0.050	-0.0133
	0.000	-0.0666
0.600	0.600	+0.0061
	0.300	+0.0062
	0.200	+0.0064
	0.150	+0.0061
	0.100	+0.0037
	0.050	-0.0128
	0.000	-0.0664
0.300	0.300	+0.0059
	0.200	+0.0067
	0.150	+0.0065
	0.100	+0.0039
	0.050	-0.0128
	0.000	-0.0664
0.205	0.205	+0.0069
	0.150	+0.0064
	0.100	+0.0036
	0.050	-0.0128
	0.000	-0.0662
0.155	0.155	+0.0116
	0.100	+0.0018
	0.050	-0.0157
	0.000	-0.0679
0.110	0.110	+0.0187
	0.050	-0.0168
	0.000	-0.0710
0.059	0.059	+0.0178
	0.000	-0.0686
0.018	0.018	-0.0140

Table number A_3.28	Test number 26F(A)	
Mean test-piece rim distance from die (in.)	Distance along test-piece from die (in.)	Mean test-piece diameter relative to standard (in.)
1.000	1.000	+0.0077
	0.600	+0.0064
	0.300	+0.0062
	0.200	+0.0066
	0.150	+0.0065
	0.100	+0.0039
	0.050	-0.0091
	0.000	-0.0587
0.600	0.600	+0.0078
	0.300	+0.0064
	0.200	+0.0069
	0.150	+0.0064
	0.100	+0.0042
	0.050	-0.0091
	0.000	-0.0585
0.300	0.300	+0.0078
	0.200	+0.0061
	0.150	+0.0060
	0.100	+0.0040
	0.050	-0.0091
	0.000	-0.0583
0.192	0.192	+0.0106
	0.150	+0.0070
	0.100	+0.0024
	0.050	-0.0108
	0.000	-0.0592
0.151	0.151	+0.0174
	0.100	+0.0036
	0.050	-0.0148
	0.000	-0.0620
0.097	0.097	+0.0292
	0.050	-0.0098
	0.000	-0.0668
0.053	0.053	+0.0292
	0.000	-0.0588
0.012	0.012	-0.0175

SPLAY MEASURMENT DATA - FREE REDRAWING

Table number A_3.29	Test number 27F(A)	
Mean test-piece rim distance from die (in.)	Distance along test-piece from die (in.)	Mean test-piece diameter relative to standard (in.)
1.000	1.000	+0.0043
	0.600	+0.0039
	0.300	+0.0037
	0.200	+0.0038
	0.150	+0.0042
	0.100	+0.0033
	0.050	-0.0036
	0.000	-0.0480
0.600	0.600	+0.0039
	0.300	+0.0037
	0.200	+0.0040
	0.150	+0.0042
	0.100	+0.0035
	0.050	-0.0036
	0.000	-0.0484
0.292	0.292	+0.0040
	0.200	+0.0041
	0.150	+0.0043
	0.100	+0.0036
	0.050	-0.0033
	0.000	-0.0483
0.193	0.193	+0.0043
	0.150	+0.0049
	0.100	+0.0036
	0.050	-0.0034
	0.000	-0.0483
0.142	0.142	+0.0071
	0.100	+0.0041
	0.050	-0.0045
	0.000	-0.0487
0.098	0.098	+0.0159
	0.050	-0.0057
	0.000	-0.0517
0.057	0.057	+0.0234
	0.000	-0.0518
0.022	0.022	+0.0121

Table number A_3.30	Test number 28F(A	
Mean test-piece rim distance from die (in.)	Distance along test-piece from die (in.)	Mean test-piece diameter relative to standar (in.)
1.000	1.000	-0.0040
	0.600	+0.0009
	0.300	+0.0008
	0.200	+0.0007
	0.150	-0.0009
	0.100	-0.0096
	0.050	-0.0328
	0.000	-0.0840
0.600	0.600	-0.0028
	0.300	+0.0014
	0.200	+0.0008
	0.150	-0.0007
	0.100	-0.0090
	0.050	-0.0320
	0.000	-0.0835
0.302	0.302	-0.0029
	0.200	-0.0002
	0.150	-0.0006
	0.100	-0.0090
	0.050	-0.0316
	0.000	-0.0831
0.200	0.200	+0.0022
	0.150	-0.0043
	0.100	-0.0142
	0.050	-0.0353
	0.000	-0.0854
0.153	0.153	+0.0076
	0.100	-0.0132
	0.050	-0.0394
	0.000	-0.0877
0.104	0.104	+0.0104
	0.050	-0.0334
	0.000	-0.0889
0.054	0.054	+0.0019
	0.000	-0.0809
0.017	0.017	-0.0559

SPLAY MEASURMENT DATA - FREE REDRAWING

Table number A_3.31	Test number 29F(A)	
Mean test-piece rim distance from die (in.)	Distance along test-piece from die (in.)	Mean test-piece diameter relative to standard (in.)
1.000	1.000	-0.0001
	0.600	-0.0008
	0.300	-0.0006
	0.200	-0.0014
	0.150	-0.0023
	0.100	-0.0079
	0.050	-0.0277
	0.000	-0.0787
0.600	0.600	+0.0003
	0.300	-0.0010
	0.200	-0.0010
	0.150	-0.0019
	0.100	-0.0077
	0.050	-0.0278
	0.000	-0.0780
0.302	0.302	+0.0015
	0.200	-0.0013
	0.150	-0.0022
	0.100	-0.0080
	0.050	-0.0280
	0.000	-0.0786
0.205	0.205	+0.0080
	0.150	-0.0027
	0.100	-0.0132
	0.050	-0.0331
	0.000	-0.0811
0.155	0.155	+0.0165
	0.100	-0.0097
	0.050	-0.0376
	0.000	-0.0856
0.107	0.107	+0.0215
	0.050	-0.0289
	0.000	-0.0870
0.055	0.055	+0.0163
	0.000	-0.0745
0.014	0.014	-0.0565

Table number A_3.32	Test number 30F(A)	
Mean test-piece rim distance from die (in.)	Distance along test-piece from die (in.)	Mean test-piece diameter relative to standard (in.)
1.000	1.000	-0.0005
	0.600	+0.0001
	0.300	+0.0005
	0.200	+0.0004
	0.150	-0.0007
	0.100	-0.0067
	0.050	-0.0266
	0.000	-0.0770
0.600	0.600	-0.0020
	0.300	+0.0004
	0.200	+0.0003
	0.150	-0.0008
	0.100	-0.0065
	0.050	-0.0267
	0.000	-0.0773
0.293	0.293	+0.0011
	0.200	+0.0004
	0.150	-0.0009
	0.100	-0.0067
	0.050	-0.0270
	0.000	-0.0774
0.196	0.196	+0.0078
	0.150	-0.0001
	0.100	-0.0114
	0.050	-0.0320
	0.000	-0.0808
0.147	0.147	+0.0159
	0.100	-0.0057
	0.050	-0.0352
	0.000	-0.0844
0.097	0.097	+0.0199
	0.050	-0.0234
	0.000	-0.0840
0.053	0.053	+0.0143
	0.000	-0.0719
0.011	0.011	-0.0720

SPLAY MEASURMENT DATA - FREE REDRAWING

Table number A_3.33	Test number 31F(A)	
Mean test-piece rim distance from die (in.)	Distance along test-piece from die (in.)	Mean test-piece diameter relative to standard (in.)
1.000	1.000	0.0000
	0.600	+0.0004
	0.300	+0.0004
	0.200	+0.0006
	0.150	+0.0002
	0.100	-0.0026
	0.050	-0.0173
	0.000	-0.0671
0.600	0.600	+0.0002
	0.300	+0.0005
	0.200	+0.0005
	0.150	+0.0002
	0.100	-0.0025
	0.050	-0.0175
	0.000	-0.0672
0.294	0.294	+0.0008
	0.200	+0.0006
	0.150	+0.0002
	0.100	-0.0024
	0.050	-0.0173
	0.000	-0.0670
0.194	0.194	+0.0031
	0.150	+0.0005
	0.100	-0.0040
	0.050	-0.0187
	0.000	-0.0674
0.150	0.150	+0.0091
	0.100	-0.0043
	0.050	-0.0229
	0.000	-0.0705
0.093	0.093	+0.0182
	0.050	-0.0157
	0.000	-0.0742
0.046	0.046	+0.0169
	0.000	-0.0622
0.011	0.011	-0.0377

Table number A_3.34	Test number 32F(A)	
Mean test-piece rim distance from die (in.)	Distance along test-piece from die (in.)	Mean test-piece diameter relative to standard (in.)
1.000	1.000	-0.0012
	0.600	-0.0002
	0.300	-0.0002
	0.200	0.0000
	0.150	-0.0001
	0.100	-0.0015
	0.050	-0.0119
	0.000	-0.0584
0.600	0.600	-0.0004
	0.300	-0.0011
	0.200	+0.0001
	0.150	+0.0001
	0.100	-0.0015
	0.050	-0.0121
	0.000	-0.0588
0.292	0.292	-0.0012
	0.200	+0.0001
	0.150	0.0000
	0.100	-0.0013
	0.050	-0.0117
	0.000	-0.0579
0.188	0.188	+0.0015
	0.150	+0.0003
	0.100	-0.0016
	0.050	-0.0121
	0.000	-0.0581
0.137	0.137	+0.0063
	0.100	-0.0010
	0.050	-0.0159
	0.000	-0.0609
0.091	0.091	+0.0139
	0.050	-0.0127
	0.000	-0.0653
0.048	0.048	+0.0157
	0.000	-0.0578
0.018	0.018	-0.0094

SPLAY MEASURMENT DATA - FREE REDRAWING

Table number $A_3.35$	Test number 33F(A)	
Mean test-piece rim distance from die (in.)	Distance along test-piece from die (in.)	Mean test-piece diameter relative to standard (in.)
1.000	1.000	-0.0025
	0.600	-0.0005
	0.300	-0.0010
	0.200	-0.0009
	0.150	-0.0008
	0.100	-0.0014
	0.050	-0.0073
	0.000	-0.0514
0.600	0.600	-0.0019
	0.300	-0.0006
	0.200	-0.0007
	0.150	-0.0004
	0.100	-0.0011
	0.050	-0.0068
	0.000	-0.0500
0.303	0.303	-0.0017
	0.200	-0.0001
	0.150	-0.0002
	0.100	-0.0007
	0.050	-0.0067
	0.000	-0.0490
0.203	0.202	-0.0016
	0.150	-0.0003
	0.100	-0.0006
	0.050	-0.0069
	0.000	-0.0521
0.158	0.158	-0.0008
	0.100	-0.0008
	0.050	-0.0071
	0.000	-0.0496
0.111	0.111	+0.0044
	0.050	-0.0112
	0.000	-0.0523
0.067	0.067	+0.0124
	0.000	-0.0583
0.035	0.035	+0.0115

Table number	Test number	
Mean test-piece rim distance from die (in.)	Distance along test-piece from die (in.)	Mean test-piece diameter relative to standard (in.)
1.000	1.000	
	0.600	
	0.300	
	0.200	
	0.150	
	0.100	
	0.050	
	0.000	
0.600	0.600	
	0.300	
	0.200	
	0.150	
	0.100	
	0.050	
	0.000	
	0.200	
	0.150	
	0.100	
	0.050	
	0.000	
	0.150	
	0.100	
	0.050	
	0.000	
	0.100	
	0.050	
	0.000	
	0.050	
	0.000	
	0.000	

REDRAW LOAD MEASUREMENT DATA - FREE REDRAWING

Table number A_3. 36	Test number 1F (B)
Test piece rim distance from die (in.)	Redraw load (tonf.)
1.00	1.32
0.71	1.32
0.46	1.31
0.28	1.30
0.21	1.26
0.16	1.20
0.13	1.18
0.09	1.17
0.08	1.17
0.06	1.05
0.02	0.78

Table number A_3. 37	Test number 2F (B)
Test piece rim distance from die (in.)	Redraw load (tonf.)
1.00	1.33
0.74	1.32
0.50	1.32
0.29	1.32
0.21	1.30
0.17	1.25
0.10	1.22
0.08	1.22
0.05	1.10
0.00	0.86
-	-

Table number A_3. 38	Test number 3F (B)
Test piece rim distance from die (in.)	Redraw load (tonf.)
1.00	1.64
0.69	1.64
0.42	1.63
0.25	1.62
0.20	1.60
0.16	1.54
0.13	1.50
0.10	1.46
0.07	1.50
0.05	1.36
0.00	0.92

Table number A_3. 39	Test number 3F (G)
Test piece rim distance from die (in.)	Redraw load (tonf.)
1.00	1.64
0.72	1.64
0.44	1.64
0.20	1.62
0.17	1.60
0.13	1.54
0.10	1.48
0.07	1.50
0.06	1.45
0.00	1.02
-	-

REDRAW LOAD MEASUREMENT DATA - FREE REDRAWING

Table number A_3. 40	Test number 4F(B)
Test piece rim distance from die (in.)	Redraw load (tonf.)
1.00	1.65
0.58	1.62
0.31	1.62
0.20	1.61
0.16	1.58
0.12	1.51
0.08	1.46
0.04	1.50
0.00	1.33
-	-
-	-

Table number A_3. 41	Test number 5F(B)
Test piece rim distance from die (in.)	Redraw load (tonf.)
1.00	1.50
0.72	1.50
0.42	1.49
0.20	1.49
0.14	1.46
0.10	1.42
0.05	1.35
0.03	1.36
0.00	1.42
-0.03	1.36
-0.06	1.21
-0.07	0.74

Table number A_3. 42	Test number 6F(B)
Test piece rim distance from die (in.)	Redraw load (tonf.)
1.00	1.52
0.72	1.52
0.40	1.52
0.20	1.52
0.10	1.50
0.07	1.44
0.04	1.42
0.01	1.44
-0.02	1.36
-0.06	1.14
-	-

Table number A_3. 43	Test number 7F(B)
Test piece rim distance from die (in.)	Redraw load (tonf.)
1.00	1.05
0.74	1.06
0.33	1.05
0.21	1.04
0.17	1.00
0.10	0.93
0.07	0.95
0.02	0.62
-	-
-	-
-	-

REDRAW LOAD MEASUREMENT DATA - FREE REDRAWING

Table number A_3. 44	Test number 7F(G)
Test piece rim distance from die (in.)	Redraw load (tonf.)
1.00	1.08
0.77	1.08
0.56	1.08
0.33	1.08
0.20	1.07
0.15	1.03
0.11	0.98
0.08	0.95
0.06	0.96
0.04	0.87
0.00	0.65

Table number A_3. 45	Test number 8F(B)
Test piece rim distance from die (in.)	Redraw load (tonf.)
1.00	1.04
0.64	1.03
0.38	1.03
0.23	1.03
0.15	1.025
0.11	0.98
0.05	0.93
0.02	0.96
-0.03	0.82
-0.08	0.61
-	-

Table number A_3. 46	Test number 9F(B)
Test piece rim distance from die (in.)	Redraw load (tonf.)
1.00	1.01
0.80	1.00
0.50	0.995
0.25	0.995
0.15	0.98
0.12	0.95
0.08	0.90
0.04	0.87
0.00	0.90
-0.01	0.93
-0.04	0.86
-0.08	0.72

Table number A_3. 47	Test number 10F(B)
Test piece rim distance from die (in.)	Redraw load (tonf.)
Spurious results. Test-piece developed misalignment during redraw.	

REDRAW LOAD MEASUREMENT DATA - FREE REDRAWING

Table number A_3. 48	Test number 11F(B)
Test piece rim distance from die (in.)	Redraw load (tonf.)
1.00	0.89
0.59	0.89
0.30	0.89
0.20	0.88
0.16	0.85
0.12	0.80
0.10	0.79
0.07	0.82
0.04	0.69
0.02	0.46
-	-

Table number A_3. 49	Test number 11F(G)
Test piece rim distance from die (in.)	Redraw load (tonf.)
1.00	0.86
0.71	0.86
0.44	0.86
0.25	0.86
0.16	0.85
0.13	0.83
0.11	0.80
0.06	0.76
0.04	0.77
0.03	0.69
0.00	0.50

Table number A_3. 50	Test number 12F(B)
Test piece rim distance from die (in.)	Redraw load (tonf.)
1.00	0.86
0.76	0.86
0.55	0.855
0.31	0.855
0.17	0.85
0.13	0.84
0.11	0.82
0.09	0.79
0.04	0.765
0.01	0.79
0.00	0.74

Table number A_3. 51	Test number 13F(B)
Test piece rim distance from die (in.)	Redraw load (tonf.)
1.00	0.81
0.71	0.805
0.45	0.80
0.22	0.80
0.14	0.785
0.10	0.765
0.07	0.745
0.04	0.72
0.01	0.74
-0.01	0.745
-0.03	0.68
-0.05	0.59
-0.07	0.48

REDRAW LOAD MEASUREMENT DATA - FREE REDRAWING

Table number A_3. 52	Test number 14F(B)
Test piece rim distance from die (in.)	Redraw load (tonf.)
1.00	0.795
0.69	0.795
0.42	0.795
0.17	0.795
0.10	0.78
0.05	0.75
0.02	0.745
0.00	0.75
-0.04	0.70
-0.09	0.555
-	-

Table number A_3. 53	Test number 15F(B)
Test piece rim distance from die (in.)	Redraw load (tonf.)
1.00	0.54
0.61	0.54
0.31	0.54
0.17	0.53
0.12	0.52
0.10	0.50
0.08	0.32
0.03	0.17
-	-
-	-
-	-

Table number A_3. 54	Test number 15F(G)
Test piece rim distance from die (in.)	Redraw load (tonf.)
1.00	0.52
0.70	0.525
0.45	0.53
0.26	0.535
0.15	0.535
0.12	0.525
0.09	0.50
0.06	0.42
0.00	0.22
-	-
-	-

Table number A_3. 55	Test number 16F(B)
Test piece rim distance from die (in.)	Redraw load (tonf.)
1.00	0.51
0.69	0.51
0.38	0.51
0.15	0.50
0.11	0.49
0.09	0.47
0.05	0.45
0.04	0.46
0.03	0.40
0.00	0.31
-	-

REDRAW LOAD MEASUREMENT DATA - FREE REDRAWING

Table number A_3. 56	Test number 17F(B)
Test piece rim distance from die (in.)	Redraw load (tonf.)
1.00	0.51
0.77	0.51
0.53	0.505
0.28	0.505
0.11	0.505
0.07	0.49
0.05	0.47
0.01	0.46
-0.01	0.48
-0.02	0.42
-0.03	0.38
-0.05	0.29

Table number A_3. 57	Test number 18F(B)
Test piece rim distance from die (in.)	Redraw load (tonf.)
1.00	0.50
0.67	0.50
0.42	0.50
0.21	0.51
0.08	0.51
0.04	0.50
0.00	0.49
-0.02	0.50
-0.06	0.44
-0.08	0.35
-	-

Table number A_3. 58	Test number 19F(B)
Test piece rim distance from die (in.)	Redraw load (tonf.)
1.00	0.82
0.77	0.80
0.52	0.80
0.32	0.80
0.22	0.79
0.14	0.76
0.10	0.74
0.06	0.70
0.00	0.62
-	-
-	-

Table number A_3. 59	Test number 20F(B)
Test piece rim distance from die (in.)	Redraw load (tonf.)
1.00	1.50
0.75	1.50
0.51	1.50
0.32	1.50
0.25	1.49
0.20	1.44
0.16	1.38
0.13	1.35
0.08	1.35
0.05	1.14
0.00	0.73

REDRAW LOAD MEASUREMENT DATA - FREE REDRAWING

Table number $A_3.60$	Test number 20F(G)
Test piece rim distance from die (in.)	Redraw load (tonf.)
1.00	1.52
0.76	1.52
0.51	1.52
0.33	1.52
0.23	1.52
0.18	1.47
0.15	1.40
0.12	1.36
0.10	1.36
0.07	1.23
0.00	0.77

Table number $A_3.61$	Test number 21F(B)
Test piece rim distance from die (in.)	Redraw load (tonf.)
1.00	1.03
0.76	1.02
0.50	1.02
0.33	1.02
0.22	1.02
0.17	0.99
0.14	0.97
0.10	0.93
0.06	0.95
0.04	0.86
0.00	0.52

Table number $A_3.62$	Test number 21F(G)
Test piece rim distance from die (in.)	Redraw load (tonf.)
1.00	1.07
0.63	1.07
0.40	1.07
0.30	1.07
0.22	1.07
0.16	1.04
0.11	1.00
0.08	0.95
0.06	0.96
0.05	0.89
0.04	0.77

Table number $A_3.63$	Test number 22F(B)
Test piece rim distance from die (in.)	Redraw load (tonf.)
1.00	0.79
0.69	0.79
0.43	0.79
0.25	0.79
0.19	0.785
0.14	0.76
0.12	0.73
0.09	0.72
0.05	0.73
0.04	0.68
0.00	0.46

REDRAW LOAD MEASUREMENT DATA - FREE REDRAWING

Table number A_3. 64	Test number 22F(G)
Test piece rim distance from die (in.)	Redraw load (tonf.)
1.00	0.78
0.63	0.78
0.33	0.78
0.23	0.78
0.16	0.77
0.11	0.74
0.08	0.71
0.05	0.685
0.04	0.66
0.03	0.57
0.00	0.36

Table number A_3. 65	Test number 23F(B)
Test piece rim distance from die (in.)	Redraw load (tonf.)
1.00	0.465
0.60	0.46
0.32	0.46
0.16	0.46
0.14	0.45
0.13	0.445
0.10	0.42
0.07	0.21
0.02	0.07
-	-
-	-

Table number A_3. 66	Test number 23F(G)
Test piece rim distance from die (in.)	Redraw load (tonf.)
1.00	0.485
0.59	0.475
0.33	0.475
0.17	0.48
0.11	0.475
0.09	0.445
0.06	0.345
0.00	0.19
-	-
-	-
-	-

Table number A_3. 67	Test number 24F(B)
Test piece rim distance from die (in.)	Redraw load (tonf.)
1.00	1.10
0.68	1.08
0.46	1.08
0.30	1.08
0.20	1.08
0.16	1.06
0.11	1.02
0.07	1.00
0.05	0.95
0.01	0.74
-	-

REDRAW LOAD MEASUREMENT DATA - FREE REDRAWING

Table number A_3. 68	Test number 25F(B)
Test piece rim distance from die (in.)	Redraw load (tonf.)
1.00	0.95
0.77	0.94
0.54	0.94
0.30	0.94
0.16	0.94
0.11	0.90
0.05	0.86
0.01	0.66
-	-
-	-
-	-

Table number A_3. 69	Test number 26F(B)
Test piece rim distance from die (in.)	Redraw load (tonf.)
1.00	1.62
0.74	1.62
0.46	1.61
0.28	1.61
0.20	1.58
0.15	1.53
0.10	1.43
0.07	1.46
0.05	1.36
0.00	1.05
-	-

Table number A_3. 70	Test number 26F(G)
Test piece rim distance from die (in.)	Redraw load (tonf.)
1.00	1.66
0.62	1.66
0.32	1.66
0.20	1.66
0.14	1.60
0.11	1.52
0.08	1.50
0.06	1.47
0.05	1.32
0.00	0.82
-	-

Table number A_3. 71	Test number 27F(B)
Test piece rim distance from die (in.)	Redraw load (tonf.)
1.00	0.96
0.73	0.96
0.51	0.97
0.29	0.97
0.17	0.97
0.14	0.96
0.11	0.92
0.08	0.89
0.07	0.905
0.04	0.745
0.00	0.31

REDRAW LOAD MEASUREMENT DATA - FREE REDRAWING

Table number A_3. 72	Test number 27F(G)
Test piece rim distance from die (in.)	Redraw load (tonf.)
1.00	0.94
0.90	0.96
0.75	0.98
0.58	0.98
0.40	0.99
0.25	0.99
0.14	1.00
0.08	0.94
0.06	0.86
0.00	0.54
-	-

Table number A_3. 73	Test number 28F(B)
Test piece rim distance from die (in.)	Redraw load (tonf.)
1.00	0.244
0.69	0.244
0.44	0.230
0.24	0.230
0.19	0.225
0.15	0.219
0.10	0.212
0.08	0.215
0.06	0.205
0.00	0.167
-	-

Table number A_3. 74	Test number 29F(B)
Test piece rim distance from die (in.)	Redraw load (tonf.)
1.00	0.316
0.79	0.316
0.58	0.315
0.39	0.315
0.27	0.313
0.22	0.305
0.17	0.290
0.14	0.285
0.10	0.290
0.06	0.260
0.00	0.205

Table number A_3. 75	Test number 29F(G)
Test piece rim distance from die (in.)	Redraw load (tonf.)
1.00	0.34
0.76	0.34
0.53	0.34
0.33	0.34
0.23	0.337
0.18	0.325
0.14	0.315
0.11	0.30
0.09	0.305
0.06	0.273
0.01	0.198

REDRAW LOAD MEASUREMENT DATA - FREE REDRAWING

Table number A_3. 76	Test number 30F(B)
Test piece rim distance from die (in.)	Redraw load (tonf.)
1.00	0.340
0.78	0.340
0.53	0.338
0.33	0.335
0.24	0.332
0.20	0.321
0.15	0.310
0.12	0.302
0.12	0.308
0.05	0.280
0.00	0.235

Table number A_3. 77	Test number 31F(B)
Test piece rim distance from die (in.)	Redraw load (tonf.)
1.00	0.205
0.69	0.205
0.49	0.205
0.28	0.205
0.19	0.200
0.14	0.195
0.11	0.186
0.07	0.192
0.05	0.170
0.00	0.105
-	-

Table number A_3. 78	Test number 31F(G)
Test piece rim distance from die (in.)	Redraw load (tonf.)
1.00	0.205
0.66	0.205
0.39	0.205
0.20	0.205
0.15	0.20
0.12	0.191
0.08	0.18
0.07	0.182
0.04	0.164
0.01	0.13
-	-

Table number A_3. 79	Test number 32F(B)
Test piece rim distance from die (in.)	Redraw load (tonf.)
1.00	0.155
0.85	0.155
0.65	0.158
0.45	0.158
0.28	0.158
0.16	0.155
0.11	0.148
0.07	0.142
0.04	0.148
0.03	0.138
0.00	0.112

REDRAW LOAD MEASUREMENT DATA - FREE REDRAWING

Table number A3. 80	Test number 32F(G)
Test piece rim distance from die (in.)	Redraw load (tonf.)
1.00	0.15
0.58	0.15
0.35	0.15
0.17	0.15
0.12	0.143
0.10	0.134
0.09	0.134
0.03	0.115
0.01	0.068
-	-
-	-

Table number A3. 81	Test number 33F(B)
Test piece rim distance from die (in.)	Redraw load (tonf.)
1.00	0.090
0.81	0.090
0.59	0.092
0.43	0.092
0.27	0.095
0.15	0.095
0.12	0.092
0.11	0.088
0.07	0.090
0.05	0.067
0.00	0.035

Table number A3. 82	Test number 33F(G)
Test piece rim distance from die (in.)	Redraw load (tonf.)
1.00	0.092
0.73	0.095
0.48	0.095
0.30	0.095
0.20	0.095
0.14	0.095
0.10	0.090
0.07	0.080
0.03	0.058
0.01	0.035
-	-

Table number	Test number
Test piece rim distance from die (in.)	Redraw load (tonf.)

TABLE A_3. 83.

SPLAY MEASUREMENT TEST PROGRAMME - FREE PROFILE DATA

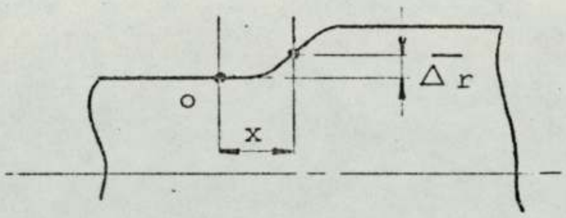

Test number	1F(P)	2F(P)	3F(P)	4F(P)	5F(P)	6F(P)	7F(P)
x (in.)	$\overline{\Delta r}$(in.)	$\overline{\Delta r}$(in.)	$\overline{\Delta r}$(in.)	$\overline{\Delta r}$(in.)	$\overline{\Delta r}$(in.)	$\overline{\Delta r}$(in.)	$\overline{\Delta r}$(in.)
0	0	0	0	0	0	0	0
0.025	-	0.0001	0	0.0001	0.0001	0.0001	-
0.050	0	0.0008	0.0008	0.0007	0.0006	0.0007	0.0001
0.075	0	0.0033	0.0038	0.0031	0.0027	0.0033	0.0003
0.100	0.0006	0.0090	0.0102	0.0097	0.0102	0.0074	0.0012
0.125	0.0021	0.0210	0.0237	0.0246	0.0216	0.0164	0.0045
0.150	0.0057	0.0455	0.0505	0.0565	0.0448	0.0294	0.0134
0.175	0.0144	0.0692	0.0749	0.0798	0.0664	0.0435	0.0307
0.200	0.0311	0.0862	0.0909	0.0942	0.0868	0.0589	0.0624
0.225	0.0571	0.0969	0.1005	0.1032	0.0986	0.0743	0.0853
0.250	0.0770	0.1039	0.1063	0.1084	0.1053	0.0887	0.0978
0.275	0.0910	0.1083	0.1093	-	0.1093	0.1001	0.1055
0.300	0.1004	0.1105	0.1108	0.1124	-	0.1074	0.1095
0.325	0.1068	0.1113	0.1115	-	0.1123	0.1121	0.1113
0.350	0.1107	-	-	0.1132	-	0.1148	-
0.375	-	0.1116	0.1117	-	0.1128	-	0.1120
0.400	0.1131	-	-	-	-	0.1169	-
0.425	-	0.1115	-	-	-	-	0.1121
0.450	0.1134	-	-	-	-	0.1174	-
0.475	-	-	-	-	-	-	0.1120
0.500	0.1133	-	-	-	-	-	-
0.525	-	-	-	-	-	-	0.1119

TABLE A_3. 84.

SPLAY MEASUREMENT TEST PROGRAMME - FREE PROFILE DATA

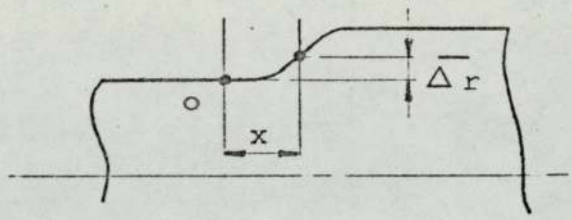

Test number	8F(P)	9F(P)	10F(P)	11F(P)	12F(P)	13F(P)	14F(P)
x (in.)	$\overline{\Delta r}$(in.)	$\overline{\Delta r}$(in.)	$\overline{\Delta r}$(in.)	$\overline{\Delta r}$(in.)	$\overline{\Delta r}$(in.)	$\overline{\Delta r}$(in.)	$\overline{\Delta r}$(in.)
0	0	0	0	0	0	0	0
0.025	0	0.0002	0.0002	-	-	0.0001	0.0001
0.050	0.0003	0.0009	0.0014	0	0.0001	0.0006	0.0011
0.075	0.0015	0.0038	0.0048	0	0.0002	0.0028	0.0045
0.100	0.0057	0.0113	0.0122	0.0005	0.0017	0.0079	0.0125
0.125	0.0165	0.0267	0.0241	0.0027	0.0068	0.0242	0.0254
0.150	0.0429	0.0518	0.0383	0.0098	0.0185	0.0482	0.0399
0.175	0.0747	0.0766	0.0532	0.0242	0.0473	0.0743	0.0550
0.200	0.0932	0.0931	0.0687	0.0524	0.0808	0.0925	0.0699
0.225	0.1030	0.1029	0.0841	0.0816	0.0977	0.1032	0.0852
0.250	0.1088	0.1083	0.0973	0.0973	0.1063	0.1088	0.0986
0.275	0.1115	0.1111	0.1062	0.1057	0.1108	0.1113	0.1069
0.300	0.1124	0.1122	0.1119	0.1097	0.1125	-	0.1118
0.325	0.1128	0.1126	0.1149	0.1112	0.1129	0.1124	0.1142
0.350	-	-	0.1163	-	-	-	-
0.375	0.1129	0.1128	-	0.1119	0.1130	0.1126	0.1155
0.400	-	-	0.1170	-	-	-	-
0.425	-	-	-	0.1119	-	-	0.1157
0.450	-	-	-	-	-	-	-
0.475	-	-	-	-	-	-	-
0.500	-	-	-	-	-	-	-
0.525	-	-	-	-	-	-	-

TABLE A_3. 85.

SPLAY MEASUREMENT TEST PROGRAMME - FREE PROFILE DATA

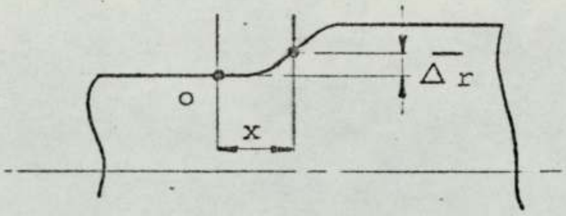

Test number	15F(P)	16F(P)	17F(P)	18F(P)	19F(P)	20F(P)	21F(P)
x (in.)	$\overline{\Delta r}$(in.)	$\overline{\Delta r}$(in.)	$\overline{\Delta r}$(in.)	$\overline{\Delta r}$(in.)	$\overline{\Delta r}$(in.)	$\overline{\Delta r}$(in.)	$\overline{\Delta r}$(in.)
0	0	0	0	0	0	0	0
0.025	-	-	0.0001	0.0001	0.0001	0	0.0001
0.050	0.0002	0	0.0007	0.0009	0.0005	0.0003	0.0009
0.075	0.0002	0	0.0037	0.0053	0.0023	0.0018	0.0050
0.100	0.0013	0.0006	0.0132	0.0153	0.0061	0.0052	0.0132
0.125	0.0058	0.0040	0.0312	0.0297	0.0139	0.0122	0.0310
0.150	0.0163	0.0135	0.0567	0.0451	0.0300	0.0271	0.0612
0.175	0.0371	0.0373	0.0821	0.0595	0.0533	0.0539	0.0852
0.200	0.0764	0.0770	0.0992	0.0747	0.0723	0.0749	0.0968
0.225	0.0966	0.0976	0.1073	0.0897	0.0877	0.0897	0.1067
0.250	0.1064	0.1073	-	0.1020	0.0981	0.0992	0.1108
0.275	0.1103	0.1109	0.1117	0.1088	0.1052	0.1055	0.1125
0.300	0.1114	0.1119	-	0.1120	0.1101	0.1093	-
0.325	-	-	0.1121	0.1132	0.1130	0.1113	0.1133
0.350	0.1120	0.1124	-	-	0.1145	-	-
0.375	-	-	0.1120	0.1137	-	0.1127	0.1133
0.400	0.1118	-	-	-	0.1154	-	-
0.425	-	-	-	0.1137	-	0.1130	-
0.450	-	-	-	-	0.1156	-	-
0.475	-	-	-	-	-	-	-
0.500	-	-	-	-	-	-	-
0.525	-	-	-	-	-	-	-

TABLE A_3. 86.

SPLAY MEASUREMENT TEST PROGRAMME - FREE PROFILE DATA

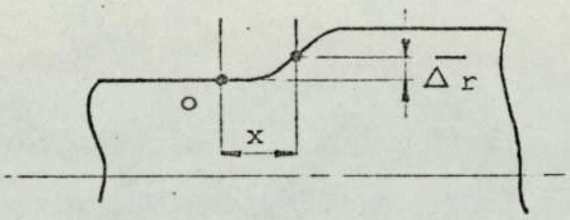

Test number	22F(P)	23F(P)	24F(P)	25F(P)	26F(P)	27F(P)	28F(P)
x (in.)	$\overline{\Delta}$ r(in.)	$\overline{\Delta}$ r(in.)	$\overline{\Delta}$ r(in.)	$\overline{\Delta}$ r(in.)	$\overline{\Delta}$ r(in.)	$\overline{\Delta}$ r(in.)	$\overline{\Delta}$ r(in.)
0	0	0	0	0	0	0	0
0.025	0	0.0001	0	0.0002	0	0	0.0001
0.050	0.0004	0.0008	0.0006	0.0009	0	0.0003	0.0005
0.075	0.0022	0.0035	0.0026	0.0042	0.0003	0.0017	0.0023
0.100	0.0076	0.0108	0.0083	0.0119	0.0016	0.0062	0.0067
0.125	0.0193	0.0256	0.0206	0.0284	0.0060	0.0161	0.0151
0.150	0.0429	0.0564	0.0448	0.0578	0.0155	0.0366	0.0324
0.175	0.0757	0.0903	0.0700	0.0824	0.0356	0.0723	0.0575
0.200	0.0949	0.1048	0.0875	0.0969	0.0680	0.0956	0.0763
0.225	0.1053	0.1109	0.0989	0.1058	0.0904	0.1062	0.0900
0.250	0.1104	-	0.1057	0.1105	0.1027	0.1103	0.0993
0.275	0.1126	0.1129	0.1094	0.1127	0.1093	-	0.1054
0.300	-	-	-	0.1135	-	0.1120	0.1094
0.325	0.1133	0.1133	0.1117	-	0.1133	-	-
0.350	-	-	-	0.1137	-	0.1121	0.1129
0.375	0.1134	0.1132	0.1120	-	0.1139	-	-
0.400	-	-	-	0.1137	-	0.1120	0.1134
0.425	0.1132	-	0.1120	-	0.1138	-	-
0.450	-	-	-	0.1136	-	-	0.1134
0.475	-	-	0.1119	-	-	-	-
0.500	-	-	-	-	-	-	-
0.525	-	-	-	-	-	-	-

TABLE A_3. 87.

SPLAY MEASUREMENT TEST PROGRAMME - FREE PROFILE DATA

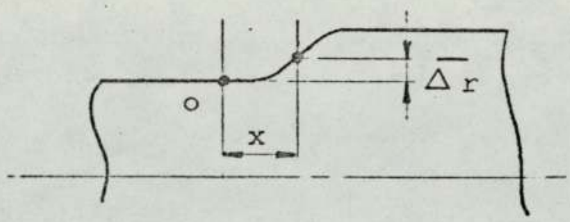

Test number	29F(P)	30F(P)	31F(P)	32F(P)	33F(P)		
x (in.)	$\overline{\Delta r}$(in.)	$\overline{\Delta r}$(in.)	$\overline{\Delta r}$(in.)	$\overline{\Delta r}$(in.)	$\overline{\Delta r}$(in.)	$\overline{\Delta r}$(in.)	$\overline{\Delta r}$(in.)
0	0	0	0	0	0		
0.025	0	0.0001	0.0001	0	0.0002		
0.050	0.0004	0.0005	0.0014	0.0004	0.0005		
0.075	0.0018	0.0023	0.0051	0.0022	0.0013		
0.100	0.0057	0.0051	0.0140	0.0074	0.0051		
0.125	0.0138	0.0139	0.0321	0.0190	0.0153		
0.150	0.0307	0.0301	0.0532	0.0428	0.0323		
0.175	0.0580	0.0533	0.0854	0.0759	0.0659		
0.200	0.0786	0.0723	0.0980	0.0943	0.0934		
0.225	0.0921	0.0877	0.1054	0.1039	0.1054		
0.250	0.1011	0.0981	0.1092	0.1086	0.1105		
0.275	0.1067	0.1052	0.1108	0.1104	-		
0.300	-	0.1101	-	-	0.1123		
0.325	0.1114	0.1130	0.1116	0.1113	-		
0.350	-	0.1145	-	-	0.1129		
0.375	0.1122	-	0.1117	0.1111	-		
0.400	-	0.1154	-	-	0.1124		
0.425	0.1122	-	-	-	-		
0.450	-	0.1156	-	-	-		
0.475	-	-	-	-	-		
0.500	-	-	-	-	-		
0.525	-	-	-	-	-		

SPLAY MEASUREMENT DATA - CONSTRAINED REDRAWING

Table number A_3.88	Test number 1C(A)	
Mean test-piece rim distance from die (in.)	Distance along test-piece from die (in.)	Mean test-piece diameter relative to standard (in.)
0.300	0.300	+0.0026
	0.200	+0.0030
	0.150	+0.0031
	0.100	+0.0034
	0.075	+0.0031
	0.050	+0.0022
	0.025	-0.0012
	0.000	-0.0241
0.200	0.200	+0.0035
	0.150	+0.0033
	0.100	+0.0034
	0.075	+0.0031
	0.050	+0.0023
	0.025	-0.0011
	0.000	-0.0245
0.153	0.153	+0.0036
	0.100	+0.0035
	0.075	+0.0032
	0.050	+0.0023
	0.025	-0.0012
	0.000	-0.0244
0.101	0.101	+0.0045
	0.075	+0.0039
	0.050	+0.0021
	0.025	-0.0015
	0.000	-0.0245
0.073	0.073	+0.0072
	0.050	+0.0031
	0.025	-0.0024
	0.000	-0.0247
0.049	0.049	+0.0192
	0.025	+0.0022
	0.000	-0.0253
0.024	0.024	+0.0249
	0.000	-0.0239
-0.003	-0.003	-0.0095

Table number A_3.89	Test number 2C(A)	
Mean test-piece rim distance from die (in.)	Distance along test-piece from die (in.)	Mean test-piece diameter relative to standard (in.)
0.300	0.300	+0.0020
	0.200	+0.0024
	0.150	+0.0023
	0.100	+0.0024
	0.075	+0.0021
	0.050	+0.0016
	0.025	-0.0026
	0.000	-0.0280
0.200	0.200	+0.0023
	0.150	+0.0026
	0.100	+0.0025
	0.075	+0.0022
	0.050	+0.0016
	0.025	-0.0024
	0.000	-0.0277
0.147	0.147	+0.0023
	0.100	+0.0026
	0.075	+0.0024
	0.050	+0.0020
	0.025	-0.0025
	0.000	-0.0284
0.103	0.103	+0.0028
	0.075	+0.0026
	0.050	+0.0016
	0.025	-0.0026
	0.000	-0.0281
0.075	0.075	+0.0038
	0.050	+0.0018
	0.025	-0.0026
	0.000	-0.0274
0.053	0.053	+0.0131
	0.025	-0.0022
	0.000	-0.0281
0.028	0.028	+0.0186
	0.000	-0.0271
0.002	0.002	+0.0112

SPLAY MEASUREMENT DATA - CONSTRAINED REDRAWING

Table number $A_3.90$	Test number 3C(A)	
Mean test-piece rim distance from die (in.)	Distance along test-piece from die (in.)	Mean test-piece diameter relative to standard (in.)
0.300	0.300	+0.0037
	0.200	+0.0028
	0.150	+0.0028
	0.100	+0.0030
	0.075	+0.0028
	0.050	+0.0019
	0.025	-0.0028
	0.000	-0.0284
0.200	0.200	+0.0038
	0.150	+0.0030
	0.100	+0.0029
	0.075	+0.0026
	0.050	+0.0019
	0.025	-0.0029
	0.000	-0.0279
0.153	0.153	+0.0041
	0.100	+0.0032
	0.075	+0.0027
	0.050	+0.0019
	0.025	-0.0027
	0.000	-0.0277
0.103	0.103	+0.0056
	0.075	+0.0035
	0.050	+0.0016
	0.025	-0.0031
	0.000	-0.0272
0.081	0.081	+0.0079
	0.050	+0.0022
	0.025	-0.0037
	0.000	-0.0280
0.054	0.054	+0.0173
	0.025	-0.0020
	0.000	-0.0281
0.027	0.027	+0.0231
	0.000	-0.0261
0.007	0.007	+0.0108

Table number $A_3.91$	Test number 4C(A)	
Mean test-piece rim distance from die (in.)	Distance along test-piece from die (in.)	Mean test-piece diameter relative to standard (in.)
0.300	0.300	+0.0037
	0.200	+0.0031
	0.150	+0.0032
	0.100	+0.0034
	0.075	+0.0030
	0.050	+0.0019
	0.025	-0.0032
	0.000	-0.0279
0.200	0.200	+0.0036
	0.150	+0.0033
	0.100	+0.0034
	0.075	+0.0031
	0.050	+0.0020
	0.025	-0.0031
	0.000	-0.0282
0.152	0.152	+0.0036
	0.100	+0.0035
	0.075	+0.0030
	0.050	+0.0018
	0.025	-0.0032
	0.000	-0.0281
0.097	0.097	+0.0057
	0.075	+0.0040
	0.050	+0.0015
	0.025	-0.0035
	0.000	-0.0284
0.073	0.073	+0.0092
	0.050	+0.0035
	0.025	-0.0040
	0.000	-0.0285
0.048	0.048	+0.0200
	0.025	+0.0009
	0.000	-0.0233
0.028	0.028	+0.0233
	0.000	-0.0271
0.010	0.010	+0.0135

SPLAY MEASUREMENT DATA - CONSTRAINED REDRAWING

Table number A3.92	Test number 5C(A)	
Mean test-piece rim distance from die (in.)	Distance along test-piece from die (in.)	Mean test-piece diameter relative to standard (in.)
0.300	0.300	+0.0026
	0.200	+0.0024
	0.150	+0.0020
	0.100	+0.0026
	0.075	+0.0022
	0.050	+0.0009
	0.025	-0.0064
	0.000	-0.0348
0.200	0.200	+0.0027
	0.150	+0.0026
	0.100	+0.0027
	0.075	+0.0026
	0.050	+0.0010
	0.025	-0.0064
	0.000	-0.0350
0.153	0.153	+0.0030
	0.100	+0.0026
	0.075	+0.0022
	0.050	+0.0010
	0.025	-0.0064
	0.000	-0.0356
0.101	0.101	+0.0048
	0.075	+0.0026
	0.050	0.0000
	0.025	-0.0073
	0.000	-0.0364
0.075	0.075	+0.0097
	0.050	+0.0014
	0.025	-0.0088
	0.000	-0.0370
0.056	0.056	+0.0161
	0.025	-0.0072
	0.000	-0.0381
0.033	0.033	+0.0188
	0.000	-0.0363
0.014	0.014	+0.0126

Table number A3.93	Test number 6C(A)	
Mean test-piece rim distance from die (in.)	Distance along test-piece from die (in.)	Mean test-piece diameter relative to standard (in.)
0.300	0.300	+0.0022
	0.200	+0.0016
	0.150	+0.0016
	0.100	+0.0017
	0.075	+0.0014
	0.050	+0.0003
	0.025	-0.0041
	0.000	-0.0301
0.200	0.200	+0.0021
	0.150	+0.0016
	0.100	+0.0016
	0.075	+0.0013
	0.050	+0.0002
	0.025	-0.0044
	0.000	-0.0302
0.153	0.153	+0.0021
	0.100	+0.0018
	0.075	+0.0013
	0.050	+0.0003
	0.025	-0.0043
	0.000	-0.0311
0.105	0.105	+0.0033
	0.075	+0.0019
	0.050	+0.0002
	0.025	-0.0044
	0.000	-0.0305
0.074	0.074	+0.0063
	0.050	+0.0013
	0.025	-0.0054
	0.000	-0.0301
0.057	0.057	+0.0166
	0.025	-0.0037
	0.000	-0.0318
0.037	0.037	+0.0234
	0.000	-0.0319
0.009	0.009	+0.0035

SPLAY MEASUREMENT DATA - CONSTRAINED REDRAWING

Table number A_3.94	Test number 7C(A)	
Mean test-piece rim distance from die (in.)	Distance along test-piece from die (in.)	Mean test-piece diameter relative to standard (in.)
0.300	0.300	+0.0040
	0.200	+0.0033
	0.150	+0.0034
	0.100	+0.0035
	0.075	+0.0029
	0.050	+0.0011
	0.025	-0.0071
	0.000	-0.0356
0.200	0.200	+0.0035
	0.150	+0.0031
	0.100	+0.0035
	0.075	+0.0031
	0.050	+0.0013
	0.025	-0.0066
	0.000	-0.0350
0.149	0.149	+0.0039
	0.100	+0.0036
	0.075	+0.0030
	0.050	+0.0011
	0.025	-0.0068
	0.000	-0.0350
0.103	0.103	+0.0066
	0.075	+0.0036
	0.050	+0.0002
	0.025	-0.0076
	0.000	-0.0351
0.073	0.073	+0.0132
	0.050	+0.0037
	0.025	-0.0087
	0.000	-0.0361
0.049	0.049	+0.0201
	0.025	-0.0029
	0.000	-0.0367
0.033	0.033	+0.0205
	0.000	-0.0347
0.015	0.015	+0.0139

Table number A_3.95	Test number 8C(A)	
Mean test-piece rim distance from die (in.)	Distance along test-piece from die (in.)	Mean test-piece diameter relative to standard (in.)
0.300	0.300	+0.0002
	0.200	0.0000
	0.150	+0.0002
	0.100	+0.0001
	0.075	-0.0005
	0.050	-0.0025
	0.025	-0.0117
	0.000	-0.0423
0.200	0.200	+0.0001
	0.150	-0.0001
	0.100	0.0000
	0.075	-0.0005
	0.050	-0.0026
	0.025	-0.0117
	0.000	-0.0423
0.150	0.150	+0.0005
	0.100	-0.0002
	0.075	-0.0008
	0.050	-0.0026
	0.025	-0.0118
	0.000	-0.0429
0.100	0.100	+0.0036
	0.075	+0.0006
	0.050	-0.0032
	0.025	-0.0123
	0.000	-0.0428
0.077	0.077	+0.0097
	0.050	-0.0010
	0.025	-0.0132
	0.000	-0.0427
0.053	0.053	+0.0153
	0.025	-0.0100
	0.000	-0.0438
0.035	0.035	+0.0166
	0.000	-0.0425
0.018	0.018	+0.0115

SPLAY MEASUREMENT DATA - CONSTRAINED REDRAWING

Table number $A_3.96$	Test number 9C(A)	
Mean test-piece rim distance from die (in.)	Distance along test-piece from die (in.)	Mean test-piece diameter relative to standard (in.)
0.300	0.300	-0.0003
	0.200	-0.0001
	0.150	+0.0001
	0.100	+0.0005
	0.075	+0.0004
	0.050	-0.0010
	0.025	-0.0055
	0.000	-0.0300
0.200	0.200	0.0000
	0.150	+0.0005
	0.100	+0.0006
	0.075	+0.0004
	0.050	-0.0009
	0.025	-0.0057
	0.000	-0.0310
0.147	0.147	0.0000
	0.100	+0.0007
	0.075	+0.0004
	0.050	-0.0010
	0.025	-0.0048
	0.000	-0.0316
0.101	0.101	+0.0016
	0.075	+0.0009
	0.050	-0.0008
	0.025	-0.0059
	0.000	-0.0313
0.073	0.073	+0.0054
	0.050	+0.0007
	0.025	-0.0066
	0.000	-0.0316
0.047	0.047	+0.0192
	0.025	+0.0006
	0.000	-0.0333
0.029	0.029	+0.0213
	0.000	-0.0311
0.006	0.006	+0.0006

Table number $A_3.97$	Test number 10C(A)	
Mean test-piece rim distance from die (in.)	Distance along test-piece from die (in.)	Mean test-piece diameter relative to standard (in.)
0.300	0.300	-0.0012
	0.200	-0.0009
	0.150	-0.0006
	0.100	-0.0005
	0.075	-0.0010
	0.050	-0.0027
	0.025	-0.0100
	0.000	-0.0383
0.200	0.200	-0.0019
	0.150	-0.0006
	0.100	-0.0004
	0.075	-0.0008
	0.050	-0.0026
	0.025	-0.0098
	0.000	-0.0383
0.147	0.147	-0.0020
	0.100	-0.0003
	0.075	-0.0007
	0.050	-0.0026
	0.025	-0.0098
	0.000	-0.0383
0.105	0.105	+0.0005
	0.075	-0.0001
	0.050	-0.0026
	0.025	-0.0100
	0.000	-0.0384
0.075	0.075	+0.0074
	0.050	-0.0003
	0.025	-0.0108
	0.000	-0.0390
0.051	0.051	+0.0156
	0.025	-0.0063
	0.000	-0.0396
0.028	0.028	+0.0154
	0.000	-0.0365
0.016	0.016	+0.0076

SPLAY MEASUREMENT DATA - CONSTRAINED REDRAWING

Table number A_3.98	Test number 11C(A)	
Mean test-piece rim distance from die (in.)	Distance along test-piece from die (in.)	Mean test-piece diameter relative to standard (in.)
0.300	0.300	-0.0009
	0.200	-0.0010
	0.150	-0.0009
	0.100	-0.0009
	0.075	-0.0016
	0.050	-0.0039
	0.025	-0.0133
	0.000	-0.0444
0.200	0.200	-0.0013
	0.150	-0.0008
	0.100	-0.0007
	0.075	-0.0013
	0.050	-0.0040
	0.025	-0.0131
	0.000	-0.0439
0.150	0.150	-0.0008
	0.100	-0.0007
	0.075	-0.0014
	0.050	-0.0040
	0.025	-0.0131
	0.000	-0.0437
0.097	0.097	+0.0027
	0.075	+0.0001
	0.050	-0.0040
	0.025	-0.0131
	0.000	-0.0436
0.075	0.075	+0.0091
	0.050	-0.0014
	0.025	-0.0144
	0.000	-0.0445
0.046	0.046	+0.0152
	0.025	-0.0073
	0.000	-0.0454
0.030	0.030	+0.0138
	0.000	-0.0417
0.010	0.010	-0.0025

Table number A_3. 99	Test number 12C(A)	
Mean test-piece rim distance from die (in.)	Distance along test-piece from die (in.)	Mean test-piece diameter relative to standard (in.)
0.300	0.300	+0.0082
	0.200	+0.0063
	0.150	+0.0067
	0.100	+0.0069
	0.075	+0.0067
	0.050	+0.0050
	0.025	-0.0002
	0.000	-0.0252
0.200	0.200	+0.0082
	0.150	+0.0071
	0.100	+0.0068
	0.075	+0.0063
	0.050	+0.0049
	0.025	-0.0004
	0.000	-0.0255
0.152	0.152	+0.0086
	0.100	+0.0073
	0.075	+0.0064
	0.050	+0.0046
	0.025	0.0000
	0.000	-0.0266
0.097	0.097	+0.0113
	0.075	+0.0084
	0.050	+0.0044
	0.025	-0.0017
	0.000	-0.0256
0.068	0.068	+0.0170
	0.050	+0.0096
	0.025	-0.0025
	0.000	-0.0274
0.051	0.051	+0.0282
	0.025	+0.0039
	0.000	-0.0276
0.033	0.033	+0.0331
	0.000	-0.0271
0.014	0.014	+0.0235

SPLAY MEASUREMENT DATA - CONSTRAINED REDRAWING

Table number A_3.10	Test number 13C(A)	
Mean test-piece rim distance from die (in.)	Distance along test-piece from die (in.)	Mean test-piece diameter relative to standard (in.)
0.300	0.300	+0.0003
	0.200	+0.0037
	0.150	+0.0037
	0.100	+0.0038
	0.075	+0.0039
	0.050	+0.0035
	0.025	-0.0012
	0.000	-0.0240
0.200	0.200	+0.0009
	0.150	+0.0038
	0.100	+0.0037
	0.075	+0.0035
	0.050	+0.0031
	0.025	-0.0019
	0.000	-0.0284
0.145	0.145	0.0000
	0.100	+0.0040
	0.075	+0.0036
	0.050	+0.0027
	0.025	-0.0039
	0.000	-0.0336
0.100	0.100	0.0000
	0.075	+0.0033
	0.050	+0.0026
	0.025	-0.0023
	0.000	-0.0280
0.080	0.080	+0.0004
	0.050	+0.0026
	0.025	-0.0019
	0.000	-0.0282
0.055	0.055	+0.0094
	0.025	-0.0024
	0.000	-0.0281
0.030	0.030	+0.0135
	0.000	-0.0297
0.013	0.013	+0.0049

Table number A_3.10	Test number 14C(A)	
Mean test-piece rim distance from die (in.)	Distance along test-piece from die (in.)	Mean test-piece diameter relative to standard (in.)
0.300	0.300	+0.0068
	0.200	+0.0054
	0.150	+0.0058
	0.100	+0.0062
	0.075	+0.0057
	0.050	+0.0040
	0.025	-0.0023
	0.000	-0.0295
0.200	0.200	+0.0068
	0.150	+0.0060
	0.100	+0.0062
	0.075	+0.0057
	0.050	+0.0039
	0.025	-0.0020
	0.000	-0.0293
0.147	0.147	+0.0069
	0.100	+0.0070
	0.075	+0.0064
	0.050	+0.0046
	0.025	-0.0013
	0.000	-0.0288
0.102	0.102	+0.0100
	0.075	+0.0079
	0.050	+0.0043
	0.025	-0.0020
	0.000	-0.0295
0.075	0.075	+0.0171
	0.050	+0.0087
	0.025	-0.0032
	0.000	-0.0303
0.052	0.052	+0.0270
	0.025	+0.0028
	0.000	-0.0324
0.029	0.029	+0.0293
	0.000	-0.0272
0.015	0.015	+0.0214

SPLAY MEASUREMENT DATA - CONSTRAINED REDRAWING

Table number $A_3.102$	Test number 15C(A)	
Mean test-piece rim distance from die (in.)	Distance along test-piece from die (in.)	Mean test-piece diameter relative to standard (in.)
0.300	0.300	+0.0067
	0.200	+0.0053
	0.150	+0.0056
	0.100	+0.0060
	0.075	+0.0055
	0.050	+0.0033
	0.025	-0.0036
	0.000	-0.0309
0.200	0.200	+0.0069
	0.150	+0.0059
	0.100	+0.0060
	0.075	+0.0056
	0.050	+0.0032
	0.025	-0.0035
	0.000	-0.0315
0.160	0.160	+0.0074
	0.100	+0.0062
	0.075	+0.0054
	0.050	+0.0032
	0.025	-0.0037
	0.000	-0.0316
0.114	0.114	+0.0097
	0.075	+0.0062
	0.050	+0.0029
	0.025	-0.0040
	0.000	-0.0313
0.086	0.086	+0.0140
	0.050	+0.0041
	0.025	-0.0047
	0.000	-0.0315
0.063	0.063	+0.0234
	0.025	-0.0034
	0.000	-0.0324
0.043	0.043	+0.0294
	0.000	-0.0340
0.023	0.023	+0.0279

Table number $A_3.103$	Test number 16C(A)	
Mean test-piece rim distance from die (in.)	Distance along test-piece from die (in.)	Mean test-piece diameter relative to standard (in.)
0.300	0.300	+0.0071
	0.200	+0.0053
	0.150	+0.0054
	0.100	+0.0055
	0.075	+0.0050
	0.050	+0.0022
	0.025	-0.0082
	0.000	-0.0393
0.200	0.200	+0.0070
	0.150	+0.0060
	0.100	+0.0057
	0.075	+0.0049
	0.050	+0.0021
	0.025	-0.0075
	0.000	-0.0382
0.150	0.150	+0.0075
	0.100	+0.0061
	0.075	+0.0049
	0.050	+0.0019
	0.025	-0.0071
	0.000	-0.0379
0.103	0.103	+0.0110
	0.075	+0.0069
	0.050	+0.0017
	0.025	-0.0073
	0.000	-0.0376
0.077	0.077	+0.0180
	0.050	+0.0056
	0.025	-0.0082
	0.000	-0.0377
0.055	0.055	+0.0253
	0.025	-0.0044
	0.000	-0.0388
0.029	0.029	+0.0258
	0.000	-0.0350
0.008	0.008	+0.0056

SPLAY MEASUREMENT DATA - CONSTRAINED REDRAWING

Table number A_3.104		Test number 17C(A)
Mean test-piece rim distance from die (in.)	Distance along test-piece from die (in.)	Mean test-piece diameter relative to standard (in.)
0.300	0.300	-0.0005
	0.200	+0.0011
	0.150	+0.0013
	0.100	+0.0017
	0.075	+0.0018
	0.050	+0.0010
	0.025	-0.0046
	0.000	-0.0289
0.200	0.200	-0.0002
	0.150	+0.0014
	0.100	+0.0017
	0.075	+0.0019
	0.050	+0.0008
	0.025	-0.0049
	0.000	-0.0304
0.150	0.150	-0.0004
	0.100	+0.0017
	0.075	+0.0018
	0.050	+0.0006
	0.025	-0.0051
	0.000	-0.0308
0.101	0.101	+0.0015
	0.075	+0.0010
	0.050	-0.0006
	0.025	-0.0062
	0.000	-0.0320
0.072	0.072	+0.0063
	0.050	+0.0003
	0.025	-0.0083
	0.000	-0.0328
0.047	0.047	+0.0213
	0.025	0.0000
	0.000	-0.0329
0.023	0.023	+0.0210
	0.000	-0.0277
0.003	0.003	-0.0088

Table number A_3.105		Test number 18C(A)
Mean test-piece rim distance from die (in.)	Distance along test-piece from die (in.)	Mean test-piece diameter relative to standard (in.)
0.300	0.300	-0.0026
	0.200	0.0000
	0.150	0.0000
	0.100	+0.0004
	0.075	+0.0002
	0.050	-0.0023
	0.025	-0.0091
	0.000	-0.0383
0.200	0.200	-0.0024
	0.150	+0.0005
	0.100	+0.0007
	0.075	+0.0007
	0.050	-0.0009
	0.025	-0.0084
	0.000	-0.0377
0.150	0.150	-0.0023
	0.100	+0.0011
	0.075	+0.0010
	0.050	-0.0007
	0.025	-0.0081
	0.000	-0.0373
0.106	0.106	-0.0008
	0.075	+0.0007
	0.050	-0.0013
	0.025	-0.0089
	0.000	-0.0374
0.075	0.075	+0.0058
	0.050	-0.0005
	0.025	-0.0111
	0.000	-0.0384
0.058	0.058	+0.0142
	0.025	-0.0096
	0.000	-0.0404
0.036	0.036	+0.0171
	0.000	-0.0401
0.024	0.024	+0.0140
0.013	0.013	+0.0033

SPLAY MEASUREMENT DATA - CONSTRAINED REDRAWING

Table number A_3.106	Test number 19C(A)	
Mean test-piece rim distance from die (in.)	Distance along test-piece from die (in.)	Mean test-piece diameter relative to standard (in.)
0.300	0.300	-0.0017
	0.200	+0.0004
	0.150	+0.0007
	0.100	+0.0009
	0.075	+0.0006
	0.050	-0.0015
	0.025	-0.0109
	0.000	-0.0414
0.200	0.200	-0.0011
	0.150	+0.0009
	0.100	+0.0011
	0.075	+0.0009
	0.050	-0.0016
	0.025	-0.0106
	0.000	-0.0406
0.148	0.148	-0.0008
	0.100	+0.0012
	0.075	+0.0010
	0.050	-0.0014
	0.025	-0.0106
	0.000	-0.0407
0.097	0.097	+0.0025
	0.075	+0.0007
	0.050	-0.0030
	0.025	-0.0116
	0.000	-0.0419
0.075	0.075	+0.0098
	0.050	-0.0002
	0.025	-0.0133
	0.000	-0.0421
0.045	0.045	+0.0159
	0.025	-0.0073
	0.000	-0.0451
0.024	0.024	+0.0111
	0.000	-0.0392
0.009	0.009	-0.0041

Table number A_3.107	Test number 20C(A)	
Mean test-piece rim distance from die (in.)	Distance along test-piece from die (in.)	Mean test-piece diameter relative to standard (in.)
0.300	0.300	+0.0009
	0.200	+0.0004
	0.150	+0.0005
	0.100	+0.0006
	0.075	+0.0005
	0.050	+0.0004
	0.025	-0.0017
	0.000	-0.0241
0.200	0.200	+0.0010
	0.150	+0.0012
	0.100	+0.0007
	0.075	+0.0008
	0.050	+0.0002
	0.025	-0.0019
	0.000	-0.0241
0.147	0.147	+0.0004
	0.100	+0.0010
	0.075	+0.0010
	0.050	+0.0005
	0.025	-0.0013
	0.000	-0.0238
0.103	0.103	+0.0019
	0.075	+0.0019
	0.050	+0.0008
	0.025	-0.0011
	0.000	-0.0224
0.075	0.075	+0.0031
	0.050	+0.0015
	0.025	-0.0012
	0.000	-0.0228
0.053	0.053	+0.0143
	0.025	-0.0005
	0.000	-0.0232
0.028	0.028	+0.0252
	0.000	-0.0242
0.002	0.002	-0.0075

SPLAY MEASUREMENT DATA - CONSTRAINED REDRAWING

Table number A_3.108	Test number 21C(A)	
Mean test-piece rim distance from die (in.)	Distance along test-piece from die (in.)	Mean test-piece diameter relative to standard (in.)
0.300	0.300	+0.0027
	0.200	+0.0007
	0.150	+0.0013
	0.100	+0.0010
	0.075	+0.0007
	0.050	0.0000
	0.025	-0.0048
	0.000	-0.0324
0.200	0.200	+0.0026
	0.150	+0.0010
	0.100	+0.0010
	0.075	+0.0010
	0.050	+0.0005
	0.025	-0.0045
	0.000	-0.0320
0.157	0.157	+0.0034
	0.100	+0.0011
	0.075	+0.0008
	0.050	+0.0002
	0.025	-0.0044
	0.000	-0.0311
0.103	0.103	+0.0042
	0.075	+0.0020
	0.050	+0.0005
	0.025	-0.0040
	0.000	-0.0301
0.078	0.078	+0.0087
	0.050	+0.0026
	0.025	-0.0038
	0.000	-0.0292
0.057	0.057	+0.0211
	0.025	-0.0013
	0.000	-0.0296
0.035	0.035	+0.0260
	0.000	-0.0299
0.013	0.013	+0.0169

Table number $A_3$109	Test number 22C(A)	
Mean test-piece rim distance from die (in.)	Distance along test-piece from die (in.)	Mean test-piece diameter relative to standard (in.)
0.300	0.300	+0.0007
	0.200	-0.0005
	0.150	-0.0007
	0.100	-0.0004
	0.075	-0.0005
	0.050	-0.0009
	0.025	-0.0042
	0.000	-0.0298
0.200	0.200	+0.0007
	0.150	0.0000
	0.100	-0.0005
	0.075	-0.0006
	0.050	-0.0008
	0.025	-0.0041
	0.000	-0.0291
0.153	0.153	+0.0002
	0.100	+0.0002
	0.075	-0.0002
	0.050	-0.0008
	0.025	-0.0038
	0.000	-0.0277
0.102	0.102	+0.0009
	0.075	+0.0007
	0.050	+0.0002
	0.025	-0.0031
	0.000	-0.0280
0.074	0.074	+0.0036
	0.050	+0.0012
	0.025	-0.0030
	0.000	-0.0266
0.058	0.058	+0.0173
	0.025	-0.0015
	0.000	-0.0271
0.028	0.028	+0.0234
	0.000	-0.0273
0.010	0.010	+0.0149

SPLAY MEASUREMENT DATA - CONSTRAINED REDRAWING

Table number A_3.110	Test number 23C(A)	
Mean test-piece rim distance from die (in.)	Distance along test-piece from die (in.)	Mean test-piece diameter relative to standard (in.)
0.300	0.300	+0.0009
	0.200	+0.0004
	0.150	+0.0005
	0.100	+0.0007
	0.075	+0.0005
	0.050	+0.0002
	0.025	-0.0028
	0.000	-0.0278
0.200	0.200	+0.0009
	0.150	+0.0005
	0.100	+0.0007
	0.075	+0.0007
	0.050	+0.0004
	0.025	-0.0026
	0.000	-0.0274
0.156	0.156	+0.0009
	0.100	+0.0009
	0.075	+0.0008
	0.050	+0.0005
	0.025	-0.0025
	0.000	-0.0267
0.106	0.106	+0.0013
	0.075	+0.0011
	0.050	+0.0006
	0.025	-0.0022
	0.000	-0.0267
0.078	0.078	+0.0044
	0.050	+0.0018
	0.025	-0.0023
	0.000	-0.0264
0.056	0.056	+0.0167
	0.025	-0.0022
	0.000	-0.0274
0.036	0.036	+0.0242
	0.000	-0.0293
0.015	0.015	+0.0202

Table number A_3.111	Test number 24C(A)	
Mean test-piece rim distance from die (in.)	Distance along test-piece from die (in.)	Mean test-piece diameter relative to standard (in.)
0.300	0.300	+0.0002
	0.200	0.0000
	0.150	0.0000
	0.100	+0.0001
	0.075	+0.0001
	0.050	-0.0008
	0.025	-0.0078
	0.000	-0.0375
0.200	0.200	+0.0004
	0.150	+0.0001
	0.100	+0.0001
	0.075	+0.0001
	0.050	-0.0006
	0.025	-0.0074
	0.000	-0.0367
0.145	0.145	+0.0008
	0.100	+0.0002
	0.075	+0.0001
	0.050	-0.0008
	0.025	-0.0073
	0.000	-0.0357
0.097	0.097	+0.0017
	0.075	+0.0006
	0.050	-0.0007
	0.025	-0.0071
	0.000	-0.0383
0.069	0.069	+0.0104
	0.050	+0.0031
	0.025	-0.0078
	0.000	-0.0348
0.045	0.045	+0.0180
	0.025	-0.0020
	0.000	-0.0355
0.022	0.022	+0.0188
	0.000	-0.0296
0.010	0.010	+0.0120

REDRAW LOAD MEASUREMENT DATA - CONSTRAINED REDRAWING

Table Number A_3. 112	Test Number 1C(B)
Test piece rim distance from die (in.)	Redraw load (tonf.)
0.400	0.415
0.265	0.410
0.165	0.410
0.112	0.412
0.082	0.410
0.065	0.405
0.047	0.375
0.041	0.380
0.023	0.375
0.017	0.357
0.005	0.330
-0.012	0.250

Table Number A_3. 113	Test Number 1C(G)
Test piece rim distance from die (in.)	Redraw load (tonf.)
0.395	0.443
0.264	0.443
0.146	0.443
0.064	0.443
0.050	0.440
0.040	0.422
0.027	0.405
0.014	0.394
0.005	0.370
0.000	0.290
-	-
-	-

Table Number A_3. 114	Test Number 2C(B)
Test piece rim distance from die (in.)	Redraw load (tonf.)
0.400	0.282
0.245	0.284
0.120	0.284
0.083	0.282
0.065	0.278
0.048	0.271
0.040	0.276
0.024	0.266
0.000	0.250
-0.005	0.252
-0.024	0.215
-	-

Table Number A_3. 115	Test Number 3C(B)
Test piece rim distance from die (in.)	Redraw load (tonf.)
0.396	0.365
0.245	0.365
0.143	0.365
0.090	0.360
0.080	0.350
0.053	0.345
0.024	0.333
0.012	0.324
-0.005	0.303
-0.024	0.295
-0.036	0.220
-	-

REDRAW LOAD MEASUREMENT DATA - CONSTRAINED REDRAWING

Table Number A_3. 116	Test Number 3C(G)
Test piece rim distance from die (in.)	Redraw load (tonf.)
0.400	0.415
0.265	0.415
0.186	0.415
0.125	0.415
0.075	0.422
0.050	0.410
0.040	0.396
0.030	0.383
0.012	0.396
0.000	0.370
-0.005	0.367
-0.024	0.250

Table Number A_3. 117	Test Number 4C(B)
Test piece rim distance from die (in.)	Redraw load (tonf.)
0.400	0.415
0.270	0.420
0.155	0.415
0.100	0.412
0.080	0.410
0.063	0.396
0.048	0.386
0.023	0.396
0.012	0.367
0.000	0.342
-0.012	0.350
-0.023	0.284

Table Number A_3. 118	Test Number 5C(B)
Test piece rim distance from die (in.)	Redraw load (tonf.)
0.400	0.376
0.260	0.376
0.170	0.380
0.100	0.380
0.071	0.370
0.054	0.360
0.030	0.364
0.005	0.344
0.000	0.324
-0.010	0.265
-	-
-	-

Table Number A_3. 119	Test Number 5C(G)
Test piece rim distance from die (in.)	Redraw load (tonf.)
0.400	0.404
0.255	0.404
0.178	0.404
0.113	0.410
0.075	0.410
0.054	0.404
0.046	0.396
0.036	0.384
0.012	0.384
0.000	0.350
-0.018	0.297
-	-

REDRAW LOAD MEASUREMENT DATA - CONSTRAINED REDRAWING

Table Number A_3. 120	Test Number 6C(B)
Test piece rim distance from die (in.)	Redraw load (tonf.)
0.400	0.495
0.251	0.495
0.150	0.492
0.106	0.495
0.080	0.490
0.064	0.470
0.045	0.460
0.030	0.470
-0.005	0.410
-0.016	0.283
-	-
-	-

Table Number A_3. 121	Test Number 7C(B)
Test piece rim distance from die (in.)	Redraw load (tonf.)
0.396	0.458
0.228	0.458
0.136	0.455
0.096	0.452
0.076	0.450
0.060	0.435
0.048	0.425
0.024	0.435
0.012	0.422
0.000	0.383
-	-
-	-

Table Number A_3. 122	Test Number 8C(B)
Test piece rim distance from die (in.)	Redraw load (tonf.)
0.400	0.490
0.250	0.494
0.166	0.496
0.107	0.494
0.075	0.477
0.054	0.462
0.036	0.470
0.017	0.450
0.000	0.422
-0.017	0.390
-	-
-	-

Table Number A_3. 123	Test Number 9C(B)
Test piece rim distance from die (in.)	Redraw load (tonf.)
0.600	0.376
0.370	0.376
0.220	0.380
0.125	0.380
0.098	0.380
0.076	0.370
0.064	0.357
0.054	0.346
0.038	0.346
0.017	0.330
0.005	0.303
0.000	0.197

REDRAW LOAD MEASUREMENT DATA - CONSTRAINED REDRAWING

Table Number A_3.124	Test Number 10C(B)
Test piece rim distance from die (in.)	Redraw load (tonf.)
0.396	0.330
0.257	0.330
0.156	0.330
0.096	0.330
0.087	0.325
0.066	0.313
0.044	0.305
0.024	0.305
0.000	0.270
-	-
-	-
-	-

Table Number A_3. 125	Test Number 11C(B)
Test piece rim distance from die (in.)	Redraw load (tonf.)
0.400	0.330
0.235	0.330
0.130	0.330
0.080	0.317
0.054	0.305
0.030	0.305
0.000	0.270
-0.024	0.198
-	-
-	-
-	-
-	-

Table Number A_3. 126	Test Number 12C(B)
Test piece rim distance from die (in.)	Redraw load (tonf.)
0.600	0.710
0.415	0.705
0.220	0.700
0.135	0.700
0.105	0.700
0.086	0.685
0.071	0.650
0.060	0.650
0.043	0.625
0.028	0.625
0.000	0.440
-	-

Table Number A_3. 127	Test Number 12C(G)
Test piece rim distance from die (in.)	Redraw load (tonf.)
0.400	0.670
0.260	0.670
0.160	0.665
0.126	0.660
0.105	0.660
0.084	0.665
0.060	0.660
0.047	0.650
0.030	0.610
0.017	0.600
0.000	0.480
-	-

REDRAW LOAD MEASUREMENT DATA - CONSTRAINED REDRAWING

Table Number A_3. 128	Test Number 13C(B)
Test piece rim distance from die (in.)	Redraw load (tonf.)
0.396	0.362
0.240	0.370
0.132	0.373
0.083	0.366
0.054	0.353
0.025	0.330
0.000	0.323
-0.018	0.245
-	-
-	-
-	-
-	-

Table Number A_3. 129	Test Number 14C(B)
Test piece rim distance from die (in.)	Redraw load (tonf.)
0.400	0.640
0.300	0.640
0.204	0.635
0.107	0.630
0.082	0.615
0.063	0.585
0.030	0.580
0.000	0.500
-	-
-	-
-	-
-	-

Table Number A_3. 130	Test Number 14C(G)
Test piece rim distance from die (in.)	Redraw load (tonf.)
0.400	0.710
0.275	0.715
0.167	0.700
0.110	0.700
0.072	0.710
0.048	0.685
0.042	0.670
0.030	0.655
0.021	0.650
0.000	0.535
-	-
-	-

Table Number A_3. 131	Test Number 15C(B)
Test piece rim distance from die (in.)	Redraw load (tonf.)
0.396	0.720
0.270	0.710
0.163	0.700
0.120	0.700
0.090	0.690
0.065	0.665
0.054	0.650
0.030	0.650
0.018	0.640
0.000	0.525
-	-
-	-

REDRAW LOAD MEASUREMENT DATA - CONSTRAINED REDRAWING

Table Number A_3. 132	Test Number 16C(B)
Test piece rim distance from die (in.)	Redraw load (tonf.)
0.400	0.640
0.292	0.640
0.178	0.640
0.118	0.630
0.093	0.610
0.062	0.580
0.030	0.585
0.006	0.530
0.000	0.460
-	-
-	-
-	-

Table Number A_3. 133	Test Number 16C(G)
Test piece rim distance from die (in.)	Redraw load (tonf.)
0.400	0.630
0.210	0.630
0.125	0.625
0.080	0.630
0.054	0.610
0.036	0.590
0.018	0.580
0.012	0.515
0.018	0.365
-	-
-	-
-	-

Table Number A_3. 134	Test Number 17C(B)
Test piece rim distance from die (in.)	Redraw load (tonf.)
0.600	0.800
0.370	0.800
0.282	0.790
0.182	0.785
0.105	0.785
0.100	0.780
0.074	0.765
0.060	0.740
0.048	0.740
0.023	0.700
0.000	0.590
-	-

Table Number A_3. 135	Test Number 18C(B)
Test piece rim distance from die (in.)	Redraw load (tonf.)
0.396	0.690
0.270	0.690
0.167	0.685
0.120	0.685
0.090	0.680
0.072	0.670
0.053	0.640
0.030	0.645
0.018	0.630
0.000	0.590
-	-
-	-

REDRAW LOAD MEASUREMENT DATA - CONSTRAINED REDRAWING

Table Number A_3. 136	Test Number 19C(B)
Test piece rim distance from die (in.)	Redraw load (tonf.)
0.400	0.740
0.286	0.740
0.185	0.745
0.113	0.750
0.082	0.725
0.046	0.700
0.023	0.700
0.000	0.640
-0.018	0.560
-	-
-	-
-	-

Table Number A_3. 137	Test Number 20C(B)
Test piece rim distance from die (in.)	Redraw load (tonf.)
0.400	0.082
0.282	0.082
0.194	0.084
0.118	0.084
0.075	0.085
0.058	0.080
0.041	0.075
0.018	0.075
0.005	0.071
-0.018	0.065
-	-
-	-

Table Number A_3. 138	Test Number 20C(G)
Test piece rim distance from die (in.)	Redraw load (tonf.)
0.400	0.085
0.250	0.085
0.132	0.085
0.068	0.083
0.036	0.082
0.027	0.078
0.020	0.078
0.013	0.075
0.005	0.070
0.000	0.060
-	-
-	-

Table Number A_3. 139	Test Number 21C(B)
Test piece rim distance from die (in.)	Redraw load (tonf.)
0.400	0.052
0.227	0.052
0.120	0.052
0.096	0.052
0.072	0.050
0.047	0.048
0.025	0.047
0.018	0.044
0.000	0.040
-	-
-	-
-	-

REDRAW LOAD MEASUREMENT DATA - CONSTRAINED REDRAWING

Table Number A_3. 140	Test Number 22C(B)
Test piece rim distance from die (in.)	Redraw load (tonf.)
0.400	0.078
0.269	0.078
0.174	0.078
0.092	0;078
0.072	0.075
0.047	0.072
0.025	0.072
0.018	0.070
0.000	0.060
-0.005	0.060
-0.021	0.050
-	-

Table Number A_3. 141	Test Number 22C(G)
Test piece rim distance from die (in.)	Redraw load (tonf.)
0.400	0.075
0.194	0.075
0.100	0.075
0.065	0.075
0.044	0.071
0.020	0.070
0.010	0.065
0.000	0.055
-	-
-	-
-	-
-	-

Table Number A_3. 142	Test Number 23C(B)
Test piece rim distance from die (in.)	Redraw load (tonf.)
0.400	0.076
0.250	0.076
0.154	0.076
0.107	0.076
0.083	0.076
0.076	0.075
0.060	0.072
0.037	0.072
0.024	0.069
0.000	0.063
-	-
-	-

Table Number A_3. 143	Test Number 24C(B)
Test piece rim distance from die (in.)	Redraw load (tonf.)
0.400	0.075
0.226	0.075
0.140	0.074
0.120	0.074
0.078	0.072
0.065	0.070
0.035	0.069
0.017	0.069
0.000	0.060
-0.017	0.042
-	-
-	-

REDRAW LOAD MEASUREMENT DATA - CONSTRAINED REDRAWING

Table Number A_3. 144	Test Number 24C(G)
Test piece rim distance from die (in.)	Redraw load (tonf.)
0.400	0.082
0.255	0.080
0.175	0.080
0.110	0.080
0.065	0.080
0.030	0.074
0.006	0.072
0.000	0.067
-0.024	0.052
-	-
-	-
-	-

Table Number	Test Number
Test piece rim distance from die (in.)	Redraw load (tonf.)

Table Number	Test Number
Test piece rim distance from die (in.)	Redraw load (tonf.)

Table Number	Test Number
Test piece rim distance from die (in.)	Redraw load (tonf.)

A_3. 7. Ancillary tests in splay-measurement programme.

(a) Tensile tests.

Short lengths of test-piece tubing in each material, size and prior cold work condition were retained for tensile tests. The most direct method of testing was on a length of test-piece tube, but it was found that an extensometer could not be satisfactorily attached to tube wall thicknesses less than 0.019 in. An alternative was to obtain test specimens by cutting rings from tubes, slitting, and opening out. This method was rejected on the grounds that additional bending strains would be introduced in the thicker tubes, and it was considered improper to use the ring-test method for thin tubes and the conventional method for thick tubes. A further alternative was to cut longitudinal strip test specimens from tube walls, but this procedure was tedious involving machine slitting to give the necessary accuracy on specimen width.

The testing problem was overcome by following the direct tube-testing procedure but introducing a modification for thinner walled test-pieces, where an inner plug was used to enable the necessary extensometer gripping pressure to be generated. The device is shown in FIG. A_3.10. The plug body (1) was a loose fit in the tube (2) and carried two end collars which were interchangeable and 0.005 in. smaller than the tube bore. Distance between the collars was just less than the extensometer gauge length. The lower collar was locked in position but the upper collar (3) was free to slide as the test-piece elongated.

Before conducting a test with the plug, the test-piece was dimpled and marked with reference line X in a simple jig. The plug was then inserted, located against the dimple, and the extensometer attached using line X as a reference. Tensile testing was then carried out conventionally using end plugs (4) for gripping. The method proved easy to apply and gave results consistent with those on thicker-walled tubes.

Tests were conducted on a 50 Tonf. Denison machine using a Mercer extensometer model 2 B150 with a 2 in. gauge length, strain rate

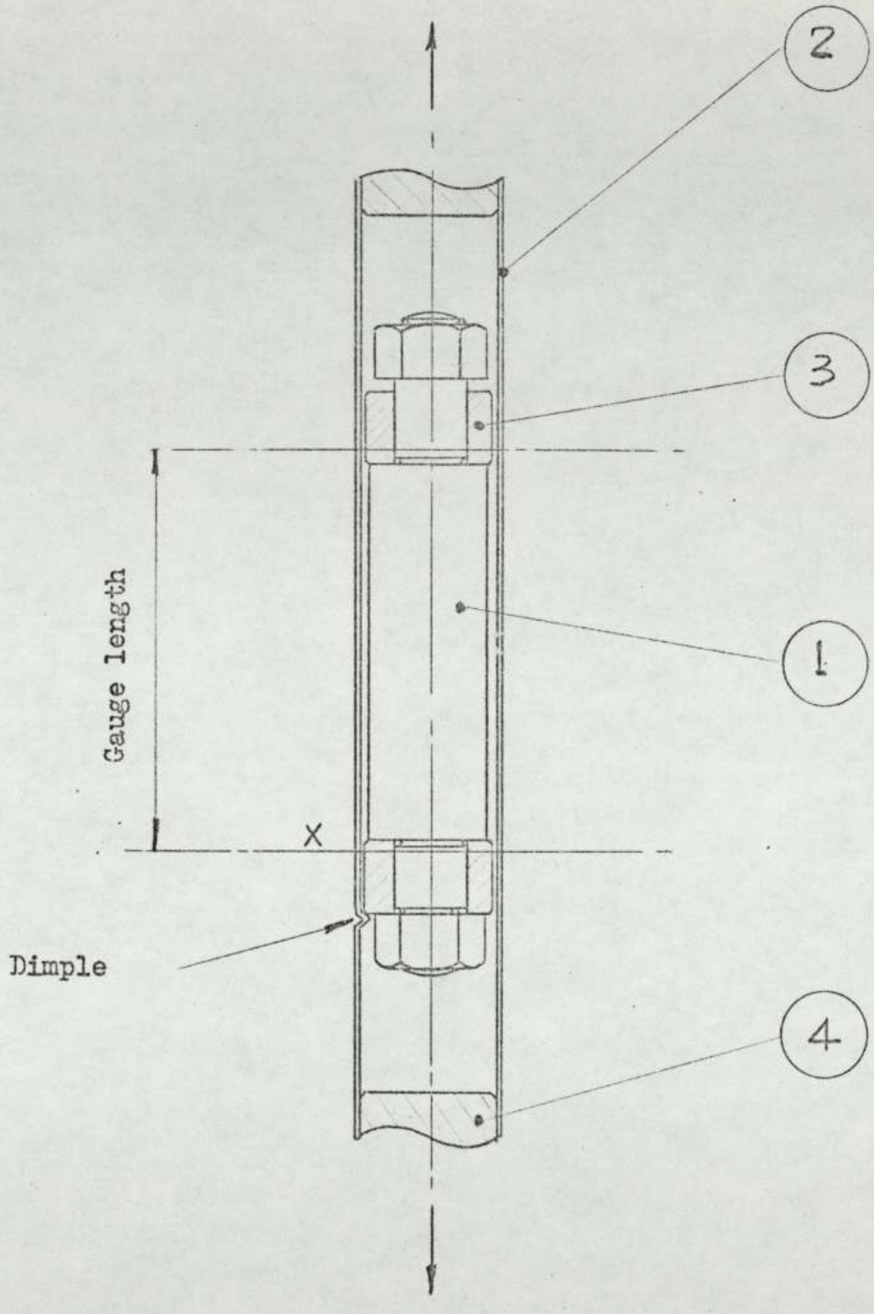

FIG. A_3.10. TENSILE TESTING THIN-WALLED TUBE WITH INNER PLUG being adjusted to suit simultaneous reading of load-meter and extensometer. Results are plotted in FIGS. A_3. 11 - A_3.14.

(b) Plane-strain compression tests.

The Watts and Ford indentation test was used. In this test a flat strip testpiece is compressed between two aligned, overhanging anvils, and indentation depth and load measured in increments. Tool and test-piece geometry may be arranged so that strain across the strip width is approximately zero. For this condition load-indentation data provided by the test are readily converted into an equivalent stress-strain curve. The test has proved reliable and reproducible and is now regarded as a standard method of obtaining stress-strain data to large plastic strains.

Evaluation of test specimen and tooling geometry.

Conditions laid down for plane strain compression testing are;

$$2 < \frac{b}{t} < 4$$

$$6 \leq \frac{W}{b}$$

where b = anvil breadth

t = specimen thickness

W = specimen width

The smallest permissible value of $\frac{W}{t}$ was therefore 12/1. An expression relating $\frac{W}{t}$ to t was derived for specimens cut from the wall of a tube, and the four hollow sizes used for making splay-measurement test-pieces were then examined to find a suitable $\frac{W}{t}$, t combination. It was concluded that a specimen 0.030 in. thick, 0.60 in. wide $\left(\frac{W}{t} = 20\right)$ could be obtained from all hollows.

To cover the strain range corresponding to splay test-piece cold-work (0 - 67 %) it was required to indent specimens to a thickness below 0.010 in. Applying the $\frac{b}{t}$ test condition three anvils sizes were evaluated;

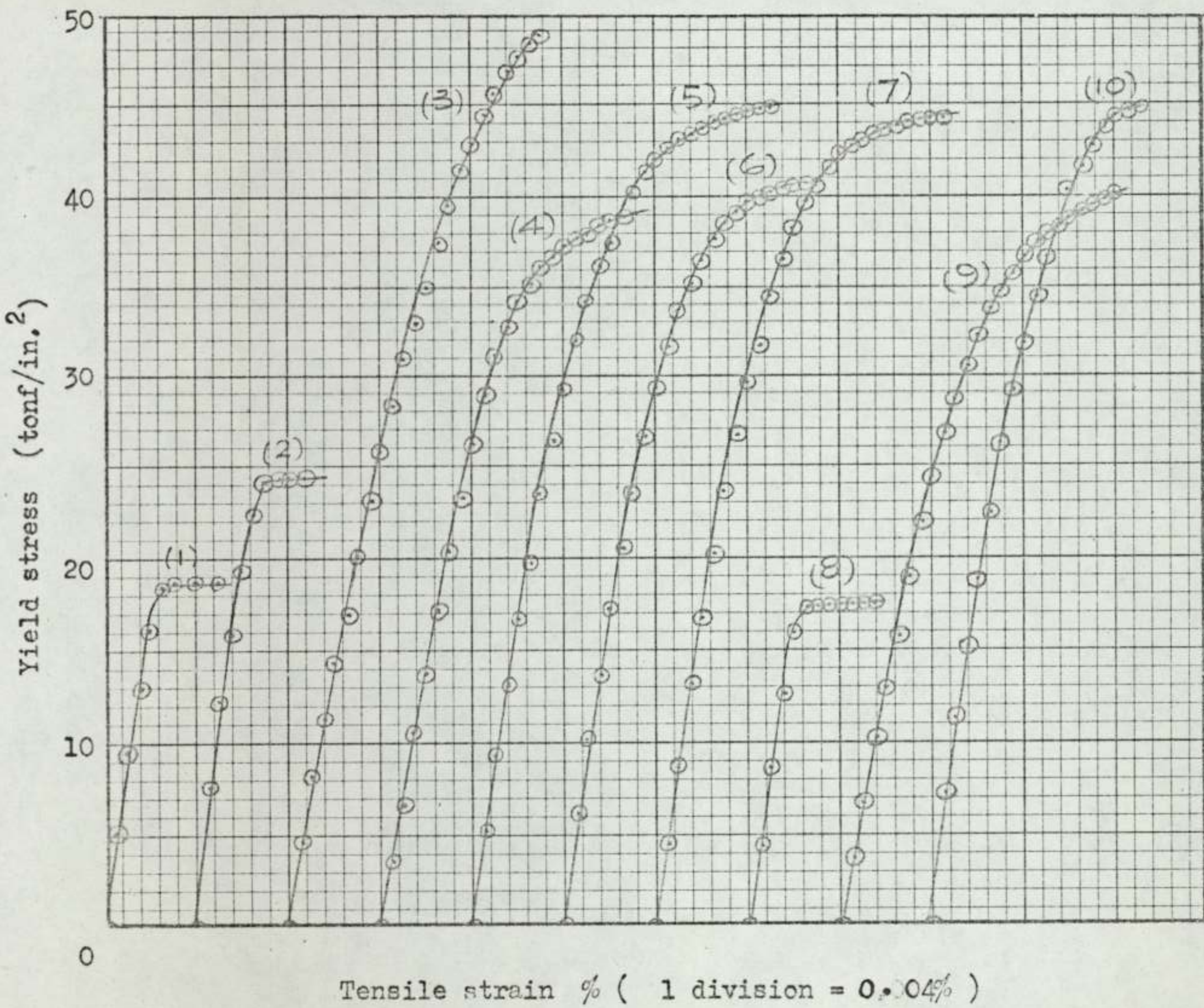

Curve number.	Prior cold-work (nominal) %	Nominal test-piece dimensions (in.)	
		°/dia.	Wall thk.
1	0	0.750	0.040
2	0	0.750	0.030
3	50	0.750	0.030
4	50	0.750	0.025
5	50	0.750	0.019
6	50	0.750	0.0125
7	50	0.750	0.0095
8	0	0.750	0.0075
9	50	0.750	0.0075
10	67	0.750	0.0075

FIG. A_3.11 TENSILE TEST DATA ON SPLAY-MEASUREMENT TEST MATERIAL. LOW CARBON STEEL.

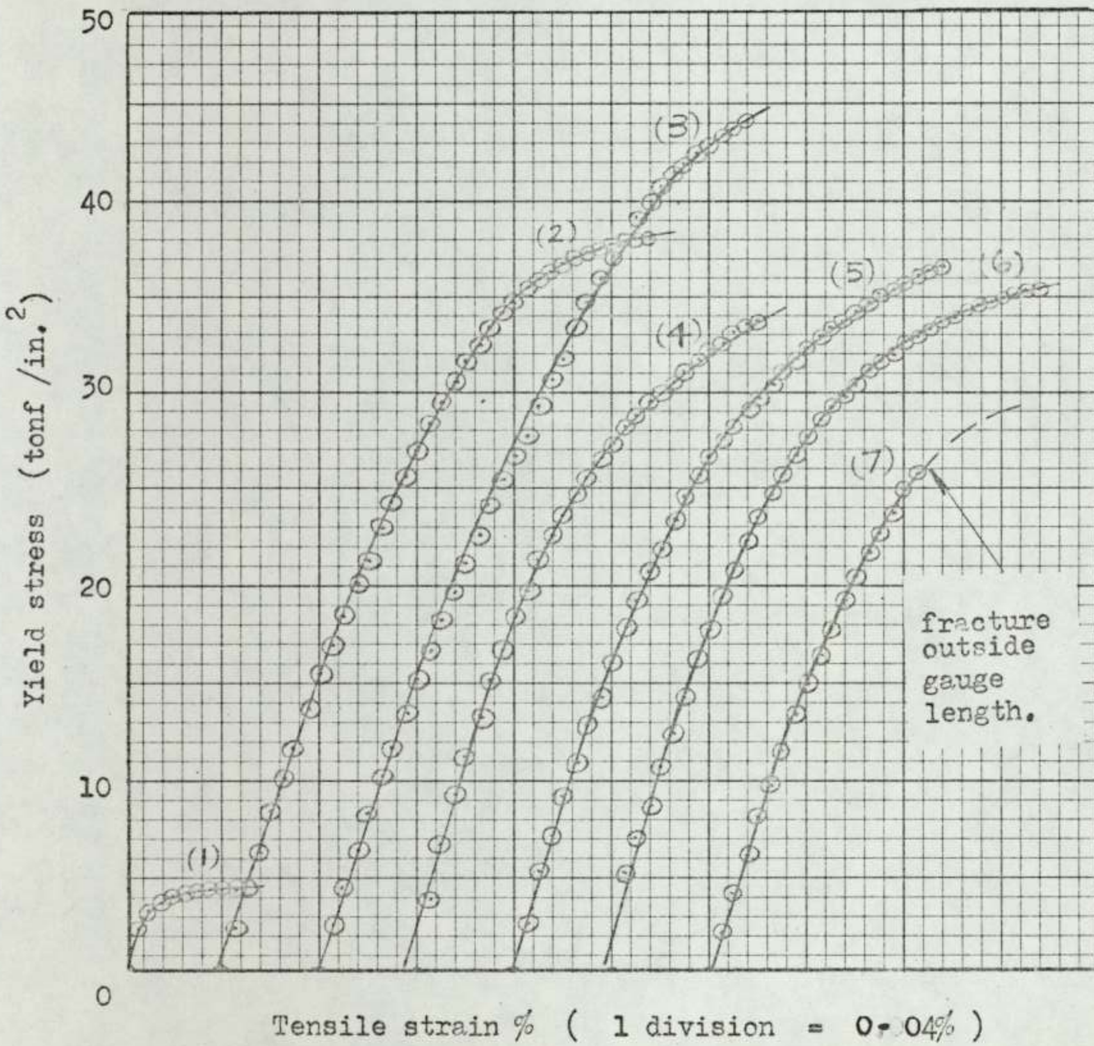

Curve number	Prior cold-work (nominal) %	Nominal test-piece dimensions (in.)	
		o/dia.	Wall thk
1.	0	0.750	0.0375
2.	50	0.750	0.0375
3.	67	0.750	0.0375
4.	50	0.750	0.025
5.	50	0.750	0.019
6.	50	0.750	0.0125
7.	50	0.750	0.0095

FIG. A_3.12 TENSILE TEST DATA ON SPLAY MEASUREMENT TEST MATERIAL. 70/30 BRASS.

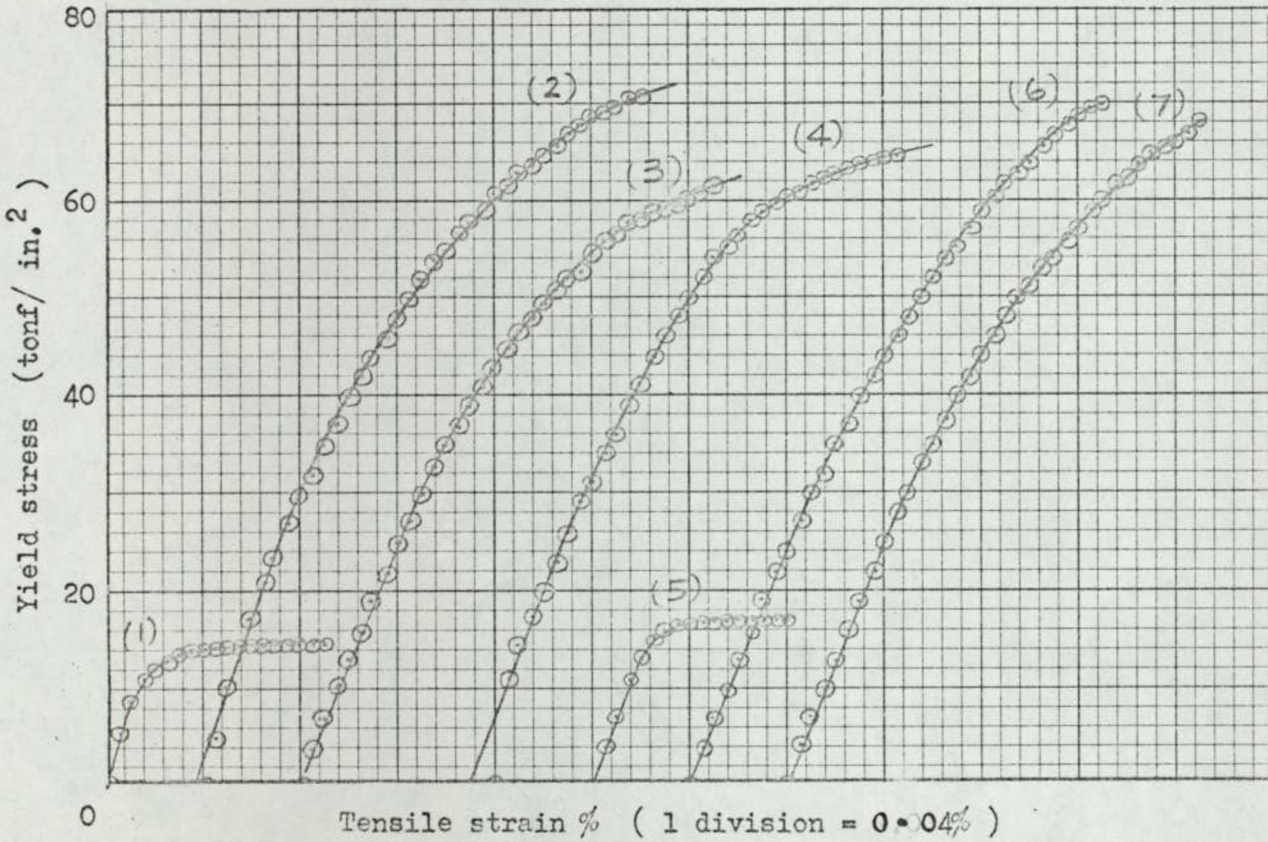

Curve number	Prior cold-work (nominal) %	Nominal test-piece dimensions (in.)	
		o/dia.	Wall thk
1	0	0.750	0.025
2	50	0.750	0.019
3	50	0.750	0.0125
4	50	0.750	0.0095
5	0	0.750	0.0075
6	50	0.750	0.0075
7	67	0.750	0.0075

FIG.A_3.13 TENSILE TEST DATA ON SPLAY-MEASUREMENT TEST MATERIAL. T304 STAINLESS STEEL.

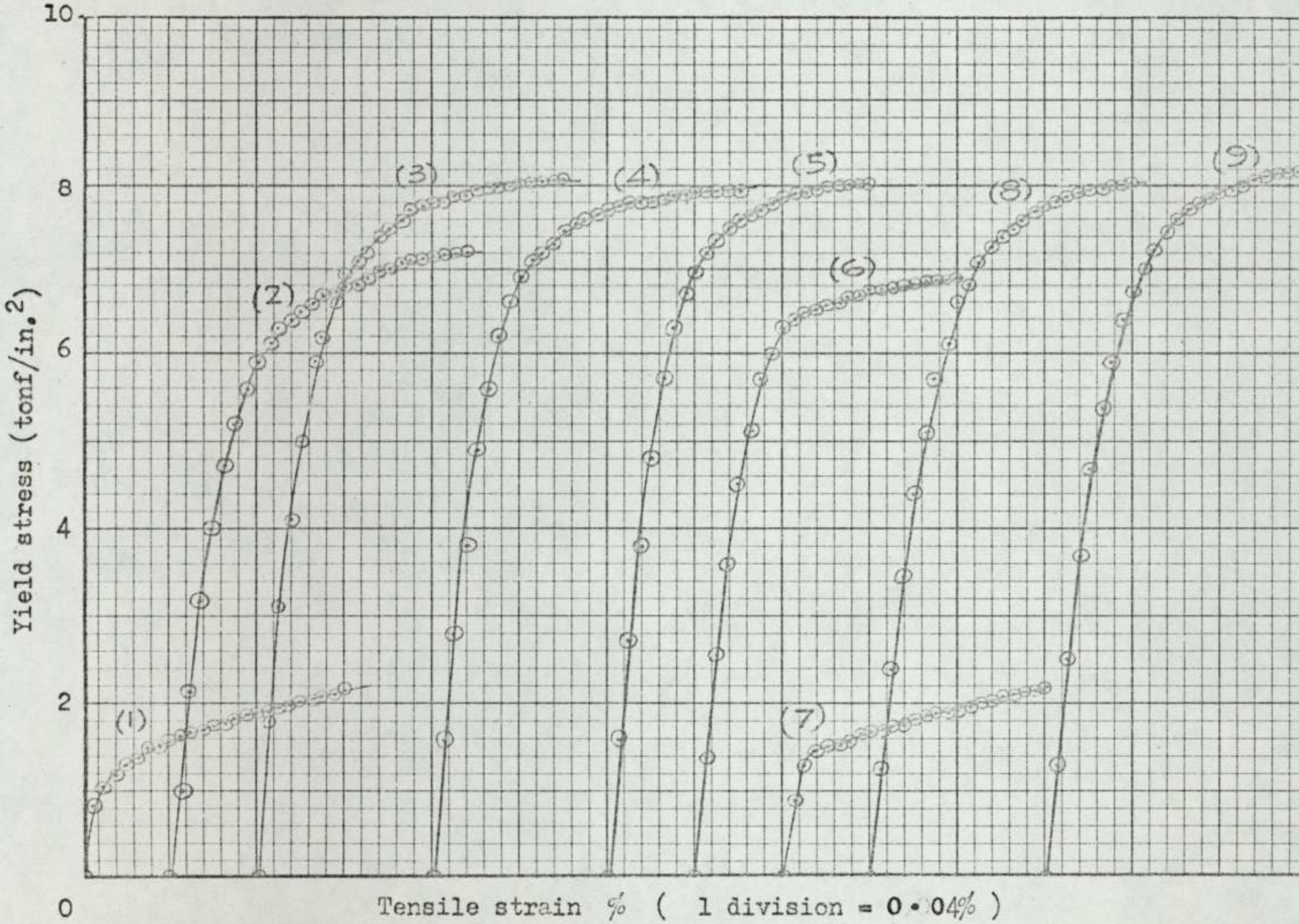

Curve number	Prior cold-work (nominal)	Nominal test-piece dimensions (in.)	
	%	o/dia.	Wall thk
1	0	0.750	0.0375
2	50	0.750	0.0375
3	67	0.750	0.0375
4	50	0.750	0.025
5	50	0.750	0.019
6	50	0.750	0.0125
7	0	0.750	0.0075
8	50	0.750	0.0075
9	67	0.750	0.0075

FIG. A_3.14 TENSILE TEST DATA ON SPLAY - MEASUREMENT TEST MATERIAL. ALUMINIUM.

Anvil breadth (b) in.	maximum specimen thickness (t) in.	minimum specimen thickness (t) in.
0.090	0.045	0.0225
0.050	0.025	0.0125
0.025	0.0125	0.0063

The smallest value of $\frac{W}{b}$ was thus $0.60/0.090 = 6.7$ which complied with the test condition $\frac{W}{b} \geq 6$

Manufacture of test specimens.

Specimens were machined from the four hollows using the following procedure;

(1) Each hollow length (6 in.) was machined with four external equi-spaced flats slightly wider than the finished specimen width.

(2) The hollows were then slit along the edges of the flats to the specimen width, using a straddle mill.

(3) The severed strips were removed from the parent hollow and clamped on a jig with the flat faces downwards. The inner face (corresponding to the bore of the hollow) was then machined to give the required specimen wall thickness.

A hardness check comparison made between specimens and hollows revealed that work-hardening had occurred in the specimens during machining. All specimens were therefore annealed before compression testing.

Subpress for plane-strain compression testing.

The subpress, illustrated in FIG. A_3.15, was an existing die-set which had been arranged for plane strain compression testing. The dial gauge was used to ensure that the test specimen was correctly re-positioned after removal for measurement and re-lubrication. It also served as a means of estimating strain increments during testing.

Before commencing tests the upper platen was fitted with central ball housing to ensure central load application. Also, guides were introduced to ensure that the specimen was always squarely located

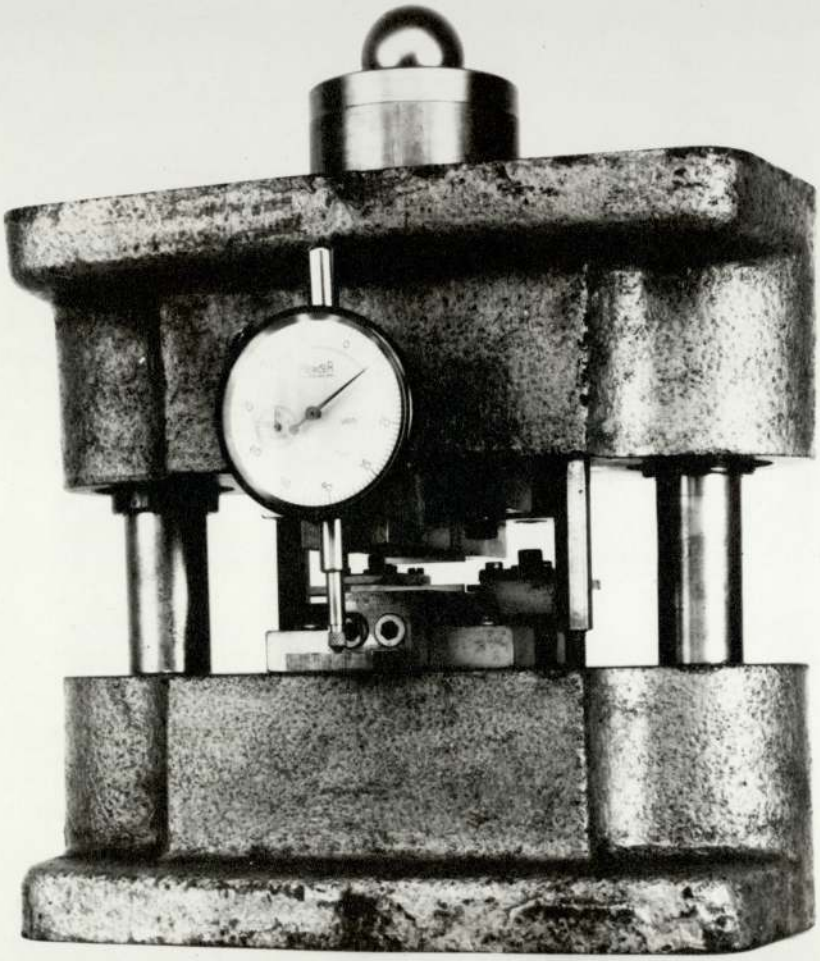

FIG. A_3.15 SUBPRESS FOR PLANE-STRAIN COMPRESSION TESTS.

to the compression anvils. In FIG. A_3.15 the upper platen is shown lifted clear by a screwed rod situated at the front right-hand side of the unit. This proved to be a useful means of platen separation for specimen removal and re-entering. During loading the rod was screwed down clear of the top platen.

<u>Testing procedure.</u>

Tests on low carbon steel, stainless steel and brass specimens were conducted on a 50 Tonf Denison testing machine at Tube Investments Limited. This machine proved too insensitive for aluminium tests which were carried out on a 5000 kg. Instron testing machine at Aston University.

The lubricant used for all materials was Rocol A.S.P. molybdenum disulphide grease.

Testing for each material proceeded as follows;

(1) After specimen lubrication, approximately 20 initial indentations were made with the 0.090 in. broad anvils, the deepest indentation corresponding to the limit of the required strain range. The intermediate indentations were selected to provide approximately even coverage of the range. On completing indentation the specimen was removed from the sub-press and the root thickness of each indentation accurately measured with a pin-headed micrometer.

(2) The specimen was re-lubricated and entered into the subpress with the shallowest indentation aligned with the anvils. The top platen was then lowered under load to provide about 5 % plastic strain, the corresponding load being noted on the test machine load-meter. Afterwards the specimen was removed and the new indented thickness measured. Thus the total strain and corresponding load to cause yielding was known for that particular indentation.

(3) The specimen was re-lubricated and the testing procedure repeated, indentations of roughly 5 % plastic strain being made eventually in all original indentations. At the appropriate $\frac{b}{t}$ ratio anvils were changed

in compliance with the test condition $2 < \frac{b}{t} < 4$

Test results.

Plane-strain yield stress was evaluated by dividing indentation load by the appropriate platen contact area b.w. Curves were then drawn of yield-stress against natural strain for each material, and appear as the upper curves in FIGS. A_3.16 - A_3.19. Plane-strain values of stress and strain σ, ε were then converted to equivalent stress and strain $\bar{\sigma}, \bar{\varepsilon}$, by the relationships;

$$\bar{\sigma} = \frac{\sqrt{3}}{2} . \sigma$$

$$\bar{\varepsilon} = \frac{2}{\sqrt{3}} . \varepsilon$$

These results appear as the lower curves in FIGS. A_3.16 - A_3.19.

(c) Combined results.

Stress-strain curves obtained from the uniaxial tensile tests (FIGS.A_3.11 - A_3.14) were fitted to the equivalent stress-strain curves, the point of tangency being identified by a letter representing each individual test-piece. The tables which accompany FIGS. A_3.16 - A_3.19 provide a means of comparison between the actual prior-strain (as given by the tests), and the nominal prior-strain.

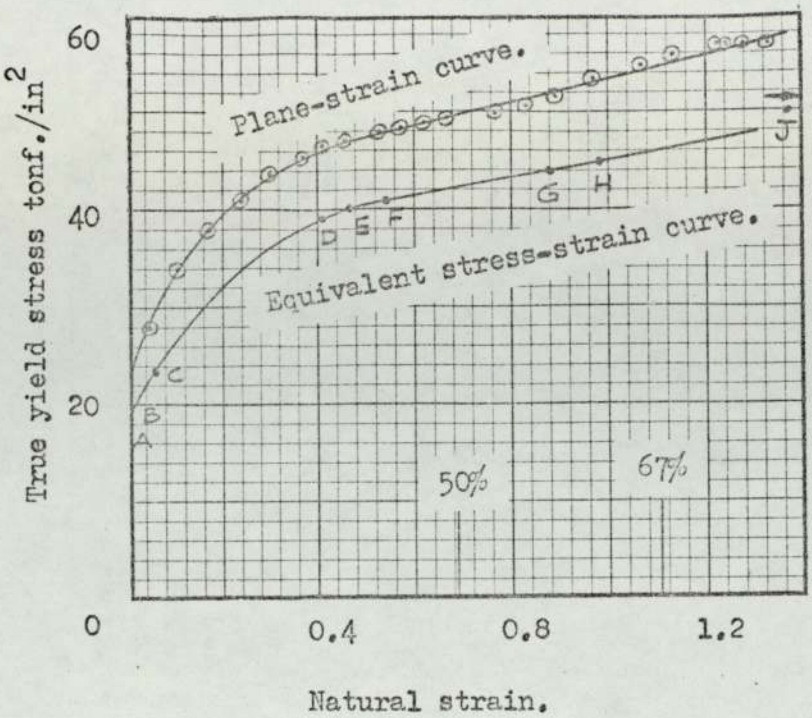

Code letter.	Prior cold-work. %	Nominal test-piece dimensions (in.)	
		o/dia.	Wall thk.
A	0	0.750	0.0075
B	0	0.750	0.040
C	0	0.750	0.030
D	50	0.750	0.025
E	50	0.750	0.0075
F	50	0.750	0.0125
G	50	0.750	0.0095
H	50	0.750	0.019
	67	0.750	0.0075
J	50	0.750	0.030

FIG. A3.16 SPLAY MEASUREMENT TEST PROGRAMME. TEST MATERIAL STRESS-STRAIN DATA. LOW CARBON STEEL.

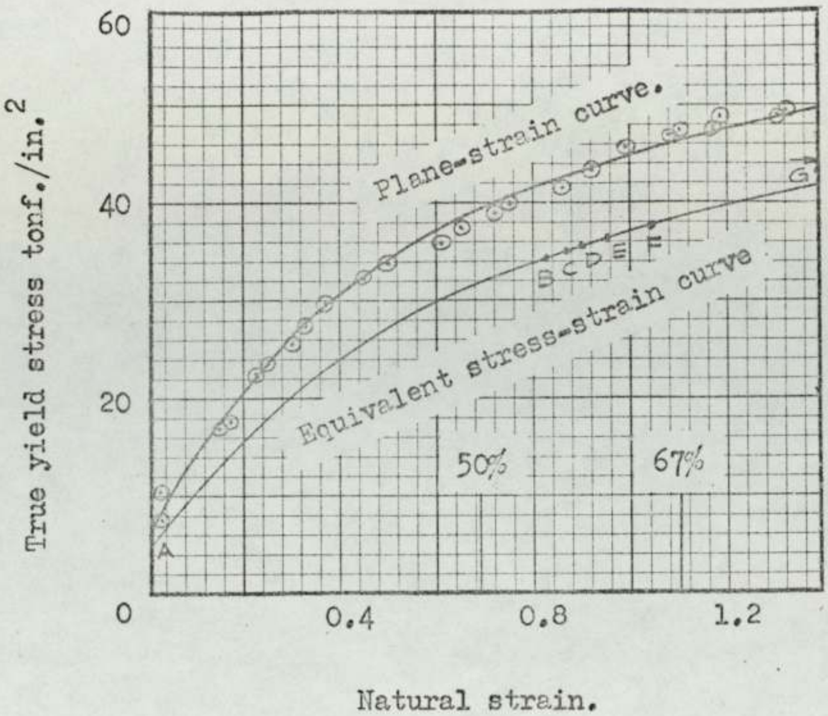

Code letter	Prior cold-work %	Nominal test-piece dimensions (in.)	
		°/dia.	Wall thk
A	0	0.750	0.0375
B	50	0.750	0.025
C	50	0.750	0.0095
D	50	0.750	0.0125
E	50	0.750	0.019
F	50	0.750	0.0375
G	67	0.750	0.0375

FIG.A_3.17 SPLAY MEASUREMENT TEST PROGRAMME. TEST MATERIAL STRESS-STRAIN DATA. 70/30 BRASS.

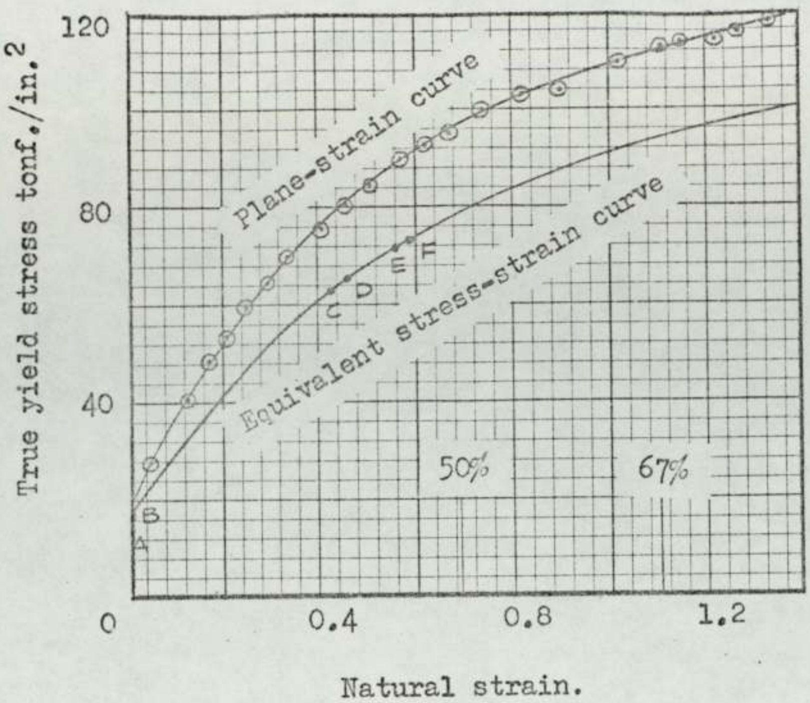

Code letter	Prior cold-work (nominal) %	Nominal test-piece dimensions (in.)	
		°/dia.	Wall thk
A	0	0.750	0.025
B	0	0.750	0.0075
C	50	0.750	0.0125
D	50	0.750	0.0095
E	67	0.750	0.0075
F	50	0.750	0.0075
	50	0.750	0.019

FIG. A_3.18 SPLAY MEASUREMENT TEST PROGRAMME. TEST MATERIAL STRESS-STRAIN DATA. T304 STAINLESS STEEL.

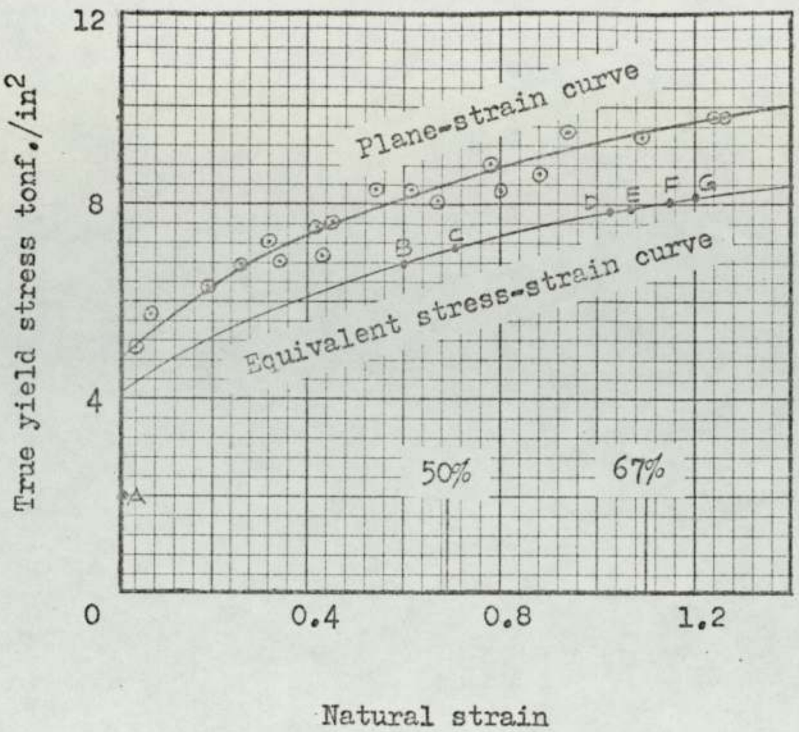

Code letter	Prior cold-work (nominal) %	Nominal test-piece dimensions (in.)	
		o/dia	Wall thk.
A	0	0.750	0.0375
	0	0.750	0.0075
B	50	0.750	0.0125
C	50	0.750	0.0375
D	50	0.750	0.025
E	50	0.750	0.019
	50	0.750	0.0075
F	67	0.750	0.0375
G	67	0.750	0.0075

FIG. A_3.19 SPLAY MEASUREMENT TEST PROGRAMME. TEST MATERIAL STRESS-STRAIN DATA. ALUMINIUM

A_4 THIRD EXPERIMENTAL PROGRAMME - PROVING TESTS.

A_4.1. Chemical analysis of cup material.

Low carbon steel.

Carbon	-	0.050 %
Silicon	-	0.007 %
Manganese	-	0.35 %
Sulphur	-	0.016 %
Phosphorus	-	0.006 %

70/30 brass.

Copper	-	69 %
Zinc	-	30.5 %

Aluminium.

Manganese	-	0.3 %
Silicon	-	0.2 %
Copper	-	0.01 %
Ferrite	-	0.03 %

$A_{4}.2$. Tabulated proving-test programme results.

TABLE A_4.1. DIMENSIONS OF CUPS FOR PROVING TESTS.

Redraw number	Cup material	Trimmed cup length (in.)	Distance below trimmed cup rim ($\frac{1}{8}$ in. intervals)	Wall thickness (in.)	Outside diameter (in.)
I	Steel.	2.3/8	0	0.043	3.244
			1	0.042	
			2	0.041	3.237
			3	0.040	
			4	0.039	3.235
			5	0.0385	
			6	0.038	3.232
			7	0.0376	
			8	0.0376	3.231
			9	0.0373	
			10	0.0368	3.231
I	Alum.	2.3/8	0	0.0445	3.248
			1	0.044	
			2	0.043	3.245
			3	0.042	
			4	0.0405	3.238
			5	0.0395	
			6	0.039	3.235
			7	0.0385	
			8	0.0375	3.232
			9	0.0372	
			10	0.0366	3.232
2	Steel.	3	0	0.044	2.581
			1	0.043	
			2.	0.0416	2.573
			3	0.0405	
			4	0.0397	2.574
			5	0.0395	
			6	0.039	2.574
			7	0.0384	
			8	0.038	2.574
			9	0.0375	
			10	0.0375	2.574
2	Brass	3	0	0.0445	2.593
			1	0.0435	
			2	0.0423	2.576
			3	0.0412	
			4	0.0406	2.574
			5	0.0403	
			6	0.040	2.574
			7	0.040	
			8	0.0395	2.575
			9	0.039	
			10	0.0384	2.574

TABLE - $A_4.2$.

PROVING TEST PROGRAMME - SPLAY AND REDRAW-LOAD DATA.

Test number	1P			2P			3P			4P		
Cup rim distance from die (in.)	(A) Cup rim splay %	(B) Redraw load (tonf.)	(G) Guided redraw load (tonf.)	(A) Cup rim splay %	(B) Redraw load (tonf.)	(G) Guided redraw load (tonf.)	(A) Cup rim splay %	(B) Redraw load (tonf.)	(G) Guided redraw load (tonf.)	(A) Cup rim splay %	(B) Redraw load (tonf.)	(G) Guided redraw load (tonf.)
2.	0	-	Peak load = 5.17 tonf.	0	1.31	Cup fractured at load = 2.16 tonf.	0	3.47	-	0	1.28	-
1.3/8	-	-		-	-		-	-	4.08	-	-	1.65
1.	0	4.80		0.03	1.77		0	4.50	-	0	1.76	-
7/8	-	-		-	-		-	-	4.27	-	-	1.79
5/8	-	-		-	-		-	-	-	-	-	1.81
9/16	-	-		-	-		-	-	-	-	-	1.85
1/2	0.06	4.80		0.06	2.10		0.15	4.94	4.52	0.15	2.00	1.85
7/16	0.09	5.15		0.43	2.17		1.32	4.85	-	1.26	1.96	1.89
3/8	0.71	5.25		1.70	2.15		2.16	4.76	4.56	2.24	1.93	1.92
5/16	2.49	5.00		3.48	2.03		2.76	4.76	4.54	2.80	1.89	1.99
1/4	3.80	4.94		3.97	1.99		3.16	4.70	4.58	3.15	2.00	1.93
3/16	3.74	5.15		4.04	2.06		3.26	4.80	4.58	3.28	2.00	1.89
1/8	2.09	4.70		2.43	2.15		2.64	4.90	4.43	2.82	2.00	1.93
1/16	-0.40	4.30		0.49	2.17		1.32	4.57	4.46	0.49	1.72	1.93
0	-	-		-	1.96		-	2.90	4.56	0	0.84	1.93

TABLE - A_4.3.

PROVING TEST PROGRAMME - SPLAY AND REDRAW-LOAD DATA.

Test number	5P		6P		7P		8P	
Cup rim distance from die (in.)	(A) Cup rim splay (%)	(B) Redraw load (tonf.)	(A) Cup rim splay (%)	(B) Redraw load (tonf.)	(A) Cup rim splay (%)	(B) Redraw load (tonf.)	(A) Cup rim splay (%)	(B) Redraw load (tonf.)
2	0	3.32	0	1.19	0	2.97	0	1.12
1	0	3.53	0	1.27	0	3.04	0.06	1.26
1/2	0	3.74	0.06	1.37	0.03	3.23	1.20	1.42
7/16	0	3.82	1.41	1.37	0.83	3.23	1.97	1.42
3/8	0.71	3.76	2.70	1.36	2.00	3.18	2.77	1.42
5/16	2.40	3.72	3.82	1.33	2.65	3.18	3.32	1.42
1/4	3.20	3.72	4.28	1.39	2.98	3.18	3.44	1.42
3/16	3.50	3.72	-	1.41	2.86	3.18	3.41	1.42
1/8	3.08	3.70	2.70	1.44	1.35	3.18	2.80	1.42
1/16	1.36	3.76	-0.06	1.46	-1.75	2.75	0.19	1.39
0	-	3.25	-	1.28	-	1.74	-	1.25

TABLE - A_4.4.

PROVING TEST PROGRAMME - SPLAY AND REDRAW-LOAD DATA.

Test number	Cup rim distance from die (in.)		(A) Cup rim splay (%)		(B) Redraw load (tonf)
	Ears	Valleys	Ears	Valleys	
9P	-	2	-	-	-
	-	1	-	-	5.11
	5/8	1/2	0	0	5.60
	9/16	7/16	0.03	0.22	5.69
	1/2	3/8	0.37	1.00	5.61
	7/16	5/16	1.79	2.34	5.36
	3/8	1/4	3.62	3.14	5.40
	9/32	3/16	5.04	3.14	5.65
	7/32	1/8	6.10	2.28	5.27
	1/8	1/16	6.35	-	-
	-	0	-	-	-
10p	2	2	0	0	1.65
	1	1	0.03	0.03	2.05
	1/2	1/2	0.22	0.22	2.29
	7/16	7/16	1.48	1.48	2.39
	3/8	3/8	2.40	2.40	2.35
	5/16	5/16	2.98	2.98	2.25
	1/4	1/4	3.30	3.30	2.20
	3/16	3/16	2.78	2.78	2.29
	1/8	1/8	2.37	2.37	2.40
	1/16	1/16	1.90	1.90	2.40
	0	0	-	-	2.20

TABLE - A_4.5.

PROVING TEST PROGRAMME - SPLAY AND REDRAW-LOAD DATA.

Test number	11P		12P		13P		14P	
Cup rim distance from die (in.)	(A) Cup rim splay (%)	(B) Redraw load (tonf.)	(A) Cup rim splay (%)	(B) Redraw load (tonf.)	(A) Cup rim splay (%)	(B) Redraw load (tonf.)	(A) Cup rim splay (%)	(B) Redraw load (tonf.)
2	0	3.29	0	2.72	0	2.71	0	2.91
1	0	3.75	0	3.70	0	3.13	0.04	3.62
1/2	0.04	3.94	0.04	4.10	0.04	3.40	0.12	3.82
7/16	0	3.94	0.16	4.10	0.12	3.40	0.35	3.88
3/8	0.16	3.97	0.46	4.10	0.62	3.42	1.00	3.85
5/16	1.51	3.87	2.12	4.05	2.17	3.29	2.55	3.70
1/4	3.20	3.60	3.60	3.79	2.86	3.18	3.43	3.51
3/16	3.94	3.45	4.50	3.58	3.10	3.15	3.70	3.42
1/8	3.82	3.45	4.35	3.53	3.02	3.10	3.40	3.42
1/16	1.74	3.15	2.51	3.36	0.77	2.71	1.62	3.42
0	-	1.45	-	2.33	-	1.55	-	2.34

TABLE - A_4.6.

PROVING TEST PROGRAMME - SPLAY AND REDRAW-LOAD DATA.

Test number	15P		16P		17P		18P	
Cup rim distance from die (in.)	(A) Cup rim splay (%)	(B) Redraw load (tonf.)	(A) Cup rim splay (%)	(B) Redraw load (tonf.)	(A) Cup rim splay (%)	(B) Redraw load (tonf.)	(A) Cup rim splay (%)	(B) Redraw load (tonf.)
2	0	3.50	0	2.94	0	2.60	0	2.77
1	0	3.60	0	3.88	0	2.91	0.04	3.56
1/2	0	3.67	0	4.16	0	3.27	0	3.78
7/16	0	3.71	0	4.19	0	3.30	0.08	3.83
3/8	0	3.71	0	4.19	0	3.30	0.08	3.83
5/16	0	3.71	0	4.27	0.04	3.30	-	3.88
1/4	0.04	3.75	0	4.11	0.08	3.37	0.15	3.88
3/16	0.08	3.81	0.27	-	0.19	3.37	0.46	3.91
1/8	0.35	3.81	1.12	4.20	1.05	3.28	1.31	3.91
1/16	2.13	3.75	2.63	4.07	1.82	3.15	2.43	3.81
0	2.94	3.50	3.25	3.60	2.32	3.10	2.81	3.57
-1/32	-	3.30	-	-	-	-	-	-
-1/16	-	3.15	3.60	-	2.48	-	2.92	3.70
-1/8	-	-	-	-	0.62	-	1.70	-

TABLE - A_4.7.

PROVING TEST PROGRAMME - SPLAY AND REDRAW LOAD DATA.

Test number	Cup rim distance from die (in.)		(A) Cup rim splay (%)		(B) Redraw load (tonf.)
	Ears	Valleys	Ears	Valleys	
19P	-	2.	-	-	3.68
	1.5/8	1.1/2	0	0	-
	1.1/8	1.	0	0	3.98
	5/8	1/2	0	0	4.20
	9/16	7/16	0	0	4.20
	1/2	3/8	0	0.12	4.20
	7/16	5/16	0.77	1.31	4.37
	3/8	1/4	2.82	2.74	4.27
	5/16	3/16	4.81	3.28	4.10
	1/4	1/8	6.16	2.70	3.88
	5/32	1/16	6.16	0.39	3.83
	-	0	-	-	2.58
20P	3/4	3/4	Cup fractured.		

TABLE - A_4.8

PROVING TEST PROGRAMME - SPLAY AND REDRAW-LOAD DATA.

Test number	21P		22P	
Cup rim distance from die (in.)	(A) Cup rim splay %	(B) Redraw load (tonf.)	(A) Cup rim splay %	(B) Redraw load (tonf.)
2.	0	-	0	2.97
1.	0	2.52	0.04	3.10
1/2	0.35	2.90	0.50	3.33
7/16	0.62	2.90	0.97	3.33
3/8	1.28	2.83	1.55	3.25
5/16	1.70	2.68	1.97	3.20
1/4	2.10	2.60	2.40	3.05
3/16	2.29	2.53	2.62	2.97
1/8	1.90	2.60	2.44	2.97
1/16	-0.97	2.68	-0.54	3.10
0	-	2.33	-	3.05

TABLE - A_4.9.

PROVING TEST PROGRAMME - HOLD-DOWN LOAD DATA.

Test number.		Hold-down load (tonf)	Test number.		Hold-down load (tonf)
1P	(B)	1.50-1.70	12P	(B)	1.30-1.60
	(G)	1.50			
2P	(B)	1.25-1.45	13P	(B)	1.30-1.65
	(G)	1.20			
3P	(B)	1.10-1.30	14P	(B)	1.20-1.50
	(G)	1.10-1.40			
4P	(B)	1.25-1.50	15P	(B)	1.35-1.60
	(G)	1.25-1.50			
5P	(B)	1.25-1.50	16P	(B)	1.25-1.50
6P	(B)	1.40-1.50	17P	(B)	1.50-1.60
7P	(B)	1.25-1.50	18P	(B)	1.25-1.50
8P	(B)	1.50-1.60	19P	(B)	1.25-1.60
9P	(B)	1.30-1.50	20P	(B)	Cup fractured.
10P	(B)	1.20-1.35	21P	(B)	0
11P	(B)	1.10-1.40	22P	(B)	0

TABLE A_4.10 TENSILE TEST RESULTS ON BLANKS FOR PROVING - TEST CUPS.

Material	Test piece orientation relative to rolling direction (deg.)	0.2 % proof stress. Tonf./in^2.
Aluminium.	0	4.35
	0	4.44
	45	4.70
	45	4.38
	90	4.50
	90	4.57
70/30 brass.	0	12.45
	0	12.80
	45	12.60
	45	12.75
	90	13.00
	90	13.00
Low carbon steel.	Random	11.65
		11.85
		12.10
		12.10
		11.42
		11.65

A_5. JUSTIFICATION OF THEORETICAL ASSUMPTIONS

$A_5$1. Constant cup wall length during splaying

In developing the 'tangential' and 'hyperbolic' theories of splaying it was assumed that the effected wall length l_o remained constant throughout. It is true that the volume $2\pi r_o . t_o . l_o$ must be constant, but during the splay phase it cannot be assumed without justification that the current length of wall l undergoes no change from its initial value l_o. In the splay phase elements above the current neutral point are splaying under the action of a high tensile circumferential stress which is largely responsible for yielding, although the possibility of a small radial stress cannot be precluded except at the very rim. As a result of the stress condition, currently splayed elements will tend to increase in circumferential length, shorten in radial length, and become thinner. The strain ratios will be approximately $-\varepsilon_1' = -\varepsilon_2 = \frac{1}{2}\varepsilon_3$. Below the current neutral point the reverse straining situation will occur under the action of a high compressive circumferential stress σ_3. Although a tensile stress σ_1 will be present due to radial drawing it will at this stage be small compared with σ_3 and therefore exert little influence on the strain ratios which will be approximately $\varepsilon_1 = \varepsilon_2 = -\frac{1}{2}\varepsilon_3$.

It is thus seen that the effects of splaying and radial drawing during the splay-phase have opposing influence in changing the wall length involved in splaying such that they tend to be self-cancelling. The quantitative effect on the wall length l is analysed below in respect to the 'tangential' theory. Similar results appertain tothe 'hyperbolic' theory. FIG A_5.1 illustrates the situation just before maximum splaying occurs, when the plane of steady-state bending has rotated through an angle θ. At point A the current wall thickness $t > t_o$, whilst at the rim $t < t_o$. The element located at r_o will have thickness t_o since this particular element has thinned in splaying and afterwards thickened by an equal amount of radial drawing. The thickness strain at A is given approximately by $\ln \frac{\hat{t}}{t_o} = \frac{1}{2} \ln \frac{r_o}{r_o - R_o(1-\cos\theta)}$

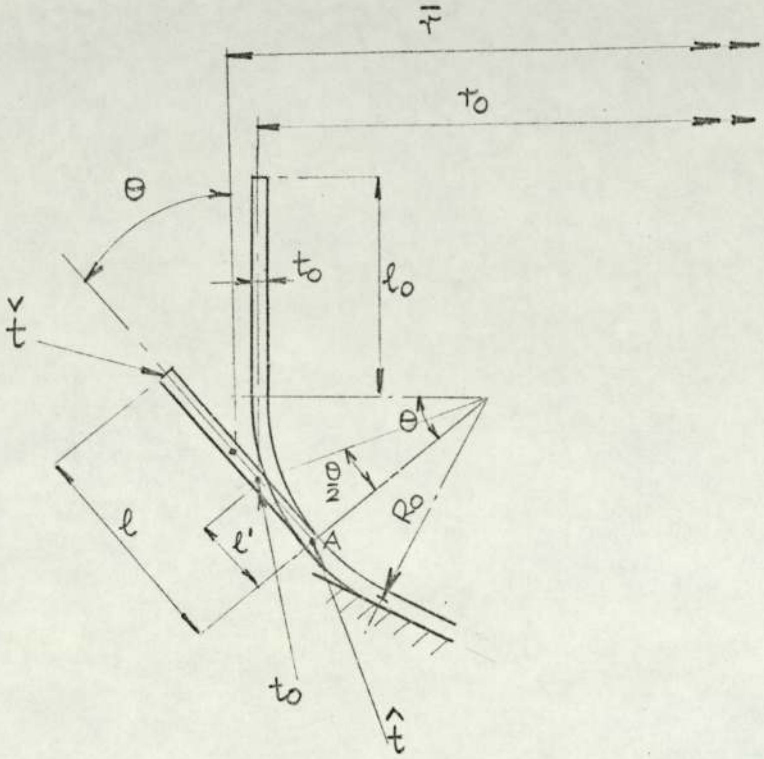

FIG $A_5 1$. NOMENCLATURE FOR CALCULATING THE TRUE UNBENT CUP WALL LENGTH IN TANGENTIAL SPLAYING giving $$\hat{t} \simeq t_o\left[1 + \frac{1}{2}\,\frac{R_o}{r_o}\left(1 - \cos\theta\right)\right] \qquad \text{———} \quad A_5.1$$

The length $\ell' = R_o \tan\theta/2$, and assuming that thickness varies uniformly over ℓ

$$\frac{\hat{t} - t_o}{R_o \tan\frac{\theta}{2}} = \frac{t_o - \check{t}}{\ell - R_o\tan\frac{\theta}{2}}$$

or $$\check{t} = t_o\left[1 - \frac{1}{2}\,\frac{R_o}{r_o}\left(1 - \cos\theta\right)\left(\frac{\ell - R_o\tan\frac{\theta}{2}}{R_o\tan\frac{\theta}{2}}\right)\right] \qquad \text{———} \quad A_5.2$$

Now the volume of the splayed cup wall = $2\pi.\bar{r}.a$ were $\bar{r}$ is the radius to the centroid of the section, and a = the section area. It can be shown that,

$$\bar{r} = \frac{\ell\sin\theta}{2}\left[\frac{1 + \frac{R_o}{r_o}\left(1-\cos\theta\right)\left(\frac{1}{2} - \frac{\ell}{3R_o\tan\frac{\theta}{2}}\right)}{1 + \frac{R_o}{r_o}\left(1-\cos\theta\right)\left(\frac{1}{2} - \frac{\ell}{4R_o\tan\frac{\theta}{2}}\right)}\right] + r_o - R_o\left(1-\cos\theta\right)$$

and

$$a = t_o.\ell\left[1 + \frac{R_o}{r_o}\left(1-\cos\theta\right)\left(\frac{1}{2} - \frac{\ell}{4R_o\tan\theta/2}\right)\right]$$

Equating of initial and current volumes leads to the expression,

$$\frac{\ell_o}{\ell} = \left[1 + \frac{R_o}{r_o}\left(1-\cos\theta\right)\left(\frac{1}{2} - \frac{\ell}{3R_o\tan\theta/2}\right)\right]\left\{\frac{\ell\sin\theta}{2r_o} + \frac{\left[1 - \frac{R_o}{r_o}\left(1-\cos\theta\right)\right]\left[1 + \frac{R_o}{r_o}\left(1-\cos\theta\right)\left(\frac{1}{2} - \frac{\ell}{4R_o\tan\theta/2}\right)\right]}{\left[1 + \frac{R_o}{r_o}\left(1-\cos\theta\right)\left(\frac{1}{2} - \frac{\ell}{3R_o\tan\theta/2}\right)\right]}\right\} \qquad A_5.3$$

Equation $A_5.3$ is not readily solved in terms of $\frac{R_o}{r_o}, \frac{\ell}{R_o}, \theta$.

However to observe the effect of a change in wall length on splaying two situations were investigated representing severe splaying with thin-walled and thick-walled cups. Using the expression for maximum tangential rim-splay based on ℓ_o , a value of θ was determined for the two situations (1) $R_o/t_o = 4$, $r_o/t_o = 48$, and (2) $R_o/t_o = 4$, $r_o/t_o = 12$. Values of ℓ/ℓ_o were then found from equation $A_5.3$ by successive approximation, commencing with $\ell = \ell_o$ in the right-hand side. In both cases it was found l/l_o = •995, i.e. during the splay-phase the wall length tended to shorten very slightly. The effect on maximum rim splay was: as follows;

(1) Thin-walled cup

$$\hat{\Delta s}_{(l_o)} = 5.52\ \%$$
$$\hat{\Delta s}_{(l)} = 5.48\ \%$$

Error = 0.73 % on $\hat{\Delta s}_{(l_o)}$

(2) Thick-walled cup

$$\hat{\Delta s}_{(l_o)} = 6.6\ \%$$
$$\hat{\Delta s}_{(l)} = 6.6\ \%$$

Error = 0

The reason for the improved result with lower t_o/t_o ratios is that the term $\frac{R_o}{r_o}$ predominates in the expression for splaying, and a slight change in the term $\frac{l_o}{r_o}$ is therefore of less significance.

It was concluded that the errors involved in using l_o to determine splaying are not serious, and are justifiable in view of the simplifications so obtained.

$A_5 2$ Change in zone geometry below the plane of previous steady-state bending

When developing tangential and hyperbolic splay theories it was assumed that during the splay-phase the cup wall currently below point A (FIG A_5.2) would remain bent to radius R_O, and would not unbend as constraint exercised by the cup rim region diminished. The purpose of this appendix is to provide justification for that assumption.

Suppose that during splaying the cup wall below A unbent to some radius $R_O' > R_O$ such that the point A moved outwards to a radius $r > r_O$. Now this particular element has previously bent to R_O when A was at A_O, and therefore must unbend from this radius. Therefore bending work is equal to that in the steady-state, and hence the total specific work for the element on reaching the die at B must exceed that in steady-state. On the hypothesis that splaying is associated with a decrease in process work such a situation is unlikely to be valid. It could be argued that the zone geometry may change such that die contact takes place above point B and therefore that overall radial drawing work for t the element may decrease below steady-state. This does not alter the fact that on reaching B the elemental work would have exceeded that of steady-state. It would seem therefore that any unbending of the wall below A could only be accommodated provided elements do not splay i.e. those elements below A cannot exceed a radius $r > r_O$. This possibility is now investigated.

FIG $A_5$2. shows the splay situation after the element at A_O, when splaying commenced, has moved into the zone to A via the path R_O, θ. Suppose that some unbending had occurred below A such that the element had traversed an alternative path and is currently located at A', the instantaneous radius of bending being R_O'. The position of A' along the arc $A'B$ is given by the volume constancy condition $V_{AB} = V_{A'B}$. Since $R_O' > R_O$ it follows $(\alpha - \theta') < (\alpha - \theta)$. It is seen that the element has received less radial drawing work in

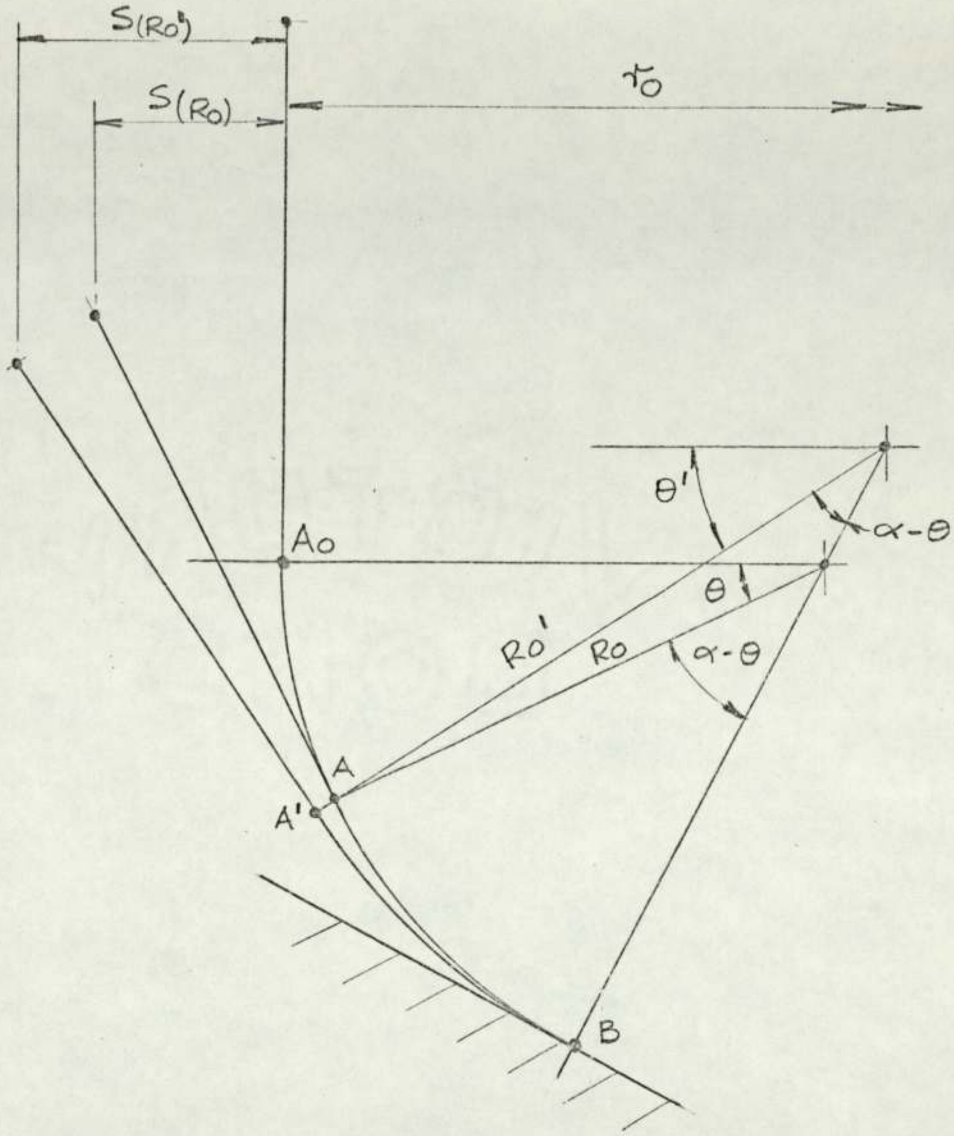

FIG A_5.2 ZONE GEOMETRY DURING SPLAYING reaching A' than in reaching A. However the work of elements $r < r_o$ cannot be considered in isolation from the remainder of the cup wall above A or A', and in deforming to radius R_o' appreciably greater bulk work is involved in splaying and subsequent radial drawing than if the radius remained constant at R_o. It was therefore considered reasonable to assume constant curvature below point A throughout the splay-phase.